

**Study of Allene-Based Ligands for Transition Metal  
Complexes – Synthesis and Applications in  
Catalysis and as Metallodrugs**



**Hanna Katarzyna Maliszewska**

The thesis is submitted in partial fulfilment of the requirements for the  
degree of Doctor of Philosophy

at

University of East Anglia, Norwich

School of Chemistry

March 2021

## Declaration

The research in this thesis is, to the best of my knowledge, original and my own work except where due references have been made.

Parts of this work have been published:

*“Allene-derived metal complexes: synthesis and first applications in catalysis”*, H. K. Maliszewska, D. L. Hughes, M. P. Muñoz, *Dalton Trans.* **2020**, 49, 4034-4038.

Hanna Maliszewska

March 2021

## Abstract

From being regarded as a chemical curiosity the allene functional moiety emerged as one of very useful synthetic tools of modern organic chemistry over the past few decades. Inherent axial chirality of the allene skeleton makes it especially attractive in the context of highly demanded new asymmetric synthesis methods. This doctoral thesis explores the use of the allene group as a backbone in a new ligand scaffold for the synthesis of novel allene-derived transition metal complexes for applications in catalysis and as metallodrugs.

Examples of optically active allene-containing complexes equipped mainly with phosphorus-based donor groups have been developed in the past decade and some of them have been found to act as catalysts in asymmetric transformations. However, the field remains highly underexplored.

This doctoral study presents the development and synthesis of new allene-based ligand candidates as well as the use of reported examples in unprecedented settings. These ligands were used to prepare a range of novel symmetric, non-symmetric, neutral and cationic complexes with Pd, Pt and Au metal centres. Depending on the nature of the metal used, the allene-based ligands could retain their cumulene system in the new organometallic compounds. While in the presence of others, the cyclisation afforded new carbene-type complexes (Figure 1). The new series of organometallic compounds were extensively characterised including techniques such as HR-MS, X-ray diffraction, variable temperature NMR spectroscopy and cyclic voltammetry.

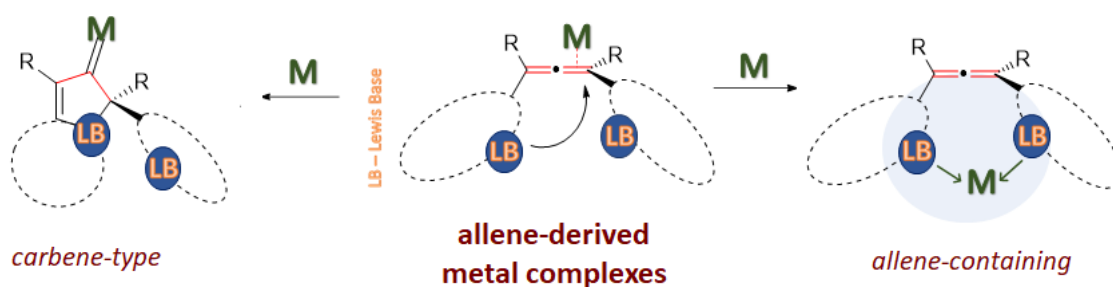


**Figure 1** Two classes of allene-derived metal complexes.

The synthesis of allene-derived metal complexes was followed by the investigation of their catalytic activity and bioactivity. The new compounds performed well as catalysts in Heck reaction, cyclisation of 1,6-enynes or metal-catalysed nucleophilic addition to allenes. Preliminary testing of the antimicrobial properties of new complexes showed their high toxicity towards bacteria and fungi with one hit compound currently being evaluated in *in vivo* models. The antiproliferative properties against MDA-MB-231 human breast adenocarcinoma cancer

cell line was probed, showing cytotoxicity in a low micromolar range for selected compounds. The new allene-derived complexes were also found to interact with non-canonical DNA secondary structures such as i-motif and G-quadruplex, giving a first look at potential mechanism of action of these metallodrug candidates.

Preparation of optically enriched allene-based ligands for the asymmetric version of the project was also briefly explored.



## **Access Condition and Agreement**

Each deposit in UEA Digital Repository is protected by copyright and other intellectual property rights, and duplication or sale of all or part of any of the Data Collections is not permitted, except that material may be duplicated by you for your research use or for educational purposes in electronic or print form. You must obtain permission from the copyright holder, usually the author, for any other use. Exceptions only apply where a deposit may be explicitly provided under a stated licence, such as a Creative Commons licence or Open Government licence.

Electronic or print copies may not be offered, whether for sale or otherwise to anyone, unless explicitly stated under a Creative Commons or Open Government license. Unauthorised reproduction, editing or reformatting for resale purposes is explicitly prohibited (except where approved by the copyright holder themselves) and UEA reserves the right to take immediate 'take down' action on behalf of the copyright and/or rights holder if this Access condition of the UEA Digital Repository is breached. Any material in this database has been supplied on the understanding that it is copyright material and that no quotation from the material may be published without proper acknowledgement.

## Acknowledgments

I would like to thank the Faculty of Science, University of Anglia (UEA), for funding the PhD studentship that allowed me to carry out this doctoral research. This work would have never been accomplished without the input from a number of brilliant collaborators and colleagues both at UEA and externally to whom I am deeply grateful. In particular, I extend my thanks to Dr David Hughes (UEA) for crystallographic analyses of a number of structures presented in the thesis and Dr J. Christensen (UK National Crystallography Service, University of Southampton) for analysis of structure **141**. To Dr Abdula-Sada (University of Sussex) and National Mass Spectrometry Facility (Swansea) for HR-MS analyses. To Stephen Boyer (London Metropolitan University) for elemental analysis. To the Fielden group (UEA) for help with cyclic voltammetry and X-ray crystallography training. To Dr Colin Macdonald (UEA) for help with NMR experiments. I am very grateful to the Waller group (UCL, formerly UEA), in particular to Dr Zoë Waller, Dr Mahmoud Abdelhamid and Ying Xia, for the analyses of the interactions of our compounds and DNA. My deep thanks go to the Marin group (UEA), Dr Maria J. Marin and Carla Arnau del Valle for the training and collaboration on cell culturing and cytotoxicity assays and help with UV-Vis and fluorescence spectroscopy. Thanks to MChem student Tino Freestone for the synthesis of fluorinated ligand **97e**. Finally thanks to the Community for Open Antimicrobial Drug Discovery (CO-ADD, University of Queensland, Australia) for carrying out the antimicrobial assays.

There is no doubt that my PhD degree has been so far one of the most formative experiences, but also one of the most stimulating and enjoyable. This was possible thanks to a great number of amazing people that I had met along the way and I would like to take this opportunity to express my deepest thanks to them. I would like to thank all the kind and helpful people from the Schools of Chemistry and Pharmacy at UEA, in particular faculty members who guided my academic journey since my master's degree. Thanks to Prof. Andrew Cammidge for his mentorship especially in my first year at UEA and to the whole faculty of Organic Department. I am very grateful to my second supervisor Dr Chris Richards for all his insights and suggestions to improve my research. Likewise, thanks to Dr Zoë Waller, Dr John Fielden, Dr Rianne Lord and Dr Maria J. Marin from other departments who were always ready with their assistance whenever I had doubts about less familiar aspects of chemistry.

My experience wouldn't be the same if not for some brilliant people I had a chance to work with in the Muñoz group. Thanks to Dr José Miguel Alonso Gomez for his continuous, invaluable presence and support. I am also very grateful to Dr Lewis Williams for his guidance in the later stages of the project. Thanks to other students doing their research in the group, both undergrads and postgrads. Especially thanks to my fellow PhD students Andreas

Apostolides and Carla Arnau del Valle for sharing their experiences with me. In particular, Carla was not only a great colleague always finding time to help me with the research but also a great friend outside of the lab. I will always look back with fond memories on all the fun times we shared with Carla and Carlos Juan Carot.

Of course my biggest thanks go to Dr Maria Paz Muñoz. Paz, it is difficult to name all the things I am grateful for! Thanks for being a great mentor during my masters and for encouraging me and believing in my potential to pursue further study. I am not sure if I would have decided to do a PhD without the great experience I had in your lab. Thank you for not only being a teacher and a role model to me, but also for making me feel as a valued colleague and a team-member. Thank you for your constant support, helping me to build my confidence, all your advice, guidance, discussions and time that helped me to develop professionally and personally.

Last but definitely not least, I would like to thank my family. I would never be where I am now without the love and support from my parents Beata and Ireneusz Dyk, my sisters Maria and Amelia, my godmother Marta Ciesielska, my new family Marzena, Jacek and Sandra Maliszewscy and most importantly my husband Konrad Maliszewski. Thank you all!

**Abbreviations and Acronyms**

A - Adenine

AAA – Asymmetric Allylic Alkylation

Acac - Acetylacetone

AcOEt – Ethyl acetate

AIDS – Acquired Immune Deficiency Syndrome

Anal. – Elemental Analysis

ASAP – Atmospheric Solid Analysis Probe

BINAP - 2,2'-Bis(diphenylphosphino)-1,1'-binaphthalene

Bipy – 2,2'-Bipyridine

BLA – Bond Length Alternation

Boc - *tert*-Butyloxycarbonyl

brs – broadened signal

BSA - Bis(trimethylsilyl)acetamide

C - Cytosine

CAAC carbenes - Cyclic Alkyl Amino Carbene

Cat. – Catalyst

CC<sub>50</sub> – concentration at 50% cytotoxicity

CD – Circular Dichroism

CIP priority rules – Cahn-Ingold-Prelog priority rules

CO-ADD – Community for Open Antimicrobial Drug Discovery

Conv. - Conversion

COSY – Correlation Spectroscopy

CTB - CellTiter-Blue®

CV – Cyclic voltammetry

d – doublet

DBU - 1,8-Diazabicyklo[5.4.0]undek-7-en

DCC - *N,N'*-Dicyclohexylcarbodiimide

DCD model – Dewar-Chat-Duncanson model

DFT – Density Functional Theory

DIAD - Diisopropyl azodicarboxylate

DIBAL - Diisobutylaluminum hydride

DMAP - 4-Dimethylaminopyridine

DMEM - Dulbecco's Modified Eagle Medium  
 DMF – Dimethylformamide  
 DMP - Dess–Martin Periodinane  
 DMSO – Dimethyl Sulfoxide  
 DNA – Deoxyribonucleic Acid  
 E1 – Elimination reaction  
 EA – Elemental Analysis  
 EDG – Electron Donating Group  
 EDTA - Ethylenediaminetetraacetic Acid  
 ee – enantiomeric excess  
 EI – Electron Impact  
 equiv. - equivalent  
 ES – Experimental Section  
 ESI – Electrospray Ionisation  
 EWG – Electron Withdrawing Group  
 FBS – Fetal Bovine Serum  
 FID - Fluorescent Intercalator Displacement  
 FMO – Frontier Molecular Orbital  
 FRET - Förster Resonance Energy Transfer  
 G – Guanine  
 G +ve – Gram-positive bacteria  
 G -ve – Gram-negative bacteria  
 Gem – geminal  
 HC<sub>10</sub> – concentration at 10% haemolytic activity  
 HEG – Hexaethylene Glycol  
 HMBC – Heteronuclear Multiple Bond Coherence Spectroscopy  
 HOMO – Highest Occupied Molecular Orbital  
 HPLC – High Performance Liquid Chromatography  
 HR-MS – High Resolution Mass Spectrometry  
 HSQC – Heteronuclear Single Quantum Coherence Spectroscopy  
 HWE reaction - Horner-Wadsworth-Emmons  
 IC<sub>50</sub> - Half maximal inhibitory concentration  
 IR – Infrared Spectroscopy  
*J* – coupling constant in NMR spectroscopy

L – Ligand  
 L-AA – L-Ascorbic Acid  
 LB – Lewis base  
 LG – Leaving Group  
 LiHMDS - Lithium bis(trimethylsilyl)amide  
 m - multiplet  
 M – Metal atom or complex  
 MIC – Minimum Inhibitory Concentration  
 Min – Minute  
 mit - Mitoxantrone  
 Mol - Mole  
 MS – Mass Spectrometry  
 Ms – Mesyl group  
 MTT - 3-(4,5-dimethylthiazol-2-yl)-2,5-diphenyltetrazolium bromide  
 MW - Microwave  
 NHC carbenes – N-Heterocyclic carbenes  
 NIS - N-Iodosuccinimide  
 NMR – Nuclear Magnetic Resonance  
 NOESY – Nuclear Overhauser Effect Spectroscopy  
 NSI – Nanospray Ionisation  
 Nu – Nucleophile  
 O – Oxidation process  
 ORTEP - Oak Ridge Thermal Ellipsoid Plot  
 PBS-B – Phosphate-buffered saline for biological applications  
 Pet – Petroleum ether  
 ppm – parts per million  
*p*TsOH – *para*-Toluenesulfonic acid  
 Py - Pyridine  
 q – quartet  
 R – generic group (H, alkyl, aryl)  
 rt – room temperature  
 s – singlet  
 S<sub>E</sub>Ar – Electrophilic Aromatic Substitution  
 SM – Starting Materials

S<sub>N</sub>2 – Nucleophilic substitution

SOD – superoxide dismutase

SSTD NMR – Spin Saturation Transfer Differences Nuclear Magnetic Resonance

t – triplet or time

T – Thymine or Temperature

T<sub>m</sub> – melting temperature

TBAF - Tetrabutylammonium Fluoride

Tf - Triflate

TFA – Trifluoroacetic acid

Th - Thiophene

THF – Tetrahydrofuran

THT -Tetrahydrothiophene

TLC – Thin Layer Chromatography

TMEDA - *N,N,N',N'*-Tetramethylethylenediamine

TMS - Trimethylsilyl

TO – Thiazole orange

Tol – Toluene

TrxR – Thioredoxin reductase

Ts – Tosyl group

UV-Vis – Ultraviolet-Visible spectroscopy

X - heteroatom

XRD – X-ray diffraction

2D – two-dimensional

3D – three-dimensional

**Table of Contents**

<b>Declaration</b> .....	<b>2</b>
<b>Abstract</b> .....	<b>3</b>
<b>Acknowledgments</b> .....	<b>5</b>
<b>Abbreviations and Acronyms</b> .....	<b>7</b>
<b>Table of Contents</b> .....	<b>11</b>
<b>I. Introduction</b> .....	<b>13</b>
<b>I a. Allenes – a class of unsaturated compounds</b> .....	<b>13</b>
<b>I b. Allenes and transition metals</b> .....	<b>19</b>
<b>II. Aims and objectives</b> .....	<b>28</b>
<b>III. Allene-containing ligand candidates</b> .....	<b>30</b>
<b>III a. Introduction</b> .....	<b>30</b>
III a. 1. Synthesis of allenes.....	30
III a. 2. Synthesis of allene-containing ligands.....	35
<b>III b. Results and Discussion</b> .....	<b>40</b>
III b. 1. Bis(pyridyl)allenes.....	41
III b. 2. Bis(phosphine)allenes.....	45
III b. 3. Bis(thienyl)allenes.....	46
III b. 4. Bis( $\alpha$ -amino)allenes.....	56
III b. 5. Miscellaneous methods.....	60
<b>III c. Conclusions</b> .....	<b>63</b>
<b>IV. Allene-derived metal complexes – synthesis and fundamental studies</b> .....	<b>65</b>
<b>IV a. Introduction</b> .....	<b>65</b>
<b>IV b. Results and Discussion</b> .....	<b>76</b>
IV b. 1. Preliminary experiments.....	77
IV b. 2. Palladium complexes with bis(pyridyl)allenes.....	80
IV b. 3. Platinum complexes with bis(pyridyl)allenes.....	85
IV b. 4. Gold complexes with bis(pyridyl)allenes.....	92
<b>IV c. Conclusions</b> .....	<b>108</b>



---

<b>V.</b>	<b>Applications in catalysis</b> .....	<b>111</b>
<b>V a.</b>	<b>Introduction</b> .....	<b>111</b>
<b>V b.</b>	<b>Results and Discussion</b> .....	<b>113</b>
V b. 1.	Tsuji-Trost reaction .....	113
V b. 2.	Mizoroki-Heck cross-coupling reaction .....	118
V b. 3.	Cyclisation and alkoxy cyclisation of 1,6-enynes .....	121
V b. 4.	Metal-catalysed nucleophilic addition to allenes .....	133
<b>V c.</b>	<b>Conclusions</b> .....	<b>137</b>
<b>VI.</b>	<b>Bioactivity of allene-derived metal complexes</b> .....	<b>139</b>
<b>VI a.</b>	<b>Introduction</b> .....	<b>139</b>
<b>VI b.</b>	<b>Results and Discussion</b> .....	<b>146</b>
VI b. 1.	Stability studies .....	146
VI b. 2.	Antibacterial and antifungal activity .....	150
VI b. 3.	Antiproliferative activity against cancerous cells .....	153
VI b. 4.	Towards the mechanism of action – studies of the interactions with DNA .....	160
<b>VI c.</b>	<b>Conclusions</b> .....	<b>170</b>
<b>VII.</b>	<b>Resolution of precursors to allene ligands</b> .....	<b>172</b>
<b>VII a.</b>	<b>Introduction</b> .....	<b>172</b>
<b>VII b.</b>	<b>Results and Discussion</b> .....	<b>173</b>
<b>VII c.</b>	<b>Conclusions</b> .....	<b>178</b>
<b>VIII.</b>	<b>Conclusions</b> .....	<b>179</b>
<b>IX.</b>	<b>Future research directions</b> .....	<b>180</b>
<b>X.</b>	<b>Experimental Section</b> .....	<b>181</b>
<b>XI.</b>	<b>References</b> .....	<b>290</b>

## I. Introduction

This thesis is structured in the following way: Chapter I serves as an introduction to the chemistry and history of the allene functional group which is the focal point of the study. It also introduces the reader to the subject of allene-transition metals interactions and reactivity. After the section outlining the aims and objectives of the project (Chapter II) we come to the chapters describing the experimental work and findings of the study. Each of these chapters begins with the review of relevant literature serving as an introduction and reference point to the results presented in the second part of the chapter. Thus, Chapter III and IV discuss synthetic investigations into the preparation of allene-based ligands and corresponding transition metal complexes. Chapters V and VI turn to the study of applications of allene-derived metal complexes as catalysts and drug candidates, respectively. The last section, Chapter VII, is concerned with the development of the asymmetric version of the allene ligands. The work is concluded with the summary of the study and brief discussion of the future research directions.

### I a. Allenes – a class of unsaturated compounds

Allene or 1,2-propadiene **1** (Figure 2, a) is the parent compound of a larger family of organic compounds, allenes, characterised by the occurrence of two adjacent, non-conjugated double bonds in a molecule joined to the same carbon atom. The number of consecutive, contiguous double bonds can be larger than two and compounds with three and more directly joined unsaturations are termed cumulenes (Figure 2, b-c).<sup>[1,2]</sup> Cumulenes with as many as nine successive double bonds have been prepared, although the stability of the compounds diminishes with increased C=C chain length.

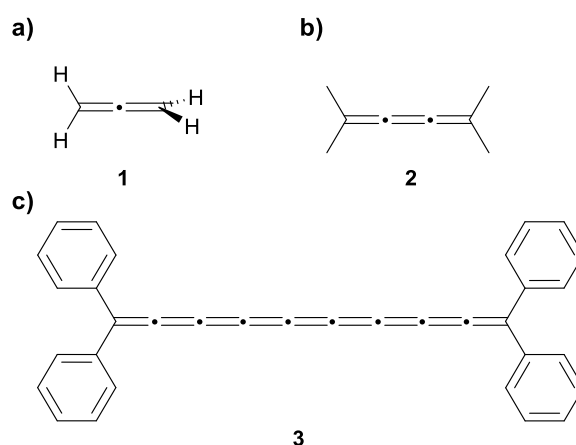


**Figure 2** Structures of different cumulenes: a) 1,2-propadiene (**1**); b) tetramethyl[3]cumulene (**2**); c) tetraphenyl[9]cumulene (**3**).

The structure of the allene skeleton with its unusual stereochemistry was predicted as early as 1875 by van't Hoff.<sup>[3]</sup> Since then it was regarded as highly unstable and not likely to be experimentally accessible. However, the first synthesis of the allene-containing compound in the laboratory, glutinic acid **4** (Figure 3, a), was achieved only two years later.<sup>[4]</sup> Although, due to the lack of suitable analytical techniques the structure of glutinic acid was not confirmed till 1954.<sup>[5]</sup> It was also discovered that allenes occur in nature with the first isolated allene-containing natural product being mycomycin **5** (Figure 3, b) - a fungal metabolite with high antibiotic activity.<sup>[6,7]</sup> In fact, many more natural products isolated at the turn of the 19<sup>th</sup> and 20<sup>th</sup> century were confirmed to feature allene or cumulene moieties only much later.<sup>[8]</sup>

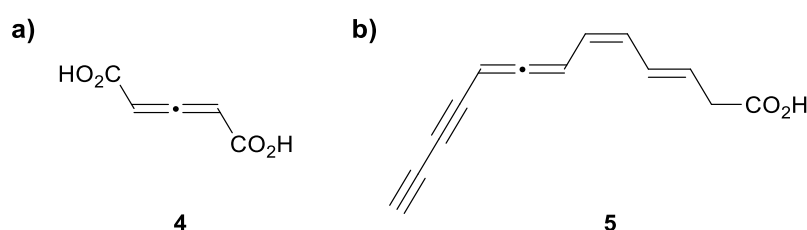


**Figure 3** First allenic compounds: a) synthetic glutinic acid (**4**); b) natural product mycomycin (**5**).

A couple more milestones in the development of allene chemistry were marked in the first half of the 20<sup>th</sup> century. The first review on allene chemistry was published in 1928 and the first chiral allene was synthesised in 1935.<sup>[9,10]</sup> The area enjoyed a steady progress throughout the rest of the 20<sup>th</sup> century<sup>[11–13]</sup> with a real spike of interest of the community in the 21<sup>st</sup> century evidenced by the thousands of articles published on the topic every year.

The most distinctive structural feature of the allene functional group is the orthogonal relationship of its  $\pi$ -bonds (Figure 4, a). The central carbon atom of the allene is found in  $sp$  hybridisation with both terminal ones being  $sp^2$ -hybridised and a  $C=C=C$  angle of  $180^\circ$ . The molecule can be viewed as an extended tetrahedron formed by the two perpendicular planes within. Perpendicular arrangement of the  $p$ -orbitals prevents the overlap and hence the lack of conjugation in the system. This classic description of the allene's orbitals has recently been updated.<sup>[14,15]</sup> It has been proposed on the basis of quantum chemical computations that  $p$ -orbitals in cumulene systems form helical frontier molecular orbitals (FMOs) (Figure 4, b). In symmetrically substituted allenes there are three  $C_2$  axis of symmetry.

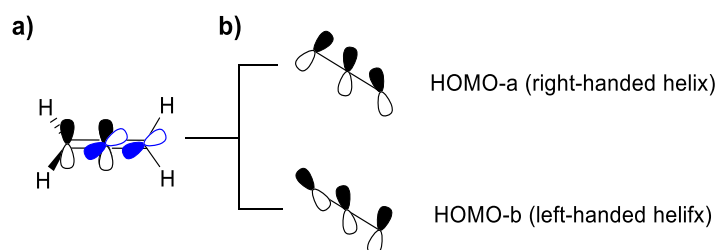


**Figure 4** Orbital description of the allene molecule: a) classic representation of the perpendicular p-orbitals; b) helical topology of the FMOs.

The C=C bond lengths in the allene were determined to be slightly shorter compared to that in ethene, 1.31 vs 1.33 Å, respectively.<sup>[11]</sup> This contraction is rationalised by a hyperconjugation of C-H  $\sigma$ -bonds with the distal  $\pi$ -bond.  $\sigma$ - $\pi$  Interaction of that type are favourable thanks to the alignment on the same plane and as a result the allene double bond shares a partial triple bond character. The H-C-H dihedral angle in the parent allene was determined at 118.2°.<sup>[12]</sup> These values might be subjected to variations when substituted allenes are concerned. In longer cumulenes, the consecutive double bonds have been found to have different bond distances, the phenomenon known as bond length alternation (BLA).<sup>[2]</sup>

A special sub-group within the class are bent allenes (Figure 5, a).<sup>[16–19]</sup> Found, for example, in cyclic compounds, they exhibit distinct structural features to their linear congeners. Bent allenes arise also due to the packing effects in the crystal lattice that forces the non-linear geometry, for example, in the acyclic allene **7** (Figure 5, b). The C=C=C angle in such compounds can be severely diminished and there is a debate about a character of such compounds (bent allene vs carbodicarbene vs zwitterion).<sup>[20–22]</sup> The bending of the allene disturbs and weakens its  $\pi$ -system.<sup>[15]</sup> Depending on the electronic features an polarisation of the molecule the central carbon atom can acquire carbene or dicarbanionic character.<sup>[20]</sup>

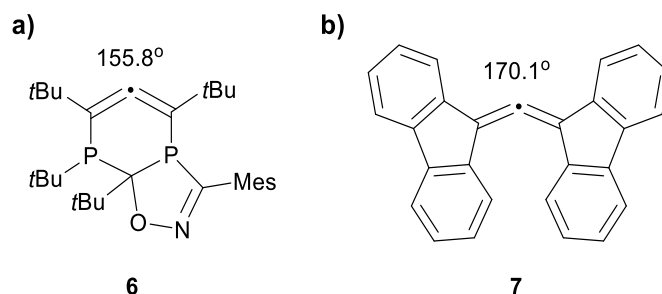


**Figure 5** Examples of bent allenes: a) **6** - inside a ring;<sup>[18]</sup> b) **7** - acyclic bent allene.<sup>[16]</sup>

In general, allenes are more reactive than other unsaturated compounds with non-cumulated double bonds. For example, the allene was found to be less energetically favourable

than its propyne isomer with 2.1 kJ energy difference.<sup>[23]</sup> However, some factors such as substitution can skew the isomerisation equilibrium in favour of non-thermodynamic allene species.

As a consequence of a rigid geometry of the allene skeleton this group of compounds possesses inherent axial chirality originally predicted by van't Hoff.<sup>[3]</sup> Contrary to the more common central chirality stemming from the presence of a stereogenic centre(s) in a molecule, allenes' chirality comes from a spatial arrangement around an axis in allenes with at least two substituents, one on each termini. The first homologue with that feature is 1,3-dimethylallene **8**. It does not have any mirror planes within the molecule and hence two non-superimposable mirror images can be drawn (Figure 6, a). The configuration of the enantiomers can be assigned by looking at the molecule along the main C=C=C axis (Figure 6, b) and determining the priority of the substituents with the Cahn-Ingold-Prelog rules. The configuration is determined by the direction you need to go from a group of lower priority on the front carbon atom to the group of higher priority on the back carbon atom.

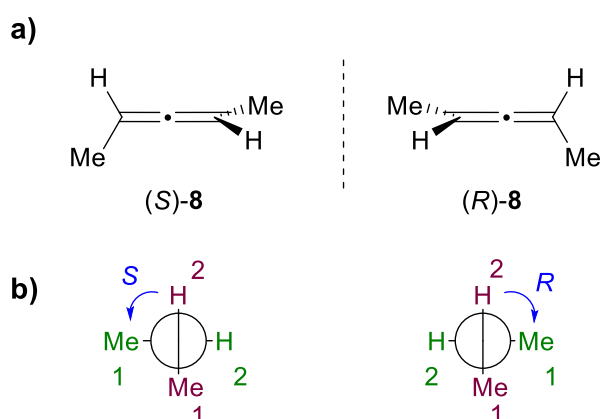


**Figure 6** Stereochemistry of allenes: a) two enantiomers of 1,3-dimethylallene (**8**); b) Newman projection of 1,3-dimethylallene with priority assigned according to CIP priority rules.

The first analytical techniques that allowed the detection of the allene functionalities and in particular differentiate them from the isomeric alkynes were infrared (IR) and Raman spectroscopies. From the three vibrational modes of the allene: bending, symmetric stretching and asymmetric stretching, the latter is especially useful as a diagnostic appearing as a strong band at 1930-1980  $\text{cm}^{-1}$  in an IR spectrum.<sup>[11]</sup> For comparison, the stretching frequency of an isolated double bond and triple bond are typically found at around 1650 and 2200  $\text{cm}^{-1}$ , respectively. The allene range is largely unaffected by the substitution changes, however it can move to shorter wavenumbers in fluoroallenes.<sup>[11]</sup> Characterisation of allenes with nuclear magnetic resonance technique revealed that resonances of their vinyl-type protons are displaced upfield (4.5-5.5 ppm) compared to olefin compounds, the shift attributed to a

shielding effect of the sp-hybridised central carbon atom.<sup>[11]</sup> Additionally, the values of the  $^4J_{\text{H-H}}$  coupling constants across the allene skeleton are unusually high for this type of long range coupling, probably due to  $\sigma$ - $\pi$  C-H/C=C interactions mentioned previously in the discussion of the allene bond lengths. The characteristic peak of a central carbon atom of the allene in  $^{13}\text{C}$  NMR spectra is typically found at 200-220 ppm, however it can be substantially shifted upfield in substituted allenes or longer cumulenes. The range for the terminal carbon atoms is more similar to standard alkene range (100-150 ppm). UV-Vis spectroscopy is a method of choice for the analysis of longer cumulenes.<sup>[1]</sup>

Currently, allenes enjoy an indisputable place among essential synthetic intermediates and building blocks in organic chemistry.<sup>[24-27]</sup> Unique structure and properties of allenes allowed to utilise their chemistry in challenging areas of asymmetric synthesis,<sup>[28,29]</sup> axial-to-central chirality transfer,<sup>[30]</sup> novel carbon coordination chemistry<sup>[31]</sup> or material science.<sup>[32]</sup> What is more, allenes' relevance is underlined by their occurrence in as many as 150 natural products isolated and characterised up to 2004.<sup>[8]</sup>

Natural products bearing allene (cumulene) moieties can be divided into three main classes: linear allenes, allenic carotinoids and terpenoids and bromoallenes (Figure 7, a-d); most of which were isolated in a non-racemic form.<sup>[8,33-36]</sup> The interesting properties of allenic compounds prompted many efforts for their total syntheses.<sup>[37-39]</sup> Stemming from the natural product chemistry, non-natural allene-containing compounds became attractive targets due to their desirable pharmacological activity. For example, allene-bearing steroids, amino acids, nucleoside analogues or prostaglandins have been prepared and tested for their inhibitory or antiviral properties.<sup>[40-43]</sup> A few allenic compounds, such as Enprostil **13** (inhibitor of gastric acid secretion), can even be found on the market (Figure 7, e).<sup>[44]</sup>

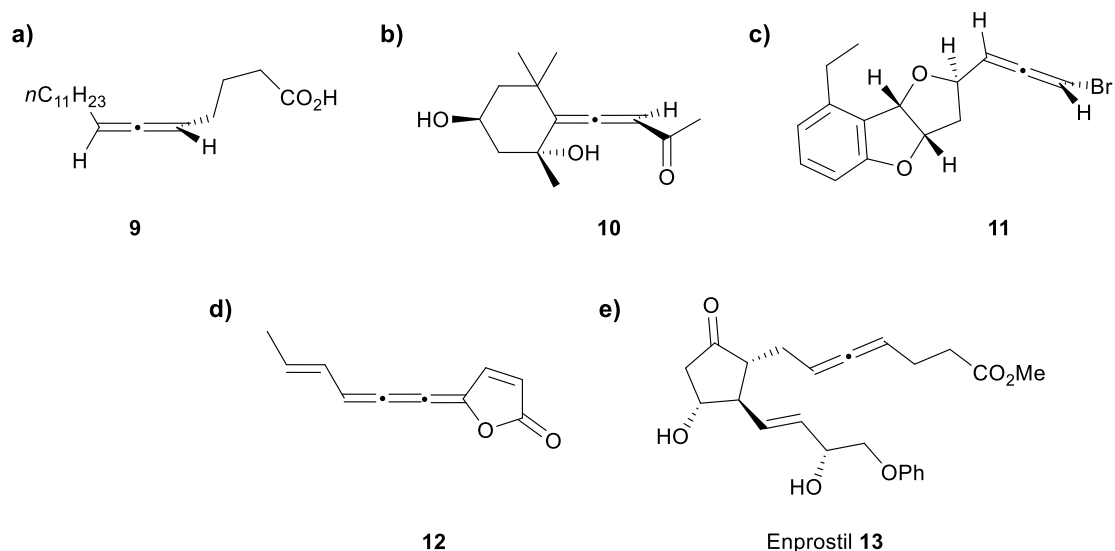
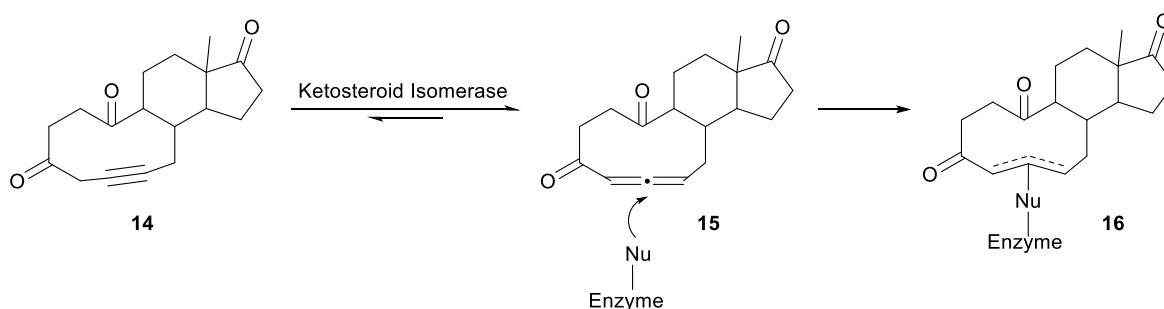


**Figure 7** Allene/cumulene natural and non-natural products: a) laballenic acid (**9**); b) grasshopper ketone (**10**); c) panacene (**11**); d) naturally occurring cumulene (**12**); e) Enprostil (**13**).

The mechanism of action of most allenic therapeutics is poorly understood, but their activity is mostly linked to inhibition of enzymes. The model of “mechanism-based inhibition” was proposed where “suicide substrates” irreversibly react with residues of the enzymes and disrupt their activity.<sup>[45]</sup> Latent allenic “suicide substrates” are often uncovered from acetylenic precursors in the course of normal catalytic activity of the enzyme. Such highly reactive allenic species, usually with electron-withdrawing substituents, act as Michael acceptors towards nucleophilic groups of the enzyme. For example, acetylenic steroid **14** has been found to inhibit an action of ketosteroid isomerase enzyme derived from *Pseudomonas testosteroni* (Scheme 1).<sup>[46]</sup> Allenic ketone **15** was believed to act as a substrate for the enzyme following the isomerisation from its acetylenic precursor **14**. Then, in the active site, the electrophilic **15** was thought to undergo Michael addition with nucleophilic amino acid residues of the enzyme.



**Scheme 1** Example of proposed mechanism of action of allene-based drugs.

## I b. Allenes and transition metals

Allenes can act as  $\pi$ -ligands when interacting with transition metals similarly to olefins or alkynes.<sup>[47,48]</sup> Structural similarities of these unsaturated ligands allow to describe the allene-transition metal bonding according to the Dewar-Chatt-Duncanson<sup>[49,50]</sup> (DCD) molecular orbital model developed for alkenes and alkynes.<sup>[48]</sup> Thus, for alkyne ligands, there are four principal orbital interactions that contribute to bonding (Figure 8, a).<sup>[51]</sup> Overlap of in-plane  $\pi$  orbitals of the ligand with an empty orbital of the metal of suitable symmetry forms a  $L \rightarrow M$   $\sigma$  bond.  $\pi$ -Symmetric interaction of filled metal d orbital to antibonding  $\pi^*$  orbital of the ligand results in  $M \rightarrow L$  shift of electron density known as back-donation or back-bonding. The remaining interactions,  $L \rightarrow M$   $\pi$  donation and  $M \rightarrow L$   $\delta$  back-donation, contribute to bonding in a lesser extent. In fact, typically,  $\sigma$  interaction and  $\pi$  back-bonding account for up to ~65% and ~25% contribution, respectively. Therefore, alkyne (and olefins or allenes) ligands are regarded as strong two-electron  $\sigma$  donors and rather weak  $\pi$  acceptors. Some computational studies also suggest that the bonding in such complexes has not-negligible electrostatic character.<sup>[52]</sup> The metal-allene bonding can be represented as monodentate- $\pi$  (**17**) and bidentate- $\sigma$  (**18**) type at the two ends of bond types' continuum depending on an individual character of metal and ligand fragments (Figure 8, b).<sup>[48]</sup> In non-symmetrically substituted allenes, the interaction with a metal can be achieved with either of the non-identical double bonds, often depending on the steric hindrance around the particular bond. This can lead to a fluxional behaviour in solution, where the metal fragment moves between the two available double bonds (see page 23).

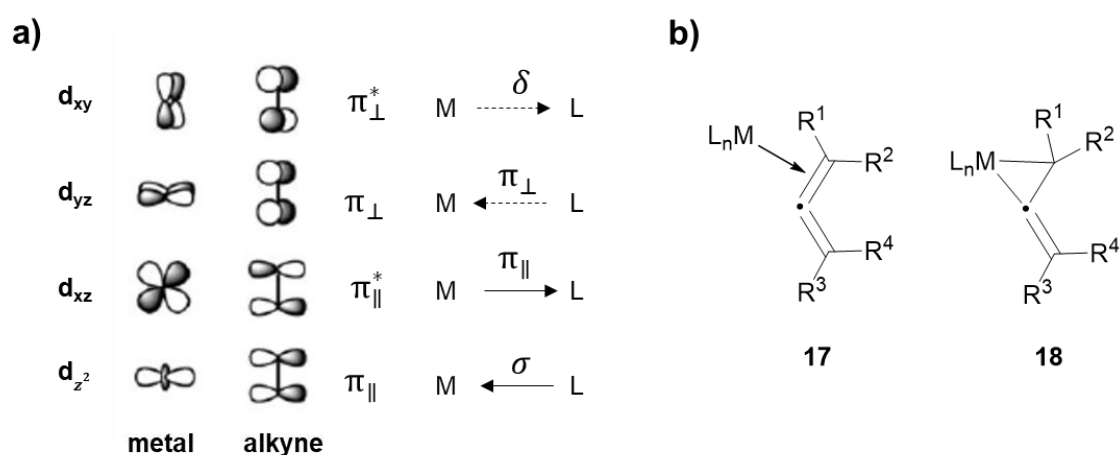


**Figure 8** a) Orbital description of alkyne-transition metal interaction according to DCD model;<sup>[51]</sup> b) allene-transition metal bonding representations.

Important implication of the  $\pi$ -ligands-metal bonding is the shift of electron density into  $\pi^*$  antibonding orbitals and resulting elongation and bending of the multiple bond. Actually,



these parameters can be used to assess the extent of the back-bonding. In general, more electron rich metal fragments capable of significant back-donation cause more pronounced bond elongation and more severe bending of the ligand. Perhaps the most important consequence of the bonding, however, is a net depletion of electron density from the ligand. Therefore, metal-bonded unsaturated ligands undergo electrophilic activation by coordination to the metal, becoming susceptible to nucleophilic attack, one of the most studied reactivities of these systems.<sup>[53]</sup>

Different types of allene-metal complexes have long been invoked as intermediates or transition states in chemical reactions. However, in recent years more and more isolated and characterised examples have allowed for a better understanding of their chemistry. Metal-allene complexes can be divided into two sub-categories in respect to their coordination mode to the metal centre (Figure 9). The first category comprises  $\eta^2$  complexes (**19-21**) in which one of the allene's double bonds is bonded to the metal. It is possible that the contribution of the carbon atoms in that bond is not equivalent. As a result, the slipped structures (**20** and **21**) can occur favouring one side over the other depending on the substitution pattern of the allene and character of the metal centre and its ligands. In the second category, we find  $\eta^1$  complexes with the metal bonded to the central carbon atom of the allene skeleton. These complexes can be represented as  $\sigma$  allylic cations (**22**), zwitterionic carbenes (**23**) and bent allenes (**24**).

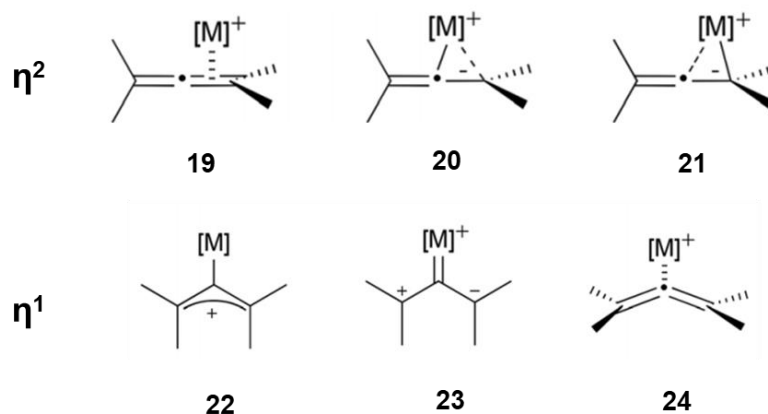


**Figure 9** Allene-transition metal coordination modes.<sup>[54]</sup>

Computational studies have been performed to investigate the relative stability of different types of allene-metal complexes. In particular, the ground states, interconversions and racemisation process in Au-allene complexes, relevant for this thesis, have been widely studied.<sup>[54–57]</sup> For example, for (*R*)-1,3-dimethylallene **8** in the presence of AuBr<sub>3</sub>, four structures converged as minima (Figure 10, a). Two similar  $\eta^2$  structures were found along with two non-linear  $\eta^1$  complexes. The latter were less stable planar **22**-type and the least stable bent allene **24**-type species. The use of different metal fragments (AuCl<sub>3</sub>, PtCl<sub>2</sub>) allowed to

locate more type **24** structures, but as in the previous case the type **19-21** complexes were found as ground states. As an additional illustration, complexes of allene **8** and  $[\text{Au}(\text{PMe}_3)]^+$ , (*R*)-**25a** and (*R*)-**25b**, were more stable than  $\eta^1$  allylic **26b** with other C(2)-coordinated structures found only as transition states (**26a**, **26c**, **27a-b**) (Figure 10, b). The energy barrier for the stereomutation between the species depended on the allylic strain of respective transition states (see **26a** vs **26c**).

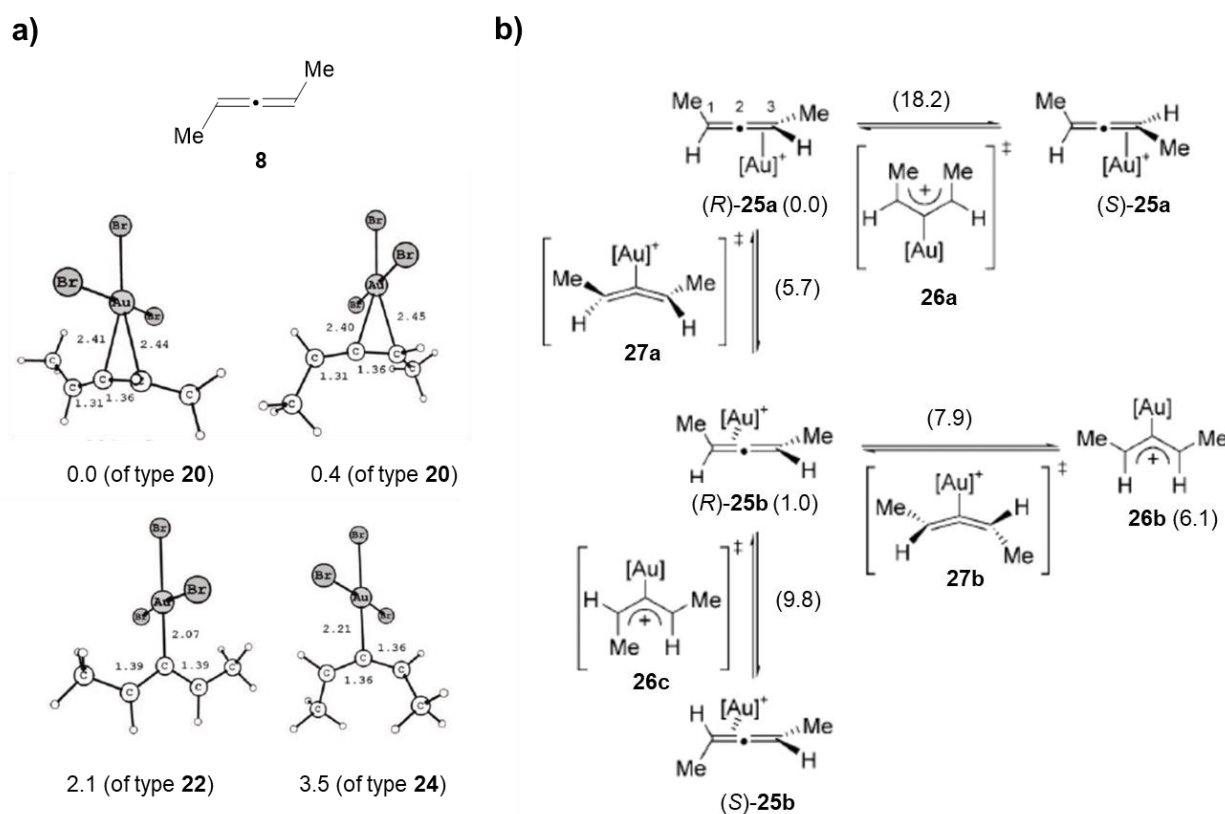


**Figure 10** Relative stability of Au-allene complexes according to computational studies: a) minima for allene **8** and  $\text{AuBr}_3$ ; b) complexation of allene **8** and  $[\text{Au}(\text{PMe}_3)]^+$  (relative enthalpies in  $\text{kcal}\cdot\text{mol}^{-1}$ ).<sup>[54]</sup>

It was envisioned that the disfavoured  $\eta^1$  coordination could be promoted by the presence of stabilising EDG substituent on the allene. Thus, for acetate- (**28**) and vinyl-substituted (**30**) allenes, the allylic cations **29a** and **31** were determined as ground states (Figure 11, a-b). Interestingly, in case of acetate allene **28**, the bent complex **29b** was of similar energy to  $\eta^2$  **29c** and **29d**.

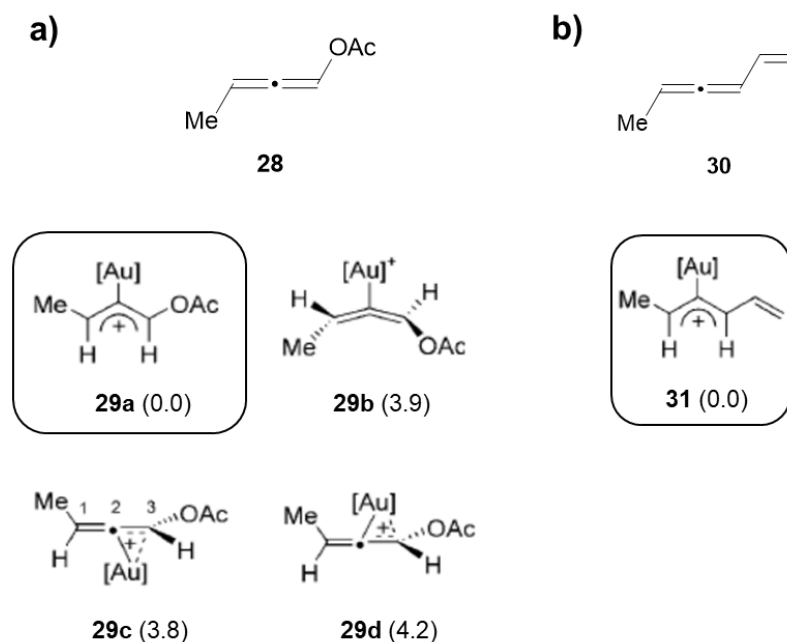


**Figure 11** Relative stability of Au complexes of EDG-substituted allenes according to computational studies: a) for acetate-allene **28**; b) for vinyl-allene **30** (relative enthalpies in kcal·mol<sup>-1</sup>).<sup>[64]</sup>

Allene-metal complexes can exhibit interesting dynamic behaviour in solution. Described first for Fe complexes,<sup>[58,59]</sup>  $\eta^2$  allene-metal complexes have been found to display novel type of valence tautomerism. It has been proposed that the metal fragment of the complex can move between the two double bonds of the allene and their respective faces in an eight-shaped manner (Figure 12, a) with a low activation energy for the tetramethyl(allene)-Fe complex **33** (Figure 12, a).<sup>[58]</sup> Similar behaviour was reported for Au  $\eta^2$ -allene complexes disclosed by Widenhoefer and co-workers.<sup>[60]</sup> The authors observed coordination of the Au fragment to the less substituted double bond of 1,1-dimethylallene. Temperature dependent NMR experiments revealed the diastereotopic character of the allenyl methyl groups. The differentiation of these substituents was ascribed to fluxional sliding of the Au fragment between orthogonal  $\pi$ -faces of the allene. Migration of AuL<sub>n</sub> was proposed to proceed *via*  $\eta^1$ -intermediate or transition state **34a/34b** (Figure 12, b) in which the Au is positioned at 45° relative to the orthogonal  $\pi$ -faces and not the  $\eta^1$ -allylic cation.  $\pi$ -Face exchange was also found to play a role in the Au-catalysed racemisation of allenes.<sup>[56,57]</sup> The study of the in solution fluxional behaviour of Pt-allene complexes with the use of novel SSTD NMR method<sup>[61]</sup> reported by our group consolidated and expanded previous understanding of the phenomenon.<sup>[62]</sup> The rotational ( $\pi$ -face exchange) and helical (movement between double bonds) components of the metal fragment migrations were confirmed to proceed intramolecularly through  $\eta^1$  intermediates. The differences in determined activation energies for the fluxional behaviour of reported Pt-allene complexes in comparison with other metal complexes were proposed to be a factor influencing the disparity in their reactivity.

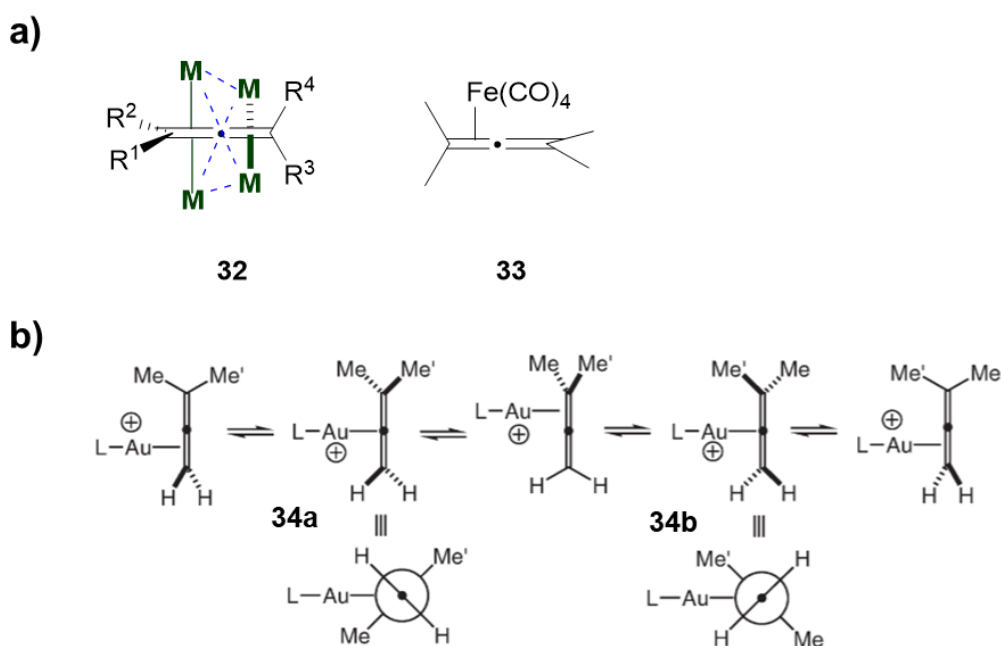


**Figure 12** a) Model of a fluxional behaviour of allene-transition metal complexes in solution first described for **33**; b) fluxional behaviour of AuL(**34**) complex (L = P(*t*Bu)<sub>2</sub>o-biphenyl).<sup>[60]</sup>

As supported by computational analysis, the most stable  $\eta^2$ -allene complexes are also the most prevalent and accessible in the laboratory. Therefore, a number of Ir, Fe, Rh, Pd, Pt or Mo examples have been prepared and characterised.<sup>[48]</sup> The allene-metal coordination process is evidenced by the decrease of the C=C=C stretching frequencies in the IR spectra and the shift of peaks in the NMR spectra in comparison to the free allene ligand. Crystallographic analysis of  $\eta^2$ -allene species (**35**, Figure 13, a) uncovered important structural information about these compounds exemplified by the complexes **35a-e** (Table 1). **35a-e** fit well with the description of slipped structures of **20/21**-type where the metal centre is located at the unequal distance from the carbon atoms of the coordinated double bond depending on the specific features of the system.

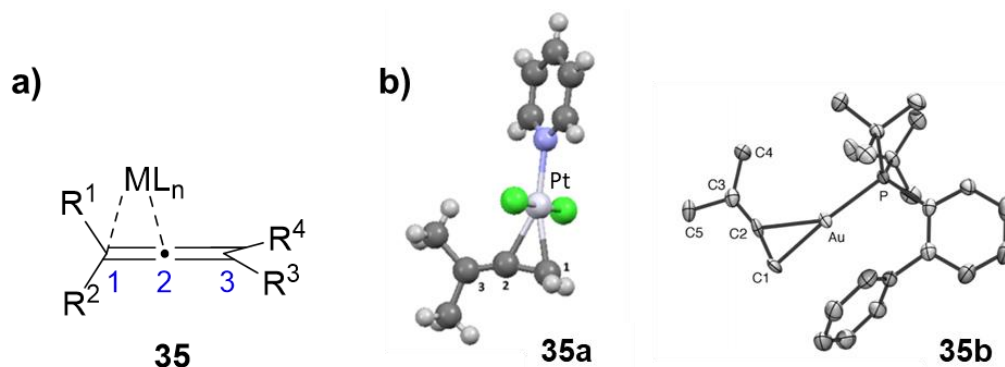


**Figure 13** Examples of  $\eta^2$ -allene metal complexes a) general structure (**35**); b) Pt(II)-**35a**<sup>[62]</sup> and Au(I)-**35b**<sup>[60]</sup> complexes of 1,1-dimethylallene.

**Table 1** Selected solid state parameters of complexes **35a-e**.

	$\eta^2$ complex	C <sup>1</sup> =C <sup>2</sup> [Å]	C <sup>2</sup> =C <sup>3</sup> [Å]	C <sup>1</sup> -M [Å]	C <sup>2</sup> -M [Å]	C <sup>1</sup> =C <sup>2</sup> =C <sup>3</sup> [deg.]	Ref.
1	<b>1</b> (R <sup>1-4</sup> = H; ML <sub>n</sub> = -)	1.31	1.31	-	-	180°	[11]
2	<b>35c</b> (R <sup>1-4</sup> = H; ML <sub>n</sub> = Pd(PPh <sub>3</sub> ) <sub>2</sub> )	1.40	1.30	2.12	2.07	148.3	[63]
3	<b>35d</b> (R <sup>1-3</sup> = H; R <sup>4</sup> = +PPh <sub>3</sub> ; ML <sub>n</sub> = Pt(PPh <sub>3</sub> ) <sub>2</sub> )	1.473	1.343	2.102	1.943	136.2	[64]
4	<b>35e</b> (R <sup>1-4</sup> = Me; ML <sub>n</sub> = PtCl <sub>2</sub> ; dimer)	1.37	1.36	2.25	2.07	151.4	[65]
5	<b>35a</b> (R <sup>1-2</sup> = H; R <sup>3-4</sup> = Me; ML <sub>n</sub> = Pt(py)Cl <sub>2</sub> )	1.382	1.293	2.138	2.108	159.7	[62]
6	<b>35b</b> (R <sup>1-2</sup> = H; R <sup>3-4</sup> = Me; ML <sub>n</sub> = AuL) <sup>a</sup>	1.340	1.311	2.191	2.306	165.0	[60]

<sup>a</sup> L = P(*t*Bu)<sub>2</sub>*o*-biphenyl.

Some general trends can be distinguished, for example, for different metal centres. Thus, Au complexes tend to bond closer to the external carbon atom of the double bond (entry 6, Table 1) whereas Pd or Pt complexes to the internal one (entries 2-5, Table 1). It has been proposed that the asymmetric binding in the case of Pt complexes might be caused by the back-bonding interaction of the metal and antibonding  $\pi^*$  orbital of the non-coordinated double bond. Additionally, the double bonds in the coordination sphere of the metals (C<sup>1</sup>=C<sup>2</sup>) are substantially elongated in comparison to the free allene bond (entry 1, Table 1). Whereas, the remaining C<sup>2</sup>=C<sup>3</sup> bond is usually affected to a much lesser extent. The allene skeletons in **35a-e** are considerably distorted with the C<sup>1</sup>=C<sup>2</sup>=C<sup>3</sup> backbones strongly deviated from linear geometry (entry 1 vs entries 2-6, Table 1). This data supports strong  $\sigma$ -donating and weak  $\pi$ -accepting character of the  $\pi$ -allene ligands similar to their alkene and alkyne equivalents.

$\eta^1$ -Allene complexes remain much more experimentally elusive compared to their  $\eta^2$  congeners. From the three possible  $\eta^1$ -coordination modes, types **22** and **23**, are still largely considered in terms of reaction intermediates and/or transition states. However, a growing number of reports discusses the synthesis and characterisation of bent allene type complexes **24**.<sup>[20,66-68]</sup> As mentioned before, the allenic character of these compounds has been disputed as carbodicarbene in nature. Carbodicarbene compounds were envisioned as resonance forms of so called “push-push” substituted allenes (**37**), contrarily to “push-pull” allenes (**36**) with carbene character at a central carbon atom (Figure 14, a).<sup>[20]</sup> Structures of the **37** type feature a localisation of two lone electron pairs at the central carbon atom giving them the dicarbanionic character. Carbodicarbenes (L<sub>2</sub>C), also called carbones, are divalent C(0) compounds (Figure 14, b). Their bonding situation is sometimes compared to that of a metal with the ligands in the coordination sphere (L→C(0), donor-acceptor bonds), with good  $\sigma$ -donor ligands (e.g. (NHC)-carbenes) stabilising the carbodicarbene structure.

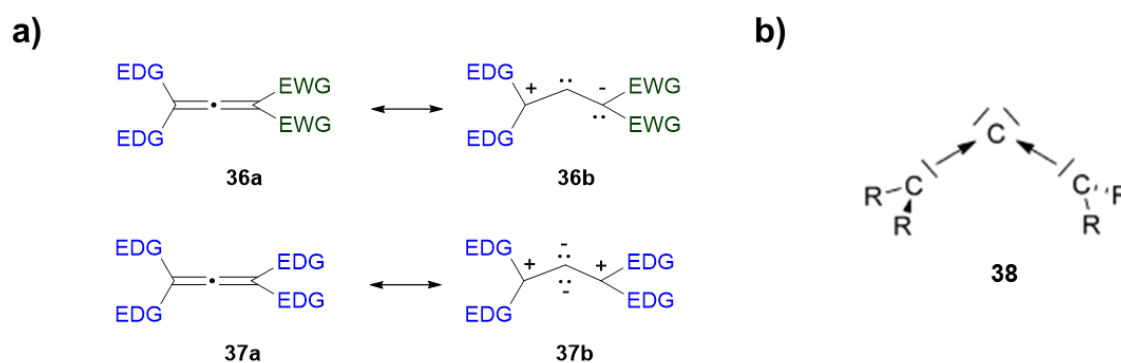
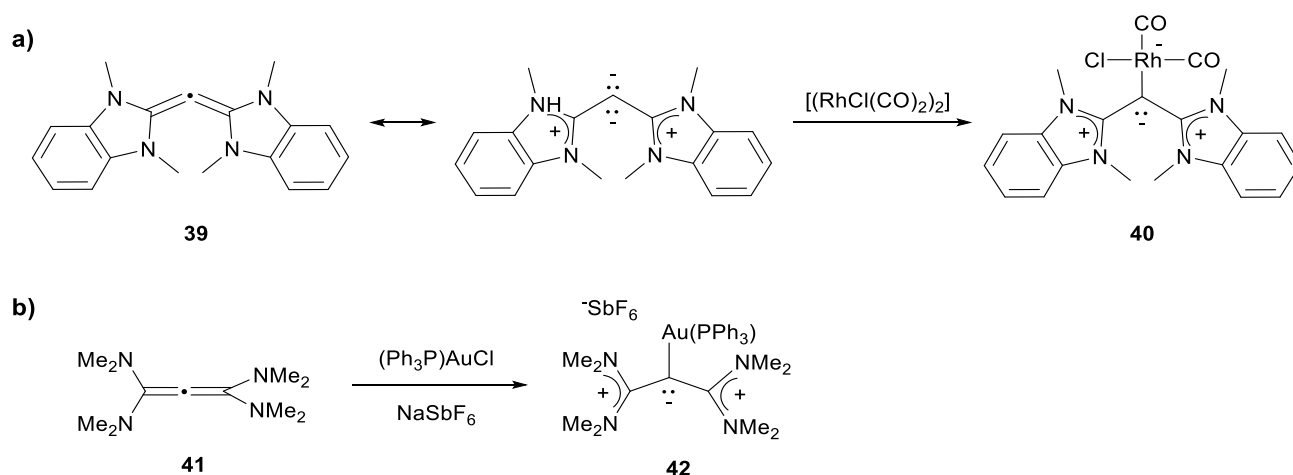


**Figure 14** General structures of: a) “push-pull”-**36** and “push-push”-**37** allenes; b) carbene **38**.

Inherent geometry of carbones, such as their non-linearity and lack of orthogonal planes distinguish them from classic allenic structures. For example, Bertrand and co-workers prepared (NHC)-substituted bent allene/carbodicarbene Rh(I) complex **40** (Scheme 2, a).<sup>[20]</sup> The three carbon atom core of the complex was found at extremely bent angle of 121.2(7)°, compared to 134.8(2)° in the free ligand. The latter was found to be a strong  $\sigma$ -donor, as determined by the stretching frequencies of the carbonyl ligands in **40**. Another example is Au(I) complex **42** disclosed by Fürstner and co-workers prepared in a reaction of tetraminoallene **41** termed as “hidden carbene” (Scheme 2, b).<sup>[69]</sup>



**Scheme 2** Synthesis of carbodicarbene complexes of: a) Rh(I); b) Au(I).

A different class of allene-containing organometallics constitute allenyl type complexes **43** (Figure 15, a).<sup>[70,71]</sup> Allenyl complexes can be described as  $\sigma$ -bonded, vinyl-type  $\eta^1$  species where bonding to the metal does not generally disrupt the geometry of the allene fragment. Allenylmetal compounds are usually synthesised *via* metal-halogen exchange or more commonly by deprotonation of propargylic precursors. Allenyl complexes are often in equilibrium with their propargylic counterparts, however, they are the typically favoured tautomers on account of stronger allenyl-metal bond (Figure 15, b).<sup>[72]</sup> Allenylmetal complexes

are employed as very useful synthetic reagents in stoichiometric and catalytic reactions, for instance, allenylpalladium reagents used in cross-coupling reactions. Additional advantage of their use is the potential utilisation of the chiral information of the allene component. Isolation and structural characterisation of many transition metal-allenyl  $\eta^1$  complexes showed their straightforward coordination mode demonstrated in Pt(II) and Ru(II) complexes **45a** and **45b** (Figure 15, c).<sup>[73,74]</sup> The double bond distances and C=C=C angles of the allene skeletons in such compounds remain very similar to those in non-coordinated allenes. For Pt square planar complexes, the allene ligand usually sits perpendicularly to the metal coordination sphere.

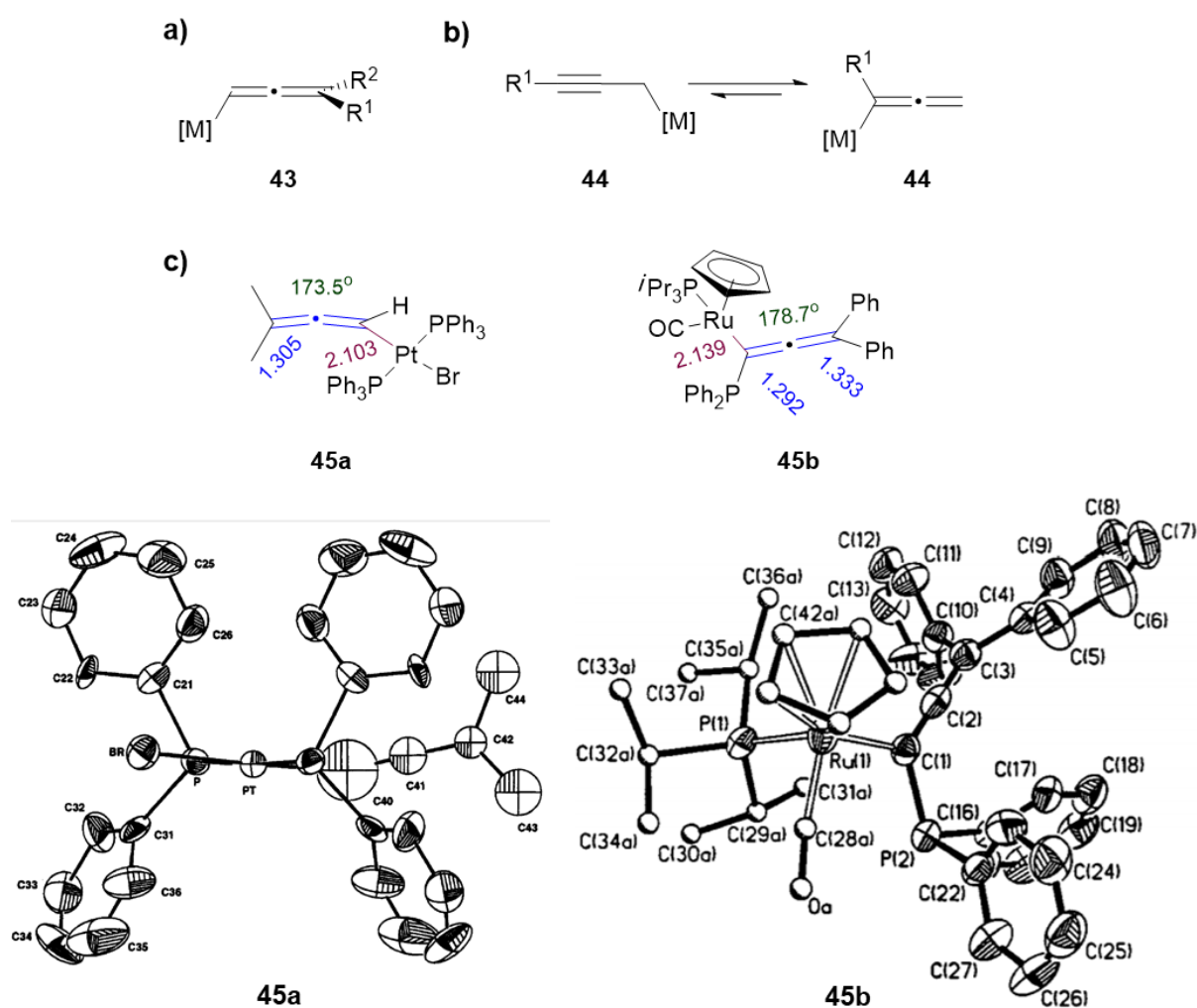


**Figure 15** Allenylmetal complexes: a) general structure **43**; b) propargyl/allenylmetal equilibrium; c) isolated examples of Pt(II)-**45a**<sup>[73]</sup> and Ru(II)-**45b**.<sup>[74]</sup>

Allenylidene complexes (**46**, Figure 16, a) do not formally contain the allene functional group, however, their cumulene character is noteworthy.<sup>[75,76]</sup> The propadienylidene carbene organic fragment (**47**, Figure 16, b) in these compounds is inherently unstable, nevertheless, it can be stabilised by the coordination to a transition metal.

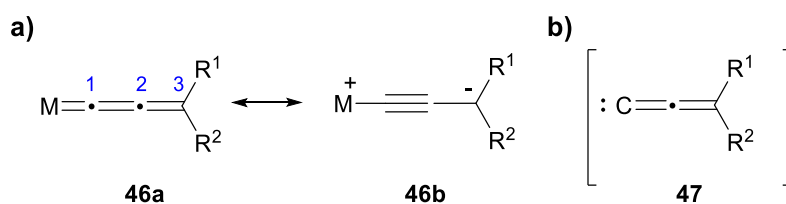


**Figure 16** a) Resonance forms of allenylidene metal complex **46**; b) propadienyliidene unit **47**.

Many examples of Ti-, Fe-, W-, Pd-, Os-, Au-, Ru- *etc.* allenylidene ( $C_3$  fragment) and longer homologs ( $C_4$ - $C_6$  fragments) have been prepared to date.<sup>[75]</sup> The standard synthetic methods for allenylidenes' synthesis involve use of vinylidene or propargyl precursors. Features such as rigid linear structure and characteristic bands corresponding to  $C=C=C$  stretching frequencies in the infrared spectra are reminiscent of the classic cumulene systems. On the other hand, solid state parameters determined for this class of compounds are quite distinct from typical allenes or allene-metal complexes. For example, C(1)-C(2) and C(2)-C(3) bond distances lay outside typical double bond region thanks to possible resonance forms of **46**. The carbene character of C(1) is supported by M-C(1) bond lengths typically found in a 1.806-2.185 Å range. C(1) is also the most deshielded carbon atom of the  $C_3$  skeleton according to  $^{13}C$  NMR analyses and common site of nucleophilic attacks. Some examples of allenylidene complexes with their crystal structures are shown below (Figure 17).<sup>[77,78]</sup>

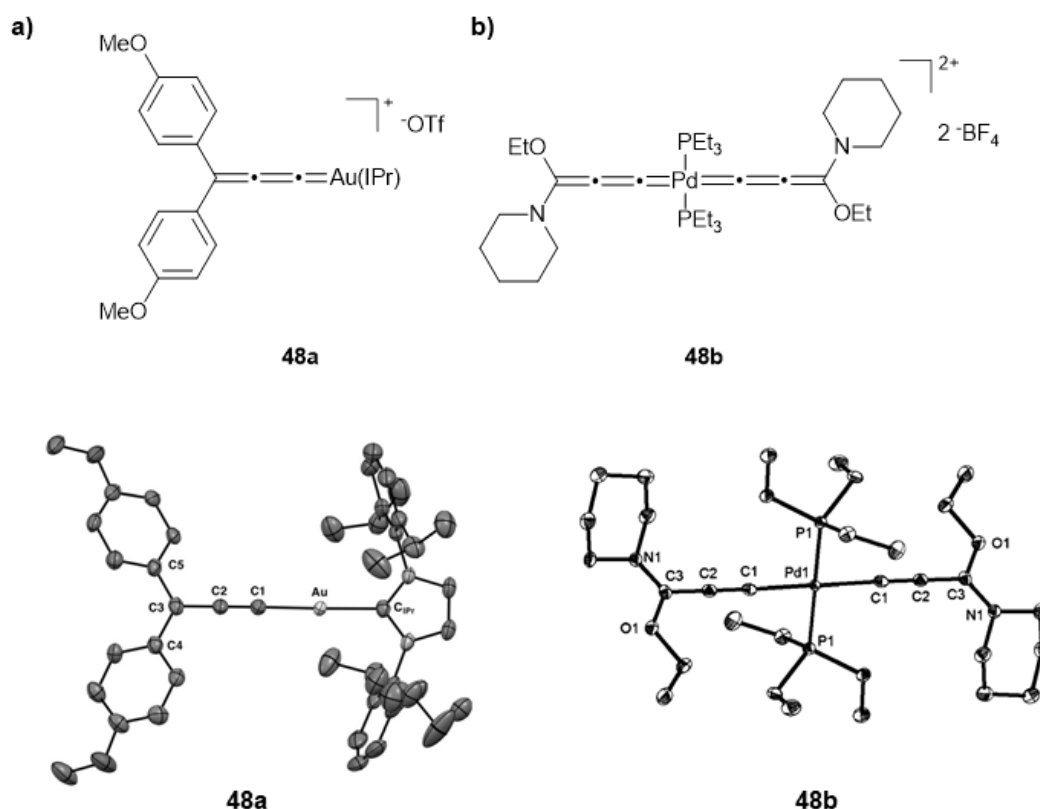


**Figure 17** Examples of cationic allenylidene complexes: a) Au-**48a**;<sup>[77]</sup> b) Pd-**48b**.<sup>[78]</sup>



## II. Aims and objectives

The aim of the study presented in this doctoral thesis was to explore the use of allene-based compounds as novel ligands for transition metal complexes and investigate the applications of resulting organometallic systems. Figure 18 illustrates the main project objectives.

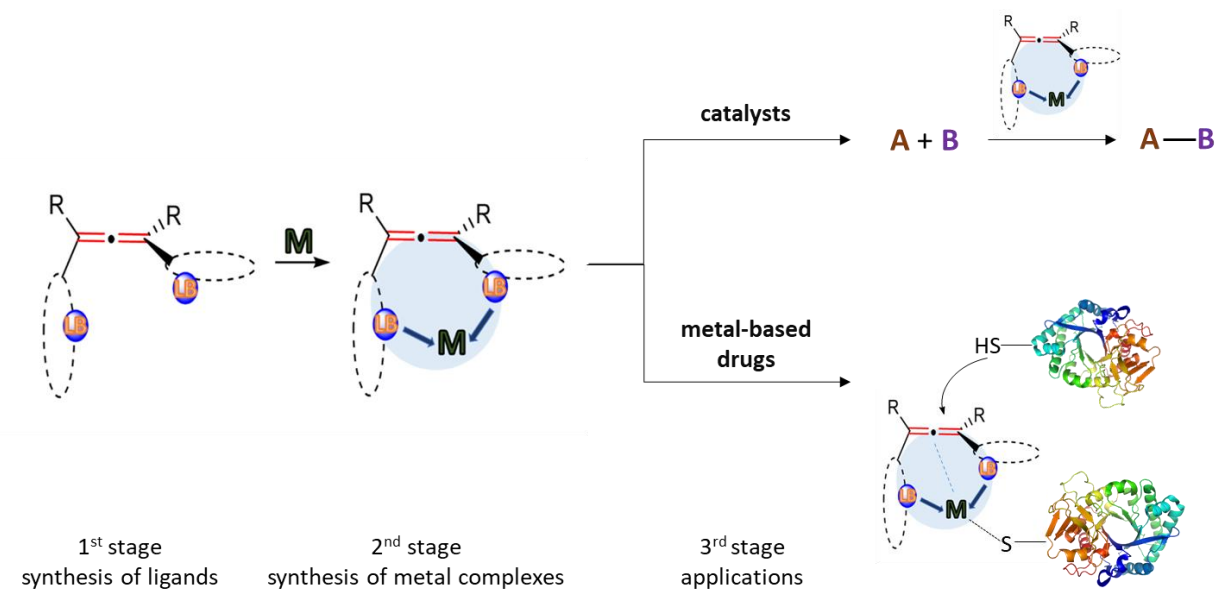


**Figure 18** Project objectives (LB – Lewis base).

The first stage of the project encompasses the synthesis of tetrasubstituted allene ligands equipped with two donor-type substituents in a 1,3-relationship. These Lewis-basic groups are designed as primary sites of interaction with metals, contrary to the allene-metal complexes where the allene double bonds are coordinated to metals (see Section I b.). The allene group used as backbone of the ligand has an important structural role that determines the geometry of the ligand and can be a source of chirality in the system. Such arrangement creates a special pocket within the ligand ready to accommodate a metal centre. Donor substituents could be heteroatom-based groups such as phosphines or amines directly bonded to the allene or alternatively a donor site could be a part of cyclic substituent (inside the ring like nitrogen atom in the pyridine or on the ring like the methoxy group in anisole). Throughout this work, terms “allene-based” or “allene-containing” ligands refer to this ligand architecture.

The behaviour of allene-based ligands in the presence of metals is investigated in the second stage of the project. The successful ligand candidates are envisioned to act as bidentate or tridentate (with allene participation) chelate systems that could increase the stability of challenging metal centres in the new complexes. One of the biggest challenges in the synthesis of allene-containing metal complexes is the susceptibility of the allene group to undergo intramolecular nucleophilic attack of one of its Lewis basic groups promoted by the

presence of a metal. This can result in a loss of crucial allene-supported backbone and thus the nucleophilicity of the substituents and the character of the metal centre have to be adequately adjusted. The steric bulk of the remaining groups around the allene core could increase the stability of the ligand. Full characterisation of all new allene-derived metal species will follow.

Finally, in the last stage of the study allene-derived metal complexes are investigated for their potential applications. Unique structural features of the new compounds such as  $C_2$  symmetry of the allene make them interesting candidates for applications in catalysis. Additionally, interesting 3D geometries and the dual character of these new organometallics, present them as candidates for metal-based drugs as the interactions with intracellular targets needed to realise their biological action could stem from both the presence of the metal centre as well as the allene core. As seen before in Section I a. the mechanism of action of most pharmacologically active allene compounds is attributed to their reaction with nucleophilic residues in the cell that undergo addition to the allene skeleton. These studies can help to uncover the structure-activity relationship of the new compounds, in particular the influence of the ligand substitution pattern, complex stoichiometry or symmetry.

### III. Allene-containing ligand candidates

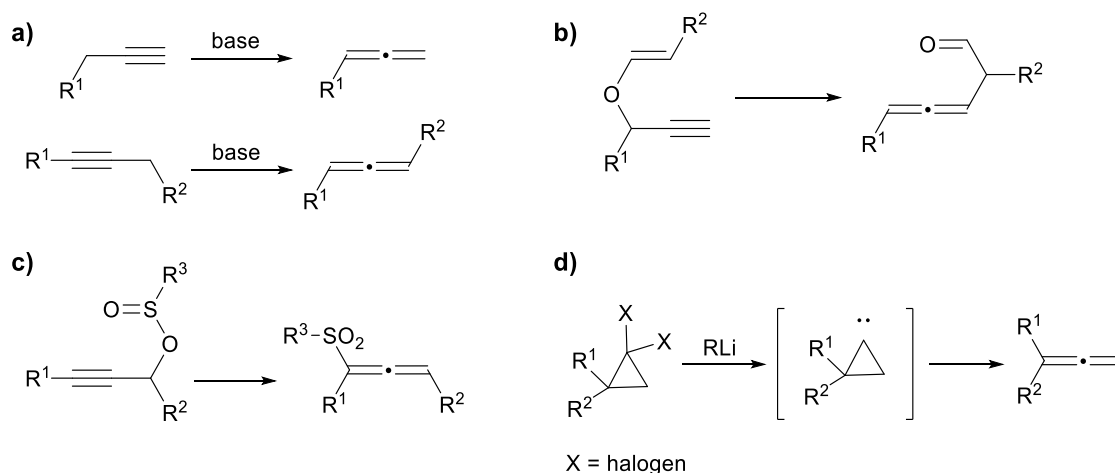
#### III a. Introduction

##### III a. 1. Synthesis of allenes

The wide adoption of the allene functionality as a common element in the organic chemist's toolbox was accompanied by the rapid development of many methodologies for allenes' synthesis in recent decades.<sup>[71,79–81]</sup> A brief overview of major synthetic approaches for the synthesis of allenes from alkenes and alkynes including all classic reaction types will be given here, with a particular emphasis on methods used for the synthesis of tetrasubstituted allene-based ligand candidates. Methods where allene or allenyl-compounds are used as substrates are not covered. For the discussion on the enantioselective synthesis of allenes, see Chapter VII.

##### - Rearrangement reactions

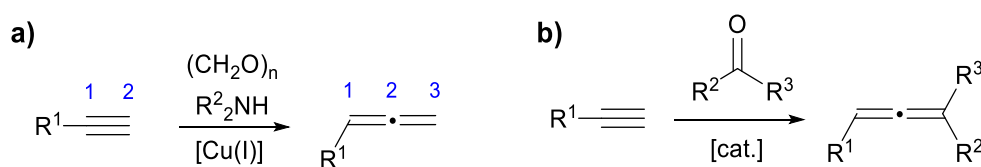
Thermal or base-induced prototropic rearrangement of terminal or internal alkynes readily yields mono- or disubstituted allenes, respectively (Scheme 3, a). Allenes with a variety of different substituents can be accessed by this method.<sup>[82–86]</sup> Sigmatropic rearrangements are also widely used in the synthesis of allenes. [3,3]-sigmatropic reactions such as Claisen-, Cope- or metal-catalysed rearrangements of propargyl substrates have been used in the synthesis of allenyl carbonyl compounds in particular (Scheme 3, b).<sup>[87–93]</sup> Similarly, [2,3]-sigmatropic rearrangement of propargyl sulfenates, sulfinates or phosphites is a good method for a generation of heteroatom-substituted allenes in a concerted manner (Scheme 3, c).<sup>[94–97]</sup> Different type of rearrangements, for example, Doering-Moore-Skatteböl carbene rearrangement of *gem*-dihalocyclopropanes with alkali metals, alkyllithium or Grignard reagents can also be used for the synthesis of allenes (Scheme 3, d).<sup>[98–100]</sup>



**Scheme 3** Rearrangement reactions to make allenes: a) prototropic rearrangement; b) Claisen rearrangement; c) [2,3]-sigmatropic rearrangement; d) Doering-Moore-Skattebøl carbene rearrangement.

- Homologation reactions

Common methods for a double bond formation such as Wittig or Horner-Wadsworth-Emmons reactions can be applied to the synthesis of allenes.<sup>[101,102]</sup> But perhaps the most widely used homologation method is the Crabbé reaction, where terminal alkynes are converted to monosubstituted allenes under Cu-catalysis (Scheme 4, a).<sup>[103,104]</sup> The original method of reaction of acetylenes with paraformaldehyde in the presence of amine has been extensively developed, in particular by the Ma group, to make a use of other carbonyl compounds such as other aldehydes and ketones to access di- and tri-substituted products (Scheme 4, b).<sup>[105,106]</sup>

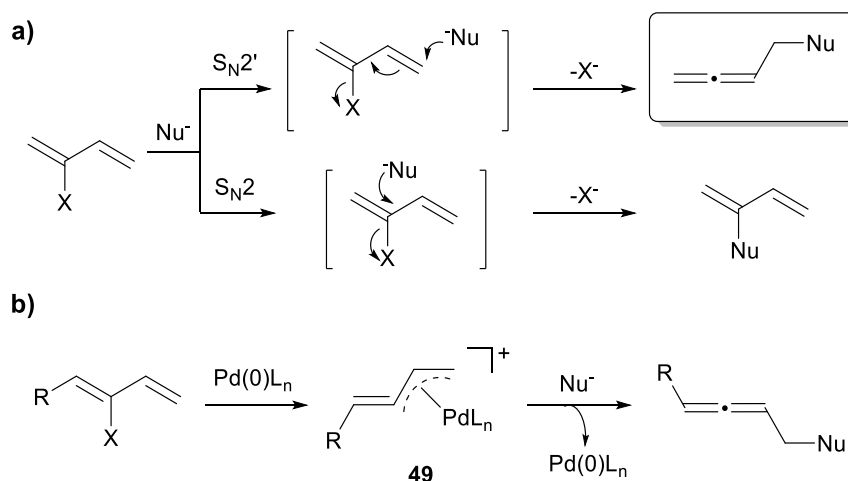


**Scheme 4** Homologation reactions to make allenes: a) Crabbé reaction with paraformaldehyde; b) homologation with aldehydes and ketones.

- Substitution reactions

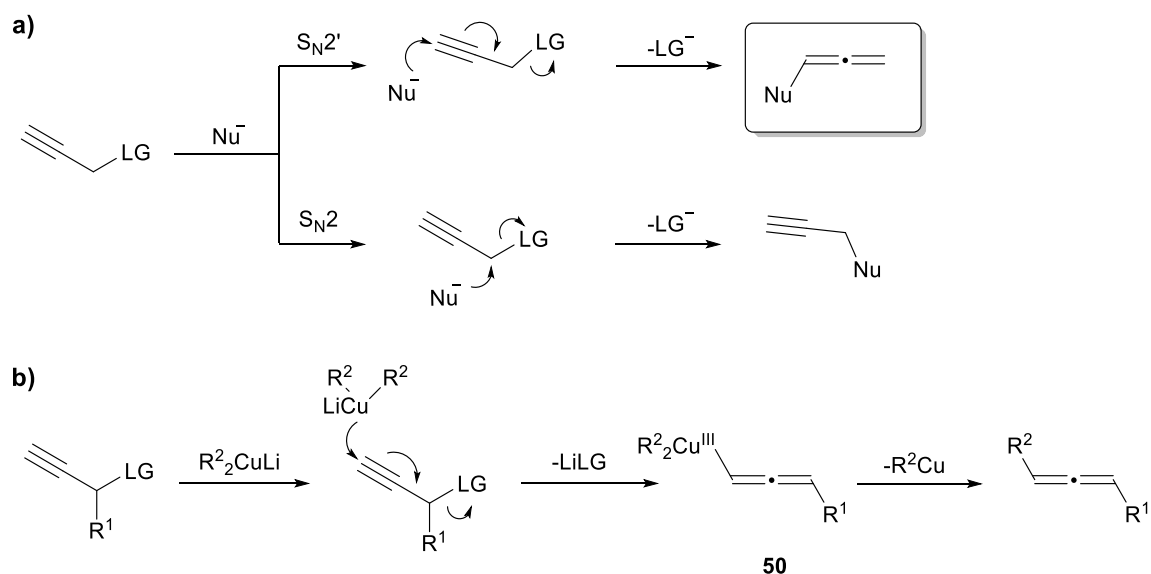
This class of reactions is one of the most common ways to access the allene functionality, especially when fully substituted allenes are needed. Substitutions resulting in an allene formation proceed through  $\text{S}_{\text{N}}2'$  mechanism and are mainly used with 2-halo-1,3-butadienes<sup>[107,108]</sup> and propargyl compounds<sup>[109–111]</sup> starting materials. Reaction of the former and related 2-substituted 1,3-butadienes such as 2-phosphates can proceed through already

mentioned  $S_N2'$  mechanism or in competing  $S_N2$  manner (Scheme 5, a).<sup>[112,113]</sup> The selectivity of the reaction is highly dependent on the reaction conditions. Grignard reagents and soft carbon nucleophiles under Cu and Pd catalysis have been employed to promote the  $S_N2'$ -type transformations.<sup>[114,115]</sup> In the case of Pd catalysis, the cycle is believed to proceed through the key intermediate (alkylidene- $\pi$ -allyl)Pd **49** complex (Scheme 5, b).<sup>[107]</sup>



**Scheme 5** Substitution of 2-halo-1,3-butadienes: a) competing pathways; b) schematic of Pd-catalysed  $S_N2'$  reaction.

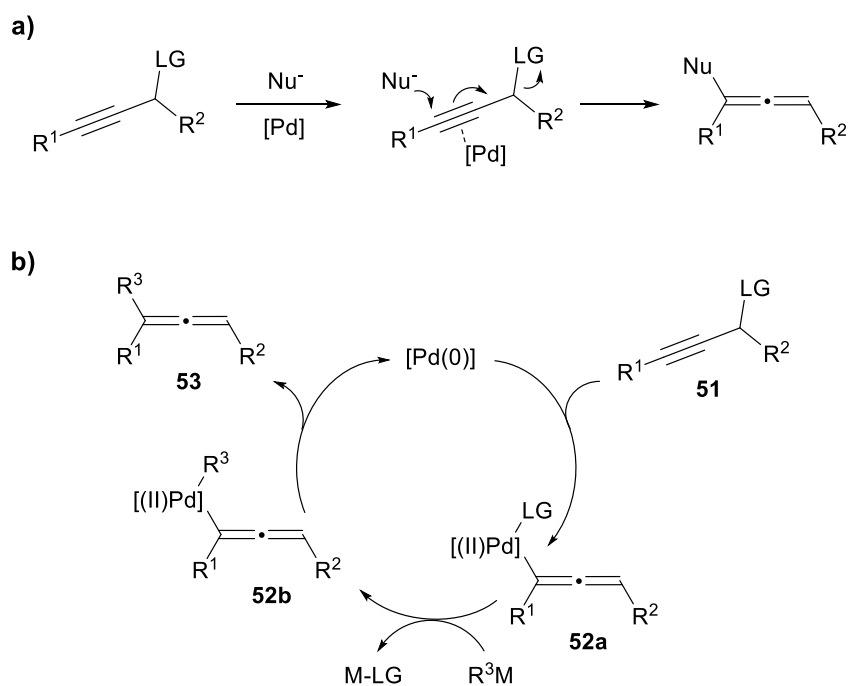
Even more extensively studied and perhaps the most common methodologies are the substitution reactions on propargyl compounds. The competition between the two substitution modes,  $S_N2'$  vs  $S_N2$ , can also be observed (Scheme 6, a). One of the first examples of this method was the reaction of propargylic esters with stoichiometric organocuprates (e.g.  $R_2CuLi$ ).<sup>[116]</sup> The methodology was later extended to other starting materials such as propargyl triflates, mesylates, oxiranes, sulfonates or halides.<sup>[117–119]</sup> The reaction is postulated to proceed *via*  $\sigma$ -Cu(III) species **50** that releases the allene product upon reductive elimination (Scheme 6, b).<sup>[120]</sup> The scope of the nucleophiles also increased to include Grignard or organozinc reagents.<sup>[121–123]</sup>



**Scheme 6** Substitution of propargyl compounds: a) competing pathways; b) mechanism of reaction with organocuprates.

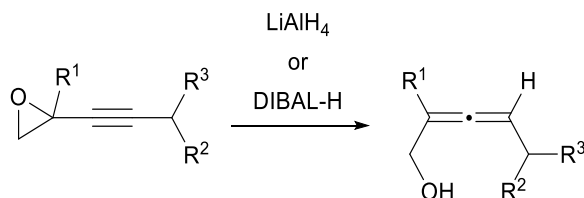
Further developments saw the Cu(I)-mediated reaction refined to the catalytic version often with improved yields and selectivities.<sup>[124,125]</sup> Other metals have also been reported to catalyze this transformation. From them, Pd is nowadays the most commonly employed transition metal in catalytic  $S_N2'$  nucleophilic substitutions of propargyl compounds with some examples of Ni-, Fe- or Ir-catalysis.<sup>[71,81,126–129]</sup> Substrate scope includes propargyl electrophiles equipped with leaving groups such as: esters, halides, carbonates, sulfonates or epoxides. A range of various, often organometallic, nucleophilic partners has been used with good results. For example, Grignard, organozinc, organoboron or organoaluminium reagents have been used.

The reaction mechanism can generally be viewed as an electrophilic activation of the triple bond by the Pd catalyst towards the formal  $S_N2'$  attack of nucleophiles (Scheme 7, a). In more detail, it can be described as a Pd(0)/Pd(II) catalytic cycle resembling that of classic cross-coupling reactions, in particular with organometallic nucleophiles. The cycle is postulated to proceed *via* ( $\sigma$ -allenyl)Pd(II) intermediate **52a** derived from oxidative addition of Pd(0) species to propargyl electrophile **51** (scheme 5, b).<sup>[130,131]</sup> In this step, the propargyl unit rearranges to the allene skeleton in a  $S_N2'$  manner. Subsequent transmetalation with the organometallic reagent and reductive elimination releases the substituted allene product **53** (Scheme 7, b). In fact, cross-coupling reactions can be distinguished as another sub-category of allenes' synthesis methods.<sup>[132–134]</sup>



**Scheme 7** Pd-catalysed  $S_N2'$  substitution of propargyl electrophiles: a) general reaction scheme; b) postulated catalytic cycle.

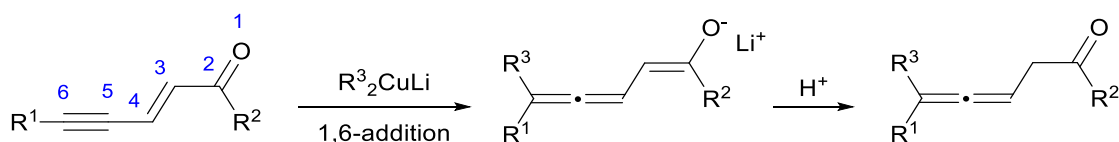
Additionally, reduction of propargyl electrophiles with hydrides ( $\text{LiAlH}_4$ , DIBAL-H *etc.*) and some transition metal catalysed reductions are known to proceed *via*  $S_N2'$  mechanism (Scheme 8).<sup>[135,136]</sup>



**Scheme 8** Reduction of propargyl electrophiles with hydrides to make allenes.

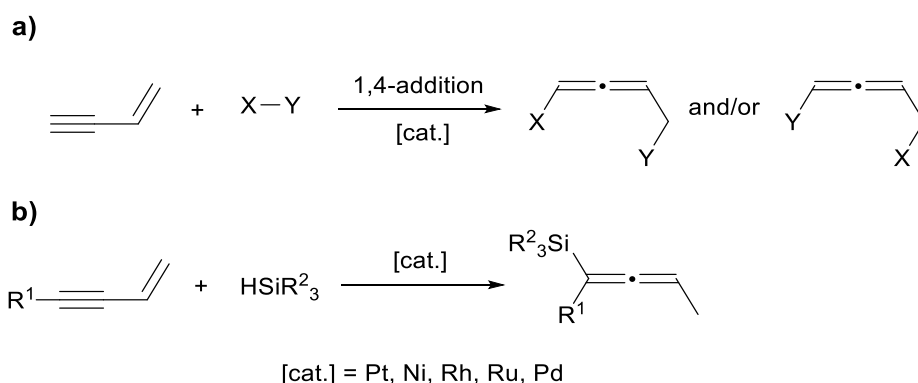
#### - Addition reactions

Addition of organocuprates to conjugated enynes is a standard method for the synthesis of allenes (Scheme 9).<sup>[137,138]</sup> The anticipated 1,6-regioselectivity is normally favoured by the presence of EWG substituents at the double bond of the substrate, whereas their presence on the triple bond usually leads to a 1,4-addition pathway resulting in formation of conjugated dienes. Allene-forming 1,8-, 1,10- or even 1,12-cuprate additions to extended enynes have been reported.<sup>[139]</sup>



**Scheme 9** 1,6-Organocuprate addition to conjugated enynes to make allenes.

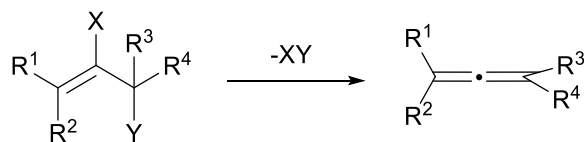
Another popular variant of the reaction is the transition metal catalysed 1,4-addition to conjugated enynes (Scheme 10, a). Common methods include Pt-, Ni-, Rh-, Ru- or Pd-catalysed additions of hydrosilanes or hydroboranes yielding allenyl silanes and allenyl boranes, respectively (Scheme 10, b).<sup>[140–143]</sup> 1,4-additions can also occur in an intramolecular manner affording functionalised allenes.<sup>[144]</sup>



**Scheme 10** 1,4-Addition to conjugated enynes to make allenes: a) general reaction scheme; b) metal-catalysed addition of hydrosilanes.

#### - Elimination reactions

1,2-Elimination reactions are another good method for the synthesis of allenes (Scheme 11).<sup>[145]</sup> Highly substituted allenes can be accessed this way, for example, by dehydrohalogenation or dehydration of vinyl or allylic starting materials. Base- and metal-promoted reactions have been reported in that regard.<sup>[146–148]</sup>



**Scheme 11** 1,2-Elimination of olefins to make allenes.

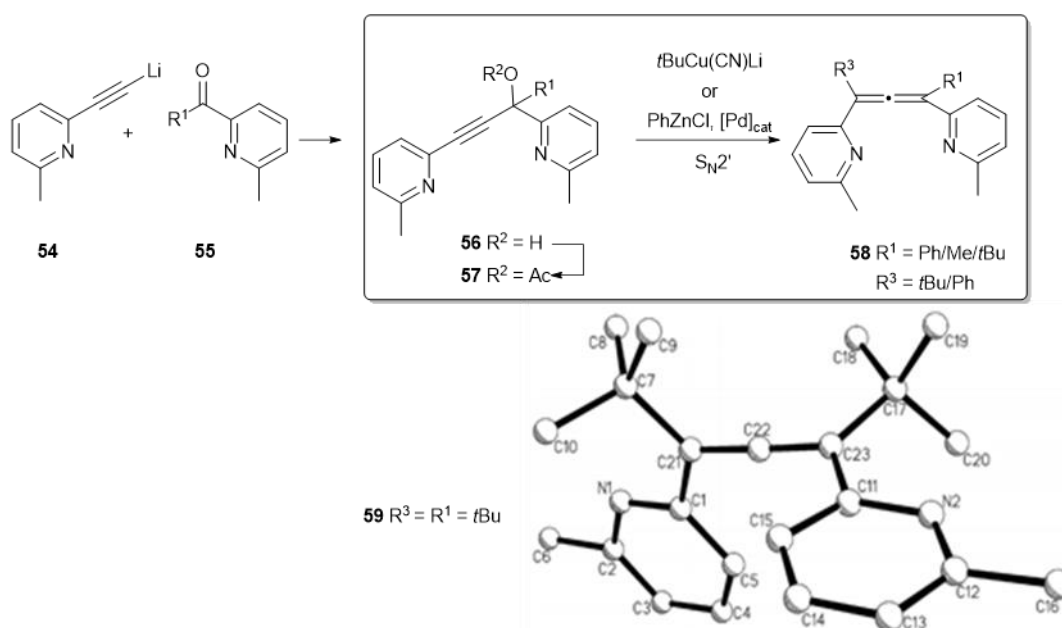
### III a. 2. Synthesis of allene-containing ligands

This section describes allene-containing ligands with general structural features outlined in the project objectives section (page 28). These allenes are equipped with donor-type substituents



used for binding to metals and the allene core provides the general shape of the ligand. A small number of reported allene-containing ligands that emerged since 2008 are presented below.

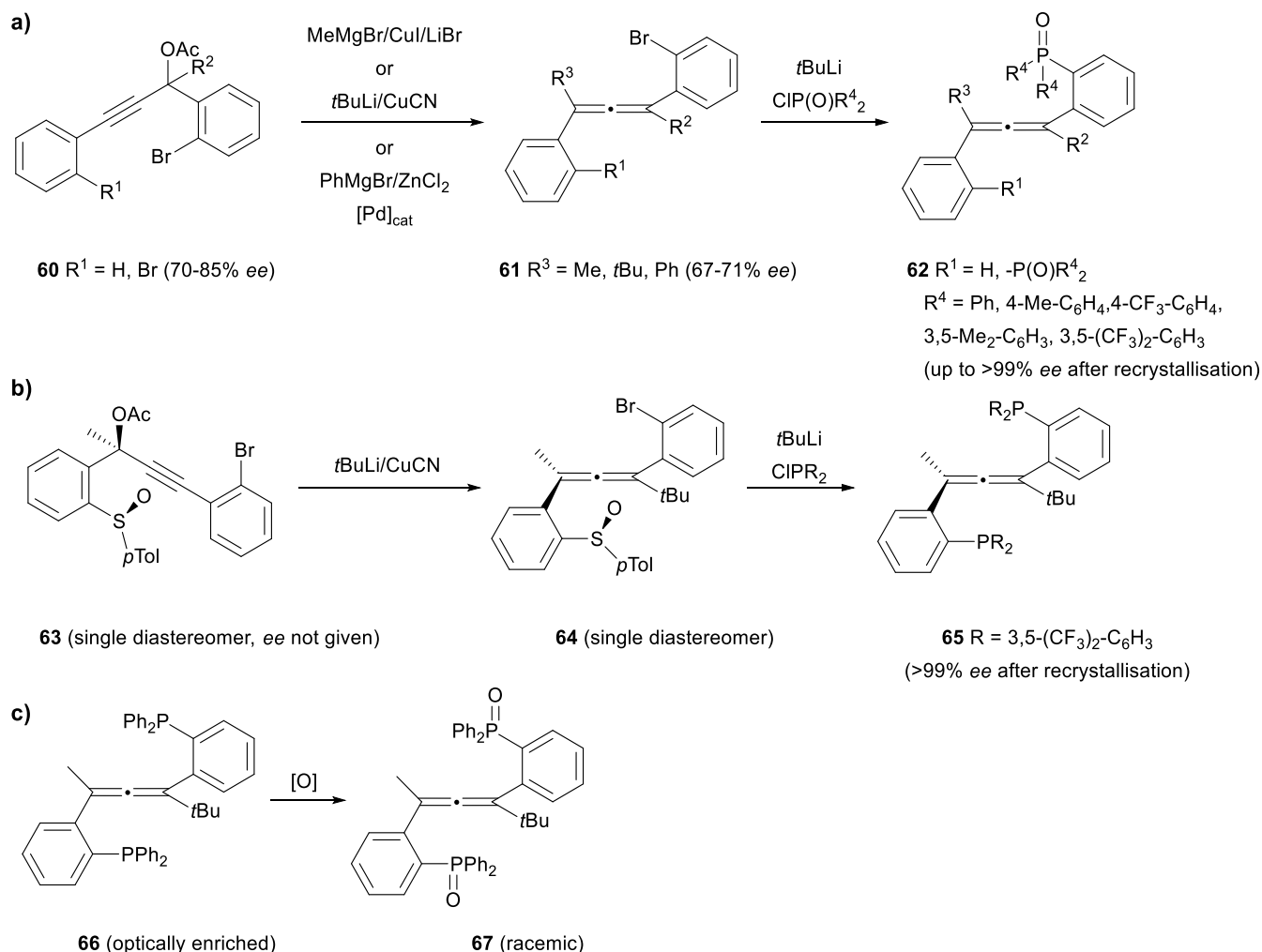
In the majority of examples, the authors followed very similar synthetic strategy to generate their respective ligands. Typically, tetrasubstituted allenes were formed in the  $S_N2'$ -substitution on propargylic electrophiles. Thus, the first example of the synthesis of axially chiral ligands for transition metal complexes based on the allene backbone was reported by Krause group.<sup>[149]</sup> The authors chose bis(pyridyl)allene as the key motif for the ligand's design and successfully synthesised several derivatives corresponding to the general structure **58** (Scheme 12). The key step of the synthesis,  $S_N2'$ -displacement, was achieved either by reaction with *t*-butylcuprate or phenylzinc reagents under Pd-catalysis. Starting materials for this transformation were obtained by esterification reaction of tertiary propargyl alcohols, initially synthesised by addition of lithium acetylides to pyridyl ketones (Scheme 12). Additionally, the synthesis of an enantioenriched bis(pyridyl)allene derivative was achieved from enantiomerically pure ester (*ee*  $\geq$  99%), obtained by HPLC separation of the precursor propargyl acetate. Bis(*t*-butyl)derivative **59** was characterised by X-ray crystallography (Scheme 12) and displayed the two pyridyl units supported on the allene skeleton with nitrogen atoms facing away from the anticipated metal-coordinating pocket.



**Scheme 12** Synthesis of bis(pyridyl)allenes and crystal structure of allene **59**.<sup>[149]</sup>

A range of optically active mono- and bis(phosphine oxides) supported on an allene framework was prepared utilising a similar synthetic approach by Ready and co-workers.<sup>[150]</sup> Asymmetric addition of terminal alkynes to the corresponding ketones or resolution of racemic tertiary alcohols followed by acylation furnished optically active starting materials **60** for  $S_N2'$ -

substitution with organocuprate or arylzinc halides reagents. The resulting tetrasubstituted allenes **61** were subsequently treated with *t*BuLi and diarylchlorophosphine oxides to form final products **62** (Scheme 13, a). These allenes were used as organocatalysts in an asymmetric epoxide ring opening reaction.

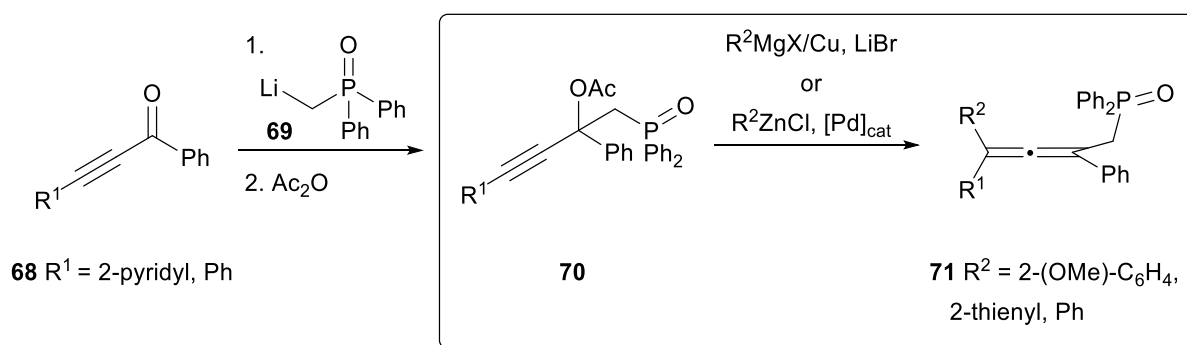


**Scheme 13** Allene-containing ligands from Ready's group: a) synthesis of mono- and bis(phosphine oxide)allenes; b) synthesis of phosphine allenes; c) rapid oxidation of phosphine allenes.

The same authors continued their work on phosphorus-based allene ligands in asymmetric catalysis, switching their attention to allene-containing phosphines (**65**) (Scheme 13, b).<sup>[151]</sup> Starting material **63** was prepared by stereoselective addition of lithiated acetylene to the ketone containing sulfoxide group with a fixed stereochemistry acting as a chiral auxiliary and then acylated.<sup>[152]</sup> The key feature in the subsequent synthesis from the single diastereomer of acetate **63** was the presence of electron-withdrawing groups on the phosphine. This electronic arrangement played a pivotal role for the stability and stereochemical integrity of the ligand. Successful generation of enantiomerically pure ligands such as **65**, having highly electron-accepting substituents on phosphorus, was possible

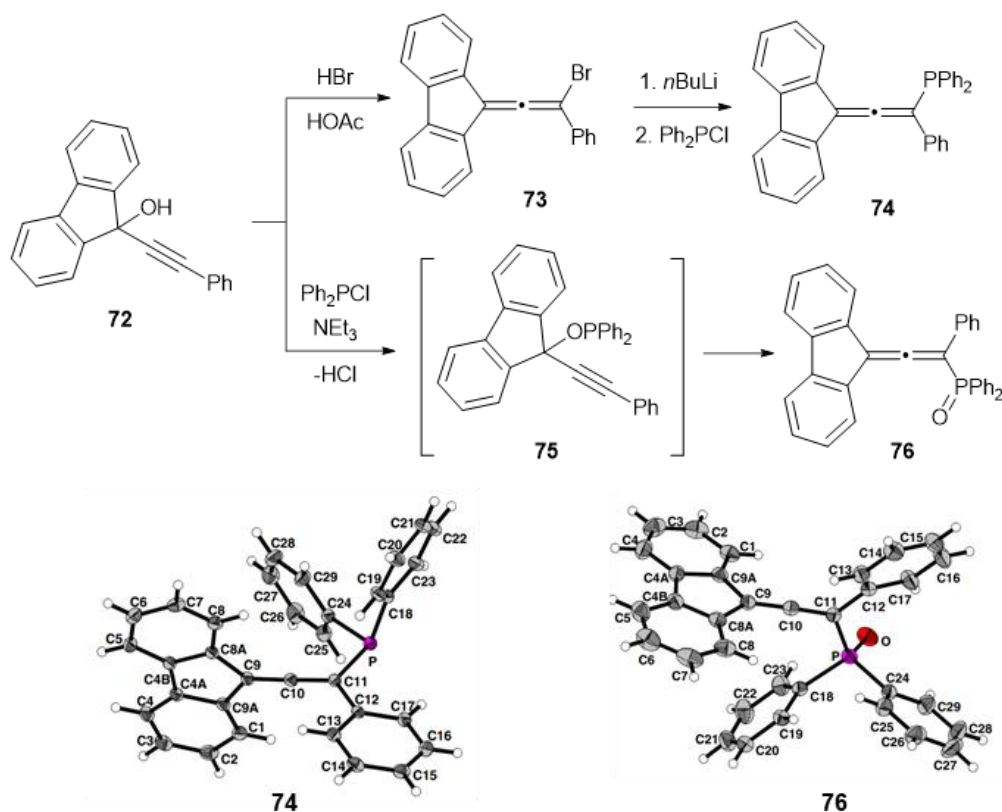
whereas derivatives such as **66** underwent prompt oxidation to **67** (with racemisation) upon exposure to air (Scheme 13, c). This was a strange observation considering the stability of other triaryl phosphines. The authors conducted a separate study investigating the cause of this unusual oxidation.<sup>[153]</sup> They proposed that a phosphine group in the ligand can cyclize onto the allene core giving an achiral zwitterionic phosphonium species that is easily oxidised with molecular oxygen.

The Fensterbank group chose an alkyl-tethered phosphine oxide moiety as a principal donor site in the design of their ligands and consequently carried out the synthesis of several allenes with described characteristics in a typical  $S_N2'$  manner (Scheme 14).<sup>[154]</sup> Tertiary alcohol precursors were obtained by somewhat different synthetic route to the previously described, namely, by the addition of lithium methyldiphenylphosphine oxide **69** to ynones **68**.



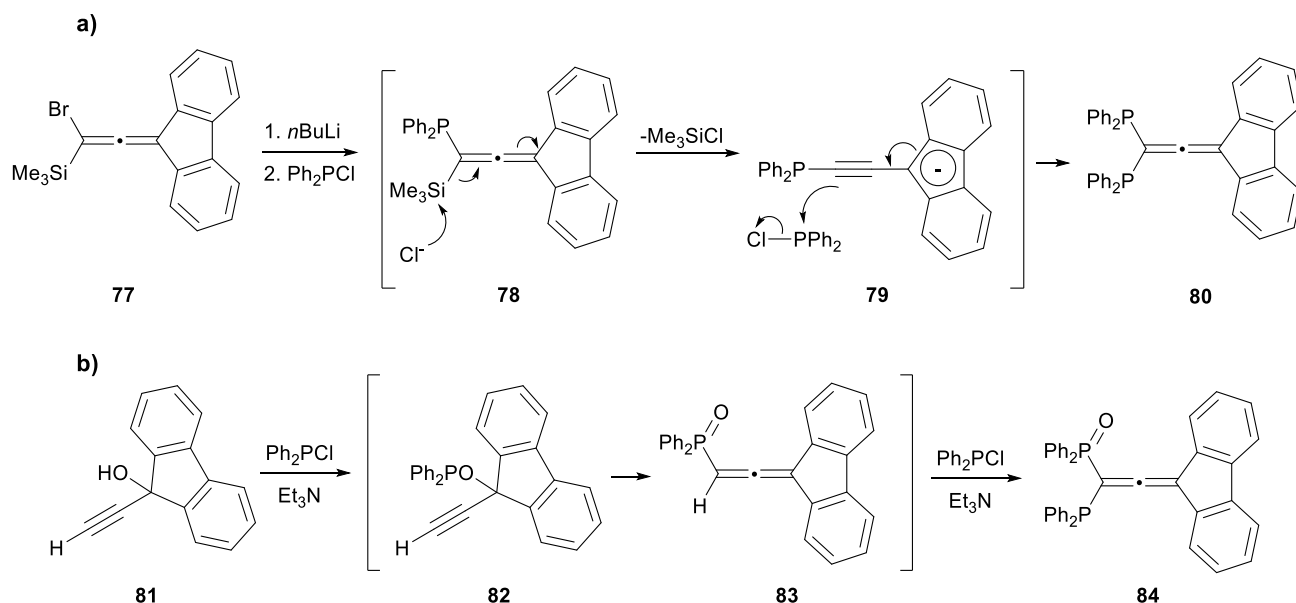
**Scheme 14** Fensterbank's synthesis of (phosphine oxide)allenes.

Allene-containing ligands have also been synthesized by methods other than  $S_N2'$ -displacement. An early example comes from the McGlinchey group, studying fluorenylidene-containing allenes and derivatives. The authors described the synthesis of phosphine- and phosphine oxide(fluorenyl)allene ligands **74** and **76**, where the phosphorus atom is directly bonded to the allene (Scheme 15). Both compounds were prepared from propargyl alcohol **72**, the former *via* bromoallene **73** and the latter *via* [2,3]-sigmatropic rearrangement of intermediate **75**.



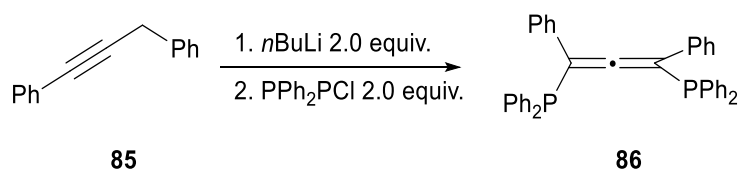
**Scheme 15** Synthesis of mono-phosphine and phosphine oxide(fluorenyl)allenes and crystal structures of **74** and **76**.<sup>[155]</sup>

Somewhat similar strategy was later used by the same group to obtain bis(phosphine)- and phosphine(phosphine oxide)allene ligands **80** and **84** (Scheme 16).<sup>[156]</sup> The formation of **80** was proposed to proceed *via* stabilised 14 $\pi$ -electron aromatic intermediate **79** resulting from the elimination of the silyl group from the preceding allene intermediate **78** (Scheme 16, a). While **84** was formed after initial [2,3]-sigmatropic rearrangement of **82** followed by the deprotonation of **83** and attack on another Ph<sub>2</sub>PCl molecule (Scheme 16, b).



**Scheme 16** Proposed mechanism for the synthesis of: a) 1,1-bis(phosphine)allene **80**; b) 1,1-phosphine(phosphine oxide)allene **84**.

The last reported example was proposed by Fensterbank and co-workers in 2016 and also featured a bis(phosphine)allene design with phosphines placed directly onto the allene skeleton.<sup>[157]</sup> The authors took advantage of an older report<sup>[158]</sup> to readily access 1,3-bis(phosphine)allene **86** in a one-step reaction from alkyne **85** *via* prototropic rearrangement (Scheme 17).



**Scheme 17** Synthesis of 1,3-bis(phosphine)allene **86**.

### III b. Results and Discussion

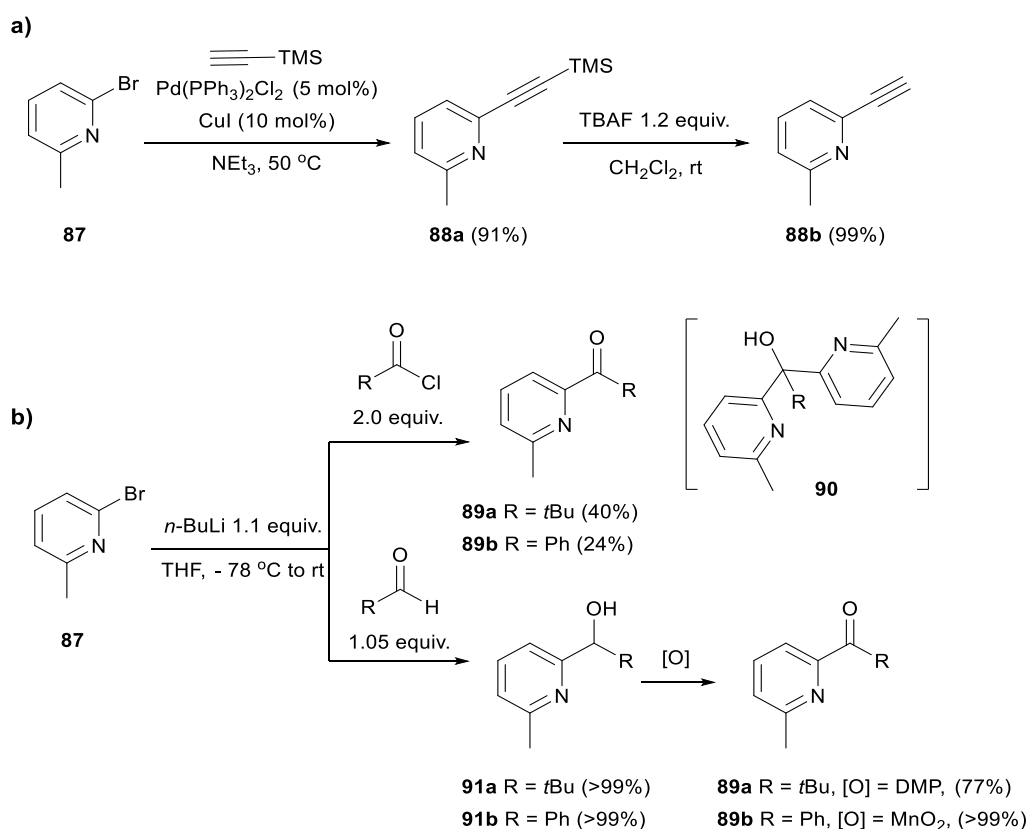
We started the synthesis of a series of allene-containing ligands with the selection of initial synthetic targets and fitting preparative approaches. Relevant literature review (see also Section IV a.) demonstrated that the most successful complex-forming allene ligands were equipped with nitrogen (pyridines) and phosphine donor units. What is more, the allenes needed to be at least tri- but better yet tetrasubstituted and the remaining substituents on the allene backbone tended to be quite bulky, e.g. *t*-butyl or phenyl groups.

As the starting point, we attempted the reproduction of some of the results from the cited studies with a rationale that the complexation properties and applications of some of the

reported ligands had been very limited. Consequently, we chose Krause's bis(pyridyl)allenes<sup>[149]</sup> as the main synthetic objective with some attention paid to bis(phosphine) ligands reported by Fensterbank group.<sup>[157]</sup> Based on the insights gained from these initial attempts, we followed with the synthesis of unprecedented allene-containing ligands.

### III b. 1. Bis(pyridyl)allenes

The synthesis of bis(pyridyl)allenes postulated by Krause began with the addition of lithiated alkynyl(pyridines) to pyridyl ketones. When unsubstituted (alkynyl)pyridines were used the overall efficiency of the synthesis decreased, therefore a methyl-substituted pyridine derivative was employed.<sup>[127]</sup> This methyl group also seemed necessary to increase the stability of the final allene structures. Thus, we prepared 6-methyl-2-ethynylpyridine **88b** from commercially available bromopyridine **87** and TMS-acetylene in a Sonogashira cross-coupling reaction. The deprotection of TMS-protected intermediate **88a** afforded compound **88b** with overall 90% yield over the two steps (Scheme 18, a).

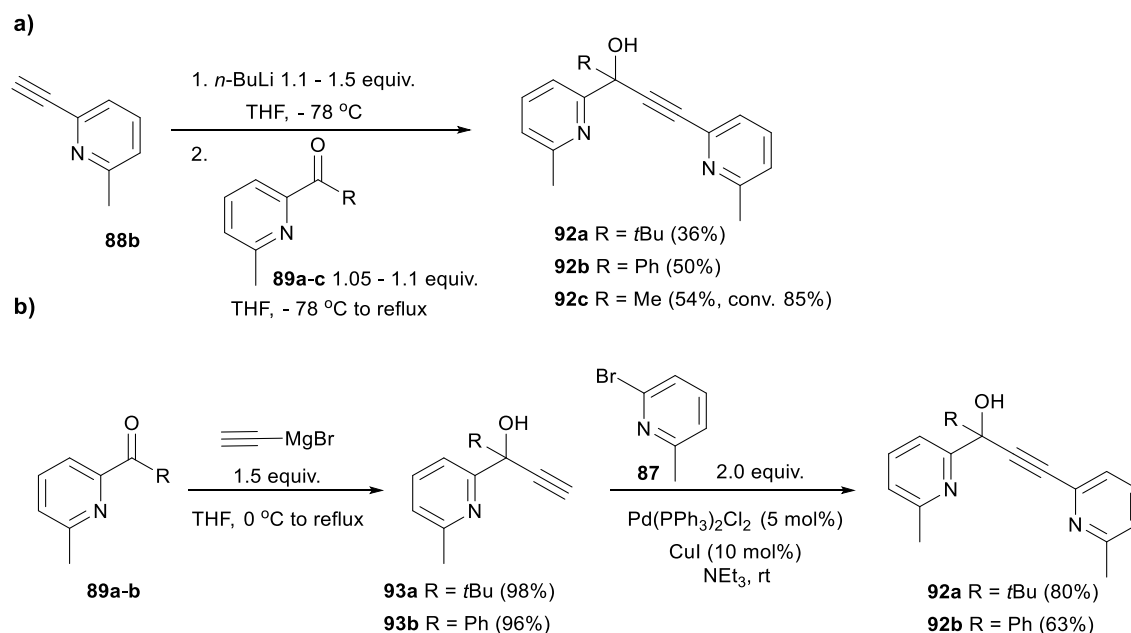


**Scheme 18** Synthesis of pyridyl: a) acetylene **88b**; b) ketones **89a-b**.

Pyridyl ketone derivatives were synthesised next. The choice of the second substituent on the ketone determined one of the substituents in the final allene product. Initially, we tried one-step protocol with the addition of 6-methyl-2-bromopyridine **87** reacted with *n*-BuLi

(lithium-halogen exchange) to the corresponding acid chloride.<sup>[159]</sup> The displacement of the chloride yielded desired *t*-butyl- (**89a**) and phenyl- (**89b**) ketones, albeit in moderate yields (Scheme 18, b). Despite the fact that in both cases an excess of the acid chloride was used, the double addition of the pyridyl unit that formed tertiary alcohol **90** was occurring competitively. Also, products of the *n*-BuLi attack on the carbonyl were observed. Isolation of the pure products was thus hampered by the resulting complex reaction mixtures. To overcome the disadvantages arising from this approach, we shifted our attention to a very similar yet two-step method.<sup>[160]</sup> This time, lithiated pyridine was added to the corresponding aldehyde and we observed quantitative formation of pyridyl alcohols **91a-b**. Secondary alcohols **91a-b** were readily oxidized with DMP<sup>[161]</sup> or MnO<sub>2</sub><sup>[162]</sup> to the corresponding ketones **89a-b** (Scheme 18, b).

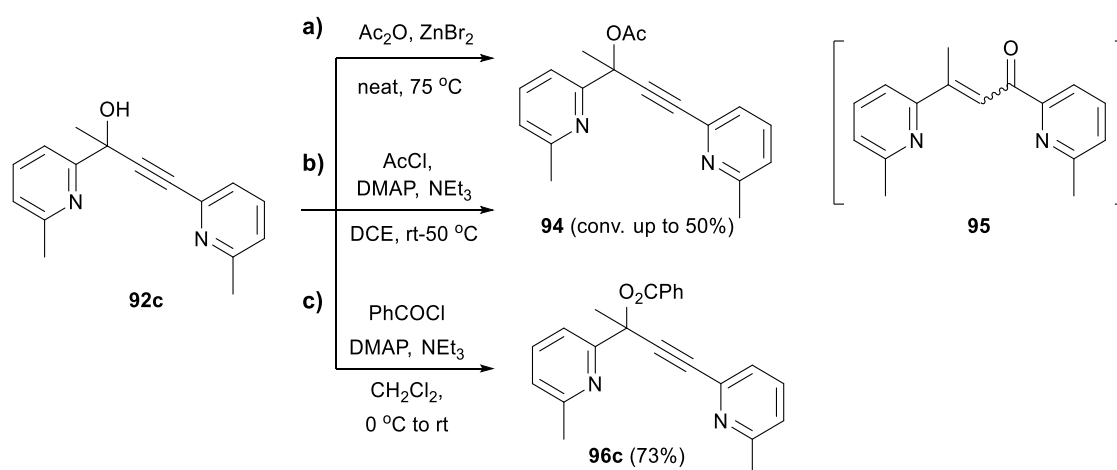
The synthesis of the propargyl alcohols followed. Alkyne **88b** was deprotonated with *n*-BuLi solution and reacted with the two previously synthesised ketones and additional commercially available methyl ketone **89c**. The formation of congested tertiary alcohols **92a-c** proceeded with difficulty even under refluxing conditions (Scheme 19, a). We tested an alternative strategy to access **92a-b** next. The challenging tertiary centre was formed first with the addition of smaller Grignard nucleophile, ethynylmagnesium bromide, to the ketone in excellent yield (Scheme 19, b, **93a-b**). Afterwards, we introduced the second pyridyl group in a Sonogashira cross-coupling affording **92a-b** in higher yields.



**Scheme 19** Synthesis of bis(pyridyl)propargyl alcohols **92a-c** by addition of: a) lithiated acetylene; b) Grignard reagent.

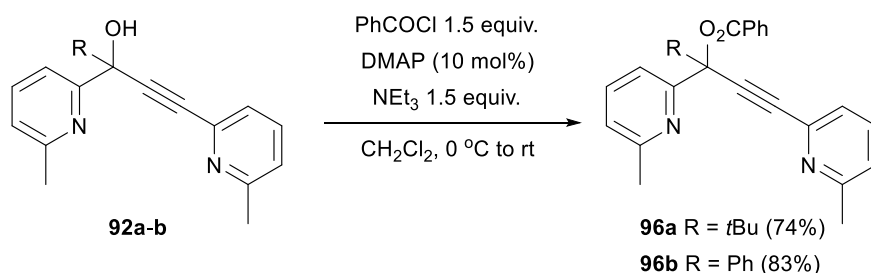
The esterification of the resulting bis(pyridyl)alcohols was similarly challenging. The reported conditions of the reaction with sterically hindered substrates<sup>[149]</sup> and acetic anhydride

catalsed by DMAP or zinc salts resulted only in modest conversion of the starting material **92c**. What is more, the main product seemed to be ketone **95** formed by a rearrangement of the alcohol (Scheme 20, a). Subsequently, we tested more reactive coupling partners. Use of a DMAP-catalysed esterification method developed for structurally similar pyridine N-oxides with benzoyl chloride<sup>[163]</sup> modified to the use of acetyl chloride, however, resulted in only partial conversion to the ester **94**. Complete conversion was crucial in that particular reaction as alcohol/ester mixture was practically inseparable. Fortunately, when we used benzoyl chloride the corresponding benzoate ester **96c** was formed in good yield (Scheme 20, c).



**Scheme 20** Optimisation of esterification conditions for alcohol **92c**.

The same conditions were applied to the remaining alcohols and gave esters **96a** and **96b** in 74% and 83% yield, respectively (Scheme 21).

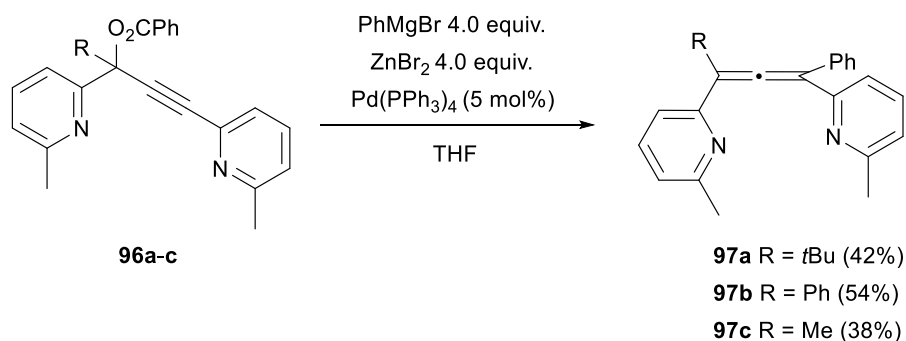


**Scheme 21** Esterification of alcohols **92a-b**.

Resulting esters **96a-c** were direct precursors to the allenic target molecules. The key step in the synthesis was thus Pd-catalysed substitution<sup>[149]</sup> on propargyl benzoate esters with an organozinc nucleophile, phenylzinc bromide. The latter is initially prepared from the Grignard reagent phenylmagnesium bromide and  $\text{ZnBr}_2$ . The success of the reaction requires highly anhydrous conditions and the use of thoroughly dry zinc salt. Additionally, the temperature range and reaction times had to be optimised for each substrate to achieve an



optimal yield of the allenic product. Consequently, we obtained three derivatives of bis(pyridyl)allenes (**97a-c**); allene **97c** has not been previously reported (Scheme 22).



**Scheme 22** Synthesis of allenes **97a-c** in  $S_N2'$  reaction.

We serendipitously discovered that some of the bis(pyridyl)allenes exhibit some fluorescent properties. Specifically, we characterised the fluorescent behaviour of allene **97b** (Figure 19). We detected that **97b** has a strong absorption band between 250 – 350 nm (Figure 19, a). We observed the strongest fluorescence emission at 530 nm in the visible range when **97b** was excited at 281 nm (Figure 19, b). We did not pursue the utilisation of this phenomenon much further in the project, however it proved quite useful in the future coordination studies. The visible loss of fluorescence of the bis(pyridyl)allene solutions was usually a sign of reaction completion in reactions with metal salts, as allene-derived metal complexes (from either class, see Chapter IV) were not fluorescent.

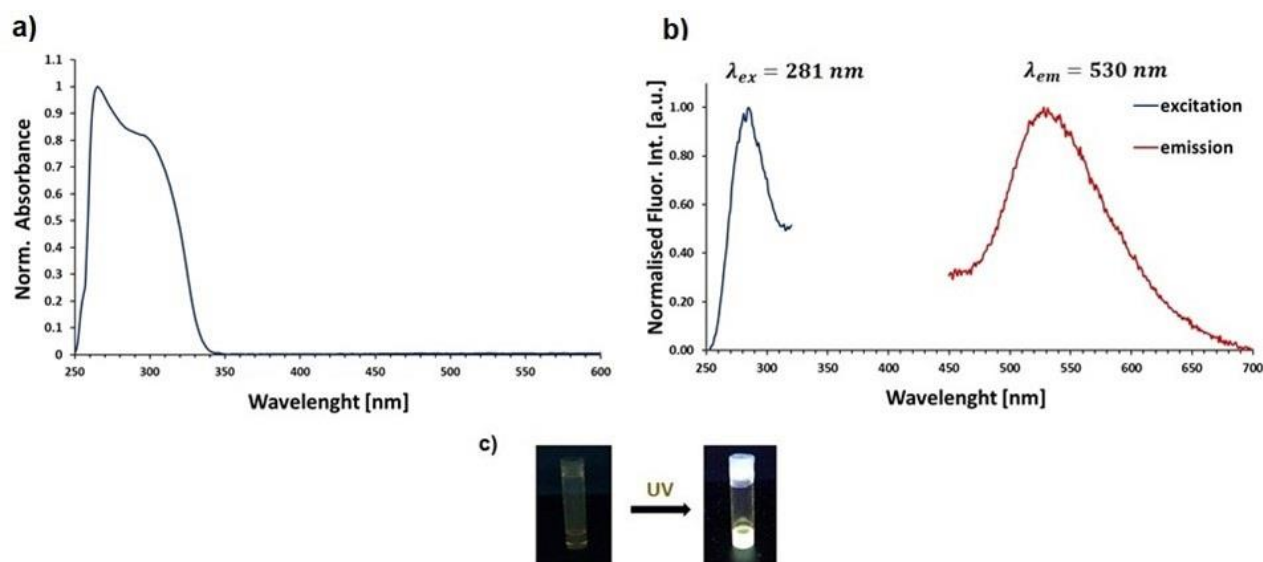
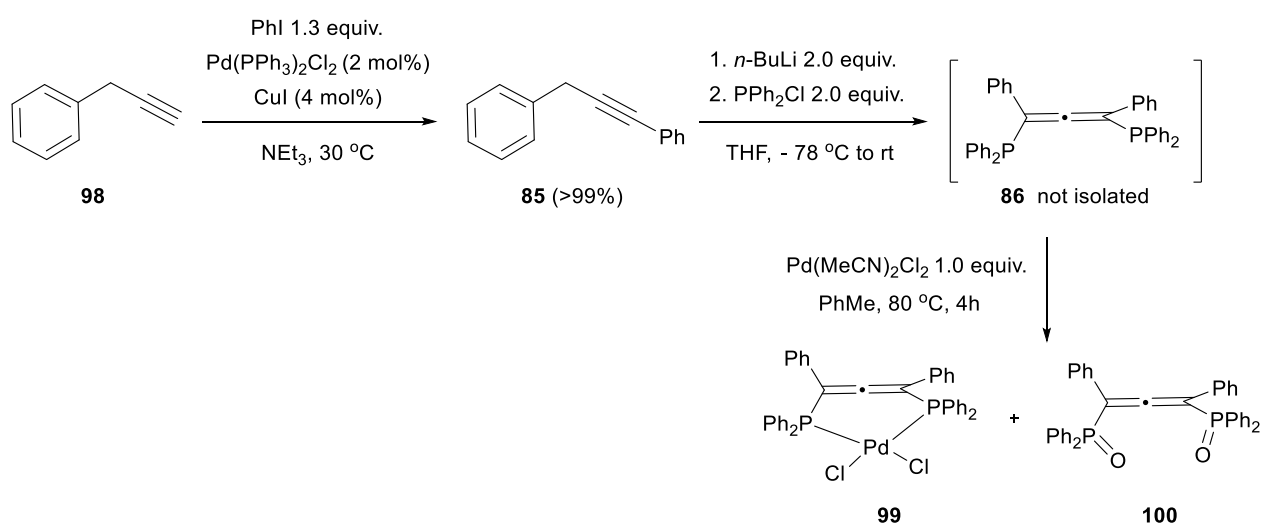


**Figure 19** UV-Vis characterisation of bis(pyridyl)allene **97b**: a) absorbance spectrum (0.05 mM in DMSO) b) normalised fluorescence intensity (0.05 mM in DMSO) c) solution of **97b** in  $\text{CH}_2\text{Cl}_2$  under UV light.

### III b. 2. Bis(phosphine)allenes

One of the previously discussed allenic ligands, namely, bis(phosphine)allene **86**, seemed to be of interest as the next synthetic target. First of all, preliminary studies carried out by Fensterbank and co-workers revealed that this ligand readily forms complexes with metals such as Pd(II), Pt(II) or Au(I) (see Section IV a.).<sup>[157]</sup> Secondly, the two-step synthesis of compound **86** rendered it very accessible. We decided to prepare **86** to study its extended coordination properties and novel applications.

We attempted the preparation of **86** according to a reported procedure.<sup>[157]</sup> Firstly, Sonogashira cross-coupling reaction of commercially available 3-phenyl-1-propyne **98** and iodobenzene quantitatively yielded alkyne **85**.<sup>[164]</sup> Then, the latter was reacted with 2 equiv. of *n*-BuLi and chlorodiphenylphosphine (Scheme 23).



**Scheme 23** Attempted synthesis of bis(phosphine)allene **86**.

The isolation of pure allene **86** proved to be very challenging. The proposed method of purification, recrystallisation from the mixture of water and ethanol as well as other solvent mixtures were unsuccessful, as was purification by column chromatography. However, the analysis of aliquots of impure reaction mixture suggested that the allene product was formed as determined by the characteristic peak of the central allene carbon atom at over 200 ppm in the <sup>13</sup>C NMR spectrum. Unfortunately, the <sup>31</sup>P NMR analysis indicated that the product contained phosphine oxide moieties rather than phosphine groups, suggesting formation of a **100**-type product. Contrarily to the reported properties of compound **86** it appeared to be rather air unstable. We subsequently tried *in situ* formation of a complex to avoid the oxidation of bis(phosphine)allene **86** during the work-up (Scheme 23). To test this approach we chose the already reported Pd(II) complex **99**. After the allene formation step, 1 equiv. of Pd(MeCN)<sub>2</sub>Cl<sub>2</sub> was added to the crude reaction mixture kept under inert atmosphere. Heating at 80 °C in

toluene followed, and postulated air stable complex **99** was isolated by recrystallisation. Nevertheless, the resulting solid was found (NMR and mass spectrometry analyses) to contain the bis(phosphine oxide)allene **100** as the main component with only trace quantities of **99**.

It seemed that highly anaerobic conditions would be necessary to avoid rapid oxidation of allene **86**. Combined with the difficulty in handling, **86** became less attractive in terms of envisioned applications. Unless the design was altered, for example, by placing more electron accepting groups in the phosphine moiety to thwart the oxidation, the ligand seemed to be unsuitable for further use and was not investigated further.

### III b. 3. Bis(thienyl)allenes

As the next ligand candidate we chose the general structure of bis(thienyl)allene **101** (Figure 20). Their use as ligands for transition metal complexes has not been reported to date. Tailored particularly for Au complexation, the choice of sulphur-based substituents for the ligands was supported on well-known Au-S affinity, which could promote effective coordination. We argued that similarity between thiophene and pyridine rings would allow for the synthesis of bis(thienyl)allenes in a manner related to already optimised route for bis(pyridyl)allenes.

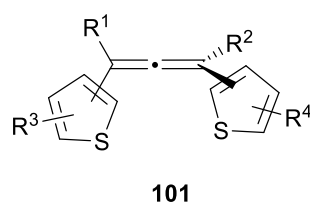
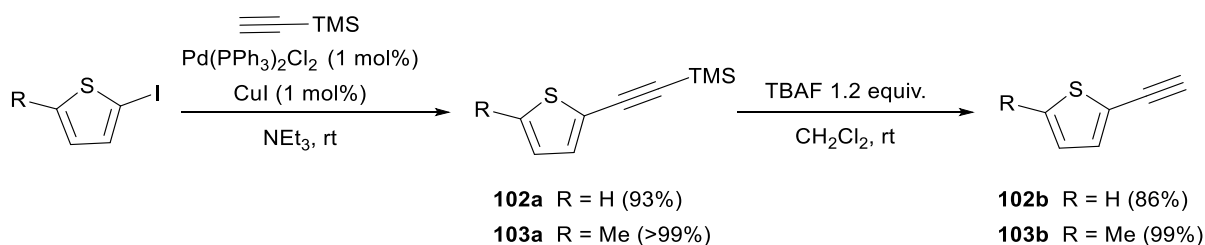


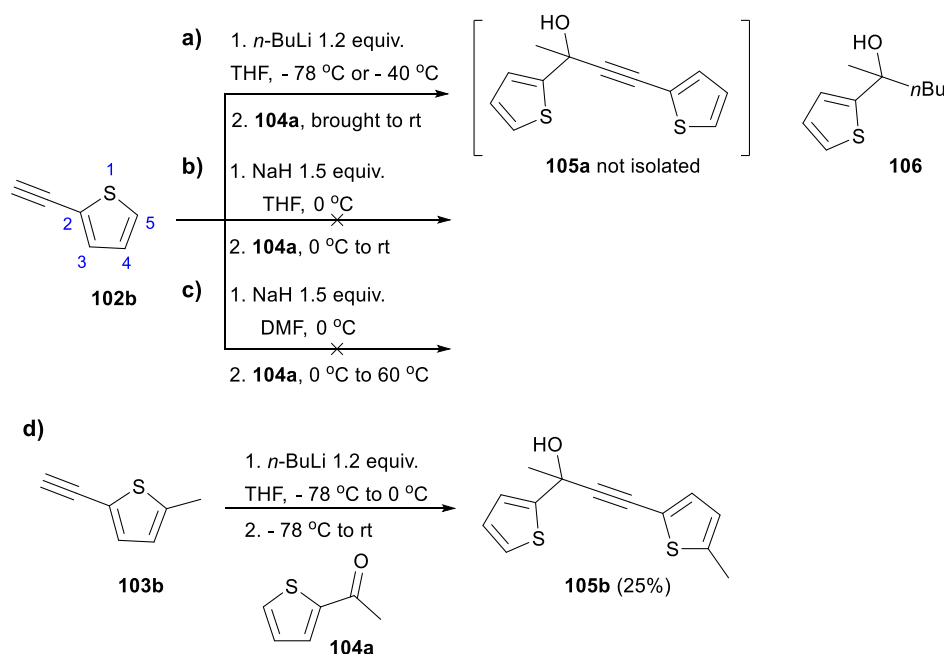
**Figure 20** General structure of bis(thienyl)allene **101** ligand.

We firstly attempted the synthesis of **101** derivatives *via* previously used synthetic route beginning with the addition of lithiated ethynylthiophenes to thienyl ketones. Consequently, ethynylthiophenes **102-103b** were prepared from corresponding iodothiophenes in the Sonogashira cross-coupling reaction with TMS-acetylene followed by TBAF deprotection (Scheme 24).<sup>[165]</sup>



**Scheme 24** Synthesis of thienyl acetylenes **102-103b**.

In the following step, alkyne **102b** was subjected to deprotonation with *n*-BuLi base and reacted with commercially available methylthienyl ketone **104a** under standard conditions (THF, -78 °C, Scheme 25, a). However, the expected propargyl alcohol product **105a** was not formed. Instead, we recovered the starting materials together with the product of *n*-butyl addition to the ketone (**106**). The same reaction carried out at -40 °C gave very similar result. This time, we observed one more product in the resulting mixture which suggested that in fact deprotonation of **102b** might have occurred but in the 5-position of the thiophene ring and not in the acetylenic proton. NaH base was tested in the same reaction to prevent the ambiguous deprotonation and the attack of the base on the carbonyl of the ketone. An initial experiment of deprotonation of **102b** with sodium hydride gave promising result when quenching with D<sub>2</sub>O showed clear incorporation of deuterium in the acetylenic position. Nevertheless, when we reacted **102b** with the ketone only starting materials were recovered (Scheme 25, b, c).

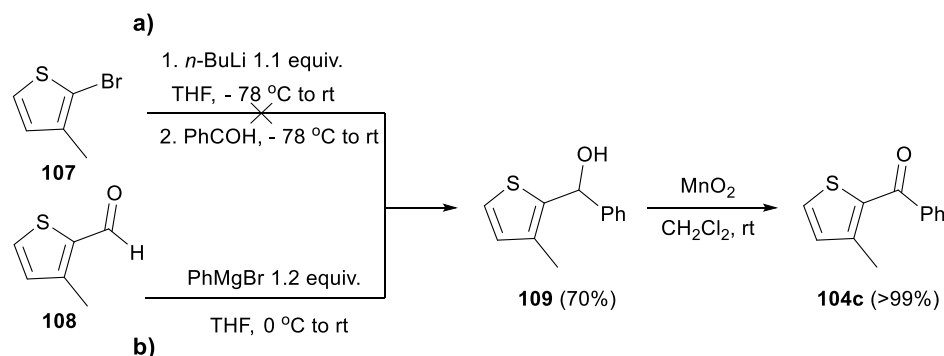


**Scheme 25** Synthesis of propargyl alcohols from alkyne: a-c) **102b**; d) **103b**.

We expected the reaction with alkyne **103b** to be more straightforward as its potential site of unwanted deprotonation was blocked with a methyl substituent. However, when reacted with *n*-BuLi and ketone **104a** at -78 °C only unreacted starting materials were isolated. In turn, when during deprotonation the reaction was allowed to warm to 0 °C the alcohol product **105b** was formed to some extent (Scheme 25, d).

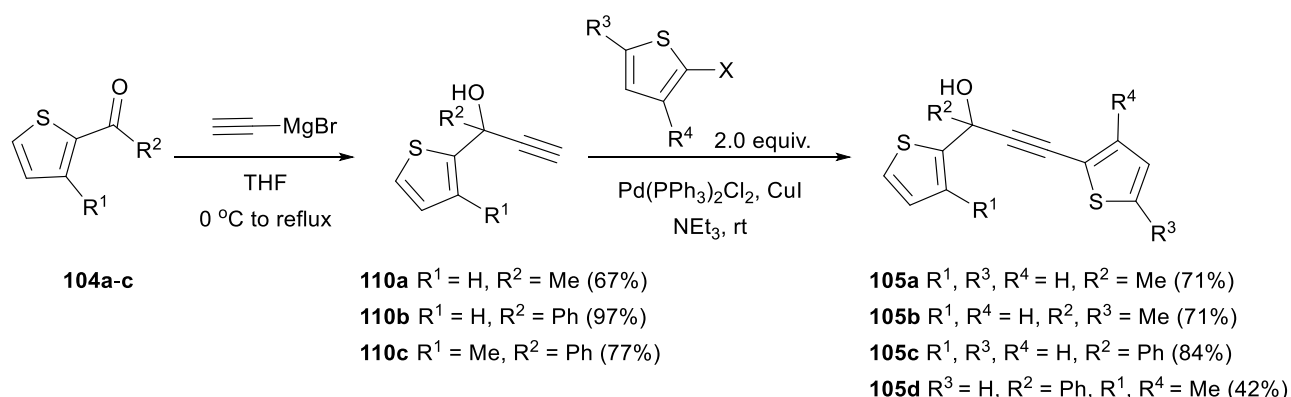
As the addition of (thienyl)acetylenes to ketones proved to be quite problematic and inefficient we subsequently tried the alternative Grignard addition to ketones, because that approach had given better results in the case of pyridine analogues. The reactions were carried out with commercially available ketones **104a-b** and synthesised **104c** (Scheme 26). We could

not access **104c** by the lithiation of the bromothiophene **107** followed by addition to benzaldehyde as that gave a complex reaction mixture (Scheme 26, a). Instead, reaction of thiophenecarboxyaldehyde **108** with a Grignard reagent yielded alcohol **109** that was then converted to ketone **104c** in quantitative yield (Scheme 26, b).



**Scheme 26** Preparation of thienyl ketone **104c** from: a) bromothiophene **107**; b) thienyl aldehyde **108**.

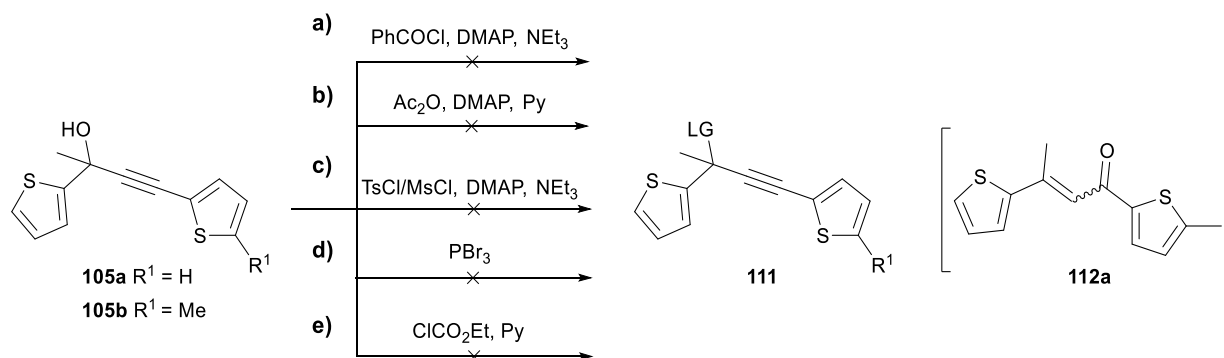
Addition of ethynylmagnesium bromide in refluxing THF to ketones **104a-c** readily afforded tertiary alcohols **110a-c** (Scheme 27). Subsequent Sonogashira coupling resulted in successful isolation of a series of bis(thienyl)alcohols **105a-d** with different substitution pattern.



**Scheme 27** Two-step preparation of bis(thienyl)propargyl alcohols **105a-d**.

Surprisingly, the esterification conditions with PhCOCl established for the pyridine analogues of **105** appeared to be unviable in the next step (Scheme 28, a). Next, we tried the conditions of DMAP-catalysed coupling with acetic anhydride, unfortunately replicating the results of the previous experiment (Scheme 28, b). In light of the unsuccessful esterification attempts, we tried to transform the alcohol into some other leaving groups. However, DMAP-catalysed reaction with tosyl or less bulky mesyl chlorides<sup>[166]</sup> did not afford expected substitution products (Scheme 28, c). Although we observed full conversion of the starting material, isolation of expected product **111** was not achieved. On the other hand, carrying the

reaction at 0 °C instead of room temperature in order to avoid any competing transformations of the forming product completely retarded the substitution.

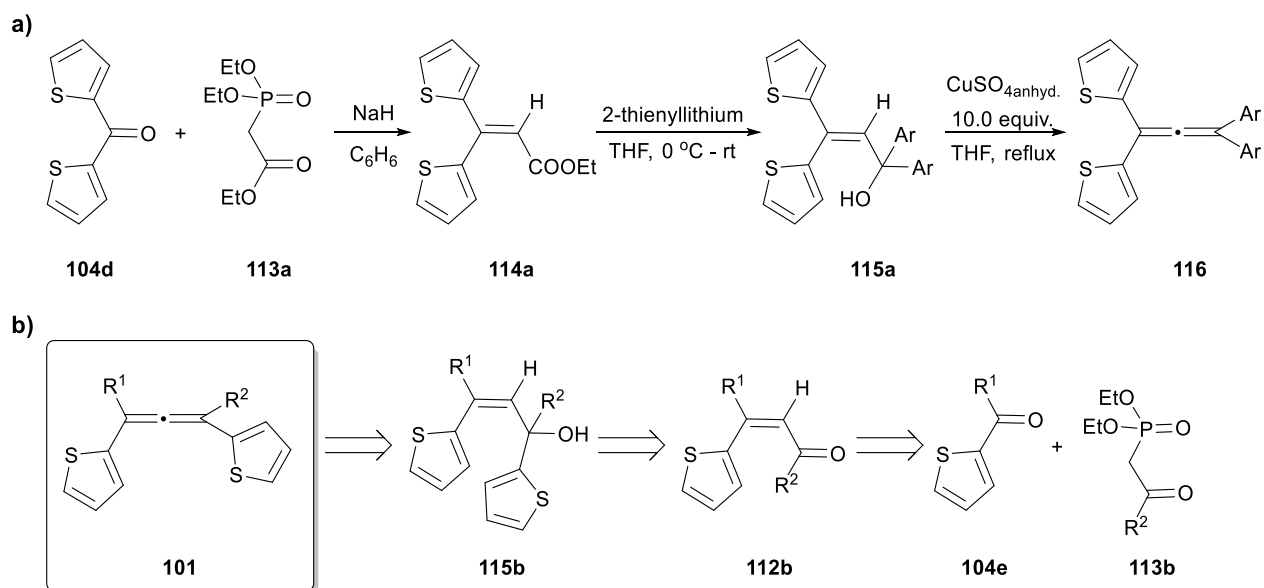


**Scheme 28** Attempts to introduce a good leaving group in alcohols **105a-b**.

We also attempted the substitution of the hydroxyl group for a bromide. Reaction of **105b** with PBr<sub>3</sub>, however, did not yield the expected bromo-derivative. The only product isolated by column chromatography separation appeared to be ketone **112a** deriving from the rearrangement of the starting material itself (Scheme 28, d). The last attempt to incorporate a leaving group into **105b** was the reaction with ethyl chloroformate to furnish carbonate ester (Scheme 28, e), which is another common precursor in the synthesis of allenes.<sup>[167]</sup> This experiment once again yielded very complex reaction mixture from which we could not isolate the expected carbonate.

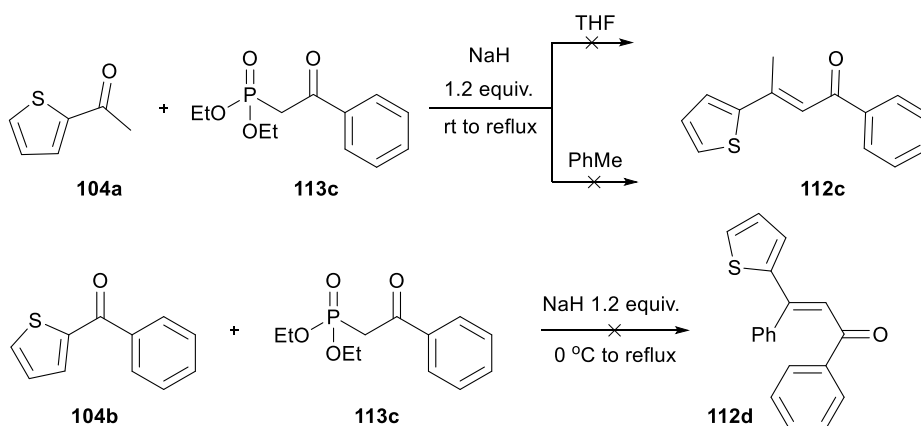
Due to the unsatisfactory progress with this type of transformation we sought another strategy to access bis(thienyl)allenes where the use of LG-containing precursors was not necessary. We took advantage of another reported method to access fully substituted allene skeletons, namely dehydration of 1,1,3,3-substituted allylic alcohols.<sup>[145]</sup>

Oda and co-workers<sup>[168]</sup> achieved the synthesis of bis- and tetrakis(2-thienyl)allenes by Lewis acid mediated dehydration of alcohols of the type **115a** (Scheme 29, a). We envisioned that a starting material with two thiophene rings in 1,3-relationship under similar reaction conditions could afford target structure **101**. This could be achieved, for instance, by replacing the partners in preceding Horner-Wadsworth-Emmons (HWE) reaction. Especially, exchanging the ester group in the phosphonate **113a** for a ketone (**113b**) would allow us to obtain two different substituents on the allene terminus *via*  $\alpha,\beta$ -unsaturated ketone **112b** and alcohol **115b** (Scheme 29, b).



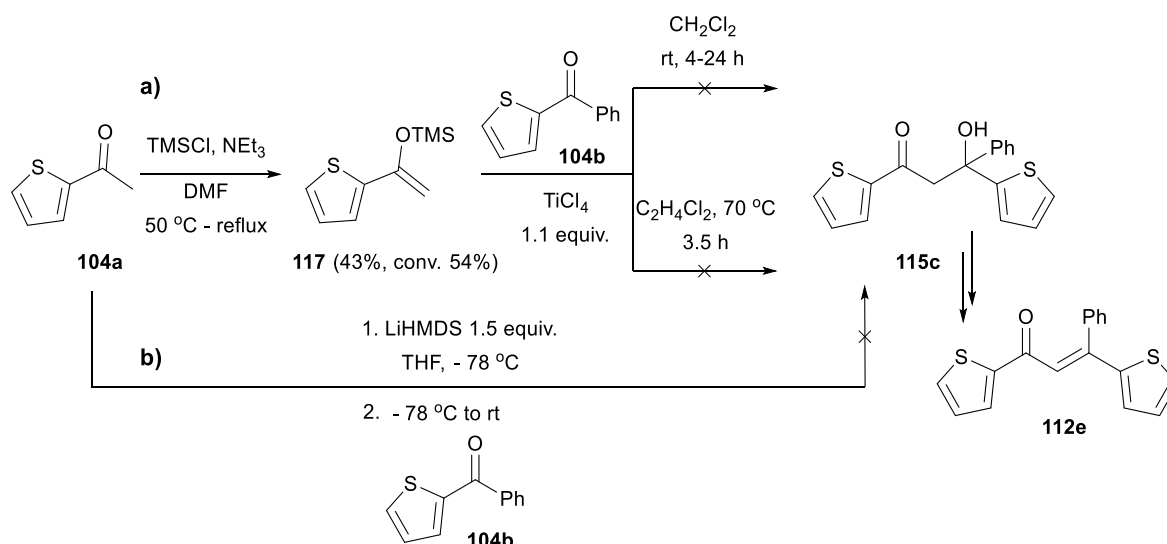
**Scheme 29** Synthesis of thienylallenes: a) Oda's methodology; b) retrosynthetic analysis for the target bis(thienyl)allenes **101**.

Starting with the HWE reaction, we reacted two commercially available thienyl ketones **104a** and **104b** with commercial diethyl benzoylmethylphosphonate **113c**. The use of similar to reported reaction conditions, however, did not promote formation of expected conjugated ketones **112c-d** and only starting materials were recovered (Scheme 30).



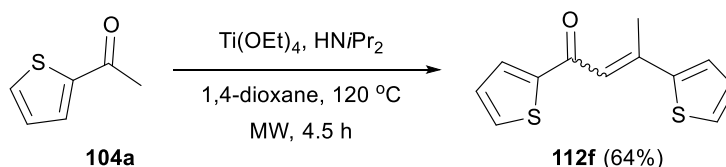
**Scheme 30** Attempted preparation of conjugated ketones *via* Horner-Wadsworth-Emmons reaction.

As an alternative, we tested the aldol reaction of silyl enol ether **117** of ketone **104a** (Scheme 31, a). Unfortunately, the reaction with ketone **104b** in two different sets of conditions did not work. A direct aldol cross-condensation of ketones **104a** and **104b** with LiHMDS used as a base was also unsuccessful (Scheme 31, b). The negative results of HWE and aldol reactions prompted us to look for yet another method for the synthesis of  $\alpha,\beta$ -unsaturated carbonyl compounds.



**Scheme 31** Attempted preparation of conjugated ketones *via* aldol reactions: a) with silyl enol ether **117**; b) *via* enolate.

Unexpectedly, when doing a literature search in a different area of the project (see Section III b. 5.) we found that reaction of ketone **104a** in the presence of Ti(IV) had been reported to yield  $\alpha,\beta$ -unsaturated ketone **112f** (Scheme 32), which was the compound targeted before in the HWE reaction. Self-condensation of **104a** to form **112f** promoted by Ti(IV) worked well, in good agreement to known reactivity of ketones with  $\alpha$ -acidic protons.<sup>[169]</sup>

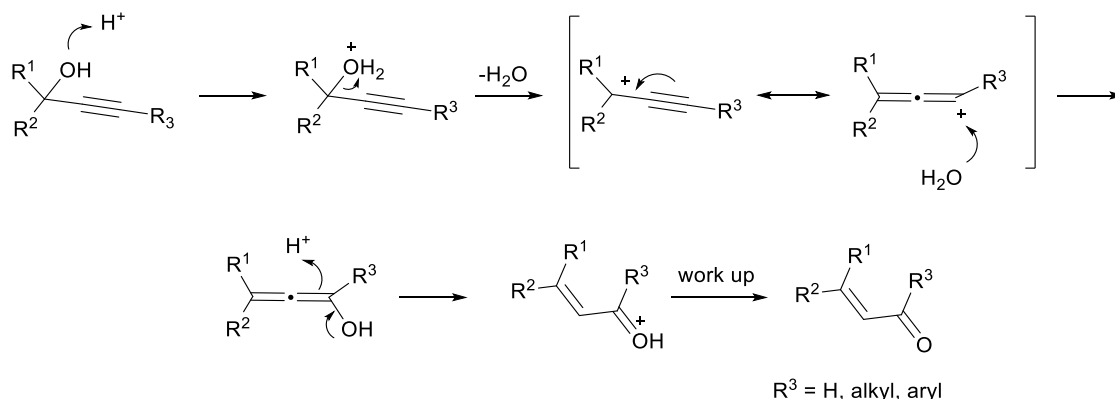


**Scheme 32** Self-condensation of ketone **104a** in the presence of Ti(OEt)<sub>4</sub>.

However, by default, this method could not be extended to enones with all aromatic substituents, so we tried to find a more general method for the construction of this type of compounds. The next methodology we investigated was the Meyer-Schuster rearrangement.<sup>[170]</sup> An advantage of this method laid in the use of propargylic alcohols as starting materials, the synthesis of which had already been optimised. Meyer-Schuster rearrangement is an acid catalysed reaction with both protic and Lewis acids working as catalysts. The reaction starts with the protonation of the alcohol followed by loss of a water molecule in an E1 manner, to afford a carbocation which is subsequently trapped by another water molecule (Scheme 33). After tautomerization of the resulting enol, the  $\alpha,\beta$ -unsaturated carbonyl compound is revealed. Depending on the structure of the starting material, terminal

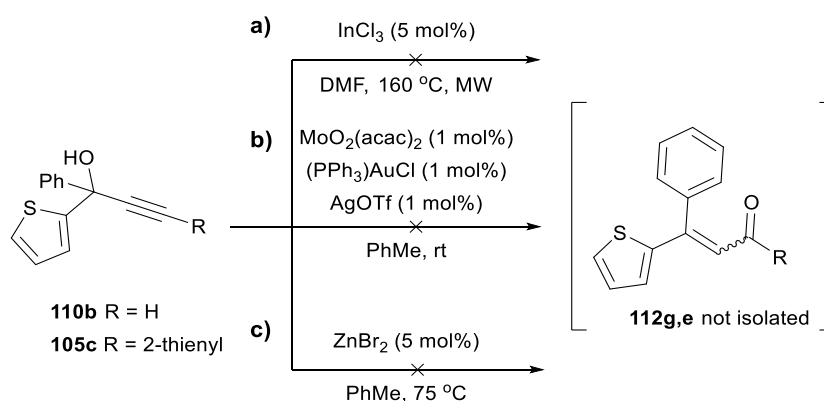


vs internal alkyne, this can be either aldehyde or ketone. In fact, this type of reaction was probably responsible for the formation of the unwanted product **95** shown in the Scheme 20.



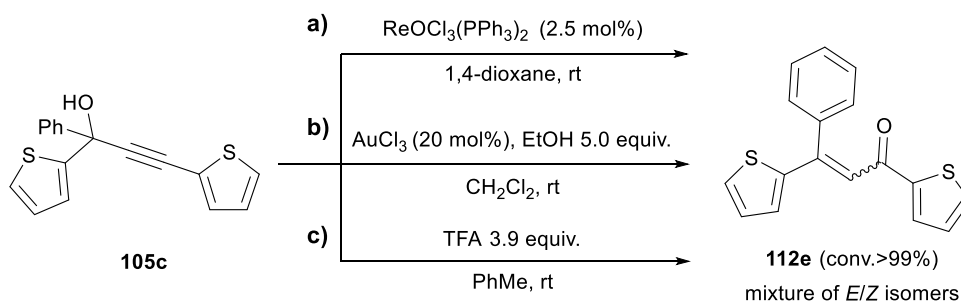
**Scheme 33** Mechanism of the Meyer-Schuster rearrangement.

Initially, alcohols **110b** and **105c** were subjected to different Lewis acids (Scheme 34, a-c) to find working reaction conditions. However, In-, Mo/Au- or Zn-catalysis did not seem to promote the reaction.<sup>[171,172]</sup>



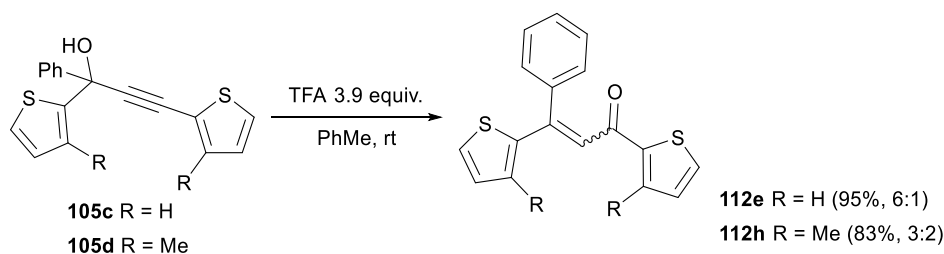
**Scheme 34** Attempted preparation of  $\alpha,\beta$ -unsaturated carbonyl compounds via Meyer-Schuster rearrangement.

Gratifyingly, the three sets of conditions we tried next: Re(V), Au(III) and trifluoroacetic acid catalysis, resulted in complete conversion of alcohol **105c** to unsaturated ketone **112e** (Scheme 35, a-c).<sup>[173–175]</sup>



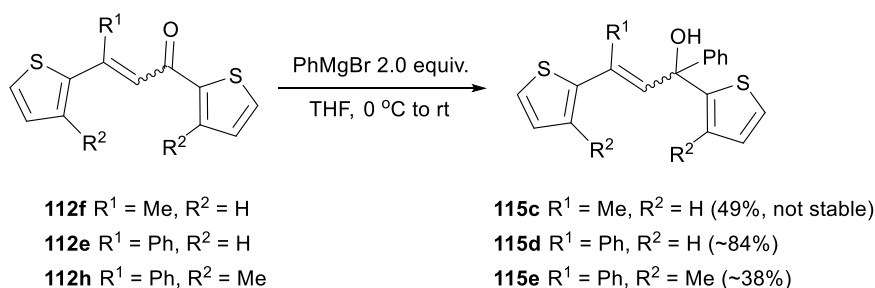
**Scheme 35** Synthesis of  $\alpha,\beta$ -unsaturated ketone **112e** via Meyer-Schuster rearrangement.

The TFA experiment was chosen as the reaction of choice affording brightly yellow products **112e,h** with the highest *E/Z* selectivity and in excellent yields (Scheme 36). Isomeric purity of the products, though, was not a primary concern at this point as the stereochemical information of this intermediate compound will be eventually lost in the following steps.



**Scheme 36** TFA-promoted Meyer-Schuster rearrangement of alcohols **105c-d**.

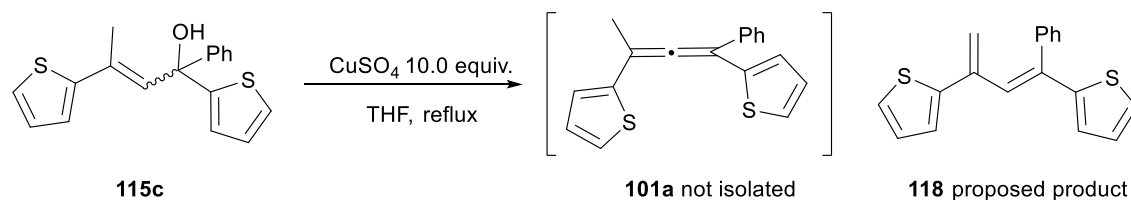
Introduction of the last substituent was carried out by addition of  $\text{PhMgBr}$ , to afford alcohols **115c-e** (Scheme 37). These allylic alcohols proved to be quite reactive and challenging to purify. Nevertheless, **115c-e** could be now used in the final step of the synthesis, namely 1,2 dehydration, to form the target allene skeleton.



**Scheme 37** Preparation of tertiary allylic alcohols **115c-e** via Grignard addition.

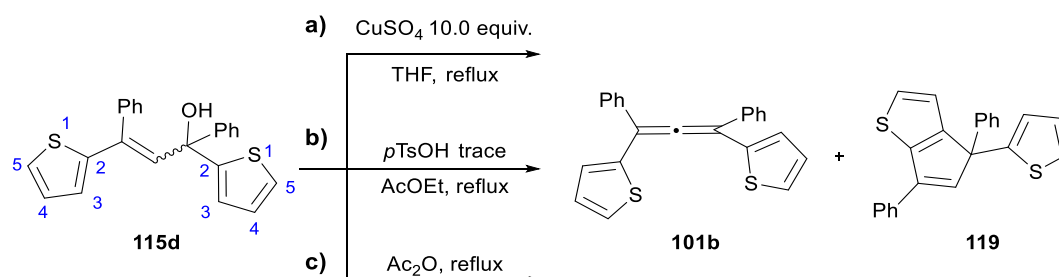
At first, **115c** was subjected to original conditions of dehydration with anhydrous  $\text{CuSO}_4$  in refluxing THF (Scheme 38).<sup>[168]</sup> This reaction proceeded with full conversion of the starting material but spectral analysis of the isolated product did not correspond to the expected allene

structure **101a**. The analysis indicated that dehydration might have occurred with the participation of the methyl group present in the structure possibly resulting in butadiene **118**.



**Scheme 38** CuSO<sub>4</sub>-promoted dehydration of alcohol **115c**.

We hoped that alcohols **115d** and **115e** lacking protons available in  $\gamma$ -position to the hydroxyl group would favour 1,2-dehydration to form the allene. Starting with **115d**, once more CuSO<sub>4</sub> was used to facilitate the dehydration (Scheme 39, a). The analysis of the reaction mixture revealed the presence of two compounds characterised as the expected allene **101b** and cyclopenta[b]thiophene derivative **119** in 1:1 ratio and 44% total yield. Neither compound has been previously reported although formation of analogous bicyclic products has been sometimes observed in reactions of thienyl-substituted allenes.<sup>[176]</sup> Formation of **119** might be accounted for by the attack of one of the thiophene rings' C(3) carbon atoms on the intermediate carbocation or *via* the allene as an intermediate. The isolation of the allene from above mixture was thwarted by the fact that both compounds unsurprisingly exhibited identical polarity.



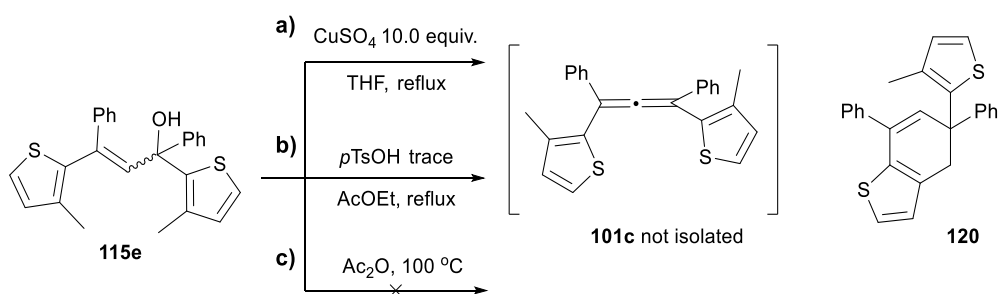
		<b>101b:119</b>	<b>Conv. (%)</b>	<b>Yield (%)</b>
a)	CuSO <sub>4</sub>	1:1	70%	44
b)	<i>p</i> TsOH	7:1	>95%	50
c)	Ac <sub>2</sub> O	1:2	>98%	95 <sup>a</sup>

<sup>a</sup> Crude mixture.

**Scheme 39** Dehydration of alcohol **115d**.

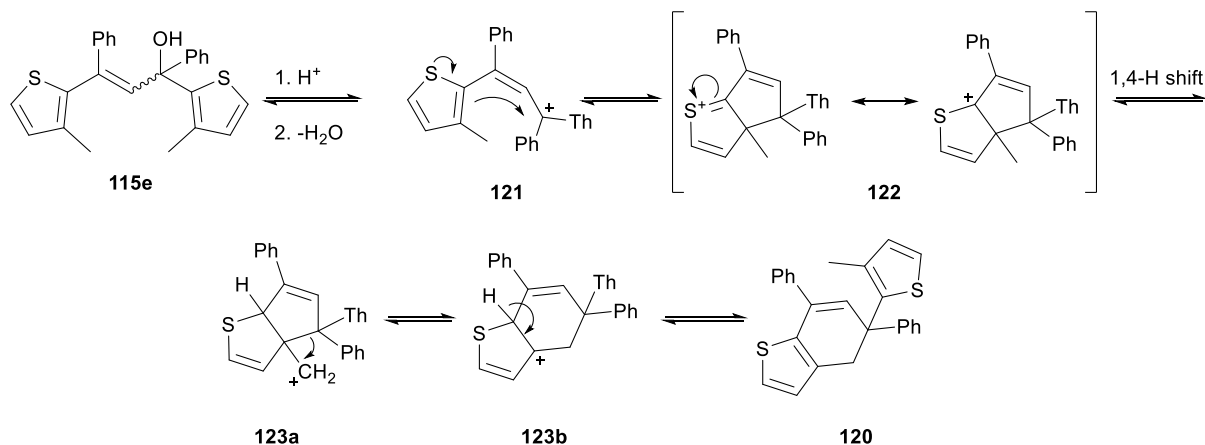
Following the first positive result where we observed formation of the desired allene, we looked for more selective dehydration conditions. To that end, reactions in the presence of traces of *p*-toluenesulfonic acid and acetic anhydride were carried out (Scheme 39, b-c).<sup>[177,178]</sup> We observed very good conversions in both instances, but much better selectivity in favour of the allene **101b** was observed in the reaction with *p*TsOH.

Although thiophene is nucleophilic on both  $\alpha$ - and  $\beta$ -carbons to the sulphur atom, the intramolecular nucleophilic attack as observed on Scheme 39 could only take place through C(3) position due to the geometry of the allene. Consequently, alcohol **115e** with both thiophenes blocked in the C(3) positions by a methyl group, seemed to be substantially less susceptible to a carbocyclisation observed before. Nonetheless, when subjected to the same three sets of reaction conditions no allene product was isolated (Scheme 40, a-c).



**Scheme 40** Dehydration of alcohol **115e**.

Excluding the  $\text{Ac}_2\text{O}$  experiment where decomposition occurred (Scheme 40, c), the only product we isolated and then fully characterised from the dehydration attempt was compound **120**. It seems that even the protection of the reactive position on a thienyl group was not effective enough to prevent the unwanted cyclisation. Generation of **120** might be explained perhaps by the series of sequential carbocation rearrangements depicted on Scheme 41.



**Scheme 41** Proposed mechanism for a formation of **120**.

Bis(thienyl)allenes proved to be very challenging targets. Despite using multiple strategies, we could not find an optimal synthetic methodology for the efficient synthesis and isolation of the desired allenes, mainly due to high reactivity of majority of obtained bis(thienyl) compounds. The difference in reactivity and stability between thienyl and pyridyl allenes could be supported by good  $\pi$ -nucleophilicity of thiophenes vs preferred nucleophilicity of nitrogen's

lone pair of electrons in pyridines as measured in Mayr's nucleophilicity scales.<sup>[179,180]</sup> Nevertheless, the behaviour of single isolated allene **101b** in the presence of metals was tested and the results will be covered in Section IV b. 1.

#### III b. 4. Bis( $\alpha$ -amino)allenes

Aliphatic amino- and polyamino-compounds have long been established as one of the main classes of ligands for transition metal complexes.<sup>[181–183]</sup> They have been successfully applied as part of organometallic systems in the myriad of catalytic<sup>[184,185]</sup> and biomedical<sup>[186,187]</sup> contexts. However, to the best of our knowledge there are no examples of allene-based amine-containing ligands in the literature at the moment. These type of structures (**124**, Figure 21) could constitute an important class of ligands complementary to previously reported bis(pyridyl)allenes.

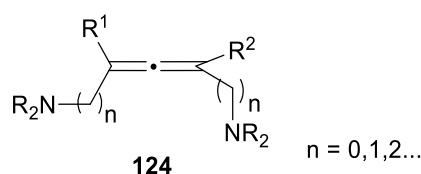
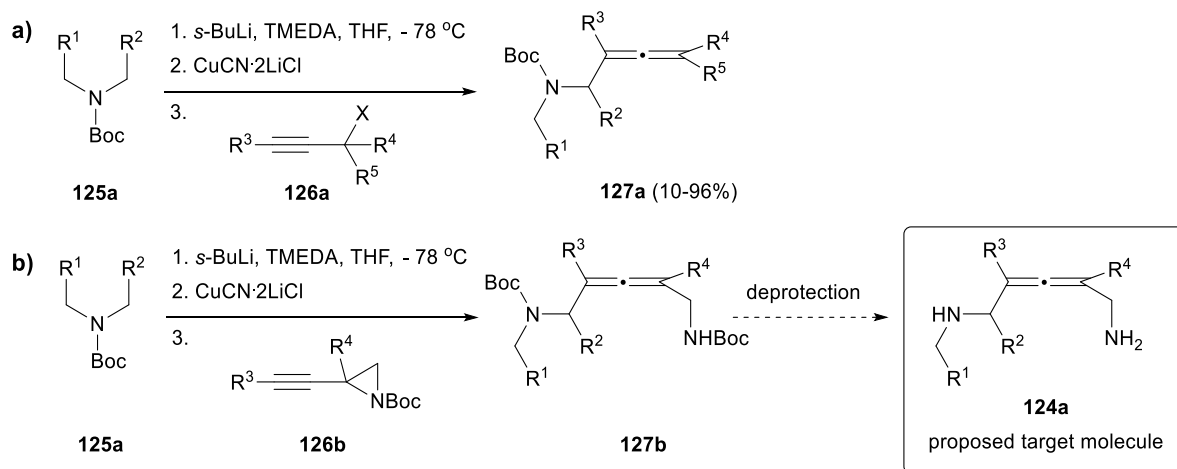


**Figure 21** General structure of bis(amino)allene ligand **124**.

Lack of the applications of structures analogous to that on Figure 21 might stem from the considerable difficulty in their preparation. In fact, there are hardly any tetrasubstituted bis(amino)allenes to be found in the literature. Additionally, when we consider possible variations in the structure of **124**, more challenges arise. The amine moieties in the molecule could be directly bonded to the allene skeleton ( $n = 0$ ) or be separated by a chain of varying length ( $n = 1, 2, \dots$ ). The choice of the chain length will have a notable impact on the synthetic strategy and will influence the size of the target pocket where a metal centre will be situated and thus the bite angle of the complex. The number of carbon atoms separating the amine from the core would also determine the size of the ring formed if undesirable cyclisation within the ligand occurred, thus 5- and 6-membered rings should be avoided. At the beginning, we ruled out the structure with  $n = 0$ , as potentially too challenging to access. We chose the bis( $\alpha$ -amino)allene skeleton where  $n = 1$  as a target molecule in a compromise of all the factors mentioned.

This choice was strongly supported by the fact that there was an existing methodology that could be adapted to furnish bis( $\alpha$ -amino)allenes from readily available starting materials. Dieter and co-workers<sup>[188]</sup> proposed the synthesis of ( $\alpha$ -amino)allenes **127a** from propargyl precursors **126a** where the amine group was introduced as an organocopper reagent. Lithiation of protected secondary cyclic or acyclic amines **125a** followed by reaction with a

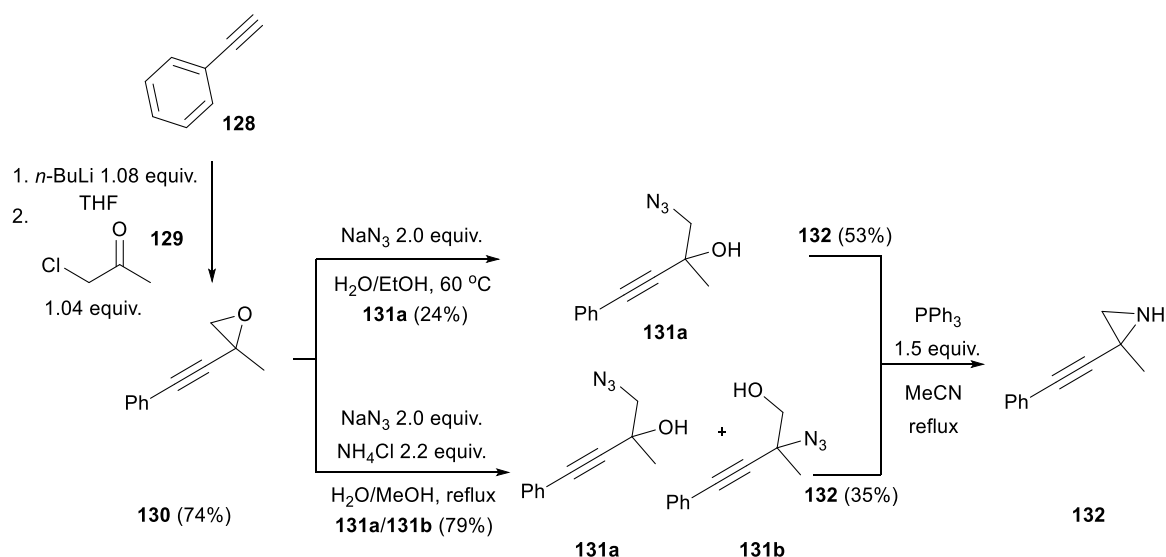
copper salt formed reactive nucleophilic species that could then displace the leaving group of the propargyl compound **126a** in a  $S_N2'$  manner (Scheme 42, a).



**Scheme 42** Preparation of aminoallenes: a) Dieter's synthesis of ( $\alpha$ -amino)allenes **127a**; b) our modification to access bis( $\alpha$ -amino)allenes **127b/124a**.

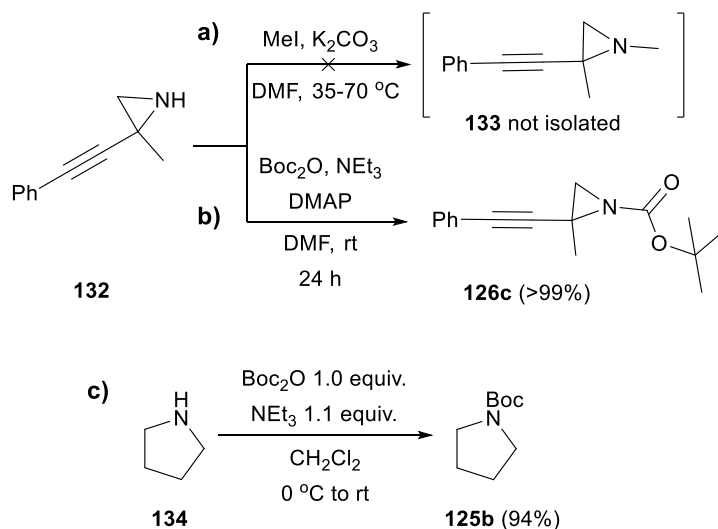
Our modification of Dieter's methodology relied on a use of alkynylaziridine **126b** as propargyl starting material (Scheme 42, b). This alteration would give us an advantage of both having a leaving group, opening aziridine ring, and providing a second amine group for the target structure at the same time. The successful use of propargyl aziridines in very similar context has been evidenced, for example, by Ohno and co-workers.<sup>[189]</sup> The method would still remain closely related to the original report where propargyl oxiranes were successfully used in a similar manner. Resulting allene **127b** could be used directly in the complexation experiments or be deprotected first to uncover both amine units (**124a**).

The preparation of starting materials for the Dieter's reaction followed. We made the aziridine component according to the Blum-Ittah reaction,<sup>[190]</sup> in which epoxides are converted to the respective aziridines with the use of  $\text{NaN}_3$  and  $\text{PPh}_3$ . The two-step reaction: azido alcohol formation and finishing ring closure can be done as a one-pot reaction, but in this case the intermediate azido alcohol **131a** was isolated (Scheme 43). Alternative reaction conditions yielded mixture of regioisomers of **131a/131b**, but the overall yield of aziridine **132** was improved. The preceding epoxide **130** was prepared in good yield from phenylacetylene **128** and chloroacetone **129**.<sup>[191]</sup>



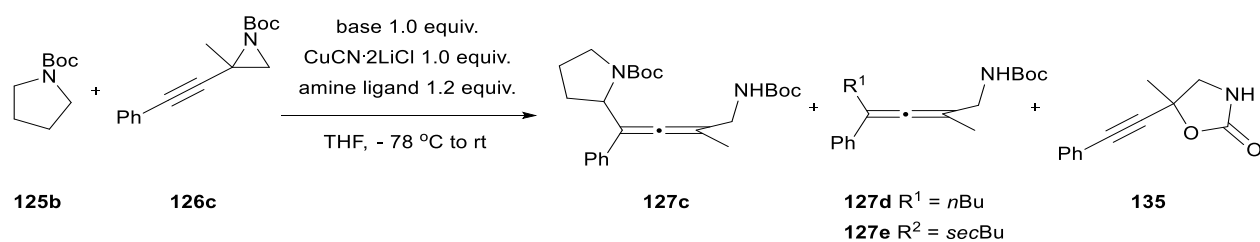
**Scheme 43** Preparation of aziridine **132** via Blum-Ittah reaction.

Subsequent protection of **132** completed the preparation of propargyl aziridine. Surprisingly, alkylation with MeI was not achieved. However, quantitative formation of Boc-protected derivative **126c** was achieved under mild conditions (Scheme 44, a-b). We chose pyrrolidine as the amine nucleophile for the reaction with the propargyl aziridine. Pyrrolidine was readily Boc-protected under standard conditions in excellent yield (Scheme 44, c).



**Scheme 44** Protection of starting materials: a) aziridine **132**; b) pyrrolidine **134**.

With the starting materials in hand, we carried out the modified Dieter's reaction. Scheme 45 illustrates a general reaction scheme and summary of optimisation efforts.



	Base	Amine	CuCN·2LiCl	126c (%)	127c <sup>a</sup> (%)	127d-e <sup>b</sup> (%)	135 (%)
1	<i>n</i> -BuLi	-	+	-	-	57	-
2	<i>sec</i> -BuLi	TMEDA	-	~80	-	-	-
3	<i>sec</i> -BuLi	TMEDA	+	-	-	25	15
4	<i>sec</i> -BuLi	(-)-sparteine	+	-	29	16	-

<sup>a</sup> **127c**~50:50 mixture of diastereoisomers and/or rotamers. <sup>b</sup> **127d** or **127e**.

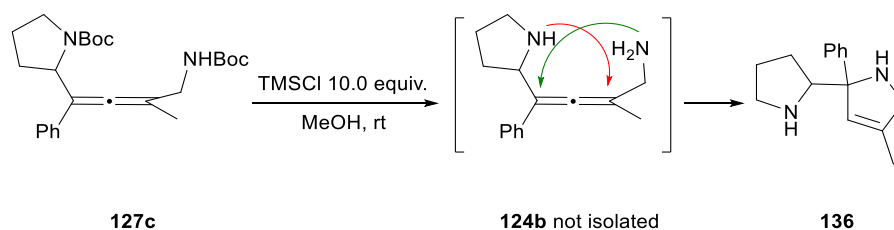
**Scheme 45** Synthesis of aminoallenes with organocuprate nucleophiles.

The only product we isolated from the first attempt of the reaction was allene **127d**. Formation of **127d** resulted from an attack of the nucleophilic base onto the propargyl starting material (Scheme 45, entry 1). The next run, with original *sec*-BuLi and TMEDA (*N,N,N',N'*-tetramethylethane-1,2-diamine), but no copper source resulted only in the recovery of the starting material (Scheme 45, entry 2), whereas in the presence of copper complex, again *sec*-BuLi substituted allene **127e** was formed (Scheme 45, entry 3). Additionally, some of the aziridine **126c** was recovered as oxazolidinone **135**, perhaps formed by opening of the aziridine by a water molecule followed by an attack on the carbamate's carbonyl group. The use of an amine ligand was an important factor in the reaction conditions as it is responsible for stabilisation of an intermediate organolithium species formed after deprotonation of the amine starting material. We swapped the TMEDA ligand for another common ligand used in such deprotonations, an alkaloid (-)-sparteine.<sup>[192]</sup> This resulted in generation of desired allene **127c**, albeit in moderate yield. This time allene **127e** was formed as a by-product as well.

Overall, we successfully established the conditions for the generation of bis( $\alpha$ -amino)allenes with sufficient efficiency to produce the ligand candidate compounds in the amounts needed for preliminary coordination studies. Provided their good performance in those experiments, further optimisation towards better selectivity and yields would be merited.

Lastly, allene **127c** was subjected to the Boc deprotection conditions taking into account the presence of the allene core in the molecule. Thus, we replaced standard trifluoroacetic acid conditions with *in situ* generated methanolic HCl (Scheme 46).<sup>[188]</sup> The isolated product did not contain any Boc moieties, however it also lacked the allene group. One of the amine substituents attacked the allene core forming a cyclic product. Closer analysis of the product pointed towards compound **136** as the only product. Similar cyclisations are known to occur, but usually some catalysis is required (e.g. Au(I)).<sup>[188]</sup>





**Scheme 46** Boc-deprotection of bis(amino)allene **127c**.

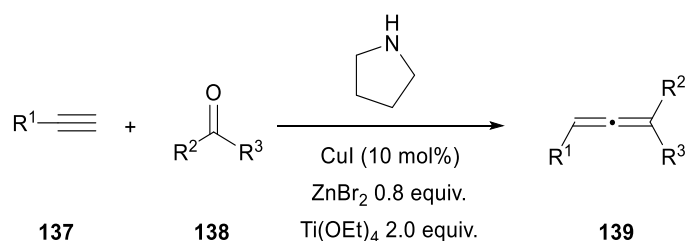
This reaction concluded our investigation into the synthesis of unprecedented bis( $\alpha$ -amino)allenes. The first compound of this series, **127c**, was subsequently tested for its ability to act as ligand in transition metal complexes in its protected form (see Section IV b. 1.). Results of these experiments determined further development of the series.

The next section, closing the chapter on the synthesis of ligand candidates will give a short account of a few methodologies we tested in order to access envisaged allene-containing structures from simpler than previously used starting materials.

### III b. 5. Miscellaneous methods

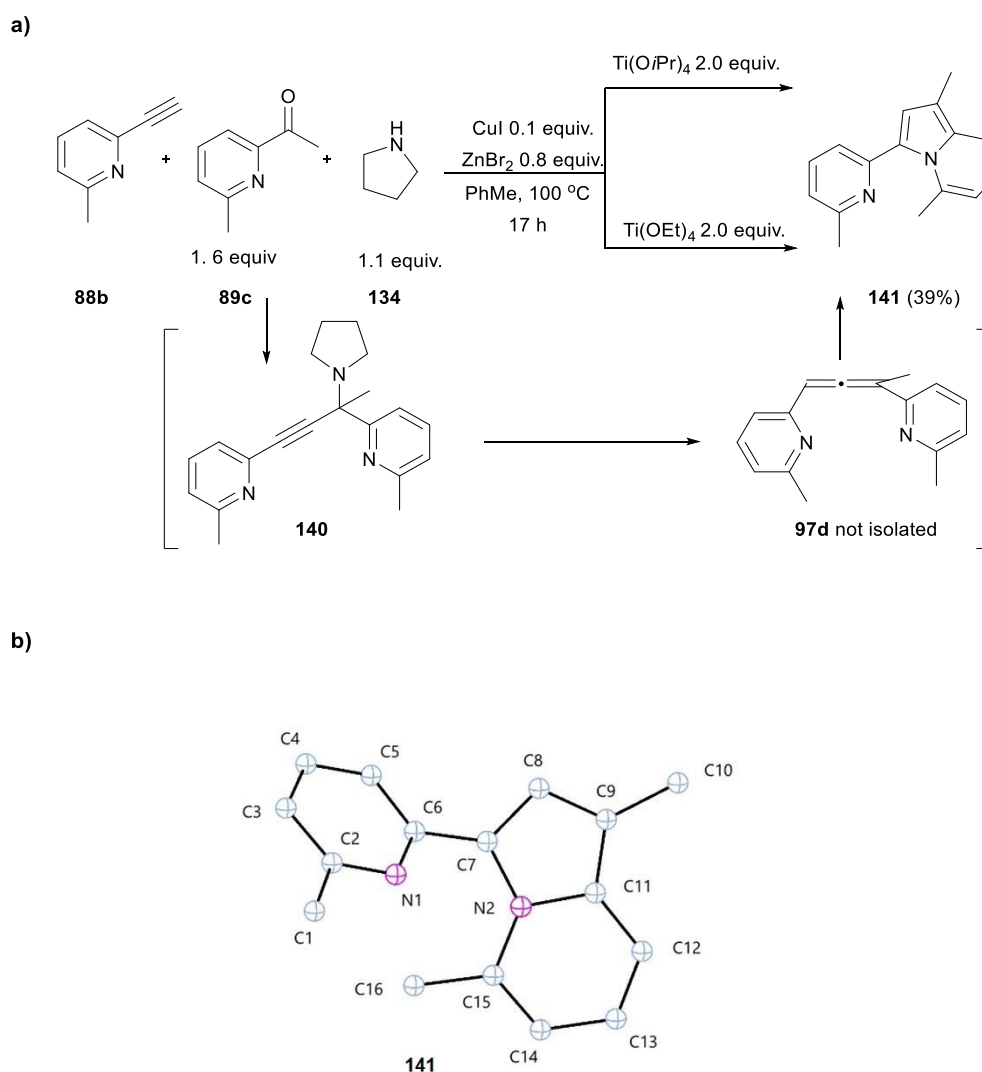
To build heavily decorated allenes similar to the ones in the project objectives usually quite complex precursor molecules are required. As seen in the preceding sections the synthesis of such precursors is not a trivial task and it presents a significant challenge of multistep syntheses. A number of methodologies have been developed to overcome these limitations where more readily available starting materials are directly converted to highly substituted allenes.<sup>[80,193–196]</sup> We applied some of these methods to the synthetic problems presented in the previous sections, albeit without very satisfying results. Nevertheless, we obtained some valuable insights regarding other parts of the project from these experiments making them worth recounting here.

Ma and co-workers<sup>[197]</sup> had proposed a synergistic 3-metal catalytic system promoting the formation of allenes from terminal alkynes and ketones *via* propargyl amines generated *in situ* (Scheme 47).



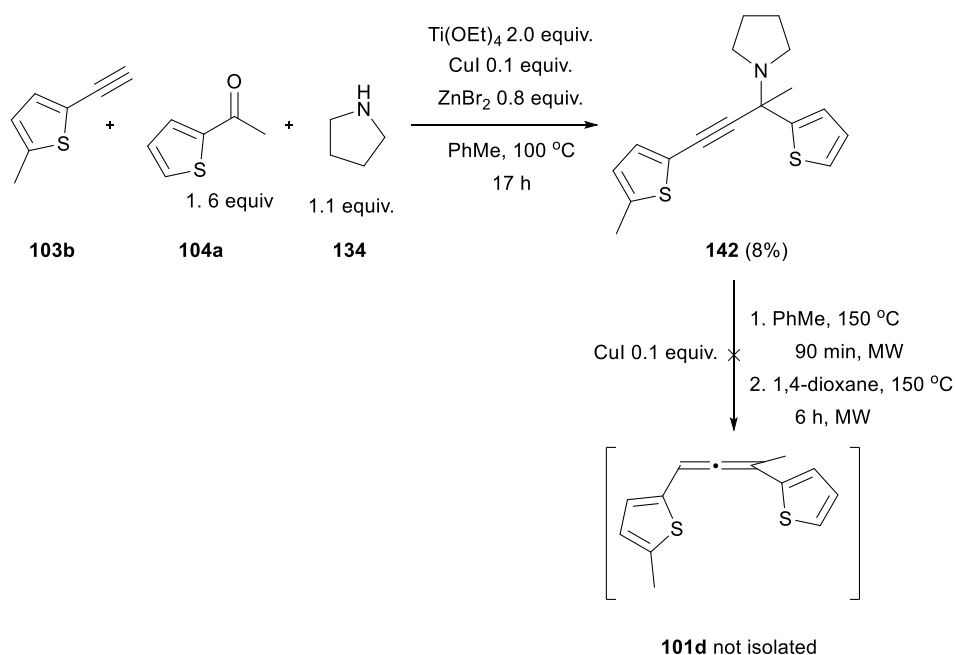
**Scheme 47** Ma's methodology for the synthesis of di- and tri-substituted allenes.

Above conditions were applied to the pyridine-based starting materials **88b** and **89c**, due to some of the difficulties encountered in the preparation of the propargyl derivatives needed as allene precursors (Scheme 48). Interestingly, instead of expected allene **97d**, the product isolated from the reaction was N-fused heterocycle **141**, which structure was unambiguously confirmed by X-Ray analysis. The result, albeit inexpedient, was in agreement with known reactivity of pyridine-substituted propargyl compounds in the presence of Cu and other metals.<sup>[198]</sup> The cyclisation mechanism for that reaction postulates an allene intermediate, which in this case seemed to be readily susceptible to further reaction. In order to confirm formation of the allene intermediate and avoid the cyclisation we replaced the pyridyl ketone **89c** with non-nucleophilic benzaldehyde. However, we obtained a very complex reaction mixture as a result.



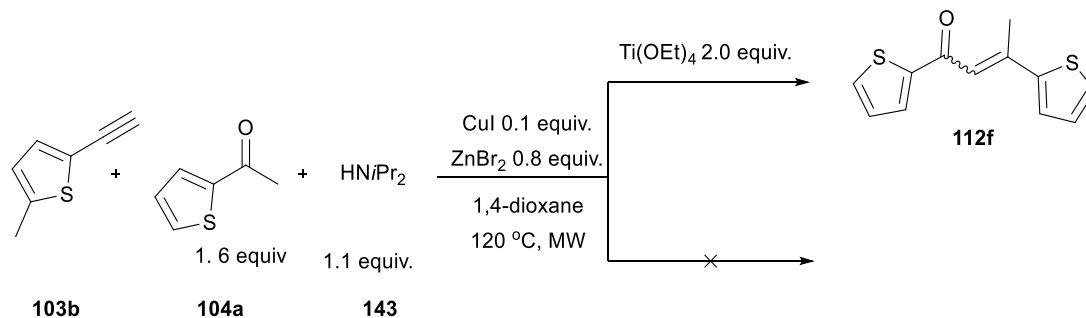
**Scheme 48** Ma's reaction with pyridyl starting materials: a) reaction scheme; b) ORTEP representation of X-ray structure of compound **141** (Hs omitted).

We also applied Ma's methodology to thienyl starting materials. In this case, circumventing the preparation of leaving group-containing propargyl substrates would be even more attractive considering the difficulties encountered in their synthesis (see Section III b. 3.). Scheme 49 shows a reaction carried out with thiophene-containing substrates resulting in formation of **142** in agreement with postulated intermediate in the reaction mechanism. In theory, **142** should be transformed to the expected allene product **101d** in the presence of Cu, for instance, similarly to reactivity encountered in the Crabbé homologation reaction.<sup>[103,104]</sup> However, even under microwave assisted conditions, commonly used in the synthesis of allenes, this reaction was unsuccessful.



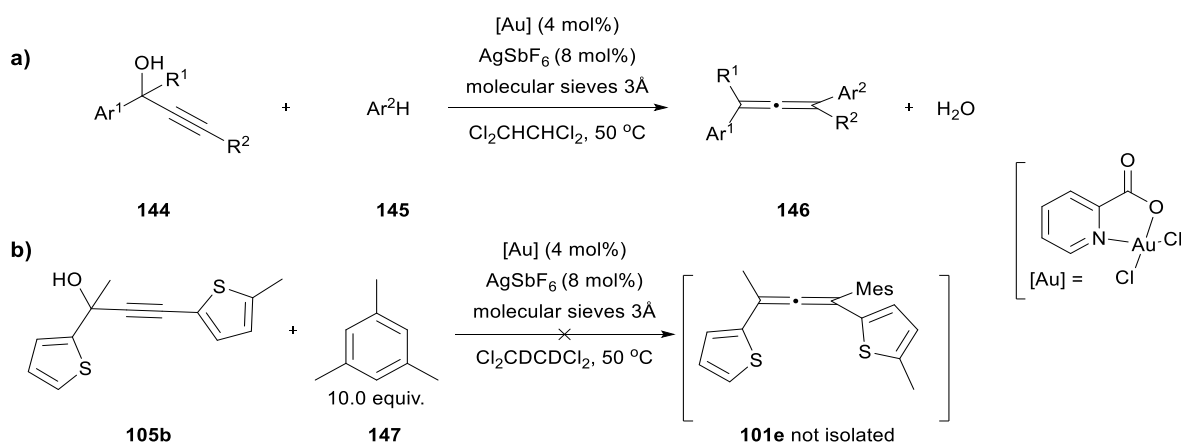
**Scheme 49** Ma's reaction with thienyl starting materials.

The reaction was repeated with *i*- $\text{Pr}_2\text{NH}$  **143**, because we argued that it would be more labile and more easily displaced from the intermediate than pyrrolidine (Scheme 50). This MW variant of the reaction afforded bright yellow product identified as conjugated ketone **112f**. It seemed that under these conditions the predominant process was a self-condensation of ketone **104a** promoted by the presence of  $\text{Ti}(\text{IV})$ .<sup>[169]</sup> On the other hand, the reaction repeated without the addition of  $\text{Ti}(\text{OEt})_4$  did not initiate at all. These results differed from the expected outcome, but they were useful in a different part of the project (see page 51). On the whole,  $\text{Ti}/\text{Cu}/\text{Zn}$  catalytic system was quite incompatible with the required starting materials.



**Scheme 50** Modified Ma's reaction with thienyl starting materials.

Next, we tried the Au(III)-catalysed reaction of propargylic alcohols reported by Li and co-workers<sup>[199]</sup> on alcohol **105b** synthesised before (Scheme 51, a-b). Regrettably, all the attempts on the reaction resulted in decomposition of the material.

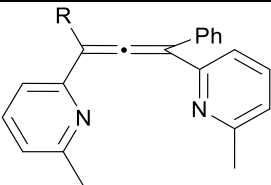
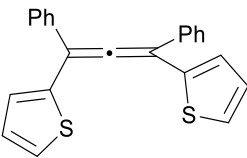
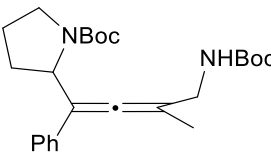


**Scheme 51** Synthesis of allenes from propargyl alcohols: a) Au-catalysed Li's reaction; b) Li's reaction with alcohol **105b**.

### III c. Conclusions

This chapter summarised our work directed towards the synthesis of novel classes of ligands for transition metal complexes based on the allene skeleton. The syntheses of several possible architectures were investigated with N-, S- and P-coordinating units. We successfully obtained the racemic series of bis(pyridyl)allenes (Table 2, entry 1, Section III b. 1.) along with the first example of completely new bis( $\alpha$ -amino)allene (Table 2, entry 3, Section III b. 4.). Moreover, bis(thienyl)allene was accessed (Table 2, entry 2, Section III b. 3.) after a considerable synthetic effort. We also briefly considered phosphine-based ligands (Section III b. 2.), but we ruled them out due to their heightened reactivity. The last section, Section III b. 5., looked at the methodologies that attempt to access the target molecules from simpler precursors.

**Table 2** Allene-containing ligands prepared in the first stage of the project.

Entry	Section	Ligands
1	III b. 1.	 <b>97a-c</b> R = <i>t</i> Bu, Ph, Me
2	III b. 3.	 <b>101b</b>
3	III b. 4	 <b>127c</b>

All successful ligand candidates, particularly nitrogen-based bis(pyridyl)allenes, were carried to the next part of the project described in the following chapter. Chapter IV discusses the results of the exploration of coordination properties of new ligands with various metal centres, such as Pt, Pd, Au and Ru. Characterisation and structural properties of new metal complexes are also discussed.

## IV. Allene-derived metal complexes – synthesis and fundamental studies

### IV a. Introduction

Small number of the literature examples of the allene-containing compounds used as ligands cited in Chapter III is further reflected in a limited number of the corresponding transition metal complexes. Since 2008 only a handful of such studies has emerged. Thus, the literature concerning allene-derived complexes can be presented in its entirety to showcase current developments in the area.

The very first examples of the synthesis of allene-containing ligands and then metal complexes came from Krause group in 2008 with their bis(pyridyl)allene ligand design.<sup>[149]</sup> Preliminary experiments on the complexation properties of bis(pyridyl)allenes were carried out with the use of various Cu(I) and Ag(I) salts. The results obtained from electrospray mass spectrometry and temperature dependant NMR spectroscopy analyses revealed that the formation of 1:1 complexes of **148a** type took place regardless of the metal to ligand ratio (Figure 22). In particular, NMR-monitored reaction of bis(*t*-butyl) ligand **59** with 2 equiv. of [Cu(MeCN)<sub>4</sub>]PF<sub>6</sub> resulted in a mixture of **148a** type complex characterised by the shift of its *t*Bu (1.23 vs 1.29 ppm) and Me (2.65 vs 2.47 ppm) peaks in reference to the free ligand which was also present in the solution in a 1:1 ratio to the complex. This result suggested formation of a symmetric complex with single resonances for *t*Bu- and Me-groups, however the Cu(I) compounds were not fully characterised.

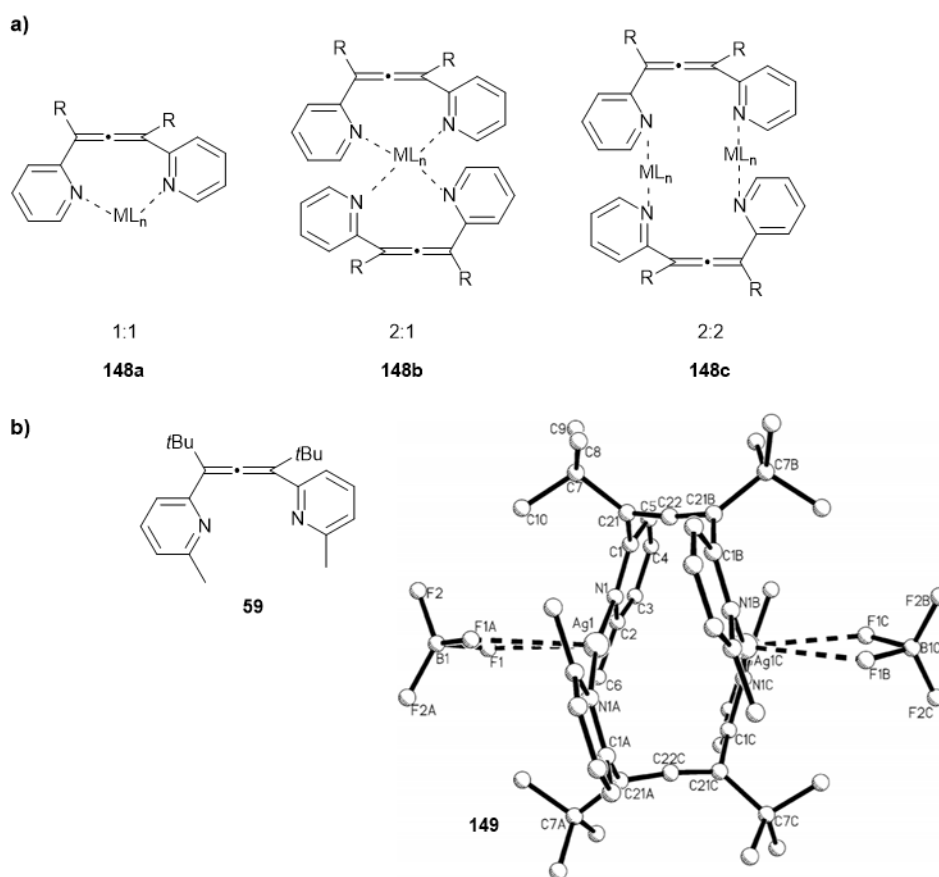


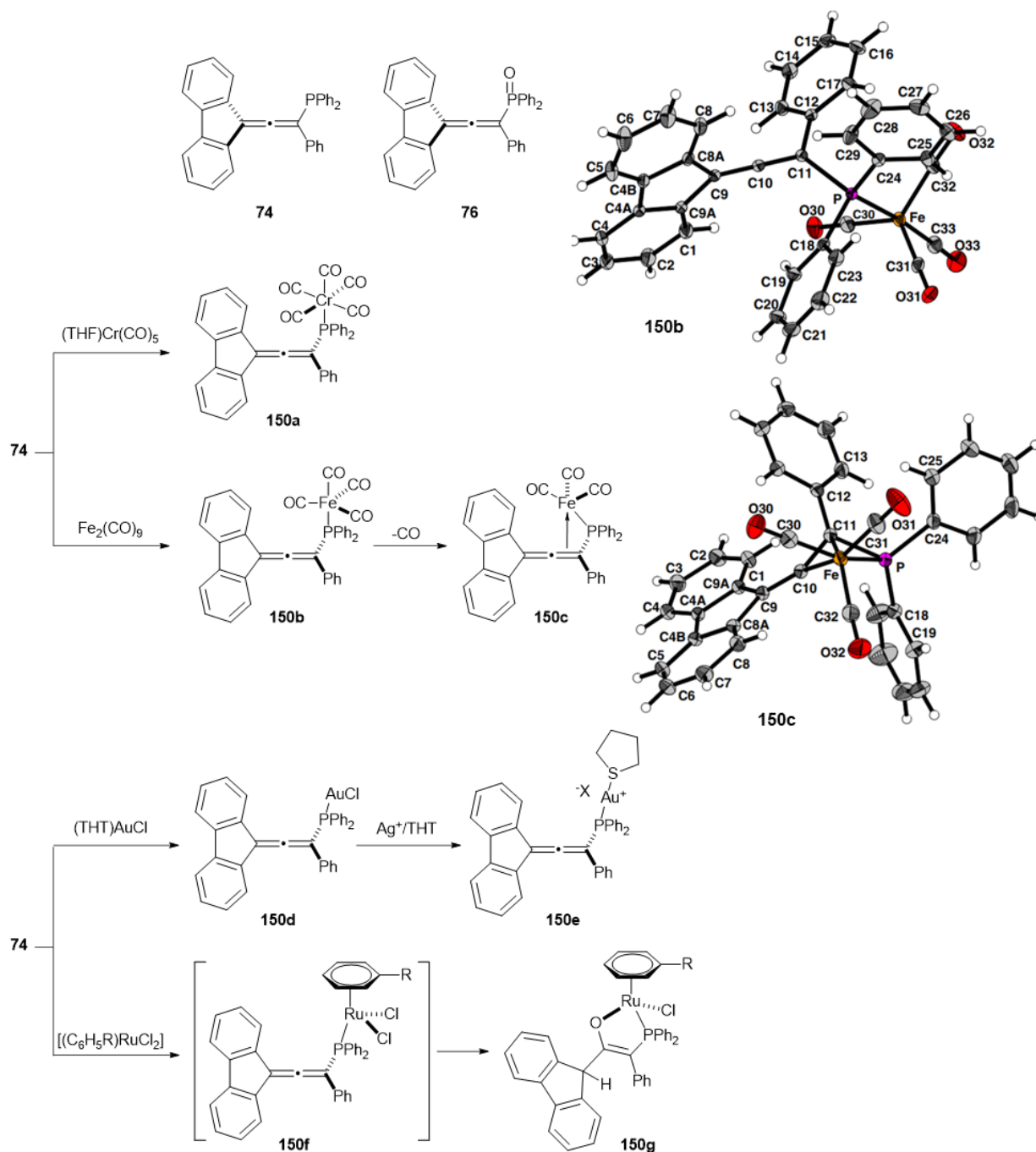
**Figure 22** Bis(pyridyl)allenes and metals: a) some possible modes of metal coordination; b) bis(*t*-butyl)allene **59** and the crystal structure of its 2:2 complex with AgBF<sub>4</sub> (**149**).<sup>[149]</sup>

The authors claimed that 2:1 and 2:2 ligand to metal complexes were not observed in solution. However, bis(*t*-butyl)-substituted allene **59** reacted with silver tetrafluoroborate to form a 2:2 complex of the **148c** type as determined by X-ray crystallography analysis (**149**, Figure 22). The authors suggested that the disagreement between solution and solid-state results might arise from a preferential crystallisation of the complex with 2:2 stoichiometry. Further development of these ligands or any applications of their complexes were not reported in the original study or later.

The same year McGlinchey and co-workers disclosed first examples of allene ligands containing phosphorus-based donor groups and their complexes with Cr, Fe and Au.<sup>[155]</sup> In the pursuit of fluorenylidene-derived allenes as precursors for the synthesis of tetracenes the group prepared mono phosphine- and phosphine oxide-containing fluorenyl(allenes) **74** and **76** (Scheme 52). **74** was subsequently reacted with a series of metal complexes precursors, starting with (THF)Cr(CO)<sub>5</sub> to yield Cr-**150a** complex with mono coordination to the phosphine moiety. Analogous product **150b** was obtained after reaction of **74** with Fe<sub>2</sub>(CO)<sub>9</sub>, although this time monocoordinated **150b** was thermally unstable and readily lost one carbonyl ligand to form bidentate complex **150c**. The latter also featured η<sup>2</sup> coordination of the closer double bond

of the allene group in the freed coordination site. The linear allene unit in **150b** ( $178.4^\circ$ ) became heavily distorted in **150c** ( $138.6^\circ$ ) with a C(10) peak on  $^{13}\text{C}$  NMR shifting from 207.9 ppm to 167.3 ppm. Ligand **74** also formed 1:1 Au(I) linear complexes **150d** and **150e**, however, it did not produce the expected Ru complex **150f**. In this case, the allene core was not maintained and the ruthenacycle **150g** was isolated. The authors proposed that initially formed **150f** underwent loss of a chloride ligand that was replaced by the double bond of the allene in the coordination sphere of Ru. Then, the activated double bond was attacked by a molecule of water and eventually, the newly introduced oxygen atom coordinated to Ru. The coordination properties of phosphine oxide analogue **76** were not discussed.

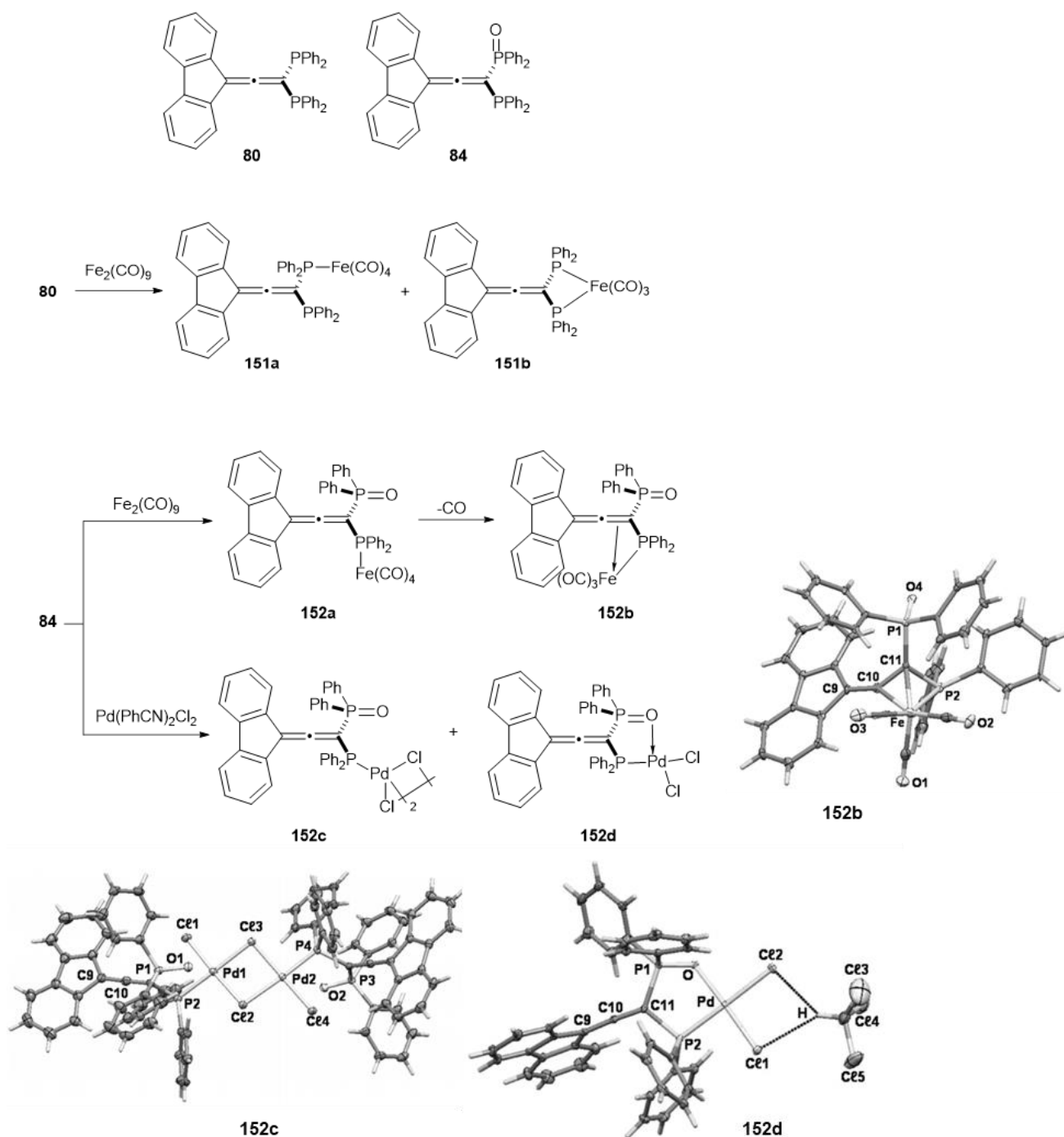




**Scheme 52** Phosphine- (**74**) and phosphine oxide (**76**) fluorenyl(allene) ligands and metal complexes of ligand **74** (THT = tetrahydrothiophene;  $\text{X} = \text{PF}_6^-$  or  $\text{ClO}_4^-$ ;  $\text{R} = \text{CH}_2\text{NHCO}(\text{C}_6\text{H}_4)\text{NO}_2$ ); crystal structures of **150b-c**.<sup>[155]</sup>

The authors later expanded their fluorenyl(allene) work preparing two more ligand candidates: bis(phosphine)allene **80** and mixed phosphine(phosphine oxide) allene **84** (Scheme 53).<sup>[156]</sup> These ligands differed from the general trend of allene ligands' design by having the donor-type groups in 1,1- not 1,3-relationship. However, they displayed interesting

coordination behaviour. Reaction of **80** with  $\text{Fe}_2(\text{CO})_9$  yielded two species: monodentate **151a** and symmetric bidentate **151b** in a 5:2 ratio, evidenced by NMR analysis. On the other hand, behaviour of mixed ligand **84** with the same metal salt was found to be parallel to that of mono(phosphine)allene **74**, excluding any  $-\text{Ph}_2\text{P}=\text{O}$ -metal interaction. Interestingly, when **84** was exposed to  $\text{Pd}(\text{PhCN})_2\text{Cl}_2$ , it also formed different 2:2 and 1:1 products, none of which involved the allene in the coordination sphere (Scheme 53). Minor product **152c** was characterised as a chloride-bridged dimer with exclusive Pd-coordination to the phosphine group. The analysis of major **152d** showed instead that Pd centre formed bonds to both -O and -P atoms in the respective substituents. No applications of the resulting series of fluorenyl(allene)-containing complexes were discussed by the authors.



**Scheme 53** Fluorenyl(allenes) **80** and **84** and their metal complexes; crystal structures of **152b-d**.<sup>[156]</sup>

Phosphine-containing allenes reported by Ready and co-workers were found to act as successful ligands for transition metals.<sup>[151]</sup> Phosphine groups in these ligands were not directly bonded to the allene but placed on its aryl substituents. It is noteworthy that this was the first study which demonstrated that optically pure allene-based ligands can coordinate to different metal centres and maintain their chemical integrity and optical activity. Thanks to this feature, allene-containing scaffolds emerged as suitable ligands for catalysis, importantly in the asymmetric version. Coordination experiments with ligand (S)-**65** yielded a 1:1 complex **153**

with Rh(I), (*S*)-**65** acting as a tridentate ligand with both phosphorus atoms and one of the allene double bonds coordinating to the metal centre (Figure 23). The C=C=C angle of the allene became distorted to 148° forcing it into helical-like conformation wrapping around Rh centre. Enantioenriched Rh(I) complexes were successfully employed as catalysts in an asymmetric addition of arylboronic acids to  $\alpha$ -keto esters (see Section V a.).

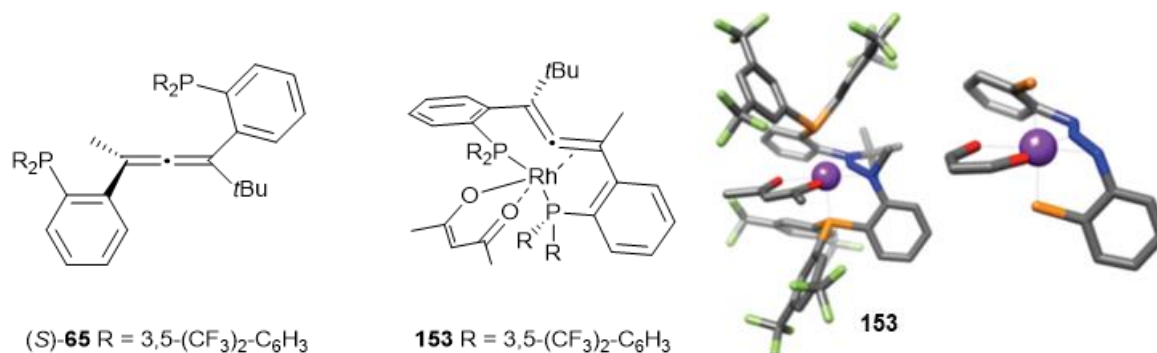


**Figure 23** Optically pure bis(phosphine)allene **65** and its Rh complex; X-ray structure of **153**.<sup>[151]</sup>

Amongst other isolated and characterised complexes of allene-containing phosphines, were structures in which monophosphine **154** coordinated to Ag(I) and Pt(II) complexes with 1:1 stoichiometry (Figure 24). The coordination sphere in both complexes differed substantially. Nearly exclusive interaction between Ag(I) centre and phosphine site was observed in the first case of **155a** with the C=C=C angle of the allene remaining almost unchanged at 179°. The square-planar (**154**)PtCl<sub>2</sub> complex **155b**, on the other hand featured the interaction of both phosphine and allene components with the metal centre. In the latter complex the resulting allene C=C=C angle became heavily distorted and decreased to 152°. Interestingly, when bisphosphine ligand **65** was exposed to PtCl<sub>2</sub> a reaction took place, where a Pt-C covalent bond was formed with the central carbon of the allene, combined with the elimination of the HCl molecule (Figure 24).

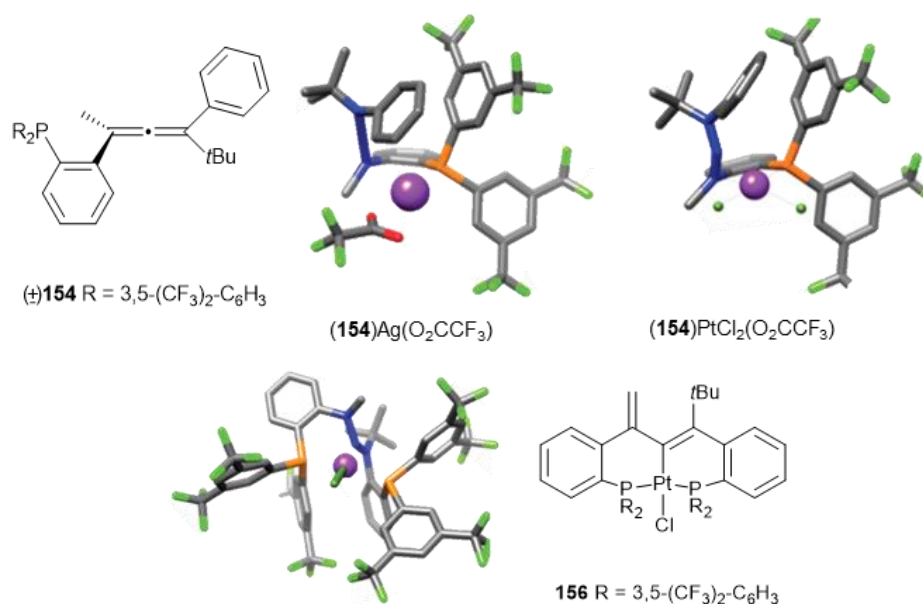
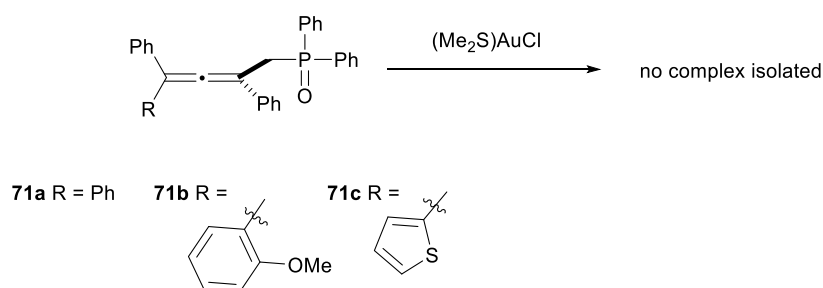


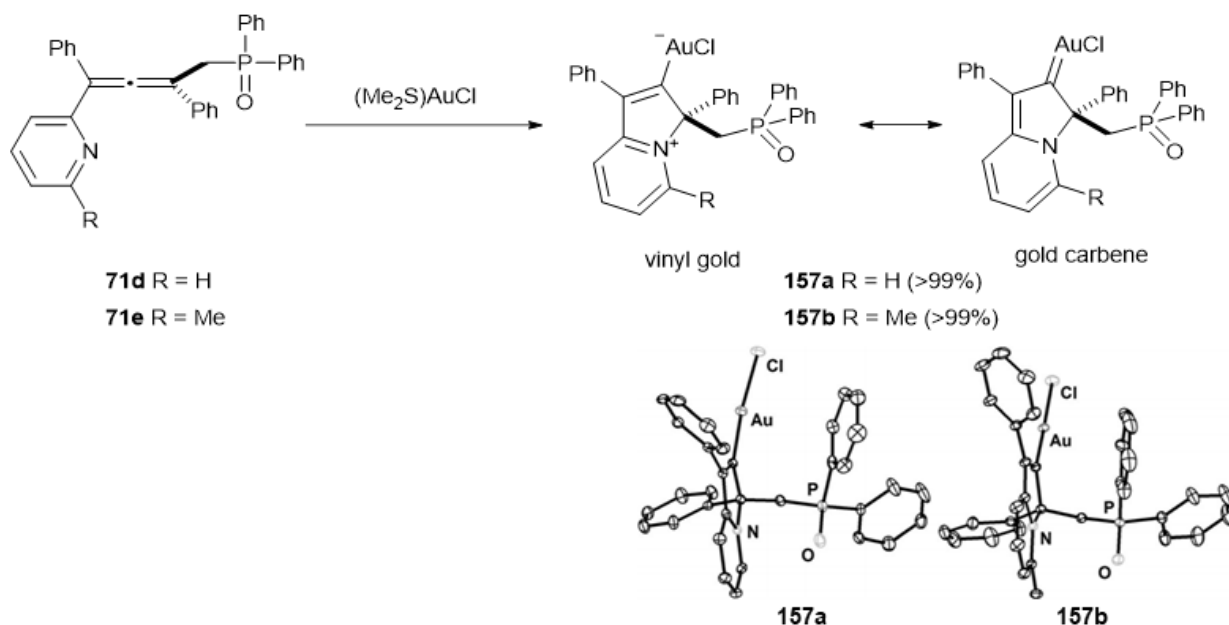
**Figure 24** Monophosphine allene **154** and crystal structures of its Ag and Pt complexes.<sup>[151]</sup>

In 2015, the Fensterbank group progressed the investigation into the area of the novel class of allene-containing ligands with a special interest in the potential formation of complexes with Au and their reactivity.<sup>[154]</sup> However, when first compounds **71a-c**, containing a phosphine oxide as a donor, were subjected to Au(I) coordination conditions, the formation of the corresponding complexes was not observed (Scheme 54).



**Scheme 54** Reaction of phosphine oxide ligands **71a-c** with Au(I).

As the Lewis basicity of allenes **71a-c** proved not sufficient for them to act as effective ligands, the attention of the study was shifted to phosphine oxides with a pyridyl(allene) unit. The choice of this particular substituent referred to Krause's pioneering work, in which it was shown that pyridyl(allene) ligands are suitable for complexation with transition metals.<sup>[149]</sup> Thus, allenes **71d** and **71e** quantitatively reacted with (Me<sub>2</sub>S)AuCl to yield complexes **157a** and **157b** (Scheme 55).

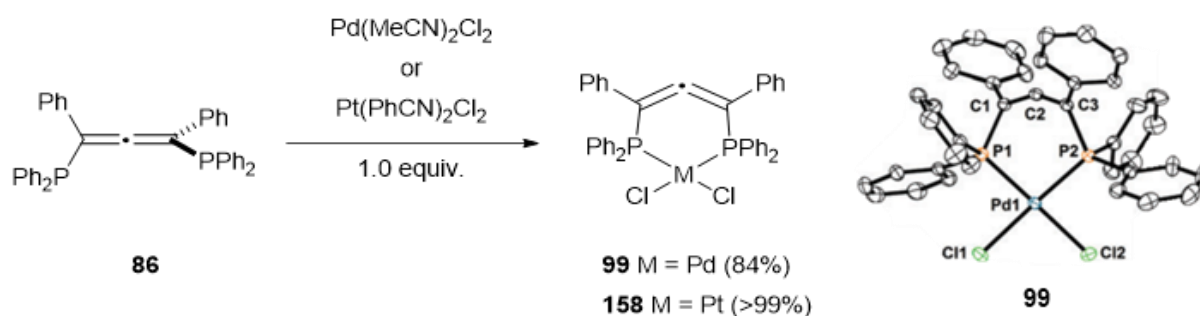


**Scheme 55** Reaction of phosphine oxide(pyridyl) allenes **71d-e** with Au(I); X-ray structures of products **157a-b**.<sup>[154]</sup>

The origin of these complexes can be attributed to the attack of the pyridine group onto the allene moiety. This reactivity was observed earlier in Cu-catalysis,<sup>[198,200]</sup> but stoichiometric, metal-containing products had not been isolated in that context. The new Au compounds did not feature any coordination of the phosphine oxide moiety to the metal centre. These results, similar to McGlinchey's studies, showed again that phosphine oxide group is a poor choice for a donor group in allene-based ligands. Isolation of complexes **157a** and **157b** was particularly interesting as Au-carbene complexes lacking the stabilising heteroatom in the  $\alpha$ -position were little known.<sup>[201–203]</sup> In fact, the dual carbene/vinyl character of the compounds was studied more closely. Therefore, functionalisation of **157a** and **157b** was attempted (protodeauration, addition of electrophilic halide source) in a manner known to occur in vinyl-Au compounds. However, the complexes proved to be quite unreactive in that regard. DFT calculations also suggested electron accepting character of the indolizinium part of the complex, resembling the classic back-bonding character of the carbene complexes. However, the bond order analysis was more consistent with proposed vinyl representation, suggesting a dual character. The application of these complexes has not been reported so far.

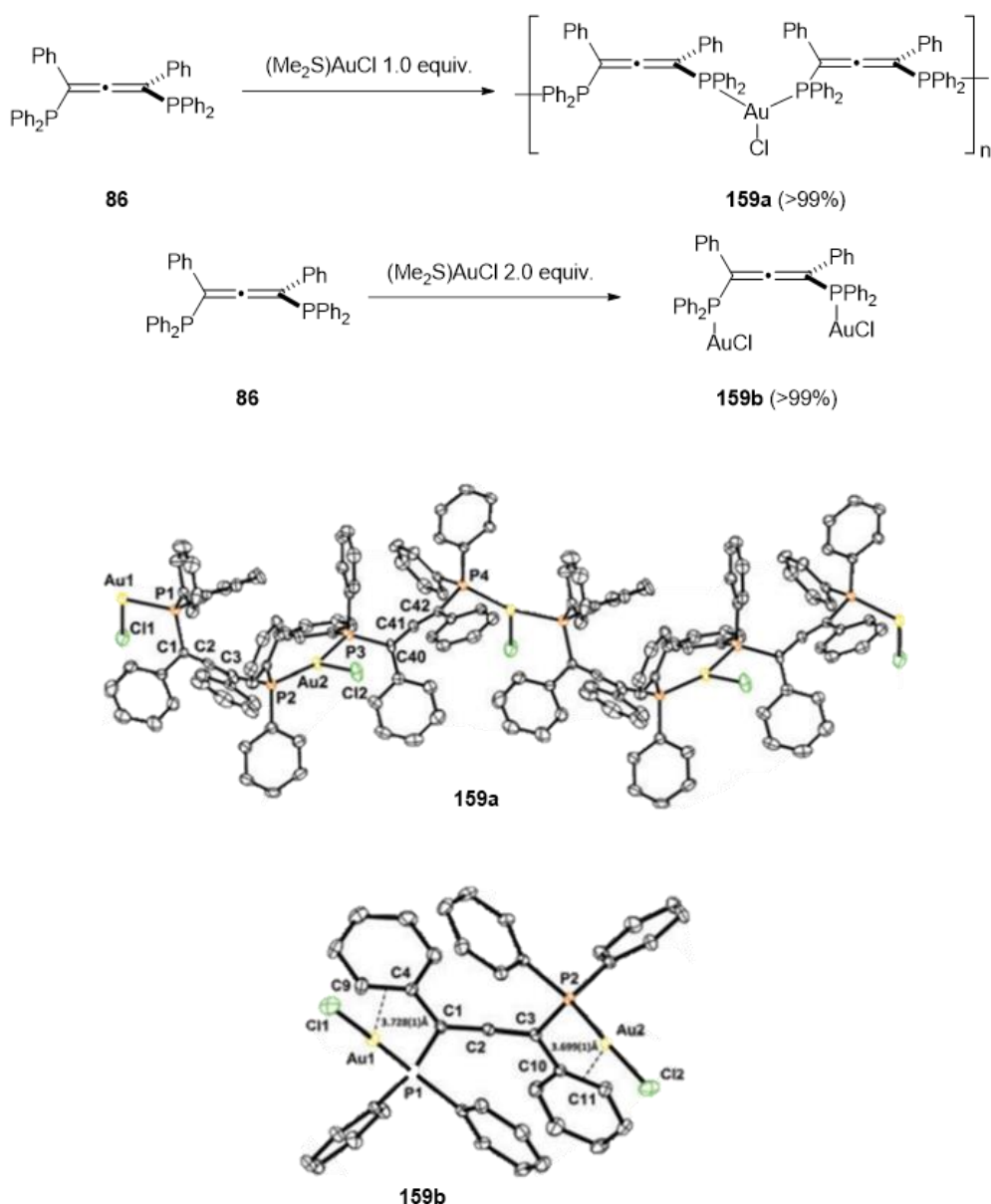
A year later, the same group proposed yet another framework for phosphorus-substituted allenic ligand, this time focusing on bis(phosphine)allenes and their susceptibility towards the coordination to precious metals.<sup>[157]</sup> Ligand **86** in which one phosphine group is directly bonded to each terminal carbon atom of the allene core was used and the study of its unknown coordination properties followed. Firstly, it was found that **86** can form 1:1 mononuclear complexes with Pd(II) and Pt(II) centres (Scheme 56). Isolated complexes of both

metals, **99** and **158**, appeared to have square planar geometry with the allene C=C=C angle being substantially bent to 151.3° and 151.8°, respectively. Also, Pt(II) complex **158** proved to be unstable at room temperature.



**Scheme 56** Synthesis of Pd- and Pt complexes of bis(phosphine)allene **86**; crystal structure of complex **99**.<sup>[157]</sup>

Secondly, as in the case of allene-containing phosphine oxides, ligand **86** was tested for coordination to Au(I) centres. Depending on the ligand to metal ratio, the formation of complexes with different stoichiometry was observed (Scheme 57). Reaction of allene ligand **86** with 1 equiv. of  $(\text{Me}_2\text{S})\text{AuCl}$  afforded mononuclear, polymeric structure **159a**, while reaction with 1:2 ligand to metal ratio yielded dinuclear complex **159b**. XRD analysis of the latter complex revealed that only phosphine moieties were involved in the coordination to Au, excluding possible Au-allene coordination.

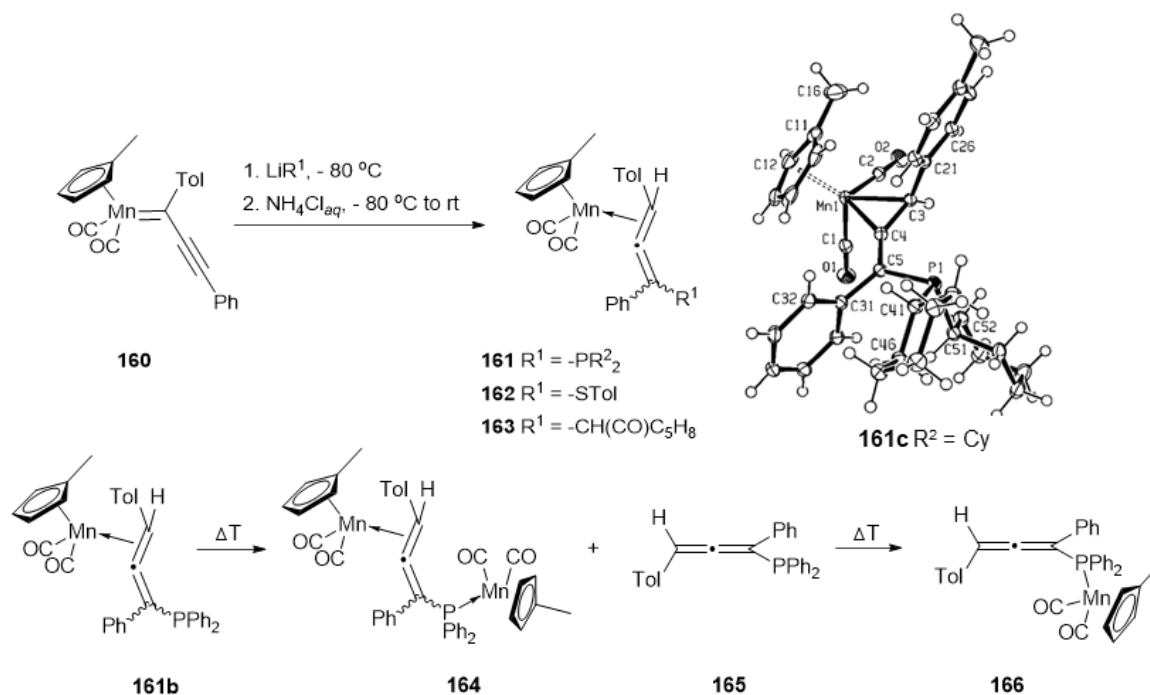


**Scheme 57** Au(I)-complexes of ligand **86** and their X-ray structures.<sup>[157]</sup>

HPLC resolution furnished compound **159b** in enantiomerically pure form ( $ee \geq 98\%$ ). Enantiomer (*aR*)-(+)-**159b** was then tested in asymmetric catalysis in cycloisomerisation of 1,6-enynes (see Section V a.).

One more example of structurally relevant allene-containing complexes has been reported to form in somewhat different to standard ligand/metal reaction setting by Lugan & Lavigne and co-workers.<sup>[204]</sup> The study focused on the synthesis of Mn( $\eta^2$  allene) complexes from Mn-carbene precursors and nucleophiles (Scheme 58). It was observed that upon thermal rearrangement **161**-type complexes can form monodentate phosphine(allene) Mn complexes such as **166**. The rearrangement was believed to proceed *via* initial formation of dinuclear **164** and free allene **165**, eventually leading to **166** in a very good yield.





**Scheme 58**  $\eta^2$ - and P-coordinated Mn-allene complexes.<sup>[204]</sup>

To the best of our knowledge, this short review exhausts the examples of allene-derived complexes reported to date. Presented studies give valuable information as to the factors influencing the stability and activity of allene-containing ligands and complexes, such as spatial congestion around the allene backbone or choice of substituents acting as an effective Lewis bases in resulting complexes.

#### IV b. Results and Discussion

The previous sections described the syntheses of several allene-based ligand candidates and their complexation with metals, but the scope and applications reported so far remain limited. Considering the potential of these type of new metal complexes in (asymmetric) catalysis and in the unexplored area of their uses as metallodrugs, we decided to select some of the previously reported candidates for further thorough scrutiny of their coordination properties with selected transition metals of interest and the resulting outcomes are presented next. In particular, metals such as Au, Pt and Pd were explored due to their known catalytic and medicinal activity. Initial testing of all the prospective ligands with series of different metal sources was followed by a more in-depth study of the bis(pyridyl)allenes' complexation with aforementioned metals.

Within the bis(pyridyl)allenes, the  $C_2$ -symmetric compound **97b** (see Scheme 22) was chosen as a probe for all the coordination experiments. This choice allowed us to simplify the analysis of the resulting organometallic products by reduction of the complexity of emerging

NMR spectra. Additionally, the maintained or broken symmetry in new compounds supplied preliminary information about the number of active coordination sites within the ligand. The synthetic methodology established for compound **97b** was next extended to the remaining bis(pyridyl) ligands. Non-symmetric **97a** was used as a main counterpart to produce analogous series of complexes. In most, and especially in more challenging examples, the complexation reaction conditions were routinely tested first with related model ligands (bipy, TMEDA) to minimise the loss of precious allene compounds.

In general, I initially assessed the success of the complexation experiment by the change of colour of the reacting mixture and with the use of  $^1\text{H}$  NMR spectra showing a shift of signals in relation to a free ligand spectrum. Further characterisation followed, usually including  $^{13}\text{C}$  NMR, high resolution mass spectrometry (HR-MS) and elemental analysis (EA) that helped to propose new structures and reveal the ligand to metal ratios. In some cases, the structural information was also complemented by the data from additional techniques such as heteronuclear and 2D NMR, X-ray diffraction or cyclic voltammetry.

As a general rule all the new allene-containing ligands discussed in Chapter III were presented without highlighting the stereochemistry of the allene. Chapter III was focused on different synthetic methodologies to access the allene-containing ligands and all the structures were prepared as racemates. However, in this chapter I want to emphasise the geometry of the allene ligand and its pocket for metal coordination. Consequently, all the structures presented below highlight the 3D arrangement of the allene, although they were prepared as racemates and therefore the absolute configuration is not given. Each new allene-derived metal complex in the thesis was given a unique number for the ease of reference.

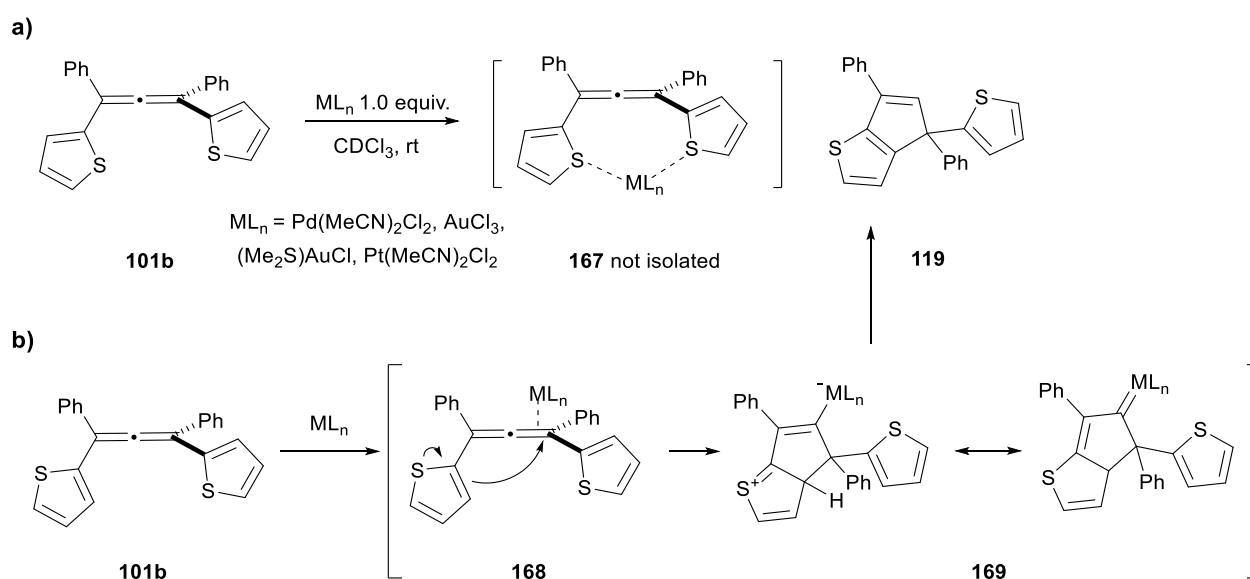
#### IV b. 1. Preliminary experiments

I began the initial assessment of the allene-containing ligand candidates by exposing all three general architectures of the ligand to various metal salts used commonly as precursors to more complex metal complexes. Thus, the allenes **97a**, **101b** and **127c** were reacted with 1 equiv. of different Pd-, Pt-, Ru- and Au-compounds in a range of solvents and conditions.

In case of bis(thienyl)allene **101b** none of the experiments yielded the allene-metal complex of the **167**-type (Scheme 59, a). Instead, in all instances, allene **101b** activated by the metal, fully reacted to give compound **119** with a cyclopenta[b]thiophene core, without a metal present in the structure. I observed a generation of **119** before (Scheme 39, Chapter III) in the allene formation step in the presence of Cu or under acidic conditions. Formation of this product could come from a similar process to the observed in the previously reported N-fused Au(I) compounds in which a vinyl-metal/metal carbene type structure could be proposed as intermediate (**169**, Scheme 59, b). This time, however, the carbocyclisation in **168** took place

and not the heteroatom attack. In the case of the thiophene, the **157**-type complex was not observed in any of the experiments (see Scheme 55). Instead, protodemetalation of analogue **169** could readily occur, perhaps explained by the inferior stabilisation effect of sulphur over the metal carbene and recovery of aromaticity by loss of the proton in the C(3) position of the attacking thiophene (option not available in the pyridine analogues). On the other hand, I observed the same type of metal-free product in case of trisubstituted bis(pyridyl)allene **97d** (Scheme 48) under Cu/Zn/Ti conditions.

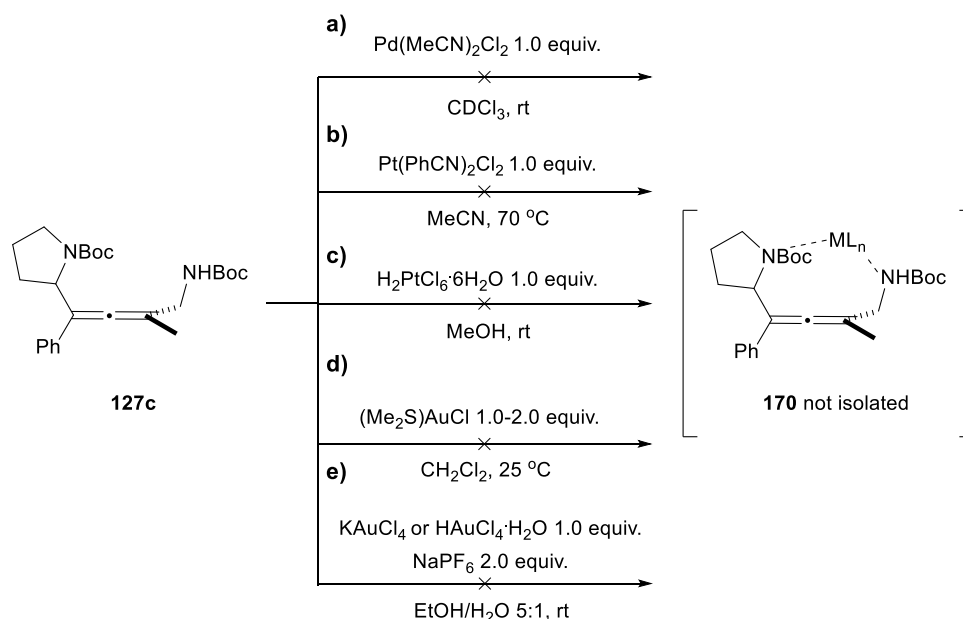
Overperforming nucleophilicity of the thiophene ring, even when the reactive 3-position on the ring had been blocked as seen previously, seems to be a factor excluding it from the successful use as allene-containing ligand.



**Scheme 59** Bis(thienyl)allene **101b** in the presence of metals: a) observed product **119**; b) proposed mechanism for a formation of **119**.

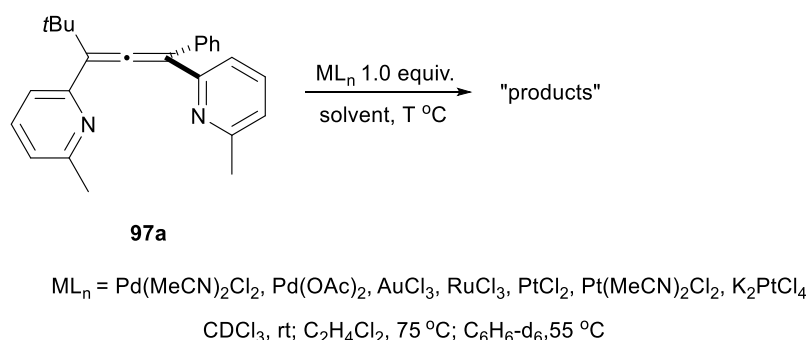
Boc-protected bis(amino)allene **127c** was similarly reacted with a selection of metal salts as depicted in the Scheme 60. All these reactions resulted in either the recovery of the unreacted **127c** ( $\text{Pt}(\text{PhCN})_2\text{Cl}_2$ ,  $\text{KAuCl}_4$ ) or decomposition of the ligand under the reaction conditions ( $\text{Pd}(\text{MeCN})_2\text{Cl}_2$ ,  $\text{H}_2\text{PtCl}_6$ ,  $(\text{Me}_2\text{S})\text{AuCl}$ ,  $\text{HAuCl}_4$ ). Perhaps presence of the Boc-protecting groups deactivated the amines too much against the complexation by engaging the lone electron pair of nitrogen atoms into resonance stabilisation with Boc's carbonyl. On the contrary, if the ligand lost the protecting groups under the complexation conditions we could expect it to undergo competitive cyclisation similar to that observed in the Scheme 46 instead of metal coordination.

As the model bis(amino)allene ligand **127c** was unable to form any distinct coordination complexes with the chosen metals of interest I decided not to pursue work on this ligand type further.



**Scheme 60** Bis(amino)allene **127c** in the presence of metals.

Lastly, I examined the bis(pyridyl)allene structure to establish if the scope of previously reported complexation (Cu(I), Ag(I))<sup>[149]</sup> could be extended to more relevant metal centres. Allene **97a** was exposed to a series of metal salts in 1:1 ratio, first in chloroform at room temperature and then when I did not observe any visual changes and no shift of the signals on the NMR spectra, in C<sub>2</sub>H<sub>4</sub>Cl<sub>2</sub> and C<sub>6</sub>D<sub>6</sub> at elevated temperatures (Scheme 61).



**Scheme 61** Bis(pyridyl)allene **97a** in the presence of metals.

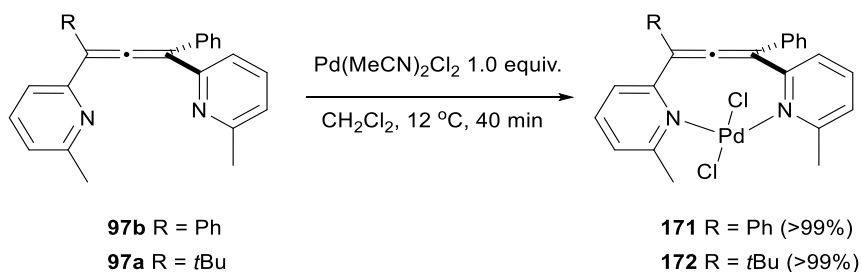
These experiments revealed that **97a** readily forms new Pd(II) compounds at rt, but only in the presence of a Pd source with neutral accompanying labile ligands, the allene backbone seems to withstand the reaction. Also, reaction with AuCl<sub>3</sub> appeared to yield the allene-metal complex, however the product was not very stable in solution. The remaining

examples, in particular with the Pt salts, proved to be quite unreactive and in all cases, **97a** was recovered intact. However, these results indicated that bis(pyridyl)allene contrary to the two previous ligand candidates is much more robust and can be explored under more challenging conditions without the loss of its chemical integrity.

The promising results of the initial coordination experiments with bis(pyridyl)allene **97a** prompted us towards more thorough studies of the behaviour of its derivatives in the presence of metals and these results are documented in the following sections.

#### IV b. 2. Palladium complexes with bis(pyridyl)allenes

In line with the first exploratory experiments, we reacted the  $C_2$ -symmetric allene **97b** with 1 equiv. of  $\text{Pd}(\text{MeCN})_2\text{Cl}_2$  in  $\text{CH}_2\text{Cl}_2$  (Scheme 62). Upon reaction completion, the product was isolated as a red powder in quantitative yield and characterised by NMR.



**Scheme 62** Preparation of Pd complexes **171-172**.

Spectral analysis typical for all complexation experiments of **171** followed and will serve as an exemplary case here. Thus,  $^1\text{H}$  NMR spectra of free ligand **97b** and proposed complex **171** were recorded in the same solvent and temperature and compared (Figure 25, a). We can see on the spectrum of a free ligand that a number of magnetic environments in the aromatic region is reduced from factual 16 to only 6, as could be expected considering the symmetry of the molecule. Similarly, the signals corresponding to two pyridyl methyl groups appear as single peak at 2.58 ppm. Spectrum of complex **171** shares all these similarities with a major difference being the chemical shift of the peaks. In particular, the peak of methyl groups situated in close proximity to a reaction centre was shifted significantly downfield to 3.17 ppm ( $\Delta\delta = +0.59$  ppm).

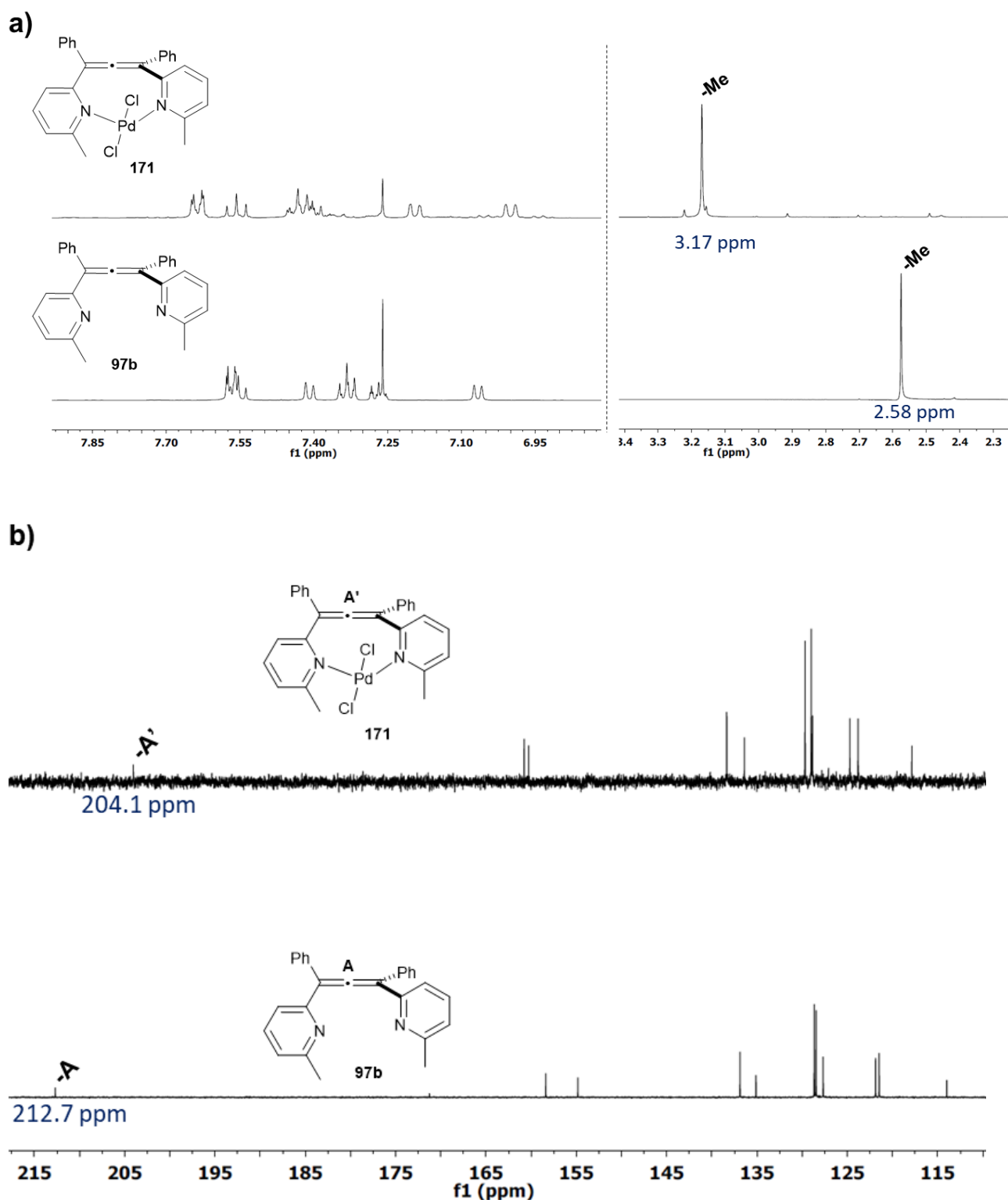


**Figure 25** Comparison of NMR spectra of the free ligand **97b** and its Pd complex **171**: a)  $^1\text{H}$  NMR expansion of regions at 2.3-3.6 ppm and 6.9-7.9 ppm; b)  $^{13}\text{C}$  NMR expansion of region at 110-215 ppm.

These results suggest formation of a symmetric complex with bidentate chelation of the Pd to both pyridyl groups. Further evidence came from  $^{13}\text{C}$  NMR spectrum, where all the

signals moved but the symmetry remained unchanged (Figure 25, b). The allene central carbon atom peak in the characteristic range around 200 ppm was still present, but slightly shifted upfield from 212.7 ppm in the free allene spectrum (A) to 204.1 ppm (A') in **171**. This suggested that the allene core of the ligand was maintained in the complexation process and was not substantially involved in an interaction with the metal centre.

I obtained analogous results for ligand **97a** that quantitatively formed complex **172** under the same reaction conditions (Scheme 62), as can be judged from spectra presented on Figure 26. The inherent lack of symmetry in **97a** (the overlap of the two methyl peaks in the free ligand was coincidental) was translated to its Pd complex **172**.

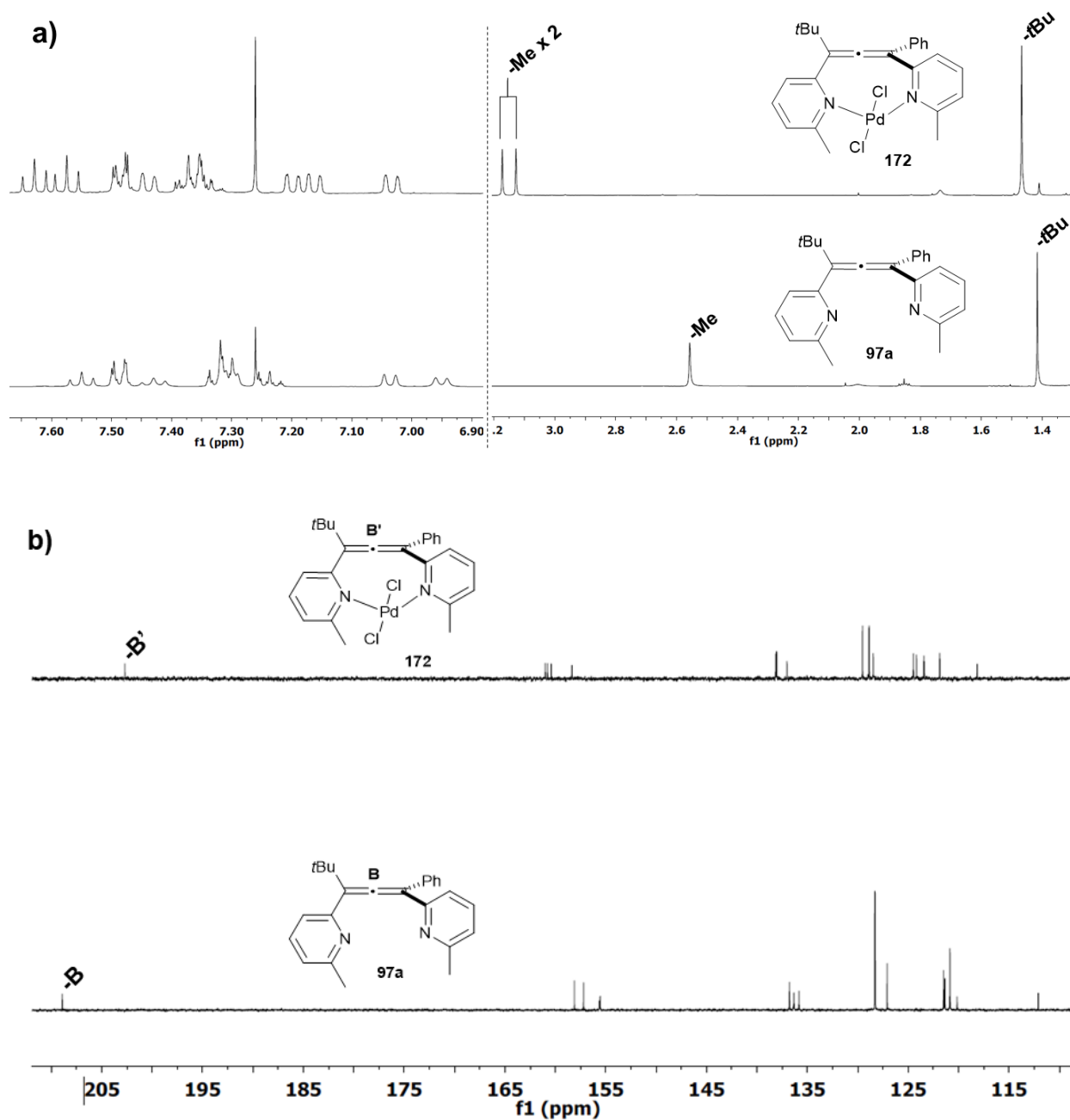


**Figure 26** Comparison of NMR spectra of the free ligand **97a** and its Pd complex **172**: a)  $^1\text{H}$  NMR expansion of regions at 1.3-3.3 ppm and 6.9-7.8 ppm; b)  $^{13}\text{C}$  NMR expansion of region at 110-212 ppm.

Results from HR-MS and EA analyses further supported the proposed structures and confirmed the ligand to metal ratio at 1:1. For example, isotopic pattern characteristic for Pd-containing species was found to be in perfect agreement with the theoretical peak for **172** (Figure 27).



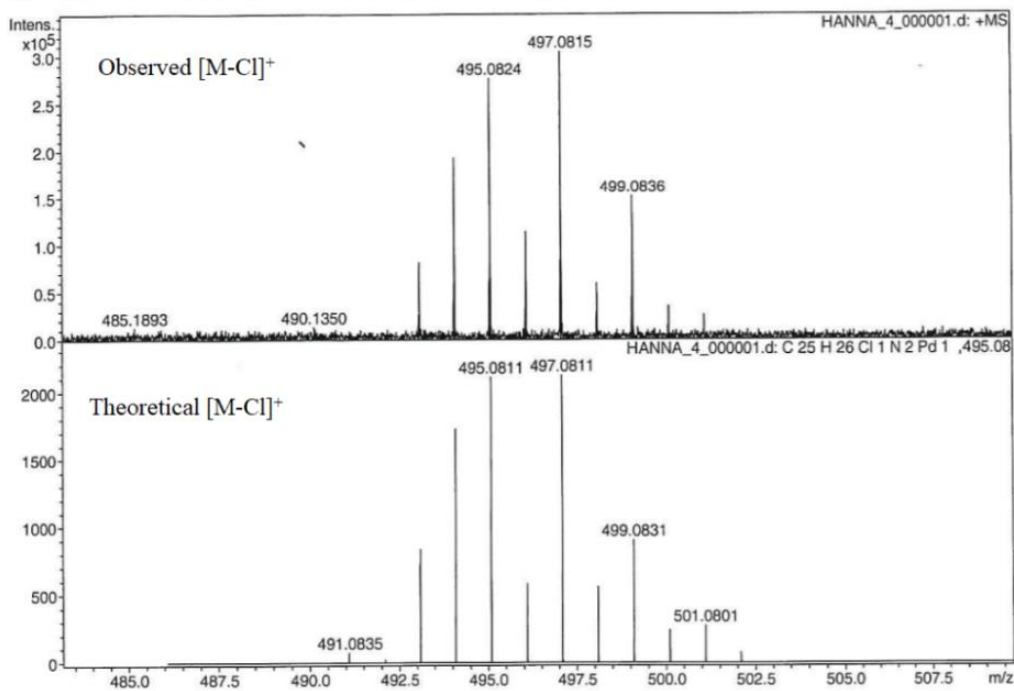


**Figure 27** Fragment of high resolution mass spectrum (ESI) of complex **172** showing peaks corresponding to the  $[M-Cl]^+$  ion.

I obtained good quality crystals of **172** from vapour diffusion of *n*-hexane/ $CH_2Cl_2$  at 4 °C. Structure of non-symmetric complex **172** was thus also unambiguously confirmed with X-ray crystallography (Figure 28).

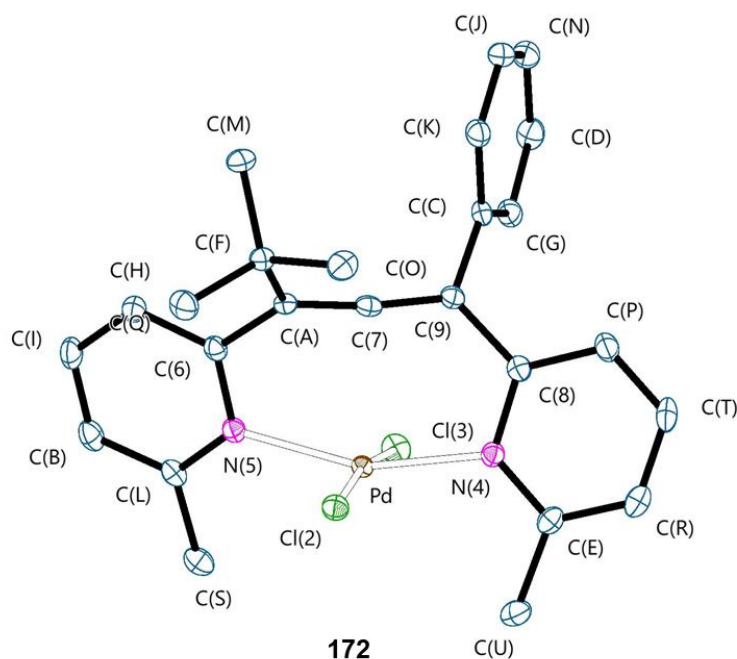


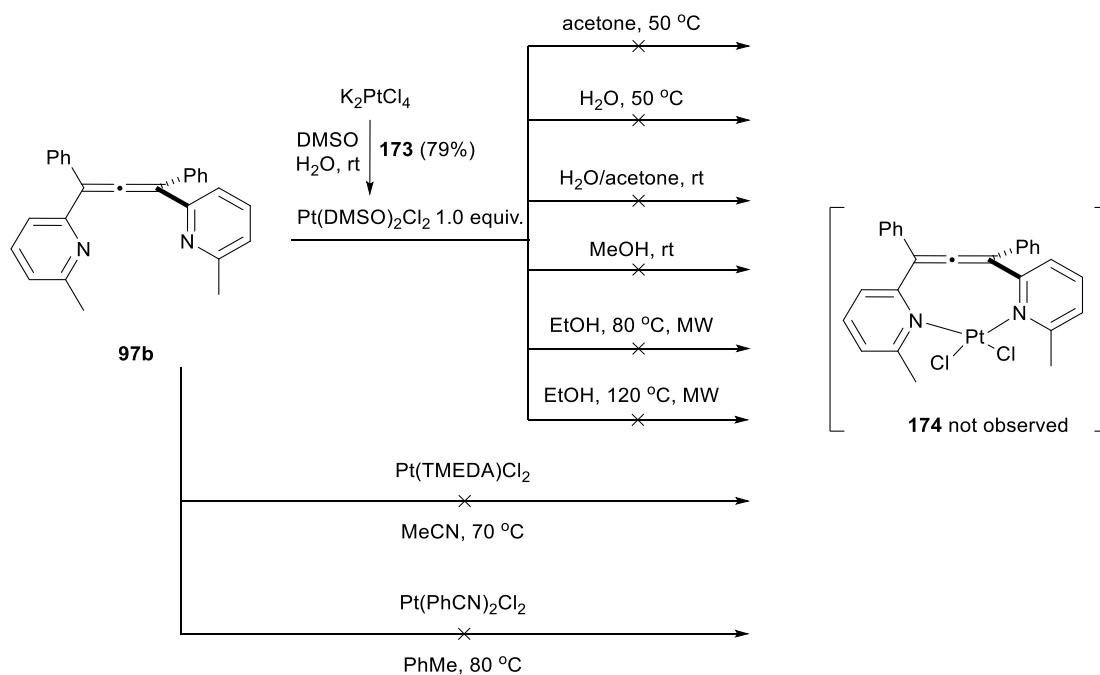
**Figure 28** ORTEP representation of the X-ray structure of complex **172** (Hs omitted).

When looking at the structure **172** we can clearly see the undisturbed allene unit with the C(A)-C(7)-C(9) angle measured at 172.3°. Similarly, the typical double bond distances of the allene found at 1.321(2) Å and 1.322(2) Å are indicative of a non-metal bonded allene group. As we expected, the nitrogen atoms of both pyridines are facing inwards the ligand's pocket and are engaged in bonding to the Pd, with bond lengths of Pd-N(5) 2.0489(1) Å and Pd-N(4) 2.0269(1) Å. Overall, the perpendicular arrangement of the allene ligand is maintained and Pd is enclosed within. **172** features very slightly distorted square planar geometry typical for Pd(II) complexes. The coordination sphere is completed by two chloride ligands equally distanced from the metal centre (2.3300(4) Å and 2.3203(5) Å). Interestingly, bis(pyridyl)allene ligand is bonded to Pd in a *trans* arrangement. There are only few examples of such bidentate, *trans*-spanning ligands based on pyridyl groups reported to date.<sup>[205,206]</sup> Formation of *trans* isomers of complexes with our ligands might have beneficial consequences for their use in catalysis. For example, *trans*-spanning pyridyl ligands have been observed to be more active catalyst in Heck coupling reaction.<sup>[207]</sup>

Although I could not obtain good enough crystals of the symmetric **171** to perform the crystallographic analysis, we have assigned *trans* geometry to that complex based on the similarity of the remaining characterisation data. In particular, the shift of the peaks corresponding to the central carbon atom of the allene in <sup>13</sup>C NMR in both **172** and **171** vs free ligand changed to a similar degree (6.1 ppm and 8.6 ppm, respectively). We can contrast these observations with the data reported for *cis*-bis(phosphine)allene Pd(II) complex **99** (see Scheme 56). In **99**, the *cis* arrangement was combined with a heavy bend of the allene core and a change of 16.6 ppm on <sup>13</sup>C NMR.

### IV b. 3. Platinum complexes with bis(pyridyl)allenes

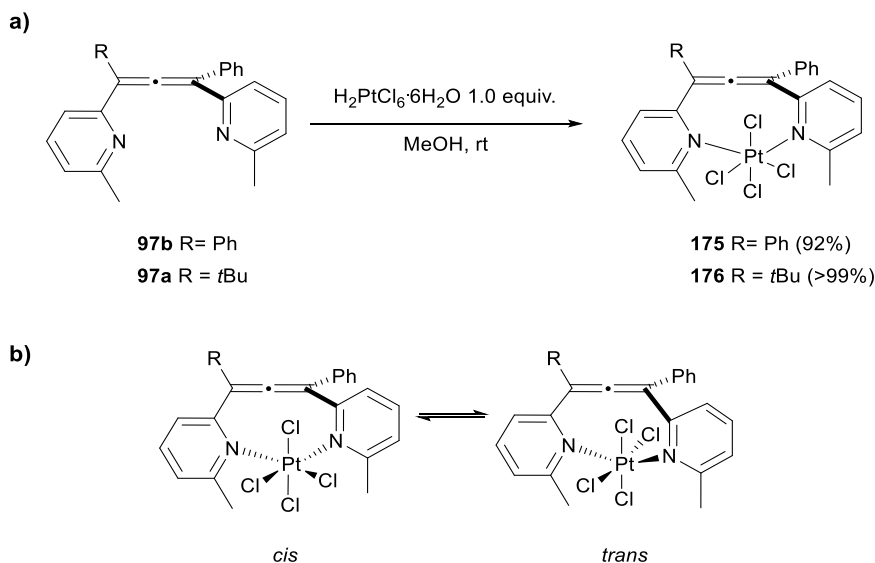
I tried to overcome initial failure to form Pt(II) bis(pyridyl)allene complexes in reactions with salts such as PtCl<sub>2</sub>, Pt(MeCN)<sub>2</sub>Cl<sub>2</sub> and K<sub>2</sub>PtCl<sub>4</sub> with the use of a Pt source with more labile ligands that would be more readily displaced by the allene ligand. Thus, *cis*-Pt(DMSO)<sub>2</sub>Cl<sub>2</sub> was prepared from K<sub>2</sub>PtCl<sub>4</sub> and used in further screening (Scheme 63). However, reaction of ligand **97b** with 1 equiv. of *cis*-Pt(DMSO)<sub>2</sub>Cl<sub>2</sub> in acetone, water or alcohol solvents at room and elevated temperatures led to recovery of the unreacted ligand in most cases. I did not observe any reaction in the presence of Pt(TMEDA)Cl<sub>2</sub> or Pt(PhCN)<sub>2</sub>Cl<sub>2</sub> either.



**Scheme 63** Reaction of ligand **97b** with Pt(II) precursors.

These results seem to be counterintuitive when compared to Pd experiments with the same ligand in light of the respective effective ionic radii of  $\text{Pd}^{2+}$  and  $\text{Pt}^{2+}$ . For the 4-coordinate square geometries the  $\text{Pt}^{2+}$  radius is actually smaller ( $0.74\text{ \AA}$  against  $0.78\text{ \AA}$ ) than that of  $\text{Pd}^{2+}$ .<sup>[208]</sup> In theory the formation of a complex with a ligand with the same bite angle should be even more favourable, but that was not the case. For better comparison, we could estimate the size of the ligand pocket using X-ray data of our Pd complex **172** and Krause's Ag complex **149** (see Figure 22). The size, measured as a distance between the nitrogen atoms of the two pyridines was found at  $4.008\text{ \AA}$  in **172** and  $4.953\text{ \AA}$  for **149**. Another insight deriving from the ionic radii comparison was a notable size difference of 6-coordinate  $\text{Pt}^{4+}$  and  $\text{Pt}^{2+}$  ions at  $0.77\text{ \AA}$  and  $0.94\text{ \AA}$ , respectively. We thought that we could potentially access the complex with a smaller Pt centre more easily. I tested this assumption in the reaction of **97b** with a Pt(IV) salt  $\text{H}_2\text{PtCl}_6 \cdot 6\text{H}_2\text{O}$  (Scheme 64, a). Gratifyingly, the reaction at room temperature in methanol resulted in a formation of a pale orange powder in 92% yield. This powder was a new Pt(IV) complex **175** with 1:1 ligand to metal stoichiometry confirmed by  $^1\text{H}$ ,  $^{13}\text{C}$  NMR, HR-MS and EA analyses. Noteworthy, spectra of the new compound were still characterised by an increased symmetry indicative of a bidentate nature of the ligand. The data also suggested that the allene core did not participate in the metal complexation. I obtained even better result with the non-symmetric ligand **97a** which was fully reacted to its Pt(IV) complex **176** (Scheme 64). I encountered some initial difficulty during the characterisation of **176** with  $^{13}\text{C}$  NMR (very small signal response even for highly concentrated samples). The spectrum was enhanced by the use of variable temperature version of the experiment. I established the desired temperature

at 75 °C by a series of  $^1\text{H}$  experiments in which I observed a significant improvement of resolution compared to a spectrum recorded at ambient temperature.



**Scheme 64** Pt(IV) complexes **175-176**: a) preparation; b) structures of *cis* and *trans* isomers.

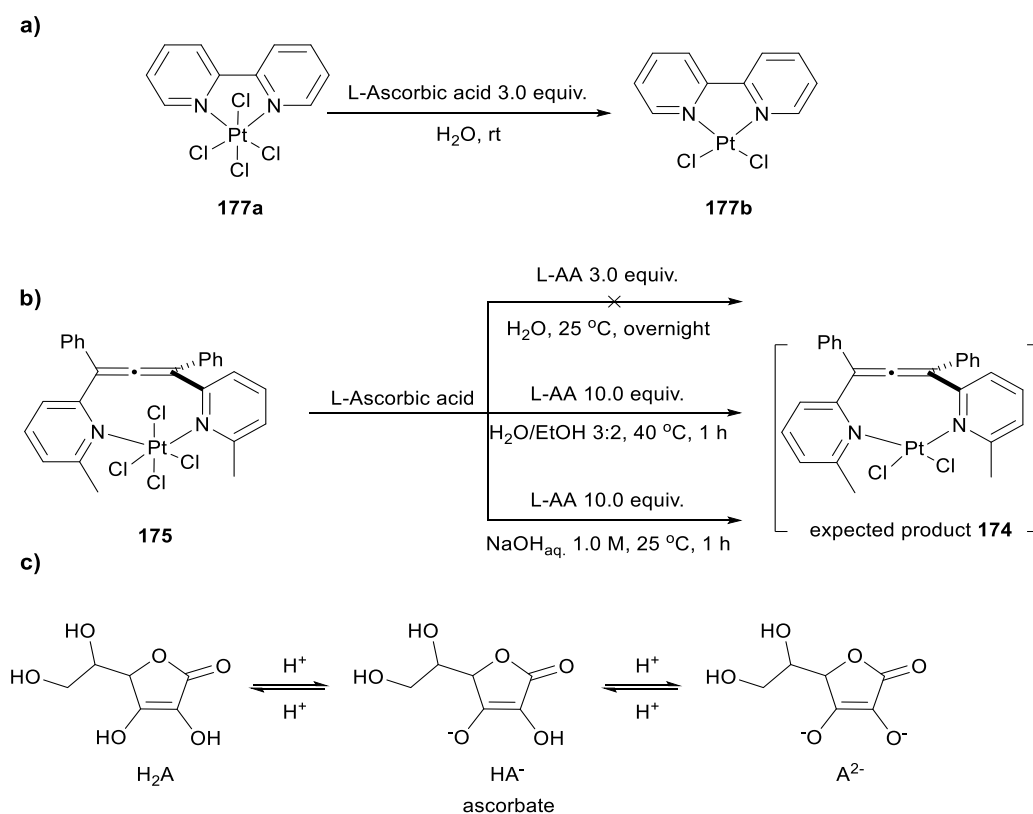
Both complexes **175-176** were only soluble in DMSO, with **175** not being very stable in a solution over longer periods of time (see Section VI b. 1.). This posed a problem for obtaining good crystals that would allow us to determine the structures with certainty. However, we proposed an octahedral geometry of the metal centre typical for Pt(IV) complexes and draw the structures as *cis* isomers in this case. The *trans* isomer would require one of the chloride ligands to be placed directly in the space between Pt atom and the centre of the allene or a distortion of the octahedral geometry. Although, the NMR data indicates that the allene environment did not substantially change in **175-176** compared to free ligands we cannot completely rule out either isomer. Perhaps, the broadening of signals observed on the NMR spectra is a reflection of the equilibrium between the *cis/trans* isomers (Scheme 64, b).<sup>[209]</sup>

The synthesis of the novel Pt(IV) bis(pyridyl)allene complexes brought a twofold advantage. First of all, Pt(IV) complexes have been extensively studied as pro-drugs for anticancer therapy (see Section VI a.).<sup>[210–212]</sup> Pt(IV) compounds are considered as potential precursors to the active Pt(II) species and are designed to circumvent some of the undesired side effects of the latter. Hence, the cytotoxicity and redox chemistry of **175-176** would be of much interest. Secondly, Pt(IV) compounds can be used as synthetic precursors to more challenging Pt(II) equivalents by means of chemical or electrochemical reduction. I investigated the reduction problem next.

The literature concerning the reduction of Pt(IV) complexes is strongly linked to their anticancer reactivity and was mainly developed in biologically relevant settings. Therefore, the

main reported reducing agents used for chemical reductions are those found in significant concentrations in the intracellular environment, such as ascorbic acid, glutathione or L-cysteine.<sup>[210]</sup>

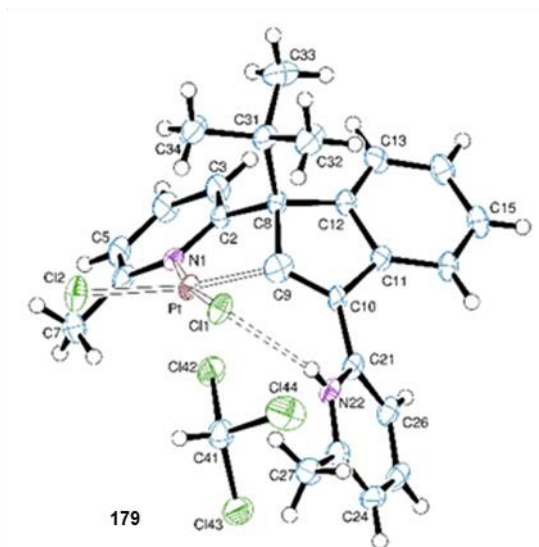
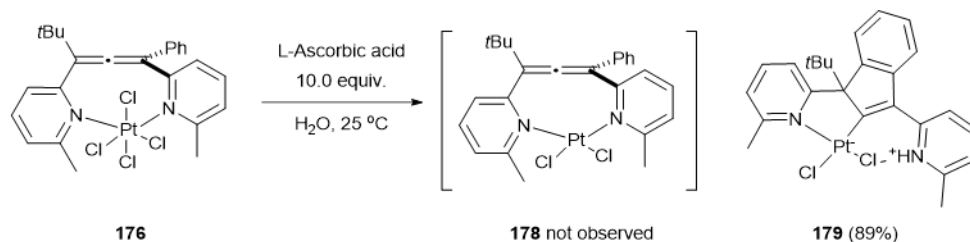
As a starting point, I chose the ascorbic acid reduction and validated it on Pt(bipy)Cl<sub>4</sub> model (Scheme 65, a). Reaction of **177a** with 3 equiv. of L-ascorbic acid successfully produced Pt(II) analogue **177b**, confirmed by excellent agreement of NMR data with literature values. Compound **175** was then subjected to the same and modified conditions (Scheme 65, b). The reaction in water or water/ethanol mixture gave very inconsistent results. I always isolated a product in trace amounts that hindered full characterisation. Next, I carried out the reaction in increased pH media and in larger excess of the reductant to improve the issues of efficiency and reproducibility. A higher pH environment was thought to influence an equilibrium of different forms of the ascorbic acid in solution, favouring the dianion believed to be the active species in the reaction (Scheme 65, c). Although the yields improved slightly I could not establish the identity of the product with confidence.



**Scheme 65** Reduction of Pt(IV) complexes with ascorbic acid: a) model bipy complex **177a**; b) bis(pripyl)allene complex **175**; c) ascorbic acid forms in solution.

On the contrary, non-symmetric **176** was readily reduced in aqueous media in the presence of 10 equiv. of ascorbic acid (Scheme 66). Surprisingly, the isolated product was not

Pt(II) analogue of **176** of the **178** type, but a hexacyclic platinumacylce **179** isolated as an orange solid in 89% yield. **179** was fully characterised, including X-ray structure determination.

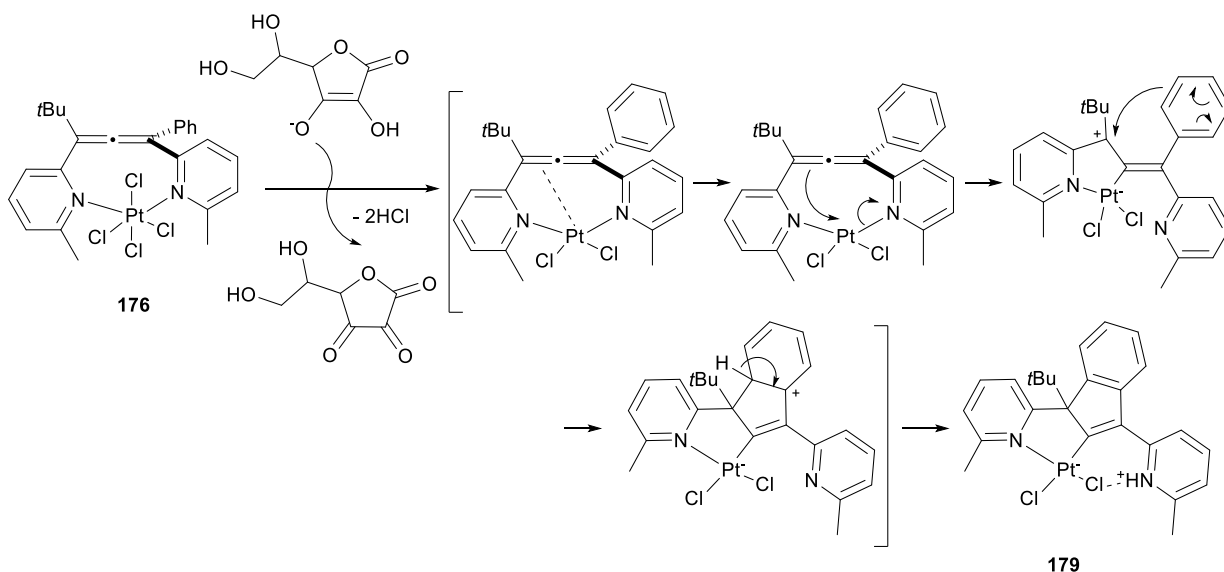


**Scheme 66** Reduction of Pt(IV) complex **176**; ORTEP representation of the X-ray structure of product **179** (thermal ellipsoids drawn at 50% probability level).

**179** crystallised in a triclinic  $P\bar{1}$  space group. Interestingly, it was not the pyridine substituent that attack the allene backbone, but a phenyl group, resulting in a formation of indene-type core of a new complex. Pt was found in a near square planar geometry, chelated by the N(1) atom of the pyridine and C(9) – former central carbon atom of the allene. The Pt-C(9) bond distance was found at 1.963(5) Å. The coordination sphere was completed by two chloride ligands, one of which was an acceptor of good intramolecular hydrogen bond with a pyridinium group not bonded to the metal centre, N(22)-H(22)...Cl(1) at 2.33(9) Å.

We can view the formation of **179** from its Pt(IV) precursor **176** as a cyclometallation process with characteristic establishment of a new metal-carbon  $\sigma$ -bond *via* transition metal-mediated bond activation.<sup>[213]</sup> The large majority of cyclometallation reactions involve activation of C-H bonds, however the examples with C-O, C-Si or like in our example activation of a C-C bonds are known. In general, cyclometallation is initiated by coordination of the metal centre by a donor group present in a molecule, for example, the pyridyl groups in **176**. The process is terminated by the subsequent bond activation closing the metallacyclic product. In case of

platinacycles, typically five-membered ringed products are formed *via* C-H ( $sp^2$ ,  $sp^3$ ) activation. C,P-, C,N-Chelating or pincer C,N,C-, N,C,N- *etc.* platinacycles examples are common. Interestingly, N,N-coordinated Pt-bipy complexes have been found to undergo cycloplatination to less common C,N-chelates *via* so called “rollover” mechanism.<sup>[214,215]</sup> In case of **176**, such process involving activation of the double bond of the allene skeleton was perhaps accompanied by a  $S_EAr$ -type attack of the phenyl substituent. A tentative mechanism for the formation of **179** assuming the initial Pt(IV)/Pt(II) reduction is proposed on the Scheme 67.



**Scheme 67** Proposed mechanism for the formation of platinacycle **179**.

I also investigated both **175** and **176** by cyclic voltammetry (CV) to gain additional insight into the reduction process. The results for both compounds were much alike and will be describe here in detail for **176**. I observed three reduction peaks below -1.0 V on the first voltammogram of **176** recorded in the direction of positive E values (Chart 1, a). We assigned the cathodic peak **A** at -1.1 V to a Pt(IV)/Pt(II) reduction event, whereas peaks **B-C** in more negative potential range perhaps arose from the reductions of the allene ligand fragment. When the experiment was run in the opposite direction we could also observe an oxidation event. I determined by narrowing the range of potential window to **A** peak only (Chart 1, b), that the new anodic oxidation peak **A'** at 0.06 V was associated with **A** (Chart 1, c). Initial Pt(IV)/Pt(II) reduction was probably followed by partial re-oxidation of resulting Pt(II) species. However, such re-oxidation would not lead to the original Pt(IV) complex, because in that case we would see a more symmetric voltammogram, corresponding to a classic two electron reversible process. What is more, the irreversible Pt(IV)/Pt(II) reduction is usually combined with a loss of two axial chloride ligands (electrochemical-chemical process) and therefore regeneration of the initial analyte is not likely. The corresponding values for **A** and **A'** peaks for complex **175** under the same experimental conditions were -1.0 V and 0.19 V, respectively.

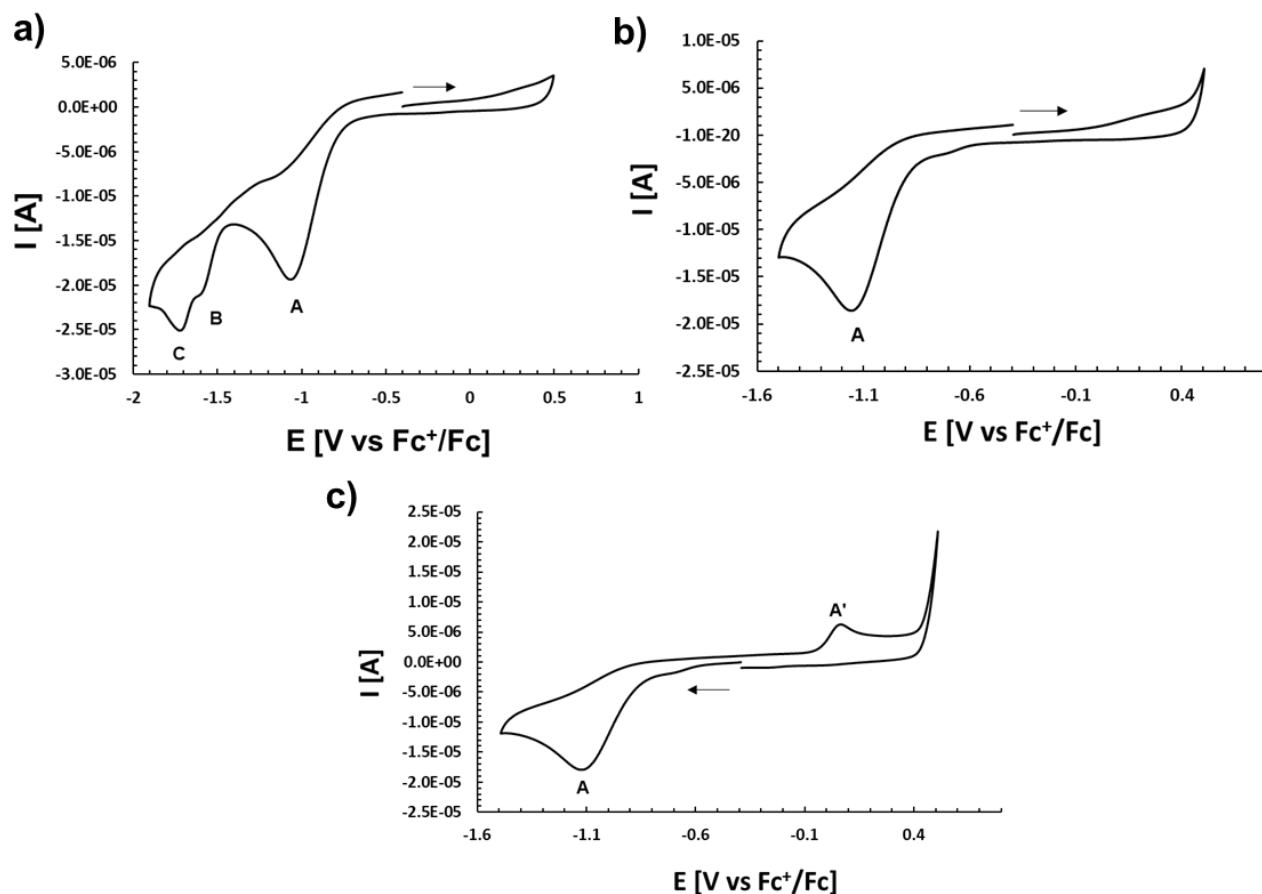


**Chart 1** Voltammograms of a solution of **176** at 1.6 mM, in 0.1 M (*n*-Bu<sub>4</sub>N)(PF<sub>6</sub>) DMSO solution with a scan rate of 100 mV/s at rt at a glassy carbon working electrode. Potentials referenced to ferrocene internal standard.

Very similar CV profiles were observed in a reported study focusing on the identification of the products of electrochemical reduction of three promising Pt(IV) drug precursors (Figure 29).<sup>[216]</sup> In particular, the reduction potential value of -0.964 V for dichloro-compound **180** and its oxidation potential values are in good agreement with those observed for **176** and **175**. Interestingly, the study found that only **180** was cleanly reduced to its Pt(RNCH<sub>2</sub>CH<sub>2</sub>NR)(Py)<sub>2</sub> analogue, whereas **181** and **182** underwent more complicated reaction pathways.

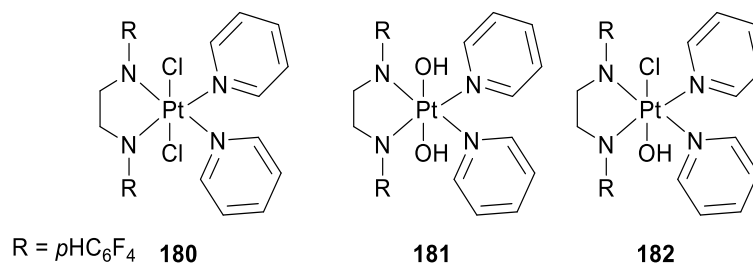


**Figure 29** Pt(IV) complexes studied as anticancer prodrugs.



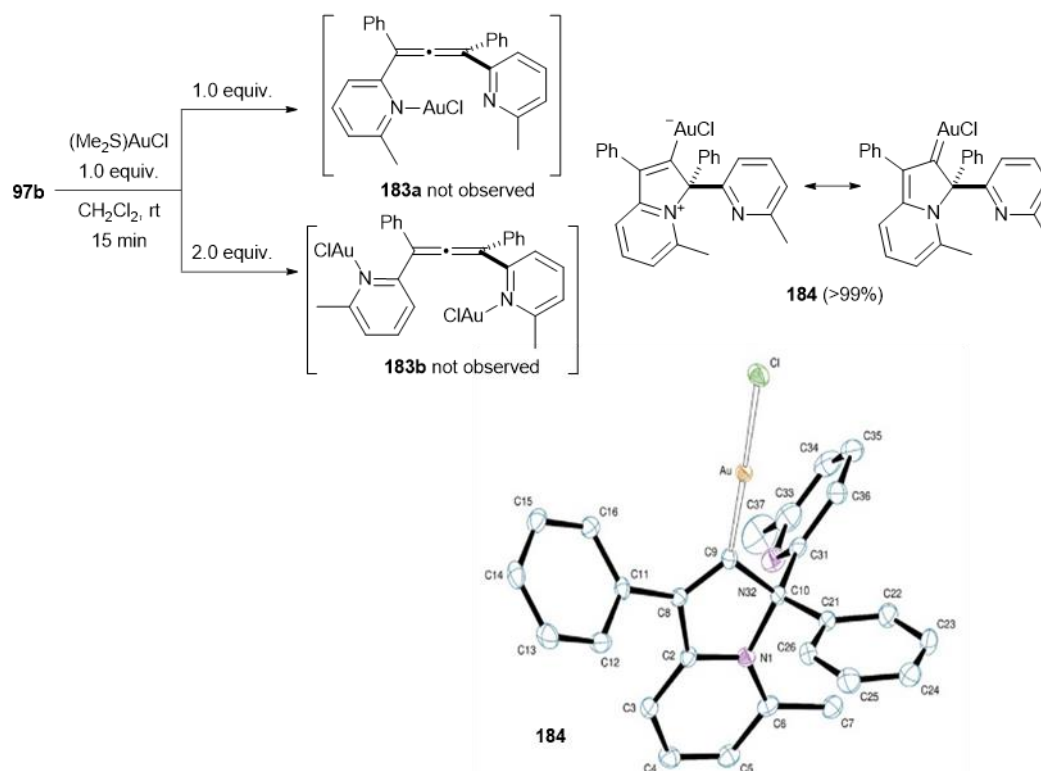
Baik and co-workers used a mixed electrochemical/computational approach to study several Pt(IV) compounds of general structure  $\text{Pt}(\text{NH}_3)_2\text{Cl}_2\text{L}_2$  ( $\text{L} = \text{Cl}^-$ ,  $\text{CH}_3\text{COO}^-$ ,  $\text{CHCl}_2\text{COO}^-$ ) and shed more light onto the details of their reduction process to Pt(II) analogues.<sup>[217]</sup> The authors established that the commonly observed 2-electron, irreversible reduction proceeds in a stepwise manner. First, one electron transfer produces a metastable six coordinate Pt(III) intermediate. The latter, upon addition of a second electron loses two axial ligands (L) forming the Pt(II) species. In general, this description also fits the reduction process observed for **175** and **176**.

The reduction of six coordinate Pt(IV) compounds to four coordinate Pt(II) species is believed to proceed through an irreversible loss of two axial ligands and the influence of the character of those ligands on the reduction potential of Pt(IV) complexes has been studied.<sup>[218–222]</sup> For example, Choi and co-workers observed a correlation of reduction rates and reduction potentials and the electron-withdrawing character and bulkiness of the axial ligands in a series of Pt(IV) complexes.<sup>[221]</sup> The more bulky and electron withdrawing the ligand the higher the rate and the more positive the potential of the reduction. Thus, the observed reduction potential range varied from  $-0.884$  V for  $\text{Pt}(\text{2HNCH}_2\text{CH}_2\text{NH}_2)(\text{OH})_2\text{Cl}_2$  to  $-0.09$  V for Pt(diaminocyclohexane) $\text{Cl}_4$  complex. The reduction potential values for **176** and **175** with two chloride axial ligands each ( $-1.1$  V,  $-1.0$  V) might seem surprisingly negative in comparison suggesting some other factors at play decreasing their aptitude for electrochemical reduction. Interestingly, although the chemical reduction of **176** with ascorbic acid, of much more positive oxidation potential ( $+0.56$  V under same conditions used for the CV of Pt complexes),<sup>[221]</sup> might seem unfeasible, it took place nonetheless, and similar behaviour of other Pt(IV) complexes was observed elsewhere.<sup>[223]</sup> The quite negative reduction potentials of **175** and **176** might prove advantageous for their stability under physiological conditions and in consequence for their use as pro-drugs. To confirm the structures of the products of the electrochemical reduction of **175** and **176**, future work with these complexes might include bulk electrolysis experiments that would enable us to isolate enough quantity of the products to carry out extended characterisation.

#### IV b. 4. Gold complexes with bis(pyridyl)allenes

As in the case of Pd and Pt, there are no reported examples of Au bis(pyridyl)allene coordination compounds. Consequently, we describe the first syntheses of Au(I)- and Au(III)-complexes with those ligands here, building on the promising reactivity observed in the reaction with  $\text{AuCl}_3$ . I began a systematic study of the behaviour of bis(pyridyl)allenes in the presence of Au with probing their propensity to form Au(I) compounds. Thus, allene **97b** was reacted respectively with 1 and 2 equiv. of  $(\text{Me}_2\text{S})\text{AuCl}$  in  $\text{CH}_2\text{Cl}_2$  at room temperature (Scheme 68). Due to the linear coordination of Au(I), we expected formation of **183a**-type complex with Au

centre captured by one of the pyridyl groups or 2:1 complex **183b** resembling Fensterbank's Au(I)-bis(phosphine) complex **159b**.<sup>[157]</sup> However, irrespective of the variance in the conditions, after 15 min I quantitatively isolated the same product **184** from both experiments. Full characterisation of **184** uncovered an interesting result, with the first obvious observation being the lack of symmetry in the product.



**Scheme 68** Reaction of ligand **97b** with Au(I); ORTEP representation of X-ray structure of complex **184** (Hs omitted, thermal ellipsoids drawn at 50% probability level).

Au seemed to activate one of the allene's double bonds towards attack from the nitrogen atom of a pyridine ring onto the allene terminus ultimately leading to a formation of **184**.<sup>[201]</sup> This result resembled the reactivity I encountered with the thiophene and amino ligands, where the donor substituents acted as nucleophiles ready to attack the activated allene. I also saw the same type of reactivity with the trisubstituted bis(pyridyl)allene **97d** (see Scheme 48) under the trimetallic catalytic system Cu/Zn/Ti. However, in that case the product did not feature metal bonding. This reactivity of **97b** with Au(I) was also interesting when we reflect on the behaviour of bis(pyridyl)allenes in the presence of other coinage metals such as Cu and Ag. For those, Krause and co-workers proposed the allene-containing structures.<sup>[149]</sup> In any case, protodemetalation did not occur in this experiment and I obtained **184** as a complex that exhibits a bicyclic core with the Au bonded to the former central carbon atom of the allene. The structure can be depicted in its two resonance forms of a zwitterionic vinyl-Au or a neutral carbene. Conjugation with heteroatoms in the  $\alpha$ -position to C(9) is normally needed for

stabilisation of this electron deficient carbon for successful isolation of metal carbene complexes.<sup>[224,225]</sup> Interestingly the heteroatom in our new complexes is not in such proximity to C(9) but still provides high level of stabilisation. In fact, similar longer range heteroatom conjugation in Au(I) complexes has been observed in compounds isolated by, for example, Hammond and Fürstner (**185-186**, Figure 30).<sup>[201,202]</sup> The remaining pyridyl group of our new complexes sits on a newly created stereogenic centre and does not participate in the metal coordination. Good quality crystals of **184** were grown (CH<sub>2</sub>Cl<sub>2</sub>/cyclohexane), which allowed us to unambiguously determine the structure with X-ray crystallography (*vide infra* for discussion). Structure **184** shows similar features to the Au(I)-**157** derived from (pyridyl)(phosphine oxide)allene reported by Fensterbank and co-workers.<sup>[154]</sup>

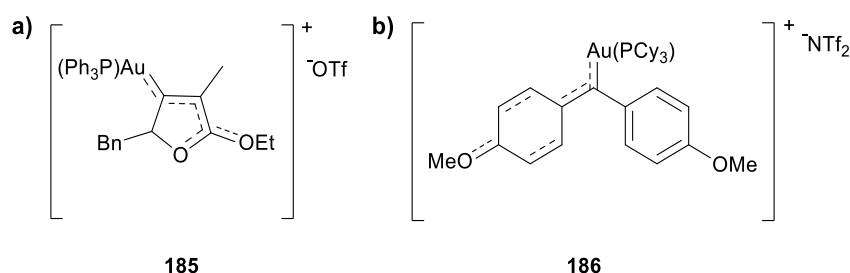
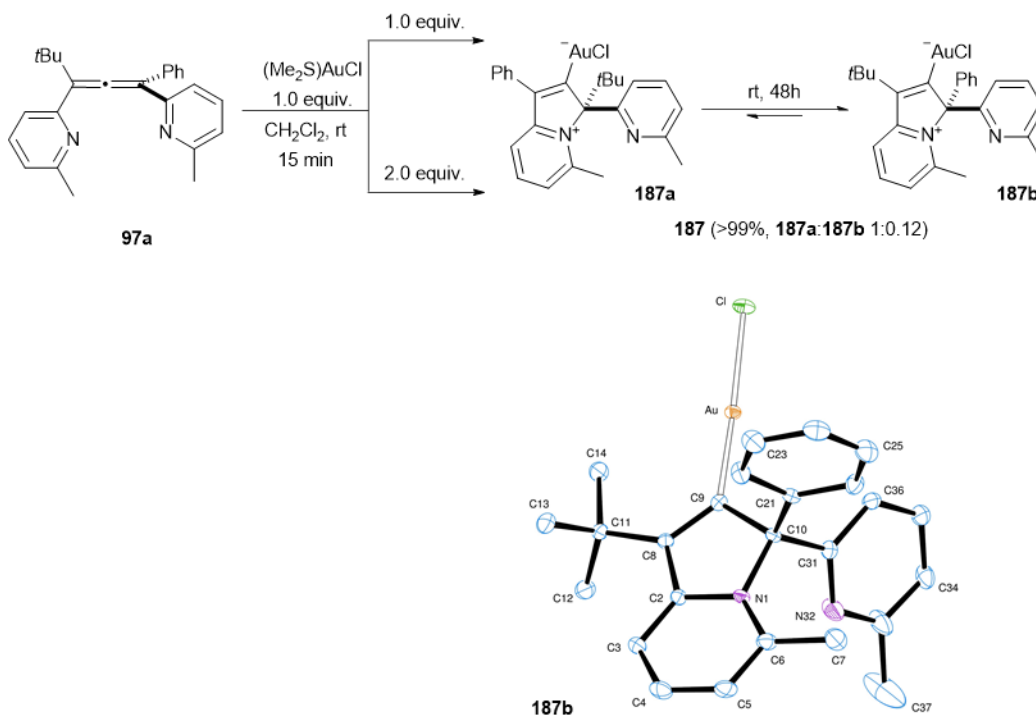


**Figure 30** Heteroatom-stabilised Au(I) carbenoids reported by: a) Hammond's group; b) Fürstner's group.

When I subjected allene **97a** to the same reaction conditions, again it was fully transformed to carbene-type compound **187**. With a non-symmetric ligand such as **97a**, the two pyridyl groups, which are not equivalent, cyclised onto the allene with different rates resulting in an isomeric mixture isolated at 1:0.12 ratio of **187a**:**187b** products (Scheme 69).



**Scheme 69** Reaction of ligand **97a** with Au(I); ORTEP representation of X-ray structure of complex **187b** (Hs omitted, thermal ellipsoids drawn at 50% probability level).

The structures of **187a** and **187b** were assigned on the basis of NMR (including HMBC and NOESY experiments) and XRD analysis of the isomer **187b**. I observed that the isomeric ratio changed in a solution over time to >99% of **187b** (Scheme 69). These experiments showed that isomer **187a** with *t*Bu- and pyridyl groups on the  $sp^3$  carbon atom was the kinetic product in the reaction and isomerised to the more favourable thermodynamic isomer **187b**. This process might be promoted because of the more sterically challenging environment of the tetrahedral carbon in **187a** compared to **187b**. I performed a series of  $^1\text{H}$  NMR experiments tracking the change in concentration of both species in the solution (Figure 31, a-b). I determined the ratio by comparison of integration of the pyridyl signals at 6.79 ppm (**187a**) and at 8.49 ppm (**187b**) in the aromatic region (Figure 31, b). Then I calculated the concentrations of **187a** and **187b** at specific time intervals from known initial concentrations of the sample and corresponding isomeric ratio.

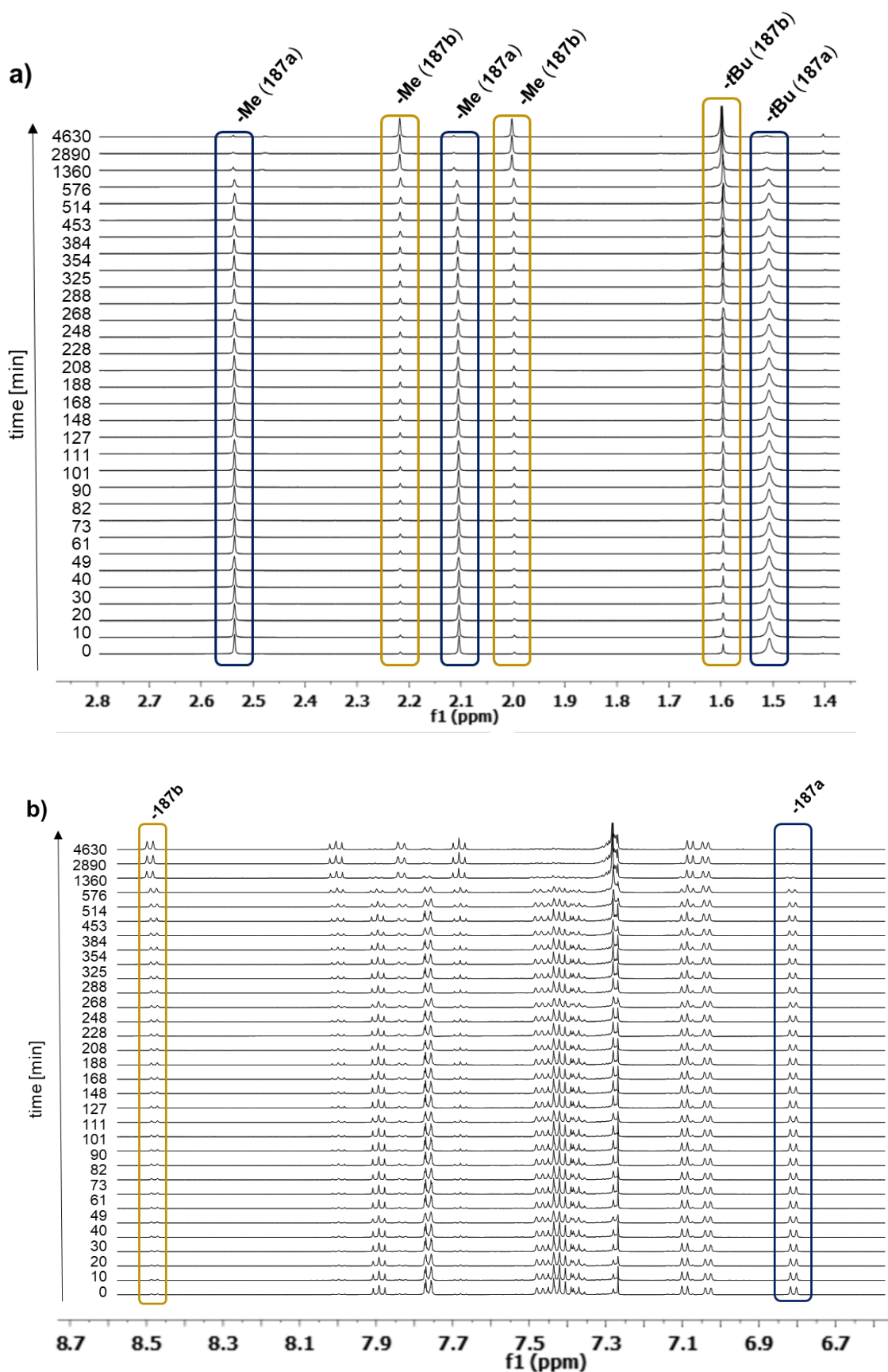


**Figure 31** Periodic  $^1\text{H}$  NMR experiment of mixture **187a/187b**: a) expansion of 1.4-2.8 ppm region; b) expansion of 6.6-8.6 ppm region.

The corresponding concentrations of **187a/187b** were plotted vs time till the total disappearance of the **187a** isomer (Chart 2, a). This data allowed us to determine the first order rate constant of isomerisation at  $k_{\text{isom}} = 1 \times 10^{-5} \text{ s}^{-1}$  by straight line approximation on the plot of  $\ln[187a]$  vs time (Chart 2, b).

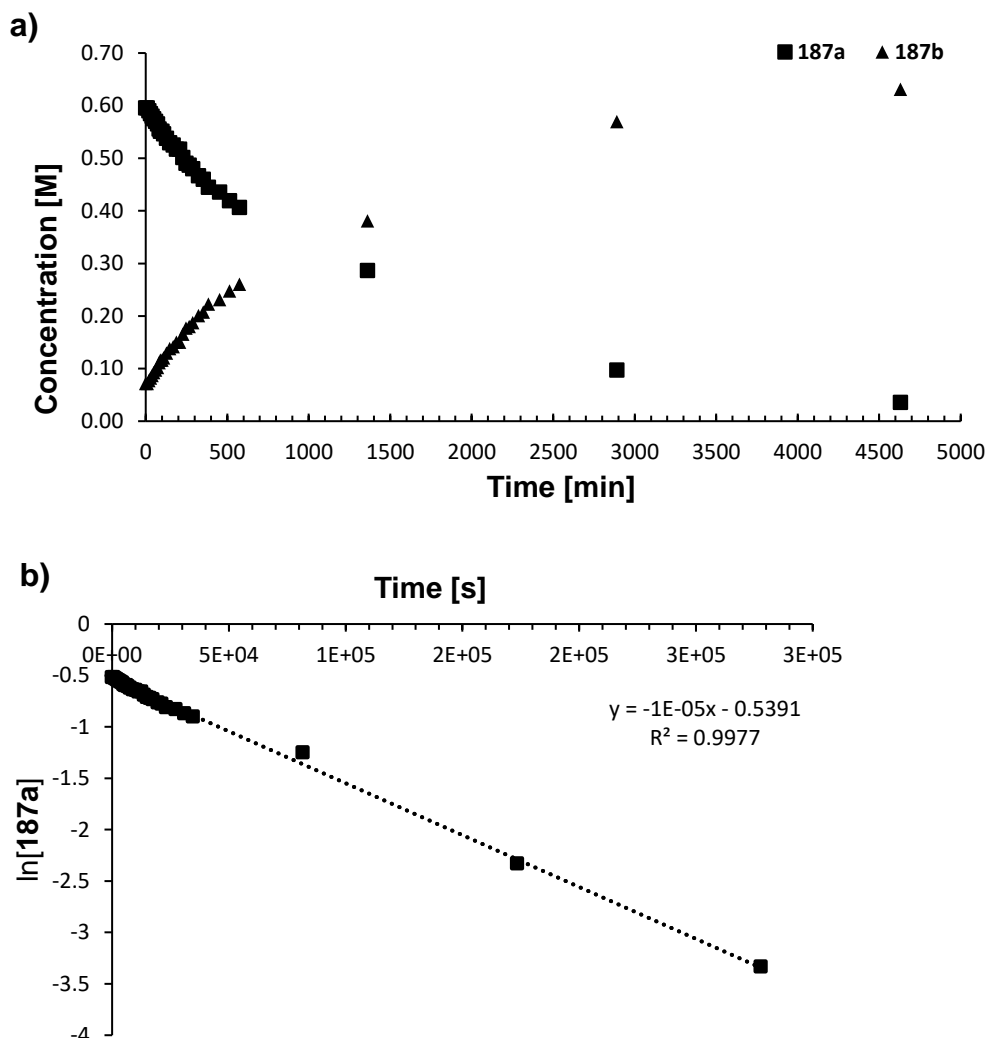
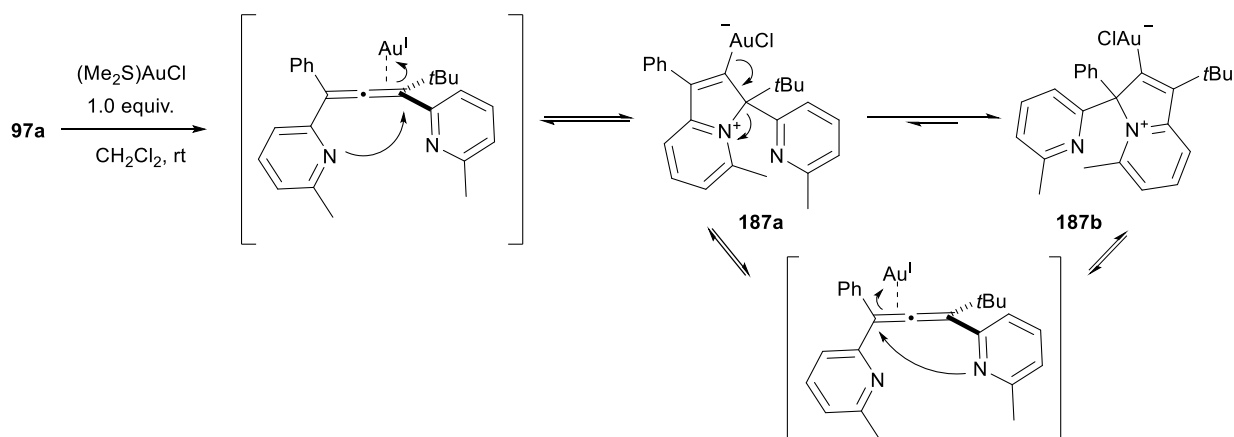


**Chart 2** Isomerisation of **187a/187b**: a) plot of the change of concentration of both species in the solution vs time; b) plot of  $\ln[187a]$  vs time used to establish rate constant and order of the isomerisation.

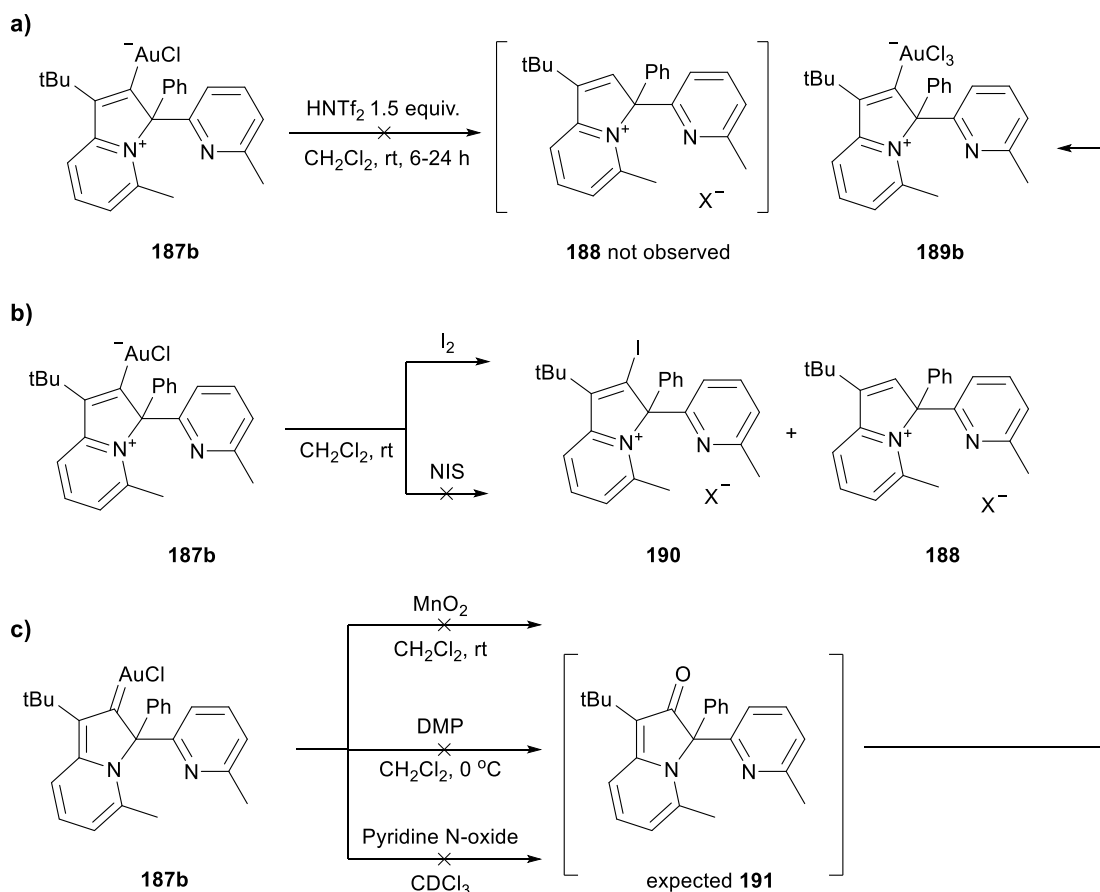
The equilibration process can be seen as a reversible cyclisation/ring opening reaction, with the AuCl fragment moving across the allene system (Scheme 70). Non-static interaction of AuCl fragment with the double bonds of the allene resembles fluxional behaviour of  $\eta^2$ -allene Au complexes (see Section I b.).



**Scheme 70** Proposed mechanism of the isomerisation of **187a/187b**.

I investigated the carbene/vinyl-Au character of **187a-b** in a series of functionalisation attempts (Scheme 71). For example, to probe the vinyl-Au character, **187b** was reacted with HNTf<sub>2</sub>. This strong acid is commonly generated *in situ* and involved in protodemetalation of vinyl-Au(I) intermediates in reactions catalysed by Au(I) cationic complexes that are generated by chloride abstraction using AgNTf<sub>2</sub> and I used it to simulate those catalytic conditions. However, complex **187b** did not undergo the expected protodemetalation (Scheme 71, a). In contrast, the reaction led mainly to decomposition after long times with isolation of small amounts of **189b**, the Au(III) analogue of **187b**, confirmed by X-ray crystallography. Although isolation of this Au(III) complex was unexpected, the oxidation of Au(I) carbene complexes to Au(III) hydride species has been observed by Bertrand and co-workers with triflic acid.<sup>[226]</sup> Other oxidation methods for Au(I) complexes involve the use of halogens or proceed *via* oxidative addition.<sup>[227,228]</sup>

Other electrophilic reagents (such as electrophilic halogenated compounds) have shown to react with vinyl-metal complexes, to give the corresponding vinyl-halogen derivatives. Reaction of complex **187b** with iodine resulted in a mixture of products that appeared to contain vinyl iodide **190** and protodemetalation product **188**, whereas milder conditions of NIS ended up with complete decomposition (Scheme 71, b). Related NIS-induced cyclisation of pyridyl(allenes) to 2-iodoindolizines has been reported recently without the involvement of metals or formation of the vinyl-Au complexes.<sup>[229]</sup>



**Scheme 71** Attempted functionalisation of complex **187b**: a) protodeauration with acid; b) reaction with electrophiles; c) oxidation.

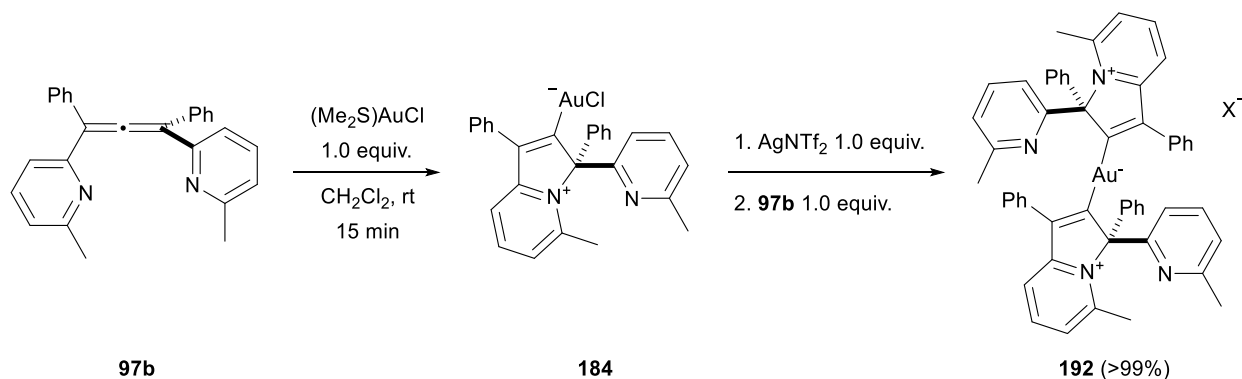
On the other hand, metal carbenes have been reported to oxidise to the corresponding carbonyls, so to probe the carbene character, I attempted to oxidise complex **187b** using common oxidising agents. However, all oxidation efforts resulted in recovery of unaltered starting material (Scheme 71, c). Only under acidic conditions of Dess-Martin reagent I saw traces amounts of Au(III) complex **189b** similar to the reaction with HNTf<sub>2</sub>.

The predominant robustness of **187b** under presented conditions and mixed results of the derivatisation seemed to confirm the true dual carbene/vinyl-Au nature of new compounds rather than point to either one of them. This inference is further supported by the solid-state analysis of this new family of complexes (*vide infra*, page 107).

Another way to functionalise the new Au(I) complexes could be achieved not through replacement of the metal centre but by ligand exchange in the Au coordination sphere. For instance, we could access interesting extended 3D architectures by replacement of the chloride ligand for one more bis(pyridyl)allene ligand to form a complex resembling those from cyclic (alkyl)(amino)carbene (CAAC)<sup>[230]</sup> or *N*-heterocyclic carbene (NHC)<sup>[231]</sup> classes. I carried



out such reaction with complex **184** (Scheme 72). After initial formation, **184** was exposed to 1 equiv. of  $\text{AgNTf}_2$  followed by another equivalent of allene **97b**.

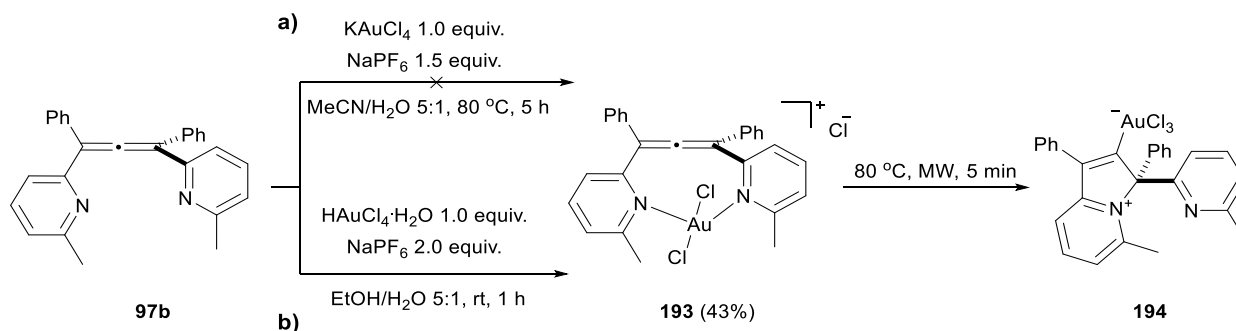


**Scheme 72** Preparation of 2:1 complex **192**.

The yellow solid that was formed was analysed by NMR and HR-MS and we proposed structure **192** for the product. The mass spectrometry analysis pointed to the 2:1 ligand to metal ratio in the product. Similarly, both  $^1\text{H}$  and  $^{13}\text{C}$  NMR spectra showed two distinct, but analogous ligand units. Each of them shared many similarities to the spectrum of 1:1 complex **184**, such as peaks corresponding to the stereogenic carbon atoms at 98.94 ppm and 94.92 ppm for **192**, and 97.5 ppm in **184** on the  $^{13}\text{C}$  NMR spectrum. The peaks corresponding to carbene-type carbon atoms in **192** (208.5 and 208.0 ppm), however, moved significantly downfield compared to the same peak in **184** (191.3 ppm). Such pronounced shift might be an additional proof that Au centre in **192** features a second ligand significantly different to the chloride one in **184**. The fact that the spectra of **192** are not fully symmetric might be caused by restricted rotation of its substituents in a highly congested environment or perhaps very distinct vinyl/carbene character of the ligands. This observation is quite unusual as similar dimeric Au complexes of (NHC)-carbenes typically have symmetric spectra.<sup>[232–234]</sup> **192** could be crystallised, however poor diffraction of resulting crystals did not allow us to confirm the structure with X-ray crystallography.

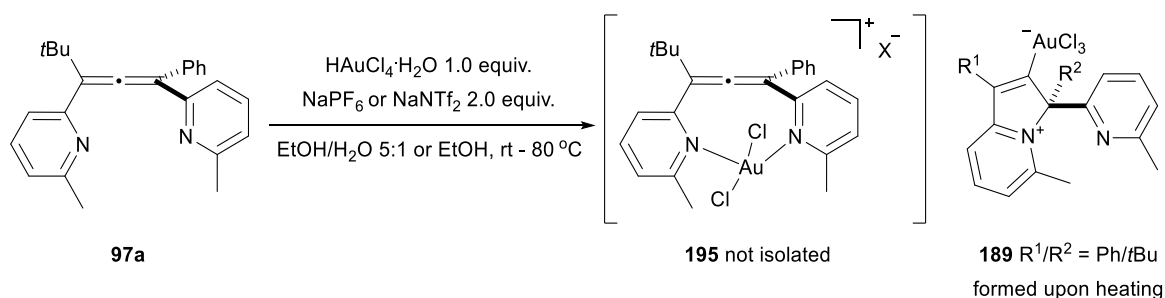
Next I investigated the complexation of bis(pyridyl)allenes with Au(III) salts. To begin with, allene **97b** was reacted with two cationic Au(III) sources,  $\text{KAuCl}_4$  and  $\text{HAuCl}_4$  hydrate (Scheme 73). Both reaction mixtures contained  $\text{NaPF}_6$  furnishing a counterion for an anticipated cationic complex that would facilitate crystallisation of the product. The first experiment with  $\text{KAuCl}_4$  in an acetonitrile/water mixture at 80 °C yielded a very complex reaction mixture. However, reaction with  $\text{HAuCl}_4$  in an aqueous ethanol at room temperature, promoted the formation of a dark orange solid that precipitated from the reaction in 43% yield, with a proposed symmetric structure **193**. Elemental analysis of this complex suggested that actually the counterion of **193** was a chloride anion. When the reaction under these conditions was

pushed by microwave heating to improve the yield, after only 5 min at 80 °C, **193** was completely transformed into bright yellow powder identified as **194**, the Au(III) equivalent to Au(I) carbene-type compounds that we saw earlier. Depending on a slight change in reaction conditions, room temperature vs heating, we could access two very different classes of Au(III) compounds from the same starting materials.



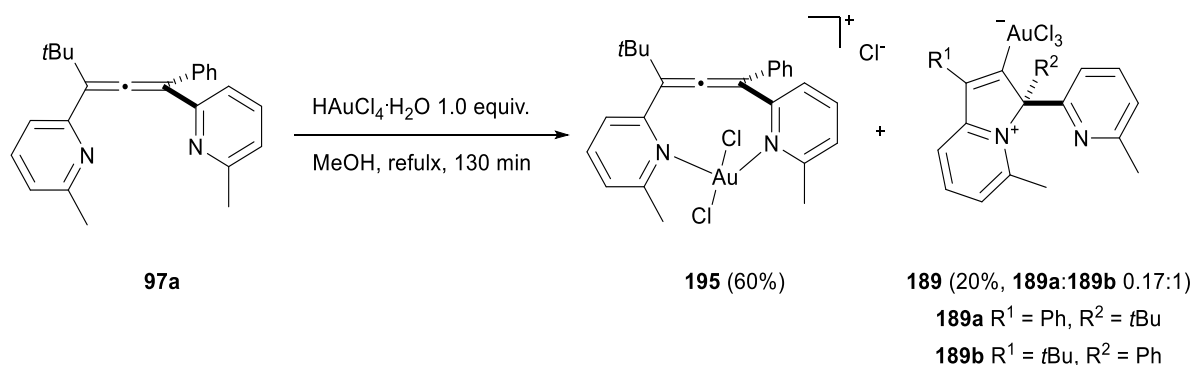
**Scheme 73** Reaction of ligand **97b** with Au(III).

The optimised conditions applied to non-symmetric **97a**, however, did not afford expected **195** and further variation in the conditions allowed us to pinpoint only carbene-type **189** that was always forming at elevated temperatures (Scheme 74).



**Scheme 74** Reaction of ligand **97a** with Au(III).

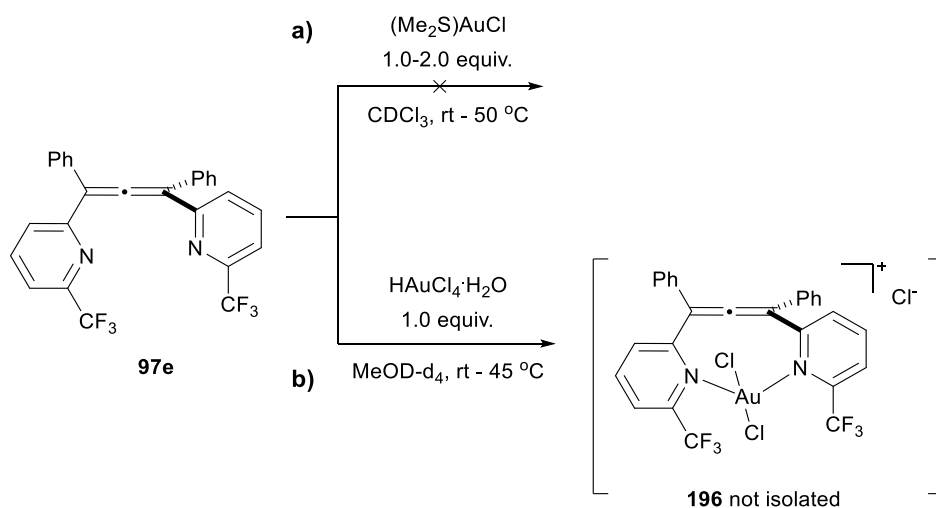
I could gain better control over the reaction with **97a** with a simple switch to refluxing methanol. Separation of bright yellow precipitate furnished carbene-type **189** in 20% yield and 0.17:1 isomeric ratio, whereas allene-containing **195** left in solution was recovered after concentration of the filtrate (60% yield, Scheme 75). Reaction of symmetric bis(pirydyl)allene **97b**, substituted with two phenyl groups, in methanol, on the other hand, produced only the carbene compound **194**. The formation of *N,N*-chelating complexes such as **193** and **195** in Au(III) experiments that were inaccessible in corresponding Au(I) reactions underpins the different character of these Au species. In particular, we observed the carbophilic preference of Au(I) compounds for coordination to  $\pi$ -system<sup>[60,235,236]</sup> vs the preference of Au(III) for  $\sigma$ -donative ligands.



**Scheme 75** Reaction of ligand **97a** with Au(III) in MeOH.

The fact that we could isolate allene-containing Au complexes with bis(pyridyl)allene ligands prompted us to investigate these type of Au complexes further. We argued that modification of our ligands' structure might favour allene-containing complexes and not the carbene-type products. For example, increase of a steric bulk around the allene core or decrease of the nucleophilicity of the pyridyl groups could disfavour metal-induced cyclisation. We decided to explore the latter variant and prepare a modified ligand with EWG substituents situated on both pyridine groups. We chose a symmetric -CF<sub>3</sub> substituted structure **97e** (Scheme 76) as a close analogue to the original methylated ligand. As a result **97e** was prepared utilising the same synthetic strategy modified to the use of fluorinated starting materials.<sup>[237]</sup>

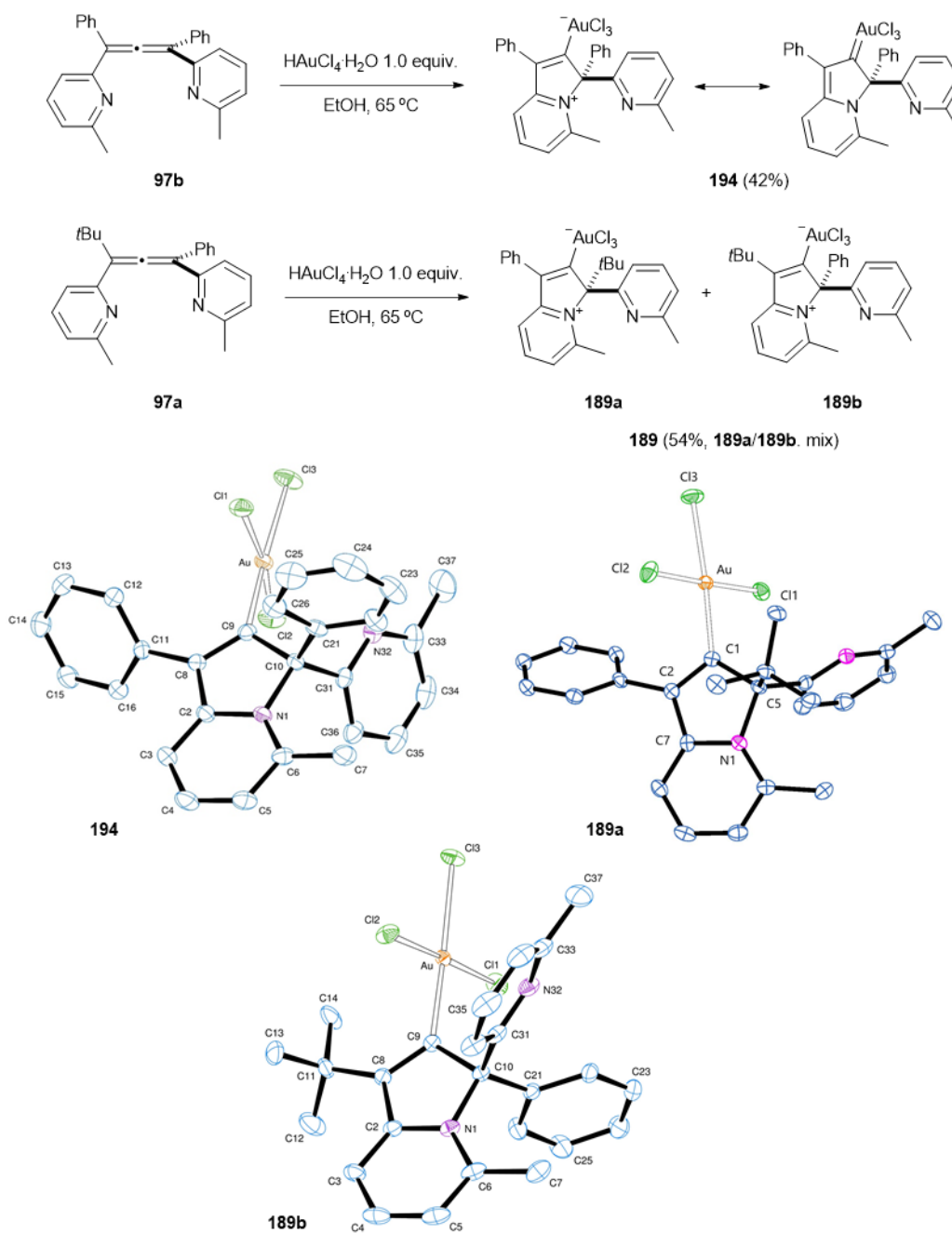
Then, I reacted ligand **97e** with 1 and 2 equivalents of (Me<sub>2</sub>S)AuCl and monitored the progress by <sup>1</sup>H and <sup>19</sup>F NMR spectroscopy (Scheme 76, a). Initial reaction at rt and then at elevated temperature always resulted in the recovery of unreacted starting materials even after several days. I observed similarly sluggish reactivity in the reaction with Au(III) salt (Scheme 76, b). This time, however, I could see very slow reaction of **97e** to a non-symmetric product, which could again arise from the pyridine cyclisation. Full characterisation of this product was not feasible due to very small quantities obtained. Symmetric bidentate complex **196** was never observed and even after 5 days of reaction ligand **97e** constituted over 50% of the reaction mixture.



**Scheme 76** Reaction of fluorinated bis(pyridyl)allene ligand **97e** with Au: a) with Au(I) precursor; b) with Au(III) precursor.

Deactivation of the pyridines by an inductive depletion of their electron density in the robust ligand **97e** proved not only to mostly thwart the nucleophilicity of the ligand but also completely stopped any metal coordination. More modifications will be needed to strike a finer balance between these two reactivities.

I accomplished the deliberate synthesis of Au(III) carbene-type complexes **189** and **194** in ethanol at 65 °C (Scheme 77). Full characterisation of **189** and **194** revealed many structural similarities with their Au(I) counterparts and recently reported Au(III)-indolizine compounds reported by Ho, Tse, Wong and co-workers obtained from propargyl pyridines.<sup>[238]</sup> The exact isomeric ratio of isolated products **189a/189b** was dependent on the reaction time. However, the ratio of the two species seemed to remain constant when left in solution for long periods of time (Figure 32).



**Scheme 77** Preparation of carbene-type Au(III) complexes **189** and **194** and ORTEP representation of their X-ray structures (Hs omitted, thermal ellipsoids drawn at 50% probability level).

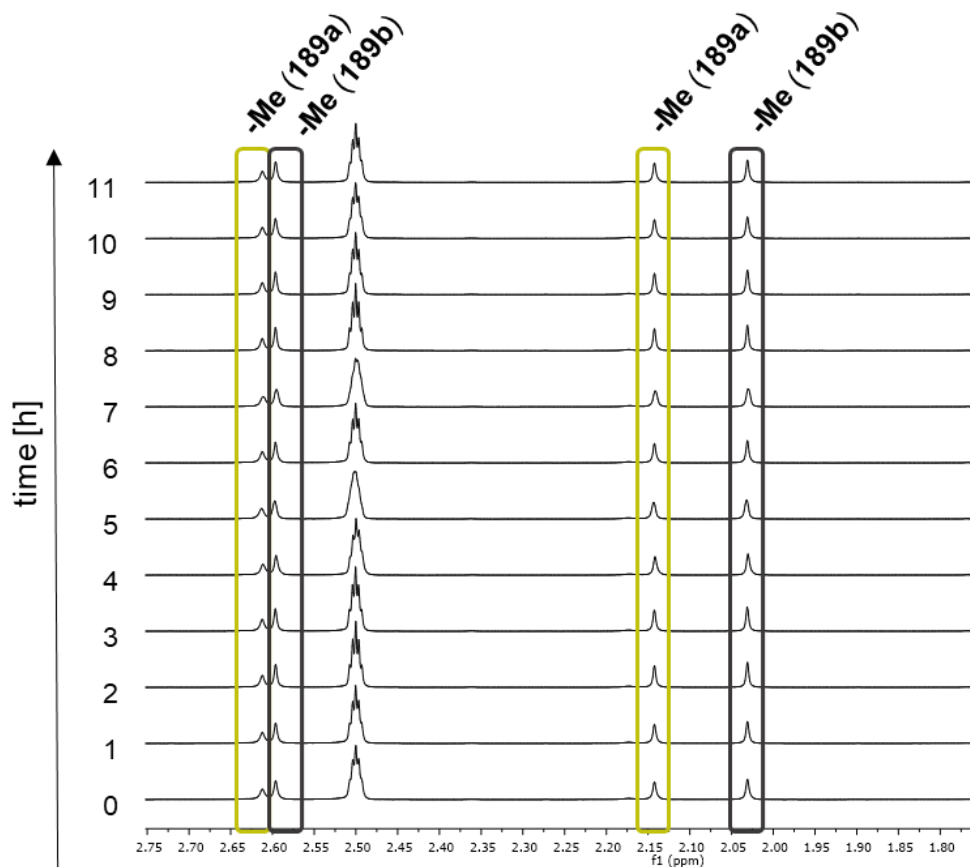


**Figure 32** Periodic  $^1\text{H}$  NMR experiment of the mixture **189a/189b**, expansion of aliphatic region 1.8-2.7 ppm.

All compounds with a carbene-type structure besides **187a** yielded good quality crystals that allowed us to collect the solid state data by X-ray diffraction. Contrarily, crystals of the complexes that were proposed to feature the original bis(pyridyl)allene motif were much more difficult to obtain. To induce better crystal packing and/or stabilise the less robust complexes featuring the allenes I attempted to exchange their counterions for anions such as  $\text{Ph}_4\text{B}^-$ ,  $\text{Tf}_2\text{N}^-$  or  $\text{TsO}^-$  due to their increased size and non-nucleophilic properties, but that strategy turned out to be ineffective. I also tried co-crystallisation methods with poly-halogenated compounds such as pentafluoriodobenzene. Such co-crystallisation partners have been found to promote crystallisation of halogen-containing species thanks to formation of halogen bonding.<sup>[239]</sup> Unfortunately, these attempts did not improve the quality of desired crystals. We tentatively assigned square planar geometry to both allene-supported complexes **193** and **195** and represent them as *trans* isomers in analogy to the Pd complexes.

Crystal structures of the Au carbene-type complexes are gathered in the Figure 33, with all the key solid-state parameters collected in Table 3.

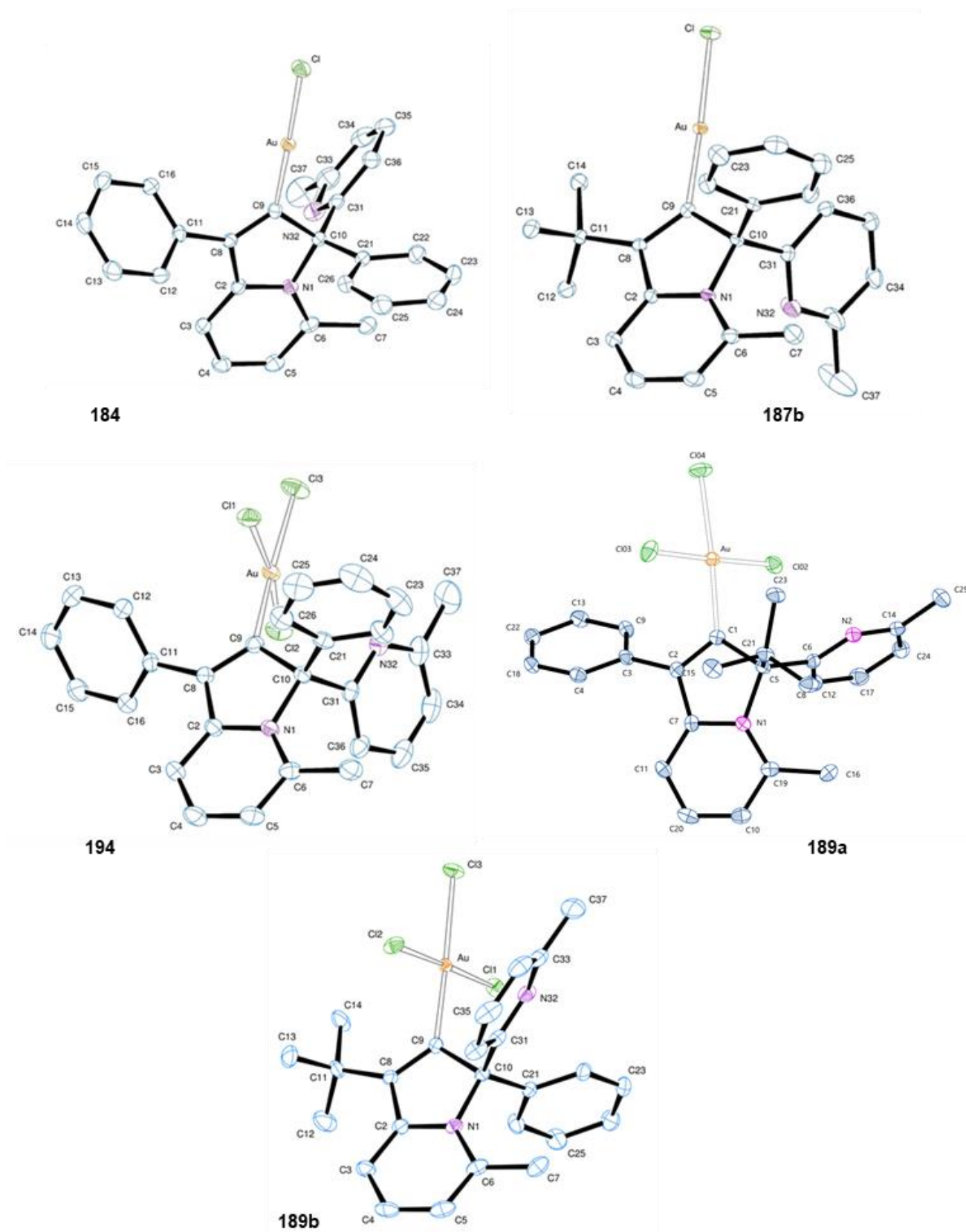


**Figure 33** ORTEP representation of X-ray structures of complexes **184**, **187b**, **194** and **189** (Hs omitted, thermal ellipsoids drawn at 50% probability level).

**Table 3** Selected crystallographic data for complexes **184**, **187b**, **194** and **189**.

	<b>184</b>	<b>187b</b>	<b>194</b>	<b>189a</b>	<b>189b</b>
X-ray source	Mo-K $\alpha$	Mo-K $\alpha$	Mo-K $\alpha$	Mo-K $\alpha$	Mo-K $\alpha$
Crystal system	Monoclinic	Tetragonal	Monoclinic	Monoclinic	Monoclinic
Space group	P 2 <sub>1</sub> /n	P 4 <sub>1</sub>	P 2 <sub>1</sub> /c	P 2 <sub>1</sub> /n	P 2 <sub>1</sub> /n
Au-C [Å]	1.986(3)	1.997(3)	2.004(2)	2.038(3)	2.020(2)
			(1) 2.2819(7)	(2) 2.2833(7)	(1) 2.2889(6)
Au-Cl [Å]	2.3031(7)	2.3068(7)	(2) 2.2900(7)	(3) 2.2869(8)	(2) 2.2927(6)
			(3) 2.3502(6)	(4) 2.3481(7)	(3) 2.3475(6)
C-Au-Cl angle [°]	177.29(8)	177.11(9)	176.99(7)	175.70(4)	176.95(7)
			C(1)-Au-Cl(1)	C(1)-Au-Cl(2)	C(9)-Au-Cl(1)
			88.94(7)	91.89(8)	91.79(7)
			C(1)-Au-Cl(3)	C(1)-Au-Cl(3)	C(9)-Au-Cl(2)
			89.13(7)	89.74(8)	86.94(7)
Selected angles [°]	-	-	Cl(1)-Au-Cl(2)	Cl(2)-Au-Cl(4)	Cl(1)-Au-Cl(3)
			90.93(2)	88.54(3)	91.26(2)
			Cl(3)-Au-Cl(2)	Cl(3)-Au-Cl(4)	Cl(2)-Au-Cl(3)
			91.42(2)	89.80(3)	90.01(2)
			Cl(1)-Au-Cl(3)	Cl(2)-Au-Cl(3)	Cl(1)-Au-Cl(2)
			171.72(2)	178.30(3)	178.41(2)

All the members of the new family of Au carbene-type compounds are built on a bicyclic indolizine-type core with Au atom bonded to a former central carbon atom of the allene that now neighbours a new stereogenic centre. As expected for Au(I) compounds the geometry around the metal centre was found to be close to linear (177.11(9) $^{\circ}$ -177.29(8) $^{\circ}$ ), whereas Au(III) compounds featured near square planar arrangement (e.g. please see selected angles in **194**, Table 3). Au(I)-C bond distances in **184** and **187b** of 1.986(3)-1.997(3) Å can be placed in a lower range of those reported for related Au(I) carbenes, for example they were comparable to Fensterbank's<sup>61</sup> **157a** and **157b** values of 1.993(4) Å and 1.984(2) Å, respectively. Whereas corresponding values in Au(I) vinyl compounds are typically significantly higher.<sup>[201,240–242]</sup> In case of Au(III) complexes, there are much fewer reports dealing with the synthesis of related systems. The Au-C distances in **194**, **189a** and **189b** found at 2.004(2)-2.038(3) Å were comparable to those reported by Ho, Tse, Wong and co-workers (1.993(5)-2.030 Å).<sup>[238]</sup> Additionally, when the Au(III)-C bond lengths of **194**, **189a** and **189b** are compared with better documented Au(III) (NHC)-carbenes they fit in the mid-range of

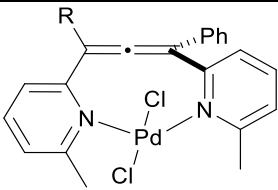
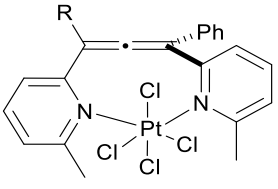
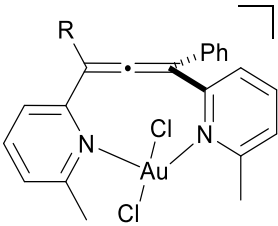
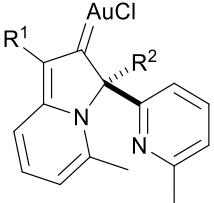
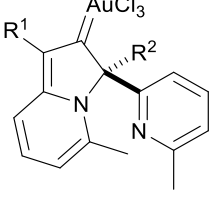
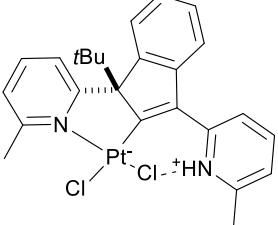


previously published values.<sup>[243–245]</sup> And these values are slightly shorter when juxtaposed with the reported Au(III)-vinyl bond distances.<sup>[246,247]</sup>

### **IV c. Conclusions**

The bis(pyridyl)allenes emerged as the most robust and versatile ligand candidates from the three main ligand architectures under investigation. The complexation studies revealed some discrepancy in the reactivity of different derivatives of bis(pyridyl)allene skeleton, pointing to the differences in their electronic and steric properties and/or bite angle values. We achieved not reported to date complexation of those ligands with Pd(II), Pt(IV), Pt(II), Au(I) and Au(III), affording a series of 11 (13 including isomers) novel metal complexes (Table 4). The trifluoromethyl-substituted ligand did not promote formation of the allene-containing complexes.

**Table 4** Summary of the novel allene-derived complexes prepared in the second stage of the project.

Entry	Complex	Section	Structure
allene-containing complexes	1	171-172	IV b. 2.
			 <p>171 R = Ph 172 R = <i>t</i>Bu</p>
	2	175-176	IV b. 3.
		 <p>175 R = Ph 176 R = <i>t</i>Bu</p>	
3	193,195	IV b. 4.	 <p>193 R = Ph 195 R = <i>t</i>Bu</p>
carbene-type complexes	4	184, 187a-b	IV b. 4.
			 <p>184 R<sup>1</sup> = R<sup>2</sup> = Ph 187a R<sup>1</sup> = Ph, R<sup>2</sup> = <i>t</i>Bu 187b R<sup>1</sup> = <i>t</i>Bu, R<sup>2</sup> = Ph</p>
	5	194, 189a-b	IV b. 4.
		 <p>194 R<sup>1</sup> = R<sup>2</sup> = Ph 189a R<sup>1</sup> = Ph, R<sup>2</sup> = <i>t</i>Bu 189b R<sup>1</sup> = <i>t</i>Bu, R<sup>2</sup> = Ph</p>	
6	179	IV b. 3.	 <p>179</p>

In general, the new complexes can be grouped in the two main classes, namely, allene-based bidentate complexes such as **171** or **175** (Table 4, entries 1-3) and allene-derived carbene-type compounds of **184** type (Table 4, entries 4-6). All new compounds were fully characterised and their properties were studied.

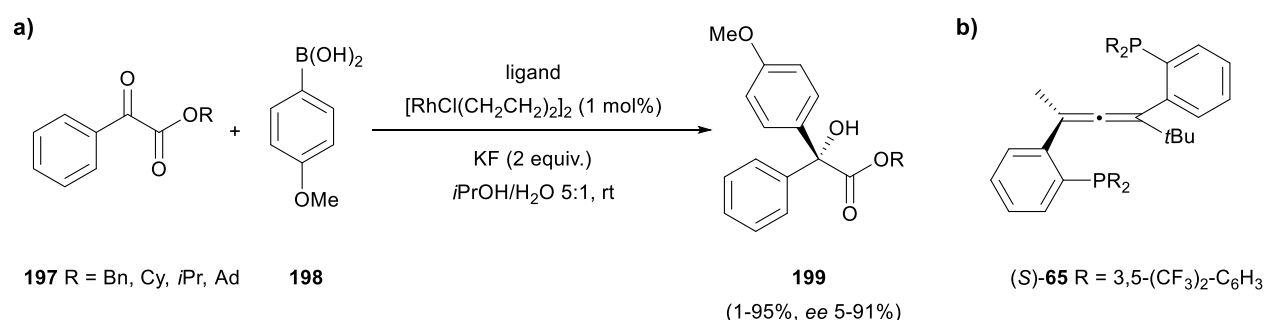
In the next chapters we will examine the first applications of all new metal complexes, starting with their use as catalysts in several benchmark reactions.

## V. Applications in catalysis

### V a. Introduction

The syntheses of novel allene-derived metal complexes have rarely been accompanied by the discussion of potential applications of such new systems (see Section IV a.). However, some authors recognised that the presence of (chiral) allene ligand(s) in a complex coupled with unique geometries of the final structures creates an interesting opportunity for (asymmetric) catalysis with these compounds. So far, the field of catalysis is the only area where these materials have been utilised and the applicability is very limited to date.

Thus, Ready and co-workers used their allene-containing phosphine ligands (see Section III a. 2.) in the Rh(I)-catalysed addition of arylboronic acids to  $\alpha$ -keto esters, as different phosphite ligands were already known to promote this transformation in asymmetric manner (Scheme 78, a).<sup>[151,248]</sup> The screening of different enantioenriched allene ligands, metal to ligand ratios and esters uncovered that, indeed, Rh(I)-allene species can promote the asymmetric formation of tertiary alcohols in the discussed reaction.

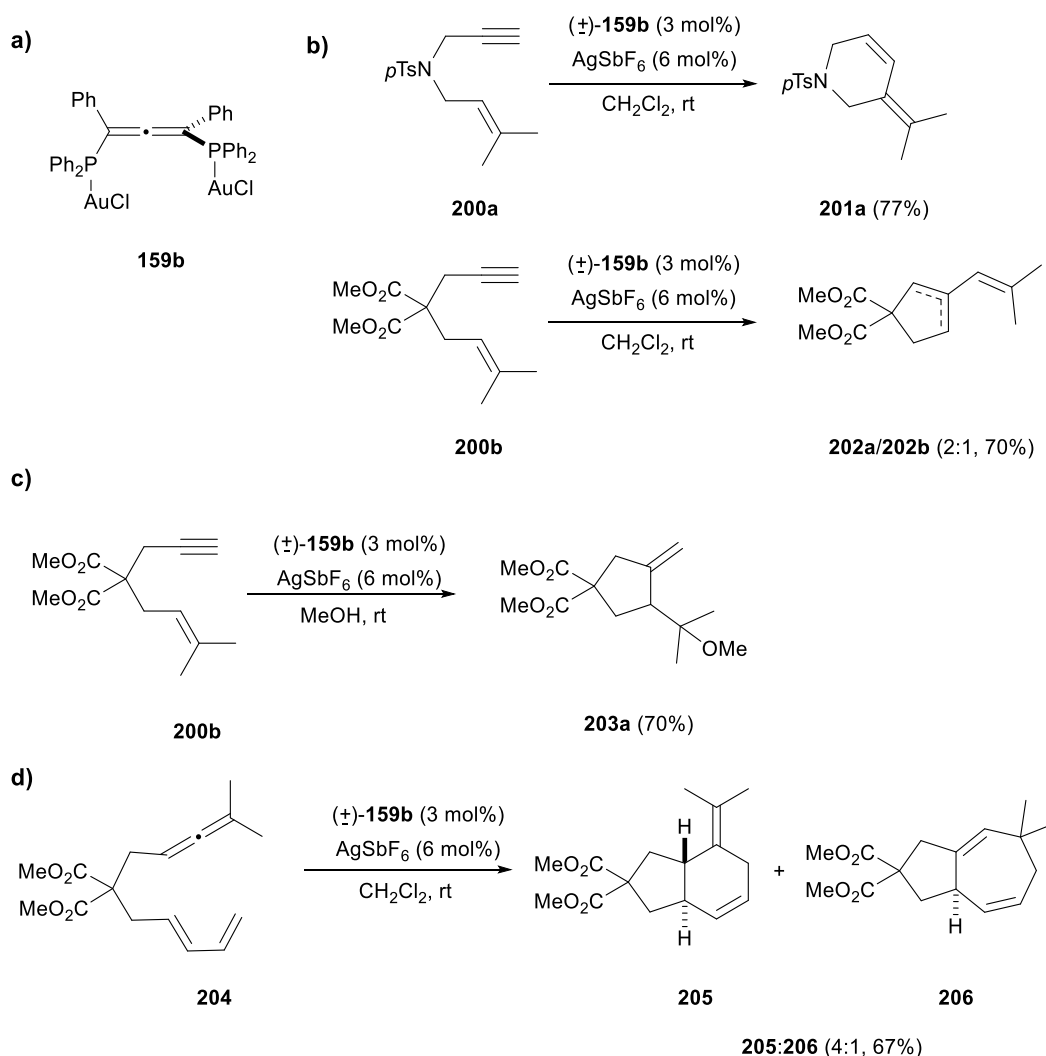


**Scheme 78** Rh(I)-catalysed addition of arylboronic acids to  $\alpha$ -keto esters: a) reaction scheme; b) best performing ligand.

The highest reactivity and stereoselectivity was achieved when cyclohexyl ester (**197**, R = Cy in Scheme 78, a) was reacted under a 1:1 catalytic system comprised of ligand **65** and the Rh(I) source yielding the corresponding alcohol in 95% yield and 91% ee. Monophosphine ligands proved to be much less selective than the bis(phosphine) congeners. Additional insights into the reaction were obtained from further screening of various derivatives of cyclohexyl  $\alpha$ -keto esters and aryl- and vinylboronic acids. In general, electron-deficient  $\alpha$ -keto esters and electron-rich arylboronic acids reacted most efficiently and with the best stereochemical control (41-98% yield, 48-95% ee).

Fensterbank and co-workers also tested the catalytic properties of their bis(phosphine)allene digold complex **159b** (Scheme 79, a).<sup>[157]</sup> First, they tested the racemic version, and they observed good reactivity in the cycloisomerisation of N- and C-tethered 1,6-

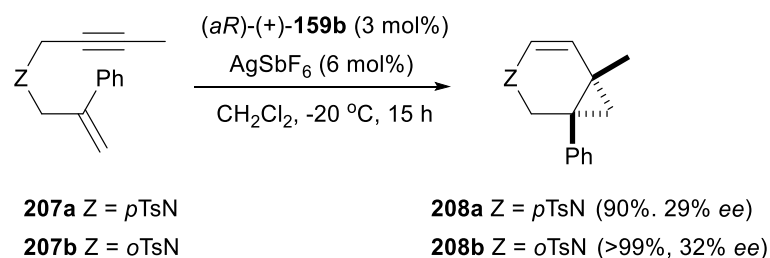
enyne using 3 mol% of the catalyst **159b** with 6 mol% of the Ag(I) salt in dichloromethane at room temperature (Scheme 79, b). When the reaction was carried out in methanol instead, the alkoxy cyclisation product **203a** was also formed in good yield (Scheme 79, c). However, previous use of simple phosphine cationic Au(I) complexes such as  $[(PPh_3)Au^+]$  at lower catalyst loadings at shorter reaction times gave similar or better yields and selectivity with these starting materials.<sup>[249]</sup> Other noteworthy reaction was the diene-allene activation of **204** resulting in two cycloadduct products, formal [4+2] compound **205** and [4+3] compound **206** generated in a 4:1 ratio (Scheme 79, d).



**Scheme 79** Reactions catalysed by Au(I) allene complex **159b**: a) structure of **159b**; b) cycloisomerisation of 1,6-enynes **200a-b**; c) alkoxy cyclisation of enyne **200b**; d) cycloaddition of diene-allene **204**.

Additionally, chiral HPLC resolution furnished complex **159** in enantiomerically pure form ( $ee \geq 98\%$ ). Enantiomer (*aR*)-(+)-**159b** was then evaluated only in the asymmetric version

of the cycloisomerisation of 1,6-enynes **207a** and **207b**, giving the corresponding bicyclic products **208a** and **208b** with high yields but only moderate enantioselectivity (Scheme 80).



**Scheme 80** Asymmetric cycloisomerisation of 1,6-enynes catalysed by (*aR*)-(+)-**159b**.

In terms of catalytic activity of carbene-type complexes characterised by a long range heteroatom stabilisation similar to complexes prepared in Chapter IV, to the best of our knowledge there are no relevant reports. However, different classes of carbene complexes, in particular Au carbenes, such as (NHC)- or (CAAC)-carbenes have been used as catalysts before in many chemical transformations and their reactivity has been reviewed.<sup>[230,250–254]</sup>

## V b. Results and Discussion

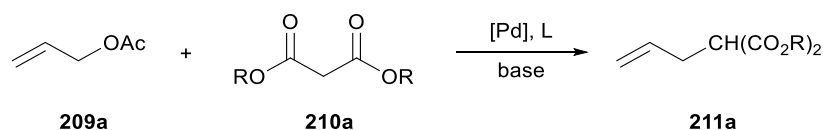
Chapter IV described the synthesis and characterisation of a small family of novel allene-derived metal complexes. Next, we present the studies exploring possible areas of application of these new compounds. The focus of this section is a preliminary examination of the catalytic activity of the new complexes in their racemic version. I tested their reactivity in a series of benchmark reactions that are commonly used in the evaluation of new catalytic systems. Pd complexes were employed in Tsuji-Trost allylic alkylation and Heck cross-coupling reactions. All complexes, but in particular Au- and Pt-ones, were also used to catalyse cycloisomerisation and alkoxy cyclisation of 1,6-enynes as well as nucleophilic addition to allenes.

Each section dedicated to a specific reaction commences with a brief overview of the transformation. The following experimental results are mostly divided into two categories to reflect the different character of the allene-containing and carbene-type complexes (see Chapter IV) and are compared to the state-of-the-art in the area.

### V b. 1. Tsuji-Trost reaction

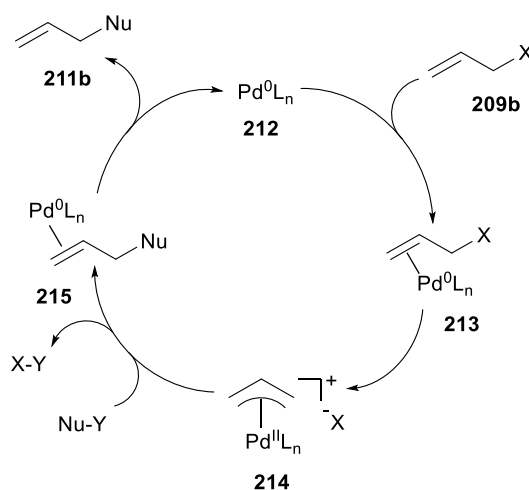
Tsuji-Trost reaction, also known as Tsuji-Trost allylation or Tsuji-Trost allylic substitution, was discovered in the Tsuji laboratory and later extended to the asymmetric variant by Trost and co-workers.<sup>[255,256]</sup> This metal-catalysed transformation typically involves the reaction of LG-containing allylic substrates and activated nucleophiles. The classic example of the Tsuji-Trost allylation is a reaction of allylic acetates with malonate-derived enolates under Pd catalysis

(Scheme 81). In fact, Pd-based catalytic systems are the most extensively studied in the context of the Tsuji-Trost reaction.



**Scheme 81** Example of Tsuji-Trost allylation.

The generally accepted mechanism for Pd-catalysed allylic substitution with “soft” nucleophiles is shown in Scheme 82. The catalytic cycle starts with Pd(0) species **212** pre-coordinating to allylic starting material **209b** resulting in a formation of  $\eta^2$  complex **213**. **213** undergoes an oxidative addition affording key  $\eta^3$  allyl Pd(II) complex **214**. In this step, the leaving group is expelled with inversion of configuration. Typically, electron-rich Pd species are necessary to facilitate the oxidative addition step and thus donor ligands such as phosphines are commonly used. Nucleophilic attack on **214** *anti* to the metal fragment forms another  $\eta^2$  complex **215** that after a de-association of Pd(0) $L_n$  from the olefin gives product **211b** and closes the catalytic cycle. Overall, the reaction proceeds with a net retention of configuration. Conversely, in the case of “hard” nucleophiles, inversion of configuration is observed. These nucleophiles attack the metal centre directly and in the reductive elimination step are transferred to the same face of the alkene from the metal fragment.

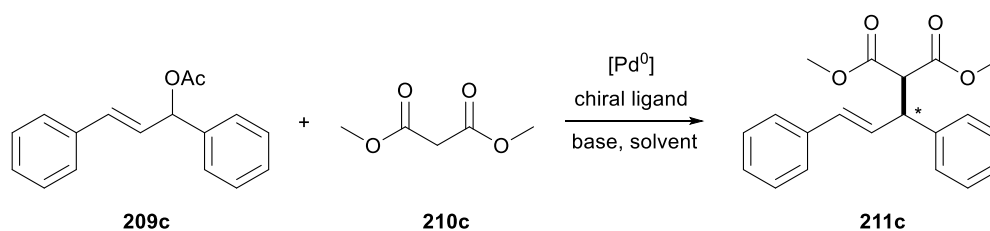


**Scheme 82** Accepted catalytic cycle for Pd-catalysed allylic substitution with “soft” nucleophiles.

The scope of the reaction typically encompasses allyl halides, acetates, carbonates, carboxylates or alcohols among others. The nucleophiles are usually stabilised carbon nucleophiles, such as aldehydes and ketones in their enolate, silyl enol or enamine form. The Pd(0) source can be used directly, although *in situ* reduction of Pd(II) catalysts is also effective.

There are two possible sites of nucleophilic attack in unsymmetrically substituted allylic substrates and the resulting  $\eta^3$  allyl complexes. Sometimes a mixture of regioisomers is obtained. The factors governing the regiochemistry of the reaction include both steric and electronic effects and the interplay of the allyl electrophile, nucleophile and ancillary ligands character. The strategies developed to achieve regiocontrol include use of intramolecular directing groups or tailored-made ligands.<sup>[257,258]</sup>

The enantioselective variant of the reaction, asymmetric allylic alkylation (AAA), has been studied extensively.<sup>[259]</sup> The enantio-discriminating step in the AAA reaction can be either the oxidative addition or the nucleophilic attack step. The former is operating when interconversion of the diastereomeric  $\pi$ -allyl complex is slower compared to the subsequent nucleophilic attack. For example, chiral catalyst can preferentially select one of the enantiotopic faces of the olefin. For symmetric, achiral  $\pi$ -allyl complexes the asymmetric induction can be guided by the presence of chiral ligands that differentiate the two termini of the allyl fragment for the nucleophilic attack step with coupled regio- and enantiocontrol. In particular, AAA benchmark reaction of 1,3-diphenylallyl acetate and dimethyl malonate (Scheme 83) is now a standard method used to assess the efficiency of asymmetric induction of newly developed chiral ligands, including pyridine-based ligands.<sup>[260,261]</sup>



**Scheme 83** Benchmark Tsuji-Trost reaction used to evaluate new chiral ligands.

I began the investigation with this standard reaction setup using 5 mol% catalyst loading (Table 5). First, I established a reference point with a reaction of a standard catalytic system  $[Pd(allyl)Cl]_2/PPh_3$  (Table 5, entry 1). Next, I used the same Pd precursor in the presence of the symmetric bis(pyridyl)allene ligand **97b** (Table 5, entry 2), however I did not observe any product formation.



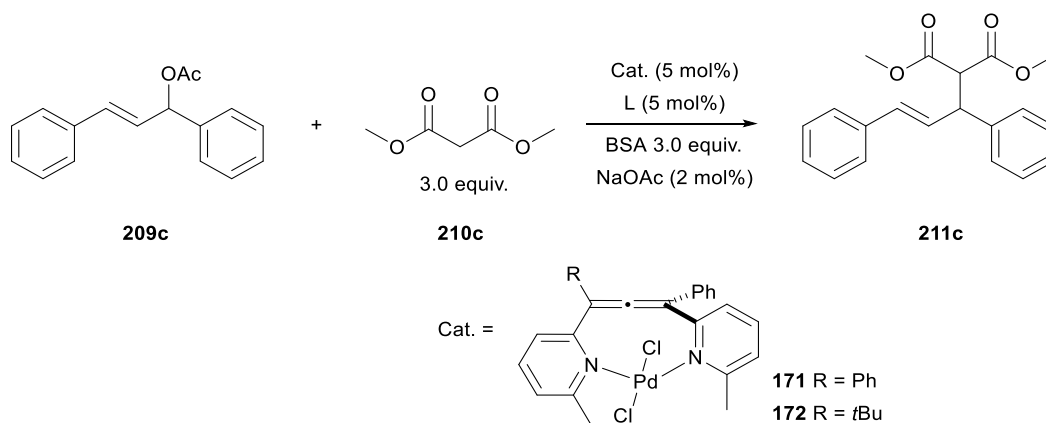
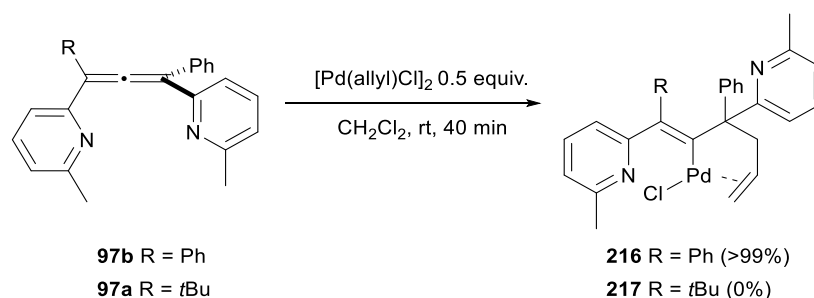


**Table 5** Model Tsuji-Trost reaction with allene-derived Pd catalysts.

Entry	Cat.	L	solvent	T (°C)	additives	Yield (%)
1	[Pd(allyl)Cl] <sub>2</sub>	PPh <sub>3</sub> <sup>a</sup>	CH <sub>2</sub> Cl <sub>2</sub>	rt	-	60
2	[Pd(allyl)Cl] <sub>2</sub>	<b>97b</b>	CH <sub>2</sub> Cl <sub>2</sub>	rt	-	-
3	<b>171</b>	-	CH <sub>2</sub> Cl <sub>2</sub>	rt	-	-
4	<b>171</b>	-	CH <sub>2</sub> Cl <sub>2</sub>	rt	NEt <sub>3</sub> <sup>b,c</sup>	-
5	<b>171</b>	-	CH <sub>2</sub> Cl <sub>2</sub>	38	HCO <sub>2</sub> NH <sub>4</sub>	-
6	<b>171</b>	-	THF	64	HCO <sub>2</sub> NH <sub>4</sub>	-
7	<b>172</b>	-	CH <sub>2</sub> Cl <sub>2</sub>	38	HCO <sub>2</sub> NH <sub>4</sub>	-

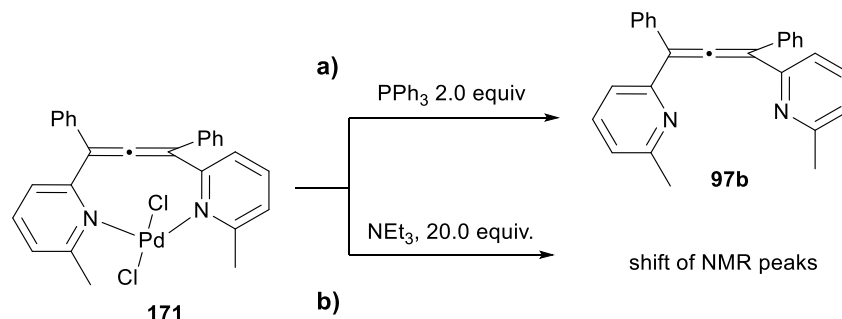
<sup>a</sup> 10 mol%. <sup>b</sup> 1.0 equiv. <sup>c</sup> [Pd] and NEt<sub>3</sub> mix beforehand.

In order to study the coordination of the ligand **97b** and [Pd(allyl)Cl]<sub>2</sub>, I carried out a stoichiometric reaction between these reagents (Scheme 84). Analysis of the quantitatively formed product **216** revealed that the allene underwent an alkylation with an allyl fragment present in the original Pd complex. Additionally, Pd which initially activated the allene, stayed bonded to the former central carbon atom (<sup>13</sup>C NMR peak of that carbon atom moved upfield to 183.3 ppm, Δδ = -29.4 ppm with respect to the allene ligand). This result confirmed the previous observation (see Section IV b. 1.) that formation of allene-containing Pd complexes requires presence of neutral accompanying ligands on the Pd precursor, and explains the lack of reactivity encountered in the alkylation reaction under these conditions (entry 2, Table 5). Ligand **97a** did not show any reactivity in the presence of stoichiometric amount of [Pd(allyl)Cl]<sub>2</sub> (Scheme 84). The lack of reactivity or loss of the allene integrity indicated that the *in situ* catalyst formation was not an effective strategy for this reaction.



**Scheme 84** Stoichiometric reaction between bis(pyridyl)allenes and  $[\text{Pd}(\text{allyl})\text{Cl}]_2$ .

Subsequently, preformed complex **171** was tested under the reaction conditions (Table 5, entry 3), but it was not active. To probe if the inactivity resulted from insufficient reduction of **171** to the active Pd(0) species needed to start the catalytic cycle, I reacted it under common conditions used to facilitate the reduction of Pd(II) catalysts in various cross-coupling reactions. Thus, in the reaction with  $\text{PPh}_3$  I detected the presence of the free allene ligand **97b** and concluded that it was being replaced in the Pd coordination sphere by the phosphine ligands (Scheme 85, a). The reaction with large excess of  $\text{NEt}_3$  (Scheme 85, b) showed slight shift of peaks corresponding to **171** on the  $^1\text{H}$  NMR spectrum, but overall the main features of the complex were maintained. **171** was then used in the Tsuji-Trost reaction in the presence of  $\text{NEt}_3$ , but its activity did not improve (Table 5, entry 4).



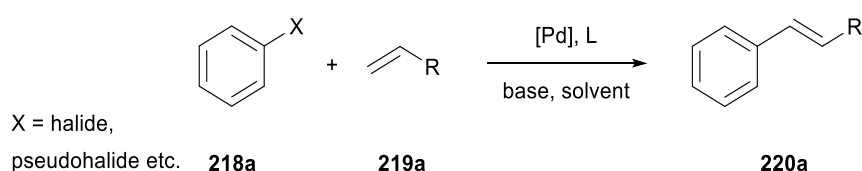
**Scheme 85** **171** under reduction conditions.

Use of additives such as ammonium formate has been shown to improve the reduction of Pd(II) pre-catalysts. However, allylic alkylation with **171** in the presence of  $\text{HCOONH}_4$  in refluxing  $\text{CH}_2\text{Cl}_2$  and THF was unsuccessful (Table 5, entries 5-6). I obtained similar result when non-symmetric complex **172** was used (Table 5, entry 7).

Either problems with the Pd(II)/Pd(0) reduction or perhaps with oxidative addition with allylic substrates might have caused the inactivity of **171** and **172** in the Tsuji-Trost alkylation. I therefore abandoned this route to focus on another important Pd-catalysed reaction.

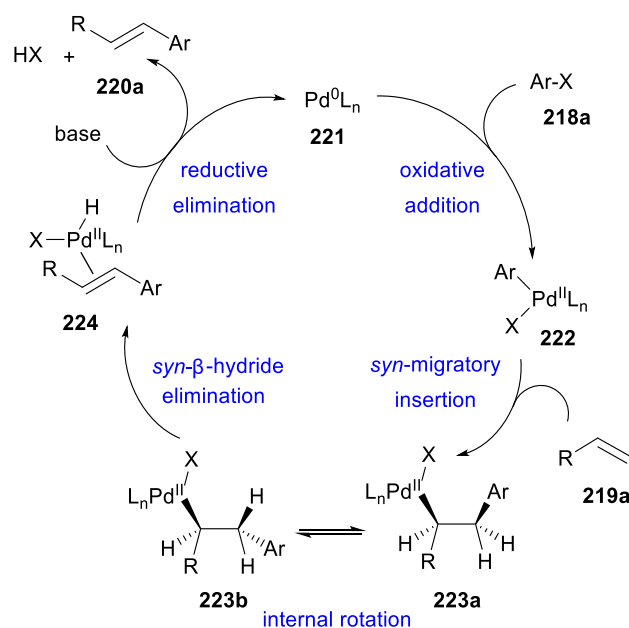
### V b. 2. Mizoroki-Heck cross-coupling reaction

Mizoroki-Heck reaction is a metal-catalysed C-C bond forming reaction, typically occurring between aryl- or vinyl halides and olefinic coupling partners (Scheme 86).<sup>[262,263]</sup> The usefulness and widespread applications of Pd-catalysed cross-coupling reactions, including the Mizoroki-Heck reaction, was recognised with the 2010 Nobel prize awarded to the pioneers in the area: R. Heck, E.-i. Negishi, and A. Suzuki.<sup>[264]</sup> Since the discovery in 1970s, the reaction has been extensively studied and improved. Some of these developments include expansion of the substrate scope beyond traditional aryl(vinyl) iodides and bromides to the so-called “pseudohalides”, such as triflates, sulfonates or diazonium salts. Moreover, milder reaction conditions have been established with decreased catalyst loadings and combination of numerous ligands. The transformation takes place predominantly between  $sp^2$ - $sp^2$  centres under Pd-catalysis. Ni-, Cu- or Rh-catalysis has also been reported.



**Scheme 86** General scheme of Mizoroki-Heck coupling.

The accepted mechanism of the Mizoroki-Heck reaction is depicted in Scheme 87. The first step in the catalytic cycle, oxidative addition, is the same as in other cross-coupling reactions (Suzuki-Miyaura, Sonogashira *etc.*). However, for Mizoroki-Heck coupling, the following steps of the mechanism differ from other cross-couplings. The cycle starts with the insertion of Pd(0) active catalytic species, sometimes after prior reduction from Pd(II) species *in situ*, into aryl(vinyl) halogen bond to form  $\sigma$ -aryl Pd(II) complex **222**. The alkene coupling partner **219a** coordinates to this Pd(II) species and undergoes insertion into Pd-C bond in a *syn* manner resulting in **223a**. The regioselectivity of this step is dictated by the character of the catalyst, the olefin and the reaction conditions. Internal rotation of **223a** sets it in the required conformation for the following *syn*- $\beta$ -hydride elimination regenerating the double bond and affording **224**. Sometimes a mixture of products results due to different stereochemical outcomes of the reaction, but for monosubstituted alkenes usually the *E* isomer of the final product is formed. Finally, base-assisted reductive elimination releases the alkene product **220a** and Pd(0) species that can begin the next turnover. The base is used stoichiometrically to facilitate the reduction and neutralise the generated equivalent of HX.



**Scheme 87** Accepted catalytic cycle for Mizoroki-Heck coupling.

High functional group tolerance and development of new intriguing variants of the reaction, e.g. intramolecular, asymmetric versions, contributed to quick acceptance of this methodology by the chemistry community. Mizoroki-Heck coupling became one of the methods of choice for complex synthetic problems, such as the total synthesis of natural products.<sup>[265]</sup> It is also extensively used in the industry, together with other C-C and C-X (X-heteroatom) bond-forming couplings.<sup>[266,267]</sup>

The catalytic asymmetric variant of the reaction was first disclosed in 1989 in the independent reports from groups of Shibasaki and Overman that demonstrated the use of chiral ligands for asymmetric induction in molecules containing prochiral centres.<sup>[268,269]</sup> The presence of the chiral influence allowed to differentiate between two “enantiofaces” of the alkene and resulted in preferential delivery of the metal fragment to one of them. The enantiotopic faces of the prochiral olefin are called *pro-S* or *pro-R* depending on which enantiomer is formed following the catalyst insertion and  $\beta$ -elimination. The best enantiocontrol is usually observed in more rigid systems. Ligands related to  $C_2$ -symmetric BINAP class perform well in this transformation and achieve formation of demanding tertiary and quaternary, including all carbon, stereogenic centres in poly- and spirocyclic products (Figure 34).<sup>[270]</sup> The asymmetric Mizorki-Heck reaction is also often used to evaluate new chiral ligands.

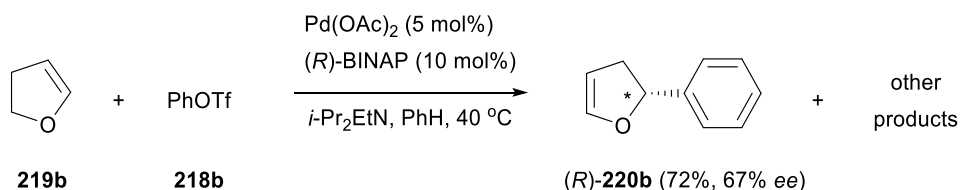


**Figure 34** Example of asymmetric Mizoroki-Heck reaction.<sup>[271]</sup>

I chose a standard coupling between styrene and aryl halides for the evaluation of new allene-derived Pd complexes in the Mizoroki-Heck coupling (Table 6). The reaction was performed under typical conditions with 2 mol% catalyst loading.

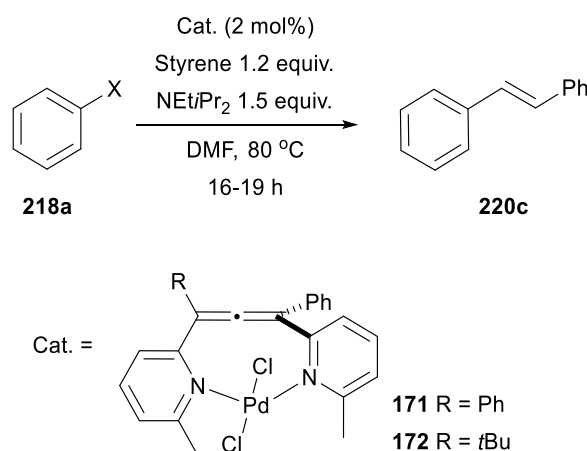


**Table 6** Mizoroki-Heck cross-coupling with allene-derived Pd catalysts.

Entry	Cat.	X	Additives	Yield (%)
1	<b>171</b>	I	$\text{HCO}_2\text{NH}_4^a$	87
2	<b>171</b>	I	-	93
3	<b>171</b>	Br	-	20
4	<b>172</b>	I	-	36
5	<b>172</b>	Br	-	-

<sup>a</sup> 10 mol%.

I observed a formation of (*E*)-stilbene **220c** in the reaction with iodobenzene catalysed by bis(phenyl)complex **171**. The use of additives ( $\text{HCO}_2\text{NH}_4$ ) was not necessary to obtain an excellent yield of the product (Table 6, entry 1 vs entry 2). The activity of **171** was substantially diminished in a reaction with bromobenzene (Table 6, entry 3). Non-symmetric complex **172** was less active giving only moderate yield of the product in the reaction with PhI (36% yield, Table 6, entry 4) and showing no activity in the coupling with PhBr (Table 6, entry 5).

Formation of the coupling product indicated that both catalysts were capable of undergoing the required Pd(II) reduction activation step as well as oxidative addition with aryl halides. It seems that more reactive coupling partners such as iodobenzene are needed to achieve best activity, which also would explain the lack of reactivity in the allylic alkylation

reaction mentioned in the previous section. The difference of activity between the two catalyst could be attributed, for example, to the steric bulk near the catalytic centre. The access of starting materials might be more hindered for the *t*-butyl substituted complex. We could also explain the discrepancy if we consider complex **171** to be in fact predominantly *cis* rather than *trans* like **172**. Although in other cross-coupling reactions the *cis* arrangement of the catalyst is necessary to complete the catalytic cycle through reductive elimination releasing the coupling product, there is no such requirement in Mizoroki-Heck coupling where the product is formed in the  $\beta$ -elimination step. In fact, *trans* complexes of Pd have been found to perform well in Mizoroki-Heck reaction.<sup>[272,273]</sup> Although, when directly compared to the *cis* congeners, the *trans* catalysts sometimes require longer induction periods and are thus less active.<sup>[272]</sup> The presumed *cis* isomer of the Pd catalyst might be more active, especially in the oxidative addition step, supporting a reasonable explanation of the different reactivity encountered in our complexes.

Although further tuning of the catalyst design is needed to increase the activity with more challenging substrates, we presented the first example of allene-derived catalytic system used in such an important process that could open further research and developments also in the asymmetric version.

### V b. 3. Cyclisation and alkoxy cyclisation of 1,6-enynes

Transition metal-catalysed carbocyclisation of enynes is a good method of accessing a wide variety of carbo-, hetero- and polycyclic products.<sup>[274–277]</sup> The reaction is based on activation of the acetylene fragment of an enyne (see Section I b.) in the presence of transition metals (Figure 35).

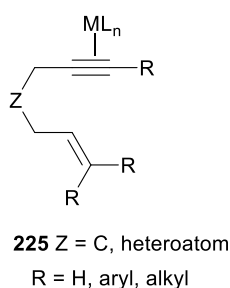
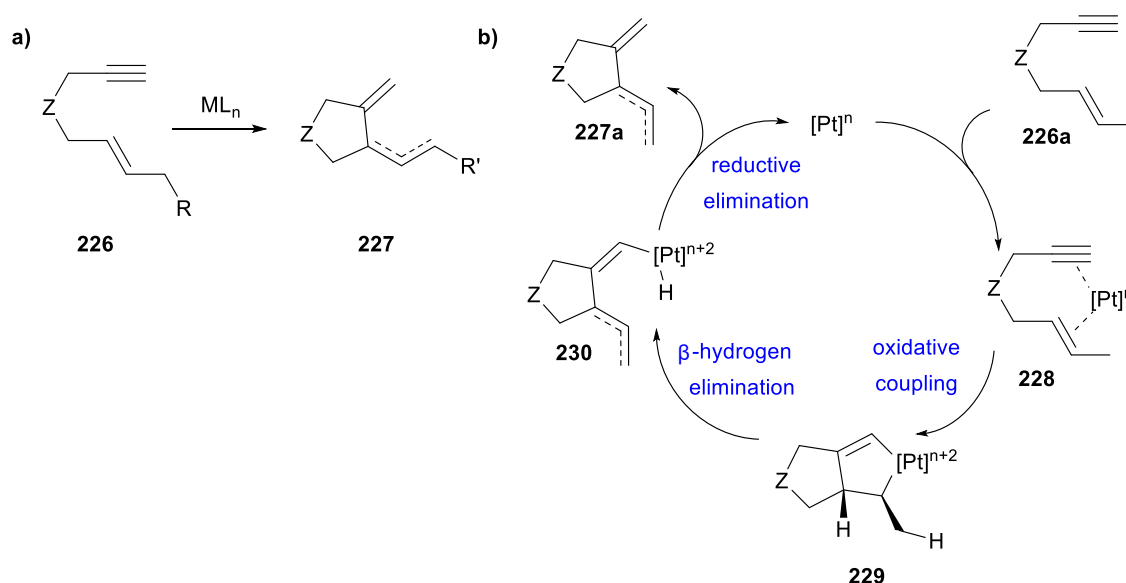


**Figure 35** Activation of enynes by transition metals.

A variety of catalysts have been explored in this transformation, for example complexes of Pd, Ru, Co, Ni, Pt,<sup>[278,279]</sup> but perhaps the most extensively studied is cationic Au(I) catalysis. Depending on the type of enyne used and the character of the catalyst, the cyclisation can operate under different mechanisms, yielding structurally varied products. The main mechanistic pathways in enyne cyclisations have been grouped as Alder-ene type

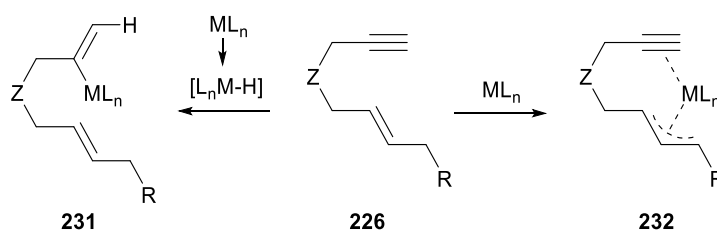
cycloisomerisation, skeletal rearrangements or cyclopropanations. These reaction variants alongside a special case of enyne alkoxy cyclisation are briefly presented below for 1,6-enynes.

Alder-ene type cycloisomerisation of 1,6-enynes (Scheme 88, a) proceeds *via* different mechanisms depending on the metal complex used. For example,  $\text{PtCl}_2$  catalysed reactions are proposed to go through key metallacycle intermediates **229** (Scheme 88, b).<sup>[275]</sup> First, the catalyst coordinates simultaneously to both unsaturations of the enyne to undergo oxidative cyclometallation affording **229**. Then, a vinyl metal complex **230** is formed by  $\beta$ -hydrogen elimination from one of the C-H bonds *cis* to the C-M bond. Finally, reductive elimination of **230** releases the cyclic diene product **227a** and regenerates the active catalyst.



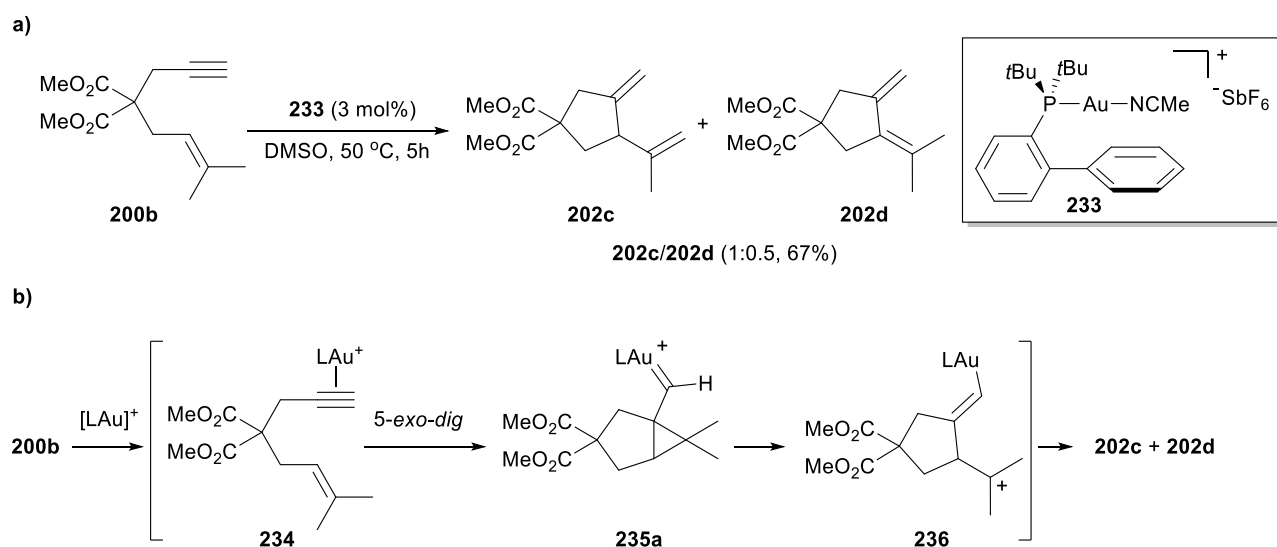
**Scheme 88** Alder-ene type cycloisomerisation of 1,6-enynes: a) general reaction scheme; b) catalytic cycle proposed for  $\text{PtCl}_2$  catalysis.

Other mechanisms for Alder-ene type reactions invoke vinyl-metal intermediates **231** (Scheme 89, left) derived from hydrometallation of the alkyne by metal hydride species, for instance generated *in situ* Pd or Ru hydrides.<sup>[280,281]</sup> Reactions with  $\pi$ -allylmetal complexes of type **232** (Scheme 89, right) proposed as intermediates are less common.



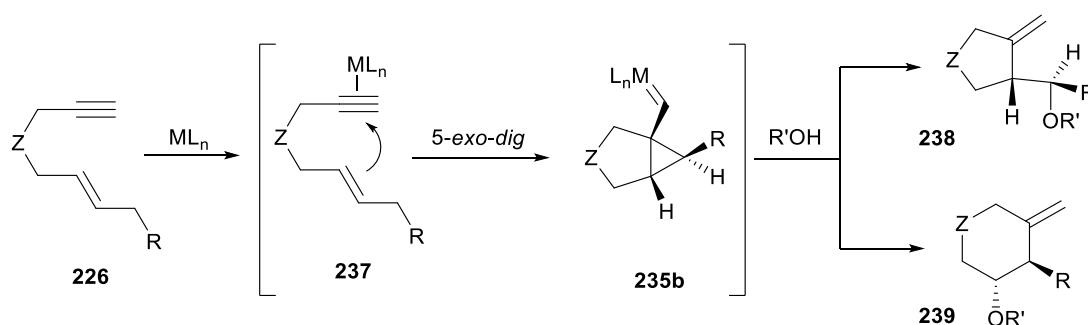
**Scheme 89** Alder-ene type cycloisomerisation *via*: vinyl-metal intermediates (left),  $\pi$ -allylmetal intermediate (right).

Interestingly, formal Alder-ene type cycloisomerisation products have also been observed in reactions catalysed by Au(I) complexes. Cyclisation of enyne **200b** afforded dienes **202c** and **202d** with 3 mol% of Au(I) phosphine catalyst **233** (Scheme 90, a).<sup>[282]</sup> However, the inability of Au(I) species to concurrently coordinate both alkyne and alkene groups makes the Alder-ene mechanism less likely. In those cases, it is suggested that the reaction goes *via* carbene intermediate **235a** obtained from 5-*exo-dig* ring closure of alkyne-coordinated complex **234** (Scheme 90, b). Ring-opening of **235a** and subsequent proton loss forms products **202c** and **202d**.



**Scheme 90** Au(I)-catalysed cycloisomerisation of enyne **200b**: a) Alder-ene products **202c/202d**; b) proposed mechanism for formation of **202c/202d** *via* carbene intermediate **235a**.

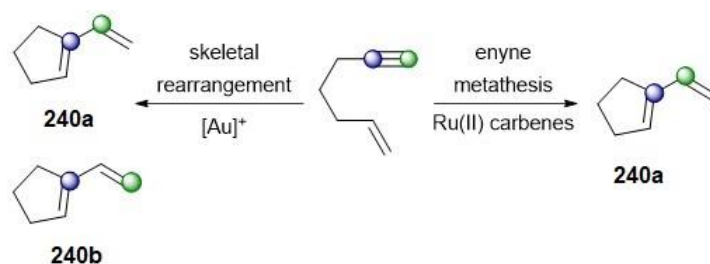
In fact, in the presence of nucleophiles such as water or alcohols, 1,6-enynes have been reported to react *via* cyclopropyl metal carbenes like **235b** to give five- or six-membered ring cyclisation/addition products (Scheme 91).<sup>[275]</sup> Inter- and intramolecular hydroxy- and alkoxy-cyclisations can be catalysed by Pt(II) or Pd(II) complexes,<sup>[283,284]</sup> although the most efficient are again Au(I)-catalysed processes.<sup>[249,275,282]</sup> The reaction is stereospecific and examples of the enantioselective version have been developed.<sup>[283,285]</sup>



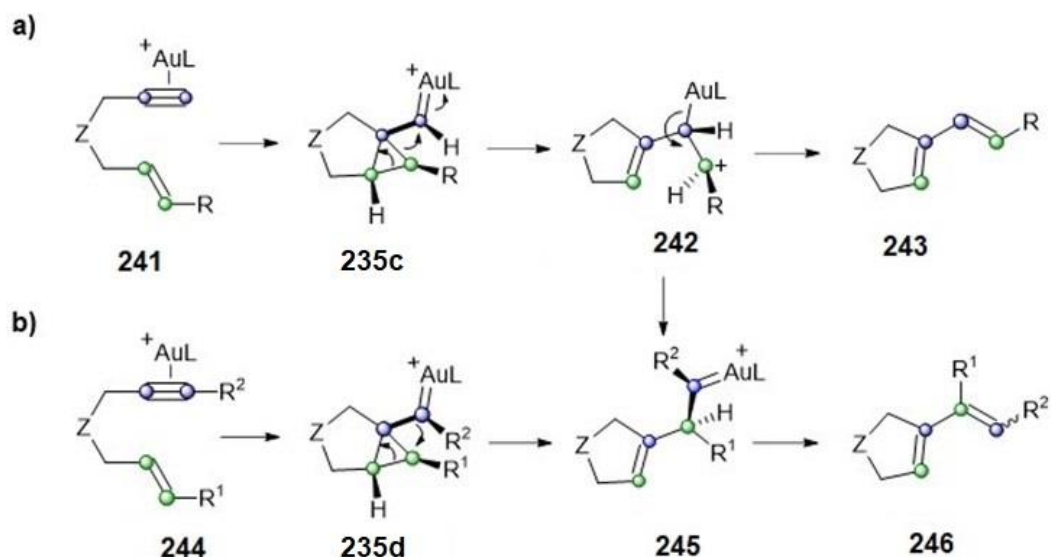


**Scheme 91** Alkoxy cyclisation of 1,6-enynes *via* carbene intermediates.

Skeletal rearrangement of 1,6-enynes is an important, atom-economic method for the synthesis of vinylcycloalkenes.<sup>[286]</sup> Two distinct reaction mechanisms have been uncovered for this transformation (Scheme 92).<sup>[274]</sup> With metal-carbene complexes the reaction proceeds by enyne metathesis mechanism. For example, Grubbs Ru(II) carbenes have been used in such way.<sup>[287]</sup> A second intramolecular mechanism was proposed for electrophilic metal complexes. This type of skeletal rearrangement is believed to yield two types of products, **240a** and **240b**, the latter with disrupted connectivity of the original carbon atoms of the acetylene moiety (Scheme 92).

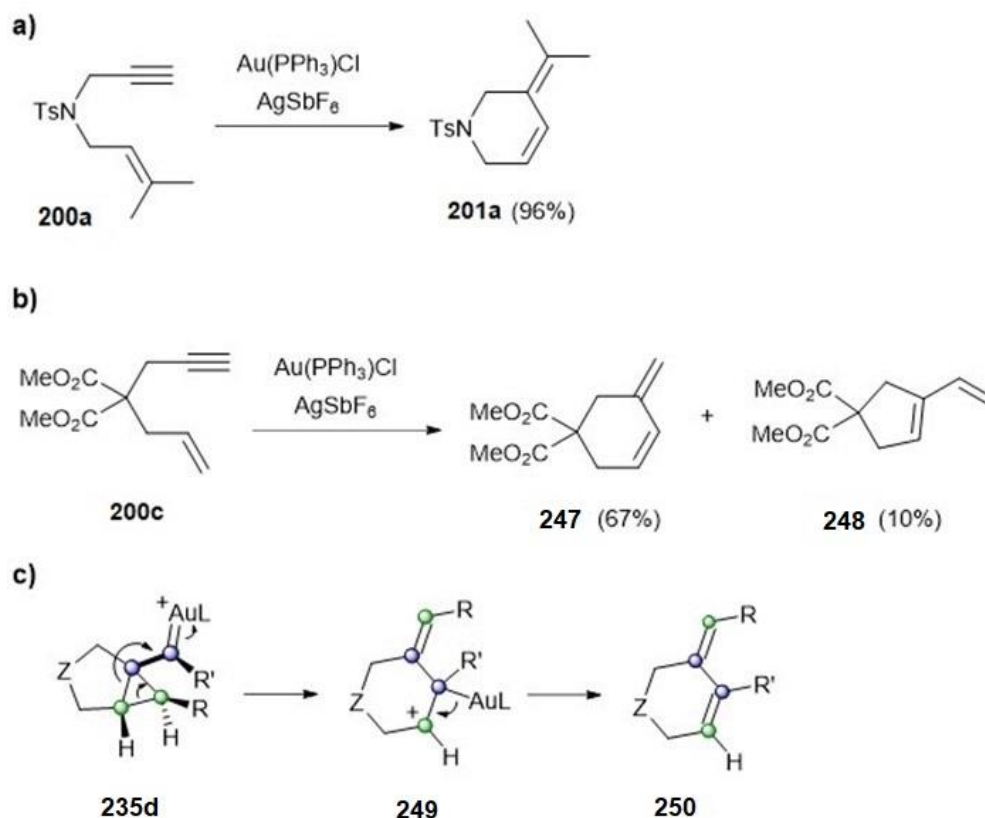
**Scheme 92** Skeletal rearrangement of 1,6-enynes.

Formation of type **240a** diene involves single cleavage of the double bond, whereas type **240b** product derives from double cleavage of the alkene and alkyne bonds. For example, for Au(I) catalysts, it has been proposed that the single cleavage mechanism goes *via* cyclopropyl Au carbene intermediate **235c** (see Scheme 91).<sup>[275]</sup> The following formation of the carbocation **242** and loss of the metal generates 1,3-diene **243** (Scheme 93, a). In the double cleavage mechanism under the same catalysis the initially formed carbene intermediate **235d** is believed to undergo dyotropic rearrangement<sup>[288]</sup> to another carbene species **245** (Scheme 93, b). After  $\alpha$ -hydrogen loss and protodemetalation, **245** would form final product **246**. The generation of **245** can also be explained by carbocationic 1,2-shift of the cyclic fragment in **242**.



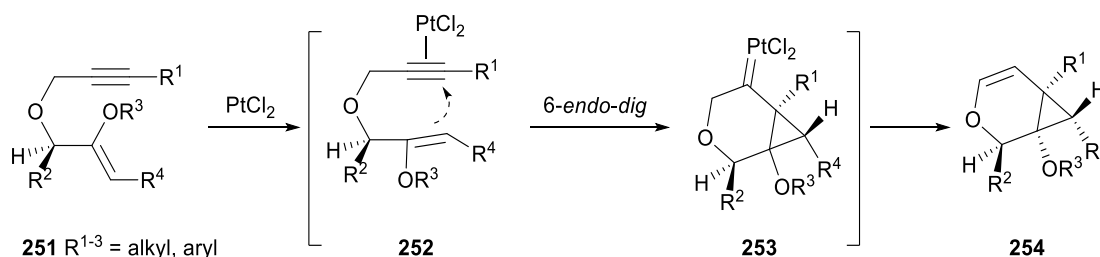
**Scheme 93** Skeletal rearrangement *via*: a) single cleavage mechanism; b) double cleavage mechanism.

Interestingly, skeletal rearrangement to six-membered products (**201a**, **247**) is also observed when the reaction proceeds by an *endo-dig* pathway. Depending on the substrates and the nature of the catalyst the reaction can be selective towards the six-membered cyclic products or give a mixture with the five-membered *exo* rearrangement products (Scheme 94, a-b).<sup>[249]</sup> Labelling experiments revealed that type **250** products are formed intramolecularly with a terminal carbon atom of the double bond of the enyne bonded to the internal carbon of the former triple bond in the product (Scheme 94, c).<sup>[289]</sup> This mechanism is related to the single cleavage mechanism in the Scheme 93.



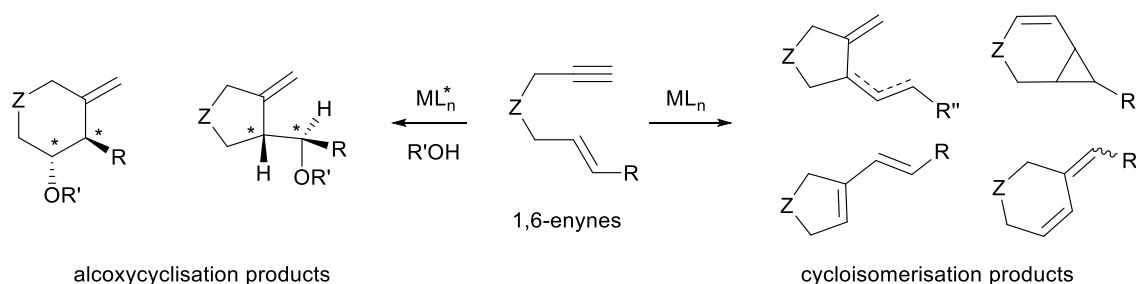
**Scheme 94** Formation of six-membered products in skeletal rearrangement of 1,6-enynes.

Carbocyclisation of heteroatom-tethered (O, N) 1,6-enynes catalysed by Pt was found to produce fused, cyclopropane bicycles. [290–292] For example, Echavarren and co-workers described cyclisation of enynes **251** under PtCl<sub>2</sub> catalysis that exclusively afforded bicyclic ethers of type **254** (Scheme 95). [292] The authors proposed that the reaction involved stereoselective 6-*endo-dig* cyclisation of η<sup>2</sup> complex **252** to Pt carbene **253**, that after β-hydrogen elimination, gave the observed products **254**.



**Scheme 95** Cycloisomerisation of 1,6-enynes to cyclopropane bicyclic products.

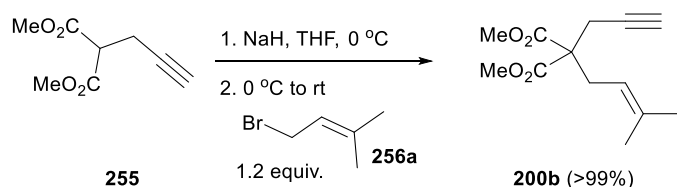
The summary of possible outcomes of the cycloisomerisation and alkoxylation of 1,6-enynes is shown in Scheme 96. As in the case of Mizoroki-Heck and Tsuji-Trost reactions, cycloisomerisation of enynes is now a standard methodology used to test new (chiral) catalytic systems.



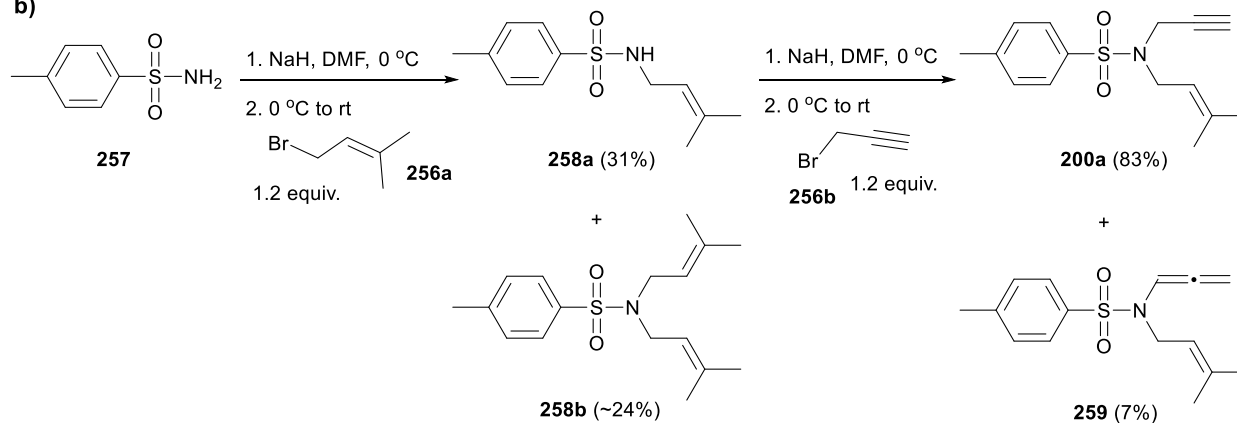
**Scheme 96** Summary of possible products of 1,6-enynes cycloisomerisation (right) and alkoxylation (left) reaction.

I prepared C- and N-tethered enynes **200b** and **200a** from  $S_N2$  reactions with prenyl (**256a**) and propargyl bromides (**256b**, Scheme 97, a-b). Interestingly, I also isolated traces of allene **259** along expected enyne **200a** in the reaction of the N-tethered enyne (Scheme 97, b). **200a-b** were subsequently used as starting materials in the screening of the new catalysts.

a)



b)



**Scheme 97** Preparation of enyne starting materials.

All the structures of the new complexes tested for their catalytic activity in enynes' reactions are listed on Figure 36 for the ease of reference (they can also be found in Appendix A).

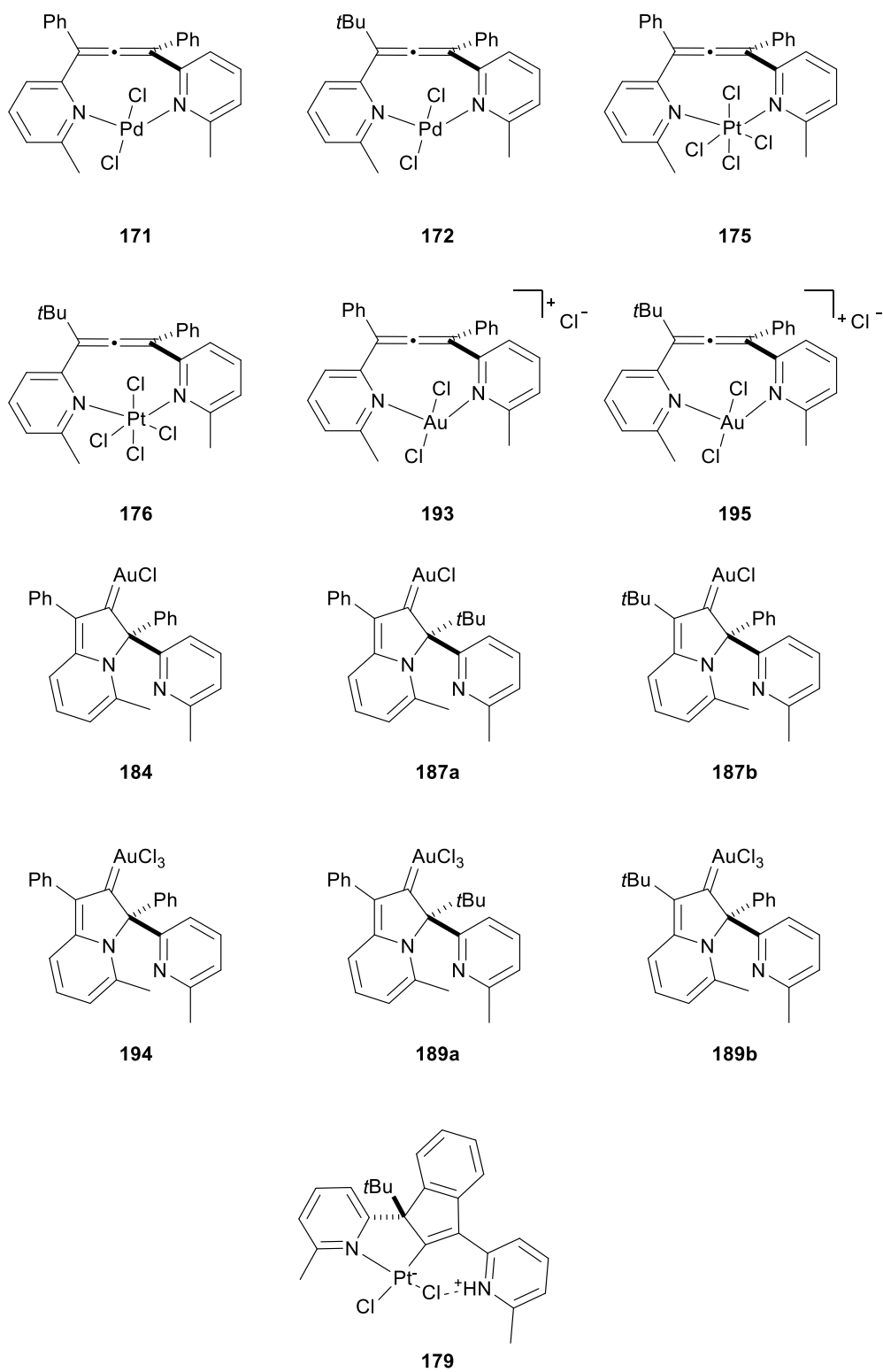


**Figure 36** Structures of new allene-derived metal complexes from the study.

Enyne **200b** was reacted under 2 mol% of the catalyst and 2.5 mol% of Ag salt (where stated) as the catalytic system. AgNTf<sub>2</sub> was used to form cationic catalytic species by chloride abstraction, and was used in a slight excess to account for its hygroscopicity. The reactions were carried out in CH<sub>2</sub>Cl<sub>2</sub> at 25 °C and in most cases for 1 h for comparison purposes (Table 7). The ratios of the starting material and the products were derived from the <sup>1</sup>H NMR spectra of the crude reaction mixtures.

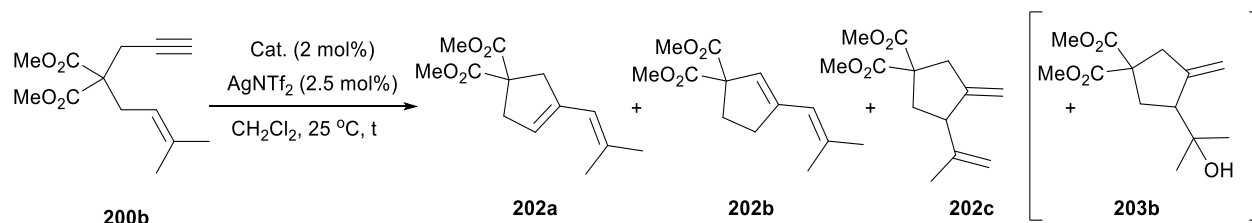


**Table 7** Cycloisomerisation of **200b** with allene-derived catalysts.

Entry	Cat.	AgNTf <sub>2</sub>	t (h)	200b	202a	202b	202c	203b	Conv. (%)	Yield (%)	
1	(Me <sub>2</sub> S) AuCl	+	1	-	1.0	1.0	-	-	>99	-	
allene-type	2	<b>171</b>	-	1	1.0	-	-	-	0	-	
	3	<b>175</b>	-	1	1.0	-	-	-	0	-	
	4	<b>171</b>	+	1	1.0	-	-	-	0	-	
	5	<b>175</b>	+	1	1.0	-	-	-	0	-	
	6	<b>172</b>	+	1	1.0	-	-	-	0	-	
	7	<b>193</b>	-	1	0.15	1.0	-	-	-	87	80
	8	<b>195</b>	-	1	0.9	1.0	-	-	53	53	
	carbene-type	9	<b>184</b>	+	1.25	-	1.0	-	-	>99	77
10		<b>187<sup>a</sup></b>	+	1	0.2	1.0	-	trace	83	83	
11		<b>187<sup>b</sup></b>	+	1	-	1.0	-	-	>99	>99 <sup>c</sup>	
12		<b>194</b>	-	1	1.0	0.6	-	-	n. is.	n. is.	
13		<b>194</b>	+	1	-	0.6	1.0	-	>99	75	
14		<b>194<sup>d</sup></b>	+	1	-	0.6	1.0	-	>99	98	
15		<b>189<sup>e</sup></b>	+	1	-	0.77	1.0	-	>99	>99	
16		<b>179</b>	-	1	1.0	-	-	0.09	n. is.	n. is.	
17		<b>179</b>	+	1	1.0	0.33	-	1.0	57	52	
18		<b>187<sup>a</sup></b>	+	4	-	1.0	-	-	>99	>99	
19		<b>179<sup>f</sup></b>	+ <sup>g</sup>	4	-	0.35	-	1.0	>99	96	

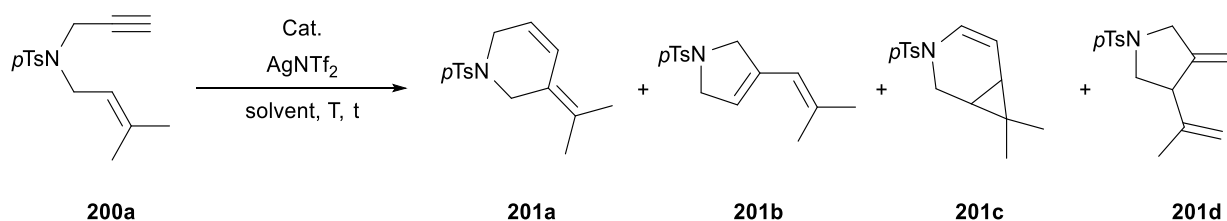
<sup>a</sup> 1:0.12 ratio **187a**:**187b**. <sup>b</sup> 100% **187b**. <sup>c</sup> 5% unidentified product. <sup>d</sup> [Ag<sup>+</sup>] added from the start. <sup>e</sup> 0.5:1.0 ratio. <sup>f</sup> 5 mol%. <sup>g</sup> 6 mol%. n. is. – not isolated (reacted further with [Ag<sup>+</sup>]) hence conv. and yield not known.

For reference, (Me<sub>2</sub>S)AuCl was used as catalyst in the first reaction resulting in a full conversion of the starting material and 1:1 mixture of isomeric skeletal rearrangement products **202a/202b** (Table 7, entry 1). Next, I tested all the new allene-containing complexes. Thus, Pd(II) and Pt(IV) complexes **171-172** and **175** were found to be completely unreactive either with or without addition of the Ag salt (Table 7, entries 2-6). Reactions with Au(III) **193** and **195** resulted in partial conversion to a single isomer of skeletal rearrangement product **202a**

isolated in 80% and 53% yield, respectively (Table 7, entries 7-8). The activity of these compounds in the absence of  $[\text{Ag}^+]$  might support their proposed cationic character. Despite not achieving full conversion, complex **193** gave a better yield and selectivity than the Au(I) bis(phosphine)allene complex **159b** reported by Fensterbank at a lower catalyst loading (Table 7, entry 7 vs Scheme 79).

Cationic carbene-type complexes performed very well in this reaction. All Au(I) complexes gave excellent results under the reaction conditions, in particular isomer **187b**, with which the diene **202a** was formed quantitatively (Table 7, entries 9-11). Au(III) analogues performed equally well with the addition of  $[\text{Ag}^+]$ , but this time a mixture of products **202a/202b** was formed (Table 7, entries 12-15). Au(III) catalysts favoured formation of isomer **202b** contrary to the Au(I) congeners promoting formation of **202a**. With further optimisation preferential use of Au(I)/Au(III) catalysts can offer complementary selectivity choice. Pt(II) **179** exhibited substantial increase of activity in the presence of  $\text{AgNTf}_2$  (Table 7, entry 16 vs entry 17). The major product in a reaction catalysed by **179** was Alder-ene type product **202c**. Full conversion was achieved for all the catalyst by prolonging the reaction time and/or increasing the catalyst loading (Table 7, entries 18-19).

The same catalyst screening was performed with N-tethered enyne **200a** under analogous reaction conditions (Table 8). In case of allene-containing complexes, I confirmed the lack of activity of Pd(II) and Pt(IV) compounds in the absence of  $\text{AgNTf}_2$  either at room temperature or at 80 °C (Table 8, entries 1-4). Previously, these complexes did not show any activity at rt, even with the addition of Ag salt (Table 7, entries 4-5). Thus, to ensure the formation of the cationic catalytic species and improve the activity, they were subsequently used with two-fold excess of  $[\text{Ag}^+]$  in toluene at 80 °C (Table 8, entries 5-8). One-hour long reactions with all the Pd(II) and Pt(IV) catalysts resulted in excellent conversions and yields. **171-172** favoured formation of a cyclopropane bicycle **201c** while **175-176** gave 6-membered skeletal rearrangement **201a** and Alder-ene **201d** as major reaction products.

**Table 8** Cycloisomerisation of **200a** with allene-derived catalysts.

Entry	Cat. (mol%)	[Ag <sup>+</sup> ] (mol%)	solvent	T (°C)	t (h)	200a	201a	201b	201c	201d	Conv. (%)	Yield (%)	
allene-type	1	<b>171</b> (3)	-	CH <sub>2</sub> Cl <sub>2</sub>	25	1.5	1.0	-	-	-	0	-	
	2	<b>175</b> (3)	-	CH <sub>2</sub> Cl <sub>2</sub>	25	1.5	1.0	-	-	-	0	-	
	3	<b>175</b> (3)	-	PhMe	80	16	1.0	-	-	-	0	-	
	4	<b>171</b> (3)	-	PhMe	80	1	1.0	-	-	-	n. is.	n. is.	
	5	<b>171</b> (3)	6.5	PhMe	80	1	-	0.6	-	1.0	0.06	>99	>99
	6	<b>172</b> (3)	6.5	PhMe	80	1	0.08	0.4	-	1.0	0.07	95	85
	7	<b>175</b> (3)	6.5	PhMe	80	1	-	0.8	0.3	0.4	1.0 <sup>a</sup>	>99	88
	8	<b>176</b> (3)	6.5	PhMe	80	1	-	1.0	0.35	0.4	1.0 <sup>a</sup>	>99	>99
	9	<b>193</b> (2)	2.5	CH <sub>2</sub> Cl <sub>2</sub>	25	1.5	1.0	0.14	0.4	0.05	-	37	36
	10	<b>195</b> (2)	2.5	CH <sub>2</sub> Cl <sub>2</sub>	25	1.5	1.0	0.08	0.25	0.03	-	26	26
carbene-type	11	<b>184</b> (3)	3.5	CH <sub>2</sub> Cl <sub>2</sub>	25	0.42	-	1.0	0.15	0.05	0.03	>99	>99
	12	<b>187<sup>b</sup></b> (2)	2.5	CH <sub>2</sub> Cl <sub>2</sub>	25	1.5	0.33	1.0	0.45	0.1	-	82	82
	13	<b>187<sup>c</sup></b> (2)	2.5	CH <sub>2</sub> Cl <sub>2</sub>	25	1.5	-	1.0	0.48	0.12	-	>99	>99
	14	<b>194</b> (2)	2.5	CH <sub>2</sub> Cl <sub>2</sub>	25	1.5	0.5	1.0	0.55	0.11	0.06 <sup>c</sup>	78	77
	15	<b>189<sup>d</sup></b> (2)	2.5	CH <sub>2</sub> Cl <sub>2</sub>	25	1.5	0.11	1.0	0.35	0.03	0.03	94	80
	16	<b>179</b> (2)	2.5	CH <sub>2</sub> Cl <sub>2</sub>	25	1.5	1.0	0.08	0.04	0.23	0.58	48	46

<sup>a</sup> 0.35 unidentified product. <sup>b</sup> 1:0.12 ratio. <sup>c</sup> 0.1 unidentified product. <sup>d</sup> 0.5:1.0 ratio. <sup>e</sup> **187b**. n. is. – not isolated (reacted further with [Ag]) hence conv. and yield not known.

I restricted the use of Au(III) allene-containing complexes to a near room temperature conditions to avoid the cyclisation to carbene species during the catalytic reaction. To promote their activity with more challenging substrate **200a**, they were tested with the addition of [Ag<sup>+</sup>] (Table 8, entries 9-10). I observed only moderate conversions after 1.5 h, although this time the major product of the reaction was the 5-membered skeletal rearrangement product **201b**.

Au carbene-type complexes showed good activity in the reaction of enyne **200a** promoting generation of skeletal rearrangement products, in particular **201a** (Table 8, 11-15). I obtained the best results in terms of conversion and yields with Au(I) complexes **184** and **187**. Pt(II) complex was again least active and catalysed formation of diene **201d**.

On the whole, all new allene-derived complexes were found to be active catalysts in enyne cyclisation reactions. For most of the allene-containing catalysts, reaction at 80 °C was necessary for good performance, but then I observed interesting preferential selectivity when switching between different metal centres (see Table 8, entries 5-10). There was not any clear activity trend between symmetric and non-symmetric catalytic species that could be easily established. Carbene-type complexes showed very good activity comparable to that of standard Au phosphine catalysts and consistent with the activity observed for (NHC)-carbene



Au complexes.<sup>[250,293,294]</sup> In particular, Au(III) and Pt(II) carbenes were active at room temperature (Table 7, entries 14-15, 19) where typical reactions with AuCl<sub>3</sub> and PtCl<sub>2</sub> require reactions in toluene at 80 °C.

Change of reaction conditions to methanol as solvent allowed us to explore the activity of allene-derive complexes in the alkoxy cyclisation of enynes (Table 9 and Table 10). The screenings were carried out with 3 mol% of catalyst loading for 24 h, at 35 °C for **200b** and 50 °C for more challenging **200a**. More sluggish alkoxy cyclisation reactions with N-tethered enyne **200a** were consistent with previous observations.<sup>[282]</sup>

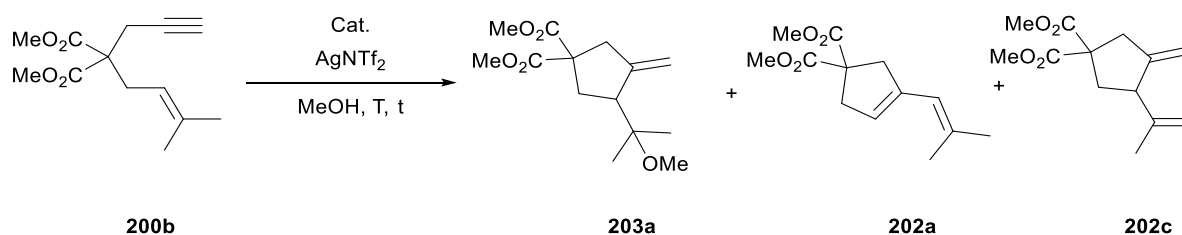


**Table 9** Alkoxy cyclisation of **200b** with allene-derived catalysts.

Entry	Cat. (mol%)	AgNTf <sub>2</sub>	T (°C)	t (h)	200b	203a	202a	202c	Conv. (%)	Yield (%)	
allene-type	1	<b>171</b> (3)	6.5	35	24	1.0	0.3	-	-	23	26
	2	<b>172</b> (3)	6.5	35	24	1.0	0.22	-	-	18	16
	3	<b>175</b> (3)	6.5	35	24	1.0	0.6	-	0.26	46	68 <sup>c</sup>
	4	<b>176</b> (3)	6.5	35	24	0.75	1.0	-	0.55	67	77 <sup>c</sup>
	5	<b>193</b> (3)	4.0	35	24	-	1.0	-	-	>99	>99
	6	<b>195</b> (3)	4.0	35	24	-	1.0	-	-	>99	96
carbene-type	7	<b>184</b> (2)	2.0	25	16	0.6	1.0	-	-	62	69
	8	<b>184</b> (4)	5.0	35	23	-	1.0	-	-	>99	>99
	9	<b>187<sup>a</sup></b> (3)	4.0	35	24	-	1.0	-	-	>99	>99
	10	<b>194</b> (3)	4.0	35	24	-	1.0	0.08	-	>99	97
	11	<b>189<sup>b</sup></b> (3)	4.0	35	24	0.1	1.0	-	-	91	91
	12	<b>179</b> (3)	4.0	35	24	0.5	1.0	-	0.2	71	71 <sup>c</sup>

<sup>a</sup> 1:0.12 ratio. <sup>b</sup> 0.5:1.0 ratio. <sup>c</sup> Total of **203a** and **202c**.

Pd(II) complexes exhibited low activity in the alkoxy cyclisation of **200b** (Table 9, entries 1-2). I observed moderate conversions with Pt(IV) compounds (Table 9, entries 3-4). For **175** and **176** formation of 5-member methoxy adduct **203a** was accompanied by isolation of Alder-ene type minor product **202c** which was previously obtained in all Pt-catalysed reactions. Complete conversions and excellent yields of **203a** were obtained with Au(III) allene-containing catalysts (Table 9, entries 5-6).

All Au carbene-type complexes performed uniformly well in this reaction (Table 9, entries 7-11) whereas **179** showed lower activity and selectivity (Table 9, entry 12).

I observed the same trend of the activity for Pd(II) and Pt(IV)-allene containing complexes in the alkoxy cyclisation of **200a** (Table 10, entries 1-4). Interestingly, Au(III) catalysts from this group showed much lower activity compared to the reaction of **200b** (Table 10 vs Table 9, entries 5-6). Carbene-type complexes also showed diminished activity in this reaction, especially in the case of Au(III) **189** and **194** (Table 10, 7-12).

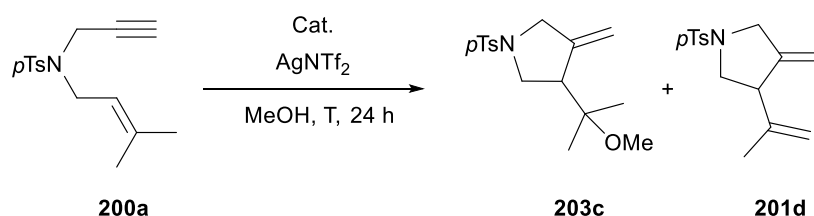


**Table 10** Alkoxy cyclisation of **200a** with allene-derived catalysts.

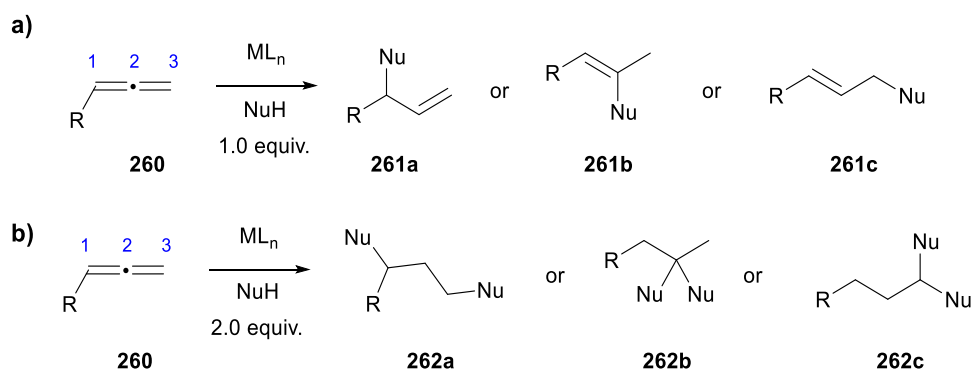
Entry	Cat. (mol%)	AgNTf <sub>2</sub>	T (°C)	200a	203c	201d	Conv. (%)	Yield (%)	
allene-type	1	<b>171</b> (3)	6.5	50	1.0	0.04	-	4	3
	2	<b>172</b> (3)	6.5	50	1.0	-	-	0	-
	3	<b>175</b> (3)	6.5	50	0.65	1.0	0.13	75	57 <sup>c</sup>
	4	<b>176</b> (3)	6.5	50	1.0	0.79	0.11	47	50 <sup>c</sup>
	5	<b>193</b> (3)	4.0	50	1.0	0.13	-	12	10
	6	<b>195</b> (3)	4.0	50	1.0	0.2	-	17	19
carbene-type	7	<b>184</b> (4)	5	35-50	0.4	1.0	-	72	76
	8	<b>184</b> (3)	4	50	0.06	1	-	95	97
	9	<b>187<sup>a</sup></b> (3)	4	50	0.85	1.0	-	54	54
	10	<b>194</b> (3)	4	50	3.4	1.0	-	22	24
	11	<b>189<sup>b</sup></b> (3)	4	50	4.5	1.0	-	18	18
	12	<b>179</b> (3)	4	50	0.8	1.0	-	56	58

<sup>a</sup> 1:0.12 ratio. <sup>b</sup> 0.5:1.0 ratio. <sup>c</sup> Plus 7% of **201d**.

Cationic Au(I) complexes were the best catalysts for cyclisation/addition reaction of enynes. This observation was consistent with previous literature findings. Both allene-based and carbene Au(III) complexes were comparably active with a C-tethered starting material but they suffered substantial loss of the activity with N-tethered enyne. Remaining Pt and in particular Pd(II) catalysts were found to be less suited for this transformation.

#### V b. 4. Metal-catalysed nucleophilic addition to allenes

Allenes, similarly to alkynes, exhibit diverse reactivity in the presence of transition metals. One of their important reactivity patterns is the nucleophilic addition to allenes.<sup>[25]</sup> Electrophilic activation of the allene double bond by a metal can lead to a wide array of addition products in the reactions with various nucleophiles (Scheme 98). The outcomes of the reaction such as single vs double addition or site of the addition is governed by the character of the allenic substrate and the catalytic system.

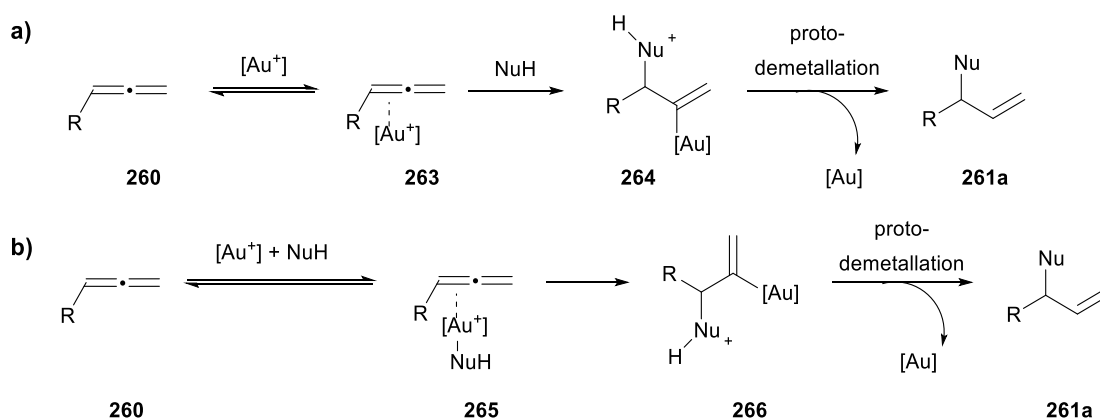


**Scheme 98** Possible outcomes of intermolecular nucleophilic addition to allenes: a) single addition; b) double addition.

Single addition to a proximal carbon atom catalysed by Au(I) or Pd(II) (C(1) in **260**, Scheme 98, a) has been typically observed for O-substituted allenes whereas N-substituted allenes such as allenamides favour addition to a distal carbon atom under Au(I) catalysis (C(3) in **260**).<sup>[26,295]</sup> Transfer of a nucleophile to a central carbon atom of the allene is rare (C(2) in **260**).<sup>[296]</sup>

In case of the double addition ((C(1) and C(3) in **260**, Scheme 98, b), bimetallic Au(I)/Pt(II) catalytic system for addition of azoles to N- and O-activated allenes was recently described by our group.<sup>[297]</sup> Pt(II) conditions with alcohol and indole nucleophiles were found to favour double distal addition to form products of **262c** type.<sup>[298–301]</sup> Double addition to the central carbon atom (C(2)) is less common.<sup>[302]</sup>

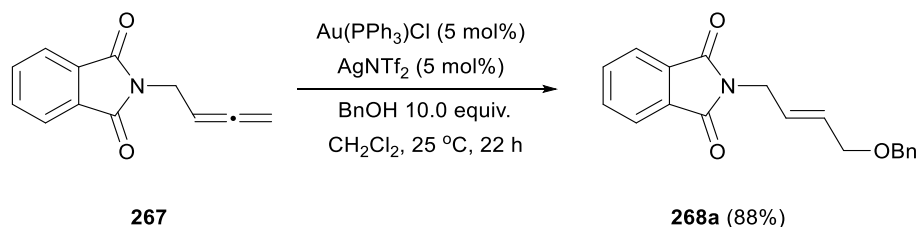
For Au(I) cationic catalysis, formation of proximal addition products of **261a** type has been proposed to proceed *via* either outer or inner sphere mechanisms (Scheme 99, a-b, respectively).<sup>[303]</sup> In the outer sphere pathway, the Au fragment first coordinates to the allene to form  $\eta^2$  complex **263** that later undergoes the nucleophilic attack in *anti* manner (**264**, Scheme 99, a). The product **261a** is released after the protodemetalation. In the inner sphere mechanism, the metal simultaneously coordinates to the nucleophile and the allene (**265**, Scheme 99, b). As a result, the nucleophile is delivered from the same side as Au in *syn* manner to form **266** that after protodemetalation gives the product. Products of the two mechanisms are identical for terminal allenes, but in case of a more substituted starting materials mixture of isomers can be obtained.



**Scheme 99** Proposed mechanism for Au(I)-catalysed nucleophilic addition to allenes: a) outer sphere pathway; b) inner sphere pathway.

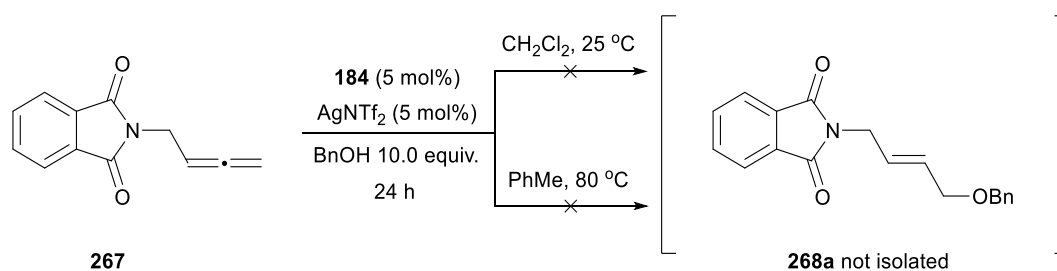
The intramolecular variant of the reaction giving access to a variety of carbo- and heterocyclic products has also been widely studied.<sup>[304]</sup> Use of enantiomerically enriched allenes can lead to a good chirality transfer to the addition products.<sup>[30]</sup>

I used phthalimide allene **267** and benzyl alcohol as our model starting materials to explore catalytic activity of the new complexes in a nucleophilic addition to allenes. I obtained one isomeric product from the distal addition under standard  $[(\text{Ph}_3\text{P})\text{Au}]^+$  catalysis (Scheme 100).



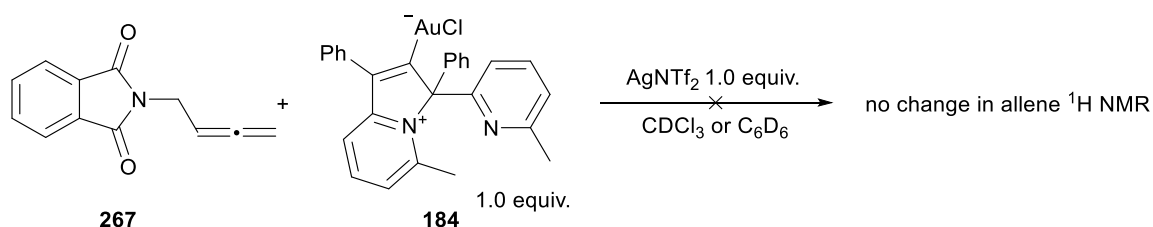
**Scheme 100** Au(I)-catalysed benzyl alcohol addition to allene **267**.

Next, I repeated the reaction using 5 mol% of the bis(phenyl) Au(I) complex **184** (Scheme 101). However, original reaction conditions of 25 °C in  $\text{CH}_2\text{Cl}_2$  or heating at 80 °C in toluene resulted in the recovery of the starting materials.



**Scheme 101** Benzyl alcohol addition to allene **267** catalysed by **184**.

I reacted **267** with 1 equiv. of cationic complex **184** to probe the interaction of the catalyst with the allene fragment (Scheme 102).  $^1\text{H}$  NMR monitoring of the reaction showed no pronounced changes in the peaks corresponding to the allene unit pointing to the weak or no interaction with the metal. In that case, lack of reactivity with the alcohol nucleophile could be explained by failure of **184** to activate the allene moiety.



**Scheme 102** Stoichiometric reaction of **267** with Au(I) complex **184**.

Other allene-derived complexes showed to be more active in the model reaction (Table 11).

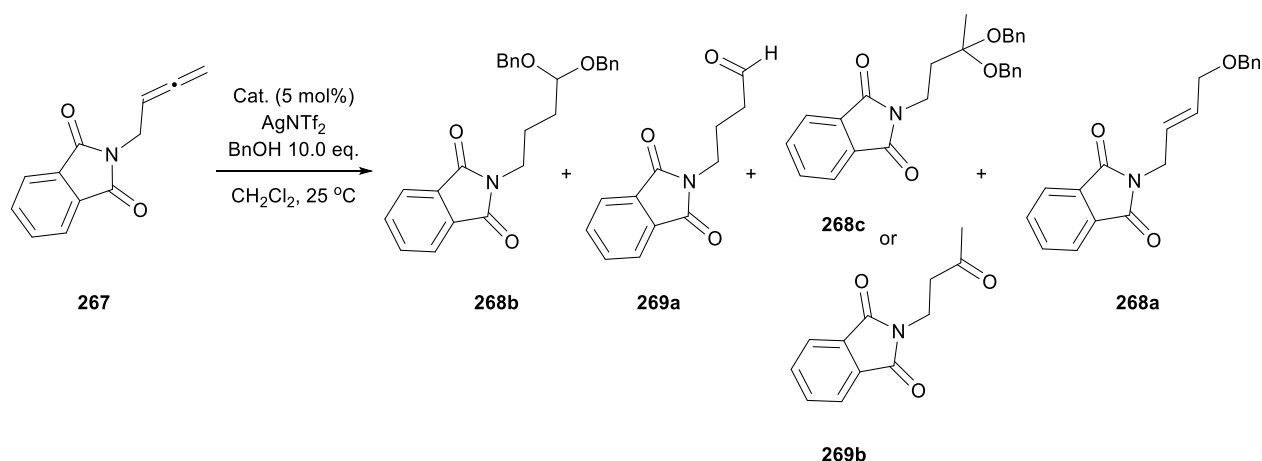


**Table 11** Addition of benzyl alcohol to allene **267** catalysed by allene-derived complexes.

Entry	Cat.	AgNTf <sub>2</sub> (mol%)	t (h)	<b>267</b>	<b>268b</b>	<b>269a</b>	<b>268c/269b</b>	<b>268a</b>	Conv. (%)
1	<b>175</b>	10	26	-	1.0	0.7	0.08	-	>99 <sup>a</sup>
2	<b>176</b>	10	27	-	1.0	0.24	0.07	-	>99 <sup>b</sup>
3	<b>195</b>	5	27	1.0	-	-	-	0.2	17
4	<b>171</b>	10	24	1.0	-	-	-	-	0
5	<b>179</b>	5	24	0.33	1.0	0.31	0.17	-	82
6	<b>194</b>	5	24	1.0	-	-	-	-	0

Table 11 shows ratios and conversions calculated from  $^1\text{H}$  NMR spectra of crude reaction mixtures. <sup>a</sup> Isolated yield 67%. <sup>b</sup> Isolated yield 61%.

Pt(IV) **175-176** were the most active from the allene-containing complexes' group (Table 11, entries 1-2). Both resulted in complete conversions and formation of the distal

double addition product – acetal **268b** corresponding to the usual reactivity with Pt(II) catalysts. **268b** was also isolated in its hydrolysed form of the aldehyde **269a**. Interestingly, a minor product of the reaction **268c** was identified as the double addition product to the central carbon atom of the allene that readily hydrolysed to ketone **269b** upon handling. This type of reactivity was previously only observed with thiol nucleophiles under Au(III) catalysis.<sup>[302]</sup> However, our allene-containing Au(III) complex **195** promoted formation of a single distal addition alkene product **268a**, albeit with low conversion (Table 11, entry 3), showing reactivity typical for Au(I) catalysis. Pd(II) **171** was completely unreactive under the reaction conditions (Table 11, entry 4).

From the other carbene-type complexes, Pt(II) **179** gave similar distribution of the regioisomeric products to those of Pt(IV) compounds with good conversion (Table 11, entry 5). On the other hand, Au(III) **194** suffered from the lack of activity similar to the Au(I) carbene-type analogue (Table 11, entry 6).

Interestingly, we showed that allene-containing catalysts can be used to catalyse reactions of allene compounds. Pt complexes were the most suitable catalysts for the addition of benzyl alcohol to allene **267**. Although cationic (NHC)-Au(I) catalytic systems have been previously observed to be active catalysts in hydration, hydroalkoxylation or hydroamination of allenes, our Au carbene-type catalysts showed no activity in the model reaction.<sup>[305–307]</sup>

### V c. Conclusions

This chapter described the first use of bis(pyridyl)allene-derived metal complexes in catalysis. The new metal complexes were used as catalysts in several benchmark reactions. Pd(II) complexes did not show any activity in the Tsuji-Trost reaction (Section V b. 1.), but they gave promising results in Mizoroki-Heck coupling (Section V b. 2.), especially with more reactive substrates. All new complexes showed moderate to excellent activity in cycloisomerisation and alkoxylation of 1,6-enynes (Section V b. 3.). Switch between catalysts based on a different metal centres allowed to achieve selectivity towards different isomeric products. Au carbene-type complexes performed particularly well in these reactions. Examples of all groups of complexes were also tested in intermolecular hydroalkoxylation of allenes (Section V b. 4.), where Pt compounds showed the best activity. In general, the influence of a character of the new catalysts over the outcome of the catalytic reactions (allene-containing vs carbene-type complexes or substitution pattern within each class) was specific to each investigated reaction. For example, pronounced difference of activity of symmetric and non-symmetric Pd complexes in Heck reaction was not observed in enyne reactions.

In the next chapter we will be looking at the use of allene-derived metal complexes in medically relevant contexts, in particular, exploring their antimicrobial and anticancer properties.

## VI. Bioactivity of allene-derived metal complexes

### VI a. Introduction

Allene-containing natural products and synthetic molecules have been demonstrated to exhibit interesting biological activity and drug action (see Section I a.). It might be relevant to consider both allene and metal fragments acting synergistically to enhance interactions with biomolecules in the investigation of the bioactivity of allene-derived metal complexes. Therefore, it is important to look at the action of metal-based drugs in more detail.

The medicinal properties of metal-based compounds have been explored for centuries.<sup>[308]</sup> The origins of the use of transition metal complexes in modern medicine is usually associated with the discovery of the anticancer activity of cisplatin, which was approved for clinical use in 1978.<sup>[309]</sup> Since then, medicinal chemistry of small, inorganic transition metal complexes developed into one of the dynamic and important areas of drug development research with more and more metal-based drugs entering pre-clinical and clinical trials.<sup>[310–314]</sup> Yet, compared to purely organic substances, the number of examples of metal-based drugs under development or available on the market is still lacking.

However, the use of organometallic and coordination metal complexes as drug candidates has some key advantages over classic organic compounds. For example, use of metal complexes allows an easy access to structures with varied geometries, extensive stereochemistry and three-dimensional shapes going beyond tetravalent tetrahedral carbon (Figure 37).<sup>[315]</sup>

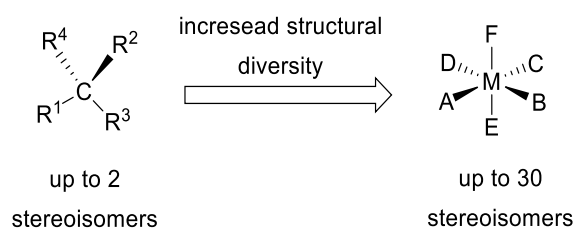


**Figure 37** Stereochemical diversity of metal coordination compounds.

The wide structural diversity can be achieved by ligand exchange reactions (varying coordination number) or redox reactions at the metal centre (change in oxidation states). Additionally, coordination to the metal can beneficially modify the pharmacological properties of existing organic drugs. Other unique properties of metal-containing species, such as Lewis acidity, radioactivity, pharmacokinetics or magnetic properties are also available for fine-tuning in the rational drug design process. Recently, it was demonstrated that metal-containing compounds are statistically more likely to be active antimicrobial and antifungal agents than



purely organic compounds (27% vs 2% of compounds showing activity in each group, respectively).<sup>[316]</sup>

Currently, the majority of transition metals and almost all classic ligand classes have already been investigated in some aspects of bioinorganic chemistry. In particular, notable therapeutic and diagnostic agents have been developed with metals such as Pt, Au, Ru, Ti, Pd, Ir, Mn, Re, Gd, Tc, Cu, Fe, Co, *etc.*<sup>[312–314,317,318]</sup> Important groups of bioactive organometallics include: metallocenes, arene-, carbonyl-, carbene-, pincer-, polynuclear- or macrocyclic complexes.<sup>[319–321]</sup> Most metal-based compounds are evaluated for their anticancer activity, although many examples also show promising broader antimicrobial cytotoxicity. Metal-based pharmaceuticals are often categorised on the basis of their mode of action.<sup>[311,322]</sup> The categories include: 1) complexes active in their inert form, 2) complexes where only some fragments are active, 3) only metal ions or their biotransformation products are active, 4) only the ligand(s) is biologically active, 5) the metal is radioactive<sup>[323]</sup> (used for radiodiagnostic imaging and radiotherapy), 7) the metal behaves as a photosensitiser<sup>[324]</sup> (in photodynamic therapy).

The different mechanisms of action of metallodrugs typically fall into one of the two categories also applicable to classic organic-based drugs: the drugs realise their action either by non-covalent, reversible interaction with the target or covalent stoichiometric binding of so-called “sacrificial” inhibitors. Interestingly, use of metal-based drugs creates a unique opportunity for catalytic mechanism of action.<sup>[325]</sup> Metallodrugs are able to induce a modification or a cleavage in the biomolecular targets in a catalytic manner and can act throughout multiple turnovers without the loss of activity.

Extensive studies of Pt complexes with anticancer properties suggested that the main target of their action is DNA.<sup>[317]</sup> However, it is now established that different classes of metallodrugs have very different molecular targets and mechanisms of action. Other identified cellular targets include proteins and enzymes or signal transduction pathways.<sup>[326,327]</sup> Recent developments in metallotherapy focus on the design of more selective agents that specifically aim at one of these targets to go beyond general non-specific cytotoxicity. For example, Mn(II) complexes have been evaluated as superoxide dismutase (SOD) mimetics<sup>[328]</sup> and Ru(II) half-sandwich complexes have been found to be potent kinase inhibitors.<sup>[329]</sup>

The research into medicinal properties of Pt- and Au-based compounds is particularly extensive and well documented.

Pt(II) chemotherapeutics are one of the most widely employed metallodrugs and are commonly used in the treatment of various types of cancer, such as testicular, ovarian, bladder, cervical or small lung cancer.<sup>[309,330]</sup> The research of Pt(II) drugs began with the serendipitous

discovery of the antiproliferative properties of cisplatin by Rosenberg.<sup>[331]</sup> Cisplatin, cis-diamminedichloridoplatinum(II) (**270**), and second- and third-generation carboplatin (**271**) and oxaliplatin (**272**, Figure 38) are the most effective Pt anticancer therapeutics currently available on the market.<sup>[332]</sup>

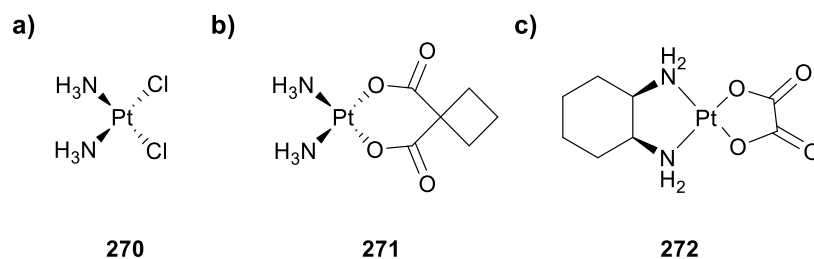


**Figure 38** Marketed Pt chemotherapeutics: a) cisplatin **270**; b) carboplatin **271**; c) oxaliplatin **272**.

These complexes feature  $d^8$  square planar Pt centre and *cis* arrangement of the two ammine ligands. The anticancer properties of Pt drugs are attributed to their interaction with DNA. Metal-induced DNA damage disrupts normal division of the cancer cells and causes cell death. Small molecules can interact with DNA in a non-covalent manner *via* intercalation (e.g. stacking interactions of planar aromatic groups), groove binding (hydrogen bonding and van der Waals interactions) or external static electronic effects (e.g. metal cations and negatively charged phosphate groups of DNA).<sup>[333]</sup> However, the accepted mechanism of the cisplatin action is covalent in nature (Figure 39, a).<sup>[317,332]</sup> Cisplatin enters the cell through diffusion or active transport *via* specific receptors. Then, it undergoes a hydrolysis activation step where its labile chloride ligands are exchanged with water molecules and produce aquated, more reactive species  $[\text{Pt}(\text{NH}_3)_2\text{Cl}(\text{H}_2\text{O})]^+$  and  $[\text{Pt}(\text{NH}_3)_2(\text{H}_2\text{O})_2]^{2+}$ . The ligand exchange process is facilitated by low intracellular concentration of chloride ions. Mono-aqua activated complex forms a monofunctional DNA adduct first, typically with the most nucleophilic site at N(7) atom of purine adenine and guanine bases (Figure 39, b). The remaining chloride ligand is replaced next by another purine residue and forms final platinated DNA crosslink. Cisplatin-DNA binding is irreversible and can afford several structurally different outcomes such as: adducts derived from intrastrand crosslinks with two nucleobases within single DNA strand, interstrand crosslinks of two different strands within one DNA molecule, N,O-chelates with the guanine molecule or DNA-protein crosslinks.<sup>[333]</sup> Other metallodrugs are also known to interact with DNA in a multifunctional way, for example, with initial intercalation followed by subsequent covalent bonding.<sup>[309]</sup>

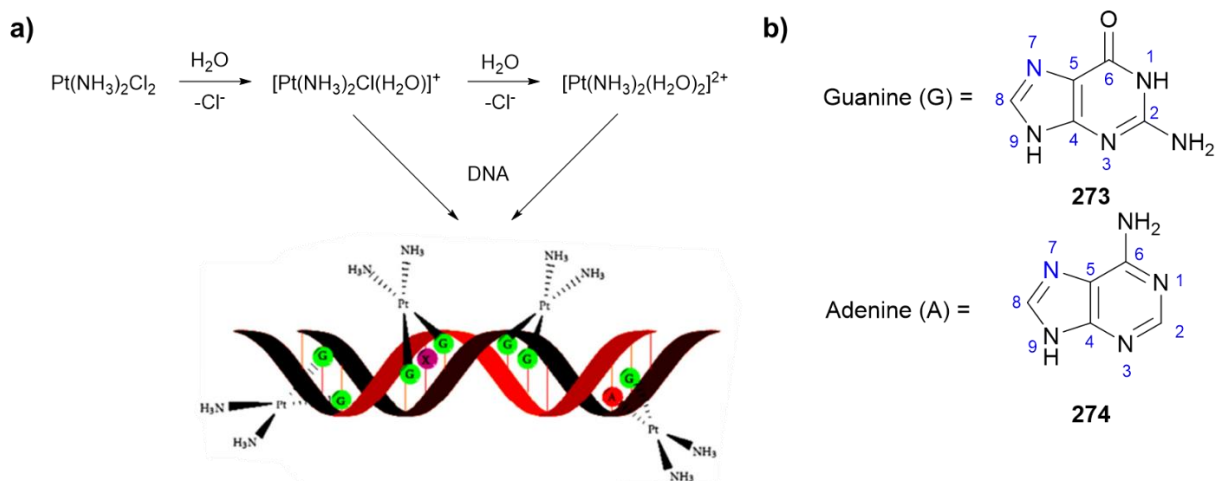


**Figure 39** Cisplatin mechanism of action: a) hydrolysis and DNA binding;<sup>[333]</sup> b) structures of purine bases.

DNA is the major molecular target for cisplatin, however it was determined that only 5-10% of its intracellular concentration can be found in the DNA fraction. The remaining cisplatin is believed to bind less specifically to other targets such as thiolated peptides, replication enzymes or RNA. This low level of selectivity is linked with serious side effects associated with Pt(II) chemotherapeutics. The other serious issue of the treatment is progressive resistance to the Pt(II) drugs. Some identified resistance mechanisms involve reduced transport of the drugs across the cell membranes or enzymatic repair of platinated lesions on DNA, for example by base excision mechanism. These concerns motivated renewed search for more active and safer Pt(II) metallodrugs over the last few decades. These efforts were also paralleled with a growingly popular approach of use of Pt(IV) complexes as antitumour agents.<sup>[210,211,330]</sup>

Pt(IV) complexes are investigated as pro-drugs to more active Pt(II) congeners thanks to their relative kinetic inertness in the ligand exchange processes. As a result, they are less prone to undesired side reactions, more suitable for oral administration and more likely to arrive at the cellular target intact. Six-coordinate, octahedral Pt(IV) centre gives an opportunity for increased structural modification in comparison to the Pt(II) analogues. It was found that modification of the ligands, especially in the axial position, can substantially alter and improve pharmacological properties of Pt(IV) complexes, such as the lipophilic/hydrophilic character. Pt(IV) prodrugs are believed to act when activated by an *in vivo* reduction to their active Pt(II) oxidation state (Figure 40, a). The process is facilitated by intracellular reducing agents such as glutathione or ascorbic acid. The reduction is usually coupled with an irreversible loss of both axial ligands (see Section IV b. 3.). The design strategies for Pt(IV) prodrugs often include complexes that upon reduction, form known Pt(II) compounds, e.g. cisplatin. The reduction rates and potentials were found to be strongly dependent on the axial, and to a lesser extent, equatorial ligands in the complexes.

Additional advantage of use of more structurally diverse and slow ligand exchanging Pt(IV) compounds is an opportunity to employ ligands that direct the drug to specific molecular targets with a presence of targeting groups. Other strategies that have been developed to improve the target selectivity include photo-activation,<sup>[334]</sup> selective reduction in a hypoxic environment of the tumour, or use of nanoparticle bonded Pt(IV) complexes.<sup>[335]</sup>

Many examples of Pt(IV) complexes have shown promising anticancer activity in *in vitro* and *in vivo* models (Figure 40, b-d).<sup>[309]</sup> However, the ongoing clinical trials have not resulted in the approval of any of the Pt(IV) therapeutics yet, often because the drugs failed to show improved survival rates when compared with the existing therapies.

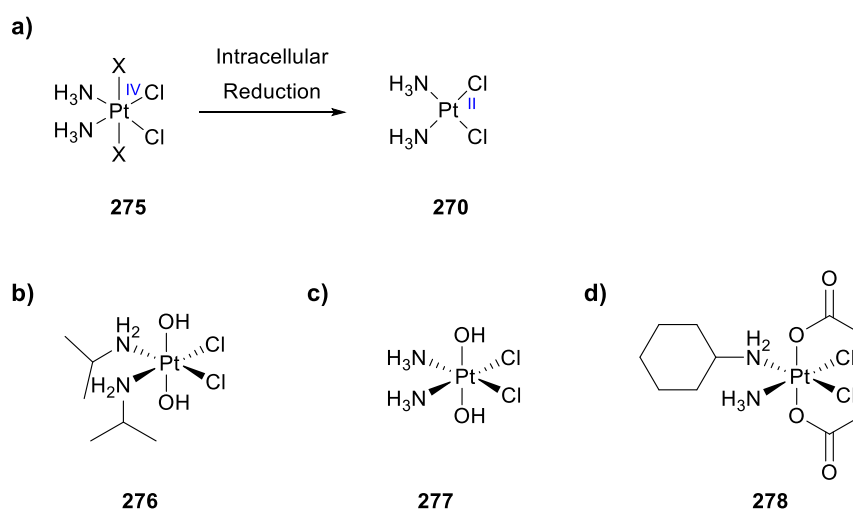


**Figure 40** Pt(IV) anticancer drugs that have entered clinical trials: a) reduction to Pt(II) analogues; b) iuprolatin **276**; c) oxoplatin **277**; d) satraplatin **278**.

The use of Au-based drugs, or chrysotherapy, in modern medicine began with the observation that the Au(I) complex  $\text{K}[\text{Au}(\text{CN})_2]$  had a bacteriostatic effect towards the bacteria that cause tuberculosis.<sup>[336]</sup> Later, Au-based medicines were proven to be effective in the symptomatic treatment of rheumatoid arthritis.<sup>[337]</sup> Early use of Au(I) thiolate complexes led to the development of the highly successful, orally administered drug Auranofin (**279**) for this disease (Figure 41, a).<sup>[308,338]</sup> Auranofin is an example of a classic two-coordinate, linear Au(I) complex with stabilising tetraacetylthioglucose and phosphine ligands. Other geometries of Au(I) complexes, such as trigonal or tetravalent tetrahedral are less stable and therefore less common. Au drugs have also been trialled in the treatment of other inflammatory disorders.

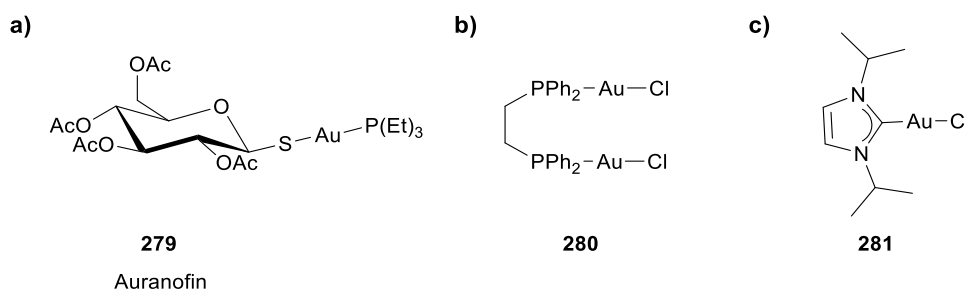


**Figure 41** Au(I) complexes with biological activity.

Au(I) metallodrugs are often considered as pro-drugs, due to facile ligand substitution reactions on the metal centre. “Soft” Au centres have a strong binding affinity for sulphur-based ligands. *In vivo* exchange reactions with thiol groups are thought to be important for the activity of Au drugs.<sup>[308,338,339]</sup> In the case of Auranofin, its ligands are believed to be readily displaced by cysteine residues of blood serum albumin. Albumin-bound Au(I) is transported across the cell membrane and arrives in the cell without a change in the oxidation state.

Anticancer activity of Au(I) complexes, including Auranofin, has also been demonstrated.<sup>[186,339]</sup> Auranofin was believed to thwart DNA replication in cancer cells in a similar mechanism of action to Pt chemotherapeutics, although it was found to be inactive in the solid tumour models. More examples of related thiolated Au(I) complexes have been tested for antitumour activity. Additionally, tertiary phosphine complexes (Figure 41, b) showed promising toxicity towards several types of cancer. These complexes were believed to act by inhibition of mitochondrial function rather than DNA binding due to a weak affinity of Au(I) to coordinate O- and N-containing ligands, such as DNA nucleobases. Other Au(I) compounds with promising anticancer activity include (NHC)- or alkynyl-complexes (Figure 41, c).<sup>[320]</sup> Their mechanism of action is usually ascribed to inhibition of Se- and S-containing enzymes such as glutathione peroxidase, cysteine protease and in particular thioredoxin reductase (TrxR). The Au(I) drug action is believed to be caused by covalent binding to the nucleophilic selenocysteine residue in the active site of TrxR.

Historically, Au(III) complexes have been regarded as too reactive and unstable for medicinal applications. However, the fact that  $d^8$  Au(III) is isoelectronic to Pt(II) and also forms square planar complexes prompted the investigation into the anticancer properties of Au(III) compounds.<sup>[186,340,341]</sup> Typically, Au(III) compounds have strong oxidant character and are readily reduced to Au(I) or even Au(0). The use of ligands that influence the reduction potential of the metal centre and the hydrolysis rates, contribute to substantial stabilisation of Au(III) complexes in aqueous physiological conditions. Studies on the mechanism of action of Au(III) drugs in cancer cells are not conclusive but point to a different mode of action to the Pt drugs. Although there is some evidence that Au(III) complexes can interact with DNA, usually it is a

weak interaction. It has been proposed that proteins, such as thiol-enzymes, might be major biomolecular targets. As such, Au(III) metallodrugs could offer an interesting alternative for treatment of cisplatin-resistant tumours.

Common trend in the preparation of stable Au(III) drug candidates is the use of multidentate ligands, including well performing bipy ligands, porphyrins and pincer ligands (Figure 42).<sup>[342–344]</sup>

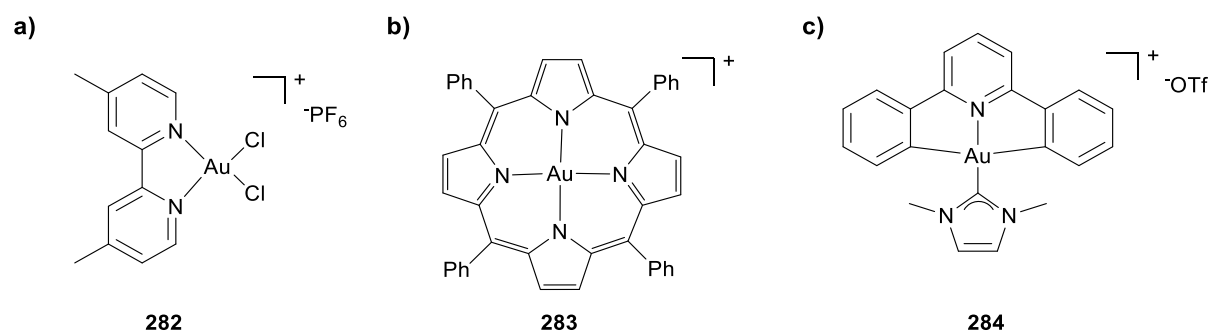


**Figure 42** Structures of Au(III) complexes investigated for anticancer applications.

Early work on Au-based therapeutics indicated their potential as antimicrobial agents, e.g. activity against tubercle bacillus. In fact, many Au compounds showed activity against a broad spectrum of microorganisms, for example parasitic *Plasmodium* causing malaria or gram-positive and gram-negative bacteria.<sup>[345,346]</sup> Although recent research in the area has not been very active, it remains crucial in the face of growing antibiotic resistance challenge and the fact that metal complexes are a very promising, new class of antimicrobials.<sup>[316]</sup>

Some studies pointed out the potential antiviral activity of Au compounds.<sup>[347,348]</sup> For example, aurocyanide  $[\text{Au}(\text{CN})_2]^-$  was found to inhibit proliferation of human immunodeficiency virus (HIV) and is investigated for AIDS treatment. Auranofin treatment produced an increase in usually declining CD4+ T cell counts in AIDS patients.

Existing limitations of the treatments involving use of metal-based drugs are still significant and are fuelling rapid developments in the area. The major drawbacks include severe side effects and acquired drug resistance. For example, Pt and Au drugs are known to cause reactions such as nephrotoxicity, neurotoxicity, adverse skin reactions, blood disorders, *etc.* The control of the selectivity towards disease-related targets is especially challenging in case of DNA-targeting drugs. DNA is ubiquitous and present in every cell in the organism rendering it a difficult target. However, its uncontrolled replication in the cancer process is the reason why more and more DNA-binding molecules are designed and synthesised. Different targeting strategies have been embedded in the design of metallodrugs to circumvent or reduce known side effects. The available extensive *in vitro* data on the bioactivity of metal-

based drugs needs to be further supported with more *in vivo* studies. The unrealised medicinal potential and documented clinical success of some metal complexes merits further attention to metallodrugs in the context of modern drug development.

## **VI b. Results and Discussion**

The previous chapter described the use of allene-derived metal complex in catalysis. Moving beyond the catalytic activity, we also investigated the new complexes for their medicinal properties. The focus of this section is the unexplored to date, use of allene-derived metal complexes as metallodrug candidates.

The biological activity of metal coordination complexes often results from combined interactions of their metal and organic fragments and cellular targets. We predicted that allene-derived metal complexes might demonstrate interesting medicinal properties thanks to their unique structural features and reactivity. In particular, we envisioned dual intracellular interaction strategy for the allene-containing complexes.<sup>[312]</sup> For these compounds, the essential activity deriving from the presence of the active metal centre is coupled with the stereochemical and chemical benefits of the allene moiety. The studies of pharmacologically active allene-based drugs and drug candidates (see Chapter I) suggest that their main mechanism of action with biological molecules is an enzyme/protein (irreversible) nucleophilic addition to the allene group. That type of reactivity is particularly favoured in metal-containing allene compounds as we have seen, for example, for Au complexes (see Chapter IV). Additionally, both allene-containing and carbene type complexes are characterised by non-flat, 3D geometry and feature N-heterocyclic groups, which is usually very important for the success of drug-like small molecules.<sup>[349]</sup> The observed robustness of the new complexes, that could be attributed to the stabilising chelate effect or heteroatom conjugation, was an incentive to test the stability of the metal centres under demanding physiological conditions.

The following sections summarise our preliminary investigations of the activity of the allene-derived complexes as inhibitors of pathogenic microorganisms' (bacteria, fungi) growth as well as human cancerous cells. One of the possible mechanisms of action of the drugs was also probed by the studies of the interaction with different DNA fragments. Details of all the assays and results provided by collaborators presented in this chapter can be found in the Experimental Section (ES).

### **VI b. 1. Stability studies**

An important feature of the drug candidates is their air and solution stability. Thus, the stability of new drug candidates is usually tested prior to any biological assays.

All new allene-derived metal complexes proved to be stable under aerobic conditions. Additionally, I have observed that carbene-type complexes could be kept in solution for a prolonged periods of time without the loss of their structural integrity (see Section IV b. 4.). However, some of the complexes containing the allene-core appeared to change in solution. In particular, I observed change of colour of NMR samples of Pt- and Au-based complexes from yellow to dark orange/red. I decided to test the stability of these compounds (Figure 43), before submitting them to the biological testing under demanding physiological conditions. Typically, the stability can be monitored by a series of periodic NMR experiments of the solution of the compound of interest in water. In case of solubility issues in aqueous solution, compounds can be dissolved in a water/organic solvent mixture or in biocompatible solvents such as DMSO or DMF.

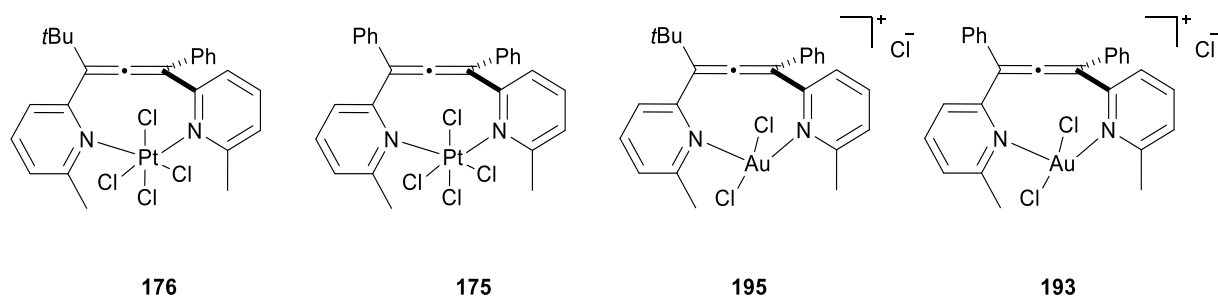


**Figure 43** Allene-containing complexes used in stability studies.

I performed a series of  $^1\text{H}$  NMR spectra for each of the four complexes **175**, **176**, **193** and **195** dissolved in DMSO. The spectra were recorded in 2 h intervals for the initial 48 h and then additional spectra were collected up to 12-13 days from the preparation of the sample. I monitored the change of the spectra in the aromatic region as well as the useful handles of the pyridyl methyl groups.

The spectrum of the *t*-butyl substituted Pt(IV) **176** remained unchanged in the 13 day period (Figure 44). There were no changes in the intensity of signals corresponding to the phenyl group (7.32-7.48 ppm) or the broadened pyridyl peaks (7.55-8.40 ppm). No new signals were observed.



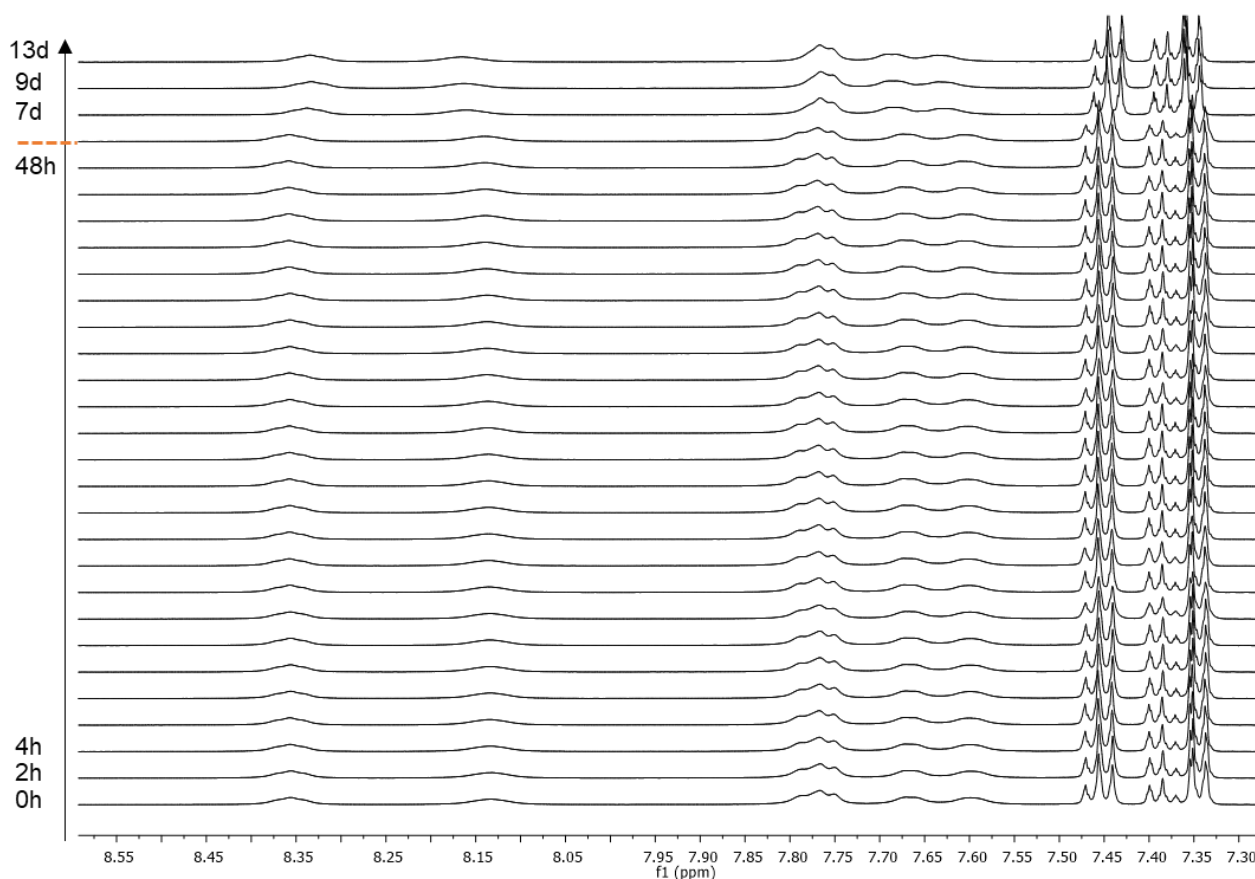


**Figure 44** Aromatic region of the  $^1\text{H}$  NMR spectrum of **176** recorded in the space of 13 days.

On the other hand, the bis(phenyl) Pt(IV) complex **175** started to decompose/react in solution after a few hours from the preparation of the NMR sample (Figure 45). At least two new unidentified species (**285a** and **285b**) started to appear on the spectrum after 6-8 h. Based on the integration of the triplet peaks corresponding to **175**, **285a** and **285b** at 8.22 (corresponding to the pyridyl proton *meta* to the methyl group), 8.30 and 8.42 ppm, respectively, I could estimate the approximate share of **175** in the mixture at different time intervals. Starting from 100% at the beginning, this share decreased to 67% after 12 h, through 54% after 24 h and 38% after 48 h. After 7 days the mixture did not contain **175** at all.

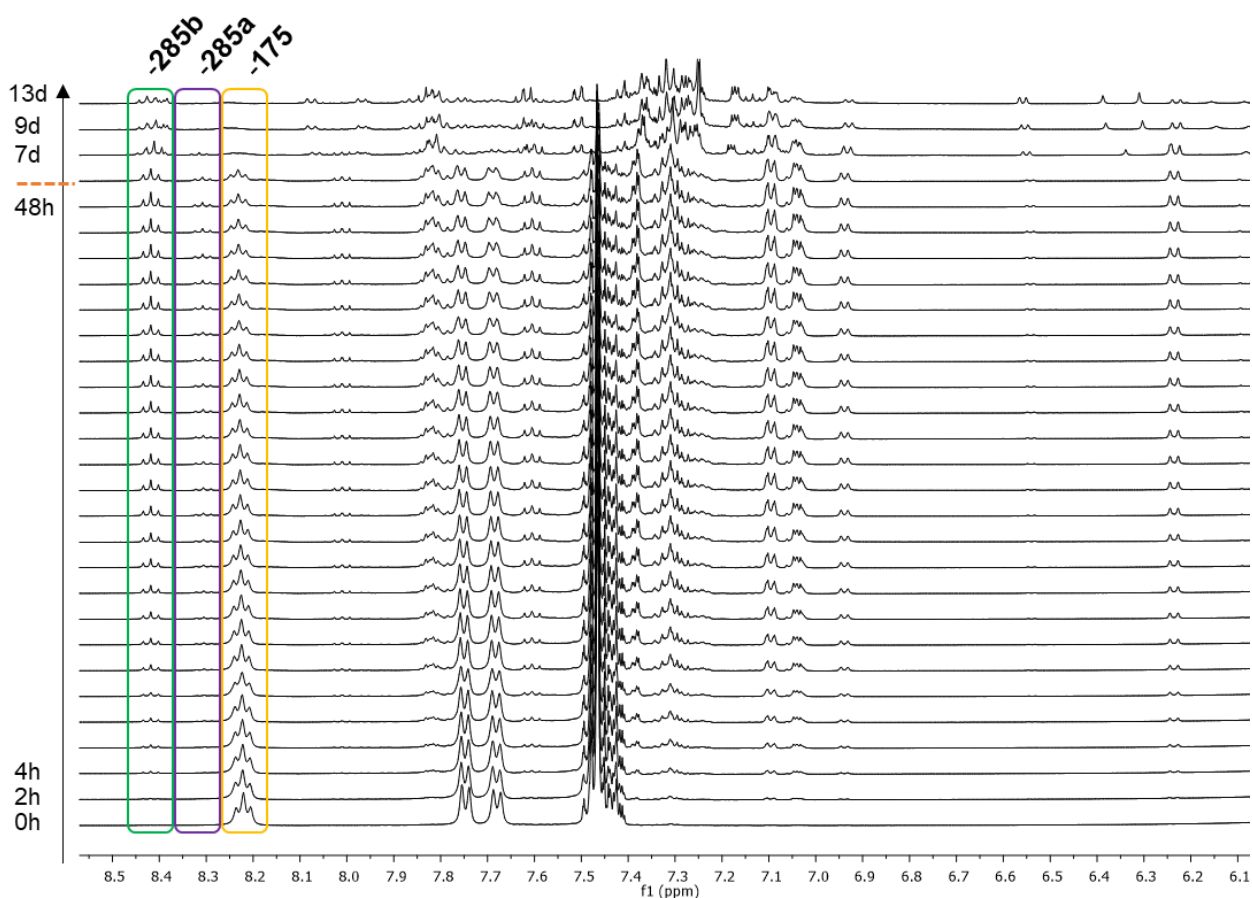


**Figure 45** Aromatic region of the  $^1\text{H}$  NMR spectrum of **175** recorded in the space of 13 days.

I observed similar trend for Au-based complexes **193** and **195**. The solution of the non-symmetric **195** remained unaltered in the period of 12 days (see ES). The symmetric **193** underwent swift changes similar to the Pt congener illustrated on the Figure 46. Spectra of the aliphatic region of **193** showed gradual decrease of the intensity of the peak at 2.60 ppm corresponding to the two methyl groups in symmetric **193**. With the disappearance of **193**, at least four other non-symmetric species started to show up on the spectra as evidenced by eight new methyl-like peaks. I identified one of this species to be the carbene-type complex **194** (methyl peaks at 2.56 and 2.12 ppm). The integration values for the methyl peaks of **193**, **194** and unidentified **286a** (2.40 ppm), **286b** (2.37 ppm), **286c** (2.32 ppm) revealed that the content of **193** in the mixture constituted around 62% after 12 h, 37% after 24 h and only around 9% after 48 h.

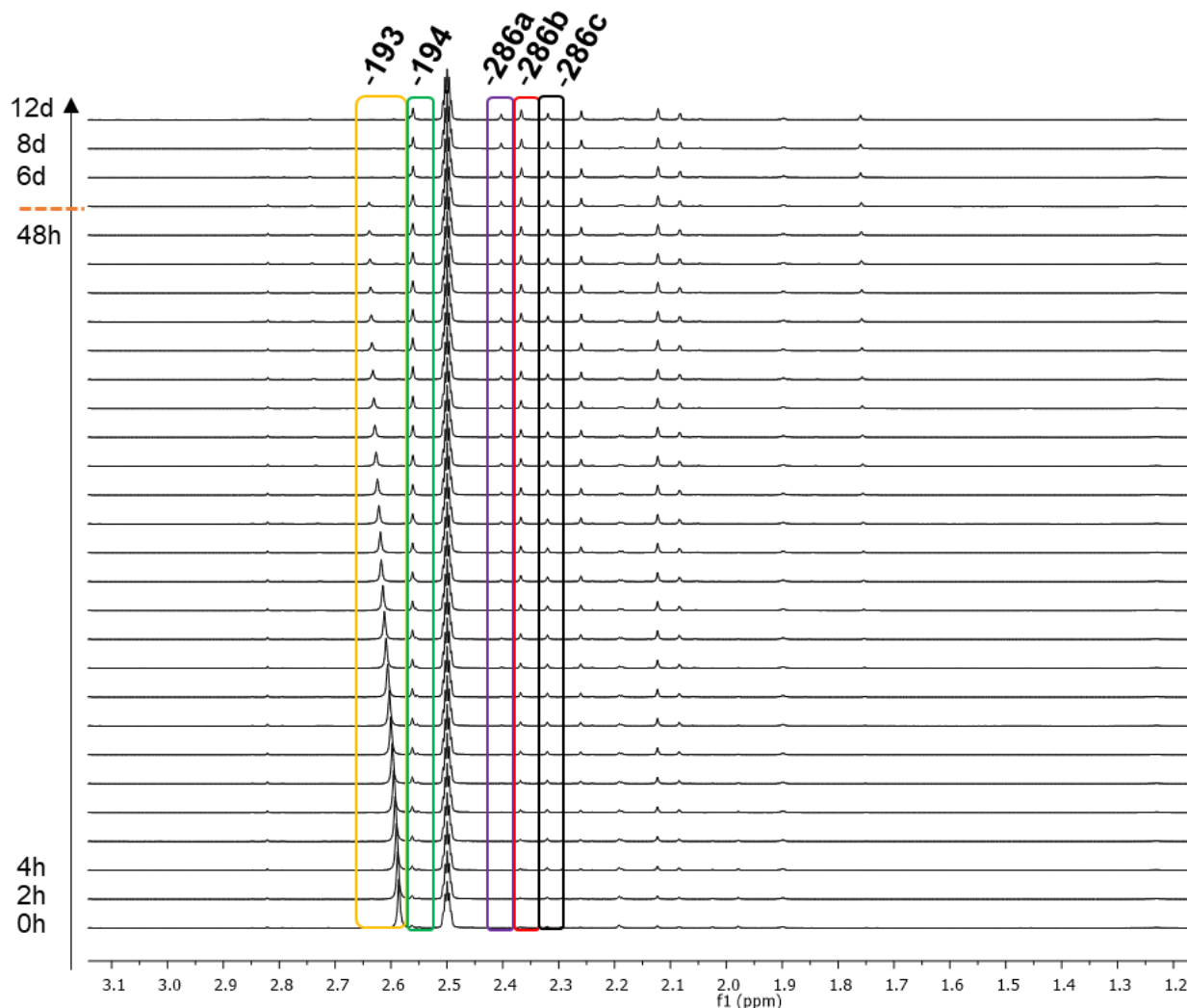


**Figure 46** Aliphatic region of the  $^1\text{H}$  NMR spectrum of **193** recorded in the space of 12 days.

The remarkable difference in stability of *t*-butyl,phenyl vs bis(phenyl) allene-containing complexes could be perhaps explained by the sterical inaccessibility of the former and/or the reactivity facilitating presence of an extra aromatic ring on the latter. These results provide valuable design information for the synthesis of analogues in the future. In terms of biological testing, it would be important to adjust the duration of the particular assays to ensure sufficient amount of the starting compounds present in case of complexes **175** and **193** and take into account their solution behaviour.

### VI b. 2. Antibacterial and antifungal activity

The results presented in this section were provided by the Community for Open Antimicrobial Drug Discovery (CO-ADD) at the University of Queensland, Australia.

Both groups of new allene-derived metal complexes as well as bis(pyridyl)allene ligands were tested for their antimicrobial activity in collaboration with CO-ADD. The routine

initial screening at the facility includes testing against microorganisms from gram-negative bacteria, gram-positive bacteria and fungi groups at single drug concentration of 32  $\mu\text{g/ml}$  (Table 12). The compounds inducing the growth inhibition of microorganisms at above 80% are deemed active (highlighted in orange, Table 12) and are subsequently tested at different drug concentrations to establish the drug dose response (also known as the hit confirmation step).

**Table 12** Percentage of growth inhibition ( $\pm 10\%$ ) of bacteria and fungi in the presence of allene-derived metal complexes and allene ligands at 32  $\mu\text{g/ml}$  of the drug.

Entry	Compound	G +ve		G -ve			Yeast	
		<i>S. aureus</i> (Sa)	<i>E. coli</i> (Ec)	<i>K. pneumoniae</i> (Kp)	<i>P. aeruginosa</i> (Pa)	<i>A. baumannii</i> (Ab)	<i>C. albicans</i> (Ca)	<i>C. neoformans</i> var. <i>grubii</i> (Cn)
allene-type	1 <b>171</b>	89.50	19.97	17.13	1.78	72.15	98.92	66.46
	2 <b>172</b>	88.65	48.49	26.24	53.44	92.24	99.78	73.68
	3 <b>176</b>	0.49	-2.56	17.84	17.75	21.87	100.22	0.49
	4 <b>175</b>	33.08	-6.04	6.61	2.90	8.76	71.29	-4.92
	5 <b>193</b>	91.03	87.82	41.8	90.52	89.96	100.22	67.40
	6 <b>195</b>	96.95	96.12	97.27	98.97	95.9	101.48	72.16
carbene-type	7 <b>184</b>	88.35	69.98	78.98	69.67	80.70	99.64	69.61
	8 <b>187<sup>a</sup></b>	89.61	89.05	91.54	92.43	91.38	99.78	69.91
	9 <b>194</b>	91.74	95.59	95.94	97.45	95.89	100.37	70.06
	10 <b>189<sup>b</sup></b>	94.08	97.73	96.07	99.65	97.27	101.04	68.25
	11 <b>179</b>	86.28	-6.04	8.7	-0.54	1.73	41.68	-8.32
ligands	12 <b>97b</b>	0.06	-3.91	4.43	19.85	6.66	2.30	-3.13
	13 <b>97a</b>	-2.65	-10.79	2.54	13.19	6.43	1.56	-2.04

<sup>a</sup> Single isomer – **187b**. <sup>b</sup> 1:0.5 ratio of **189b**:**189a**.

All complexes showed activity against at least one of the groups of microorganisms with the exception of complex **175** that was completely inactive (entry 4, Table 12). Complex **171** did not sufficiently disrupt the growth of gram-negative bacteria (entry 1, Table 12), whereas **176** and **179** were only active against fungi and gram-positive bacteria, respectively (entry 3 and 11, Table 12). Interestingly, all Au compounds from both groups of complexes exhibited antiproliferative activity across all the microorganisms' types (entries 5-10, Table 12). The screening confirmed the lack of activity of the allene ligands themselves (entries 12-13, Table 12). In total, 10 compounds (except **175**, **97a-b**) were moved to the hit confirmation stage.

Dose response of the pre-selected complexes was tested in the assays with the same microorganism species in the concentration range of 0.25 – 32  $\mu\text{g/ml}$ . These assays were used to determine the minimum inhibitory concentration (MIC) value defined as the lowest concentration of the drug at which full inhibition of the bacteria and fungi growth has been detected (inhibition > 80%), with the next highest concentration also exhibiting full growth inhibition. The compounds with MIC of 16  $\mu\text{g/ml}$  or lower were deemed active (Table 13). Additionally, cytotoxicity of new complexes was probed against human embryonic kidney cells (HEK-293) (Table 13). Cytotoxicity was expressed as a  $\text{CC}_{50}$  value – concentration at 50% cytotoxicity. The compounds with  $\text{CC}_{50}$  equal or lower than the maximum tested concentration (32  $\mu\text{g/ml}$ ) were considered toxic. Also, the haemolytic activity against human red blood cells (RBC) was determined as a  $\text{HC}_{10}$  value – concentration at 10% haemolytic activity (Table 13). Values with the “>” sign indicate a sample with no haemolytic activity or samples with  $\text{HC}_{10}$  values above the maximum tested concentration.

**Table 13** Minimum inhibitory concentration (MIC,  $\mu\text{g/ml}$ ) in a range of 0.25 - 32  $\mu\text{g/ml}$  of the drug concentration;  $\text{CC}_{50}$  (cytotoxicity,  $\mu\text{g/ml}$ ) with HEK-293 cells;  $\text{HC}_{10}$  (haemolytic activity,  $\mu\text{g/ml}$ ) with RBC cells.

Entry	Compound	G +ve		G -ve			Yeast		Human	
		<i>S. aureus</i> (Sa)	<i>E. coli</i> (Ec)	<i>K. pneumoniae</i> (Kp)	<i>P. aeruginosa</i> (Pa)	<i>A. baumannii</i> (Ab)	<i>C. albicans</i> (Ca)	<i>C. neoformans</i> var. <i>grubii</i> (Cn)	Embryonic kidney cells HEK-293 (Hk)	Red blood cells RBC (Hm)
allene-type	1 <b>171</b>	2	>32	>32	>32	>32	16	1	0.9567	>32
	2 <b>172</b>	$\leq 0.25$	>32	>32	>32	32	$\leq 0.25$	$\leq 0.25$	1.066	>32
	3 <b>176</b>	>32	>32	>32	>32	>32	32	>32	>32	>32
	4 <b>193</b>	16	32	>32	>32	>32	4	16	>32	>32
	5 <b>195</b>	16	$\leq 0.25$	>32	>32	>32	4	$\leq 0.25$	>32	$\leq 0.25$
carbene-type	6 <b>184</b>	$\leq 0.25$	>32	32	>32	32	$\leq 0.25$	$\leq 0.25$	0.6774	23.7
	7 <b>187<sup>a</sup></b>	2	>32	32	32	32	$\leq 0.25$	$\leq 0.25$	>32	>32
	8 <b>194</b>	$\leq 0.25$	16	16	>32	32	2	$\leq 0.25$	>32	19.31
	9 <b>189<sup>b</sup></b>	0.5	32	32	>32	32	2	$\leq 0.25$	>32	>32
	10 <b>179</b>	2	>32	>32	>32	>32	4	2	14.5	>32

<sup>a</sup> Single isomer – **187b**. <sup>b</sup> 1:0.5 ratio of **189b**:**189a**.

The activity of all compounds against some microorganisms' groups was confirmed in the dose response assays with the exception of **176** that exhibited no induction of growth inhibition up to 32  $\mu\text{g/ml}$  (entry 3, Table 13). From the remaining complexes only the allene-type Au(III) complex **193** and the two Au carbene-type complexes **187** and **189** derived from the non-symmetric ligand **97a** showed good antimicrobial and antifungal activity while

remaining non-toxic to human cells (entries 4, 7, 9, Table 13). However, only the latter two compounds (highlighted in yellow, Table 13) have been moved to the next stage of testing thanks to their increased activity against gram-positive bacteria and fungi.

At this stage, the antimicrobial testing was disrupted by the outbreak of the COVID-19 pandemic and more experimental data is only available for compound **189**. Thus, **189** was tested against extended panel of fungal strains (Table 14). Complex **189** was tested at two different ratios of isomers **189a** and **189b**. The former ratio was identical to that used in the previous assays whereas the latter was composed of 0.7:1 of **189b:189a**. The HC<sub>10</sub> and CC<sub>50</sub> at increased concentration range were also established (Table 14).

**Table 14** Minimum inhibitory concentration (MIC,  $\mu\text{M}$ ) of **189** against extended panel of fungal strains; HC<sub>10</sub> (haemolytic activity,  $\mu\text{M}$ ) with RBC cells; CC<sub>50</sub> (cytotoxicity,  $\mu\text{M}$ ) with HEK-293 cells.

Entry	Compound	Fungi				
		<i>Candida albicans</i> (ATCC 90028)	<i>Cryptococcus neoformans</i> (208821)	<i>Candida tropicalis</i> (ATCC 750)	<i>Candida glabrata</i> (ATCC 90030)	<i>Cryptococcus deuterogattii</i> (CBS 7750)
1	<b>189<sup>a</sup></b>	0.195-0.391	0.098-0.195	1.560-6.250	0.781-1.560	0.098-0.195
2	<b>189<sup>b</sup></b>	0.391-0.781	0.098-0.195	3.120-6.250	0.391-1.560	0.195
		Fungi			Human	
		<i>Cryptococcus deuterogattii</i> (ATCC 32609)	<i>Candida auris</i> (CBS 10913)	<i>Candida auris</i> (CBS 12373)	Red blood cells RBC (Hm)	Embryonic kidney cells HEK-293 (Hk)
3	<b>189<sup>a</sup></b>	0.024-0.049	0.391-25.000	0.006-100.000	200.000	200.000
4	<b>189<sup>b</sup></b>	0.049-0.098	0.195-0.391	0.006-100.000	200.000	200.000

<sup>a</sup> 1:05 **189b:189a**. <sup>b</sup> 0.7:1 **189b:189a**.

Both mixtures of **189** exhibited high antifungal activity in low micromolar range against majority of strains. There was not a significant difference of activity between the isomers of **189** no matter which one of them was a major component of the drug solution. **189** proved to be non-toxic and non-haemolytic up to 200  $\mu\text{M}$  of the drug concentration.

Due to its high activity and low toxicity, **189** (0.7:1) was selected for an *in vivo* evaluation in moth *Galleria Mellonella* larvae model. These experiments are currently ongoing.

### VI b. 3. Antiproliferative activity against cancerous cells

We investigated the *in vitro* anticancer activity of the new library of compounds against human breast adenocarcinoma cell line MDA-MB-231 using the CellTiter-Blue® (CTB) fluorescent

viability assay. After incubation of the cells in the presence of the drug candidate the CTB reagent was added to the treated cells. Viable cells are able to convert a redox dye resazurin present in the CTB reagent into its fluorescent derivative – resorufin (Figure 47). Under reducing conditions resorufin can be further reduced reversibly to a non-fluorescent dihydroresorufin, which can be a potential source of error when measuring the fluorescence of the treated cells.<sup>[350]</sup> Contrarily, non-viable cells do not facilitate the reduction of resazurin and do not fluoresce. The fluorescent response of the treated wells can be then measured and the percentage of the *viable* cells can be calculated in respect to the control experiment of non-treated cells. In general, the advantages of the CTB assay include high sensitivity of the fluorescence measurement compared to the colorimetric assays, decreased number of handling steps (addition, incubation, measurement) and low toxicity to cells allowing for extended periods of incubation.

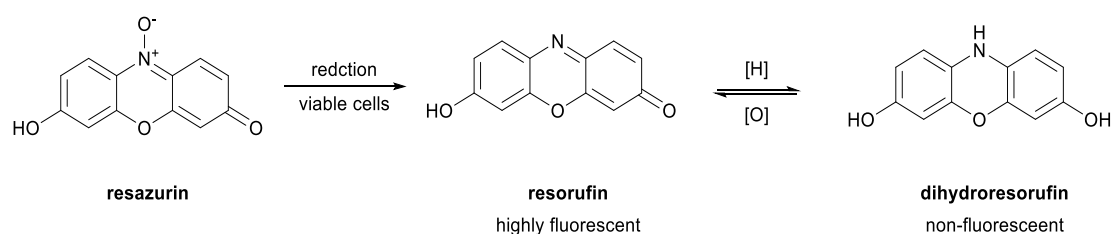


**Figure 47** Reduction of resazurin dye.

I tested both classes of complexes and allene ligands in the CTB assay. A series of 10 two-fold dilutions of each compound in DMSO in the range of 0.19 – 100  $\mu\text{M}$  was prepared. Subsequently, the MDA-MB-231 cells seeded on the 96-well plates were treated with the solutions of the drugs in technical triplicate repeat for each concentration and then they were incubated for 24 h. I chose this incubation period having in mind the solution instability of some compounds in the library (see Section VI b. 1.). After 24 h of incubation the cells were treated with the CTB reagent and the florescence was measured using a plate reader. The results of the experiment are presented as plots of the percentage of cell survival vs drug concentration – the dose response plots. The typical plot obtained for complex **193** is presented on the Figure 48.

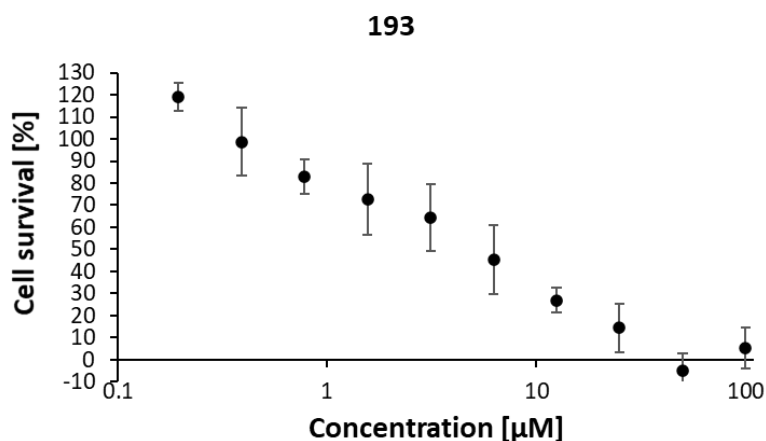


**Figure 48** CTB assay - viability of MDA-MB-231 cells treated with **193** after 24 h of incubation.

The initial experiments for all compounds in the wide concentration range (0.19 – 100  $\mu\text{M}$ ) allowed for the estimation of preliminary  $\text{IC}_{50}$  values for each compound. The  $\text{IC}_{50}$  parameter is the drug concentration value at which the *in vitro* growth of the cells is inhibited to 50%. This value is commonly used to compare the efficacy of the drug candidates. <sup>[351]</sup>

Usually, the dose response plots are characterised by the sigmoidal shape and the  $\text{IC}_{50}$  values are derived from the data points neighbouring the 50% survival mark. In our case, not all compounds gave a clear trend of diminished cell survival with the increased drug concentration (see ES). In order to facilitate the analysis, the data was also analysed using just the duplicate technical repeats from the same experiment after the rejection of the most discrepant values (see ES). Other limitation of this first experiment was the fact that the data for the control non-treated cells were also collected in just technical triplicate which was probably not sufficient to establish reliable reference point for a 100% survival and hence the experimental values for some compounds exceeded normal 0 - 100% range (see ES). However, the initial  $\text{IC}_{50}$  values could be extracted in most cases and are summarised in Table 15.



**Table 15** Initial IC<sub>50</sub> estimates for MDA-MB-231 cell line (24 h incubation) of allene-derived metal complexes and bis(pyridyl)allenes using CellTiter-Blue® assay.

	Entry	Compound	IC <sub>50</sub> [μM]
allene-type	1	<b>171</b>	0.29
	2	<b>172</b>	>100
	3	<b>176</b>	>100
	4	<b>175</b>	N/A <sup>a</sup>
	5	<b>193</b>	5.87
	6	<b>195</b>	66.12
carbene-type	7	<b>184</b>	7.00
	8	<b>187<sup>b</sup></b>	23.58
	9	<b>194</b>	10.18
	10	<b>189<sup>c</sup></b>	>100
	11	<b>179</b>	40.53
ligands	12	<b>97b</b>	>100
	13	<b>97a</b>	>100

<sup>a</sup> Lack of clear viability profile. <sup>b</sup> Single isomer – **187b**. <sup>c</sup> 1:05 **189b:189a**.

The most active compounds from the allene-type group seemed to be the symmetric Pd(II) and Au(III) compounds **171** and **193** (entry 1 and 5, Table 15). The non-symmetric congeners and both Pt(IV) complexes were substantially less toxic (entries 2-3, 6, Table 15). The lack of activity of **175** and **176** was particularly interesting as it mirrored their poor activity in the antimicrobial assays (Section VI b. 2.). Similarly, in the carbene-type class the complexes derived from the bis(phenyl)allene ligand were more active than the *t*-butyl analogues (entry 7 vs 8, 9 vs 10, Table 15). The free allene ligands did not show any antiproliferative properties (entries 12-13, Table 15), also in line with the lack of activity as antimicrobial agents. I selected the four bis(phenyl)compounds with the most promising IC<sub>50</sub> values below 20 μM for further testing (highlighted in orange in Table 15).

I proceeded to establish the exact IC<sub>50</sub> values for complexes **171**, **193**, **184** and **194** by performing the viability experiments in technical triplicate as well as two experimental repeats in a smaller concentration range on different days. Taking the example of **194** with the first IC<sub>50</sub> value found at 10.18 μM, this compound was then tested at 5 concentrations in the range of 6.125 – 12.5 μM (Figure 49).

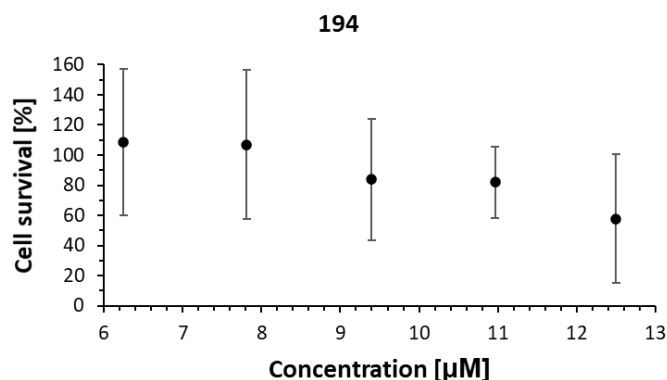


**Figure 49** CTB assay - viability of MDA-MB-231 cells treated with **194** after 24 h of incubation in 6.125 – 12.5 µM range.

As expected, I obtained close to linear response in the tested range. However, after two experimental repeats (Figure 49 and ES) I did not observe the viability dropping below 50% and therefore it was not possible to calculate the  $IC_{50}$  from these experiments. I obtained similar results for the other three compounds (see ES). Although, in this second round of testing the number of non-treated cell controls was more appropriate (>12) and the survival values mostly fell in the proper range, it might be that due to the limitations of the first experiments the tested concentration ranges of these experiments did not overlap. Additionally, in most cases I observed very large errors associated with the viability values.

The results of the CellTiter-Blue® assay were instructive, however we decided to validate these findings using different viability assay. I moved to the commonly used MTT proliferation assay and tested complexes **171**, **193**, **184** and **194** on the same cell line. The MTT assay differs from the CTB in that the cell viability is derived from the measurement of the absorbance of the MTT dye rather than the fluorescence (Figure 50). Although colorimetric MTT assay has lower sensitivity than fluorometric assays, its low cost, ease of use, rapidity and high reproducibility contributed to its widespread use in measurement of cytotoxicity.<sup>[352]</sup> Additionally, use of transparent plates necessary for the MTT assay allows to visually monitor the experiments using microscopy.

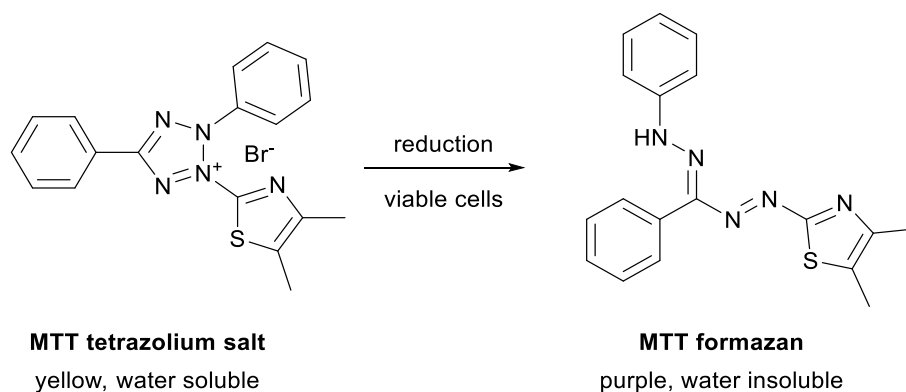


**Figure 50** Reduction of the MTT reagent.

I repeated the 24 h long experiment in the wider concentration range with the MTT assay (Figure 51 and ES). I obtained good viability vs concentration responses for all four compounds and estimated new  $IC_{50}$  values. The experimental errors were also substantially reduced in this assay, especially in the higher concentration range. This effect might result from the fact that more concentrated solutions are prepared with smaller error. Also, the smaller number of viable cells in the wells treated with higher doses of the drug might decrease the differences in absorbance readings compared to more variable wells with many cells at lower drug concentration.

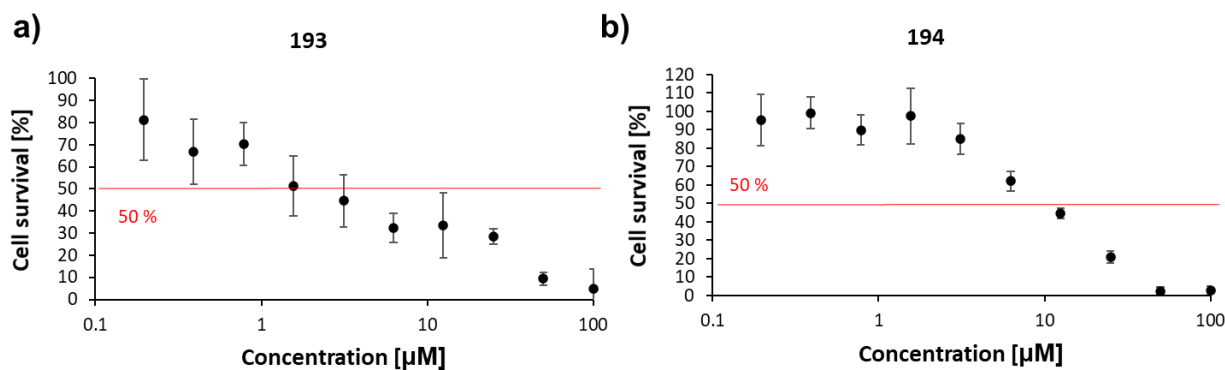


**Figure 51** MTT assay - viability of MDA-MB-231 cells treated with: a) **193**; b) **194** after 24 h of incubation.

In general, the initial estimates of the  $IC_{50}$  values in both assays were found to be in good agreement in a very similar low micromolar range.

**Table 16** Comparison of IC<sub>50</sub> values for CTB and MTT assays.

Entry	Compound	IC <sub>50</sub> CTB [μM]	IC <sub>50</sub> MTT [μM]
1	<b>171</b>	0.29	3.32 ± 1.22
2	<b>193</b>	5.87	2.50 ± 1.63
3	<b>184</b>	7.00	1.85 ± 0.40
4	<b>194</b>	10.18	14.70 ± 2.81

Subsequently, I carried out the MTT assay in restricted concentration ranges in experimental and technical triplicates to find more accurate IC<sub>50</sub> values. The sample results of these experiments are illustrated on **194** and are presented on the Figure 52. Compared to the analogous experiment with the CTB assay, the cropped concentration ranges were larger, however, to ensure that the half inhibitory concentration could be found within. The final IC<sub>50</sub> values (± standard deviation) were calculated as the mean of the three separate experimental runs and are presented in Table 16 (IC<sub>50</sub> MTT).

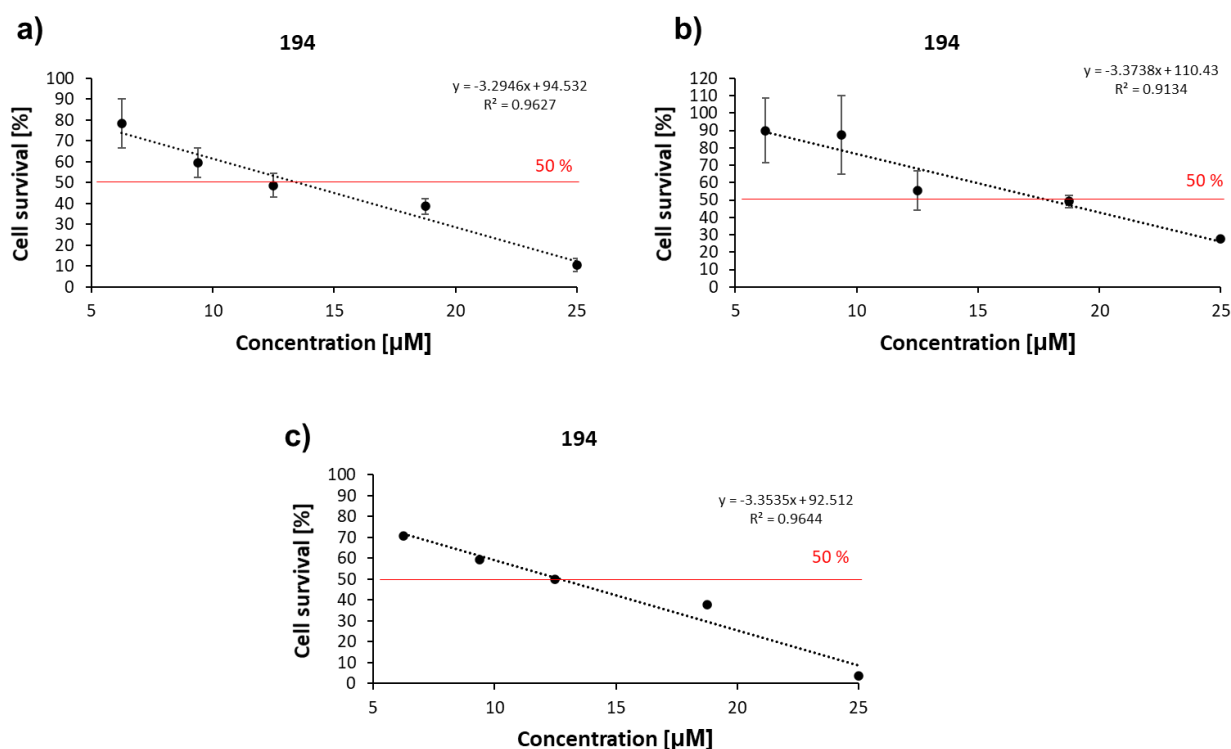


**Figure 52** MTT assay - viability of MDA-MB-231 cells treated with **194** in 6.125 – 25 μM range after 24 h of incubation: a) run 1; b) run 2; c) run 3 (experimental errors not included because some values were obtained from technical duplicates).

I confirmed significant toxicity of tested complexes against human breast cancer cell line. Particularly, two allene-containing compounds **171** and **193** and Au(I) carbene-type **184**

showed activity in the low micromolar range, whereas standard drugs e.g. cisplatin has the  $IC_{50} > 100 \mu M$  against that cell line.<sup>[353]</sup> The use of **193** might be less beneficial due to its high reactivity in solution and unknown interconversion products (Section VI b. 1.). However, results for **171** and **184** are promising. Interestingly, these compounds exemplify the two classes of allene-derived complexes and are based on Pd(II)- and Au(I)-centres that are not that well explored in the context of cancer treatment.

The good activity of the *trans* allene-containing complexes might seem surprising when we consider that most of the successful anticancer platinum-based complexes are in fact *cis* (see Figure 38). The mechanism of action of these *cis* complexes is attributed to the formation of 1,2 intrastrand crosslinks with two neighbouring nucleobases in DNA (see Figure 39), whereas the *trans* geometry of the complex does not allow for the formation of this type of crosslink. In fact, this argument was usually invoked to explain the lack of activity of the cisplatin isomer – transplatin. However, the low activity of transplatin was later accounted for by its more labile character and very facile hydrolysis under physiological conditions on route to the target.<sup>[354]</sup> The synthesis of more stable *trans* analogues with high *in vivo* antiproliferative properties pointed to the fact that other Pt-DNA adducts might be important for the high anticancer activity, for example, 1,3 intrastrand and interstrand Pt-DNA crosslinks.<sup>[355]</sup> The additional benefit of the alternative mechanism of action of the *trans* derivatives might be their effective use in cisplatin resistant cell lines.<sup>[356]</sup> This concept was extended beyond Pt-based chemotherapeutics and many other examples of *trans* coordination compounds have been found to show good activity, including Pd complexes.<sup>[357]</sup>

The anticancer testing was stopped at this point due to the time constraints of the project. Future investigation should focus on probing the cytotoxicity of the active complexes, in particular **171** and **184**, against healthy cell lines to ensure their potential for further development and safe use. At this point, we can infer from the cytotoxicity data obtained in the antimicrobial assays (Table 13) that these compounds are at least partially toxic to healthy human kidney and red blood cells at low concentrations (below  $IC_{50}$  values in case of **171** and **184**). The anticancer properties of our library of compounds could be also validated on different cancerous cell lines.

#### VI b. 4. Towards the mechanism of action – studies of the interactions with DNA

The results presented in this section were provided by Zoë Waller's group. In particular, Förster resonance energy transfer (FRET)-melting experiments for carbene-type complexes were performed by Mahmoud Abdelhamid and FRET-melting, fluorescent intercalator displacement (FID) and circular dichroism (CD) experiments of the allene-containing complexes and allene ligands were performed by Ying Xia.

Mechanism of action of many metal-based drugs is often, at least partially, ascribed to their interactions with DNA as an intracellular target (e.g. cisplatin, oxaliplatin, carboplatin).<sup>[358–362]</sup> We wanted to probe the possible source of the activity of allene-derived metal complexes by studying their interactions with different DNA types, not only with the standard double stranded helical structure, but also with non-canonical DNA secondary structures - such as G-quadruplex and i-motif, which chemistry lies within the Waller group's expertise.

The G-quadruplex is the best studied form of the quadruplex DNA and is formed in a guanine-rich regions of DNA (Figure 53, a). The formation of a tetrameric G-quadruplex structure usually requires the presence of cations that stabilise the structure.<sup>[363]</sup> The i-motif secondary structure arises in a DNA sequences rich in cytosine base repeats and its name is derived from the characteristic intercalation of the cytosine bases in its structure (Figure 53, b).<sup>[364,365]</sup> Both G-quadruplex and i-motif DNA have been recently found to play important physiological roles such as regulation of gene expression.<sup>[363,364]</sup>

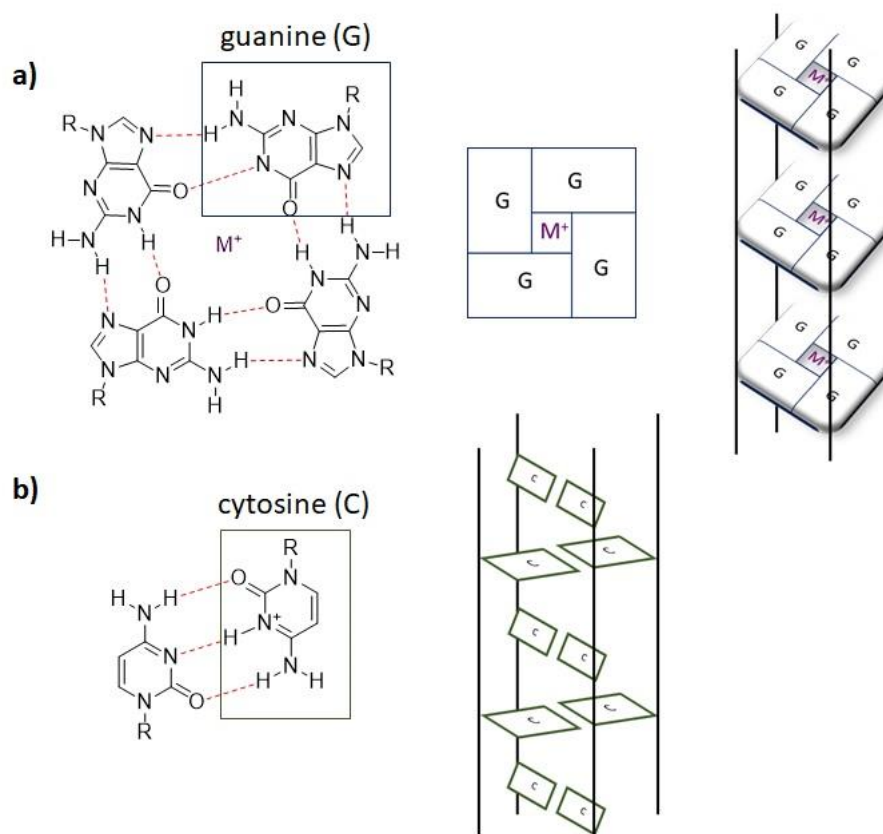


**Figure 53** Quadruplex DNA structure: a) schematic of G-quadruplex; b) schematic of i-motif.

Table 17 presents the different oligonucleotide sequences along with their predominant secondary structure used in our study to probe the interactions with complexes from the new library. These sequences are found in the human genome in promoter regions of their genes (DAP) or in the telomeric region (hTeloC, hTeloG).<sup>[366]</sup> In particular, telomeric region of DNA

and associated proteins have been linked to important functions such as DNA replication and protection against DNA damage.<sup>[367]</sup> As such, the link between dysfunctional telomeric DNA and disease e.g. cancer, is of much interest.<sup>[368]</sup>

**Table 17** Oligonucleotide sequences used in the study (T-thymine, A-adenine, G-guanine, C-cytosine, FAM-donor fluorophore 6-carboxyfluorescein and TAMRA-acceptor fluorophore 6-carboxytetramethylrhodamine – fluorescent tags (*vide infra* FRET experiments), HEG-hexaethylene glycol linker).

Entry	Name	Sequence modification – 5'→3'-modification	Secondary structure
1	DS	FAM-TATAGCTATA-HEG(18)-TATAGCTATA-TAMRA	Double-stranded
2	hTeloC	FAM-TAACCCCTAACCCCTAACCCCTAACCC-TAMRA	i-motif
3	DAP	FAM-CCCCCGCCCCCGCCCCCGCCCCGCCCC-TAMRA	i-motif
4	hif-1- $\alpha$	FAM-CGCGCTCCCGCCCCCTCTCCCTCCCGCGC-TAMRA	i-motif
5	hTeloG	FAM-GGGTTAGGGTTAGGGTTAGGG-TAMRA	G-quadruplex

One of the common techniques used to study DNA-small molecule interactions is Förster resonance energy transfer (FRET)-melting experiment. FRET-melting experiment allows for initial, high throughput screen of potential DNA binders (often called ligands). The experiment takes advantage of the Förster resonance energy transfer (FRET) phenomenon also called fluorescence resonance energy transfer.<sup>[369,370]</sup> FRET arises from the dipole-dipole intermolecular forces of molecules in close proximity. The FRET system comprises a “donor” that transfers its excitation energy to the “acceptor” in a non-radiative manner. The occurrence of FRET is dependent on the distance between the donor and the acceptor. The FRET phenomenon has been employed in the study of nucleic acids and in particular quadruplex-forming sequences.<sup>[370]</sup>

The basis of the FRET-melting experiments presented in this section is measurement of the fluorescence intensity response of the fluorescent probes (see Table 17) attached to the 5' and 3' ends of the oligonucleotide sequence. In this case, when the probes are in a small distance from each other (folded structure) the fluorescence response of the donor is transferred to the acceptor. However, upon the thermal denaturation (unfolding) of the secondary structure of DNA, the distance between the fluorophores increases, which can be measured as an increase in fluorescent intensity as a function of temperature. Routinely, the melting temperature ( $T_m$ ) where the structure is 50% folded or unfolded is established for each oligonucleotide sequence and then compared to the melting temperature of the same sequence in the presence of potential ligand, giving the value of the change in melting temperature ( $\Delta T_m$ ). A negative value of  $\Delta T_m$  (lower  $T_m$  in the presence of the ligand) indicates denaturation at lower temperature and hence destabilisation of the structure by the ligand,

whereas a positive  $\Delta T_m$  value can be interpreted as a sign of DNA stabilisation in the presence of a ligand. Therefore FRET-melting experiments are used to study thermal stability of specific DNA fragments.

The investigation began with the analysis of the carbene-type allene-derived metal complexes **179**, **184**, **187**, **189** and **194**. Each compound was tested at a range of concentrations up to 1.0  $\mu\text{M}$  which constituted 5.0 equivalents excess in respect to the DNA used at 200 nM. Higher concentrations of the complexes were not used in order to avoid non-specific interactions resulting from the sheer excess in respect to the DNA. Figure 54 shows the example of FRET-melting experiment results obtained for hTeloC i-motif-forming sequence for complexes **184** and **194**. The plots corresponding to the remaining oligonucleotide sequences and complexes can be found in the Experimental Section (page 265).

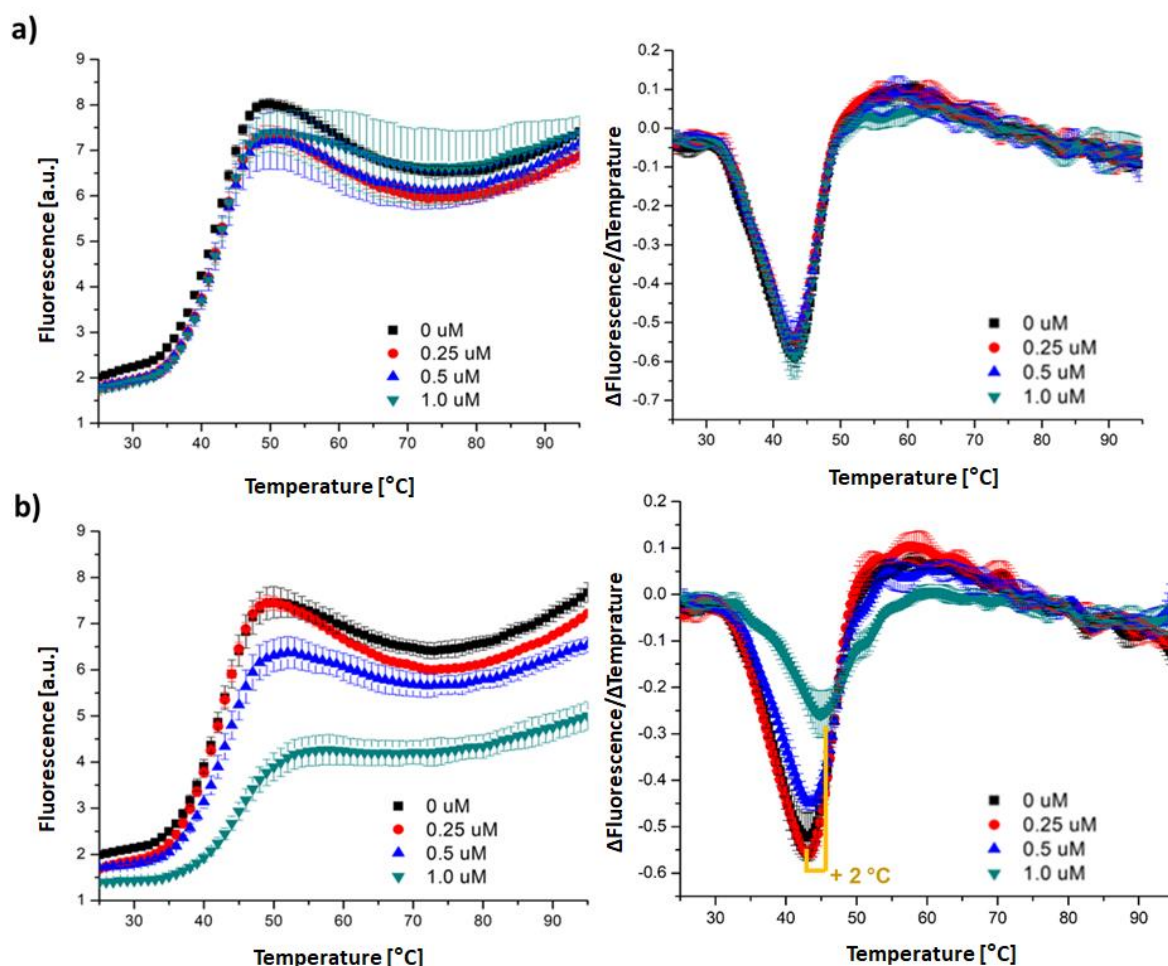


**Figure 54** FRET-melting experiments for hTeloC and complexes: a) **184**; b) **194**; melting curves (left), first derivatives of fluorescence intensity in respect to temperature (right).

The graphs on the left on Figure 54 show melting curves of the fluorophore-tagged hTeloC sequence in the presence of our complexes as well as a control curve (marked with



black squares). The melting temperatures ( $T_m$ ) can be easily read from the minima on graphs of the first derivative of the fluorescence intensity in respect to temperature (Figure 54, right). For **184**, there was no significant change in melting temperature with addition of the complex in the tested concentration range ( $\Delta T_m \approx 0$  °C, Figure 54, a). However, Au(III)-complex **194** induced stabilising effect measured as a positive change in melting temperature of + 2 °C at a concentration of 1.0  $\mu$ M (Figure 54, b). Interestingly, all the compounds, including **194**, showed no significant interaction with the remaining DNA sequences (see ES and Table 18).

**Table 18** FRET-melting experiments for carbene-type complexes.

Entry	Compound	DS	$\Delta T_m \pm 1$ [°C]			
			hTeloC	hif-1- $\alpha$	DAP	hTeloG
1	<b>184</b>	0.0	0.0	0.0	0.0	0.0
2	<b>187<sup>a</sup></b>	0.0	0.0	0.0	0.0	0.0
3	<b>194</b>	0.0	2.0	0.0	0.0	0.0
4	<b>189<sup>b</sup></b>	0.0	0.0	0.0	0.0	0.0
5	<b>179</b>	0.0	0.0	0.0	0.0	0.0

<sup>a</sup> 1:0.12 ratio **187a:187b**. <sup>b</sup> 0.5:1.0 ratio **189a:189b**.

These results suggested some possible specific interactions of **194** with the i-motif DNA over the G-quadruplex and double stranded DNAs. The origin of this effect is currently studied in our group by derivatisation of **194** and studies of structure-DNA interaction activity of its analogues as well as DNA docking modelling. The lack of evidence for the binding to any of the tested oligonucleotide sequences with other carbene-type complexes might suggest that any bioactivity observed in other assays for these compounds might not arise from a direct action of the metal complex and the DNA in the cells. The FRET-melting experiments were also performed for the allene-containing metal complexes as well as bis(pyridyl)allene ligands at a single concentration of 1.0  $\mu$ M (Table 19).

**Table 19** FRET-melting experiments for allene ligands and allene-containing complexes.

Entry	Compound	DS	$\Delta T_m \pm 1$ [°C]		
			hTeloC	hif-1- $\alpha$	hTeloG
1	<b>DMSO</b>	55	43	46	59
2	<b>97b</b>	0.0	0.0	0.0	-0.5
3	<b>97a</b>	0.0	-0.5	0.0	-1.0
4	<b>171</b>	0.0	0.0	0.0	2.0
5	<b>172</b>	0.0	0.0	0.0	-1.0
6	<b>176</b>	0.0	0.0	0.0	-1.0
7	<b>175</b>	-0.5	0.0	-0.5	-0.5
8	<b>193</b>	0.0	0.0	0.0	-0.5
9	<b>195</b>	0.0	0.0	0.0	-1.0

The majority of the allene-containing complexes and both allene ligands had no significant effect on the thermal stability of the double-stranded, i-motif or G-quadruplex sequences in the FRET-melting experiment. We observed the most pronounced response within the group for the symmetric Pd complex **171** that showed increase of the melting temperature for hTeloG of around 2 °C (entry 4, Table 19). Interestingly, Pt- and Au-based complexes, typically more associated with the mechanism of action through DNA interaction, were not found to have similar effect.

The FRET-melting results for this group of compounds were followed up with the fluorescent intercalator displacement (FID) competition assay. Carbene-type complexes will be assessed in FID assays in due course following the synthesis of more analogues.

FID assays have been developed to study binding affinity of small molecules towards different DNA secondary structures such as double-stranded, G-quadruplexes and i-motifs.<sup>[371,372]</sup> In particular, Waller and co-workers developed i-motif FID assay using thiazole orange (TO) as a fluorescent probe (Figure 55, a).<sup>[372]</sup> In the presence of DNA, the TO probe is characterised by considerable enhancement of its fluorescent response whereas when DNA is absent no significant fluorescence is observed. This difference in the fluorescence response can be interpreted in terms of binding to DNA. However, the response is only observed if a ligand binds to the same region of the DNA as the TO probe and is specific to each type of DNA. Binding to other sites is not detected. In the FID experiment, the studied DNA fragment is first equilibrated with the TO probe to reach a steady state of the fluorescent response. Subsequently, potential DNA binders are added to the system and the possible decrease of fluorescence is understood as a displacement of the thiazole orange by the tested compound in binding to the DNA fragment.

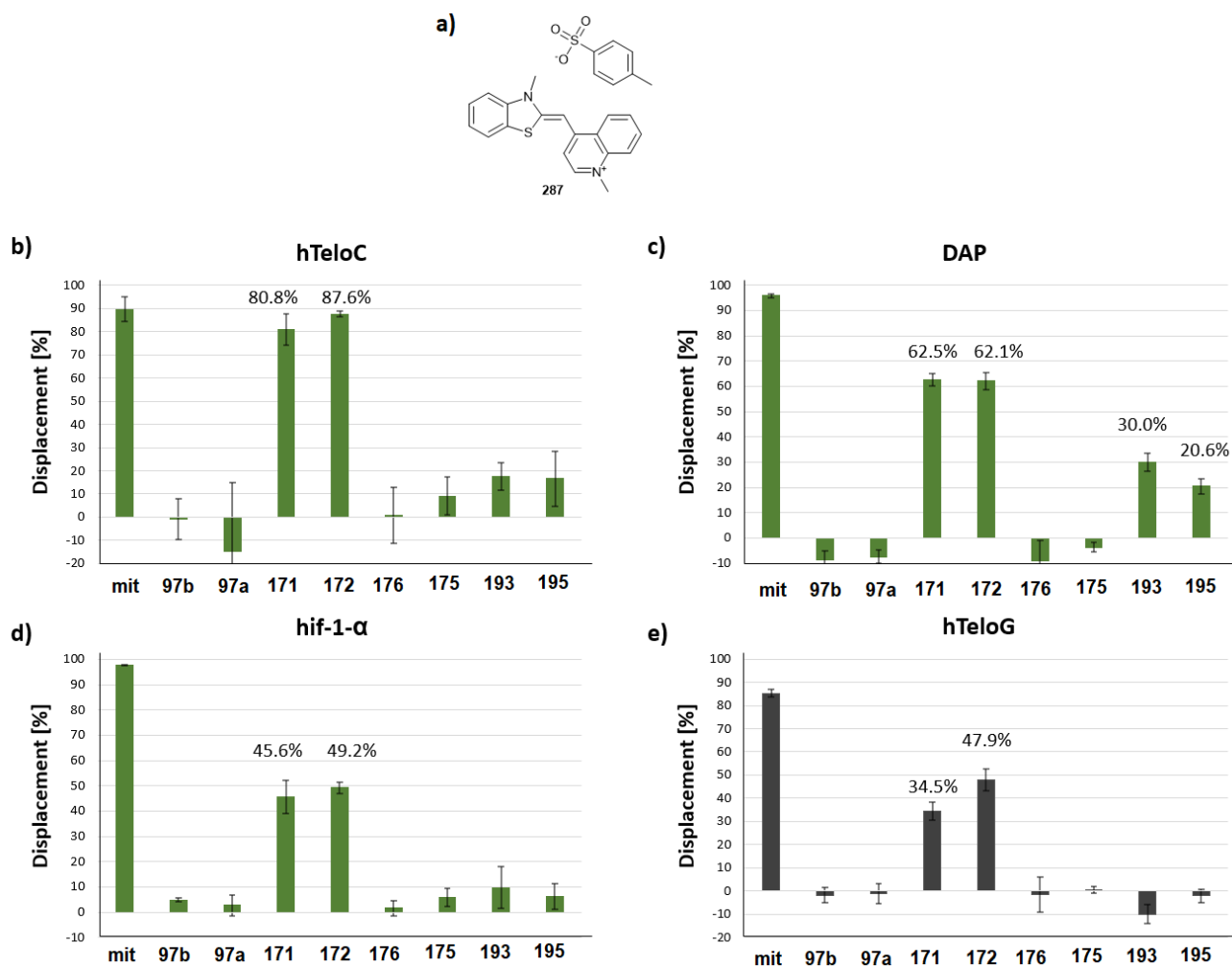


**Figure 55** a) Structure of thiazole orange **287** (TO); b-d) FID assay for allene ligands and allene-containing complexes for i-motif DNA; e) for G-quadruplex. mit = Mitoxantrone, positive control.

The compounds were tested at a single concentration of 2.5  $\mu\text{M}$  (5.0 equiv. in respect to DNA) with all three classes of DNA secondary structures and the results are partially presented on Figure 55. The data for the double-stranded DNA can be found in the Experimental Section (page 279), however none of the tested compounds showed a displacement level of over 25% (Table 20). Bis(pyridyl)allenes **97a-b** did not induce any significant displacement of the TO probe neither with the i-motif nor the G-quadruplex DNAs. This result provides further evidence that any observed bioactivity of the allene-derived metal complexes probably is not linked to the action of disassociated ligands if such de-complexation would take place under physiological conditions. Complex **171** exhibited a 34.5% displacement in the hTeloG experiment (Figure 55, e), confirming the FRET observation of its partial affinity to the G-quadruplex structure. However, its analogue **172** showed even bigger effect at 47.9%. Moreover, both Pd complexes were the most active binders for all i-motif sequences (Figure 55, b-d) reaching the displacement level of 87.6% for **172** with hTeloC (Figure 55, b). Au(III)-complexes **193** and **195** interacted with the DNA to a much lesser extent while Pt(IV)-

complexes were inactive on the level of the free allene ligands. This result further pinpoints the lack of any significant biological activity of the Pt(IV)-complexes **175-176**, that might be ascribed to problems with reduction (see Section IV b. 3. on chemical and electrochemical reduction) to active Pt(II) analogues *in situ* and/or solubility issues.<sup>[211]</sup> The results are also summarised in Table 20.

**Table 20** Summary of the FID results for allene ligands and allene-containing complexes.

Entry	Compound	DS	Displacement [%]			
			hTeloC	hif-1- $\alpha$	DAP	hTeloG
1	<b>97b</b>	9.8	-0.9	4.9	-8.6	-1.7
2	<b>97a</b>	8.1	-14.8	2.8	-7.4	-1.1
3	<b>171</b>	13.0	80.8	45.6	62.5	34.5
4	<b>172</b>	24.7	87.6	49.2	62.1	47.9
5	<b>176</b>	8.0	0.8	1.6	-8.9	-1.6
6	<b>175</b>	11.5	9.2	5.9	-3.6	0.7
7	<b>193</b>	10.6	17.6	9.8	30.0	-10.0
8	<b>195</b>	9.3	16.5	6.2	20.6	-2.1

The best Pd-based binders were further examined with circular dichroism spectroscopy (CD). Secondary structures of DNA interact with circularly polarised light in a specific manner and CD spectra are commonly used in characterisation of nucleic acids.<sup>[373]</sup> The advantages of this method include high sensitivity to conformational changes and thus very characteristic response for a particular arrangement of DNA. Typically, spectra are monitored in the region between 200-320 nm. A negative band at around 265 nm and a large positive band at around 288 nm is usually observed for an i-motif DNA. G-quadruplexes are characterised by a strong positive band at around 260 nm corresponding to the parallel forms while the antiparallel forms give a negative band at 260 nm and a positive one at 295 nm.<sup>[373]</sup> The method is also advantageous to FRET-melting, because it does not require the presence of fluorescent probes that can be a source of interference with DNA ligands.

The CD data was collected for both complexes **171** and **172** with three i-motif forming sequences (hTeloC, DAP and hif-1- $\alpha$ ) and G-quadruplex forming sequence hTeloG. A representative set of results is presented below for hTeloC DNA (remaining graphs in ES). Both complexes were first titrated against hTeloC up to 5:1 ligand to DNA ratio (Figure 56). In both cases, the characteristic i-motif peaks were observed at around 260 nm (negative) and

290 nm (positive). The increasing excess of **171** and **172** induced a visible hypochromic shift of both peaks, that is usually associated with an unfolding effect of the DNA secondary structure.

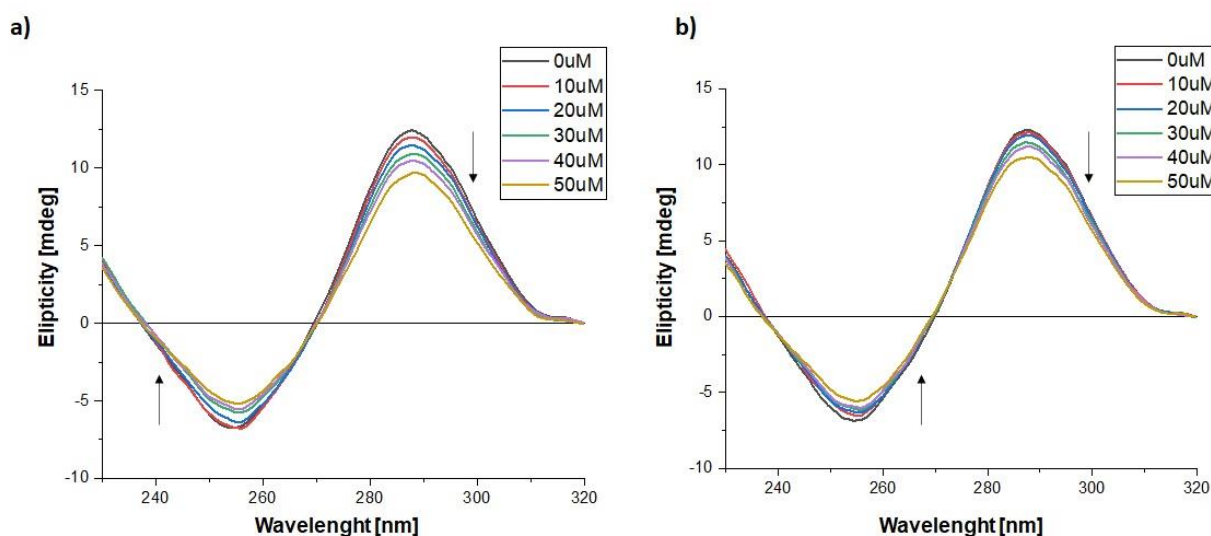


**Figure 56** CD spectra of 10  $\mu\text{M}$  hTeloC with titration up to 5.0 equiv. (50  $\mu\text{M}$ ) of: a) **171**; b) **172**.

CD-melting experiments were performed next to quantify the level of the interactions (Figure 57). In these experiments a series of CD spectra of the DNA fragment in the presence of potential binder is recorded in the range of temperatures to examine its thermal stability under these conditions. For these experiments, **171** and **172** were used in an excess of 5.0 equivalents to the hTeloC. With increasing temperature, both i-motif bands exhibited significant hypochromic as well as hypsochromic shifts that could be interpreted as an unfolding/thermal denaturation of the i-motif structure (Figure 57, a-b). The plots of normalised ellipticity vs temperature for the peak at 288 nm allowed to find the values of the melting temperature for the hTeloC sequence with (red circle) and without (black square) the Pd complexes (Figure 57, c-d), and hence the  $\Delta T_m$  value. Both complexes induced a negative  $\Delta T_m$  of - 4.0  $^{\circ}\text{C}$  and - 1.0  $^{\circ}\text{C}$  for **171** and **172**, respectively. The  $\Delta T_m$  values for remaining DNA forms are summarised in Table 21.

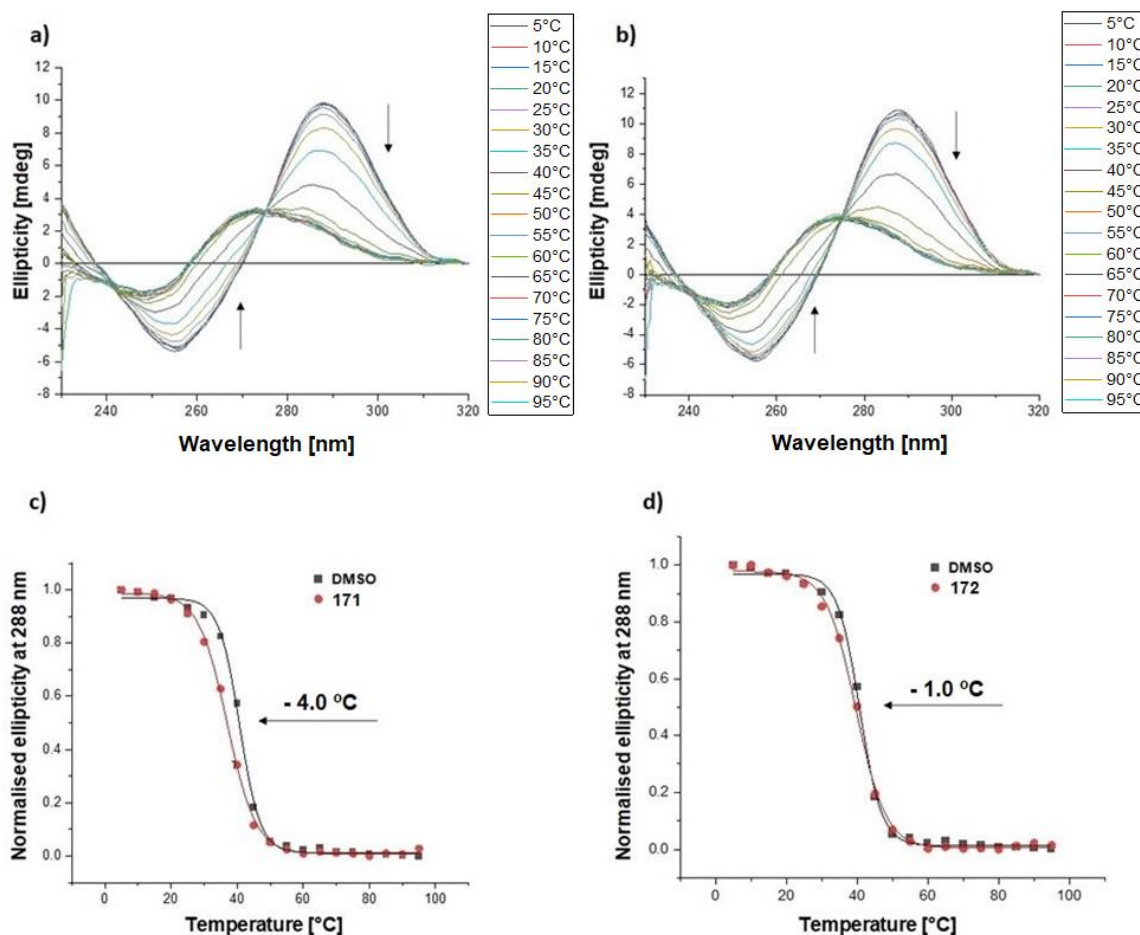


**Figure 57** CD-melting experiments (5-95 °C) of 10  $\mu\text{M}$  hTeloC with 5.0 equiv. (50  $\mu\text{M}$ ) of: a) **171**; b) **172**; c) normalised ellipticity at 288 nm of **171**; d) normalised ellipticity at 288 nm of **172**.

The  $\Delta T_m$  value for **171** in hTeloC experiment (entry 2, Table 21) was the most significant from all CD-melting profiles. This result was very interesting when connected to the significant anticancer activity exhibited by **171** (see Section VI b. 3.). It also correlates with the biggest displacement observed in FID experiments for **171** and further supports its affinity for telomeric i-motif DNA and weaker binding to the remaining DNA quadruplexes. Although **172** showed similar behaviour to **171** in the FID assay the CD-melting results pointed out that it had smaller effect on thermal stability of different DNA sequences, with the biggest effect observed for hTeloG (entry 3, Table 21). The differences between the  $\Delta T_m$  values from FRET and CD experiments (compare Table 19 vs Table 21) arise from the fact that these experiments measure different phenomena. In FRET the signal is derived from the energy transfer between fluorophores and CD measures the folding of the DNA. Because many factors can interfere with the fluorophore's signal and thus influence the final result usually the CD measurement is considered more reliable.

**Table 21** Change in melting temperature ( $\Delta T_m$ ) of hTeloC, DAP, hif-1- $\alpha$  and hTeloG measured by CD-melting experiments for **171-172**.

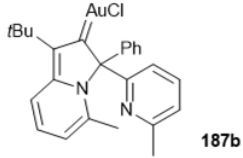
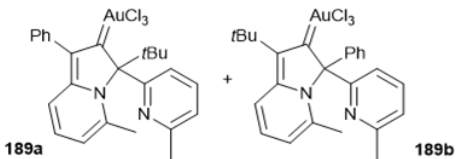
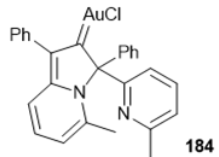
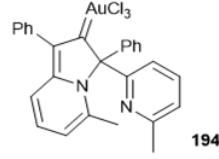
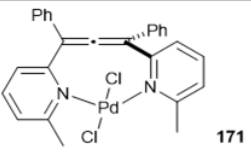
Entry	Compound	$\Delta T_m \pm 1$ [°C]			
		hTeloC	DAP	hif-1- $\alpha$	hTeloG
1	<b>DMSO</b>	41	29	25	70
2	<b>171</b>	-4.0	-1.0	0.0	-1.0
3	<b>172</b>	-1.0	-0.0	1.0	-3.0

### VI c. Conclusions

This chapter described first investigations into the biological activity of allene-derived metal complexes. The summary of the main findings is presented in Table 22. Section VI b. 1. underpinned that important for medicinal applications stability of bis(pyridyl)allene metal complexes is dependent on the nature of the ancillary substituents on the ligands. Au carbene-type complexes **187b** and **189** derived from the non-symmetric ligand **97a** showed remarkable antimicrobial activity and low toxicity for human tissue with **189** entering *in vivo* stage of testing (Section VI b. 2.). Complementary results of good anticancer activity of Pd and Au complexes **171**, **184** and **194** of symmetric ligand **97b** were presented in Section VI b. 3. These complexes showed antiproliferative activity against human breast cancer cell line in the low micromolar range. Additionally, the source of activity of the complexes was briefly investigated in DNA binding studies (Section VI b. 4.). Some of the compounds exhibiting anticancer activity were among those showing the most significant binding to quadruplex DNA, specifically **194** (Au(III)) from the carbene group and **171** Pd(II) from the allene group.

Results of this chapter clearly demonstrate that bis(pyridyl)allene-derived complexes show very promising biological activity, albeit further study is needed. These preliminary results supplemented important first information regarding the design/activity relationship in terms of both the allene ligand fragment as well as the metal centre.

**Table 22** Bioactivity of allene-derived metal complexes – summary of key findings.

Entry	Compound	Antimicrobial activity	Anticancer activity	DNA (human) interactions
1	 187b	<ul style="list-style-type: none"> <li>- G +ve bacteria</li> <li>- Fungi</li> <li>- <u>Low toxicity to human cells</u></li> </ul>	IC <sub>50</sub> > 20 μM	-
2	 189a + 189b	<ul style="list-style-type: none"> <li>- G +ve bacteria</li> <li>- Fungi</li> <li>- <u>Low toxicity to human cells</u></li> <li>- <u>In vivo testing</u></li> </ul>	IC <sub>50</sub> > 100 μM	-
3	 184	<ul style="list-style-type: none"> <li>- G +ve bacteria</li> <li>- Fungi</li> <li>- Partial toxicity to human cells</li> </ul>	IC <sub>50</sub> = 1.85 ± 0.40 μM (MDA-MB-231 cells)	-
4	 194	<ul style="list-style-type: none"> <li>- G +ve and G-ve bacteria</li> <li>- Fungi</li> <li>- Partial toxicity to human cells</li> </ul>	IC <sub>50</sub> = 14.70 ± 2.81 μM (MDA-MB-231 cells)	- Selectivity towards hTeloC i-motif (ΔTm + 2 °C in FRET)
5	 171	<ul style="list-style-type: none"> <li>- G +ve bacteria</li> <li>- Fungi</li> <li>- Partial toxicity to human cells</li> </ul>	IC <sub>50</sub> = 3.22 ± 1.22 μM (MDA-MB-231 cells)	- Binding to i-motif and G-quadruplex, in particular hTeloC (ΔTm - 4 °C in CD)

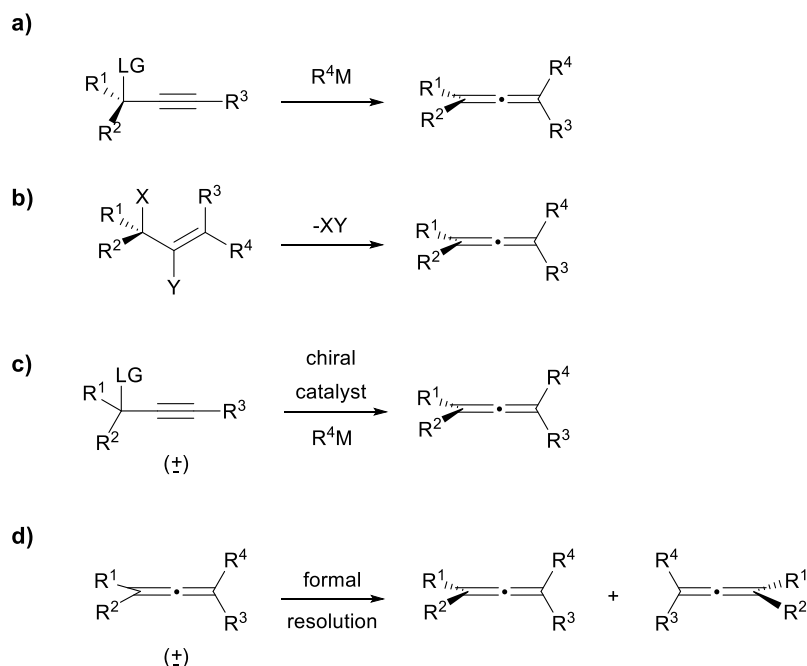
The following, last section of the thesis is looking at the development of the asymmetric version of the bis(pyridyl)allene-based systems.



## VII. Resolution of precursors to allene ligands

### VII a. Introduction

Enantioselective synthesis of allenes remains one of the important goals of modern organic chemistry.<sup>[71]</sup> Different approaches have been developed to harness axial chirality of allenes and access especially challenging tri- and tetrasubstituted optically pure allenes.<sup>[374]</sup> Non-racemic allenes can be prepared from enantiomerically enriched starting materials such as propargylic or allylic compounds with the central-to-axial chirality transfer (Scheme 103, a-b). Alternatively, stereoselective synthesis from racemic starting materials can be achieved with the use of chiral reagents or auxiliaries, but particularly effective are catalytic asymmetric reactions (Scheme 103, c).<sup>[375]</sup> Transition metal-catalysed reactions are especially prominent in catalytic enantioselective synthesis of allenes with some examples of organo- or enzymatic catalysis. Optically active allenes can be also obtained by resolution of a racemic mixture of allenic compounds (Scheme 103, d).<sup>[376,377]</sup> Different methods of resolution include chiral resolution, where the racemic allenes are reacted with optically active reagents and the resulting diastereotopic mixtures are separated on the basis of physical differences between the diastereomers, or kinetic resolution. Kinetic resolution takes advantage of the different rates of reaction of the enantiomers of the allene with a chiral reagent/catalyst. When one of the enantiomers is preferentially transformed into the product, the optical purity of the unreacted enantiomer increases.



**Scheme 103** Common approaches to enantioselective synthesis of allenes: a) from enantioenriched propargylic compounds; b) from non-racemic allylic substrates; c) synthesis from racemic substrates with chiral catalytic systems; d) resolution of racemic allenes.

## VII b. Results and Discussion

The previous chapters described the racemic synthesis of allene-containing ligands and their metal complexes as well as the proof of concept applications in catalysis and in medicinal settings. Due to the inherent axial chirality of allenes the new systems could be prepared in enantioselective manner. Such enantiomerically enriched allene-derived metal complexes could be used in asymmetric versions of tested catalytic reactions. Additionally, the bioactivity of the enantiomers could be assessed separately, potentially leading to the use of only the active ones as drug candidates.

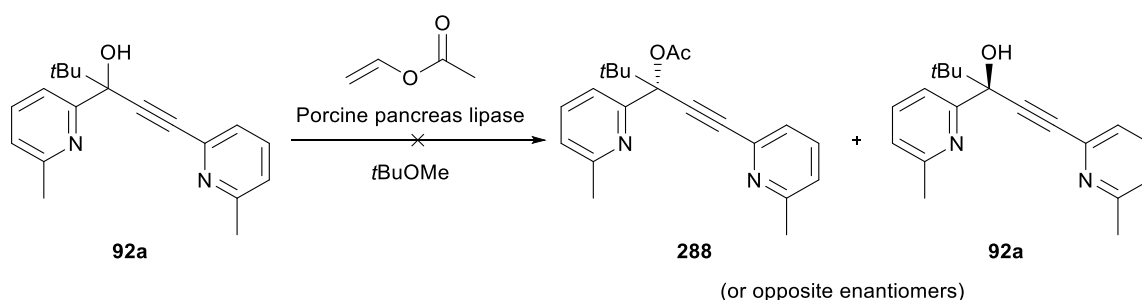
The first attempts of preparation of optically active bis(pyridyl)allenes are presented in this section. Although Krause and co-workers obtained one derivative of enantiomerically pure bis(pyridyl)allene with the HPLC separation of its ester precursor, we wanted to explore more robust chemical methods that would yield the ligands at scale, without the need of preparative HPLC.<sup>[149]</sup>

Synthesis of optically active tetrasubstituted allenes often takes advantage of the use of optically enriched propargyl compounds that undergo  $S_N2'$  reactions yielding fully substituted allenes. Preparation of enantiomerically pure propargyl alcohols is often accomplished *via* asymmetric nucleophilic addition to ketone and aldehyde precursors and resulting enantiomerically enriched alcohols are subsequently used in the synthesis of allenes.

Asymmetric addition of organometallic reagents to carbonyl compounds is typically accomplished with the use of chiral ligands.<sup>[378–381]</sup> In case of pyridine based starting materials, the best chiral inductions have been achieved using bespoke chiral ligands.<sup>[382]</sup> However, the multistep synthesis of such ligands is a substantial disadvantage to this methodology. Different approaches include resolution of racemic propargyl alcohols or esters into their enantiomers using chemical or chromatographic methods. Isolation of both enantiomers in the same process is a considerable advantage of this strategy. Thus, our first attempt to obtain optically enriched precursors to bis(pyridyl)allenes involved resolution of corresponding bis(pyridyl)propargyl alcohols.

One of the common methods of esterification of alcohols with a simultaneous chiral resolution is the use of enzymes as a chiral influence in the reaction.<sup>[383,384]</sup> In principle, in the presence of an enzyme one of the enantiomers of the alcohol undergoes esterification in much higher rate than the other, and as a result the mixture of an ester and an alcohol is obtained. These can be separated later with the use of common purification techniques. Typically, enzymatic resolution gives good results with secondary alcohols, whereas tertiary alcohols are more difficult substrates and suffer from decreased reactivity.

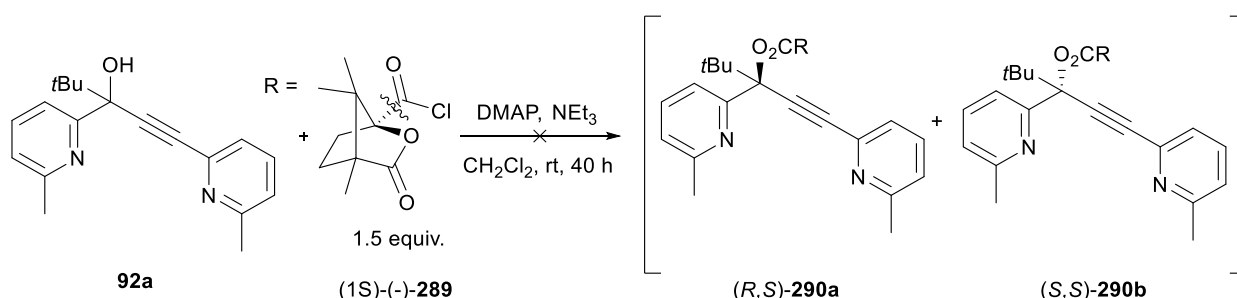
I reacted alcohol **92a** under typical conditions with vinyl acetate in the presence of lipase enzyme. I selected porcine pancreas lipase because of its documented activity with tertiary alcohols and relatively low price compared to other enzymes.<sup>[385]</sup> I did not observe any reaction, however, and recovered unreacted starting material (Scheme 104). I found similar lack of reactivity with other available pyridyl alcohols.



**Scheme 104** Attempt of enzymatic resolution of tertiary alcohol **92a**.

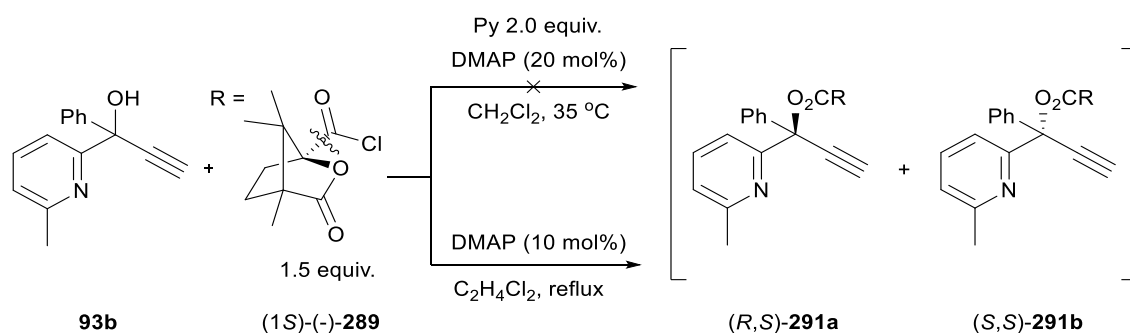
Another approach to resolution of racemic alcohols is the reaction with chiral derivatizing agent, for example, in an esterification reaction. Chiral derivatizing agents are typically used to establish the absolute configuration of chiral alcohols and amines.<sup>[386]</sup> The use of enantiomerically pure derivatizing coupling partners for resolution purposes produces a diastereomeric mixture of two ester products that can be separated after the reaction. If needed, the esters could be hydrolysed back to the alcohols, but in our case the esterified

products could be used directly in the synthesis of allenes. Thus, alcohol **92a** was reacted with 1.5 equivalents of (-)-camphanic acid chloride **289** under DMAP catalysis (Scheme 105). After 40 h I only recovered starting materials.



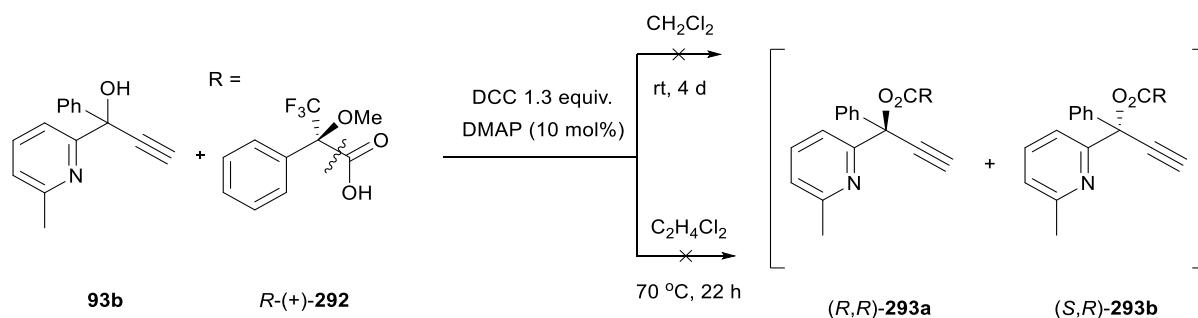
**Scheme 105** Esterification of **92a** with (1S)-(-)-camphanic acid chloride **289**.

To test if the problem was the reaction conditions used or the steric hindrance of the propargylic alcohol, I also tried the reaction on less sterically demanding tertiary alcohol **93b** with (-)-camphanic acid chloride (Scheme 106). The reaction at 35 °C in the presence of pyridine was unsuccessful. However, I observed formation of the ester in refluxing dichloroethane.<sup>[387]</sup> Although, the <sup>1</sup>H NMR analysis of an aliquot of this reaction showed no traces of the starting material and clear diastereotopic signals assigned to the expected products, I could not isolate **291**. The esterified products seemed rather unstable and all attempts of their isolation resulted in recovery of the alcohol starting material.



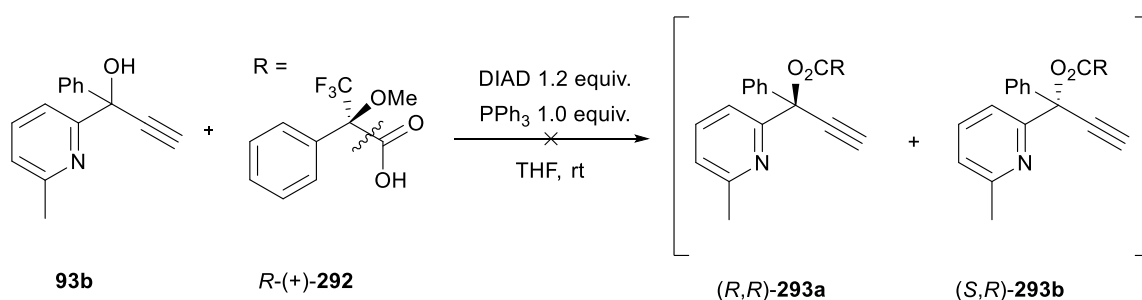
**Scheme 106** Esterification of **93b** with (1S)-(-)-camphanic acid chloride **289**.

Another classic example of derivatizing agent is  $\alpha$ -methoxy- $\alpha$ -trifluoromethylphenylacetic acid, commonly known as Mosher's acid (**292**, Scheme 107). We hoped that it would yield more stable ester products. Unfortunately, DCC promoted coupling of **93b** with (+)-Mosher's acid either at room temperature or at 70 °C resulted only in re-isolation of unreacted **93b**.



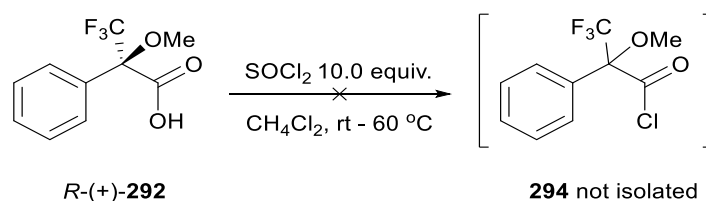
**Scheme 107** Coupling of **93b** with *R*-(+)-Mosher's acid **292**.

I did not observe any reactivity under Mitsunobu reaction conditions either (Scheme 108).<sup>[388]</sup>



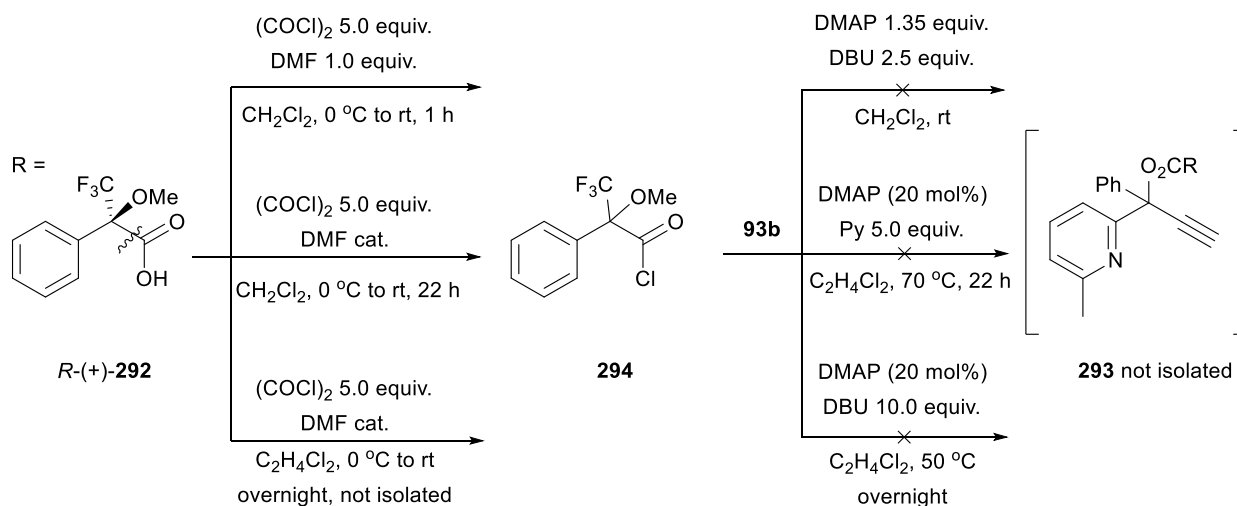
**Scheme 108** Coupling of **93b** and Mosher's acid using DIAD.

Due to the inactivity of the reaction with the Mosher's acid itself I decided to transform it into the more reactive acid chloride derivative. However, acid chloride formation with thionyl chloride did not work (Scheme 109).



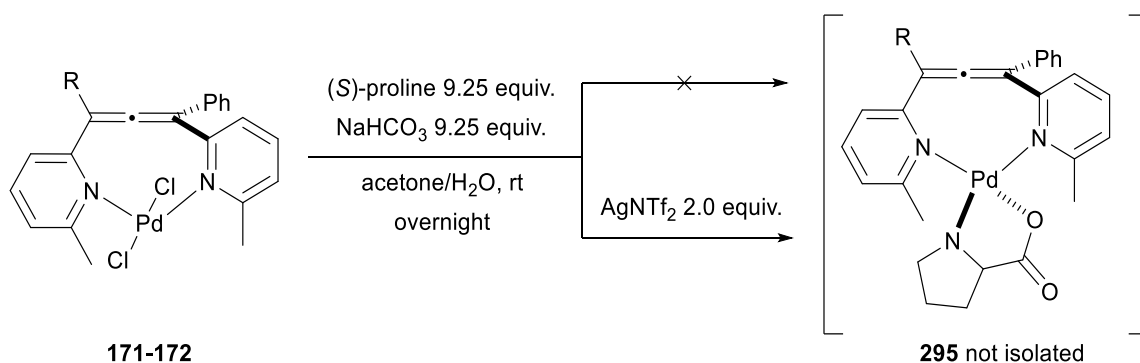
**Scheme 109** Preparation of Mosher's acid chloride with SOCl<sub>2</sub>.

I confirmed the formation of acid chloride **294** with oxalyl chloride instead (Scheme 110). However, initial attempts to isolate the intermediate Mosher's acid chloride before the reaction with **93b**, or reaction with *in situ* formation of **294**, always ended with recovery of the starting materials.



**Scheme 110** Preparation of Mosher's acid chloride **294** with  $(\text{COCl})_2$  and reaction with alcohol **93b**.

Going beyond the preparation of optically active allene ligands, some methodologies have been developed to chemically resolve metal complexes synthesised from racemic ligands. This approach could potentially overcome common problems with racemisation of allenes in the presence of metals at the stage of complex preparation. For example, palladacyclic complexes developed by Richards and co-workers were resolved using (*S*)-proline.<sup>[389]</sup> A racemic mixture of a Pd complex was expected to react with enantiomerically pure proline in a ligand exchange reaction to form two diastereomeric proline adducts. The separation of diastereoisomers followed by hydrolysis of proline adducts with HCl would yield resolved enantiomers of the starting material complex. Richards' conditions were applied to Pd allene-supported complexes **171-172**, but without any effect (Scheme 111). To facilitate the ligand exchange reaction of **171-172** with proline, the reaction was also carried out in the presence of  $\text{AgNTf}_2$ . However, the difficult separation of resulting complex reaction mixture did not yield any constructive products.



**Scheme 111** Resolution attempt of Pd complexes **171-172** with (*S*)-proline.

**VII c. Conclusions**

Asymmetric synthesis of fully substituted allenes remains a significant synthetic challenge. All the attempts of the chemical resolution of enantiomers of precursors to bis(pyridyl)allenes presented in this section were unsuccessful. The lack of reactivity of sterically demanding tertiary alcohols seemed to be a major factor contributing to the poor resolution. Pd complexes were also not resolved using a common amino acid. In the light of these observations, other approaches such as preparative HPLC or asymmetric synthesis would be needed to accomplish preparation of optically active bis(pyridyl)allenes at scale.

## VIII. Conclusions

The threefold set of objectives for this doctoral research laid out in Section II has been accomplished. I successfully prepared allene-based ligands capable of complexation to various metal centres through their Lewis basic groups and beyond and I discovered that these allene-derived metal complexes have interesting catalytic activity and bioactivity.

In the first, synthetic part of the work I identified the bis(pyridyl)allene ligand design as the most robust and versatile ligand candidate. Other ligands, decorated with thienyl, amine or phosphine groups proved to be too reactive to withstand challenging conditions of metal coordination and underwent undesired side reactions. I closely investigated the behaviour of bis(pyridyl)allenes in the presence of metals and discovered a dual mode of interaction depending on the nature of the metal itself. Reactions with Pd(II), Pt(IV) and Au(III) precursors yielded complexes in which the allene-core was preserved and the metal centre was captured by the two pyridyl groups in the ligand. With more carbophilic Au(I) (and to a certain extent Au(III)) we observed different reactivity. The activation of the allene skeleton in the presence of the metal resulted in an intramolecular attack of the pyridyl group onto the allene with a formation of a C-Au bond. I isolated a range of such stable, indolizine-based, carbene-type complexes. Allene-derived complexes of both types were fully characterised.

In the second part of the study, I investigated potential applications of the new library of complexes. In terms of their catalytic activity, I found limited applicability of Pd complexes in the Tsuji-Trost allylic alkylation. However, they showed good activity in the Mizoroki-Heck coupling. Complexes from both groups, and in particular Au(I) carbene-type compounds, could also catalyse cycloisomerisation and alkoxy cyclisation of 1,6-enynes. Pt complexes performed well as catalysts in the nucleophilic addition of alcohols to allenes.

In collaboration with UEA and external partners we also tested medicinal properties of the new complexes in three main areas: antimicrobial activity, anticancer activity and DNA interactions. Most complexes showed high toxicity towards bacteria and fungi with two Au carbenes **187b** and **189** also being non-toxic to human cells in the first screenings. Complexes derived from the symmetric ligand **97b**, (except Pt(IV) **175**) showed best antiproliferative activity towards human breast adenocarcinoma cancerous cell line. We probed the source of this activity through studies of interaction of the allene-derived complexes with different secondary structures of DNA (double stranded, i-motif, G-quadruplex) and observed preliminary selectivity of the active compounds (**194**, **171**) towards telomeric i-motif. Further biological studies are still ongoing.



## IX. Future research directions

This research project could be developed further in a number of ways to increase its impact and novelty. Starting with the design of allene-based ligands, specifically bis(pyridyl)allenes we could think about further derivatisation to accomplish new coordination behaviour. For example, the connectivity of the pyridyl groups with the allene skeleton (the nitrogen atom position) could be changed to investigate the influence on the observed cyclisation process in the presence of metals. What is more, it is easy to envision additional derivatisation of the ancillary substituents on the allene core to achieve new ligand properties. This line of research is currently investigated in our group in a related PhD project and by project students. Additionally, allenes with new types of not yet tested donor groups could be prepared and examined.

An important, not achieved so far, aspect of the project is the synthesis of optically pure allene ligands or the resulting metal complexes. In order to accomplish this, the bis(pyridyl)allenes prepared in a racemic version could be separated into their enantiomers using, for instance, preparative HPLC. Alternatively, precursors to target allenic compounds could be prepared in an asymmetric manner (e.g. asymmetric nucleophilic addition to ketones). The catalysis part of the project would benefit substantially, because the asymmetric catalysis with allene-derived complexes could be attempted.

It would be valuable to further validate the biological activity of our complexes by extension of already explored assays. For instance, testing of anticancer activity could be extended to different cancerous and healthy cell lines and with promising results move beyond *in vitro* evaluation. The source of already observed biological activity is of much interest and is an important research direction. It could be accomplished by extension of current library to study the structure/activity relationship or by molecular modelling.

**X. Experimental Section****Contents**

<b>General methods .....</b>	<b>185</b>
<b>Chapter III - Synthesis of allene-based ligands – procedures .....</b>	<b>187</b>
Compound 88a.....	187
Compound 88b.....	188
Compound 89a.....	188
Compound 89b.....	189
Compound 91a <sup>[397]</sup> .....	190
Compound 91b <sup>[397]</sup> .....	190
<b>General procedure A for the synthesis of propargyl alcohols 92a-c.....</b>	<b>191</b>
Compound 92a.....	191
Compound 92b.....	192
Compound 92c.....	193
Compound 93a <sup>[401]</sup> .....	193
Compound 93b <sup>[401]</sup> .....	194
Compound 94.....	195
<b>General procedure B for esterification of propargyl alcohols<sup>[163]</sup> .....</b>	<b>195</b>
Compound 96c.....	196
Compound 96a.....	196
Compound 96b.....	197
Compound 97a <sup>[149]</sup> .....	198
Compound 97b <sup>[149]</sup> .....	198
Compound 97c <sup>[149]</sup> .....	199
Compound 85 <sup>[164]</sup> .....	200
Compound 102a <sup>[403]</sup> .....	200
Compound 103a <sup>[403]</sup> .....	201
Compound 102b.....	201

---

Compound 103b.....	202
Compound 105b.....	202
Compound 109.....	203
Compound 104c <sup>[398]</sup> .....	204
Compound 110a <sup>[401]</sup> .....	204
Compound 110b <sup>[401]</sup> .....	205
Compound 110c <sup>[401]</sup> .....	205
Compound 105a <sup>[403]</sup> .....	206
Compound 105c.....	206
Compound 105d.....	207
Compound 112a.....	207
Compound 117 <sup>[409]</sup> .....	208
Compound 112f <sup>[197]</sup> .....	209
Compound 112e <sup>[175]</sup> .....	209
Compound 112h <sup>[175]</sup> .....	210
Compound 115c.....	211
Compound 115d.....	212
Compound 115e.....	212
Compound 101b <sup>[177]</sup> .....	213
Compound 119 <sup>[168]</sup> .....	214
Compound 120 <sup>[177]</sup> .....	214
Compound 130 <sup>[191]</sup> .....	215
Compound 131 <sup>[411]</sup> .....	216
Compound 131b <sup>[413]</sup> .....	216
Compound 132 <sup>[414]</sup> .....	217
Compound 126c <sup>[416]</sup> .....	217
Compound 125b.....	218
Compound 127c and 127e <sup>[188]</sup> .....	218
Compound 127d <sup>[188]</sup> .....	219

---

Compound 135 <sup>[188]</sup> .....	220
Compound 136 <sup>[188]</sup> .....	221
Compound 141 <sup>[197]</sup> .....	222
Compound 142 <sup>[197]</sup> .....	222
<b>Chapter IV - Synthesis of allene-derived metal complexes .....</b>	<b>223</b>
Compound 171 .....	223
Compound 172 .....	224
Compound 173 <sup>[418]</sup> .....	224
Compound 175 <sup>[419]</sup> .....	225
Compound 176 <sup>[419]</sup> .....	225
Compound 177a <sup>[419]</sup> .....	226
Compound 177b .....	226
Compound 179 .....	227
Compound 184 <sup>[157]</sup> .....	228
Compound 187 .....	228
Compound 187b .....	229
Compound 192 .....	230
Compound 193 .....	231
Compound 194 .....	231
Compound 189 and 195 .....	232
<b>Chapter IV - Isomerisation of complexes 187a and 187b – kinetic experiments .....</b>	<b>233</b>
<b>Chapter IV - Attempts to derivatise Au(I) complex 187b .....</b>	<b>233</b>
HNTf <sub>2</sub> experiment .....	233
Iodination .....	234
Oxidation experiments .....	234
<b>Chapter IV - Isomerisation of complexes 189a and 189b – kinetic experiments .....</b>	<b>234</b>
<b>Chapter IV - X-ray structure determination .....</b>	<b>235</b>
Compound 141 .....	236
Complex 172 .....	236

Complex 179.....	236
Complex 184.....	237
Complex 187b.....	238
Complex 194.....	240
Complex 189b.....	242
Complex 189a.....	242
<b>Chapter V - Catalytic experiments – preparation of starting materials and general procedures.....</b>	<b>243</b>
Compound 209c.....	243
Compound 211c.....	243
Compound 216.....	244
<b>General procedure for the Mizoroki-Heck coupling<sup>[425]</sup>.....</b>	<b>245</b>
Compound 220c.....	245
Compound 200b <sup>[427]</sup> .....	245
Compound 258a <sup>[429]</sup> .....	246
Compound 200a <sup>[429]</sup> .....	247
<b>General procedure for metal-catalysed cyclisation of enynes 200a and 200b.....</b>	<b>247</b>
Compound 202a.....	248
Compound 202b.....	248
Compound 202c.....	248
Compound 201a:201b:201c:201d 1:0.08:0.08:0.01.....	249
<b>General procedure for metal-catalysed alkoxylation of enynes 200a and 200b.....</b>	<b>249</b>
Compound 203a.....	249
Compound 203c.....	250
Compound 268a.....	250
<b>General procedure for metal-catalysed addition to allenes.....</b>	<b>251</b>
Compound 268b.....	251
Compound 269a.....	252
Compound 268c.....	252

Compound 269b.....	252
<b>Chapter VI - Stability studies.....</b>	<b>253</b>
<b>Chapter VI - Antibacterial and antifungal assays .....</b>	<b>256</b>
<b>Chapter VI - Anticancer assays.....</b>	<b>256</b>
Cell culture, passage and count .....	256
Freezing for long-term storage .....	257
<i>In vitro</i> chemosensitivity studies .....	257
CellTiter-Blue® (CTB) assay .....	258
MTT assay .....	258
<b>Chapter VI - DNA studies.....</b>	<b>266</b>
General Experimental.....	266
FRET-melting experiments.....	266
FID assay.....	279
CD-melting experiments.....	280

## General methods

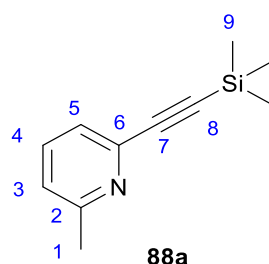
All reagents and solvents used in described syntheses were of analytical grade and purchased from commercial suppliers, including all Grignard reagents (Merck, Thermo Fisher Scientific, Fluorochem); used without further purification, unless otherwise stated. Dry solvents (anhydrous  $\geq 99.8\%$ ) were obtained directly from commercial sources.  $\text{ZnBr}_2$  was dried with a heat gun in *vacuo* until it became visibly dry. Accurate weights were obtained with a Denver Instrument SI-234 balance (230 g x 0.1 mg) for synthetic experiments and with Mettler Toledo XS205DU (81/120 g x 0.01/0.1 mg) for the preparation of stock solutions. For thin layer chromatography (TLC) technique, commercially available aluminium sheets pre-coated with silica gel (0.20 mm with fluorescent indicator UV254, Grace GM BH & Co) were used. Column chromatography was performed using silica gel 60, 0.032-0.063 mm (230-450 mesh, Alfa Aesar). Ratios of the solvents used as eluents are given in brackets. The yields of the compounds obtained as mixtures were calculated in the cases where the mixture composition was known. Non-conventional heating by microwave irradiation was performed in a Biotage Initiator<sup>+</sup> Microwave system equipment with normal absorption level, with the exception of reactions carried out in 1,4-dioxane where low level of absorption was applied. The  $^1\text{H}$  NMR and  $^{13}\text{C}\{^1\text{H}\}$  NMR spectra were recorded using a Bruker Ascend<sup>TM</sup> 500 or a Bruker

Ultrashield™ Plus 400 spectrometers (solvent given in brackets). Bruker Ultrashield™ Plus 400 spectrometer was used to record  $^{31}\text{P}$  and  $^{19}\text{F}$  spectra. Chemical shifts ( $\delta$ ) are given in parts per million (ppm) and the values of coupling constant  $J$  are given in Hertz (Hz). Abbreviations for multiplicities are as follows: s – singlet, d – doublet, t – triplet, q – quartet, m – multiplet, brs – signal broadened. Spectra were recorded at room temperature unless stated otherwise. 2D NMR experiments COSY and HSQC were performed to assign proton and carbon peaks, respectively. In some cases, they were supported with NOESY and HMBC experiments to facilitate structure elucidation. High resolution mass spectra were carried out using ESI, EI, NSI and ASAP techniques at the University of Sussex and National Mass Spectrometry Facility in Swansea. Electro Spray Ionisation (ESI) measurements were carried out on APEX II Bruker Daltonic Fourier transformer (FTMS) using Apollo ESI source. Electron Impact (EI) ionisation was performed using AutoSpec Fisons instrument. Nano Spray Ionisation (NSI) measurements were carried out on LTQ Orbitrap XL spectrometer. Atmospheric Solid Analysis Probe (ASAP) measurements were carried out Xevo G2-S spectrometer. Microanalysis was performed with Thermo Flash 2000 Elemental Analyser configured for for %CHN, at the London Metropolitan University. UV-Vis spectra were recorded using a Hitachi U-3000 spectrophotometer at rt. Quartz cuvettes with a 1 cm path length were used. Fluorescence excitation and emission spectra were obtained using an Edinburgh Instruments FS5 spectrofluorometer in quartz cuvettes with a 1 cm path length at rt. For the plate assays, absorbance and fluorescence measurements were carried out using a CLARIOstar® (BMG Labtech) microplate reader at rt. Cyclic voltammetry was performed using an Autolab PGSTAT302N potentiostat/galvanostat (Metrohm) with a three-electrode system. The glassy carbon working electrode was polished using alumina. The counter electrode was Pt, and Ag or Ag/AgCl was used as a reference electrode with ferrocene internal standard ( $\text{Fc}/\text{Fc}^+$ ) at 0.43 V vs Ag/AgCl. The electrochemical cell was purged with Ar prior and after addition of the analyte solution. For the crystal structure analysis of **141** the data was collected with Rigaku AFC<sub>11</sub> quarter chi goniometer equipped with a Rigaku Hypix 6000 detector mounted at the window of 007 HF copper rotating anode generator with Varimax optics (300 $\mu\text{m}$  focus) diffractometer. Cell determination, data collection, data reduction, cell refinement and absorption correction was performed using CrysAlisPro software.<sup>[390]</sup> Structure solution and refinement was accomplished using SHELXT and SHELXL programmes, respectively.<sup>[391,392]</sup> The crystals of **184**, **189a**, **189b**, **187a** and **172** were mounted on small loops and fixed in the cold nitrogen stream on an Rigaku Oxford Diffraction XtaLAB Synergy diffractometer, equipped with Mo-K $\alpha$  radiation, HyPix detector and a mirror monochromator. Intensity data were measured by thin-slice  $\omega$ -scans. For crystals of **194** and **179**, crystals were mounted on glass fibres and fixed in the cold nitrogen stream on an Oxford Diffraction Xcalibur-3/Sapphire3-CCD diffractometer, equipped with Mo-K $\alpha$  radiation and graphite monochromator. Intensity data

were measured by thin-slice  $\omega$ - and  $\phi$ -scans. For each sample, data were processed using the CrysAlisPro-CCD and -RED programs.<sup>[393]</sup> The structures were determined by the intrinsic phasing routines in the SHELXT program and refined by full-matrix least-squares methods, on  $F^2$ 's, in SHELXL.<sup>[391,392]</sup> The non-hydrogen atoms were refined with anisotropic thermal parameters. For **179**, the pyridinium hydrogen atom was located in a difference map and was refined freely. All other hydrogen atoms were included in idealised positions and their Uiso values were set to ride on the Ueq values of the parent carbon atoms. In the final difference map for each sample, the highest peaks were near the heavy (Au, Pt, Pd) atom. Scattering factors for neutral atoms were taken from reference.<sup>[394]</sup> Experimental details of structure determination and detailed results are listed in Table 1 and Table 2 in Appendix C. Further information can be found in Appendix C. The published X-ray structures can be found in The Cambridge Crystallographic Data Centre with the deposition numbers 1973007–1973011 and 2094617.

### Chapter III - Synthesis of allene-based ligands – procedures

#### Compound 88a

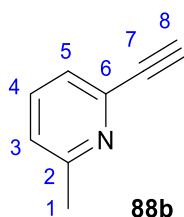


Suspension of CuI (228 mg, 0.12 mmol, 0.1 equiv.) and Pd(PPh<sub>3</sub>)Cl<sub>2</sub> (421 mg, 0.60 mmol, 0.05 equiv.) in 31 ml of triethylamine was purged with N<sub>2</sub>. 2-Bromo-6-methylpyridine **87** (2.064 g, 12.00 mmol, 1.0 equiv.) was added, followed by the slow addition of ethynyltrimethylsilane (1.882 g, 19.20 mmol, 1.6 equiv.) for a period of 1 h. The resulting reaction mixture was stirred at 50 °C for 3.5 h. Then the mixture was allowed to reach rt, diluted with dichloromethane and filtered through a pad of Celite. The solvent was removed in *vacuo* and the crude product was purified by column chromatography (Pet/AcOEt 7:1) to yield compound **88a** (2.075 g, 91%) as a brown oil.

<sup>1</sup>H NMR (500 MHz, CDCl<sub>3</sub>)  $\delta$  7.52 (t,  $J$  = 7.7 Hz, 1H, 4), 7.28 (d,  $J$  = 7.7 Hz, 1H,  $H_{Py}$ ), 7.09 (d,  $J$  = 7.7 Hz, 1H,  $H_{Py}$ ), 2.55 (s, 3H, 1), 0.26 (s, 9H, 9); <sup>13</sup>C{<sup>1</sup>H} NMR (126 MHz, CDCl<sub>3</sub>)  $\delta$  158.9 (2), 142.3 (6), 136.6 (4), 124.8 ( $C_{Py-H}$ ), 123.1 ( $C_{Py-H}$ ), 103.7 (8), 77.7 (7), 24.6 (1), -0.1 (9).

The characterisation data is in agreement with previously reported.<sup>[395]</sup>

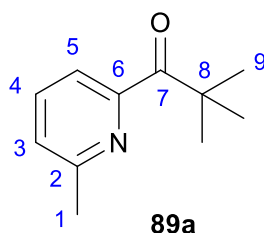


**Compound 88b**

To a solution of **88a** (2.063 g, 10.92 mmol, 1.0 equiv.) in 220 ml of dichloromethane, TBAF hydrate (3.661 g, 13.01 mmol, 1.2 equiv.) was added. After stirring at rt for 40 min, aqueous  $\text{NH}_4\text{Cl}$  was added. The organic phase was extracted with water and the combined organic layers were dried over  $\text{MgSO}_4$ , filtered and concentrated in *vacuo* to yield pure compound **88b** (1.270 g, 99%) as a brown oil.

$^1\text{H NMR}$  (500 MHz,  $\text{CDCl}_3$ )  $\delta$  7.55 (t,  $J = 7.7$  Hz, 1H, 4), 7.31 (d,  $J = 7.7$  Hz, 1H,  $H_{\text{Py}}$ ), 7.14 (d,  $J = 7.7$  Hz, 1H,  $H_{\text{Py}}$ ), 3.13 (s, 1H, 8), 2.57 (s, 3H, 1);  $^{13}\text{C}\{^1\text{H}\}$  NMR (126 MHz,  $\text{CDCl}_3$ )  $\delta$  159.2 (2), 141.6 (6), 136.7 (4), 124.7 ( $\text{C}_{\text{Py-H}}$ ), 123.5 ( $\text{C}_{\text{Py-H}}$ ), 82.9 (8), 24.6 (1). One  $\text{C}_{\text{sp}}$  signal not detected.

The characterisation data is in agreement with previously reported.<sup>[396]</sup>

**Compound 89a**

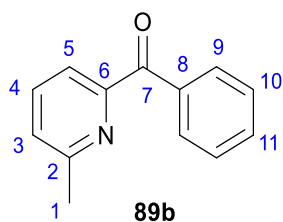
**Procedure a:**<sup>[397]</sup> To a solution of 2-bromo-6-methylpyridine **87** (1.032 g, 6.00 mmol, 1.0 equiv.) in 10.2 ml of anhydrous THF, *n*-BuLi solution in hexanes (2.96 ml, 6.60 mmol, 1.1 equiv.) was added dropwise at  $-78$  °C under inert atmosphere. The resulting deep red solution was stirred at  $-78$  °C for 1 h. Subsequently it was transferred *via* cannula to a solution of pivaloyl chloride (1.447 g, 12.00 mmol, 2.0 equiv.) in 2 ml of THF pre-cooled to  $-78$  °C. The resulting solution was stirred at  $-78$  °C for another 2 h, the colour changed to orange. The solution was slowly warmed to rt and left stirring overnight. Then, 5 ml of water was added, and the resulting mixture was poured into 50 ml of 40% aqueous NaOH solution and stirred at rt for 3.5 h. The aqueous layer was separated and extracted with  $\text{Et}_2\text{O}$  and the combined organic layers were washed with brine, dried over  $\text{MgSO}_4$ , filtered and concentrated in *vacuo*. The crude reaction

mixture was purified by column chromatography using silica gel (Pet/AcOEt 50:1) to yield compound **89a** (424 mg, 40%) as a pale yellow oil slightly contaminated with pivaloyl chloride.

**Procedure b:** To a solution of alcohol **91a** (2.452 g, 13.70 mmol, 1.0 equiv.) in 108 ml dichloromethane, the Dess-Martin periodinane (6.970 g, 16.40 mmol, 1.2 equiv.) was added at 0 °C. The reaction mixture was slowly warmed to rt. After a total of 4 h, aqueous NaHCO<sub>3</sub> was added. The aqueous layer was separated and the organic layer was washed with NaHCO<sub>3(aq)</sub>, brine, dried over MgSO<sub>4</sub>, filtered and concentrated in *vacuo*. Crude product was purified by column chromatography using silica gel (Pet/AcOEt 9:1) to yield compound **89a** (1.864 g, 77%) as a yellow oil.

**<sup>1</sup>H NMR** (500 MHz, CDCl<sub>3</sub>) δ 7.69 – 7.62 (m, 2H, *H<sub>Py</sub>*), 7.22 (dd, *J* = 7.0, 1.7 Hz, 1H, *H<sub>Py</sub>*), 2.58 (s, 3H, 1), 1.45 (s, 9H, 9); **<sup>13</sup>C{<sup>1</sup>H} NMR** (126 MHz, CDCl<sub>3</sub>) δ 207.3 (7), 156.7 (*C<sub>Py</sub>*), 154.4 (*C<sub>Py</sub>*), 136.9 (*C<sub>Py</sub>-H*), 125.4 (*C<sub>Py</sub>-H*), 120.6 (*C<sub>Py</sub>-H*), 44.4 (8), 27.8 (9), 24.5 (1); **HRMS** (ESI) (C<sub>11</sub>H<sub>16</sub>NO) [M+H]<sup>+</sup>: calcd: 178.1226; found: 178.1225.

### Compound 89b



**Procedure a:**<sup>[397]</sup> To a solution of 2-bromo-6-methylpyridine **87** (1.032 g, 6.00 mmol, 1.0 equiv.) in 10 ml of anhydrous THF, *n*-BuLi solution in hexanes (2.96 ml, 6.60 mmol, 1.1 equiv.) was added dropwise at -78 °C under inert atmosphere. The resulting deep red solution was stirred at -78 °C for 1 h. Subsequently it was transferred *via* cannula to the solution of benzoyl chloride (1.692 g, 12.00 mmol, 2.0 equiv.) in 13 ml of THF pre-cooled to -78 °C. The resulting solution was stirred at -78 °C for another 1 h, then was slowly warmed to rt and left stirring overnight. The solution changed colour to yellow. The solution was then quenched with water and the resulting mixture was poured into 20 ml of 30% aqueous NaOH solution and stirred at rt for 1 h. The aqueous layer was separated and extracted with Et<sub>2</sub>O and the combined organic layers were washed with water, brine, dried over MgSO<sub>4</sub>, filtered and concentrated in *vacuo*. The crude reaction mixture was purified by two consecutive chromatography columns using silica gel (Pet/AcOEt 94:6) to yield compound **89b** (283 mg, 24%) as a yellow oil.

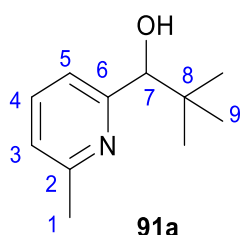
**Procedure b:**<sup>[398]</sup> To a solution of alcohol **91b** (3.033 g, 15.24 mmol, 1.0 equiv.) in 76 ml of dichloromethane, activated MnO<sub>2</sub> (5.437 g, 62.49 mmol, 4.1 equiv.) was added and the resulting suspension was stirred at rt for 24 h (monitored by TLC). The reaction mixture was

filtered through a pad of Celite and concentrated in *vacuo* to yield pure ketone **89b** (3.002 g, > 99%) as a yellow oil.

**<sup>1</sup>H NMR** (400 MHz, CDCl<sub>3</sub>) δ 8.12 – 8.07 (m, 2H, 10), 7.80 – 7.73 (m, 2H, H<sub>Py</sub>), 7.58 (t, *J* = 7.5 Hz, 1H, 11), 7.47 (t, *J* = 7.5 Hz, 2H, 9), 7.34 (dd, *J* = 6.8, 1.9 Hz, 1H, H<sub>Py</sub>), 2.63 (s, 3H, 1); **<sup>13</sup>C{<sup>1</sup>H} NMR** (101 MHz, CDCl<sub>3</sub>) δ 194.1 (7), 157.9 (C<sub>Py</sub>), 154.9 (C<sub>Py</sub>), 137.2 (4), 136.4 (8), 133.0 (11), 131.3 (2 x C<sub>Ph</sub>-H), 128.2 (2 x C<sub>Ph</sub>-H), 125.9 (C<sub>Py</sub>-H), 121.8 (C<sub>Py</sub>-H), 24.7 (1).

The characterisation data is in agreement with previously reported.<sup>[399]</sup>

### Compound 91a<sup>[397]</sup>

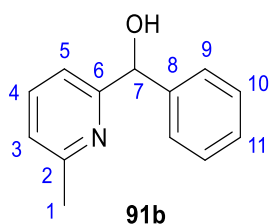


To a solution of 2-bromo-6-methylpyridine **87** (2.236 g, 13.00 mmol, 1.0 equiv.) in 19.4 ml of anhydrous THF, *n*-BuLi solution in hexanes (5.96 ml, 14.30 mmol, 1.1 equiv.) was added dropwise at -78 °C under inert atmosphere and stirred for another 20 min. Pivalaldehyde (1.48 ml, 13.65 mmol, 1.05 equiv.) was added dropwise at -78 °C and the solution was allowed to warm to rt and stirring continued for 3.5 h. NH<sub>4</sub>Cl<sub>(aq)</sub> was added and the aqueous layer was separated and extracted with dichloromethane. The combined organic layers were dried over MgSO<sub>4</sub>, filtered and concentrated in *vacuo* to yield pure alcohol **91a** (2.327 g, > 99%) as a yellow solid.

**<sup>1</sup>H NMR** (400 MHz, CDCl<sub>3</sub>) δ 7.49 (t, *J* = 7.7 Hz 1H, 4), 7.01 (d, *J* = 7.7 Hz, 1H, 5), 6.96 (d, *J* = 7.7 Hz, 1H, 3), 4.61 (d, *J* = 7.1 Hz, 1H, -OH), 4.29 (d, *J* = 7.1 Hz, 1H, 7), 2.52 (s, 3H, 1), 0.90 (s, 9H, 9); **<sup>13</sup>C{<sup>1</sup>H} NMR** (101 MHz, CDCl<sub>3</sub>) δ 159.0 (6), 156.7 (2), 135.8 (4), 121.8 (3), 119.8 (5), 80.0 (7), 36.3 (8), 26.0 (9), 24.4 (1); **HRMS** (ESI) (C<sub>11</sub>H<sub>17</sub>NONa) [M+Na]<sup>+</sup>: caclcd: 202.1202; found: 202.1201.

The characterisation data is in agreement with previously reported.<sup>[400]</sup>

### Compound 91b<sup>[397]</sup>



To a solution of 2-bromo-6-methylpyridine **87** (516 mg, 3.00 mmol, 1.0 equiv.) in 4.5 ml of anhydrous THF, *n*-BuLi solution in hexanes (1.48 ml, 3.30 mmol, 1.1 equiv.) was added dropwise at -78 °C under inert atmosphere and stirred for another 20 min. Benzaldehyde (0.32 ml, 3.2 mmol, 1.05 equiv.) was added dropwise at -78 °C and the solution was allowed to warm to rt and stirring continued for 3 h. NH<sub>4</sub>Cl<sub>(aq)</sub> was added and the aqueous layer was separated and extracted with dichloromethane. Combined organic layers were dried over MgSO<sub>4</sub>, filtered and concentrated in *vacuo*. The crude was purified by column chromatography using silica gel (AcOEt/Pet 2:3) to yield alcohol **91b** (597 mg, > 99%) as a yellow semisolid.

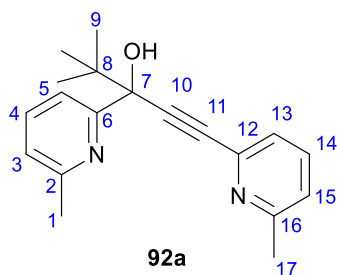
<sup>1</sup>H NMR (500 MHz, CDCl<sub>3</sub>) δ 7.49 (t, *J* = 7.7 Hz, 1H, 4), 7.40 – 7.36 (m, 2H, *H*<sub>Ph</sub>), 7.36 – 7.31 (m, 2H, *H*<sub>Ph</sub>), 7.30 – 7.25 (m, 1H, 11), 7.04 (d, *J* = 7.7 Hz, 1H, *H*<sub>Py</sub>), 6.90 (d, *J* = 7.7 Hz, 1H, *H*<sub>Py</sub>), 5.70 (brs, 2H, 7, -OH), 2.60 (s, 3H, 1); <sup>13</sup>C{<sup>1</sup>H} NMR (126 MHz, CDCl<sub>3</sub>) δ 160.0 (*C*<sub>Py</sub>), 156.7 (*C*<sub>Py</sub>), 143.5 (8), 137.3 (4), 128.6 (2 x *C*<sub>Ph-H</sub>), 127.9 (11), 127.3 (2 x *C*<sub>Ph-H</sub>), 122.0 (*C*<sub>Py-H</sub>), 118.5 (*C*<sub>Py-H</sub>), 74.6 (7), 24.3 (1).

The characterisation data is in agreement with previously reported.<sup>[399]</sup>

#### General procedure A for the synthesis of propargyl alcohols **92a-c**

To a solution of **88b** in anhydrous THF (0.2 M, 1.0 equiv.), a solution of *n*-BuLi in hexanes (1.1 equiv.) was added dropwise at -78 °C under inert atmosphere. The resulting deep red solution was stirred at -78 °C for 1 h. A solution of the corresponding pyridyl ketone (0.7 M, 1.1 equiv.) in anhydrous THF was added dropwise at -78 °C for a period of 30 min. Upon addition, the colour of the solution changed to orange. Stirring at -78 °C was continued for 1 h; then the reaction was slowly warmed to rt and left with stirring overnight (under reflux where indicated). Water was added at 0 °C. The aqueous layer was separated and extracted with Et<sub>2</sub>O, combined organic layers were dried over MgSO<sub>4</sub>, filtered and concentrated in *vacuo*. Purification by column chromatography using silica gel with the indicated mixture of Pet/AcOEt as the eluent, yielded propargyl alcohols **92a-c**.

#### Compound **92a**

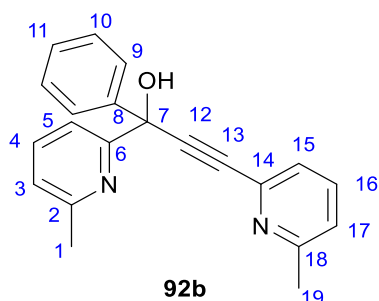


**Procedure a:** Synthesised according to **General procedure A** from alkyne **88b** (283 mg, 2.12 mmol) and ketone **89a** (412 mg, 2.33 mmol). Column chromatography (Pet/AcOEt 7:3) yielded alcohol **92a** (227 mg, 36%) as a yellow oil.

**Procedure b:** Alkyne **93a** (2.122 g, 10.45 mmol, 1.0 equiv.), Pd(PPh<sub>3</sub>)<sub>2</sub>Cl<sub>2</sub> (367 mg, 0.52 mmol, 0.05 equiv.) and CuI (200 mg, 1.05 mmol, 0.1 equiv.) were placed under inert atmosphere. 25.5 ml of triethylamine was added followed by 2-bromo-6-methylpyridine **87** (3.699 g, 20.90 mmol, 2.0 equiv.). The reaction was stirred at rt for 5 h, the reaction mixture turned black. The mixture was filtered through a pad of Celite, washed with dichloromethane and concentrated in *vacuo*. The crude product was purified by column chromatography (AcOEt/Pet 1:4 to 1:1) to yield alcohol **92a** (2.450 g, 80%) as a yellow solid.

**<sup>1</sup>H NMR** (500 MHz, CDCl<sub>3</sub>) δ 7.61 (m, 2H, *H*<sub>Py</sub>), 7.56 – 7.48 (m, 1H, *H*<sub>Py</sub>), 7.32 (d, *J* = 7.5 Hz, 1H, *H*<sub>Py</sub>), 7.13 – 7.05 (m, 2H, *H*<sub>Py</sub>), 6.25 (brs, 1H, -OH), 2.57 (brs, 3H, 1/17), 2.56 (s, 3H, 1/17), 1.07 (s, 9H, 9); **<sup>13</sup>C{<sup>1</sup>H} NMR** (126 MHz, CDCl<sub>3</sub>) δ 158.8 (*C*<sub>Py</sub>), 157.7 (*C*<sub>Py</sub>), 155.5 (*C*<sub>Py</sub>), 142.6 (*C*<sub>Py</sub>), 136.7 (4/14), 136.3 (4/14), 124.9 (*C*<sub>Py</sub>-H), 122.7 (*C*<sub>Py</sub>-H), 122.3 (*C*<sub>Py</sub>-H), 120.5 (*C*<sub>Py</sub>-H), 91.5 (10), 84.2 (11), 77.5 (7), 40.7 (8), 25.6 (9), 24.6 (1/17), 24.2 (1/17); **HRMS** (ESI) (C<sub>19</sub>H<sub>23</sub>N<sub>2</sub>O) [M+H]<sup>+</sup>: caclcd: 295.1805; found: 295.1807.

### Compound 92b

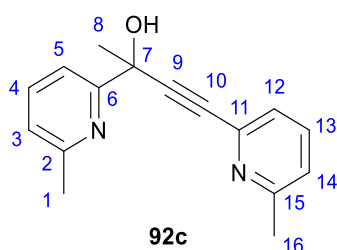


**Procedure a:** Synthesised according to **General procedure A** from alkyne **88b** (257 mg, 2.20 mmol) and ketone **89b** (477 mg, 2.42 mmol). Column chromatography (Pet/AcOEt 3:2) yielded alcohol **92b** (345 mg, 50%) as a yellow semisolid.

**Procedure b:** Alkyne **93b** (1.474 g, 6.61 mmol, 1.0 equiv.), Pd(PPh<sub>3</sub>)<sub>2</sub>Cl<sub>2</sub> (232 mg, 0.33 mmol, 0.05 equiv.) and CuI (126 mg, 0.66 mmol, 0.1 equiv.) were placed under inert atmosphere. Triethylamine (16.1 ml) was added followed by 2-bromo-6-methylpyridine **87** (1.5 ml, 13.2 mmol, 2.0 equiv.). The reaction was stirred at rt for 5 h, the reaction mixture turned black. The mixture was filtered through a pad of Celite, washed with dichloromethane and concentrated in *vacuo*. The crude product was purified by column chromatography (Pet/AcOEt/Et<sub>3</sub>N 60/39/1) to yield alcohol **92b** (1.476 g, 63%) as a yellow solid.

**<sup>1</sup>H NMR** (500 MHz, CDCl<sub>3</sub>) δ 7.76 – 7.73 (m, 2H, *H<sub>Ai</sub>*), 7.55 (q, *J* = 7.6 Hz, 2H, *H<sub>Ai</sub>*), 7.37 – 7.34 (m, 3H, *H<sub>Ph</sub>*), 7.31 – 7.27 (m, 2H, *H<sub>Py</sub>*), 7.11 (d, *J* = 7.6 Hz, 1H, *H<sub>Py</sub>*), 7.08 (d, *J* = 7.6 Hz, 1H, *H<sub>Py</sub>*) 7.05 (s, 1H, -OH), 2.61 (s, 3H, 1/19), 2.56 (s, 3H, 1/19); **<sup>13</sup>C{<sup>1</sup>H} NMR** (126 MHz, CDCl<sub>3</sub>) δ 159.6 (*C<sub>Py</sub>*), 158.9 (*C<sub>Py</sub>*), 156.0 (*C<sub>Py</sub>*), 144.0 (*C<sub>Py</sub>*), 142.2 (*C<sub>Ph</sub>*), 138.1 (*C<sub>Py</sub>-H*), 136.5 (*C<sub>Py</sub>-H*), 128.4 (2 x *C<sub>Ph</sub>-H*), 128.0 (11), 126.7 (2 x *C<sub>Ph</sub>-H*), 125.0 (*C<sub>Py</sub>-H*), 123.1 (*C<sub>Py</sub>-H*), 122.5 (*C<sub>Py</sub>-H*), 119.2 (*C<sub>Py</sub>-H*), 91.0 (12), 85.5 (13), 73.3 (7), 24.6 (1), 24.2 (19); **HRMS** (ASAP) (C<sub>21</sub>H<sub>19</sub>N<sub>2</sub>O) [M+H]<sup>+</sup>: caclcd: 315.1497; found: 315.1494.

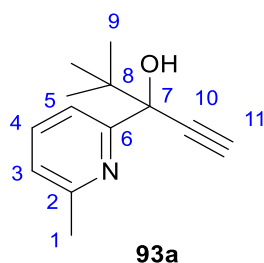
### Compound 92c



Synthesised according to **General procedure A** from alkyne **88b** (150 mg, 1.28 mmol) and ketone **89c** (190 mg, 1.41 mmol) with an overnight reflux. Column chromatography (Pet/AcOEt 2:3 to 1:1) yielded alcohol **92c** (176 mg, 54%) as a yellow oil.

**<sup>1</sup>H NMR** (500 MHz, CDCl<sub>3</sub>) δ 7.67 (t, *J* = 7.8 Hz, 1H, *H<sub>Py</sub>*), 7.52 (t, *J* = 7.5 Hz, 2H, *H<sub>Py</sub>*), 7.28 (d, *J* = 7.8 Hz, 1H, *H<sub>Py</sub>*), 7.12 (d, *J* = 7.5 Hz, 1H, *H<sub>Py</sub>*), 7.09 (d, *J* = 7.8 Hz, 1H, *H<sub>Py</sub>*), 6.11 (brs, 1H, -OH), 2.58 (s, 3H, 1/16), 2.56 (s, 3H, 1/16), 1.89 (s, 3H, 8); **<sup>13</sup>C{<sup>1</sup>H} NMR** (126 MHz, CDCl<sub>3</sub>) δ 160.4 (*C<sub>Py</sub>*), 158.8 (*C<sub>Py</sub>*), 156.4 (*C<sub>Py</sub>*), 142.3 (11), 138.0 (4), 136.4 (13), 124.8 (*C<sub>Py</sub>-H*), 122.8 (*C<sub>Py</sub>-H*), 122.5 (*C<sub>Py</sub>-H*), 117.4 (*C<sub>Py</sub>-H*), 92.3 (9), 82.8 (10), 68.4 (7), 31.9 (8), 24.6 (1), 24.2 (16); **HRMS** (ESI) (C<sub>16</sub>H<sub>17</sub>ON<sub>2</sub>) [M+H]<sup>+</sup>: caclcd: 253.1335; found: 253.1338.

### Compound 93a<sup>[401]</sup>

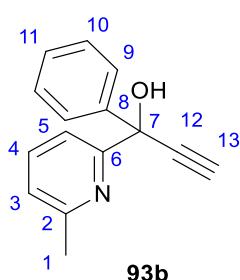


To a solution of ketone **89a** (1.876 g, 10.60 mmol, 1.0 equiv.) in anhydrous THF (42.5 ml), a commercially available solution of ethynylmagnesium bromide (31.8 ml, 0.5 M in THF, 1.5 equiv.) was added at 0 °C under inert atmosphere. The reaction mixture was warmed to rt and then heated at reflux for 3 h. After cooling to rt, the reaction was quenched with aqueous NH<sub>4</sub>Cl.

The aqueous layer was separated and extracted with dichloromethane. Combined organic layers were washed with brine, dried over  $\text{MgSO}_4$ , filtered and concentrated in *vacuo* to afford alcohol **93a** (2.119 g, 98%) as a brown solid that was used without further purification.

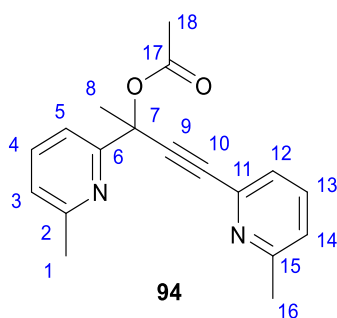
$^1\text{H NMR}$  (400 MHz,  $\text{CDCl}_3$ )  $\delta$  7.60 (t,  $J = 7.7$  Hz, 1H, 4), 7.45 (d,  $J = 7.7$  Hz, 1H,  $H_{Py}$ ), 7.09 (d,  $J = 7.7$  Hz, 1H,  $H_{Py}$ ), 6.14 (brs, 1H, -OH), 2.54 (s, 3H, 1), 2.51 (s, 1H, 11), 0.99 (s, 9H, 9);  $^{13}\text{C}\{^1\text{H}\}$  NMR (101 MHz,  $\text{CDCl}_3$ )  $\delta$  157.8 ( $C_{Py}$ ), 155.7 ( $C_{Py}$ ), 136.6 (4), 122.3 ( $C_{Py-H}$ ), 120.1 ( $C_{Py-H}$ ), 86.1 (10), 77.1 (7), 72.8 (11), 40.2 (8), 25.4 (9), 24.2 (1); HRMS (ESI) ( $\text{C}_{13}\text{H}_{18}\text{NO}$ )  $[\text{M}+\text{H}]^+$ : calcd: 204.1383; found: 204.1384.

### Compound **93b**<sup>[401]</sup>



To a solution of ketone **89b** (1.576 g, 8.00 mmol, 1.0 equiv.) in anhydrous THF (32.0 ml), a commercially available solution of ethynylmagnesium bromide (24.0 ml, 0.5 M in THF, 1.5 equiv.) was added at 0 °C under inert atmosphere. The reaction mixture was warmed to rt and then heated at reflux overnight. After cooling to rt, the reaction was quenched with aqueous  $\text{NH}_4\text{Cl}$ . The aqueous layer was separated and extracted with  $\text{Et}_2\text{O}$ . The combined organic layers were washed with brine, dried over  $\text{MgSO}_4$ , filtered and concentrated in *vacuo* to afford alcohol **93b** (1.705 g, 96%) as a black oil that was used without further purification.

$^1\text{H NMR}$  (400 MHz,  $\text{CDCl}_3$ )  $\delta$  7.70 – 7.64 (m, 2H, 9), 7.56 (t,  $J = 7.7$  Hz, 1H, 4), 7.38 – 7.32 (m, 2H, 10), 7.30 – 7.25 (m, 1H, 11), 7.19 (d,  $J = 7.7$  Hz, 1H,  $H_{Py}$ ), 7.09 (d,  $J = 7.7$  Hz, 1H,  $H_{Py}$ ), 6.95 (brs, 1H, -OH), 2.77 (s, 1H, 13), 2.60 (s, 3H, 1);  $^{13}\text{C}\{^1\text{H}\}$  NMR (101 MHz,  $\text{CDCl}_3$ )  $\delta$  159.7 ( $C_{Py}$ ), 156.1 ( $C_{Py}$ ), 143.8 (8), 138.0 (4), 128.4 (2 x  $C_{Ph-H}$ ), 128.0 (11), 126.5 (2 x  $C_{Ph-H}$ ), 122.6 ( $C_{Py-H}$ ), 118.7 ( $C_{Py-H}$ ), 86.0 (12), 74.5 (13), 72.8 (7), 24.2 (1); HRMS (ESI) ( $\text{C}_{15}\text{H}_{14}\text{NO}$ )  $[\text{M}+\text{H}]^+$ : calcd: 224.1070; found: 224.1069.

**Compound 94**

DMAP (2 mg, 0.02 mmol, 0.05 equiv.) was placed under inert atmosphere. A solution of alcohol **92c** (70 mg, 0.31 mmol, 1.0 equiv.) in pyridine (0.75 ml) was added, followed by acetic anhydride (35 mg, 0.34 mmol, 1.1 equiv.). The reaction mixture was stirred at rt for 19 h and then at 50 °C for 22 h. The mixture was quenched with water, the aqueous layer was separated and extracted with dichloromethane. The combined organic layers were dried over MgSO<sub>4</sub>, filtered and concentrated in *vacuo*. Purification by column chromatography (Pet/AcOEt 3:2 to 1:1) yielded ester **94** (39 mg, 42%) as a yellow solid contaminated with the alcohol **92c** starting material (**94**:**92c** ~ 1.4:1).

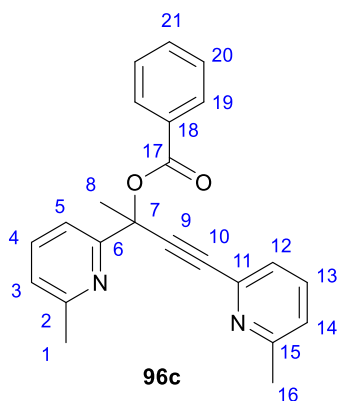
**<sup>1</sup>H NMR** (500 MHz, CDCl<sub>3</sub>) δ 7.70 (d, *J* = 7.8 Hz, 1H, *H<sub>Py</sub>*), 7.59 (t, *J* = 7.8 Hz, 1H, *H<sub>Py</sub>*), 7.56 (t, *J* = 7.8 Hz, 1H, *H<sub>Py</sub>*), 7.35 (d, *J* = 7.7 Hz, 1H, *H<sub>Py</sub>*), 7.12 (d, *J* = 7.8 Hz, 1H, *H<sub>Py</sub>*), 7.05 (d, *J* = 7.7 Hz, 1H, *H<sub>Py</sub>*), 2.58 (s, 3H, 1/16), 2.55 (s, 3H, 1/16), 2.12 (s, 3H, 18), 2.03 (s, 3H, 8); **<sup>13</sup>C{<sup>1</sup>H} NMR** (126 MHz, CDCl<sub>3</sub>) δ 169.2 (17), 158.9 (*C<sub>Py</sub>*), 158.7 (*C<sub>Py</sub>*), 158.1 (*C<sub>Py</sub>*), 137.0 (*C<sub>Py</sub>-H*), 136.7 (*C<sub>Py</sub>-H*), 125.2 (*C<sub>Py</sub>-H*), 123.2 (*C<sub>Py</sub>-H*), 122.6 (*C<sub>Py</sub>-H*), 118.1 (*C<sub>Py</sub>-H*), 77.7 (10), 75.8 (7), 29.9 (18), 24.7 (1), 24.6 (16), 21.8 (8). One C<sub>sp</sub> and C<sub>q</sub> not detected; **HRMS** (ASAP) (C<sub>18</sub>H<sub>19</sub>O<sub>2</sub>N<sub>2</sub>) [M+H]<sup>+</sup>: calcd: 295.1447; found: 295.1449.

**General procedure B for esterification of propargyl alcohols<sup>[163]</sup>**

An oven-dried round bottom flask was charged with DMAP (0.1 equiv.) and triethylamine (1.5 equiv.) and purged with N<sub>2</sub>. A solution of propargyl alcohol in anhydrous dichloromethane (0.2 M, 1.0 equiv.) was added, followed by benzoyl chloride (1.5 equiv.) added at 0 °C. The reaction mixture was warmed to rt; the progress of the reaction was monitored by TLC analysis. Upon completion water was added, the aqueous layer was separated and extracted with dichloromethane, the combined organic layers were washed with NaHCO<sub>3</sub>, brine, dried over MgSO<sub>4</sub>, filtered and concentrated in *vacuo*. Purification by column chromatography with the indicated mixture of Pet/AcOEt as the eluent yielded benzoate esters **96a-c**.



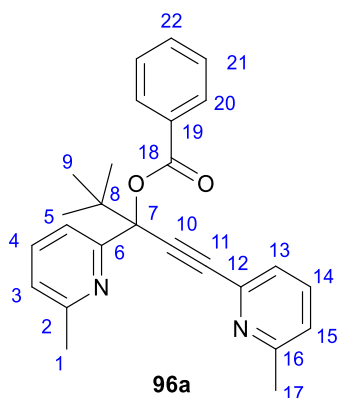
## Compound 96c



Synthesised according to **General procedure B** from alcohol **92c** (64 mg, 0.25 mmol). Stirred at rt for 1 h 40 min. Column chromatography (Pet/AcOEt 3:2) yielded ester **96c** (66 mg, 73%) as a yellow semisolid.

$^1\text{H NMR}$  (500 MHz,  $\text{CDCl}_3$ )  $\delta$  8.10 – 8.06 (m, 2H,  $H_{Ph}$ ), 7.76 (d,  $J = 7.8$  Hz, 1H,  $H_{Py}$ ), 7.61 (t,  $J = 7.7$  Hz, 1H,  $H_{Ph}$ ), 7.57 – 7.53 (m, 2H,  $H_{Py}$ ), 7.42 (t,  $J = 7.7$  Hz, 2H,  $H_{Ph}$ ), 7.36 (d,  $J = 7.7$  Hz, 1H,  $H_{Py}$ ), 7.11 (d,  $J = 7.8$  Hz, 1H,  $H_{Py}$ ), 7.06 (d,  $J = 7.7$  Hz, 1H,  $H_{Py}$ ), 2.58 (s, 3H, 1/16), 2.51 (s, 3H, 1/16), 2.21 (s, 3H, 8);  $^{13}\text{C}\{^1\text{H}\}$  NMR (126 MHz,  $\text{CDCl}_3$ )  $\delta$  164.7 (17), 158.9 ( $C_{Py}$ ), 158.7 ( $C_{Py}$ ), 158.1 ( $C_{Py}$ ), 137.0 ( $C_{Py-H}$ ), 136.7 ( $C_{Py}$ ), 133.0 ( $C_{Ph-H}$ ), 130.7 ( $C_{Py-H}$ ), 130.1 ( $C_{Ph}$ ), 130.0 (2 x  $C_{Ph-H}$ ), 128.4 (2 x  $C_{Ph-H}$ ), 125.2 ( $C_{Py-H}$ ), 123.2 ( $C_{Py-H}$ ), 122.7 ( $C_{Py-H}$ ), 118.1 ( $C_{Py-H}$ ), 76.7 (7), 29.7 (8), 24.6 (1/16), 22.8 (1/16). Two  $C_{sp}$  signals not detected; **HRMS** (ESI) ( $\text{C}_{23}\text{H}_{21}\text{N}_2\text{O}_2$ )  $[\text{M}+\text{H}]^+$ : calcd: 357.1598; found: 357.1598.

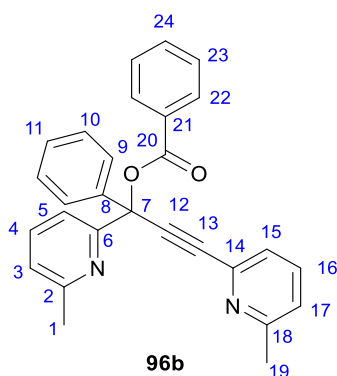
## Compound 96a



Synthesised according to **General procedure B** from alcohol **92a** (50 mg, 0.17 mmol). Stirred at rt for 2 h 40 min. Column chromatography (Pet/AcOEt/ $\text{Et}_3\text{N}$  0.73/0.25/0.02) yielded ester **96a** (50 mg, 74%) as a yellow semisolid contaminated with **92a** (**96a:92a** 3:1). The reaction is not easily scaleable, it is best to do it at a 1.0-1.5 mmol scale.

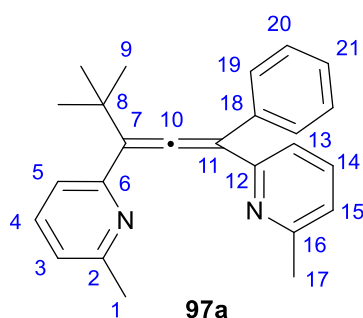
**<sup>1</sup>H NMR** (500 MHz, CDCl<sub>3</sub>) δ 8.11 – 8.08 (m, 2H, *H<sub>Ph</sub>*), 7.58 – 7.49 (m, 4H, *H<sub>Ar</sub>*), 7.45 (t, *J* = 7.7 Hz, 2H, *H<sub>Ph</sub>*), 7.34 (d, *J* = 7.7 Hz, 1H, *H<sub>Py</sub>*), 7.08 (d, *J* = 7.7 Hz, 1H, *H<sub>Py</sub>*), 7.00 (dd, *J* = 7.0, 1.2 Hz, 1H, *H<sub>Py</sub>*), 2.56 (s, 3H, 1/17), 2.43 (s, 3H, 1/17), 1.25 (s, 9H, 9); **<sup>13</sup>C{<sup>1</sup>H} NMR** (126 MHz, CDCl<sub>3</sub>) δ 164.5 (18), 156.9 (*C<sub>Py</sub>*), 155.7 (*C<sub>Py</sub>*), 135.8 (*C<sub>Py</sub>-H*), 132.8 (*C<sub>Ph</sub>-H*), 131.4 (*C<sub>Py</sub>-H*), 129.9 (2 x *C<sub>Ph</sub>-H*), 128.4 (2 x *C<sub>Ph</sub>-H*), 128.3 (*C<sub>Ph</sub>*), 125.5 (*C<sub>Py</sub>-H*), 123.2 (*C<sub>Py</sub>-H*), 121.9 (*C<sub>Py</sub>-H*), 119.9 (*C<sub>Py</sub>-H*), 84.6 (7), 41.0 (8), 26.1 (9), 25.7 (1/17), 24.7 (1/17). Two *C<sub>sp</sub>* and two *C<sub>q</sub>* not detected; **HRMS** (ESI) (C<sub>26</sub>H<sub>27</sub>N<sub>2</sub>O<sub>2</sub>) [M+H]<sup>+</sup>: caclcd: 399.2067; found: 399.2061.

### Compound 96b



Synthesised according to **General procedure B** from alcohol **92b** (945 mg, 3.01 mmol). Stirred at rt overnight. Column chromatography (Pet/AcOEt 4:1) yielded ester **96b** (1.047 g, 83%) as a yellow semisolid.

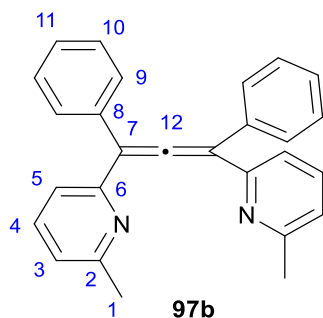
**<sup>1</sup>H NMR** (500 MHz, CDCl<sub>3</sub>) δ 8.17 – 8.14 (m, 2H, *H<sub>Ph</sub>*), 7.83 – 7.80 (m, 2H, *H<sub>Ph</sub>*), 7.76 (d, *J* = 7.8 Hz, 1H, *H<sub>Py</sub>*), 7.60 – 7.55 (m, 2H, *H<sub>Ar</sub>*), 7.53 (t, *J* = 7.8 Hz, 1H, *H<sub>Py</sub>*), 7.46 (t, *J* = 7.7 Hz, 2H, *H<sub>Ar</sub>*), 7.39 (d, *J* = 7.7 Hz, 1H, *H<sub>Py</sub>*), 7.37 – 7.33 (m, 2H, *H<sub>Ar</sub>*), 7.31 – 7.26 (m, 1H, *H<sub>Ar</sub>*), 7.10 (d, *J* = 7.7 Hz, 1H, *H<sub>Py</sub>*), 7.01 (d, *J* = 7.7 Hz, 1H, *H<sub>Py</sub>*), 2.55 (s, 3H, 1/19), 2.45 (s, 3H, 1/19); **<sup>13</sup>C{<sup>1</sup>H} NMR** (126 MHz, CDCl<sub>3</sub>) δ 164.4 (20), 158.9 (*C<sub>Py</sub>*), 158.6 (*C<sub>Py</sub>*), 158.3 (*C<sub>Py</sub>*), 142.2 (*C<sub>Py</sub>*), 141.3 (*C<sub>Ph</sub>*), 136.9 (*C<sub>Py</sub>-H*), 136.3 (*C<sub>Py</sub>-H*), 133.1 (*C<sub>Ph</sub>-H*), 130.9 (*C<sub>Ph</sub>*), 130.0 (*C<sub>Ph</sub>-H<sub>2</sub>*), 128.4 (*C<sub>Ph</sub>-H<sub>2</sub>*), 128.4 (*C<sub>Ph</sub>-H<sub>2</sub>*), 128.2 (*C<sub>Ph</sub>-H*), 126.9 (*C<sub>Ph</sub>-H<sub>2</sub>*), 125.3 (*C<sub>Py</sub>-H*), 123.1 (*C<sub>Py</sub>-H*), 122.3 (*C<sub>Py</sub>-H*), 118.2 (*C<sub>Py</sub>-H*), 88.7 (12), 87.5 (13), 80.4 (7), 24.8 (1/19), 24.6 (1/19); **HRMS** (ESI) (C<sub>28</sub>H<sub>22</sub>N<sub>2</sub>O<sub>2</sub>Na) [M+Na]<sup>+</sup>: caclcd: 441.1573; found: 441.1574.

**Compound 97a**<sup>[149]</sup>

To a suspension of  $\text{ZnBr}_2$  in anhydrous THF (0.8 M, 4.0 equiv. of  $\text{ZnBr}_2$ ), a phenylmagnesium bromide solution in  $\text{Et}_2\text{O}$  (10.0 ml, 1.0 M, 4.0 equiv.) was added dropwise at 0 °C under inert atmosphere. Stirring at 0 °C continued for 15 min, followed by 45 min at rt.  $\text{Pd}(\text{PPh}_3)_4$  (145 mg, 0.13 mmol, 0.05 equiv.) and the corresponding propargyl benzoate **96a** (996 mg, 2.50 mmol, 1.0 equiv.) in anhydrous THF (0.25 M solution of the ester) were added at 0 °C and stirring at this temperature continued for 15 min. Reaction mixture was brought to rt and stirred overnight. Water was added and the precipitate formed was filtered off. The aqueous layer of the filtrate was separated and extracted with  $\text{Et}_2\text{O}$ , the combined organic layers were dried over  $\text{MgSO}_4$  and concentrated in *vacuo*. Column chromatography (Pet/AcOEt/ $\text{NEt}_3$  93/6/1) yielded allene **97a** (264 mg, 30%) as a yellow oil.

$^1\text{H NMR}$  (400 MHz,  $\text{CDCl}_3$ )  $\delta$  7.55 (t,  $J = 7.7$  Hz, 1H,  $H_{\text{Py}}$ ), 7.49 (m, 2H,  $H_{\text{Ph}}$ ), 7.43 (t,  $J = 7.7$  Hz, 1H,  $H_{\text{Py}}$ ), 7.35 – 7.27 (m, 4H,  $H_{\text{Ar}}$ ), 7.26 – 7.21 (m, 1H,  $H_{\text{Ph}}$ ), 7.04 (d,  $J = 7.6$  Hz, 1H,  $H_{\text{Py}}$ ), 6.95 (d,  $J = 7.6$  Hz, 1H,  $H_{\text{Py}}$ ), 2.56 (s, 6H, 1/17), 1.42 (s, 9H, 9);  $^{13}\text{C}\{^1\text{H}\}$  NMR (101 MHz,  $\text{CDCl}_3$ )  $\delta$  209.0 (10), 158.1 ( $C_{\text{Py}}$ ), 157.3 ( $C_{\text{Py}}$ ), 155.7 ( $C_{\text{Py}}$ ), 155.6 ( $C_{\text{Py}}$ ), 136.8 ( $C_{\text{Py-H}}$ ), 136.3 ( $C_{\text{Py-H}}$ ), 135.8 ( $C_{\text{Ph}}$ ), 128.3 (2 x  $C_{\text{Ph-H}}$ ), 128.2 (2 x  $C_{\text{Ph-H}}$ ), 127.1 ( $C_{\text{Ph-H}}$ ), 121.5 ( $C_{\text{Py-H}}$ ), 121.4 ( $C_{\text{Py-H}}$ ), 120.9 ( $C_{\text{Py-H}}$ ), 120.9 ( $C_{\text{Py-H}}$ ), 120.2 (7), 112.1 (11), 36.3 (8), 30.3 (9), 24.8 (1/17), 24.7 (1/17); **HRMS** (ESI) ( $\text{C}_{25}\text{H}_{26}\text{N}_2\text{Na}$ ) [ $\text{M}+\text{Na}$ ] $^+$ : calcd: 377.1988 ; found: 377.1990.

The characterisation data is in agreement with previously reported.<sup>[149]</sup>

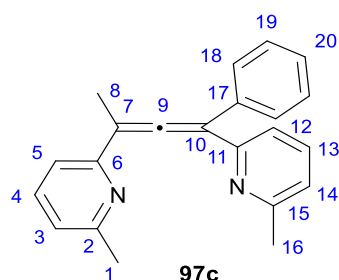
**Compound 97b**<sup>[149]</sup>

To a suspension of  $\text{ZnBr}_2$  in anhydrous THF (0.8 M, 4.0 equiv. of  $\text{ZnBr}_2$ ), a phenylmagnesium bromide solution in  $\text{Et}_2\text{O}$  (4.3 ml, 1.0 M, 4.0 equiv.) was added dropwise at 0 °C under inert atmosphere. Stirring at 0 °C continued for 30 min.  $\text{Pd}(\text{PPh}_3)_4$  (62 mg, 0.054 mmol, 0.05 equiv.) and the corresponding propargyl benzoate **96b** (447 mg, 1.07 mmol, 1.0 equiv.) in anhydrous THF (0.25 M solution of the ester) were added at 0 °C. The reaction mixture was stirred at 0 °C for 3 h. Water was added, the aqueous layer was separated and extracted with  $\text{Et}_2\text{O}$ , the combined organic layers were dried over  $\text{MgSO}_4$  and concentrated in *vacuo*. Column chromatography (Pet/AcOEt/ $\text{NEt}_3$  85/14/1) yielded allene **97b** (215 mg, 54%) as a yellow oil.

$^1\text{H NMR}$  (500 MHz,  $\text{CDCl}_3$ )  $\delta$  7.60 – 7.54 (m, 6H, 4, 9), 7.41 (d,  $J = 7.7$  Hz, 2H, 3/5), 7.37 – 7.33 (m, 4H, 10), 7.30 – 7.26 (m, 2H, 11), 7.07 (d,  $J = 7.7$  Hz, 2H, 3/5), 2.58 (s, 6H, 1);  $^{13}\text{C}\{^1\text{H}\}$  NMR (101 MHz,  $\text{DMSO-d}_6$ )  $\delta$  211.7 (12), 158.0 (2/6), 153.8 (2/6), 137.4 (4), 135.0 (8), 128.6 (9/10), 128.2 (9/10), 127.8 (11), 122.2 (3/5), 120.7 (3/5), 113.3 (7), 24.2 (1); MS (EI) ( $\text{C}_{27}\text{H}_{21}\text{N}_2$ )  $[\text{M-H}]^+$ : calcd: 373; found: 373.

The characterisation data is in agreement with previously reported.<sup>[149]</sup>

#### Compound **97c**<sup>[149]</sup>

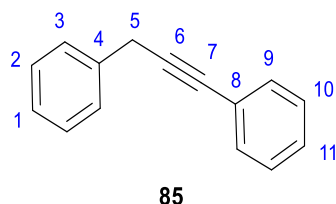


To a suspension of  $\text{ZnBr}_2$  in anhydrous THF (0.8 M, 4.0 equiv. of  $\text{ZnBr}_2$ ), a phenylmagnesium bromide solution in  $\text{Et}_2\text{O}$  (0.25 ml, 3.0 M, 4.0 equiv.) was added dropwise at 0 °C under inert atmosphere. Stirring at 0 °C continued for 30 min.  $\text{Pd}(\text{PPh}_3)_4$  (11 mg, 0.009 mmol, 0.05 equiv.) and propargyl benzoate **97c** (66 mg, 0.19 mmol, 1.0 equiv.) in anhydrous THF (0.25 M solution of the ester) was added at - 40 °C. The reaction mixture was slowly brought to rt overnight.  $\text{NH}_4\text{Cl}_{(\text{aq})}$  was added, the aqueous layer was separated and extracted with  $\text{Et}_2\text{O}$ , the combined organic layers were dried over  $\text{MgSO}_4$  followed by filtration and concentration in *vacuo*. Column chromatography (Pet/AcOEt/TEA 94:5:1) yielded allene **97c** (22 mg, 38%) as an orange oil.

$^1\text{H NMR}$  (500 MHz,  $\text{CDCl}_3$ )  $\delta$  7.54 (t,  $J = 7.7$  Hz, 1H,  $H_{\text{Py}}$ ), 7.50 – 7.43 (m, 4H,  $H_{\text{Ar}}$ ), 7.34 – 7.23 (m, 4H,  $H_{\text{Ar}}$ ), 7.05 (d,  $J = 7.7$  Hz, 1H,  $H_{\text{Py}}$ ), 6.96 (d,  $J = 7.1$  Hz, 1H,  $H_{\text{Py}}$ ), 2.57 (s, 6H, 1, 16), 2.38 (s, 3H, 8);  $^{13}\text{C}\{^1\text{H}\}$  NMR (126 MHz,  $\text{CDCl}_3$ )  $\delta$  211.3 (9), 158.3 ( $C_{\text{Py}}$ ), 158.0 ( $C_{\text{Py}}$ ), 155.3 ( $C_{\text{Py}}$ ), 154.7 ( $C_{\text{Py}}$ ), 136.9 ( $C_{\text{Ph}}$ ), 136.4 ( $C_{\text{Py-H}}$ ), 135.6 ( $C_{\text{Py-H}}$ ), 128.6 (2 x  $C_{\text{Ph-H}}$ ), 128.4 (2 x  $C_{\text{Ph-H}}$ ).

H), 127.4 ( $C_{Ph-H}$ ), 121.7 ( $C_{Py-H}$ ), 121.4 ( $C_{Py-H}$ ), 121.1 ( $C_{Py-H}$ ), 119.3 ( $C_{Py-H}$ ), 112.5 (10), 107.0 (7), 24.8 (1/16), 24.7 (1/16), 16.0 (8); **HRMS** (ESI) ( $C_{22}H_{21}N_2$ )  $[M+H]^+$ : calcd: 313.1699; found: 313.1700.

### Compound 85<sup>[164]</sup>

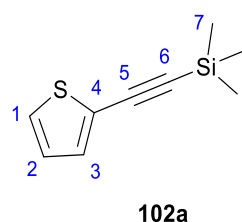


A 50 ml round bottom flask was charged with CuI (25 mg, 0.13 mmol, 0.04 equiv.), Pd(PPh<sub>3</sub>)<sub>2</sub>Cl<sub>2</sub> (45 mg, 0.06 mmol, 0.02 equiv.) and purged with N<sub>2</sub>. Triethylamine (9.0 ml) was added, followed by iodobenzene (855 mg, 4.19 mmol, 1.3 equiv.) and the solution of 3-phenyl-1-propyne **98** in 1 ml of Et<sub>3</sub>N was added dropwise. The reaction mixture was heated at 30 °C for 2 h 20 min. The resulting reaction mixture was filtered through a pad of Celite and washed with dichloromethane. Then the solvent was removed in *vacuo*. The crude was purified by column chromatography (Pet) to yield compound **85** (619 mg, > 99%) as a yellow oil.

<sup>1</sup>H NMR (400 MHz, CDCl<sub>3</sub>) δ 7.47 – 7.40 (m, 4H,  $H_{Ar}$ ), 7.37 – 7.28 (m, 5H,  $H_{Ar}$ ), 7.28 – 7.23 (m, 1H,  $H_{Ar}$ ), 3.84 (s, 2H, 5); <sup>13</sup>C{<sup>1</sup>H} NMR (101 MHz, CDCl<sub>3</sub>) δ 136.9 (4), 131.8 (2 x  $C_{Ph-H}$ ), 128.7 (2 x  $C_{Ph-H}$ ), 128.4 (2 x  $C_{Ph-H}$ ), 128.1 (2 x  $C_{Ph-H}$ ), 127.9 ( $C_{Ph-H}$ ), 126.7 ( $C_{Ph-H}$ ), 123.8 (8), 87.7 (6), 82.8 (7), 25.9 (5).

The characterisation data is in agreement with previously reported.<sup>[402]</sup>

### Compound 102a<sup>[403]</sup>



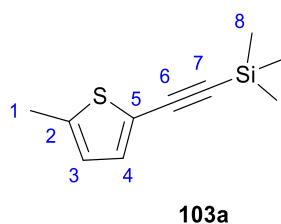
A suspension of CuI (10 mg, 0.05 mmol, 0.01 equiv.) and Pd(PPh<sub>3</sub>)<sub>2</sub>Cl<sub>2</sub> (35 mg, 0.05 mmol, 0.01 equiv.) in trimethylamine (12.6 ml) was purged with N<sub>2</sub> for 1 h. Iodothiophene (1.05 g, 5.00 mmol, 1.0 equiv.) was added, followed by ethynyltrimethylsilane (1.41 ml, 10.0 mmol, 2.0 equiv.) added in portions over the period of 90 min. The reaction mixture was stirred at rt for 2.5 h, diluted with dichloromethane and filtered through a pad of Celite. The solvent was

removed in *vacuo*. The crude was purified by column chromatography (Pet) to yield **102a** (834 mg, 93%) as a colourless oil.

$^1\text{H NMR}$  (500 MHz,  $\text{CDCl}_3$ )  $\delta$  7.24 – 7.22 (m, 2H, 1, 3), 6.96 – 6.94 (m, 1H, 2), 0.25 (s, 9H, 7);  $^{13}\text{C}\{^1\text{H}\}$  NMR (126 MHz,  $\text{CDCl}_3$ )  $\delta$  132.8 ( $\text{C}_{\text{Thr-H}}$ ), 127.4 ( $\text{C}_{\text{Thr-H}}$ ), 127.0 ( $\text{C}_{\text{Thr-H}}$ ), 123.4 (4), 98.9 (6), 97.7 (5), 0.0 (7).

The characterisation data is in agreement with previously reported.<sup>[403]</sup>

### Compound 103a<sup>[403]</sup>

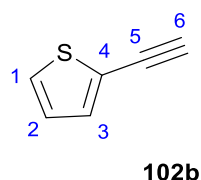


A suspension of CuI (9 mg, 0.05 mmol, 0.01 equiv.) and  $\text{Pd}(\text{PPh}_3)_2\text{Cl}_2$  (32 mg, 0.05 mmol, 0.01 equiv.) in trimethylamine (11.3 ml) was purged with  $\text{N}_2$  for 1 h. 2-Iodo-5-methylthiophene (1.008 g, 4.50 mmol, 1.0 equiv.) was added, followed by ethynyltrimethylsilane (1.27 ml, 9.00 mmol, 2.0 equiv.) added in portions over the period of 40 min. The reaction mixture was stirred at rt for 3 h, diluted with dichloromethane and filtered through a pad of Celite. The solvent was removed in *vacuo*. The crude was purified by column chromatography (Pet) to afford **103a** (878 mg, > 99%) as a yellow oil.

$^1\text{H NMR}$  (500 MHz,  $\text{CDCl}_3$ )  $\delta$  7.03 (d,  $J = 3.6$  Hz, 1H, 4), 6.61 – 6.58 (m, 1H, 3), 2.45 (d,  $J = 0.9$  Hz, 3H, 1), 0.24 (s, 9H, 8);  $^{13}\text{C}\{^1\text{H}\}$  NMR (126 MHz,  $\text{CDCl}_3$ )  $\delta$  142.3 (2), 133.1 (4), 125.3 (3), 120.9 (5), 98.2 (7), 97.8 (6), 15.5 (1), 0.1 (8).

The characterisation data is in agreement with previously reported.<sup>[404]</sup>

### Compound 102b



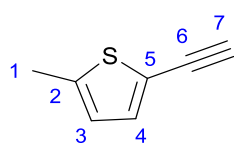
TMS protected derivative **102a** (819 mg, 4.55 mmol, 1.0 equiv.) was dissolved in dichloromethane (90.0 ml). TBAF hydrate (1.526 g, 5.46 mmol, 1.2 equiv.) was added and the reaction mixture was stirred at rt for 2 h. Then,  $\text{NH}_4\text{Cl}_{(\text{aq})}$  was added, the organic phase was

extracted with water and the combined organic layers were dried over  $\text{MgSO}_4$ , filtered and concentrated in *vacuo* to yield compound **102b** (417 mg, 86%) as a brown oil.

$^1\text{H NMR}$  (500 MHz,  $\text{CDCl}_3$ )  $\delta$  7.29 – 7.25 (m, 2H, 1, 3), 6.97 (dd,  $J = 5.2, 3.6$  Hz, 1H, 2), 3.33 (s, 1H, 6);  $^{13}\text{C}\{^1\text{H}\}$  NMR (126 MHz,  $\text{CDCl}_3$ )  $\delta$  133.2 ( $C_{\text{Thr-H}}$ ), 127.6 ( $C_{\text{Thr-H}}$ ), 127.0 (2), 122.2 (4), 81.4 (6), 77.1 (5).

The characterisation data is in agreement with previously reported.<sup>[403]</sup>

### Compound 103b



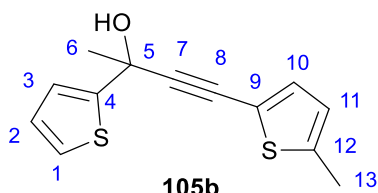
**103b**

TMS protected derivative **103a** (878 mg, 4.50 mmol, 1.0 equiv.) was dissolved in dichloromethane (50.0 ml). TBAF hydrate (1.635 g, 5.85 mmol, 1.3 equiv.) was added and the reaction mixture was stirred at rt for 1 h. Then,  $\text{NH}_4\text{Cl}_{(\text{aq})}$  was added, the organic phase was extracted with water and the combined organic layers were dried over  $\text{MgSO}_4$ , filtered and concentrated in *vacuo* to yield compound **103b** (541 mg, 99%) as a brown oil.

$^1\text{H NMR}$  (500 MHz,  $\text{CDCl}_3$ )  $\delta$  7.08 (d,  $J = 3.5$  Hz, 1H, 4), 6.62 (dq,  $J = 3.5, 1.0$  Hz, 1H, 3), 3.29 (s, 1H, 7), 2.47 (d,  $J = 1.0$  Hz, 3H, 1);  $^{13}\text{C}\{^1\text{H}\}$  NMR (126 MHz,  $\text{CDCl}_3$ )  $\delta$  142.5 (2), 133.5 (4), 125.3 (3), 119.6 (5), 80.5 (7), 77.5 (6), 15.4 (1).

The characterisation data is in agreement with previously reported.<sup>[404]</sup>

### Compound 105b



**105b**

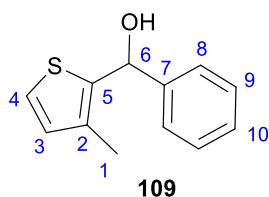
**Procedure a** (Scheme 25): To a solution of **103b** (122 mg, 0.2 M, 1.0 equiv.) in anhydrous THF, a solution of *n*-BuLi in hexanes (0.5 ml, 1.1 mmol, 1.1 equiv.) was added dropwise at  $-78$  °C under inert atmosphere. The resulting solution was stirred at  $-78$  °C for 15 min, then warmed to  $0$  °C and stirred for further 1.5 h. Ketone **104a** (139 mg, 1.10 mmol, 1.1 equiv.) was added dropwise at  $-78$  °C and the resulting solution was slowly warmed to rt overnight. Water was added at  $0$  °C and the aqueous layer was separated and extracted with dichloromethane, washed with brine; the combined organic layers were dried over  $\text{MgSO}_4$ , filtered and

concentrated in *vacuo*. Purification by column chromatography (Pet/AcOEt 20:1) yielded alkyne **105b** (61 mg, 25%) as a yellow oil.

**Procedure b** (Scheme 27): 25 ml round bottom flask was charged with **110a** (304 mg, 2.00 mmol, 1.0 equiv.), CuI (8 mg, 0.04 mmol, 0.02 equiv.) and Pd(PPh<sub>3</sub>)<sub>2</sub>Cl<sub>2</sub> (28 mg, 0.04 mmol, 0.02 equiv.) and purged with N<sub>2</sub>. Triethylamine (4.9 ml) was added, followed by 2-iodo-5-methyl-thiophene (896 mg, 4.00 mmol, 2.0 equiv.) and the resulting reaction mixture was stirred at rt overnight. Then, the mixture was diluted with dichloromethane and filtered through a pad of Celite. The solvent was removed in *vacuo*. The crude was purified by column chromatography (Pet/AcOEt 9:1) to yield compound **105b** (353 mg, 71%) as a yellow oil.

**<sup>1</sup>H NMR** (500 MHz, CDCl<sub>3</sub>) δ 7.26 (dd, *J* = 5.0, 1.3 Hz, 1H, *H*<sub>Th</sub>), 7.23 (dd, *J* = 3.6, 1.3 Hz, 1H, *H*<sub>Th</sub>), 7.05 (d, *J* = 3.4 Hz, 1H, 10), 6.97 (dd, *J* = 5.0, 3.6 Hz, 1H, *H*<sub>Th</sub>), 6.63 (dq, *J* = 3.4, 1.0 Hz, 1H, 11), 2.65 (brs, 1H, -OH), 2.47 (d, *J* = 1.0 Hz, 3H, 13), 1.97 (s, 3H, 6); **<sup>13</sup>C{<sup>1</sup>H} NMR** (126 MHz, CDCl<sub>3</sub>) δ 150.5 (4), 142.6 (12), 133.0 (*C*<sub>Th-H</sub>), 126.8 (*C*<sub>Th-H</sub>), 125.4 (*C*<sub>Th-H</sub>), 125.3 (*C*<sub>Th-H</sub>), 124.2 (*C*<sub>Th-H</sub>), 119.7 (9), 94.6 (7), 78.3 (8), 68.0 (5), 33.2 (13), 15.5 (6); **HRMS** (ASAP) (C<sub>13</sub>H<sub>13</sub>S<sub>2</sub>O) [M+H]<sup>+</sup>: calcd: 249.0408; found: 249.0408.

### Compound 109

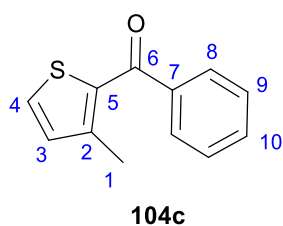


To a solution of aldehyde **108** (90% grade, 1.008 g, 8.00 mmol, 1.0 equiv.) in anhydrous THF (10 ml), a solution of phenylmagnesium bromide (9.6 ml, 1.0 M in THF, 1.2 equiv.) was added at 0 °C under inert atmosphere. The reaction mixture was warmed to rt and stirred for 3 h 10 min. NH<sub>4</sub>Cl<sub>(aq)</sub> was added, the aqueous phase was extracted with ethyl acetate and the combined organic layers were washed with brine, dried over MgSO<sub>4</sub>, filtered and concentrated in *vacuo*. Purification by column chromatography (Pet/AcOEt 7:1) afforded compound **109** (1.035 g, 70%) as a yellow oil.

**<sup>1</sup>H NMR** (400 MHz, CDCl<sub>3</sub>) δ 7.46 – 7.43 (m, 2H, 8), 7.39 – 7.35 (m, 2H, 9), 7.33 – 7.29 (m, 1H, 10), 7.16 (d, *J* = 5.0 Hz, 1H, 4), 6.82 (d, *J* = 5.0 Hz, 1H, 3), 6.08 (s, 1H, 6), 2.51 (brs, 1H, -OH), 2.22 (s, 3H, 1); **<sup>13</sup>C{<sup>1</sup>H} NMR** (126 MHz, CDCl<sub>3</sub>) δ 143.1 (*C*<sub>Ar</sub>), 141.2 (*C*<sub>Ar</sub>), 133.9 (*C*<sub>Ar</sub>), 130.3 (*C*<sub>Th-H</sub>), 128.6 (*C*<sub>Ph-H<sub>2</sub></sub>), 127.9 (10), 126.4 (*C*<sub>Ph-H<sub>2</sub></sub>), 123.7 (*C*<sub>Th-H</sub>), 70.8 (6), 14.1 (1).

The characterisation data is in agreement with previously reported.<sup>[405]</sup>

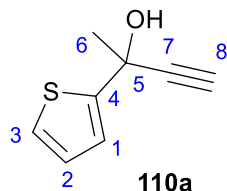


**Compound 104c**<sup>[398]</sup>

To a solution of alcohol **109** (1.035 g, 5.07 mmol, 1.0 equiv.) in dichloromethane (40.0 ml), activated MnO<sub>2</sub> (1.808 g, 20.79 mmol, 4.1 equiv.) was added and resulting suspension was stirred at rt for 26 h (monitored by TLC). Reaction mixture was filtered through a pad of Celite and concentrated in *vacuo*. Purification by column chromatography (Pet/AcOEt 13:1) afforded compound **104c** (1.024 g, > 99%, 90% pure – see **108**) as a yellow oil.

<sup>1</sup>H NMR (500 MHz, CDCl<sub>3</sub>) δ 7.83 – 7.81 (m, 2H, *H<sub>Ph</sub>*), 7.58 – 7.54 (m, 1H, 10), 7.49 (d, *J* = 4.9 Hz, 1H, *H<sub>Th</sub>*), 7.49 – 7.45 (m, 2H, *H<sub>Ph</sub>*), 7.00 (d, *J* = 4.9 Hz, 1H, *H<sub>Th</sub>*), 2.48 (s, 3H, 1); <sup>13</sup>C{<sup>1</sup>H} NMR (126 MHz, CDCl<sub>3</sub>) δ 189.8 (6), 146.0 (*C<sub>Th</sub>*), 140.1 (*C<sub>Th</sub>*), 135.1 (7), 132.3 (3/4), 132.2 (3/4), 131.0 (10), 129.2 (*C<sub>Ph-H2</sub>*), 128.4 (*C<sub>Ph-H2</sub>*), 16.9 (1).

The characterisation data is in agreement with previously reported.<sup>[405]</sup>

**Compound 110a**<sup>[401]</sup>

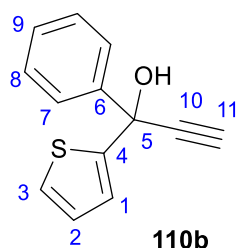
A solution of ethynylmagnesium bromide (9.0 ml, 4.5 mmol, 1.5 equiv.) in THF was added dropwise to the solution of ketone **104a** (378 mg, 3.00 mmol, 1.0 eq) in anhydrous THF (12.0 ml) at 0 °C under inert atmosphere. The resulting solution was heated at reflux for 50 min and cooled to rt. NH<sub>4</sub>Cl<sub>(aq)</sub> was added, the aqueous phase was extracted with Et<sub>2</sub>O and the combined organic layers were dried over MgSO<sub>4</sub>, filtered and concentrated in *vacuo*. The crude was purified by column chromatography (Pet/AcOEt 9:1) to yield compound **110a** (304 mg, 67%) as a yellow oil.

When reaction does not reach completion **110a** is inseparable from the ketone **104a** precursor.

<sup>1</sup>H NMR (500 MHz, CDCl<sub>3</sub>) δ 7.25 (dd, *J* = 5.1, 1.2 Hz, 1H, 1/3), 7.21 (dd, *J* = 3.6, 1.2 Hz, 1H, 1/3), 6.95 (dd, *J* = 5.1, 3.6 Hz, 1H, 2), 2.68 (s, 1H, 8), 2.67 (brs, 1H, -OH), 1.91 (s, 3H, 6); <sup>13</sup>C{<sup>1</sup>H} NMR (126 MHz, CDCl<sub>3</sub>) δ 149.9 (4), 128.2 (*C<sub>Th-H</sub>*), 125.3 (*C<sub>Th-H</sub>*), 124.3 (*C<sub>Th-H</sub>*), 86.6 (7), 72.6 (8), 67.3 (5), 33.1 (6).

The characterisation data is in agreement with previously reported.<sup>[406]</sup>

### Compound 110b<sup>[401]</sup>

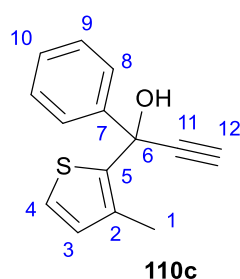


A solution of ethynylmagnesium bromide (24.0 ml, 12.0 mmol, 2.0 equiv.) in THF was added dropwise to the solution of ketone **104b** (1.128 g, 6.00 mmol, 1.0 eq) in anhydrous THF (24 ml) at 0 °C under inert atmosphere. The resulting solution was heated at reflux for 3 h and cooled to rt.  $\text{NH}_4\text{Cl}_{(\text{aq})}$  was added, the aqueous phase was extracted with  $\text{Et}_2\text{O}$  and the combined organic layers were dried over  $\text{MgSO}_4$ , filtered and concentrated in *vacuo* to yield compound **110b** (1.242 g, 97%) as a yellow oil that was used without further purification.

$^1\text{H NMR}$  (400 MHz,  $\text{CDCl}_3$ )  $\delta$  7.74 – 7.68 (m, 2H, 7), 7.41 – 7.31 (m, 3H, 8, 9), 7.27 (dd,  $J = 5.1, 1.3$  Hz, 1H, 1/3), 7.10 (dd,  $J = 3.6, 1.3$  Hz, 1H, 1/3), 6.93 (dd,  $J = 5.1, 3.6$  Hz, 1H, 2), 3.07 (brs, 1H, -OH), 2.89 (s, 1H, 11);  $^{13}\text{C}\{^1\text{H}\}$  NMR (101 MHz,  $\text{CDCl}_3$ )  $\delta$  149.7 (4), 143.8 (6), 128.4 (2 x  $C_{\text{Ph-H}}$ ), 128.4 (9), 126.6 ( $C_{\text{Th-H}}$ ), 126.3 ( $C_{\text{Th-H}}$ ), 125.8 (2 x  $C_{\text{Ph-H}}$ ), 125.7 ( $C_{\text{Th-H}}$ ), 85.9 (10), 75.1 (11), 71.9 (5).

The characterisation data is in agreement with previously reported.<sup>[407]</sup>

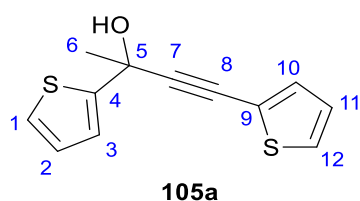
### Compound 110c<sup>[401]</sup>



A solution of ethynylmagnesium bromide (12.0 ml, 6.00 mmol, 2.0 equiv.) in THF was added dropwise to the solution of ketone **104c** (606 mg, 3.00 mmol, 1.0 eq) in anhydrous THF (12.0 ml) at 0 °C under inert atmosphere. The resulting solution was heated at reflux for 3 h and cooled to rt.  $\text{NH}_4\text{Cl}_{(\text{aq})}$  was added, the aqueous phase was extracted with  $\text{Et}_2\text{O}$  and the combined organic layers were dried over  $\text{MgSO}_4$ , filtered and concentrated in *vacuo*. The crude was purified by column chromatography (Pet/AcOEt 12:1) to yield compound **110c** (572 mg, 77%, 90% pure – see **108**) as a yellow oil.

**$^1\text{H NMR}$**  (400 MHz,  $\text{CDCl}_3$ )  $\delta$  7.68 – 7.65 (m, 2H, 8), 7.38 – 7.36 (m, 3H, 9, 10), 7.13 (d,  $J = 5.1$  Hz, 1H, 4), 6.82 (d,  $J = 5.1$  Hz, 1H, 3), 3.02 (brs, 1H, -OH), 2.90 (s, 1H, 12), 2.05 (s, 3H, 1);  **$^{13}\text{C}\{^1\text{H}\}$  NMR** (101 MHz,  $\text{CDCl}_3$ )  $\delta$  143.0 ( $C_{Ar}$ ), 140.9 ( $C_{Ar}$ ), 134.4 ( $C_{Ar}$ ), 132.0 ( $C_{Th-H}$ ), 128.5 (10), 128.4 ( $C_{Ph-H_2}$ ), 126.4 ( $C_{Ph-H_2}$ ), 122.7 ( $C_{Th-H}$ ), 84.8 (11), 75.4 (12), 71.7 (6), 14.8 (1); **MS** (EI) ( $\text{C}_{14}\text{H}_{11}\text{S}$ ) [ $\text{M}+\text{H}-\text{H}_2\text{O}$ ] $^+$ : caclcd: 211; found: 212; HRMS of corresponding peak(s) not found.

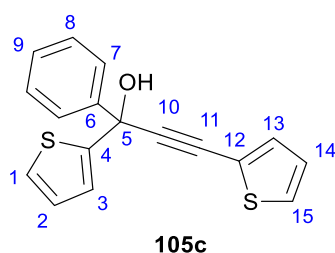
### Compound 105a<sup>[403]</sup>



A suspension of **110a** (135 mg, 0.89 mmol, 1.0 equiv.),  $\text{CuI}$  (2 mg, 0.01 mmol, 0.01 equiv.) and  $\text{Pd}(\text{PPh}_3)_2\text{Cl}_2$  (6 mg, 0.01 mmol, 0.01 equiv.) in trimethylamine (2.2 ml) was purged with  $\text{N}_2$  for 10 min. 2-Iodothiophene (374 mg, 1.78 mmol, 2.0 equiv.) was added and the reaction mixture was stirred at rt overnight. The reaction mixture was diluted with dichloromethane and filtered through a pad of Celite. The solvent was removed in *vacuo*. The crude was purified by column chromatography (Pet/AcOEt 13:1) to yield **105a** (147 mg, 71%) as a yellow oil, contaminated with inseparable ketone **104a** (**105a**:**104a** 0.8:1) precursor.

**$^1\text{H NMR}$**  (500 MHz,  $\text{CDCl}_3$ )  $\delta$  7.29 – 7.23 (m, 4H,  $H_{Th}$ ), 7.00 – 6.96 (m, 2H,  $H_{Th}$ ), 2.74 (s, 1H, -OH), 1.98 (s, 3H, 6);  **$^{13}\text{C}\{^1\text{H}\}$  NMR** (126 MHz,  $\text{CDCl}_3$ )  $\delta$  150.3 (4), 132.7 ( $C_{Th-H}$ ), 128.2 ( $C_{Th-H}$ ), 127.7 ( $C_{Th-H}$ ), 126.8 ( $C_{Th-H}$ ), 125.3 ( $C_{Th-H}$ ), 124.2 ( $C_{Th-H}$ ), 122.2 (9), 95.4 (7), 77.9 (8), 68.0 (5), 33.1 (6); **HRMS** (ASAP) ( $\text{C}_{12}\text{H}_{11}\text{OS}_2$ ) [ $\text{M}+\text{H}$ ] $^+$ : caclcd: 235.0251; found: 235.0252.

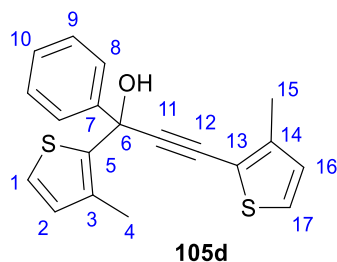
### Compound 105c



**110b** (1.07 g, 5.00 mmol, 1.0 equiv.),  $\text{CuI}$  (29 mg, 0.15 mmol, 0.03 equiv.) and  $\text{Pd}(\text{PPh}_3)_2\text{Cl}_2$  (105 mg, 0.15 mmol, 0.03 equiv.) were suspended in degassed trimethylamine (12.2 ml) under inert atmosphere. 2-Iodothiophene (2.10 g, 10.0 mmol, 2.0 equiv.) was added, the reaction mixture was stirred at rt for 5.5 h. The reaction mixture was diluted with dichloromethane and filtered through a pad of Celite. The solvent was removed in *vacuo*. The crude was purified by column chromatography (Pet/AcOEt 9:1) to yield **105c** (1.180 g, 84%) as a yellow oil.

**<sup>1</sup>H NMR** (400 MHz, CDCl<sub>3</sub>) δ 7.76 – 7.73 (m, 2H, 7), 7.42 – 7.37 (m, 2H, *H*<sub>Ar</sub>), 7.36 – 7.27 (m, 4H, *H*<sub>Ar</sub>), 7.13 (dd, *J* = 3.6, 1.3 Hz, 1H, 13), 7.01 (dd, *J* = 5.1, 3.6 Hz, 1H, *H*<sub>Th</sub>), 6.95 (dd, *J* = 5.1, 3.6 Hz, 1H, 2/14), 3.11 (s, 1H, -OH); **<sup>13</sup>C{<sup>1</sup>H} NMR** (101 MHz, CDCl<sub>3</sub>) δ 150.1 (4), 144.1 (6), 132.9 (*C*<sub>Th</sub>-H), 128.5 (2 x *C*<sub>Ph</sub>-H), 128.3 (9), 128.0 (*C*<sub>Th</sub>-H), 127.2 (*C*<sub>Th</sub>-H), 126.7 (*C*<sub>Th</sub>-H), 126.2 (*C*<sub>Th</sub>-H), 125.9 (2 x *C*<sub>Ph</sub>-H), 125.6 (*C*<sub>Th</sub>-H), 122.1 (12), 94.8 (10), 80.2 (11), 72.6 (5); **HRMS** (ESI) (C<sub>17</sub>H<sub>12</sub>OS<sub>2</sub>Na) [M+Na]<sup>+</sup>: calcd: 319.0222; found: 319.0221.

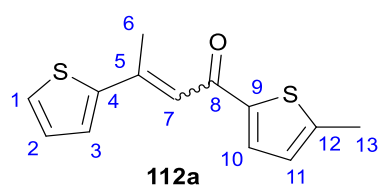
### Compound 105d



**110c** (491 mg, 2.15 mmol, 1.0 equiv.), CuI (21 mg, 0.11 mmol, 0.05 equiv.) and Pd(PPh<sub>3</sub>)<sub>2</sub>Cl<sub>2</sub> (77 mg, 0.11 mmol, 0.05 equiv.) were suspended in degassed trimethylamine (5.2 ml) under inert atmosphere. 2-Bromo-3-methylthiophene (762 mg, 4.30 mmol, 2.0 equiv.) was added and the reaction mixture was stirred at rt overnight. The reaction mixture was diluted with dichloromethane and filtered through a pad of Celite. The solvent was removed in *vacuo*. The crude was purified by column chromatography (Pet/AcOEt 7:1) to yield **105d** (293 mg, 42%, 90% pure – see **108**) as a yellow oil.

**<sup>1</sup>H NMR** (400 MHz, CDCl<sub>3</sub>) δ 7.73 – 7.70 (m, 2H, 8), 7.41 – 7.31 (m, 3H, 9, 10), 7.18 (d, *J* = 5.1 Hz, 1H, 1/17), 7.14 (d, *J* = 5.1 Hz, 1H, 1/17), 6.85 (d, *J* = 5.1 Hz, 1H, 2/16), 6.83 (d, *J* = 5.1 Hz, 1H, 2/16) 3.05 (brs, 1H, -OH), 2.35 (s, 3H, 4/15), 2.11 (s, 3H, 4/15); **<sup>13</sup>C{<sup>1</sup>H} NMR** (101 MHz, CDCl<sub>3</sub>) δ 143.6 (*C*<sub>Ar</sub>), 141.5 (*C*<sub>Ar</sub>), 137.3 (*C*<sub>Ar</sub>), 134.4 (*C*<sub>Th</sub>-H), 132.1 (*C*<sub>Ar</sub>), 129.3 (10), 128.4 (2 x *C*<sub>Ph</sub>-H), 128.3 (*C*<sub>Th</sub>-H), 126.6 (*C*<sub>Th</sub>-H), 126.5 (2 x *C*<sub>Ph</sub>-H), 122.6 (*C*<sub>Th</sub>-H), 117.5 (13), 96.3 (11), 80.3 (12), 72.6 (6), 15.2 (4/15), 14.9 (4/15); **HRMS** (ESI) (C<sub>19</sub>H<sub>16</sub>OS<sub>2</sub>Na) [M+Na]<sup>+</sup>: calcd: 347.0535; found: 347.0532.

### Compound 112a



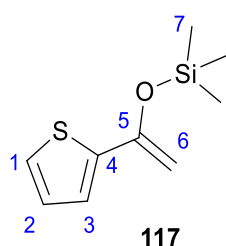
To a solution of **105b** (60 mg, 0.24 mmol, 1.0 equiv.) in THF (0.7 ml), a solution of PBr<sub>3</sub> (65 mg, 0.24 mmol, 1.0 equiv.) in THF (0.7 ml) was added dropwise at 0 °C under inert

atmosphere. The colour of the solution changed from orange to yellow upon addition. The reaction mixture was warmed to rt and stirred for 3 h and quenched with water. The aqueous phase was separated and extracted with dichloromethane. The combined organic layers were dried over MgSO<sub>4</sub>, filtered and concentrated in *vacuo*. Purification by column chromatography (Pet/AcOEt 19:1) yielded **112a** (6 mg, 10%) as a yellow semisolid.

<sup>1</sup>H NMR (500 MHz, CDCl<sub>3</sub>) δ 7.58 (d, *J* = 3.7 Hz, 1H, 10), 7.41 (dd, *J* = 3.7, 1.1 Hz, 1H, 1/3), 7.36 (dd, *J* = 5.1, 1.1 Hz, 1H, 1/3), 7.18 (q, *J* = 1.2 Hz, 1H, 7), 7.09 (dd, *J* = 5.1, 3.7 Hz, 1H, 2), 6.81 (dd, *J* = 3.7, 0.8 Hz, 1H, 11), 2.67 (d, *J* = 1.2 Hz, 3H, 6), 2.55 (d, *J* = 0.8 Hz, 3H, 13); <sup>13</sup>C{<sup>1</sup>H} NMR (126 MHz, CDCl<sub>3</sub>) δ 183.0 (8), 149.5 (5), 147.5 (C<sub>Th</sub>), 146.4 (C<sub>Th</sub>), 145.3 (C<sub>Th</sub>), 131.5 (C<sub>Th-H</sub>), 128.3 (C<sub>Th-H</sub>), 127.4 (C<sub>Th-H</sub>), 127.4 (C<sub>Th-H</sub>), 126.9 (C<sub>Th-H</sub>), 118.2 (7), 18.3 (6), 16.2 (13).

The characterisation data matches the characterisation of a derivative with an extra methyl group in the second thiophene.<sup>[408]</sup>

#### Compound 117<sup>[409]</sup>

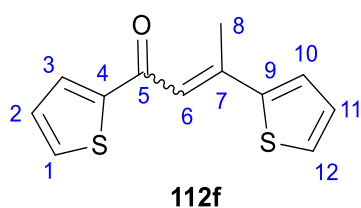


To a solution of chlorotrimethylsilane (2.25 ml, 18.0 mmol, 1.2 equiv.) in DMF (15 ml), triethylamine (5.0 ml, 36.0 mmol, 2.4 equiv.) and ketone **104a** (1.890 g, 15.00 mmol, 1.0 equiv.) were added under inert atmosphere. The reaction mixture was heated at reflux overnight. Then, the mixture was cooled to rt, diluted with AcOEt and washed twice with NaHCO<sub>3</sub>, ice water and brine. The combined organic layers dried over MgSO<sub>4</sub>, filtered and concentrated in *vacuo*. <sup>1</sup>H NMR of the aliquot of the crude showed mainly unreacted ketone. The reaction mixture was resubmitted to the same reaction conditions again and heated at 50 °C overnight. After repeated work-up and column chromatography (Pet/AcOEt 13:1) **117** (1.267 g, 43%, conv. 54%) was isolated as a yellow oil.

<sup>1</sup>H NMR (400 MHz, CDCl<sub>3</sub>) δ 7.20 – 7.16 (m, 2H, 1/3), 6.96 (dd, *J* = 5.0, 3.7 Hz, 1H, 2), 4.81 (d, *J* = 1.9 Hz, 1H, 6), 4.32 (d, *J* = 1.9 Hz, 1H, 6), 0.28 (s, 9H, 7); <sup>13</sup>C{<sup>1</sup>H} NMR (101 MHz, CDCl<sub>3</sub>) δ 151.1 (5), 142.8 (4), 127.4 (C<sub>Th-H</sub>), 125.2 (C<sub>Th-H</sub>), 124.0 (C<sub>Th-H</sub>), 90.4 (6), 0.2 (7). Trace amount of the deprotected ketone could be detected in the <sup>13</sup>C NMR spectra but not in <sup>1</sup>H.

The characterisation data is in agreement with previously reported.<sup>[410]</sup>

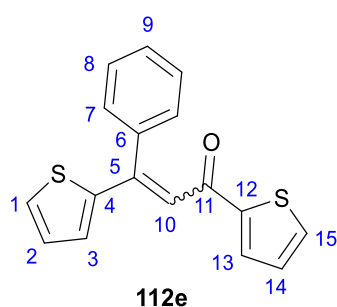
### Compound 112f<sup>[197]</sup>



A microwave vessel was charged with 1,4-dioxane (9 ml),  $\text{Ti}(\text{OEt})_4$  (1.14 g, 5.00 mmol, 1.25 equiv.), ketone **104a** (504 mg, 4.00 mmol, 1.0 equiv.) and  $i\text{Pr}_2\text{NH}$  (0.39 ml, 2.8 mmol, 0.7 equiv.) under inert atmosphere. The mixture was heated at 120 °C for 4.5 h in the The crude was filtered through a pad of silica gel, washed with AcOEt and concentrated in *vacuo*.  $^1\text{H}$  NMR of the aliquot of the crude showed a mixture of the product and unreacted ketone **104a**. The reaction mixture was resubmitted to the reaction conditions (excluding addition of 0.7 equiv. of  $i\text{Pr}_2\text{NH}$ ) and was irradiated at 120-130 °C for 4.5 h. After repeated work-up and column chromatography (Pet/dichloromethane 7:3) single isomer of **112f** (299 mg, 64%, conv.<100%) was isolated as a yellow oil.

$^1\text{H}$  NMR (500 MHz,  $\text{CDCl}_3$ )  $\delta$  7.76 (dd,  $J = 3.8, 1.0$  Hz, 1H,  $H_{\text{Th}}$ ), 7.62 (dd,  $J = 4.9, 1.0$  Hz, 1H,  $H_{\text{Th}}$ ), 7.43 (dd,  $J = 3.8, 1.0$  Hz, 1H,  $H_{\text{Th}}$ ), 7.38 (d,  $J = 5.1$  Hz, 1H,  $H_{\text{Th}}$ ), 7.24 (brs, 1H, 6), 7.15 (dd,  $J = 4.9, 3.8$  Hz, 1H, 2/11), 7.10 (dd,  $J = 5.1, 3.8$  Hz, 1H, 2/11), 2.69 (d,  $J = 1.1$  Hz, 3H, 8);  $^{13}\text{C}\{^1\text{H}\}$  NMR (126 MHz,  $\text{CDCl}_3$ )  $\delta$  183.2 (5), 148.3 (7), 147.5 ( $C_{\text{Th}}$ ), 146.2 ( $C_{\text{Th}}$ ), 133.3 ( $C_{\text{Th-H}}$ ), 131.0 ( $C_{\text{Th-H}}$ ), 128.4 ( $C_{\text{Th-H}}$ ), 128.3 ( $C_{\text{Th-H}}$ ), 127.7 ( $C_{\text{Th-H}}$ ), 127.6 ( $C_{\text{Th-H}}$ ), 118.2 (6), 18.4 (8); HRMS (ASAP) ( $\text{C}_{12}\text{H}_{11}\text{OS}_2$ )  $[\text{M}+\text{H}]^+$ : caclcd: 235.0251; found: 235.0254.

### Compound 112e<sup>[175]</sup>



To a solution of **105c** (370 mg, 1.25 mmol, 1.0 equiv.) in toluene (6.9 ml), trifluoroacetic acid (0.37 ml, 4.9 mmol, 3.9 equiv.) was added at rt under inert atmosphere. The colour of the solution instantly changed from yellow to dark green. The mixture was stirred at rt for 6 h 20 min. The crude was diluted with dichloromethane, washed with  $\text{NaHCO}_3$  three times, water

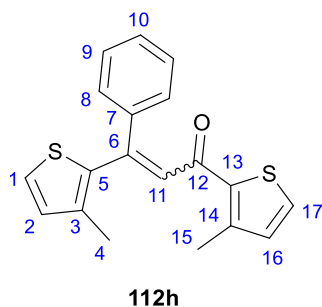
and brine. The combined organic layers were dried over  $\text{MgSO}_4$ , filtered and concentrated in *vacuo*. Purification by column chromatography (Pet/AcOEt 7:1) yielded **112e** (351 mg, 95%) as a yellow oil of inseparable mixture of geometric isomers at 6:1 ratio.

**Major isomer:**  $^1\text{H NMR}$  (500 MHz,  $\text{CDCl}_3$ )  $\delta$  7.77 (dd,  $J = 3.8, 1.1$  Hz, 1H,  $H_{Th}$ ), 7.59 (dd,  $J = 4.9, 1.1$  Hz, 1H,  $H_{Th}$ ), 7.42 – 7.38 (m, 4H,  $H_{Ar}$ ), 7.35 – 7.31 (m, 2H,  $H_{Ar}$ ), 7.29 (s, 1H, 10), 7.11 (dd,  $J = 4.9, 3.8$  Hz, 1H, 2/14), 7.03 (dd,  $J = 5.1, 3.7$  Hz, 1H, 2/14), 6.98 (dd,  $J = 3.7, 1.1$  Hz, 1H,  $H_{Th}$ );  $^{13}\text{C}\{^1\text{H}\}$  NMR (101 MHz,  $\text{CDCl}_3$ )  $\delta$  182.0 (11), 149.4 (5), 146.7 ( $C_{Th}$ ), 145.6 ( $C_{Th}$ ), 138.4 (6), 133.5 ( $C_{Th-H}$ ), 131.6 ( $C_{Th-H}$ ), 130.8 ( $C_{Th-H}$ ), 129.0 (2 x  $C_{Ph-H}$ ), 128.5 ( $C_{Th-H}$ ), 128.5 ( $C_{Th-H}$ ), 128.2 ( $C_{Th-H}$ ), 128.1 (9), 128.1 (2 x  $C_{Ph-H}$ ), 118.8 (10).

**Minor isomer:**  $^1\text{H NMR}$  (500 MHz,  $\text{CDCl}_3$ )  $\delta$  7.72 (dd,  $J = 3.8, 1.1$  Hz, 1H,  $H_{Th}$ ), 7.61 (dd,  $J = 4.9, 1.1$  Hz, 1H,  $H_{Th}$ ), 7.50 – 7.47 (m, 2H,  $H_{Ar}$ ), 7.44 (m, 4H,  $H_{Ar}$ ), 7.23 (dd,  $J = 3.7, 1.1$  Hz, 1H,  $H_{Th}$ ), 7.08 (dd,  $J = 4.9, 3.8$  Hz, 1H, 2/14), 7.00 (dd,  $J = 5.1, 3.7$  Hz, 1H, 2/14), 6.86 (s, 1H, 10);  $^{13}\text{C}\{^1\text{H}\}$  NMR (101 MHz,  $\text{CDCl}_3$ )  $\delta$  183.9 (11), 147.1 (5), 145.9 ( $C_{Th}$ ), 142.3 ( $C_{Th}$ ), 140.1 (6), 133.9 ( $C_{Th-H}$ ), 132.3 ( $C_{Th-H}$ ), 132.0 ( $C_{Th-H}$ ), 129.5 ( $C_{Th-H}$ ), 129.1 ( $C_{Th-H}$ ), 128.9 (2 x  $C_{Ph-H}$ ), 128.4 (2 x  $C_{Ph-H}$ ), 128.2 ( $C_{Ar-H}$ ), 126.9 ( $C_{Ar-H}$ ), 123.2 (10).

**MS** (EI) ( $\text{C}_{17}\text{H}_{12}\text{OS}_2$ ) [ $\text{M}$ ] $^+$ : caclcd: 296; found: 296; fragments from C(10)-C(11) bond cleavage were also observed: ( $\text{C}_{12}\text{H}_9\text{S}$ ) caclcd: 185; found: 184; ( $\text{C}_5\text{H}_3\text{OS}$ ) caclcd: 111; found: 111.

### Compound **112h**<sup>[175]</sup>

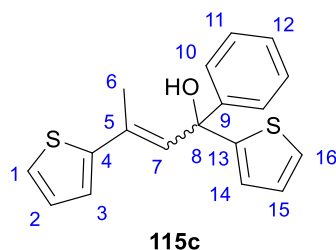


To a solution of **105d** (150 mg, 0.46 mmol, 1.0 equiv.) in toluene (2.5 ml), trifluoroacetic acid (0.14 ml, 1.8 mmol, 3.9 equiv.) was added at rt under inert atmosphere. The colour of the solution instantly changed from yellow to dark green. The mixture was stirred at rt for 3 h 20 min. The crude was diluted with dichloromethane, washed with  $\text{NaHCO}_3$  three times, water and brine. The combined organic layers were dried over  $\text{MgSO}_4$ , filtered and concentrated in *vacuo* to yield **112h** (125 mg, 83%) as a brown oil of inseparable mixture of geometric isomers at 3:2 ratio.

Spectra of both isomers are reported together, the complexity of the spectra prevented the assignment.

**<sup>1</sup>H NMR** (400 MHz, CDCl<sub>3</sub>) δ 7.42 – 7.35 (m, 9H), 7.32 – 7.30 (m, 4H), 7.28 – 7.27 (m, 1H), 7.12 (s, 1H), 6.92 – 6.85 (m, 5H), 2.55 (s, 3H), 2.51 (s, 3H), 2.06 (s, 3H), 1.99 (s, 3H); **<sup>13</sup>C{<sup>1</sup>H} NMR** (101 MHz, CDCl<sub>3</sub>) δ 184.8, 184.6, 147.8, 146.0, 145.3, 145.1, 141.1, 139.4, 138.9, 138.2, 137.7, 137.4, 134.1, 132.7, 132.6, 132.1, 130.1, 130.0, 129.9, 129.7, 129.5, 129.2, 128.8, 128.7, 128.2, 128.1, 127.8, 126.2, 126.2, 125.8, 17.0, 16.9, 16.1, 15.0; **HRMS** (ESI) (C<sub>19</sub>H<sub>16</sub>OS<sub>2</sub>Na) [M+Na]<sup>+</sup>: calcd: 347.0535; found: 347.0535.

### Compound 115c

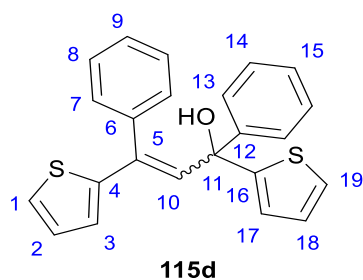


To a solution of **112f** (75 mg, 0.32 mmol, 1.0 equiv.) in anhydrous THF (1.6 ml), a solution of phenylmagnesium bromide (0.48 ml, 1.0 M in THF, 1.5 equiv.) was added at 0 °C under inert atmosphere. The reaction mixture was warmed to rt and stirred for 2.5 h. The reaction was quenched with aqueous NH<sub>4</sub>Cl. The aqueous layer was separated and extracted with Et<sub>2</sub>O. The combined organic layers were washed with brine, dried over MgSO<sub>4</sub>, filtered and concentrated in *vacuo*. Purification by column chromatography (Pet/AcOEt 19:1) afforded **115c** (49 mg, 49%) as a yellow oil.

The compound was obtained as a single isomer but was not stable enough for full characterisation.

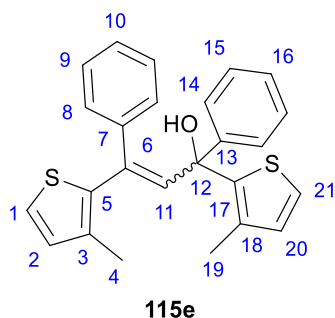
**<sup>1</sup>H NMR** (400 MHz, CDCl<sub>3</sub>) δ 7.52 – 7.48 (m, 2H, 10), 7.30 – 7.25 (m, 2H, 11), 7.23 – 7.16 (m, 2H, H<sub>Ar</sub>), 7.12 (dd, *J* = 5.1, 1.1 Hz, 1H, H<sub>Th</sub>), 7.02 (dd, *J* = 3.6, 1.1 Hz, 1H, H<sub>Th</sub>), 6.92 (dd, *J* = 5.1, 3.6 Hz, 1H, 2/15), 6.88 – 6.84 (m, 2H, H<sub>Th</sub>), 6.73 (q, *J* = 1.3 Hz, 1H, 7), 2.63 (s, 1H, -OH), 1.96 (d, *J* = 1.3 Hz, 3H, 6); **<sup>13</sup>C{<sup>1</sup>H} NMR** (101 MHz, CDCl<sub>3</sub>) δ 153.8 (C<sub>Th</sub>), 147.1 (C<sub>Th</sub>), 145.1 (9), 132.5 (5), 128.4 (2 x C<sub>Ph-H</sub>), 127.7 (C<sub>Ar-H</sub>), 127.6 (C<sub>Ar-H</sub>), 126.8 (C<sub>Ar-H</sub>), 126.8 (C<sub>Ar-H</sub>), 126.1 (2 x C<sub>Ph-H</sub>), 125.3 (C<sub>Ar-H</sub>), 124.7 (C<sub>Ar-H</sub>), 124.5 (C<sub>Ar-H</sub>), 123.9 (7), 77.0 (8), 17.8 (6).



**Compound 115d**

To a solution of **112e** (345 mg, 1.17 mmol, 1.0 equiv.) in anhydrous THF (5.9 ml), a solution of phenylmagnesium bromide (2.33 ml, 1.0 M in THF, 2.0 equiv.) was added at 0 °C under inert atmosphere. The reaction mixture was warmed to rt and stirred for 1 h. The reaction was quenched with aqueous NH<sub>4</sub>Cl. The aqueous layer was separated and extracted with Et<sub>2</sub>O. The combined organic layers were washed with brine, dried over MgSO<sub>4</sub>, filtered and concentrated in *vacuo*. Purification by column chromatography (Pet/AcOEt 12:1) afforded **115d** (370 mg, 84%) as a yellow oil of inseparable mixture of geometric isomers at 4:1 ratio.

**Major isomer:** <sup>1</sup>H NMR (400 MHz, CDCl<sub>3</sub>) δ 7.48 – 7.44 (m, 2H, *H<sub>Ar</sub>*), 7.31 (m, 5H, *H<sub>Ar</sub>*), 7.26 – 7.23 (m, 2H, 10, *H<sub>Ar</sub>*), 7.20 – 7.16 (m, 3H, *H<sub>Ar</sub>*), 6.96 – 6.91 (m, 3H, *H<sub>Ar</sub>*), 6.89 (dd, *J* = 5.1, 3.6 Hz, 1H, *H<sub>Th</sub>*), 6.57 (dd, *J* = 3.6, 1.1 Hz, 1H, *H<sub>Th</sub>*), 2.51 (s, 1H, -OH); <sup>13</sup>C{<sup>1</sup>H} NMR (101 MHz, CDCl<sub>3</sub>) δ 153.3 (*C<sub>Th</sub>*), 147.3 (*C<sub>Th</sub>*), 138.1 (*C<sub>Ph</sub>*), 135.4 (*C<sub>Ph</sub>*), 132.5 (5), 129.5 (2 x *C<sub>Ph-H</sub>*), 128.7 (*C<sub>Ar-H</sub>*), 128.6 (2 x *C<sub>Ph-H</sub>*), 128.5 (*C<sub>Ar-H</sub>*), 128.3 (2 x *C<sub>Ph-H</sub>*), 127.6 (*C<sub>Ar-H</sub>*), 127.4 (*C<sub>Ar-H</sub>*), 126.7 (*C<sub>Ar-H</sub>*), 126.3 (*C<sub>Ar-H</sub>*), 126.2 (2 x *C<sub>Ph-H</sub>*), 125.4 (*C<sub>Ar-H</sub>*), 125.2 (*C<sub>Ar-H</sub>*), 124.9 (10), 77.7 (11); **HRMS** (ASAP) (C<sub>23</sub>H<sub>17</sub>S<sub>2</sub>) [M+H-H<sub>2</sub>O]<sup>+</sup>: caclcd: 357.0772; found: 357.0770.

**Compound 115e**

To a solution of **112h** (111 mg, 0.34 mmol, 1.0 equiv.) in anhydrous THF (1.7 ml) a solution of phenylmagnesium bromide (0.68 ml, 1.0 M in THF, 2.0 equiv.) was added at 0 °C under inert atmosphere. The reaction mixture was warmed to rt and stirred for 1 h. The reaction was quenched with aqueous NH<sub>4</sub>Cl. The aqueous layer was separated and extracted with Et<sub>2</sub>O. The combined organic layers were washed with brine, dried over MgSO<sub>4</sub>, filtered and

concentrated in *vacuo*. Purification by column chromatography (Pet/AcOEt 19:1) afforded **115e** (52 mg, 38%) as a brown oil of inseparable mixture of geometric isomers at 1:0.43 ratio.

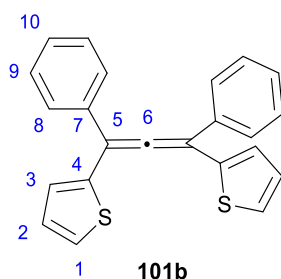
**Major isomer:**  $^1\text{H NMR}$  (400 MHz,  $\text{CDCl}_3$ )  $\delta$  7.51 – 7.45 (m, 2H,  $H_{Ph}$ ), 7.37 – 7.31 (m, 2H,  $H_{Ph}$ ), 7.31 – 7.23 (m, 6H,  $H_{Ph}$ ), 7.11 (d,  $J = 5.1$  Hz, 1H, 1/21), 7.09 (d,  $J = 5.1$  Hz, 1H, 1/21), 6.82 (d,  $J = 5.1$  Hz, 1H, 2/20), 6.78 (d,  $J = 5.1$  Hz, 1H, 2/20), 6.62 (s, 1H, 11), 2.57 (brs, 1H, -OH), 1.97 (s, 3H, 4/19), 1.97 (s, 3H, 4/19).

**Minor isomer:**  $^1\text{H NMR}$  (400 MHz,  $\text{CDCl}_3$ )  $\delta$  7.50 – 7.45 (m, 2H,  $H_{Ar}$ ), 7.37 – 7.22 (m, 9H,  $H_{Ar}$ ), 7.11 – 7.07 (m, 1H, 1/21), 6.96 (s, 1H, 11), 6.89 (d,  $J = 5.1$  Hz, 1H, 2/20), 6.85 (d,  $J = 5.1$  Hz, 1H, 2/20), 3.22 (s, 1H, -OH), 2.00 (s, 3H, 4/19), 2.00 (s, 3H, 4/19).

**Mixture of isomers:**  $^{13}\text{C}\{^1\text{H}\}$  NMR (101 MHz,  $\text{CDCl}_3$ )  $\delta$  146.6, 146.2, 144.6, 144.3, 141.5, 140.4, 139.8, 138.4, 137.4, 136.3, 134.6, 134.4, 134.3, 132.7, 132.3, 132.1, 132.1, 131.4, 130.1, 129.4, 129.3, 128.6, 128.5, 128.3, 128.2, 128.0, 127.5, 127.3, 126.7, 126.6, 126.5, 126.4, 126.2, 123.7, 122.5, 122.4, 78.2, 78.1, 15.3, 15.3, 15.2, 14.6. Assignment not performed due to the complexity of the spectrum.

**HRMS** (ESI) ( $\text{C}_{25}\text{H}_{21}\text{OS}_2$ )  $[\text{M}-\text{H}]^+$ : caclcd: 401.1028; found: 401.1029.

#### Compound **101b**<sup>[177]</sup>

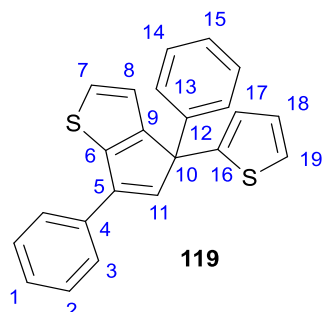


To a solution of **115d** (50 mg, 0.13 mmol, 1.0 equiv.) in AcOEt (0.5 ml), traces amounts of *p*-toluenesulfonic acid monohydrate were added. The colour of the solution changed instantly to deep blue. The mixture was heated at reflux for 15 min, then cooled to rt and diluted with AcOEt and washed with water. The organic layer was separated and dried over  $\text{MgSO}_4$ , filtered and concentrated in *vacuo*. Purification by column chromatography (Pet/AcOEt 49:1) afforded **101b** (20 mg, 43% (50% total yield counting **119**)) as an orange semisolid inseparable from **119** (**101b**:**119** 7:1).

$^1\text{H NMR}$  (400 MHz,  $\text{CDCl}_3$ )  $\delta$  7.62 – 7.58 (m, 4H, 8), 7.43 – 7.38 (m, 4H, 9), 7.38 – 7.33 (m, 2H, 10), 7.29 (dd,  $J = 5.0, 1.3$  Hz, 2H,  $H_{Th}$ ), 7.05 (m, 4H,  $H_{Th}$ );  $^{13}\text{C}\{^1\text{H}\}$  NMR (101 MHz,  $\text{CDCl}_3$ )  $\delta$  208.2 (6), 139.7 (4), 136.0 (7), 128.7 (2 x  $C_{Ph-H}$ ), 128.6 (2 x  $C_{Ph-H}$ ), 128.2 ( $C_{Ar-H}$ ), 127.7 ( $C_{Ar-H}$ ), 126.7 ( $C_{Ar-H}$ ), 125.7 ( $C_{Ar-H}$ ), 108.1 (5); **HRMS** (ASAP) ( $\text{C}_{23}\text{H}_{17}\text{S}_2$ )  $[\text{M}+\text{H}]^+$ : caclcd:

357.0772; found: 357.0762; **MS** (EI) ( $C_{23}H_{16}S_2$ )  $[M]^+$ : cacl: 356; found: 356; ( $C_{23}H_{16}S_2Na$ )  $[M+Na]^+$ : cacl: 379; found: 379.

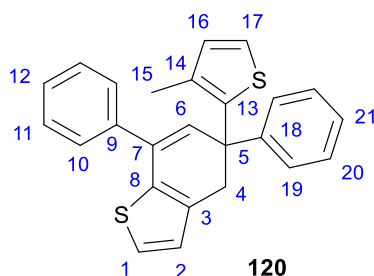
### Compound 119<sup>[168]</sup>



A solution of **115d** (100 mg, 0.27 mmol, 1.0 equiv.) in anhydrous THF (1.3 ml) was added to oven-dried (130 °C for 3 days)  $CuSO_4$  (429 mg, 2.70 mmol, 10.0 equiv.) at rt under inert atmosphere. The mixture was heated at reflux for 24 h, then cooled to rt, filtered through a pad of Celite, washed with dichloromethane and concentrated in *vacuo*. Purification by column chromatography (Pet/AcOEt 24:1) afforded **119** (21 mg, 22% (44% total yield counting **101b**)) as an orange oil inseparable from **101b** (**119:101b** 1:1).

**<sup>1</sup>H NMR** (400 MHz,  $CDCl_3$ )  $\delta$  7.82 – 7.78 (m, 2H,  $H_{Ph}$ ), 7.49 – 7.44 (m, 2H,  $H_{Ar}$ ), 7.40 – 7.33 (m, 4H,  $H_{Ar}$ ), 7.31 – 7.24 (m, 3H,  $H_{Ar}$ ), 7.21 (d,  $J = 5.1$  Hz, 1H, 7/8), 7.18 (dd,  $J = 5.1, 1.3$  Hz, 1H, 17/19), 7.10 (d,  $J = 1.5$  Hz, 1H, 11), 6.99 (dd,  $J = 3.5, 1.3$  Hz, 1H, 17/19), 6.95 (dd,  $J = 5.1, 3.5$  Hz, 1H, 18); **<sup>13</sup>C{<sup>1</sup>H} NMR** (101 MHz,  $CDCl_3$ )  $\delta$  155.5 ( $C_{Ar}$ ), 146.1 ( $C_{Ar}$ ), 142.5 ( $C_{Ar}$ ), 142.1 ( $C_{Ar}$ ), 139.5 (11), 138.5 ( $C_{Ar}$ ), 133.6 (5), 128.9 (2 x  $C_{Ph-H}$ ), 128.6 (2 x  $C_{Ph-H}$ ), 127.3 ( $C_{Ar-H}$ ), 127.3 ( $C_{Ar-H}$ ), 127.2 (2 x  $C_{Ph-H}$ ), 126.6 ( $C_{Ar-H}$ ), 126.6 (2 x  $C_{Ph-H}$ ), 125.8 ( $C_{Ar-H}$ ), 124.3 ( $C_{Ar-H}$ ), 122.8 ( $C_{Ar-H}$ ), 60.1 (10); **HRMS** (ASAP) ( $C_{23}H_{17}S_2$ )  $[M+H]^+$ : cacl: 357.0772; found: 357.0762; **MS** (EI) ( $C_{23}H_{16}S_2$ )  $[M]^+$ : cacl: 356; found: 356.

### Compound 120<sup>[177]</sup>

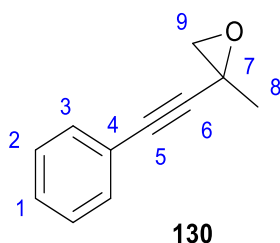


To a solution of **115e** (50 mg, 0.12 mmol, 1.0 equiv.) in AcOEt (0.5 ml), traces amount of *p*-toluenesulfonic acid monohydrate were added. The colour of the solution changed instantly to dark red. The reaction was heated at reflux for 30 min, then cooled to rt and diluted with AcOEt

and washed with water. The organic layer was separated and dried over  $\text{MgSO}_4$ , filtered and concentrated in *vacuo* to afford **120** (46 mg, 48%) as a red oil.

$^1\text{H NMR}$  (500 MHz,  $\text{CDCl}_3$ )  $\delta$  7.39 – 7.23 (m, 11H,  $H_{Ar}$ ), 6.93 (d,  $J = 5.0$  Hz, 1H,  $H_{Th}$ ), 6.64 (s, 1H,  $\delta$ ), 6.07 (d,  $J = 6.3$  Hz, 1H,  $H_{Th}$ ), 5.67 (d,  $J = 6.3$  Hz, 1H,  $H_{Th}$ ), 3.12 (d,  $J = 13.6$  Hz, 1H, 4), 3.03 (d,  $J = 13.6$  Hz, 1H, 4), 1.45 (s, 3H, 15).  $^{13}\text{C}\{^1\text{H}\}$  NMR (101 MHz,  $\text{CDCl}_3$ )  $\delta$  148.6 ( $C_{Ar}$ ), 142.6 ( $C_{Ar}$ ), 141.7 ( $C_{Ar}$ ), 140.9 ( $C_{Ar}$ ), 138.0 ( $C_{Ar}$ ), 136.3 ( $C_{Ar}$ ), 133.2 ( $\delta$ ), 131.2 ( $\gamma$ ), 130.6 ( $C_{Ar}$ -H), 129.1 (2 x  $C_{Ph}$ -H), 128.5 (2 x  $C_{Ph}$ -H), 128.4 (2 x  $C_{Ph}$ -H), 128.2 ( $C_{Ar}$ -H), 128.0 (2 x  $C_{Ph}$ -H), 127.8 ( $C_{Ar}$ -H), 127.1 ( $C_{Ar}$ -H), 125.4 ( $C_{Ar}$ -H), 122.2 ( $C_{Ar}$ -H), 57.3 (5), 39.3 (4), 28.6 (15); **HRMS** (ASAP) ( $\text{C}_{25}\text{H}_{21}\text{S}_2$ ) [ $\text{M}+\text{H}$ ] $^+$ : caclcd: 385.1085; found: 385.1078; **MS** (EI) ( $\text{C}_{25}\text{H}_{20}\text{S}_2$ ) [ $\text{M}$ ] $^+$ : caclcd: 384; found: 384.

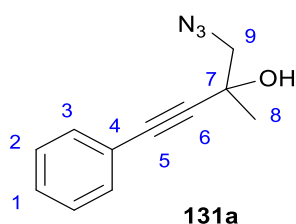
### Compound **130**<sup>[191]</sup>



To a solution of phenylacetylene **128** (510 mg, 5.00 mmol, 1.0 equiv.) in anhydrous THF (12.7 ml), a solution of *n*-BuLi in hexanes (2.26 ml, 5.40 mmol, 1.08 equiv.) was added at  $-40$  °C under inert atmosphere. The mixture was then cooled to  $-78$  °C and chloroacetone **129** (0.41 ml, 5.2 mmol, 1.04 equiv.) was added dropwise. After 10 min the reaction was slowly warmed to rt and stirred overnight. The reaction was then quenched with aqueous  $\text{NH}_4\text{Cl}$ . The aqueous layer was separated and extracted with  $\text{Et}_2\text{O}$ . Combined organic layers were dried over  $\text{MgSO}_4$ , filtered and concentrated in *vacuo*. Column chromatography (Pet/AcOEt 19:1) afforded **130** (583 mg, 74%) as a yellow oil.

$^1\text{H NMR}$  (400 MHz,  $\text{CDCl}_3$ )  $\delta$  7.45 – 7.41 (m, 2H, 3), 7.33 – 7.27 (m, 3H, 1, 2), 3.12 (dd,  $J = 5.6, 0.6$  Hz, 1H, 9), 2.85 (d,  $J = 5.6$  Hz, 1H, 9), 1.65 (brs, 3H, 8);  $^{13}\text{C}\{^1\text{H}\}$  NMR (101 MHz,  $\text{CDCl}_3$ )  $\delta$  132.0 (2/3), 128.8 (1), 128.4 (2/3), 122.3 (4), 88.5 (6), 82.2 (5), 55.9 (9), 47.8 (7), 23.2 (8).

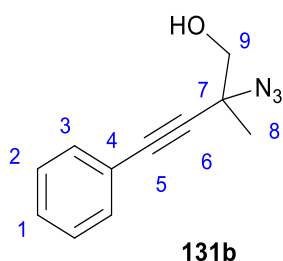
The characterisation data is in agreement with previously reported.<sup>[191]</sup>

**Compound 131**<sup>[411]</sup>

Sodium azide (130 mg, 2.00 mmol, 2.0 equiv.) was added to a suspension of epoxide **130** (158 mg, 1.00 mmol, 1.0 equiv.) in a 1:1 mixture of ethanol/water (5 ml). The mixture was heated at 60 °C for 3.5 h, then cooled to rt and concentrated in *vacuo*. The residue was dissolved in AcOEt, washed with water and brine dried over MgSO<sub>4</sub>, filtered and concentrated in *vacuo*. Purification by column chromatography (Pet/AcOEt 9:1) afforded **131a** (48 mg, 24%) as a yellow oil.

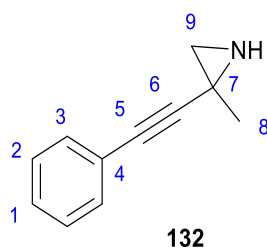
<sup>1</sup>H NMR (400 MHz, CDCl<sub>3</sub>) δ 7.49 – 7.41 (m, 2H, 3), 7.35 – 7.28 (m, 3H, 1, 2), 3.53 (d, *J* = 12.2 Hz, 1H, 9), 3.36 (d, *J* = 12.2 Hz, 1H, 9), 2.80 (brs, 1H, -OH), 1.60 (s, 3H, 8); <sup>13</sup>C{<sup>1</sup>H} NMR (101 MHz, CDCl<sub>3</sub>) δ 131.8 (2/3), 128.8 (1), 128.4 (2/3), 122.1 (4), 90.0 (6), 84.9 (5), 68.5 (7), 61.4 (9), 26.9 (8).

The characterisation data is in agreement with previously reported.<sup>[412]</sup>

**Compound 131b**<sup>[413]</sup>

A solution of epoxide **130** (1.748 g, 11.06 mmol, 1.0 equiv.) in MeOH (17.6 ml) was added to a flask charged with NH<sub>4</sub>Cl (1.302 g, 24.33 mmol, 2.2 equiv.) and NaN<sub>3</sub> (3.595 g, 55.30 mmol, 5.0 equiv.). Water (2.2 ml) was then added and the mixture was heated at reflux for 4 h. The reaction was cooled to rt, extracted with water/dichloromethane. The combined organic layers were washed with brine, dried over MgSO<sub>4</sub>, filtered and concentrated in *vacuo*. **131b** was isolated as a mixture with the other regioisomer **131a** (1:4 **131b**:**131a**, 1.769 g, 79%) and used without further purification.

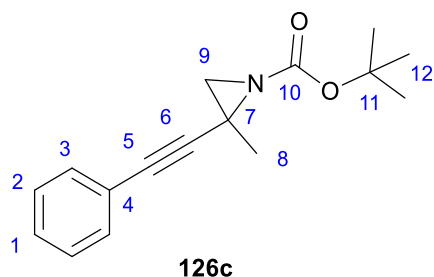
<sup>1</sup>H NMR (400 MHz, CDCl<sub>3</sub>) δ 7.68 – 7.64 (m, 2H, 3), 7.51 – 7.41 (m, 3H, 1, 2), 4.07 (d, *J* = 11.6 Hz, 1H, 9), 3.94 (d, *J* = 11.6 Hz, 1H, 9), 1.47 (s, 3H, 8).

**Compound 132**<sup>[414]</sup>

A solution of **131a** (48 mg, 0.24 mmol, 1.0 equiv.) in CH<sub>3</sub>CN (1.2 ml) was added to flask charged with PPh<sub>3</sub> (94 mg, 0.36 mmol, 1.5 equiv.) under inert atmosphere. The mixture was stirred at rt for 1 h then heated at reflux for 5 h. Then, the solvent was removed in *vacuo*. Purification by column chromatography (Pet/AcOEt 1:1) afforded **132** (20 mg, 53%) as a yellow oil.

**<sup>1</sup>H NMR** (400 MHz, CDCl<sub>3</sub>) δ 7.42 – 7.36 (m, 2H, 3), 7.31 – 7.26 (m, 3H, 1, 2), 2.28 (s, 1H, 9), 1.79 (s, 1H, 9), 1.51 (s, 3H, 8), 0.77 (brs, 1H, -NH); **<sup>13</sup>C{<sup>1</sup>H} NMR** (101 MHz, CDCl<sub>3</sub>) δ 131.8 (2/3), 128.4 (2/3), 128.3 (1), 122.8 (4), 92.2 (6), 79.0 (5), 35.7 (9), 26.0 (7), 24.1 (8).

The characterisation data is in agreement with previously reported.<sup>[415]</sup>

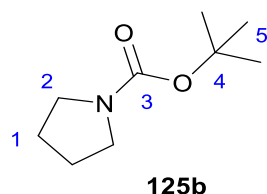
**Compound 126c**<sup>[416]</sup>

A solution of Boc<sub>2</sub>O (521 mg, 2.39 mmol, 1.5 equiv.) in DMF (8.0 ml) was added to a solution of **132** (250 mg, 1.59 mmol, 1.0 equiv.), DMAP (19 mg, 0.16 mmol, 0.1 equiv.) and Et<sub>3</sub>N (0.33 ml, 2.4 mmol, 1.0 equiv.) in DMF (8.5 ml) at 0 °C under inert atmosphere. The mixture was slowly warmed to rt and stirred overnight. Then it was diluted with AcOEt and washed with ice water several times. The combined aqueous layers were re-extracted with AcOEt. The combined organic layers were washed with brine, dried over MgSO<sub>4</sub>, filtered and concentrated in *vacuo* to obtain **126c** (409 mg, > 99%.) as a brown oil that was used without further purification. Attempts of column chromatography resulted in interconversion of **126c** to **135**.

**<sup>1</sup>H NMR** (400 MHz, CDCl<sub>3</sub>) δ 7.42 – 7.38 (m, 2H, 3), 7.32 – 7.26 (m, 3H, 1, 2), 2.64 (s, 1H, 9), 2.25 (s, 1H, 9), 1.60 (s, 3H, 8), 1.47 (s, 9H, 12); **<sup>13</sup>C{<sup>1</sup>H} NMR** (101 MHz, CDCl<sub>3</sub>) δ 160.3 (10), 131.9 (2/3), 128.6 (1), 128.4 (2/3), 122.4 (4), 88.0 (6), 81.9 (5), 81.7 (11), 39.7 (9), 34.6 (7),

28.2 (12), 23.4 (8); **HRMS** (NSI) ( $C_{16}H_{20}NO_2$ )  $[M+H]^+$ : calcd: 258.1489; found: 258.1492; a fragment from N-C(10) bond cleavage was observed ( $C_{11}H_{12}N$ )  $[M-Boc+H_2]^+$ : calcd: 158.0964; found: 158.0961; a fragment from O-C(11) bond cleavage was observed ( $C_{12}H_{12}NO_2$ )  $[M-tBu+H_2]^+$ : calcd: 202.0863; found: 202.0863.

### Compound 125b

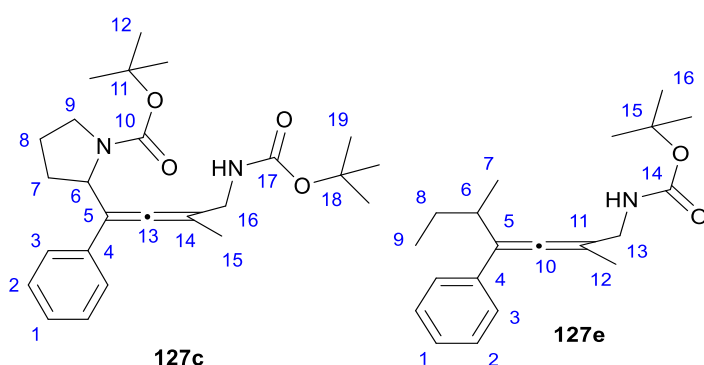


A solution of Boc<sub>2</sub>O (2.18 g, 10.0 mmol, 1.0 equiv.) in dichloromethane (4.7 ml) was added to a solution of pyrrolidine **134** (0.82 ml, 10.0 mmol, 1.0 equiv.) and Et<sub>3</sub>N (1.49 ml, 10.7 mmol, 1.07 equiv.) in dichloromethane (6.0 ml) at 0 °C under inert atmosphere. The mixture was slowly warmed to rt and stirred for 2.25 h. The it was diluted with dichloromethane, washed with water and brine. The combined organic layers were dried over MgSO<sub>4</sub>, filtered and concentrated in *vacuo* to obtain **125b** (1.603 g, 94%) as a yellow semisolid that was used without further purification.

<sup>1</sup>H NMR (400 MHz, CDCl<sub>3</sub>) δ 3.29 (m, 4H, 2), 1.81 (brs, 4H, 1), 1.44 (s, 9H, 5); <sup>13</sup>C{<sup>1</sup>H} NMR (101 MHz, CDCl<sub>3</sub>) δ 154.8 (3), 79.0 (4), 46.1 (2), 45.7 (2), 28.7 (5), 25.9 (1), 25.1 (1).

The characterisation data is in agreement with previously reported.<sup>[417]</sup>

### Compound 127c and 127e<sup>[188]</sup>



A solution of *sec*-BuLi in cyclohexane (0.57 ml, 0.80 mmol, 1.0 equiv.) was added to a solution of Boc-protected pyrrolidine **125b** (137 mg, 0.80 mmol, 1.0 equiv.) and (-)-sparteine (225 mg, 0.96 mmol, 1.2 equiv.) in anhydrous THF (1.6 ml) at -78 °C under inert atmosphere. The mixture was stirred at -78 °C for 1 h. Then, CuCN·2LiCl was prepared from pre-dried (3.5 h at 100 °C in *vacuo*) LiCl (68 mg, 1.6 mmol, 2.0 equiv.) and CuCN (72 mg, 0.80 mmol, 1.0 equiv.)

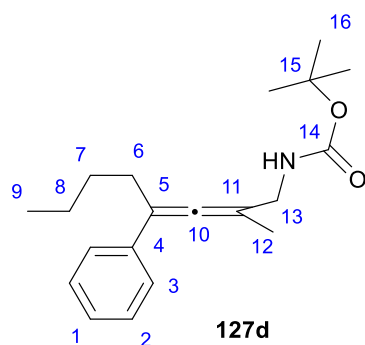
dissolved in anhydrous THF (1.6 ml). The CuCN·2LiCl solution was added to the solution of pyrrolidine at -78 °C and stirring continued for 70 min. A solution of aziridine **126c** (206 mg, 0.80 mmol, 1.0 equiv.) in anhydrous THF (0.8 ml) was added at -78 °C and reaction mixture was warmed to 0 °C. After 3 h the reaction was quenched with aqueous NH<sub>4</sub>Cl. The aqueous layer was separated and extracted with Et<sub>2</sub>O. The combined organic layers were dried over MgSO<sub>4</sub>, filtered and concentrated in *vacuo*. Purifications by column chromatography (Pet/AcOEt 4:1) afforded **127c** (98 mg, 29%) as a colourless oil and **127e** (27 mg, 16%) as a yellow oil.

Part of <sup>1</sup>H and <sup>13</sup>C{<sup>1</sup>H} NMR signals doubled due to presence of rotamers from rotation of the amide bonds or allene diastereoisomers.

**127c**: <sup>1</sup>H NMR (500 MHz, CDCl<sub>3</sub>) δ 7.34 – 7.27 (m, 4H, 2, 3), 7.23 – 7.17 (m, 1H, 1), 4.85 (m, 1H, 6), 4.62 (brs, 1H, -NH<sub>Boc</sub>), 3.78 (d, *J* = 5.7 Hz, 2H, 16), 3.45 – 3.30 (m, 2H, 9), 2.10 (m, 1H, 7/8), 1.99 – 1.90 (m, 1H, 7/8), 1.85 (m, 2H, 7/8), 1.75 (d, *J* = 3.9 Hz, 3H, 15), 1.47 (s, 9H, 12/19), 1.40 (s, 9H, 12/19); <sup>13</sup>C{<sup>1</sup>H} NMR (126 MHz, CDCl<sub>3</sub>) δ 198.9 (13), 155.9 and 155.7 (10/17), 154.3 and 154.1 (10/17), 135.9 (4), 131.9 (1), 128.4 (2/3), 127.1 (2/3), 111.8 and 110.5 (14), 104.0 and 103.5 (5), 79.3 (11/18), 79.2 (11/18), 57.8 and 57.5 (6), 46.5 and 46.1 (9), 43.6 and 43.5 (16), 32.0 and 30.9 (7), 28.7 and 28.6 (12/19), 28.5 and 28.4 (12/19), 23.5 and 22.6 (8), 17.0 and 16.8 (15); HRMS (NSI) (C<sub>25</sub>H<sub>37</sub>N<sub>2</sub>O<sub>4</sub>) [M+H]<sup>+</sup>: calcd: 429.2748; found: 429.2744.

**127e**: <sup>1</sup>H NMR (400 MHz, CDCl<sub>3</sub>) δ 7.35 (dd, *J* = 7.2, 1.5 Hz, 2H, 3), 7.30 (t, *J* = 7.2 Hz, 2H, 2), 7.19 (t, *J* = 7.2 Hz, 1H, 1), 4.60 (s, 1H, -NH), 3.79 – 3.72 (m, 2H, 13), 2.64 – 2.58 (m, 1H, 6), 1.80 (d, *J* = 6.8 Hz, 3H, 12), 1.60 – 1.49 (m, 1H, 8), 1.39 (d, *J* = 4.4 Hz, 9H, 16), 1.37 – 1.29 (m, 1H, 8), 1.09 (dd, *J* = 6.5, 5.6 Hz, 3H, 7), 0.92 (td, *J* = 7.4, 4.0 Hz, 3H, 9); <sup>13</sup>C{<sup>1</sup>H} NMR (101 MHz, CDCl<sub>3</sub>) δ 199.4 (10), 155.9 (14), 137.8 (4), 128.5 (2/3), 126.7 (1), 126.7 (2/3), 114.8 (5/11), 114.6 (5/11), 79.4 (15), 43.3 (13), 35.3 (6), 29.3 (8), 28.5 (16), 19.7 (7), 17.0 (12), 11.8 (9); HRMS (ESI) (C<sub>20</sub>H<sub>29</sub>NO<sub>2</sub>Na) [M+Na]<sup>+</sup>: calcd: 338.2091; found: 338.2089.

### Compound **127d**<sup>[188]</sup>

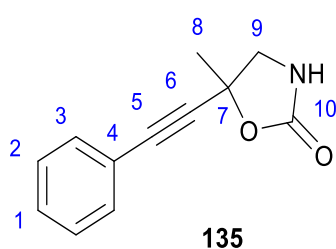




A solution of *n*-BuLi in hexanes (0.084 ml, 0.20 mmol, 1.0 equiv.) was added to a solution of Boc-protected pyrrolidine **125b** (34 mg, 0.20 mmol, 1.0 equiv.) in anhydrous THF (0.4 ml) at -78 °C under inert atmosphere. The mixture was stirred at -78 °C for 1 h. Then, CuCN·2LiCl was prepared from pre-dried (3.5 h at 100 °C in *vacuo*) LiCl (17 mg, 0.40 mmol, 2.0 equiv.) and CuCN (18 mg, 0.20 mmol, 1.0 equiv.) dissolved in anhydrous THF (0.4 ml). The CuCN·2LiCl solution was added to the solution of pyrrolidine at -78 °C and stirring continued for 50 min. A solution of aziridine **126c** (51 mg, 0.20 mmol, 1.0 equiv.) in anhydrous THF (0.4 ml) was added at -78 °C and stirring continued for 4 h at this temp. The reaction was then quenched with aqueous NH<sub>4</sub>Cl. The aqueous layer was separated and extracted with Et<sub>2</sub>O. The combined organic layers were dried over MgSO<sub>4</sub>, filtered and concentrated in *vacuo*. Purification by column chromatography (Pet/AcOEt 19:1) afforded **127d** (36 mg, 57%) as a colourless semisolid.

<sup>1</sup>H NMR (400 MHz, CDCl<sub>3</sub>) δ 7.37 (d, *J* = 7.6 Hz, 2H, 3), 7.30 (t, *J* = 7.6 Hz, 2H, 2), 7.19 (t, *J* = 7.6 Hz, 1H, 1), 4.63 (s, 1H, -NH), 3.77 – 3.71 (m, 2H, 13), 2.43 (m, 2H, 6), 1.80 (s, 3H, 12), 1.52 – 1.41 (m, 4H, 8, 7), 1.39 (s, 9H, 16), 0.93 (t, *J* = 7.1 Hz, 3H, 9); <sup>13</sup>C{<sup>1</sup>H} NMR (101 MHz, CDCl<sub>3</sub>) δ 200.0 (10), 155.9 (14), 137.6 (4), 128.4 (2/3), 126.7 (1), 126.2 (2/3), 108.4 (5/11), 101.5 (5/11), 79.4 (15), 43.4 (13), 30.4 (6), 30.2 (7), 28.5 (16), 22.6 (8), 16.9 (12), 14.1 (9); MS (EI) (C<sub>5</sub>H<sub>11</sub>NO<sub>2</sub>) [NBoc]<sup>+</sup>: caclcd: 115; found: 115; (C<sub>12</sub>H<sub>12</sub>) [M-NHBoc-C<sub>3</sub>H<sub>7</sub>]<sup>+</sup>: caclcd: 156; found: 156; HRMS of the corresponding peak(s) not found.

### Compound 135<sup>[188]</sup>

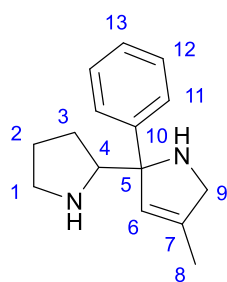


A solution of *sec*-BuLi in cyclohexane (0.14 ml, 0.20 mmol, 1.0 equiv.) was added to a solution of Boc-protected pyrrolidine **125b** (34 mg, 0.20 mmol, 1.0 equiv.) and TMEDA (28 mg, 0.24 mmol, 1.2 equiv.) in anhydrous THF (0.4 ml) at -78 °C under inert atmosphere. The mixture was stirred at -78 °C for 1 h. Then, CuCN·2LiCl was prepared from pre-dried (3.5 h at 100 °C in *vacuo*) LiCl (17 mg, 0.40 mmol, 2.0 equiv.) and CuCN (18 mg, 0.20 mmol, 1.0 equiv.) dissolved in anhydrous THF (0.4 ml). The CuCN·2LiCl solution was added to the solution of pyrrolidine at -78 °C and stirring continued for 50 min. A solution of aziridine **126c** (51 mg, 0.20 mmol, 1.0 equiv.) in anhydrous THF (0.4 ml) was added at -78 °C and the solution was slowly warmed to rt. The reaction was quenched with aqueous NH<sub>4</sub>Cl after 3 h. The aqueous

layer was separated and extracted with AcOEt. The combined organic layers were dried over MgSO<sub>4</sub>, filtered and concentrated in *vacuo*. Purification by column chromatography (Pet/AcOEt 19:1) afforded **135** (6 mg, 15%) and **127e** (16 mg, 25%) as colourless semisolids.

**135**: <sup>1</sup>H NMR (400 MHz, CDCl<sub>3</sub>) δ 7.46 – 7.41 (m, 2H, 3), 7.37 – 7.29 (m, 3H, 1, 2), 5.83 (brs, 1H, -NH), 3.89 (dd, *J* = 8.5, 0.8 Hz, 1H, 9), 3.58 (dd, *J* = 8.5, 0.8 Hz, 1H, 9), 1.83 (s, 3H, 8); <sup>13</sup>C{<sup>1</sup>H} NMR (101 MHz, CDCl<sub>3</sub>) δ 158.6 (10), 132.0 (2/3), 129.2 (1), 128.5 (2/3), 121.6 (4), 87.8 (6), 86.2 (5), 75.6 (7), 53.7 (9), 27.9 (8); HRMS (ESI) (C<sub>12</sub>H<sub>11</sub>NO<sub>2</sub>Na) [M+Na]<sup>+</sup>: calcd: 224.0628; found: 224.0681.

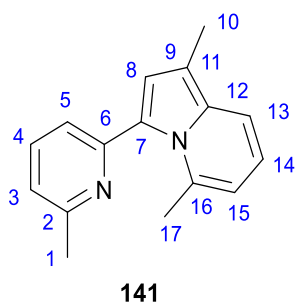
### Compound 136<sup>[188]</sup>



**136**

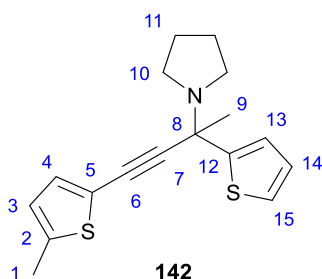
Trimethylsilyl chloride (0.04 ml, 0.3 mmol, 10.0 equiv.) was added to a solution of allene **127c** (15 mg, 0.035 mmol, 1.0 equiv.) in anhydrous MeOH (0.3 ml) at rt and the mixture was stirred at rt for 6 h. The colourless solution turned to pale pink. The reaction was then quenched with NaHCO<sub>3</sub> and diluted with dichloromethane. The organic phase was separated and washed with water, dried over MgSO<sub>4</sub>, filtered and concentrated in *vacuo* to yield **136** (4 mg, 57%) as a colourless semisolid.

<sup>1</sup>H NMR (500 MHz, CDCl<sub>3</sub>) δ 7.39 – 7.36 (m, 2H, 11), 7.33 (t, *J* = 7.6 Hz, 2H, 12), 7.30 – 7.29 (m, 1H, 13), 5.94 (d, *J* = 1.9 Hz, 1H, 6), 4.85 (t, *J* = 7.2 Hz, 1H, 4), 3.08 (t, *J* = 6.9 Hz, 1H, 1), 3.01 (d, *J* = 13.5 Hz, 1H, 9), 2.97 – 2.89 (m, 2H, 1, 9), 2.27 (m, 1H, 3), 1.98 (m, 2H, 2, 3), 1.63 – 1.56 (m, 1H, 2), 1.34 (s, 3H, 8), -NHs were not detected; <sup>13</sup>C{<sup>1</sup>H} NMR (126 MHz, CDCl<sub>3</sub>) δ 142.9 (7), 134.1 (10), 129.0 (6), 128.7 (11/12), 127.8 (13), 126.4 (11/12), 70.8 (4), 47.1 (1/9), 47.0 (1/9), 30.2 (3), 27.2 (2), 25.5 (8), C<sub>q</sub> aliphatic not detected; HRMS (NSI) (C<sub>15</sub>H<sub>21</sub>N<sub>2</sub>) [M+H]<sup>+</sup>: calcd: 229.1699; found: 229.1700.

**Compound 141**<sup>[197]</sup>

CuI (7 mg, 0.04 mmol, 0.1 equiv.) and freshly dried ZnBr<sub>2</sub> (63 mg, 0.28 mmol, 0.8 equiv.) were placed under inert atmosphere. Ti(O*i*Pr)<sub>4</sub> (199 mg, 0.70 mmol, 2.0 equiv.) in toluene (0.35 ml) was added, followed by solutions of alkyne **88b** (41 mg, 0.35 mmol, 1.0 equiv.) in toluene (0.7 ml), ketone **89c** (76 mg, 0.56 mmol, 1.6 equiv.) in toluene (0.7 ml) and pyrrolidine **134** (28 mg, 0.39 mmol, 1.1 equiv.). The mixture was heated at 100 °C for 17 h. Then, the reaction mixture was cooled to rt, filtered through a pad of silica gel, washed with acetone and concentrated in *vacuo*. Purification by column chromatography (Pet/AcOEt 6:1 to 3:2) afforded **141** (32 mg, 39%) as a white solid. Good quality single crystals were obtained by slow evaporation from dichloromethane solution at rt and were suitable for X-ray analysis (see page 235).

<sup>1</sup>H NMR (500 MHz, CDCl<sub>3</sub>) δ 7.56 (t, *J* = 7.7 Hz, 1H, 4), 7.33 (d, *J* = 7.7 Hz, 1H, 5), 7.30 (d, *J* = 8.9 Hz, 1H, 13), 7.04 (d, *J* = 7.7 Hz, 1H, 3), 6.79 (s, 1H, 8), 6.67 (dd, *J* = 8.9, 6.5 Hz, 1H, 14), 6.31 (d, *J* = 6.5 Hz, 1H, 15), 2.59 (s, 3H, 1), 2.39 (s, 3H, 17), 2.21 (s, 3H, 10); <sup>13</sup>C{<sup>1</sup>H} NMR (126 MHz, CDCl<sub>3</sub>) δ 156.6 (C<sub>Ar</sub>), 153.7 (C<sub>Ar</sub>), 135.8 (C<sub>Py-H</sub>), 135.5 (C<sub>Ar</sub>), 133.9 (C<sub>Ar</sub>), 124.3 (C<sub>Ar</sub>), 121.8 (C<sub>Py-H</sub>), 120.4 (C<sub>Py-H</sub>), 119.7 (C<sub>Py-H</sub>), 116.7 (C<sub>Py-H</sub>), 115.4 (C<sub>Py-H</sub>), 112.2 (8), 109.0 (C<sub>Ar</sub>), 24.7 (1), 23.3 (17), 10.7 (10); HRMS (ASAP) (C<sub>16</sub>H<sub>17</sub>N<sub>2</sub>) [M+H]<sup>+</sup>: calcd: 237.1392; found: 237.1395.

**Compound 142**<sup>[197]</sup>

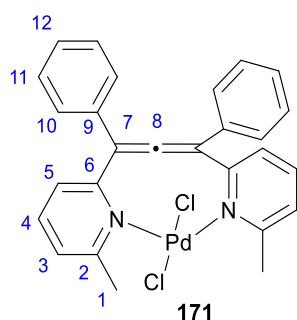
CuI (9 mg, 0.05 mmol, 0.1 equiv.) and freshly dried ZnBr<sub>2</sub> (90 mg, 0.40 mmol, 0.8 equiv.) were placed under inert atmosphere. Ti(OEt)<sub>4</sub> (228 mg, 1.00 mmol, 2.0 equiv.) in toluene (0.5 ml) was added, followed by solutions of alkyne **103b** (61 mg, 0.50 mmol, 1.0 equiv.) in toluene (1.0

ml), ketone **104a** (101 mg, 0.80 mmol, 1.6 equiv.) in toluene (1.0 ml) and pyrrolidine **134** (39 mg, 0.55 mmol, 1.1 equiv.). The mixture was then heated at 100 °C overnight. The reaction mixture was cooled to rt, filtered through a pad of silica gel, washed with acetone and concentrated in *vacuo*. Purification by column chromatography (Pet/AcOEt 19:1) afforded **142** (12 mg, 8%). Compound **142** was obtained with some inseparable impurities but was used directly in the next reaction.

**<sup>1</sup>H NMR** (400 MHz, CDCl<sub>3</sub>) δ 7.22 (d, *J* = 4.7 Hz, 2H, 13, 15), 7.04 (d, *J* = 3.5 Hz, 1H, 4), 6.92 – 6.89 (m, 1H, 14), 6.64 (dd, *J* = 3.5, 0.8 Hz, 1H, 3), 2.79 – 2.77 (m, 2H, 10), 2.68 – 2.61 (m, 2H, 10), 2.47 (s, 3H, 1), 1.81 (s, 3H, 9), 1.79 – 1.77 (m, 4H, 11); **<sup>13</sup>C{<sup>1</sup>H} NMR** (101 MHz, CDCl<sub>3</sub>) δ 151.4 (C<sub>Th</sub>), 141.7 (C<sub>Th</sub>), 132.2 (C<sub>Th-H</sub>), 125.9 (C<sub>Th-H</sub>), 125.3 (C<sub>Th-H</sub>), 124.7 (C<sub>Th-H</sub>), 124.2 (C<sub>Th-H</sub>), 118.2 (5), 92.2 (7), 77.4 (6), 60.2 (8), 48.9 (10), 33.3 (9), 23.9 (11), 15.5 (1).

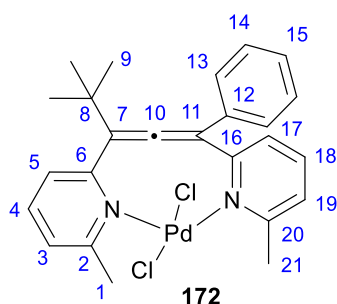
## Chapter IV - Synthesis of allene-derived metal complexes

### Compound 171



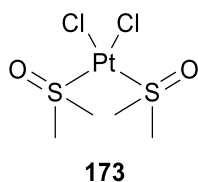
Pd(CH<sub>3</sub>CN)<sub>2</sub>Cl<sub>2</sub> (7 mg, 0.03 mmol, 1.0 equiv.) was added to a solution of allene **97b** (10 mg, 0.027 mmol, 1.0 equiv.) in dichloromethane (0.5 ml) at 12 °C. The reaction mixture changed colour from yellow to red over the course of 40 min. After that time the solution was filtered through a cotton wool plug to remove solid impurities, washed with more dichloromethane and concentrated in *vacuo* to afford **171** (14 mg, > 99%) as a red solid.

**<sup>1</sup>H NMR** (400 MHz, CDCl<sub>3</sub>) δ 7.66 – 7.61 (m, 4H, 10), 7.56 (t, *J* = 7.6 Hz, 2H, 4), 7.46 – 7.38 (m, 6H, 11, 12), 7.19 (dd, *J* = 7.6, 0.7 Hz, 2H, 3/5), 7.00 (d, *J* = 7.6 Hz, 2H, 3/5), 3.17 (s, 6H, 1); **<sup>13</sup>C{<sup>1</sup>H} NMR** (101 MHz, CDCl<sub>3</sub>) δ 204.1 (8), 160.8 (C<sub>Py</sub>), 160.3 (C<sub>Py</sub>), 138.4 (4), 136.4 (9), 129.7 (2 x C<sub>Ph-H</sub>), 129.0 (2 x C<sub>Ph-H</sub>), 128.9 (12), 124.7 (C<sub>Py-H</sub>), 123.8 (C<sub>Py-H</sub>), 117.9 (7), 26.9 (1); **HRMS** (ESI) (C<sub>27</sub>H<sub>21</sub>N<sub>2</sub><sup>106</sup>Pd) [M-Cl<sub>2</sub>-H]<sup>+</sup>: caclcd: 479.0734; found: 479.0777; **Anal.** Calcd. for C<sub>27</sub>H<sub>25</sub>N<sub>2</sub>PdCl<sub>2</sub>O<sub>1.5</sub> (**171**+1.5H<sub>2</sub>O): C 56.15, H 4.37, N 4.85; found: C 56.54, H 4.43; N 4.45.

**Compound 172**

Pd(CH<sub>3</sub>CN)<sub>2</sub>Cl<sub>2</sub> (15 mg, 0.056 mmol, 1.0 equiv.) was added to a solution of allene **97a** (20 mg, 0.056 mmol, 1.0 equiv.) in dichloromethane (0.8 ml) at 12 °C. The reaction mixture changed colour from yellow to red over the course of 40 min. After that time the solution was filtered through a cotton wool plug to remove solid impurities, washed with more dichloromethane and concentrated in *vacuo* to afford **172** (30 mg, > 99%) as a red solid. Crystals of **172** suitable for X-ray crystallography were obtained from vapour diffusion of dichloromethane/MeOH solution and *n*-Hex at 4 °C (see page 235).

**<sup>1</sup>H NMR** (400 MHz, CDCl<sub>3</sub>) δ 7.63 (t, *J* = 7.8 Hz, 1H, 4/18), 7.57 (t, *J* = 7.8 Hz, 1H, 4/18), 7.50 – 7.46 (m, 2H, 13), 7.44 (d, *J* = 7.8 Hz, 1H, *H<sub>Py</sub>*), 7.40 – 7.31 (m, 3H, 14, 15), 7.20 (dd, *J* = 7.8, 0.8 Hz, 1H, *H<sub>Py</sub>*), 7.16 (d, *J* = 7.8, 1H, *H<sub>Py</sub>*), 7.03 (d, *J* = 7.8, Hz, 1H, *H<sub>Py</sub>*), 3.17 (s, 3H, 1/21), 3.13 (s, 3H, 1/21), 1.47 (s, 9H, 9); **<sup>13</sup>C{<sup>1</sup>H} NMR** (126 MHz, CDCl<sub>3</sub>) δ 202.7 (10), 161.0 (*C<sub>Py</sub>*), 160.8 (*C<sub>Py</sub>*), 160.4 (*C<sub>Py</sub>*), 158.4 (*C<sub>Py</sub>*), 138.1 (4/18), 138.0 (4/18), 137.0 (12), 129.5 (*C<sub>Ph-H2</sub>*), 128.9 (*C<sub>Ph-H2</sub>*), 128.5 (15), 124.5 (*C<sub>Py-H</sub>*), 124.2 (*C<sub>Py-H</sub>*), 123.5 (*C<sub>Py-H</sub>*), 123.4 (*C<sub>Py-H</sub>*), 121.9 (7/11), 118.2 (7/11), 37.0 (8), 30.9 (9), 27.0 (1/21), 27.0 (1/21); **HRMS** (ESI) (C<sub>25</sub>H<sub>26</sub>N<sub>2</sub><sup>106</sup>Pd<sup>35</sup>Cl) [M-Cl]<sup>+</sup>: caclid: 495.0814; found: 495.0824.

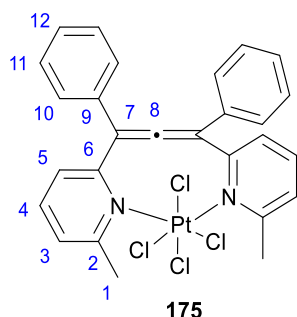
**Compound 173**<sup>[418]</sup>

K<sub>2</sub>PtCl<sub>4</sub> (1.00 g, 2.41 mmol, 1.0 equiv.) was dissolved in water (20.0 ml). The solution was filtered through a plug of cotton wool and then degassed. DMSO (0.69 ml, 9.6 mmol, 4.0 equiv.) was added. This red solution was stirred at rt in the dark for 4 h. The colour of the solution changed to yellow and a pale-yellow precipitate appeared. The precipitate was filtered off, washed with water and Et<sub>2</sub>O and dry in *vacuo* to afford **173** (799 mg, 79%) as a yellow powder.

**<sup>1</sup>H NMR** (400 MHz, DMSO-*d*<sub>6</sub>) δ 2.54 (s, 12H).

The characterisation data is in agreement with previously reported.<sup>[418]</sup>

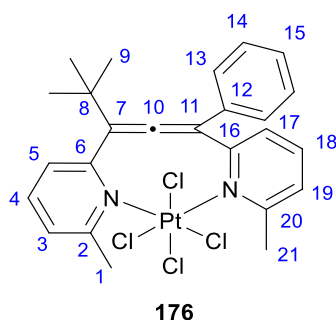
### Compound 175<sup>[419]</sup>



To a solution of  $\text{H}_2\text{PtCl}_6 \cdot 6\text{H}_2\text{O}$  (41 mg, 0.08 mmol, 1.0 equiv.) in MeOH (1.9 ml) solution of **97b** (30 mg, 0.08 mmol) in MeOH (1.9 ml) was added at rt. Upon addition, a precipitate started to form instantaneously. After 40 min of stirring at rt the solid was filtered off, washed with MeOH and dried in *vacuo* to afford **175** (53 mg, 92%) as a pale orange solid.

**<sup>1</sup>H NMR** (400 MHz, DMSO- $d_6$ )  $\delta$  8.22 (t,  $J = 7.7$  Hz, 2H, 4), 7.75 (d,  $J = 7.7$  Hz, 2H, 3/5), 7.68 (d,  $J = 7.7$  Hz, 2H, 3/5), 7.50 – 7.45 (m, 8H, 10, 11), 7.45 – 7.40 (m, 2H, 12), 2.65 (s, 6H, 1); **<sup>13</sup>C{<sup>1</sup>H} NMR** (101 MHz, DMSO- $d_6$ )  $\delta$  210.3 (8), 156.8 (4), 149.1 ( $C_{Py}$ ), 143.1 ( $C_{Py}$ ), 132.6 (9), 129.3 (2 x  $C_{Pyr-H}$ ), 129.1 (12), 127.8 (2 x  $C_{Pyr-H}$ ), 125.8 ( $C_{Pyr-H}$ ), 123.7 ( $C_{Pyr-H}$ ), 111.3 (7), 21.7 (1); **HRMS** (ESI) ( $\text{C}_{27}\text{H}_{23}^{35}\text{Cl}_3\text{N}_2^{195}\text{Pt}$ ) [ $\text{M}-\text{Cl}+\text{H}$ ]<sup>+</sup>: caclcd: 675.0575; found: 675.0565; **Anal.** Calcd. for  $\text{C}_{29.5}\text{H}_{27}\text{Cl}_9\text{N}_2\text{Pt}$  (**175**+2.5 $\text{CH}_2\text{Cl}_2$ ): C 38.52, H 2.96, N 3.05; found: C 38.55, H 3.45; N 3.25.

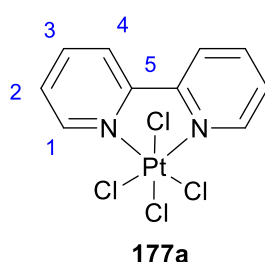
### Compound 176<sup>[419]</sup>



To a solution of  $\text{H}_2\text{PtCl}_6 \cdot 6\text{H}_2\text{O}$  (47 mg, 0.090 mmol, 1.0 equiv.) in MeOH (1.8 ml) solution of **97a** (32 mg, 0.090 mmol) in MeOH (1.8 ml) was added at rt. Upon addition a precipitate started to form instantaneously. After 40 min of stirring at rt the solid was filtered off, washed with MeOH and dried in *vacuo* to afford **176** (63 mg, > 99%) as a pale orange solid.

**$^1\text{H}$  NMR** (400 MHz, DMSO- $d_6$ )  $\delta$  8.38 (t,  $J$  = 7.9 Hz, 1H, 4/18), 8.18 (t,  $J$  = 7.8 Hz, 1H, 4/18), 7.79 (dd,  $J$  = 12.9, 7.9 Hz, 2H,  $H_{Py}$ ), 7.70 (d,  $J$  = 7.8 Hz, 1H,  $H_{Py}$ ), 7.64 (d,  $J$  = 7.8 Hz, 1H,  $H_{Py}$ ), 7.49 – 7.43 (m, 2H, 14), 7.41 – 7.36 (m, 1H, 15), 7.34 (dd,  $J$  = 5.3, 3.2 Hz, 2H, 13), 2.68 (s, 3H, 1/21), 2.66 (s, 3H, 1/21), 1.29 (s, 9H, 9);  **$^{13}\text{C}\{^1\text{H}\}$  NMR** (126 MHz, DMSO- $d_6$ , 75 °C)  $\delta$  206.3 (10), 156.3 (4/18), 156.1 (4/18), 151.3 ( $C_{Py}$ ), 150.9 ( $C_{Py}$ ), 141.3 ( $C_{Py}$ ), 139.7 ( $C_{Py}$ ), 133.7 (12), 128.5 (2 x  $C_{Pyr-H}$ ), 127.6 (15), 127.1 (2 x  $C_{Pyr-H}$ ), 124.0 ( $C_{Pyr-H}$ ), 123.2 ( $C_{Pyr-H}$ ), 122.2 ( $C_{Pyr-H}$ ), 122.1 ( $C_{Pyr-H}$ ), 118.3 (7/11), 109.1 (7/11), 35.7 (8), 29.3 (9), 22.2 (1/21), 21.7 (1/21); **HRMS** (ESI) ( $\text{C}_{25}\text{H}_{27}\text{N}_2^{194}\text{Pt}^{35}\text{Cl}_4$ ) [ $\text{M}+\text{H}$ ] $^+$ : calcd: 692.0727; found: 692.0707; **Anal.** Calcd. for  $\text{C}_{28.5}\text{H}_{33}\text{N}_2\text{PtCl}_{11}$  (**176**+3.5 $\text{CH}_2\text{Cl}_2$ ): C 34.80, H 3.38, N 2.85; found: C 34.90, H 3.61; N 3.13.

### Compound 177a<sup>[419]</sup>

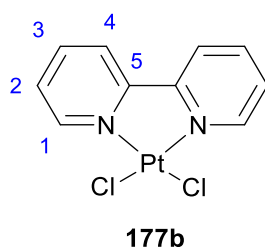


To an orange solution of  $\text{H}_2\text{PtCl}_6 \cdot 6\text{H}_2\text{O}$  (26 mg, 0.05 mmol, 1.0 equiv.) in MeOH (1.2 ml), a solution of 2,2'-bipyridine (8 mg, 0.05 mmol) in MeOH (1.2 ml) was added at rt. Upon addition a yellow suspension was formed. After 30 min of stirring at rt the solid was filtered off, washed with MeOH and dried in *vacuo* to afford **177a** (16 mg, 65%) as a yellow solid.

**$^1\text{H}$  NMR** (400 MHz, DMSO- $d_6$ )  $\delta$  8.87 (d,  $J$  = 4.8 Hz, 2H, 1), 8.63 (d,  $J$  = 8.0 Hz, 2H, 4), 8.36 (td,  $J$  = 8.0, 1.4 Hz, 2H, 3), 7.83 (m, 2H, 2).

The characterisation data is in agreement with previously reported.<sup>[420]</sup>

### Compound 177b



**Procedure a:** A white suspension of 2,2'-bipyridine (14 mg, 0.090 mmol, 1.0 equiv.) and  $\text{Pt}(\text{DMSO})_2\text{Cl}_2$  **173** (38 mg, 0.090 mmol, 1.0 equiv.) in EtOH (0.7 ml) was heated under microwave irradiation at 80 °C for 40 min. A yellow suspension was formed. The solid was

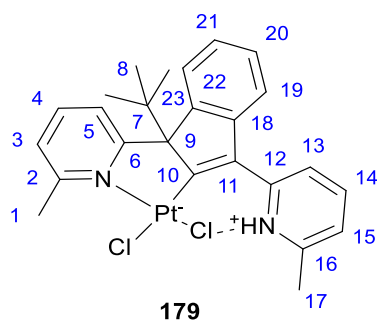
filtered off, washed with EtOH and dried in *vacuo* to afford **177b** (32 mg, 84%) as a yellow solid.

**Procedure b:**<sup>[421]</sup> L-Ascorbic acid (11 mg, 0.06 mmol, 3.0 equiv.) was added to a suspension of **177a** (11 mg, 0.02 mmol, 1.0 equiv.) in water (0.44 ml) at rt. After 90 min of stirring at rt, an orange solid was isolated by filtration, analysed by <sup>1</sup>H NMR and identified as starting material **177a**. The filtrate was left standing overnight. A small quantity of yellow precipitate crushed out, which was isolated by filtration and identified as product **177b**.

<sup>1</sup>H NMR (400 MHz, DMSO-*d*<sub>6</sub>) δ 9.49 (dd, *J* = 5.8, 0.8 Hz, 2H, 1), 8.59 (d, *J* = 7.8 Hz, 2H, 4), 8.42 (td, *J* = 7.8, 1.4 Hz, 2H, 3), 7.87 – 7.82 (m, 2H, 2).

The characterisation data is in agreement with previously reported.<sup>[422]</sup>

### Compound 179



To a solution of L-ascorbic acid (76 mg, 0.43 mmol, 10.0 equiv.) in water (0.9 ml), **176** (30 mg, 0.043 mmol, 1.0 equiv.) was added. The suspension was stirred at 25 °C for 2 h 15 min until the solid was completely dissolved and formed an orange solution. Water was removed in *vacuo* and the residue was redissolved in dichloromethane. Undissolved white residue of ascorbic acid was filtered off. The yellow filtrate was concentrated to afford **179** (24 mg, 89%) as a yellow-golden solid. Crystals of **179** suitable for X-ray crystallography were obtained by vapour diffusion of the chloroform/methanol solution with cyclohexane (see page 236).

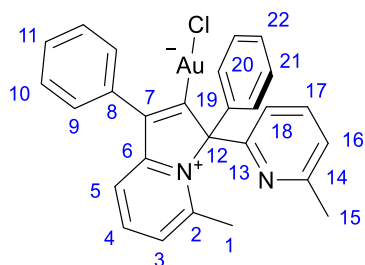
**179** gave very weak signals on <sup>13</sup>C NMR spectrum and not all expected carbon atoms were detected. Some of the missing signals were identified as cross peaks on HSQC spectrum.

<sup>1</sup>H NMR (500 MHz, DMSO-*d*<sub>6</sub>, 75 °C) δ 7.82 (t, *J* = 7.7 Hz, 1H, *H*<sub>Py</sub>), 7.69 (t, *J* = 7.7 Hz, 1H, *H*<sub>Py</sub>), 7.43 – 7.34 (m, 6H, *H*<sub>Ar</sub>), 7.32 – 7.26 (m, 2H, *H*<sub>Ar</sub>), 7.18 (d, *J* = 7.7 Hz, 1H, *H*<sub>Py</sub>), 2.53 (s, 3H, 1/17), 2.51 (s, 3H, 1/17), 1.36 (s, 9H, 8); <sup>13</sup>C{<sup>1</sup>H} NMR (126 MHz, DMSO-*d*<sub>6</sub>, 75 °C) δ 156.2, 133.9, 128.4, 127.5, 127.2, 123.5, 122.8, 121.9, 35.6, 29.3, 22.0; HRMS (ESI) (C<sub>25</sub>H<sub>26</sub>N<sub>2</sub><sup>195</sup>Pt<sup>35</sup>Cl) [M-Cl]<sup>+</sup>: calcd: 585.1434; found: 585.1452; Anal. Calcd. for



$C_{25.5}H_{30}N_2Cl_3O_{1.5}Pt$  (**179**+1.5H<sub>2</sub>O+0.5CH<sub>2</sub>Cl<sub>2</sub>): C 44.47, H 4.39, N 4.07; found: C 44.26, H 4.61; N 3.72.

### Compound **184**<sup>[157]</sup>

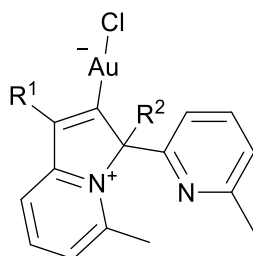


**184**

To a solution of **97b** (10 mg, 0.027 mmol, 1.2 equiv.) in dichloromethane (0.8 ml), (Me<sub>2</sub>S)AuCl (7 mg, 0.02 mmol, 1.0 equiv.) was added. Upon addition the solution changed from colourless to bright yellow. The reaction mixture was stirred at rt for 15 min and then concentrated in *vacuo* yielding **184** (16 mg, > 99%) as a yellow solid. Crystals suitable for X-ray crystallography were obtained by slow evaporation from the dichloromethane solution (see page 236).

**<sup>1</sup>H NMR** (400 MHz, CDCl<sub>3</sub>) δ 8.50 – 8.45 (m, 1H, *H<sub>Py</sub>*), 7.99 (t, *J* = 8.0 Hz, 1H, *H<sub>Py</sub>*), 7.74 (d, *J* = 7.6 Hz, 2H, *H<sub>Ph</sub>*), 7.72 – 7.67 (m, 1H, *H<sub>Py</sub>*), 7.56 (d, *J* = 8.0 Hz, 1H, *H<sub>Py</sub>*), 7.40 – 7.28 (m, 8H, *H<sub>Ph</sub>*), 7.10 (d, *J* = 7.6 Hz, 2H, *H<sub>Py</sub>*), 2.28 (s, 3H, 1/15), 2.12 (s, 3H, 1/15); **<sup>13</sup>C{<sup>1</sup>H} NMR** (101 MHz, CDCl<sub>3</sub>) δ 191.3 (19), 159.3 (*C<sub>Py</sub>*), 157.4 (*C<sub>Py</sub>*), 155.9 (*C<sub>Py</sub>*), 150.1 (*C<sub>Py</sub>*), 144.1 (7), 136.4 (*C<sub>Py</sub>*-H), 135.6 (*C<sub>Py</sub>*-H), 135.0 (*C<sub>Py</sub>*-H), 134.3 (*C<sub>Py</sub>*-H), 129.2 (*C<sub>Ph</sub>*-H), 129.0 (2 x *C<sub>Ph</sub>*-H), 128.9 (2 x *C<sub>Ph</sub>*-H), 128.7 (2 x *C<sub>Ph</sub>*-H), 128.6 (2 x *C<sub>Ph</sub>*-H), 128.1 (*C<sub>Ph</sub>*-H), 126.6 (*C<sub>Ph</sub>*), 122.7 (*C<sub>Py</sub>*-H), 121.3 (*C<sub>Ph</sub>*), 116.5 (*C<sub>Py</sub>*-H), 97.5 (12), 24.5 (1/15), 22.3 (1/15); **HRMS** (ESI) (C<sub>27</sub>H<sub>22</sub>N<sub>2</sub>Au) [M-Cl]<sup>+</sup>: caclcd: 571.1443; found: 571.1452 [M-Cl]<sup>+</sup>; **Anal.** Calcd. for C<sub>28.1</sub>H<sub>24.2</sub>N<sub>2</sub>AuCl<sub>3.2</sub> (**184**+1.1 CH<sub>2</sub>Cl<sub>2</sub>): C 48.28, H 3.49, N 4.01; found: C 48.21, H 3.48; N 4.10.

### Compound **187**



**187a** R<sup>1</sup> = Ph, R<sup>2</sup> = *t*Bu

**187b** R<sup>1</sup> = *t*Bu, R<sup>2</sup> = Ph

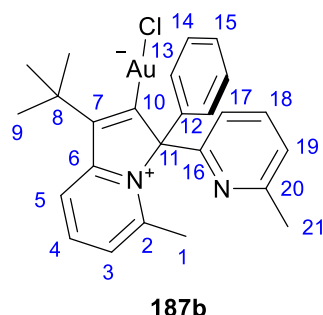
To a solution of **97a** (20 mg, 0.056 mmol, 1.0 equiv.) in dichloromethane (0.8 ml),  $(\text{Me}_2\text{S})\text{AuCl}$  (17 mg, 0.056 mmol, 1.0 equiv.) was added. Upon addition the solution changed from colourless to bright yellow. Reaction mixture was stirred at rt for 15 min and then concentrated in *vacuo* yielding **187** (33 mg, >99%) as a yellow solid. Crystals suitable for X-ray crystallography were obtained from dichloromethane solution containing iodopentafluorobenzene and layered with cyclohexane (see page 237).

Spectral analysis of **187** in 1:0.85 mixture of **187b**:**187a**.

**$^1\text{H}$  NMR** (400 MHz,  $\text{CDCl}_3$ )  $\delta$  8.46 (d,  $J = 8.0$  Hz, 1H, **187b**), 8.01 (t,  $J = 8.0$  Hz, 1H, **187b**), 7.90 (t,  $J = 7.8$  Hz, 1H, **187a**), 7.82 (d,  $J = 8.4$  Hz, 1H, **187b**), 7.75 (d,  $J = 7.1$  Hz, 2H, **187a**), 7.66 (t,  $J = 7.8$  Hz, 1H, **187b**), 7.47 – 7.31 (m, 5H, **187a**), 7.25 (m, 5H, **187b**), 7.08 – 7.00 (m, 4H, **187a-b**), 6.78 (d,  $J = 7.8$  Hz, 1H, **187a**), 2.58 (s, 3H, **187a**), 2.25 (s, 3H, **187b**), 2.13 (s, 3H, **187a**), 2.02 (s, 3H, **187b**), 1.59 (s, 9H, **187b**), 1.50 (s, 9H, **187a**);  **$^{13}\text{C}\{^1\text{H}\}$  NMR** (101 MHz,  $\text{CDCl}_3$ )  $\delta$  194.4 (**187a**), 187.7 (**187b**), 160.1 (**187b**), 159.5 (**187a**), 157.5 (**187a**), 157.2 (**187b**), 155.8 (**187a**), 155.4 (**187b**), 155.1 (**187a**), 151.0 (**187b**), 143.6 (**187a**), 143.0 (**187b**), 141.1 (**187b**), 139.2 (**187a**), 137.4 (**187a**), 136.2 (**187b**), 135.7 (**187a**), 135.0 (**187b**), 128.9 (**187a**), 128.8 (**187b**), 128.8 (**187a**), 128.4 (**187b**), 128.1 (**187a**), 126.5 (**187b**), 123.1 (**187a**), 122.4 (**187b**), 121.9 (**187a**), 121.5 (**187a**), 120.6 (**187b**), 118.7 (**187b**), 116.2 (**187a**), 102.2 (**187a**), 96.7 (**187b**), 43.2 (**187a**), 32.7 (**187b**), 31.5 (**187b**), 30.3 (**187a**), 24.7 (**187a**), 24.5 (**187b**), 22.9 (**187a**), 22.7 (**187b**).

Characterisation of a single isomer, **187b**, was attempted after the sample of **187b** had been obtained in isomerisation experiment (see page 95).

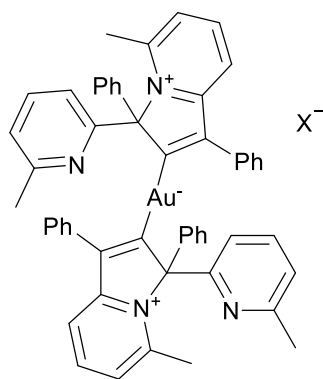
### Compound **187b**



**$^1\text{H}$  NMR** (400 MHz,  $\text{CDCl}_3$ )  $\delta$  8.50 (d,  $J = 8.0$  Hz, 1H,  $H_{Py}$ ), 8.01 (dd,  $J = 8.0, 7.7$  Hz, 1H,  $H_{Py}$ ), 7.84 (d,  $J = 7.7$  Hz, 1H,  $H_{Py}$ ), 7.68 (t,  $J = 7.7$  Hz, 1H,  $H_{Py}$ ), 7.31 – 7.26 (m, 5H,  $H_{Ph}$ ), 7.07 (d,  $J = 7.7$  Hz, 1H,  $H_{Py}$ ), 7.03 (d,  $J = 7.7$  Hz, 1H,  $H_{Py}$ ), 2.26 (s, 3H, 1), 2.03 (s, 3H, 21), 1.60 (s, 9H, 9);  **$^{13}\text{C}\{^1\text{H}\}$  NMR** (101 MHz,  $\text{CDCl}_3$ )  $\delta$  188.1 (10), 160.2 ( $C_{Py}$ ), 157.2 ( $C_{Py}$ ), 155.4 ( $C_{Py}$ ), 151.0 ( $C_{Py}$ ), 142.9 ( $C_{Py-H}$ ), 141.2 (12), 136.2 ( $C_{Py-H}$ ), 135.0 ( $C_{Py-H}$ ), 128.9 (2 x  $C_{Ph-H}$ ), 128.4 (2 x

$C_{Ph-H}$ ), 126.6 (15), 122.5 ( $C_{Py-H}$ ), 120.4 ( $C_{Py-H}$ ), 118.7 ( $C_{Py-H}$ ), 96.7 (11), 32.8 (8), 31.5 (9), 24.5 (1), 22.7 (21); **HRMS** (ESI) ( $C_{25}H_{26}N_2Au$ )  $[M-Cl]^+$ : calcd: 551.1756; found: 551.1766  $[M-Cl]^+$ ; **Anal.** Calcd. for  $C_{26.6}H_{29.2}N_2AuCl_{4.2}$  (**187b**+1.6 $CH_2Cl_2$ ): C 44.30, H 4.08, N 3.89; found: C 43.94, H 3.76; N 3.85.

### Compound 192



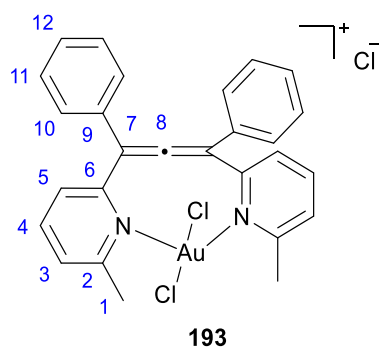
**192**

To a solution of **97b** (13 mg, 0.034 mmol, 1.05 equiv.) in dichloromethane (0.6 ml),  $(Me_2S)AuCl$  (10 mg, 0.033 mmol, 1.0 equiv.) was added. Upon addition the solution changed from colourless to bright yellow. The reaction mixture was stirred at rt for 1 h. Then,  $AgNTf_2$  (13 mg, 0.33 mmol, 1.0 equiv.) was added. A large amount of white precipitate was formed. After 5 min another portion of allene **97b** (13 mg, 0.034 mmol, 1.05 equiv.) in dichloromethane (0.4 ml) was added. After 1h of stirring at rt the reaction mixture was filtered through a pad of Celite and concentrated in *vacuo*. The resulting yellow solid was dried under *vaccum* to give 41 mg of **192** (>100%), however residual dichloromethane could not be removed.

The assignment of NMR peaks was not carried out due to complexity of the spectra.

**$^1H$  NMR** (400 MHz,  $CDCl_3$ )  $\delta$  8.09 – 8.03 (m, 2H), 7.62 – 6.97 (m, 30H), 2.29 (s, 3H), 2.22 (s, 3H), 2.10 (s, 3H), 2.04 (s, 3H);  **$^{13}C\{^1H\}$  NMR** (101 MHz,  $CDCl_3$ )  $\delta$  208.5, 208.0, 158.7, 158.6, 157.5, 157.4, 156.2, 156.0, 150.3, 149.4, 144.5, 144.5, 137.1, 137.0, 136.2, 136.0, 135.4, 135.2, 134.7, 129.2, 128.9, 128.9, 128.8, 128.6, 128.5, 128.4, 128.4, 128.1, 127.7, 127.7, 126.1, 125.4, 122.5, 122.3, 121.7, 121.7, 121.6, 121.5, 116.4, 116.3, 98.9, 98.9, 24.8, 24.4, 24.3, 22.1; **HRMS** (NSI) ( $C_{54}H_{44}N_4Au$ )  $[M-X]^+$ : calcd: 945.3226; found: 945.3225; a fragment after Au-C bond cleavage was also observed ( $C_{27}H_{22}N_2Au$ )  $[M-L-X]^+$ : calcd: 571.1443; found: 571.1431.

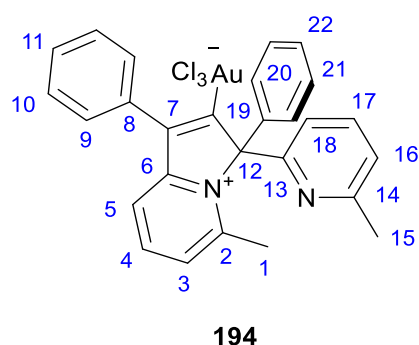
## Compound 193



A solution of allene **97b** (30 mg, 0.08 mmol, 1.0 equiv.) in EtOH (0.35 ml) was added to a solution of  $\text{HAuCl}_4 \cdot \text{H}_2\text{O}$  (27 mg, 0.08 mmol, 1.0 equiv.) in EtOH (0.35 ml) at rt followed by water (0.14 ml) and  $\text{NaPF}_6$  (27 mg, 0.16 mmol, 2.0 equiv.). After a few minutes an orange precipitate started to form. After 1 h 45 min the solid was filtered off, washed with EtOH, dried in *vacuo* to yield **193** (23 mg, 43%) as a dark orange solid.

**$^1\text{H}$  NMR** (400 MHz,  $\text{DMSO-d}_6$ )  $\delta$  8.06 (t,  $J = 7.7$  Hz, 2H, 4), 7.63 (d,  $J = 7.7$  Hz, 2H, 3/5), 7.54 (d,  $J = 7.7$  Hz, 2H, 3/5), 7.50 – 7.44 (m, 8H, 10, 11), 7.45 – 7.38 (m, 2H, 12), 2.61 (s, 6H, 1);  **$^{13}\text{C}\{^1\text{H}\}$  NMR** (101 MHz,  $\text{DMSO-d}_6$ )  $\delta$  211.1 (8), 157.3 ( $C_{Ar}$ ), 150.7 ( $C_{Ar}$ ), 141.2 ( $C_{Py-H}$ ), 133.4 (9), 129.1 (10/11), 128.7 (12), 127.9 (10/11), 124.8 ( $C_{Py-H}$ ), 122.7 ( $C_{Py-H}$ ), 112.0 (7), 22.5 (1); **HRMS** (NSI) ( $\text{C}_{27}\text{H}_{22}\text{N}_2\text{Au}^{35}\text{Cl}_2$ ) [ $\text{M-Cl}$ ] $^+$ : caclcd: 641.0820; found: 641.0816; ( $\text{C}_{27}\text{H}_{22}\text{N}_2\text{Au}$ ) [ $\text{M-3Cl}$ ] $^+$ : caclcd: 571.1443; found: 571.1429; **Anal.** Calcd. for  $\text{C}_{29}\text{H}_{26}\text{N}_2\text{AuCl}_3\text{O}$  (**193**+1.0 $\text{C}_2\text{H}_5\text{OH}$ ): C 48.19, H 3.91, N 3.88; found: C 48.57, H 3.53; N 4.11.

## Compound 194

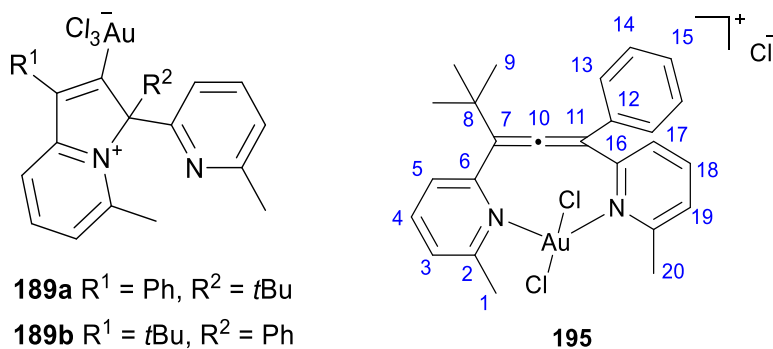


To a solution of  $\text{HAuCl}_4 \cdot x\text{H}_2\text{O}$  (18 mg, 0.053 mmol, 1.0 equiv.) in ethanol (0.8 ml), a solution of **97b** (20 mg, 0.053, 1.0 equiv.) in ethanol (0.8 ml) was added. The mixture was heated at 65 °C. After 30 min a yellow precipitate started to form. After 3 h, a yellow solid was isolated by filtration, washed with EtOH and dried in *vacuo* to yield **194** (15 mg, 42%) as a yellow solid.

Crystals suitable for X-ray crystallography were obtained by slow evaporation from the dichloromethane/methanol solution (see page 239).

**$^1\text{H}$  NMR** (400 MHz, DMSO- $d_6$ )  $\delta$  8.54 (t,  $J$  = 8.0 Hz, 1H,  $H_{\text{Py}}$ ), 7.84 (d,  $J$  = 7.7 Hz, 1H,  $H_{\text{Py}}$ ), 7.80 – 7.71 (m, 4H,  $H_{\text{Ar}}$ ), 7.61 – 7.49 (m, 4H,  $H_{\text{Ar}}$ ), 7.43 – 7.36 (m, 5H,  $H_{\text{Ar}}$ ), 7.13 (d,  $J$  = 8.0 Hz, 1H,  $H_{\text{Py}}$ ), 2.56 (s, 3H, 1/15), 2.12 (s, 3H, 1/15);  **$^{13}\text{C}\{^1\text{H}\}$  NMR** (101 MHz, DMSO- $d_6$ )  $\delta$  158.4 ( $C_{\text{Ar}}$ ), 158.2 ( $C_{\text{Ar}}$ ), 156.4 ( $C_{\text{Ar}}$ ), 154.7 ( $C_{\text{Ar}}$ ), 149.3 ( $C_{\text{Ar}}$ ), 146.7 ( $C_{\text{Ar}}$ ), 138.0 (7), 134.0 ( $C_{\text{Ar-H}}$ ), 131.6 ( $C_{\text{Ar-H}}$ ), 131.5 ( $C_{\text{Ar-H}}$ ), 129.2 ( $C_{\text{Ar-H}}$ ), 129.10 ( $C_{\text{Ar-H}}$ ), 129.0 ( $C_{\text{Ar-H}}$ ), 128.90 ( $C_{\text{Ar-H}}$ ), 128.3 ( $C_{\text{Ar-H}}$ ), 125.9 ( $C_{\text{Ar-H}}$ ), 123.3 ( $C_{\text{Ar-H}}$ ), 120.0 ( $C_{\text{Ar-H}}$ ), 118.1 ( $C_{\text{Ar-H}}$ ), 90.9 (12), 24.2 (1/15), 21.0 (1/15). The peak corresponding to C(19) was not detected.; **HRMS** (ESI) ( $\text{C}_{27}\text{H}_{22}\text{N}_2\text{Au}^{35}\text{Cl}_2$ )  $[\text{M}-\text{Cl}]^+$ : calcd: 641.0820; found: 641.0842; **Anal.** Calcd. for  $\text{C}_{27}\text{H}_{22}\text{N}_2\text{AuCl}_3$ : C 47.93, H 3.28, N 4.14; found: C 47.64, H 3.16; N 4.31.

### Compound 189 and 195



To a solution of  $\text{HAuCl}_4 \cdot \text{H}_2\text{O}$  (15 mg, 0.045 mmol, 1.0 equiv.) in methanol (0.5 ml), a solution of **97a** (16 mg, 0.045 mmol, 1.0 equiv.) in methanol (0.5 ml) was added. The mixture was heated at reflux. After 30 min a yellow precipitate started to form. After a total of 130 min, a yellow solid was isolated by filtration, washed with MeOH and dried in *vacuo* to yield **189** as 0.17:1 mixture of **189a:189b** (6 mg, 20%) as a yellow solid. The remaining filtrate was concentrated to yield **195** (18 mg, 60%) as a yellow solid. Crystals of **189a** and **189b** suitable for X-ray crystallography were obtained by vapour diffusion of dichloromethane/ $\text{CHCl}_3$  solution with cyclohexane (see page 241).

Spectral analysis of 0.5:1 mixture of **189a:189b** isomers for  $^1\text{H}$  NMR and 1:0.4 for  $^{13}\text{C}$  NMR.

**189**:  **$^1\text{H}$  NMR** (400 MHz, DMSO- $d_6$ )  $\delta$  8.58 – 8.51 (m, 1H, **189b**), 8.46 (d,  $J$  = 8.2 Hz, 1H, **189b**), 8.41 (t,  $J$  = 7.9 Hz, 1H, **189a**), 7.71 – 7.63 (m, 4H, **189a-b**), 7.58 (t,  $J$  = 7.3 Hz, 1H, **189a-b**), 7.54 – 7.46 (m, 1H, **189a**), 7.36 (t,  $J$  = 5.6 Hz, 2H, **189a-b**), 7.30 (dd,  $J$  = 7.6, 3.3 Hz, 2H, **189a-b**), 6.76 (d,  $J$  = 8.0 Hz, 1H, **189b**), 6.69 (d,  $J$  = 7.9 Hz, 1H, **189a**), 2.61 (s, 3H, **189a**), 2.60 (s, 3H, **189b**), 2.14 (s, 3H, **189a**), 2.03 (s, 3H, **189b**), 1.64 (s, 9H, **189b**), 1.54 (brs, 9H, **189a**);  **$^{13}\text{C}\{^1\text{H}\}$  NMR** (101 MHz, DMSO- $d_6$ )  $\delta$  158.1 (**189b**), 156.8 (**189b**), 156.5 (**189b**), 156.3 (**189b**),

156.1 (**189a**), 155.1 (**189b**), 154.8 (**189a**), 154.2 (**189b**), 152.7 (**189b**), 151.7 (**189b**), 150.5 (**189b**), 146.0 (**189b**), 145.2 (**189a**), 139.2 (**189a**), 139.0 (**189b**), 138.1 (**189b**), 136.8 (**189a**), 133.2 (**189a**), 132.3 (**189b**), 129.3 (**189b**), 129.0, 128.8, 127.0 (**189a**), 125.4 (**189b**), 123.3 (**189a**), 123.1, 123.1, 122.4, 120.4 (**189b**), 117.4 (**189a**), 97.4 (**189a**), 89.4 (**189b**), 43.1 (**189a**), 32.8 (**189b**), 30.0 (**189b**), 29.2 (**189a**), 24.2 (**189a**), 24.1 (**189b**), 23.9 (**189a**), 21.3 (**189b**). The peak corresponding to carbon atom bonded to Au was not detected.; **HRMS** (ESI) ( $C_{25}H_{26}N_2Au^{35}Cl_2$ ) [M-Cl]<sup>+</sup>: caclcd: 621.1130; found: 621.1160; **Anal.** Calcd. for  $C_{25}H_{26}N_2AuCl_3$ : C 45.73, H 3.99, N 4.27; found: C 45.53, H 3.83; N 4.33.

**195:** <sup>1</sup>H NMR (500 MHz, MeOD-d<sub>4</sub>) δ 8.17 (t, *J* = 7.8 Hz, 1H, 4/18), 8.11 (t, *J* = 7.8 Hz, 1H, 4/18), 7.68 (d, *J* = 7.8 Hz, 1H, *H<sub>Py</sub>*), 7.64 (d, *J* = 7.8 Hz, 1H, *H<sub>Py</sub>*), 7.59 (d, *J* = 7.8 Hz, 2H, *H<sub>Ar</sub>*), 7.47 – 7.43 (m, 2H, *H<sub>Ar</sub>*), 7.42 – 7.35 (m, 3H, *H<sub>Ar</sub>*), 2.75 (s, 3H, 1/20), 2.74 (s, 3H, 1/20), 1.36 (s, 9H, 9); <sup>13</sup>C{<sup>1</sup>H} NMR (101 MHz, MeOD-d<sub>4</sub>) δ 208.4 (10), 158.4 (*C<sub>Ar</sub>*), 158.1 (*C<sub>Ar</sub>*), 156.6 (*C<sub>Ar</sub>*), 153.0 (*C<sub>Ar</sub>*), 152.5 (*C<sub>Ar</sub>*), 144.0 (*C<sub>Py-H</sub>*), 143.2 (*C<sub>Py-H</sub>*), 134.5 (*C<sub>Py-H</sub>*), 130.3 (*C<sub>Ph-H2</sub>*), 130.0 (15), 129.0 (*C<sub>Ph-H2</sub>*), 126.7 (*C<sub>Py-H</sub>*), 126.3 (*C<sub>Py-H</sub>*), 124.5 (*C<sub>Py-H</sub>*), 120.1 (7/11), 111.5 (7/11), 37.5 (8), 30.1 (9), 22.3 (1/20), 22.1 (1/20); **HRMS** (ESI) ( $C_{25}H_{27}Cl_3N_2Au$ ) [M+H]<sup>+</sup>: caclcd: 657.0900; found: 657.0950; **Anal.** Calcd. for  $C_{25.5}H_{26.5}^{35}Cl_{4.5}N_2Au$  (**195**+0.5CHCl<sub>3</sub>): C 42.79, H 3.74, N 3.92; found: C 43.01, H 3.82, N 3.93.

#### Chapter IV - Isomerisation of complexes **187a** and **187b** – kinetic experiments

A sample of **187** in CDCl<sub>3</sub> of initial concentration of 0.067M and ratio 1:0.12 **187a**:**187b** was submitted to a series of <sup>1</sup>H NMR experiments at 10 min intervals until 2 h, then 30 min intervals until 6 h, then every hour until 10 h. The last two points were recorded at 48 and 77 h. The ratio of both species in solution was determined by comparison of integration of the signals at 6.79 ppm (**187a**) and at 8.49 ppm (**187b**). The corresponding concentrations of **187a**:**187b** were plotted vs time till the total disappearance of the **187a** isomer (see Section IV b. 4., page 97).

#### Chapter IV - Attempts to derivatise Au(I) complex **187b**

##### HNTf<sub>2</sub> experiment

To a solution of **187b** (18 mg, 0.031 mmol, 1.0 equiv.) in anhydrous dichloromethane (0.5 ml), HNTf<sub>2</sub> (13 mg, 0.046 mmol, 1.5 equiv.) was added at rt. After a few minutes, a black precipitate started to form. The starting material was consumed after 3 d of stirring at rt. The reaction mixture was filtered through Celite. The filtrate was washed twice with water and aqueous washings were then extracted back with more dichloromethane (x 3). The combined organic layers were washed with brine, dried over MgSO<sub>4</sub> and concentrated in *vacuo* to yield 8 mg of pink solid. This residue was redissolved in dichloromethane and layered with Et<sub>2</sub>O, but no

precipitation was observed. Upon slow evaporation of solvents yellow crystalline solid appear. Crystals of good quality for X-ray diffraction were isolated and analysed. The sample contained crystals of Au(III) analogue of starting material **189b** and no protodemetalation products were identified.

### **Iodination**

Reaction of **187b** (9 mg, 0.015 mmol, 1.0 equiv.) with I<sub>2</sub> (8 mg, 0.032 mmol, 2.1 equiv.) in dichloromethane (0.5 ml) resulted in complete conversion of SM within 3.5 h. Two products were isolated together as seen on <sup>1</sup>H NMR, but unsuccessful attempts of their separation hindered the full characterisation.

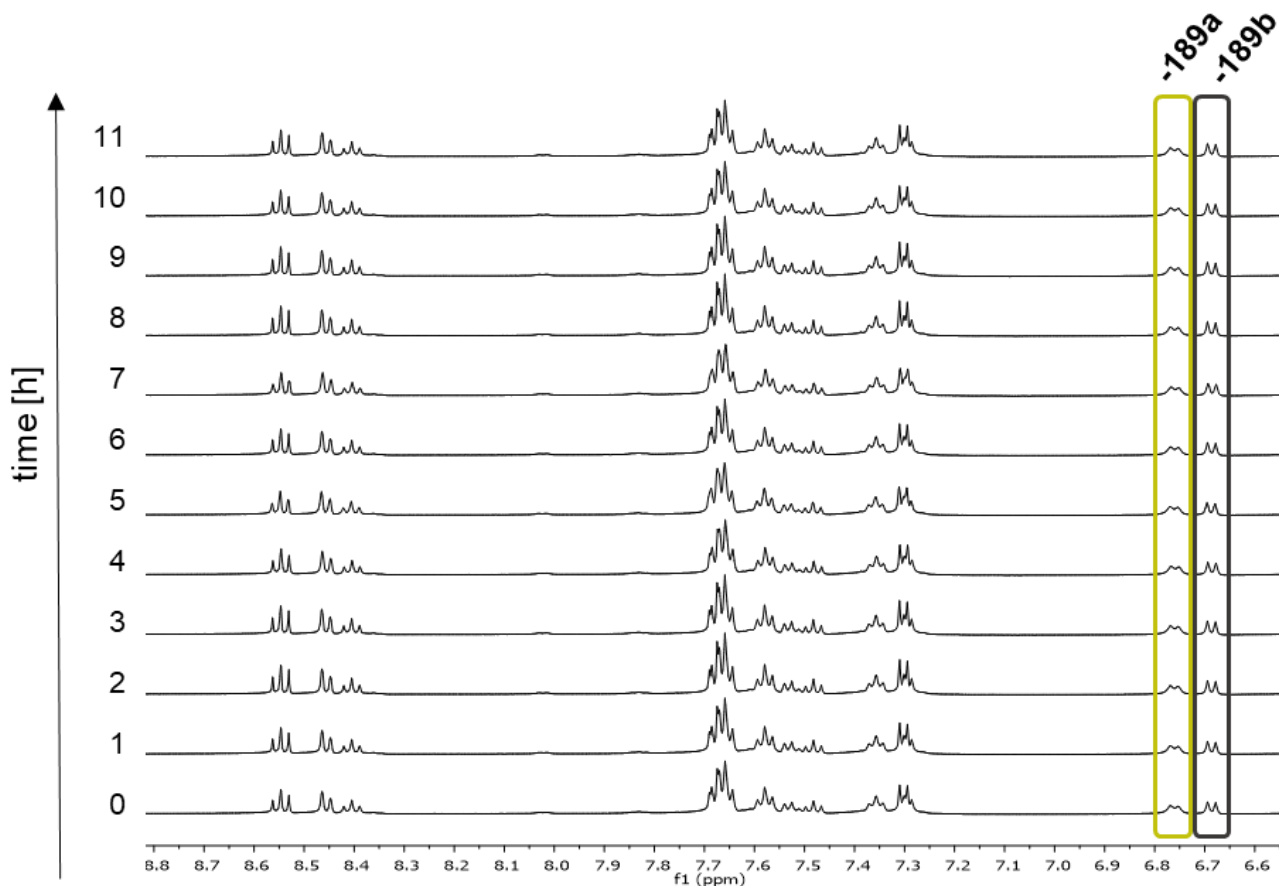
Reaction of **187b** (11 mg, 0.019 mmol, 1.0 equiv.) with NIS (5 mg, 0.021 mmol, 1.1 equiv.) in dichloromethane (0.6 ml) resulted in complete conversion of SM within 6.5 h, but analysis of the reaction mixture revealed decomposition of the material.

### **Oxidation experiments**

Prolonged reactions of **187b** (15 mg, 0.026 mmol, 1.0 equiv.) with oxidation agents such as MnO<sub>2</sub> (9 mg, 0.10 mmol, 4.1 equiv.), Dess-Martin periodinane (13 mg, 0.031 mmol, 1.3 equiv.) and pyridine N-oxide (3.4 mg, 0.035 mmol, 1.3 equiv.) in dichloromethane (0.5 ml) resulted in isolation of unreacted starting material with the exception of Dess-Martin reaction where traces of **189b** were also isolated.

### **Chapter IV - Isomerisation of complexes 189a and 189b – kinetic experiments**

A sample of **189** in DMSO-d<sub>6</sub> of initial ratio 0.75:1 **189a**:**189b** was submitted to the series of 12 <sup>1</sup>H NMR experiments with 1 h interval. The ratio of both species in solution was determined by comparison of integration of the signals at 6.76 ppm (**189b**) and at 6.69 ppm (**189a**). The observed ratio of the two species did not change in the timescale of the experiment.

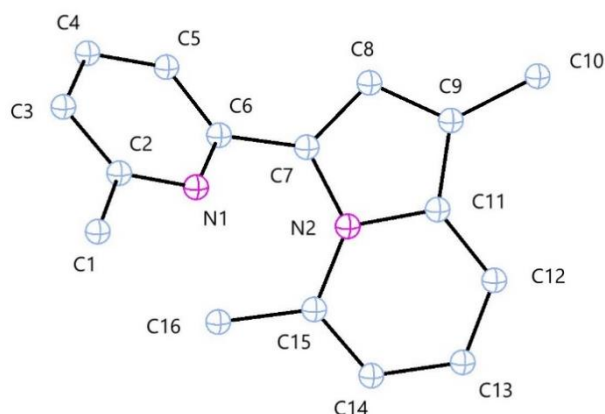


**Figure 58** <sup>1</sup>H NMR spectra of the isomerisation reaction of **189** in DMSO-d<sub>6</sub> at rt over 11 h – expansion of region from 6.5 to 9 ppm.

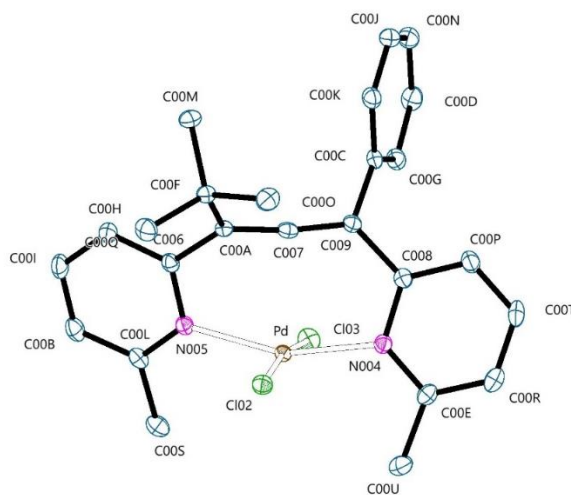
#### Chapter IV - X-ray structure determination

Data for complexes **184**, **187b**, **194**, **189b** and **179** was collected and analysed by Dr David Hughes at University of East Anglia. Data for compound **141** was collected and analysed by Dr J. Christensen at UK National Crystallography Service (University of Southampton).



**Compound 141**

**Figure 59** ORTEP representation of X-ray structure of compound **141** indicating the numbering scheme (Hs omitted). Thermal ellipsoids are drawn at the 50% probability level.

**Complex 172**

**Figure 60** ORTEP representation of X-ray structure of complex **172** indicating the numbering scheme (Hs omitted). Thermal ellipsoids are drawn at the 50% probability level.

**Complex 179**

The platinum atom shows an approximately square planar, fourfold configuration with the two chloride ligands and the chelating N(1)---C(9) group; the second nitrogen atom, N(22), is not bound to the Pt centre, but forms a pyridinium group which is the donor group in a good intramolecular hydrogen bond, N(22)-H(22)...Cl(1), Figure S12. The methine H atom of the solvent (chloroform) molecule is the donor in the C(41)-H(41)...Cl(2)#2 hydrogen bond.

The C(3)-C(4) bond lies over a neighbouring symmetry-related group with a  $\pi \dots \pi$  interaction. On the opposite side of this pyridinyl ring, one of the methyl groups of the t-butyl (intramolecular) group folds over C(2) with a short C(2)-H(34a) distance of 2.61 Å. The C(5)-H(5) bond is directed towards the centre of the C6 ring of C(11-16) of a neighbouring molecule, with the shortest H...C distance at 2.88 Å. In the pyridinium ring, a neighbouring solvent chlorine atom, Cl(43), makes a close contact with C(21) at 3.525 Å.

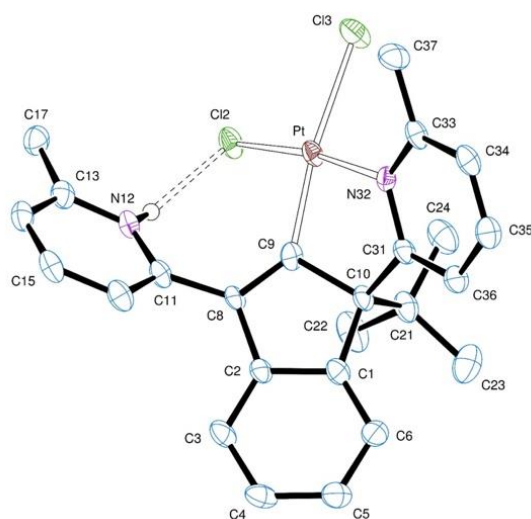


**Figure 61** ORTEP representation of a molecule of complex **179**, indicating the atom numbering scheme and the hydrogen bond (Hs omitted). Thermal ellipsoids are drawn at the 50% probability level.

### Complex 184

The principal plane of this molecule comprises the  $C_8H_3N$  ring system, with the methyl group of C(7), the Au centre, the chloride ligand and C(11) (Figure 62). The normal to the plane of the phenyl ring of C(11-16) is  $53.70(11)^\circ$  from that of the five-membered (pyrrole) ring, and C(10) has a tetrahedral arrangement with the phenyl ring of C(21) and the pyridyl ring of C(31) displaced out of the pyrrole ring plane. The ortho C(22)-H(22) group folds over the face of the pyrrole ring forming close contacts of 2.58 and 2.61 Å with C(9) and C(10).

The Au atom has an approximately linear arrangement of the chloride ligand and C(9) of the pyrrole ring.

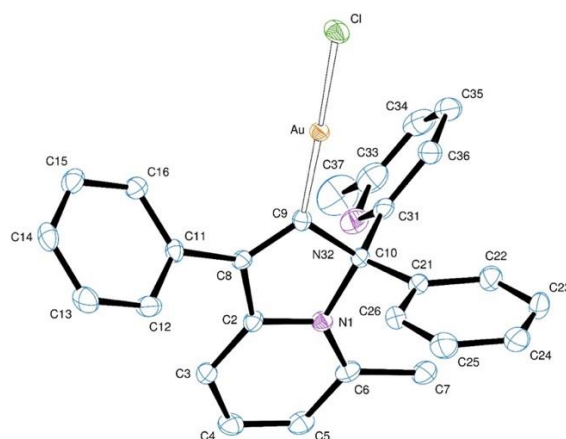


**Figure 62** ORTEP representation of a molecule of complex **184**, indicating the atom numbering scheme (Hs omitted). Thermal ellipsoids are drawn at the 50% probability level.

The shortest intermolecular contacts appear to involve the chloride ligand, with several aromatic C-H groups forming weak hydrogen bonds; the closest H...Cl distance is 2.86 Å. A view of the molecular packing is shown in Figure 63.

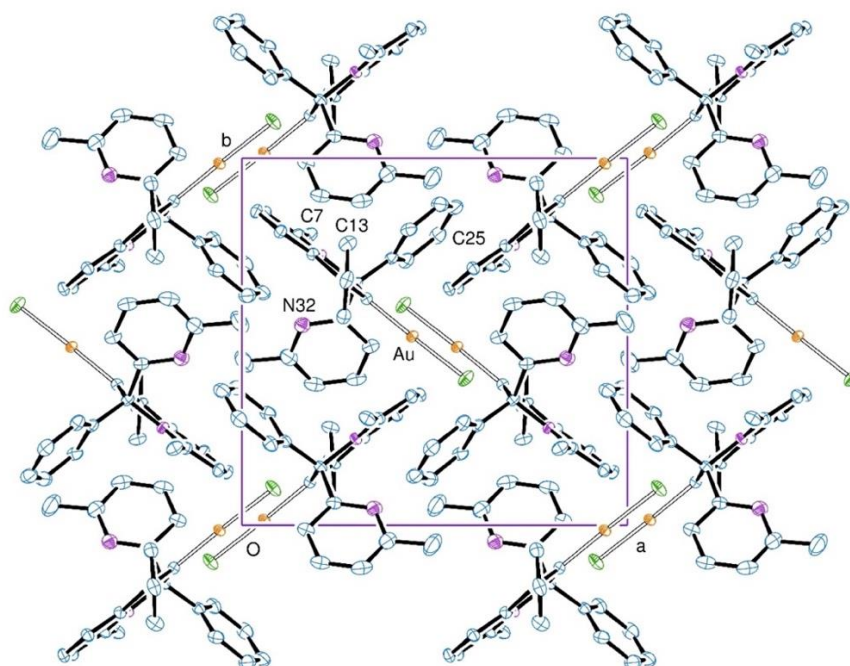


**Figure 63** View of the packing along the c axis in **184**.

### Complex 187b

Compound **187b** showed chirality, *i.e.* all the molecules are identical, each with an asymmetric centre at C(10). There were no molecules of the inverted structure/mirror image found in the selected crystal. This crystal shows polarity: all the molecules point in the same direction,

spiralling around a  $4_1$  symmetry axis. The absolute structure (Flack  $x$ ) parameter was  $-0.0125(19)$  and the correct chirality ( $S$ ) is shown in Figure 64 and Figure 65.

There is no reason for this complex to be enantiomerically pure, and perhaps there were crystals in the sample which are of the opposite enantiomer – but we were not able to detect any by the simple methods available, e.g. *via* looking for crystals with mirror-image morphologies.

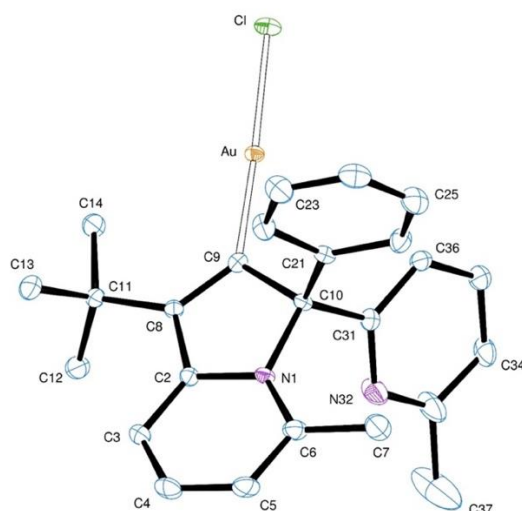


**Figure 64** ORTEP representation of a molecule of **187b**, indicating the atom numbering scheme (Hs omitted). Thermal ellipsoids are drawn at the 50% probability level.

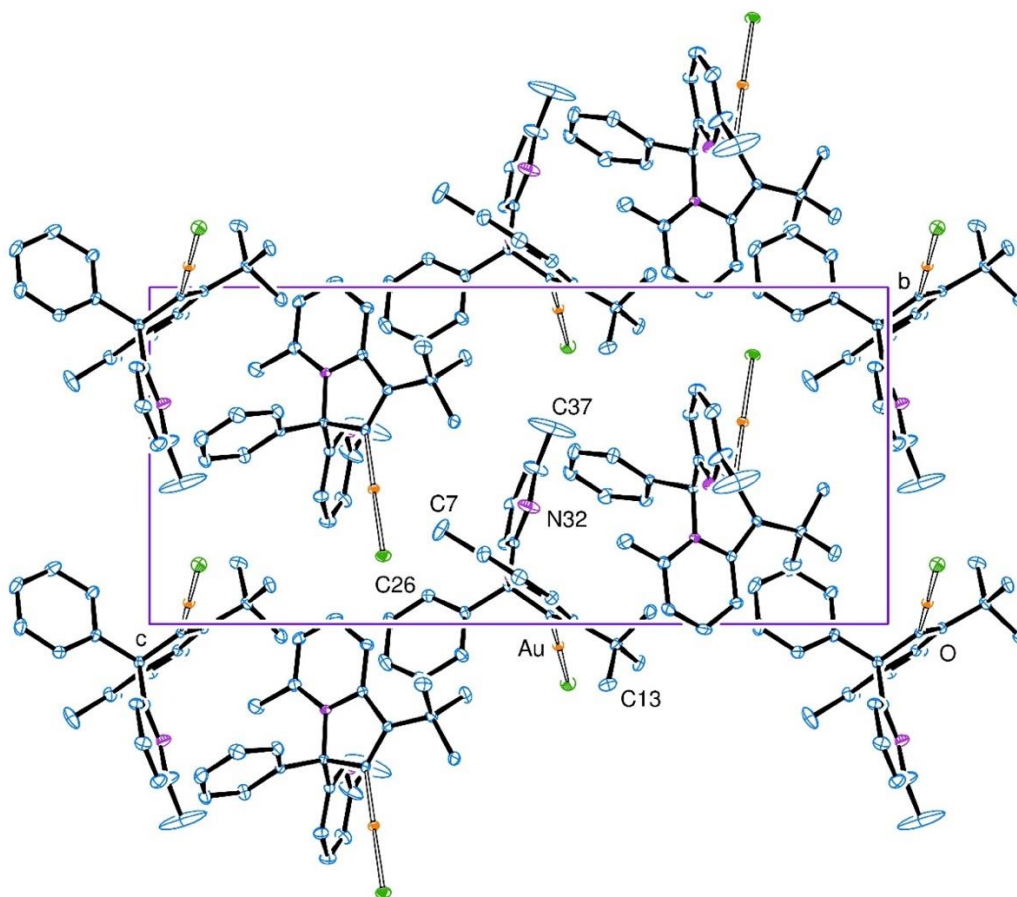
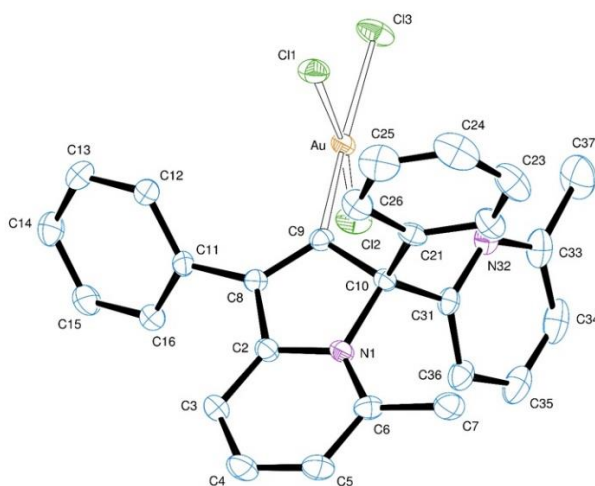


**Figure 65** View of the packing along the *a* axis in **187b**.

### Complex 194

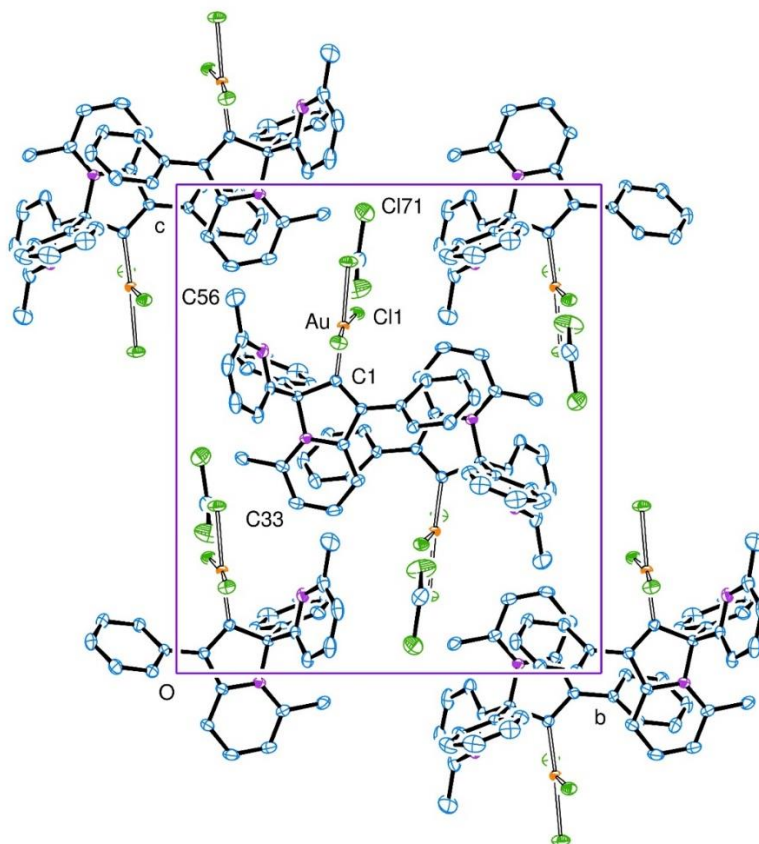
The principal plane of this molecule comprises the C<sub>8</sub>H<sub>3</sub>N ring system, with the methyl group of C(7), the Au centre, the chloride ligand and C(11) (Figure 66). The normal to the plane of the phenyl ring of C(11-16) is 53.70(11)° from that of the five-membered (pyrrole) ring, and C(10) has a tetrahedral arrangement with the phenyl ring of C(21) and the pyridyl ring of C(31) displaced out of the pyrrole ring plane. The ortho C(22)-H(22) group folds over the face of the pyrrole ring forming close contacts of 2.58 and 2.61 Å with C(9) and C(10).

The Au atom has an approximately linear arrangement of the chloride ligand and C(9) of the pyrrole ring.



**Figure 66** ORTEP representation of a molecule of **194**, indicating the atom numbering scheme (Hs omitted). Thermal ellipsoids are drawn at the 50% probability level.

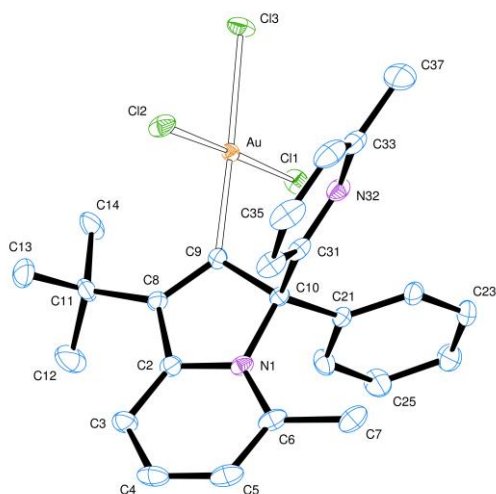
The shortest intermolecular contacts appear to involve the chloride ligand, with several aromatic C-H groups forming weak hydrogen bonds; the closest H...Cl distance is 2.86 Å. A view of the molecular packing is shown in Figure 67.



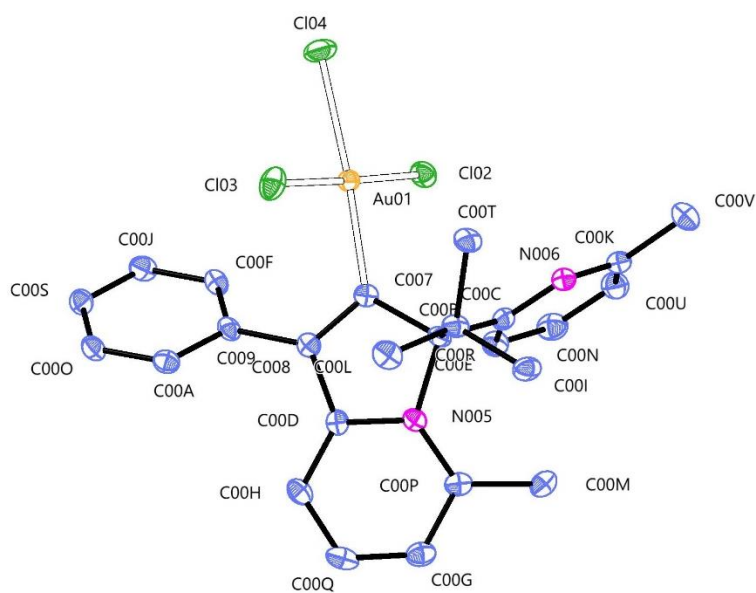
**Figure 67** View of the packing along the *a* axis in **194**.

**Complex 189b**

**189b** (Figure 68) is structurally very similar to **194**.



**Figure 68** ORTEP representation of a molecule of **189b**, indicating the atom numbering scheme (Hs omitted). Thermal ellipsoids are drawn at the 50% probability level.

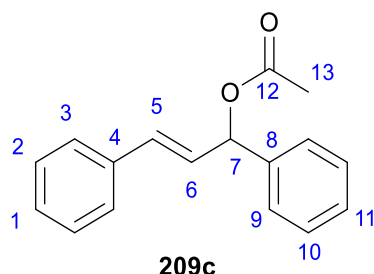
**Complex 189a**

**Figure 69** ORTEP representation of a molecule of **189a**, indicating the atom numbering scheme (Hs omitted). Thermal ellipsoids are drawn at the 50% probability level.



## Chapter V - Catalytic experiments – preparation of starting materials and general procedures

### Compound 209c

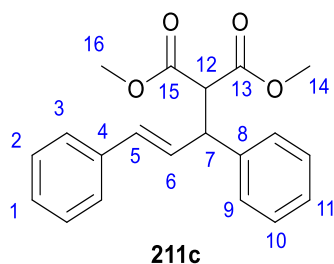


An oven-dried round bottom flask was charged with *trans*-1,3-diphenyl-2-propen-1-ol (525 mg, 2.50 mmol, 1.0 equiv.) and placed under inert atmosphere. Anhydrous dichloromethane (5.25 ml) was added, followed by Et<sub>3</sub>N (0.7 ml, 5.0 mmol, 2.0 equiv.). Acetic anhydride (0.47 ml, 5.0 mmol, 2.0 equiv.) was added at 0 °C in portions. The reaction mixture was warmed to rt and left stirring overnight. Then, it was quenched with water and the aqueous layer was separated. The organic phase was washed with NaHCO<sub>3(aq)</sub> twice, then with water and brine and dried over MgSO<sub>4</sub>, filtered and concentrated in *vacuo*. Purification by column chromatography (Pet/AcOEt 19:1) yielded **209c** (502 mg, 80%) as a colourless oil.

<sup>1</sup>H NMR (400 MHz, CDCl<sub>3</sub>) δ 7.44 – 7.35 (m, 6H, *H<sub>Ph</sub>*), 7.34 – 7.28 (m, 3H, *H<sub>Ph</sub>*), 7.27 – 7.21 (m, 1H, *H<sub>Ph</sub>*), 6.64 (d, *J* = 15.7 Hz, 1H, 5), 6.45 (d, *J* = 6.9 Hz, 1H, 7), 6.35 (dd, *J* = 15.7, 6.9 Hz, 1H, 6), 2.14 (s, 3H, 13).

The characterisation data is in agreement with previously reported.<sup>[423]</sup>

### Compound 211c



[Pd(allyl)Cl]<sub>2</sub> (2 mg, 0.005 mmol, 0.0025 equiv.) and PPh<sub>3</sub> (5 mg, 0.02 mmol, 0.1 equiv.) were placed under N<sub>2</sub>, anhydrous dichloromethane (0.5 ml) was added and the mixture stirred at rt for 30 min. Ester **209c** (50 mg, 0.20 mmol, 1.0 equiv.) in anhydrous dichloromethane (0.5 ml) was added followed by dimethyl malonate (79 mg, 0.60 mmol, 3.0 equiv.), bis(trimethylsilyl)acetamide (BSA, 0.15 ml, 0.60 mmol, 3.0 equiv.) and NaOAc (0.3 mg, 0.004 mmol, 0.02 equiv.). The reaction mixture was stirred at rt for 3 h and then quenched with

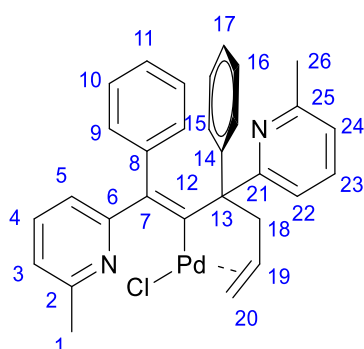


$\text{NH}_4\text{Cl}_{(\text{aq.})}$ . The organic phase was separated, washed with  $\text{NH}_4\text{Cl}_{(\text{aq.})}$  (x 3), followed by water and brine, dried over  $\text{MgSO}_4$ , filtered and concentrated in *vacuo*. Purification by column chromatography (Pet/AcOEt 6:1) yielded **211c** (39 mg, 60%) as a yellow oil contaminated with dimethyl malonate.

$^1\text{H NMR}$  (500 MHz,  $\text{CDCl}_3$ )  $\delta$  7.34 – 7.25 (m, 8H,  $H_{Ph}$ ), 7.23 – 7.19 (m, 2H, 1, 11), 6.49 (d,  $J = 15.7$  Hz, 1H, 5), 6.33 (dd,  $J = 15.7, 8.6$  Hz, 1H, 6), 4.29 – 4.23 (m, 1H, 7), 3.95 (d,  $J = 10.9$  Hz, 1H, 12), 3.70 (s, 3H, 16), 3.52 (s, 3H, 14).

The characterisation data is in agreement with previously reported.<sup>[424]</sup>

### Compound 216



**216**

$[\text{Pd}(\text{allyl})\text{Cl}]_2$  (10 mg, 0.027 mmol, 0.5 equiv.) was added to a solution of allene **97b** (20 mg, 0.053 mmol, 1.0 equiv.) in anhydrous dichloromethane (1.3 ml) at rt. The reaction mixture changed from colourless to yellow. After 40 min of stirring the solution was filtered through a cotton wool plug to remove solid impurities, washed with more dichloromethane and concentrated in *vacuo* to afford **216** (29 mg, > 99%) as an orange solid.

See Appendix A for 2D NMR spectra.

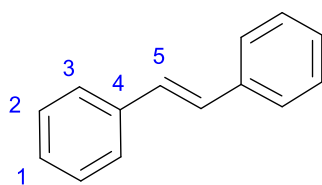
$^1\text{H NMR}$  (400 MHz,  $\text{CDCl}_3$ )  $\delta$  7.45 (t,  $J = 7.8$  Hz, 1H,  $H_{Py}$ ), 7.29 (t,  $J = 6.8$  Hz, 2H,  $H_{Ph}$ ), 7.11 (tt,  $J = 14.8, 7.6$  Hz, 8H,  $H_{Ph}$ ), 6.87 (d,  $J = 7.6$  Hz, 1H,  $H_{Py}$ ), 6.79 (t,  $J = 7.6$  Hz, 1H,  $H_{Py}$ ), 6.44 (d,  $J = 7.8$  Hz, 1H,  $H_{Py}$ ), 6.25 – 6.13 (m, 1H, 19), 5.95 (d,  $J = 7.8$  Hz, 1H,  $H_{Py}$ ), 5.83 (d,  $J = 7.6$  Hz, 1H,  $H_{Py}$ ), 5.06 (d,  $J = 10.1$  Hz, 1H, 20), 4.87 (d,  $J = 16.3$  Hz, 1H, 20), 3.17 (s, 3H, 1/26), 3.14 (m, 1H, 18), 3.12 (s, 3H, 1/26), 2.63 (dd,  $J = 13.4, 8.0$  Hz, 1H, 18);  $^{13}\text{C}\{^1\text{H}\}$  NMR (101 MHz,  $\text{CDCl}_3$ )  $\delta$  183.3 (12), 175.5 ( $C_{Ar}$ ), 169.9 ( $C_{Ar}$ ), 162.0 ( $C_{Ar}$ ), 160.7 ( $C_{Ar}$ ), 146.0 ( $C_{Ar}$ ), 141.6 ( $C_{Ar}$ ), 138.2 ( $C_{Py-H}$ ), 138.0 ( $C_{Ar-H}$ ), 136.0 (7), 133.9 (19), 130.2 ( $C_{Py-H}$ ), 129.3 ( $C_{Ar-H}$ ), 128.4 ( $C_{Py-H}$ ), 128.3 ( $C_{Ar-H}$ ), 128.1 ( $C_{Ar-H}$ ), 127.4 ( $C_{Ar-H}$ ), 127.0 ( $C_{Ar-H}$ ), 126.9 ( $C_{Ar-H}$ ), 124.1 ( $C_{Ar-H}$ ), 122.5 ( $C_{Py-H}$ ), 121.4 ( $C_{Py-H}$ ), 118.6 (20), 117.6 ( $C_{Py-H}$ ), 69.3 (13), 44.8 (18), 27.9 (1/26), 27.2 (1/26); **HRMS** (ESI) ( $\text{C}_{30}\text{H}_{27}\text{N}_2^{106}\text{Pd}$ )  $[\text{M}-\text{Cl}]^+$ : caclcd: 521.1204; found: 521.1205; **Anal.**

Calcd. for  $C_{31.4}H_{28.4}N_2PdCl_{5.2}$  (**216**+1.3CHCl<sub>3</sub>): C 52.25, H 3.97, N 3.88; found: C 52.07, H 3.96; N 4.25.

### General procedure for the Mizoroki-Heck coupling<sup>[425]</sup>

The corresponding Pd catalyst (0.005 mmol, 0.02 equiv.) and HCOONH<sub>4</sub> (0.025 mmol, 0.1 equiv.) were placed under N<sub>2</sub>. Anhydrous DMF (0.25 ml) was added, followed by aryl halide (0.25 mmol, 1.0 equiv.), *i*Pr<sub>2</sub>EtN (48mg, 0.38 mmol, 1.5 equiv.) and styrene (31 mg, 0.30 mmol, 1.2 equiv.). The reaction was heated at 80 °C for 16-19 h (overnight) and then cooled to rt, diluted with AcOEt and extracted with ice water (x 5). The organic phase was washed with brine, dried over MgSO<sub>4</sub>, filtered and concentrated in *vacuo* to yield **220c** without further purification.

### Compound 220c

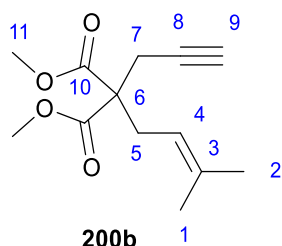


**220c**

<sup>1</sup>H NMR (400 MHz, CDCl<sub>3</sub>) δ 7.53 – 7.51 (m, 4H, 3), 7.39 – 7.33 (m, 4H, 2), 7.29 – 7.24 (m, 2H, 1), 7.12 (s, 2H, 5); <sup>13</sup>C{<sup>1</sup>H} NMR (101 MHz, CDCl<sub>3</sub>) δ 137.5 (4), 128.8 (5), 128.8 (2), 127.8 (1), 126.7 (3).

The characterisation data is in agreement with previously reported.<sup>[426]</sup>

### Compound 200b<sup>[427]</sup>



**200b**

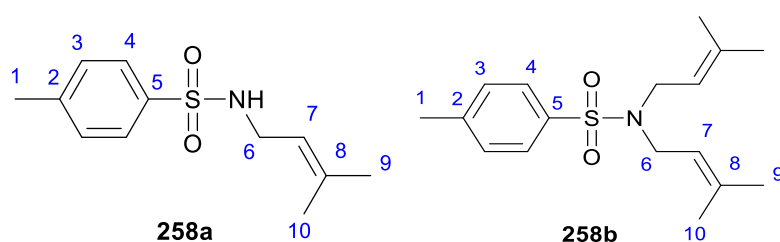
Dimethyl propargylmalonate **255** (1.02 g, 6.00 mmol, 1.0 equiv.) was added dropwise to a suspension of NaH (60% suspension in oil, 288 mg, 7.20 mmol, 1.2 equiv.) in anhydrous THF (7.7 ml) at 0 °C under N<sub>2</sub>. Evolution of gas was observed, and the solution turned bright orange. After 5 min, 3,3-dimethylallyl bromide **256a** (0.83 ml, 7.2 mmol, 1.2 equiv.) was added dropwise at 0 °C. The solution changed to a yellow suspension that was allowed to warm to rt and stirred for 5.5 h. The mixture was then quenched with water, and the aqueous layer was separated

and extracted with Et<sub>2</sub>O. The combined organic layers were dried over MgSO<sub>4</sub>, filtered and concentrated in *vacuo*. Purification by column chromatography (Pet/AcOEt 7:1) yielded **200b** (1.428 g, > 99%) as a colourless oil.

**<sup>1</sup>H NMR** (400 MHz, CDCl<sub>3</sub>) δ 4.91 – 4.85 (m, 1H, 4), 3.72 (s, 6H, 11), 2.79 – 2.75 (m, 4H, 5, 7), 1.99 (t, *J* = 2.7 Hz, 1H, 9), 1.68 (d, *J* = 1.0 Hz, 3H, 1/2), 1.64 (s, 3H, 1/2); **<sup>13</sup>C{<sup>1</sup>H} NMR** (101 MHz, CDCl<sub>3</sub>) δ 170.6 (10), 137.1 (3), 117.1 (4), 79.4 (8), 71.3 (9), 57.3 (6), 52.8 (11), 30.9 (5), 26.2 (2), 22.6 (7), 18.0 (1).

The characterisation data is in agreement with previously reported.<sup>[428]</sup>

### Compound 258a<sup>[429]</sup>



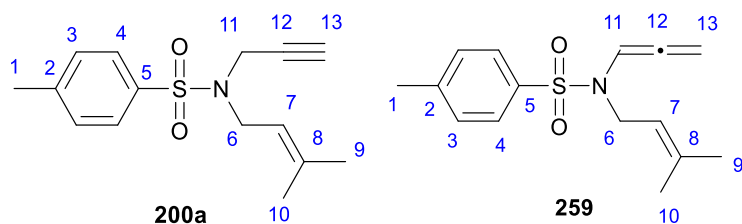
*p*-Toluenesulfonamide **257** (2.50 g, 14.6 mmol, 1.0 equiv.) in anhydrous DMF (10.0 ml) was added dropwise to a suspension of NaH (60% suspension in oil, 584 mg, 1.46 mmol, 1.0 equiv.) in anhydrous DMF (15.0 ml) at 0 °C under N<sub>2</sub>. Evolution of gas was observed. After 5 min 3,3-dimethylallyl bromide **256a** (1.70 ml, 14.6 mmol, 1.0 equiv.) was added dropwise at 0 °C. The solution was allowed to warm to rt and stirred for 22 h. The reaction was then quenched with water, and the aqueous layer was separated and extracted with AcOEt. The combined organic layers were washed with ice water (x 5) and brine, dried over MgSO<sub>4</sub>, filtered and concentrated in *vacuo*. Purification by column chromatography (Pet/AcOEt 9:1) yielded **258a** (1.078 g, 31%) as a colourless oil and **258b** (1.10 g, 24%) as a yellow oil.

**258a:** **<sup>1</sup>H NMR** (400 MHz, CDCl<sub>3</sub>) δ 7.75 (d, *J* = 7.5 Hz, 2H, 4), 7.29 (d, *J* = 7.5 Hz, 2H, 3), 5.03 (m, 1H, 7), 4.59 (brs, 1H, -NH), 3.51 (d, *J* = 6.3 Hz, 2H, 6), 2.41 (s, 3H, 1), 1.60 (s, 3H, 9/10), 1.51 (s, 3H, 9/10); **<sup>13</sup>C{<sup>1</sup>H} NMR** (101 MHz, CDCl<sub>3</sub>) δ 143.4 (2), 137.5 (5), 137.2 (8), 129.7 (3), 127.3 (4), 119.0 (7), 41.1 (6), 25.6 (9), 21.6 (1), 17.9 (10).

The characterisation data is in agreement with previously reported.<sup>[430]</sup>

**258b:** **<sup>1</sup>H NMR** (400 MHz, CDCl<sub>3</sub>) δ 7.64 – 7.59 (m, 2H, 4), 7.21 (d, *J* = 8.5, 0.6 Hz, 2H, 3), 4.92 (m, 2H, 7), 3.69 (d, *J* = 6.9 Hz, 4H, 6), 2.35 (s, 3H, 1), 1.58 (d, *J* = 0.9 Hz, 6H, 9/10), 1.50 (s, 6H, 9/10).

The characterisation data is in agreement with previously reported.<sup>[431]</sup>

**Compound 200a**<sup>[429]</sup>

**258a** (1.048 g, 4.38 mmol, 1.0 equiv.) in anhydrous DMF (10.0 ml) was added dropwise to a suspension of NaH (60% suspension in oil, 228 mg, 5.70 mmol, 1.3 equiv.) in anhydrous DMF (5.0 ml) at 0 °C under N<sub>2</sub>. Evolution of gas was observed. After 5 min propargyl bromide **256b** (80% in toluene, 0.51 ml, 4.6 mmol, 1.05 equiv.) was added dropwise at 0 °C. The colour of the solution changed from yellow to brown. The mixture was allowed to warm to rt and stirred for 3.5 h. It was then quenched with water, and the aqueous layer was separated and extracted with AcOEt. The combined organic layers were washed with ice water (x 5), and brine, dried over MgSO<sub>4</sub>, filtered and concentrated in *vacuo*. Purification by column chromatography (Pet/AcOEt 19:1) yielded **200a** (1.011 g, 83%) as a white solid and **259** (85 mg, 7%) as a yellow oil.

**200a**: <sup>1</sup>H NMR (400 MHz, CDCl<sub>3</sub>) δ 7.76 – 7.71 (m, 2H, 4), 7.29 (d, *J* = 7.9 Hz, 2H, 3), 5.13 – 5.07 (m, 1H, 7), 4.07 (d, *J* = 2.5 Hz, 2H, 11), 3.81 (d, *J* = 7.3 Hz, 2H, 6), 2.42 (s, 3H, 1), 1.98 (t, *J* = 2.5 Hz, 1H, 13), 1.72 (d, *J* = 0.9 Hz, 3H, 9/10), 1.67 (d, *J* = 0.6 Hz, 3H, 9/10); <sup>13</sup>C{<sup>1</sup>H} NMR (101 MHz, CDCl<sub>3</sub>) δ 143.5 (2), 139.2 (8), 136.3 (5), 129.5 (3), 128.0 (4), 118.1 (7), 77.2 (12), 73.5 (13), 44.1 (6), 35.5 (11), 26.0 (9), 21.7 (1), 18.0 (10).

The characterisation data is in agreement with previously reported.<sup>[432]</sup>

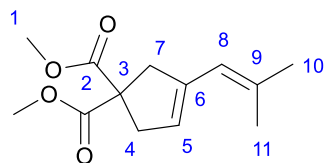
**259**: <sup>1</sup>H NMR (400 MHz, CDCl<sub>3</sub>) δ 7.69 – 7.65 (m, 2H, 4), 7.30 (d, *J* = 8.0 Hz, 2H, 3), 6.80 (t, *J* = 6.2 Hz, 1H, 11), 5.25 (d, *J* = 6.2 Hz, 2H, 13), 5.00 (m, 1H, 7), 3.76 (d, *J* = 6.6 Hz, 2H, 6), 2.42 (s, 3H, 1), 1.62 (d, *J* = 1.1 Hz, 3H, 9/10), 1.59 (s, 3H, 9/10); <sup>13</sup>C{<sup>1</sup>H} NMR (101 MHz, CDCl<sub>3</sub>) δ 201.7 (12), 143.7 (2), 136.0 (8), 136.0 (5), 129.7 (3), 127.4 (4), 119.0 (7), 100.0 (11), 87.3 (13), 44.9 (6), 25.8 (9), 21.7 (1), 18.2 (10); HRMS (ASAP) (C<sub>15</sub>H<sub>20</sub>NO<sub>2</sub>S) [M+H]<sup>+</sup>: calcd: 278.1215; found: 278.1216.

**General procedure for metal-catalysed cyclisation of enynes 200a and 200b**

The catalyst (2-3 mol%) and AgNTf<sub>2</sub> (where applicable) were placed under N<sub>2</sub> and the corresponding solvent (0.5 ml) was added. The mixture was stirred at 25 °C for 5 min. The corresponding enyne (0.1 mmol, 1.0 equiv.) in the same solvent (1.0 ml) was added. Stirring continued for indicated amount of time at indicated temperature. The reaction mixture was

filtered through a pad of Celite and concentrated in *vacuo*. The residue was analysed by  $^1\text{H}$  NMR to determine the ratio of isomeric products.

### Compound 202a

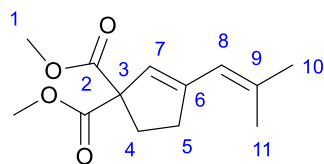


202a

$^1\text{H}$  NMR (400 MHz,  $\text{CDCl}_3$ )  $\delta$  5.72 (s, 1H, 8), 5.37 (s, 1H, 5), 3.72 (s, 6H, 1), 3.18 (d,  $J = 1.7$  Hz, 2H, 4), 3.03 (s, 2H, 7), 1.81 (s, 3H, 10/11), 1.77 (s, 3H, 10/11);  $^{13}\text{C}\{^1\text{H}\}$  NMR (101 MHz,  $\text{CDCl}_3$ )  $\delta$  172.7 (2), 138.8 (9), 135.8 (6), 124.5 (8), 120.7 (5), 59.4 (3), 52.9 (1), 43.4 (4), 40.4 (7), 27.4 (10), 19.9 (11).

The characterisation data is in agreement with previously reported.<sup>[433]</sup>

### Compound 202b



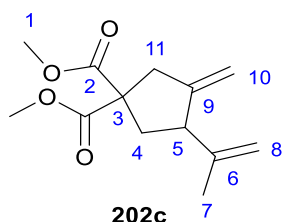
202b

In 1:0.6 mixture of **202b:202a**.

$^1\text{H}$  NMR (400 MHz,  $\text{CDCl}_3$ )  $\delta$  5.80 (s, 1H, 7), 5.59 (s, 1H, 8), 3.72 (s, 6H, 1), 2.65 (t,  $J = 6.5$  Hz, 2H, 5), 2.50 – 2.43 (m, 2H, 4), 1.83 (s, 3H, 10/11), 1.80 (s, 3H, 10/11).

The characterisation data is in agreement with previously reported.<sup>[282]</sup>

### Compound 202c



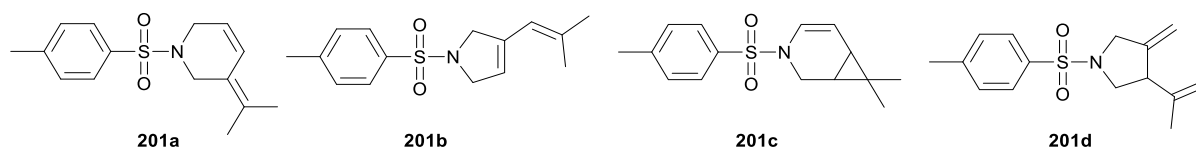
202c

In 1:0.33:1 mixture of **202c:202a:200b**.

**<sup>1</sup>H NMR** (400 MHz, CDCl<sub>3</sub>) δ 5.01 (d, *J* = 2.0 Hz, 1H, 10), 4.83 (d, *J* = 1.1 Hz, 2H, 8), 4.79 (dd, *J* = 4.4, 2.0 Hz, 1H, 10), 3.73 (s, 6H, 1), 3.31 – 3.23 (m, 1H, 5), 3.04 (d, *J* = 1.5 Hz, 1H, 11), 2.96 – 2.87 (m, 1H, 11), 2.52 (ddd, *J* = 13.0, 7.8, 1.5 Hz, 1H, 4), 2.12 (dd, *J* = 13.0, 11.3 Hz, 1H, 4), 1.64 (s, 3H, 7).

The characterisation data is in agreement with previously reported.<sup>[434]</sup>

**Compound 201a:201b:201c:201d** 1:0.08:0.08:0.01



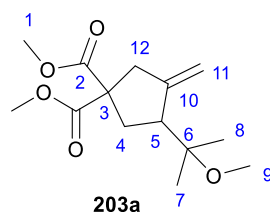
**<sup>1</sup>H NMR** (400 MHz, CDCl<sub>3</sub>) δ 7.74 – 7.70 (m, 2H, **201b**), 7.67 – 7.62 (m, 2H, **201a**), 7.33 – 7.30 (m, 2H, **201b,c**), 7.28 – 7.25 (m, 2H, **201a**), 6.59 (d, *J* = 8.4 Hz, 1H, **201c**), 6.34 (dt, *J* = 10.3, 2.1 Hz, 1H, **201a**), 5.61 (s, 1H, **201b**), 5.52 (dt, *J* = 10.3, 3.6 Hz, 1H, **201a**), 5.38 (s, 1H, **201b**), 5.06 (dd, *J* = 8.4, 4.8 Hz, 1H, **201c**), 5.01 (d, *J* = 2.1 Hz, 1H, **201d**), 4.87 – 4.85 (m, 1H, **201d**), 4.84 – 4.82 (m, 1H, **201d**), 4.80 (m, 1H, **201d**), 4.23 (d, *J* = 2.7 Hz, 2H, **201b**), 4.13 (s, 2H, **201b**), 3.90 (s, 2H, **201a**), 3.76 (s, 2H, **201a**), 3.48 (dd, *J* = 12.2, 1.5 Hz, 1H, **201c**), 3.36 (dd, *J* = 12.2, 6.0 Hz, 1H, **201c**), 2.42 (s, 3H, **201b,c**), 2.41 (s, 3H, **201a**), 1.76 (s, 3H, **201a**), 1.74 (s, 3H, **201b**), 1.66 (s, 3H, **201a**), 1.05 (s, 3H, **201c**), 1.02 (d, *J* = 1.1 Hz, 1H, **201c**), 0.97 (dd, *J* = 8.8, 4.8 Hz, 1H, **201c**), 0.73 (s, 3H, **201c**).

The characterisation data is in agreement with previously reported.<sup>[282,435,436]</sup>

### General procedure for metal-catalysed alkoxyacylation of enynes **200a** and **200b**

The catalyst (amount indicated) and AgNTf<sub>2</sub> were placed under N<sub>2</sub>, and MeOH (0.5 ml) was added. The mixture was stirred for 5 min. The corresponding enyne (0.1 mmol, 1.0 equiv.) in MeOH (1.0 ml) was added. Stirring at indicated temperature continued for 16-24 h. The reaction mixture was filtered through a pad of Celite and concentrated in *vacuo*. The residue was analysed by <sup>1</sup>H NMR to determine ratio of isomeric products.

### Compound **203a**

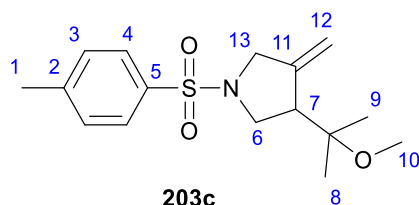


**<sup>1</sup>H NMR** (400 MHz, CDCl<sub>3</sub>) δ 5.04 – 5.01 (m, 1H, 11), 4.98 – 4.95 (m, 1H, 11), 3.72 (s, 3H, 1), 3.71 (s, 3H, 1), 3.18 (s, 3H, 9), 2.93 – 2.80 (m, 3H, 12, 5), 2.54 (ddd, *J* = 13.5, 8.5, 1.7 Hz, 1H,

4), 2.00 (dd,  $J = 13.5, 9.3$  Hz, 1H, 4), 1.17 (s, 3H, 7), 1.11 (s, 3H, 8);  $^{13}\text{C}\{^1\text{H}\}$  NMR (101 MHz,  $\text{CDCl}_3$ )  $\delta$  172.2 (2), 172.1 (2), 148.3 (10), 110.7 (11), 76.9 (6), 58.7 (3), 52.9 (1), 52.8 (1), 49.2 (5), 49.1 (9), 43.5 (12), 36.1 (4), 22.8 (9), 22.3 (8).

The characterisation data is in agreement with previously reported.<sup>[437]</sup>

### Compound 203c

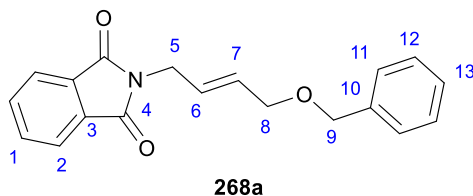


In 1:0.8 mixture of **203c**:**200a**.

$^1\text{H}$  NMR (400 MHz,  $\text{CDCl}_3$ )  $\delta$  7.75 – 7.67 (m, 2H, 4), 7.32 (d,  $J = 8.0$  Hz, 2H, 3), 5.03 (s, 2H, 12), 3.77 (s, 2H, 13), 3.39 (dd,  $J = 10.1, 4.4$  Hz, 1H, 6), 3.26 (m, 1H, 6), 3.09 (s, 3H, 10), 2.82 – 2.76 (m, 1H, 7), 2.42 (s, 3H, 1), 1.11 (s, 3H, 8/9), 1.00 (s, 3H, 8/9).

The characterisation data is in agreement with previously reported.<sup>[438]</sup>

### Compound 268a



$\text{Au}(\text{PPh}_3)\text{Cl}$  (3 mg, 0.007 mmol, 0.05 equiv.) and  $\text{AgNTf}_2$  (3 mg, 0.007 mmol, 0.05 equiv.) were placed under  $\text{N}_2$  and dichloromethane (0.3 ml) was added. The reaction mixture was stirred at 25 °C for 5 min. A solution of allene **267** (25 mg, 0.13 mmol, 1.0 equiv.) in dichloromethane (0.35 ml) was added, followed by benzyl alcohol (0.13 ml, 1.3 mmol, 10.0 equiv.). The reaction was stirred at 25 °C for 22 h, and then filtered through a pad of Celite and concentrated in *vacuo*. Column chromatography with Pet/AcOEt mixtures and dichloromethane as eluents did not allow separation of product from the excess of benzyl alcohol. Purification by column chromatography (PhMe/AcOEt 19:1) yielded **268a** (34 mg, 88%) as a white solid.

$^1\text{H}$  NMR (400 MHz,  $\text{CDCl}_3$ )  $\delta$  7.87 – 7.81 (m, 2H, 2), 7.73 – 7.68 (m, 2H, 1), 7.38 – 7.29 (m, 4H, 11, 12), 7.28 – 7.22 (m, 1H, 13), 5.89 – 5.76 (m, 2H, 6, 7), 4.48 (s, 2H, 9), 4.34 – 4.27 (m, 2H, 5), 4.00 (m, 2H, 8);  $^{13}\text{C}\{^1\text{H}\}$  NMR (101 MHz,  $\text{CDCl}_3$ )  $\delta$  168.0 (4), 138.2 (10), 134.1 (1),

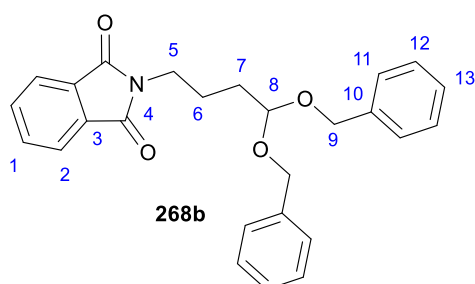
132.2 (7), 130.4 (3), 128.5 (2 x  $C_{Ph-H}$ ), 127.8 (2 x  $C_{Ph-H}$ ), 127.7 (13), 126.2 (6), 123.4 (2), 72.3 (9), 69.8 (8), 39.1 (5); **HRMS** (ASAP) ( $C_{19}H_{18}NO_3$ )  $[M+H]^+$ : caclcd: 308.1287; found: 308.1288.

The characterisation data reported for the (*Z*)-isomer of **268a** was not in agreement, hence the structure of (*E*)-isomer proposed.<sup>[439]</sup>

### General procedure for metal-catalysed addition to allenes

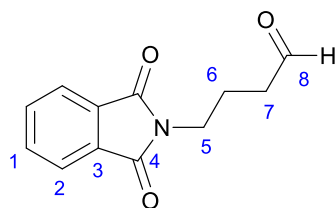
The catalyst (0.05 equiv.) and  $AgNTf_2$  (amount indicated) were placed under  $N_2$ , and dichloromethane (0.3 ml) was added. The reaction mixture was stirred at 25 °C for 5 min. A solution of allene **267** (25 mg, 0.13 mmol, 1.0 equiv.) in dichloromethane (0.35 ml) was added, followed by benzyl alcohol (0.13 ml, 1.3 mmol, 10.0 equiv.). The reaction was stirred at 25 °C for the indicated amount of time, then filtered through a pad of Celite and concentrated in *vacuo*. The ratio of products and conversions were calculated based on the  $^1H$  NMR of the crude reaction mixture or the products were isolated by column chromatography (PhMe/AcOEt 19:1).

### Compound 268b



$^1H$  NMR (500 MHz,  $CDCl_3$ )  $\delta$  7.84 (dd,  $J = 5.4, 3.0$  Hz, 2H, 2), 7.71 (dd,  $J = 5.4, 3.0$  Hz, 2H, 1), 7.34 (d,  $J = 4.4$  Hz, 8H, 11, 12), 7.31 – 7.26 (m, 2H, 13), 4.78 (t,  $J = 4.5$  Hz, 1H, 8), 4.66 (d,  $J = 11.7$  Hz, 2H, 9), 4.56 (d,  $J = 11.7$  Hz, 2H, 9), 3.72 (t,  $J = 6.5$  Hz, 2H, 5), 1.85 – 1.78 (m, 4H, 6, 7);  $^{13}C\{^1H\}$  NMR (126 MHz,  $CDCl_3$ )  $\delta$  168.5 (4), 138.2 (10), 134.0 (1), 132.2 (3), 128.5 (2 x  $C_{Ph-H}$ ), 127.9 (2 x  $C_{Ph-H}$ ), 127.7 (13), 123.3 (2), 101.8 (8), 67.5 (9), 37.8 (5), 30.9 (7), 24.1 (6); **HRMS** (NSI) ( $C_{26}H_{29}N_2O_4$ )  $[M+NH_4]^+$ : caclcd: 433.2122; found: 433.2116; a fragment from C(8)-O bond cleavage was also observed: ( $C_{19}H_{18}NO_3$ )  $[M-OBn]^+$ : caclcd: 308.1281; found: 308.1283.

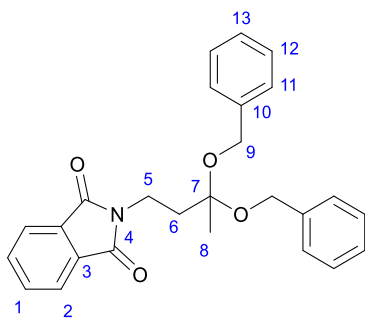


**Compound 269a****269a**

In 36.5:1.13:1.0 mixture of **BnOH**:**268b**:**269a**.

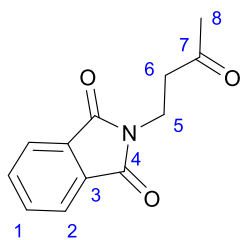
$^1\text{H NMR}$  (500 MHz,  $\text{CDCl}_3$ )  $\delta$  9.77 (s, 1H, -COH), 7.84 (m, 2H, 2), 7.75 – 7.69 (m, 2H, 1), 3.74 (t,  $J = 7.0$  Hz, 1H, 5), 2.54 (t,  $J = 7.0$  Hz, 1H, 7), 2.02 (p,  $J = 7.0$  Hz, 1H, 6).

The characterisation data is in agreement with previously reported.<sup>[440]</sup>

**Compound 268c****268c**

Product **268c** not stable enough for full characterisation and hydrolyses to **269b**.

$^1\text{H NMR}$  (500 MHz,  $\text{CDCl}_3$ )  $\delta$  7.87 – 7.82 (m, 2H, 2), 7.74 – 7.69 (m, 2H, 1), 7.40 – 7.34 (m, 8H, 11, 12), 7.30 (m, 2H, 13), 4.71 (s, 4H, 9), 3.96 (t,  $J = 7.3$  Hz, 2H, 5), 2.88 (t,  $J = 7.3$  Hz, 2H, 6), 1.25 (s, 3H, 8).

**Compound 269b****269b**

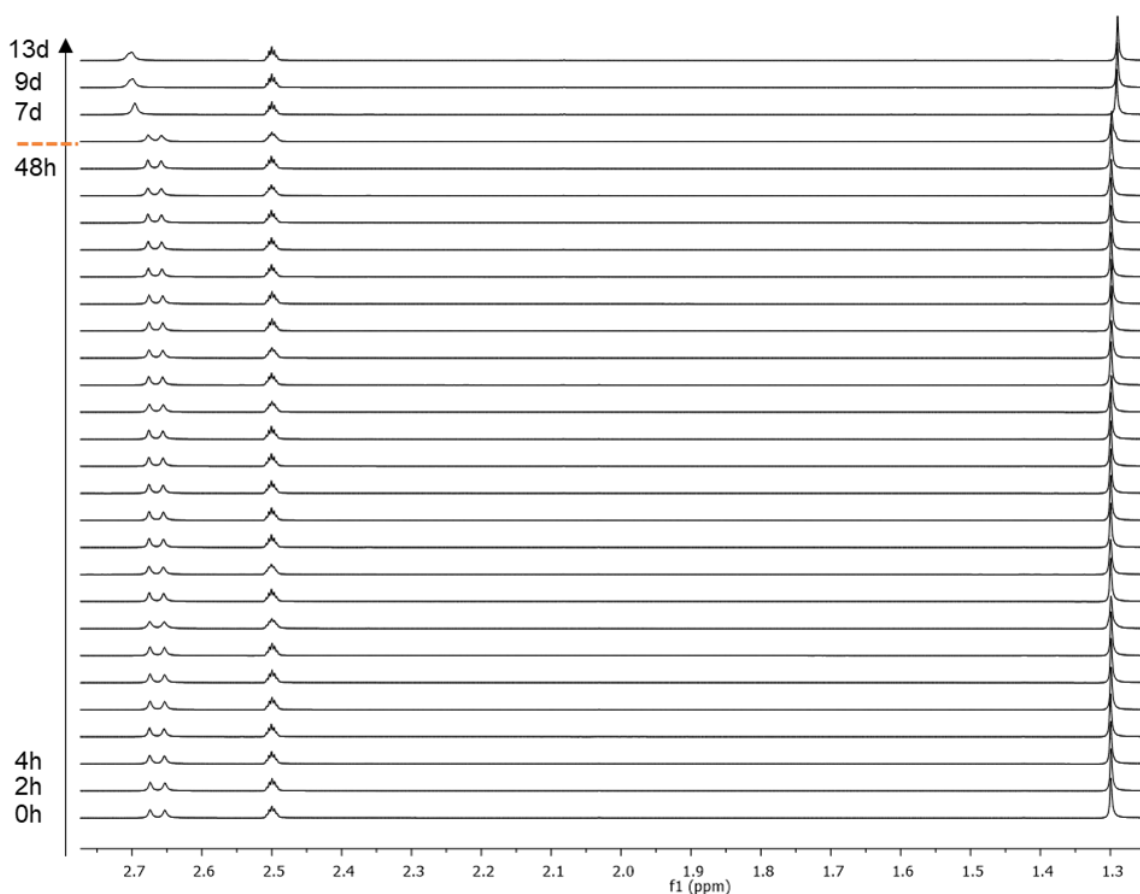
$^1\text{H NMR}$  (500 MHz,  $\text{CDCl}_3$ )  $\delta$  7.86 – 7.82 (m, 2H, 2), 7.74 – 7.69 (m, 2H, 1), 3.96 (t,  $J = 7.4$  Hz, 2H, 5), 2.88 (t,  $J = 7.4$  Hz, 2H, 6), 2.19 (s, 3H, 8).

The characterisation data is in agreement with previously reported.<sup>[441]</sup>

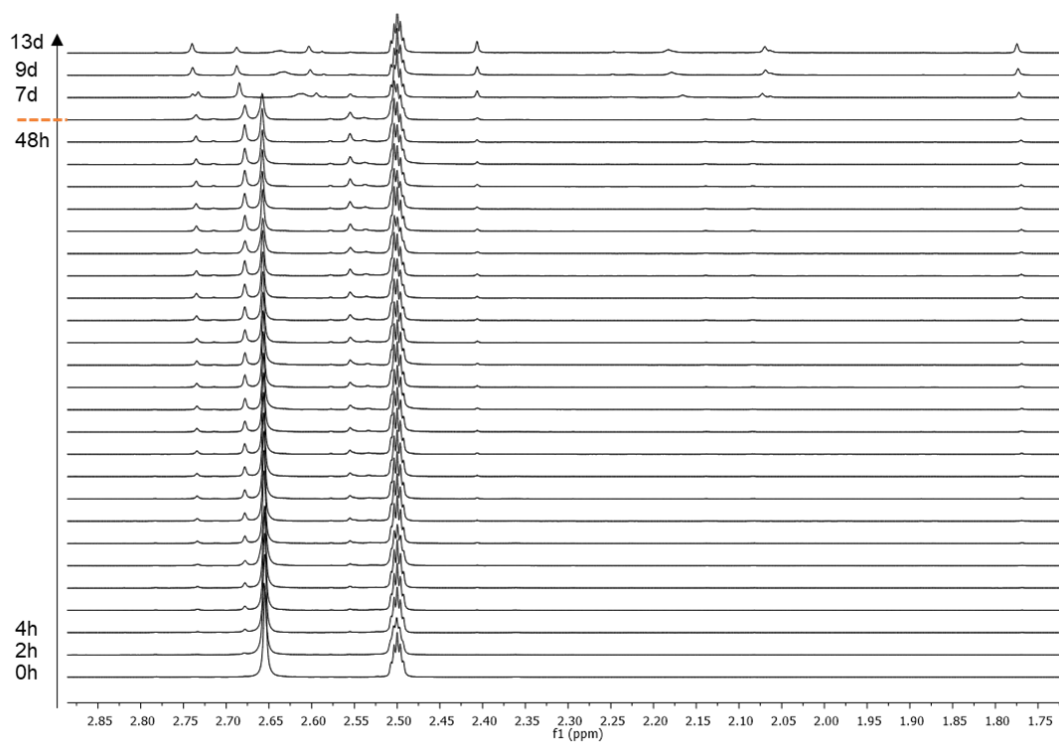
## Chapter VI - Stability studies

Samples of **176** (0.4 ml, 0.036 mmol/ml), **175** (0.4 ml, 0.035 mmol/ml), **195** (0.5 ml, 0.027 mmol/ml) and **193** (0.5 ml, 0.24 mmol/ml) in  $\text{DMSO-d}_6$  were submitted to a series of  $^1\text{H NMR}$  experiments at 2 h intervals for 48 h, then were collected once every 2-3 days for 12-13 days since the initial sample preparation.

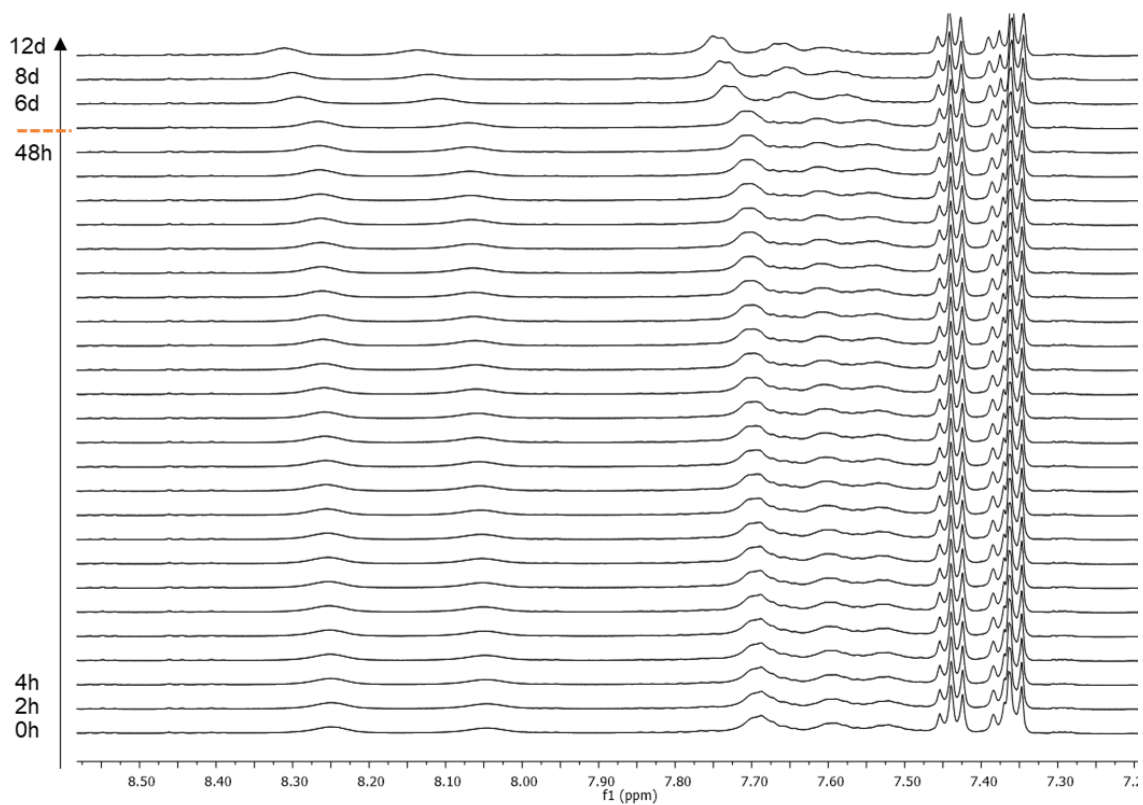
### a) Complex **176**



**Figure 70** Aliphatic region of the  $^1\text{H NMR}$  spectrum of **176** recorded in the space of 13 days.

b) Complex **175**

**Figure 71** Aliphatic region of the  $^1\text{H}$  NMR spectrum of **175** recorded in the space of 13 days.

c) Complex **195**

**Figure 72** Aromatic region of the  $^1\text{H}$  NMR spectrum of **195** recorded in the space of 12 days.

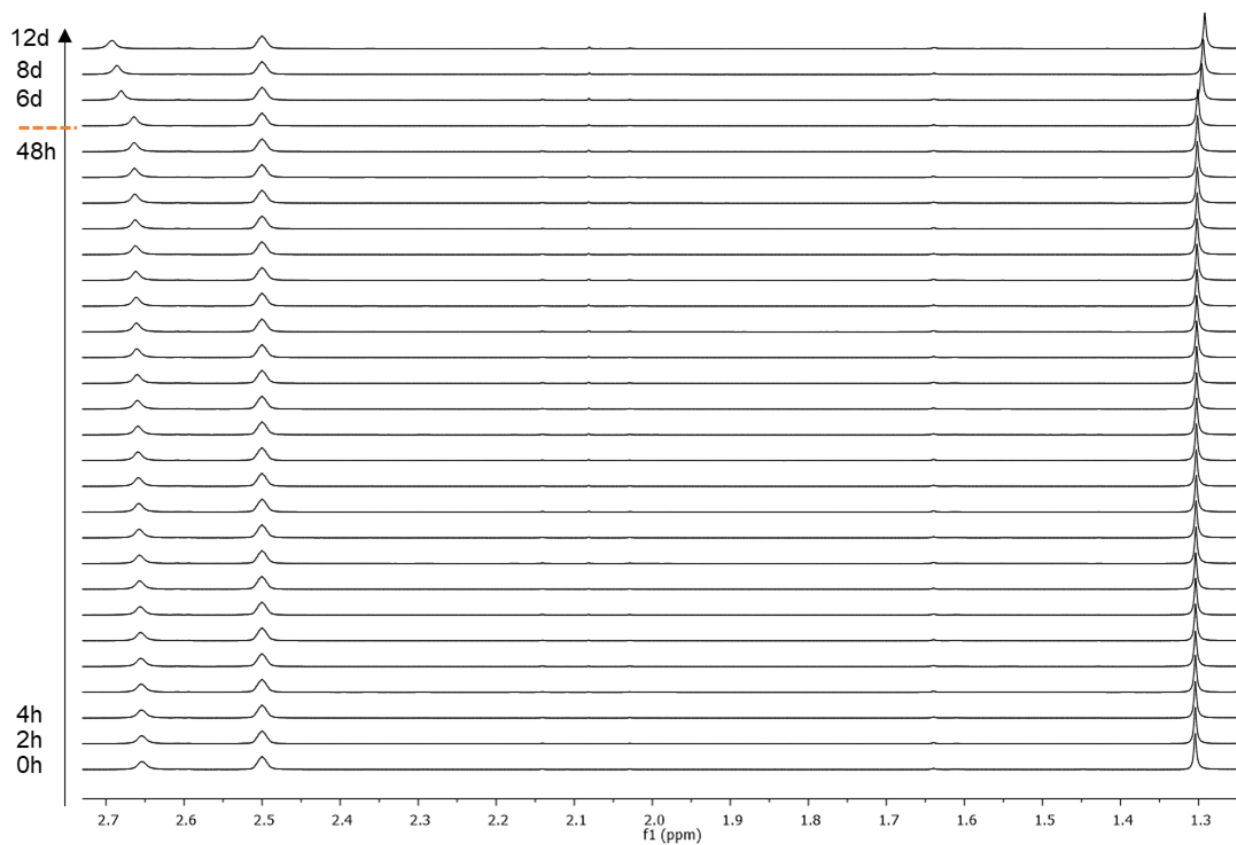


**Figure 73** Aliphatic region of the  $^1\text{H}$  NMR spectrum of **195** recorded in the space of 12 days.

d) Complex **193**

Ratio of species in solution was calculated based on integration of singlet peaks at 2.60 ppm (**193**), 2.56 ppm (**194**), 2.40 ppm (**286a**), 2.37 ppm (**286b**), 2.32 ppm (**286c**).

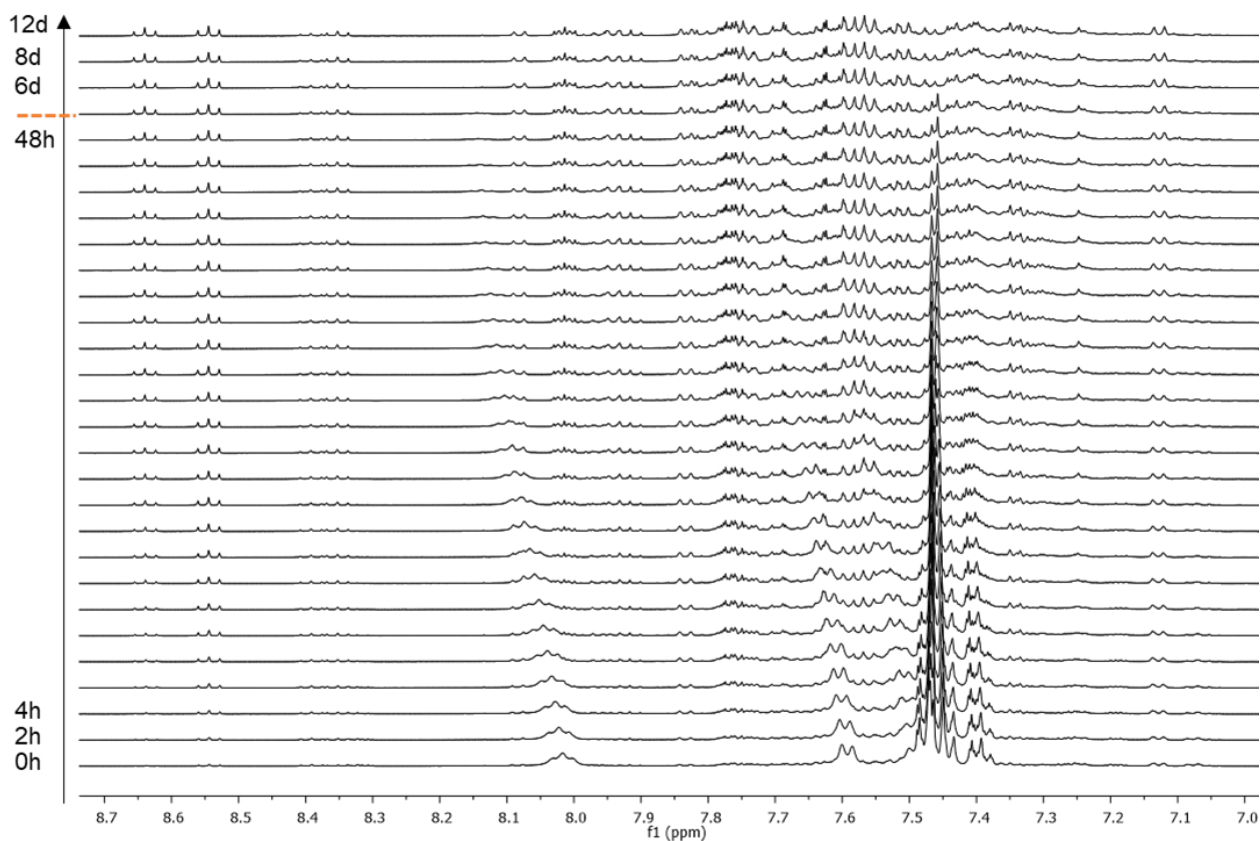


**Figure 74** Aromatic region of the  $^1\text{H}$  NMR spectrum of **193** recorded in the space of 12 days.

## Chapter VI - Antibacterial and antifungal assays

Experimental details of antibacterial and antifungal assays provided by our collaborators in CO-ADD, University of Queensland, Australia can be found in Appendix D and are presented as received.

## Chapter VI - Anticancer assays

### Cell culture, passage and count

MDA-MB-231 human breast adenocarcinoma cells were kindly provided by Dr Maria J. Marin group in the School of Chemistry, UEA. The cells were routinely cultured in high glucose DMEM phenol red-free medium supplemented with L-glutamine (1 %), FBS (10 %) and sodium pyruvate (1 mM).

MDA-MB-231 cells were defrosted by rapidly warming of two cryo tubes containing 1 ml of the cells each in a freezing medium, consisting of 9:1 complete cell culture medium and culture grade DMSO mixture, in a water bath at 37 °C. The cells were transferred to a centrifuge tube containing 8 ml of complete cell culture medium. They were centrifuged at 21 °C at 1,000 relative centrifugal force (rcf) for 5 min. Following centrifugation, the supernatant was

discarded and the pellet containing the cells was resuspended in the complete cell culture medium (12 ml) and transferred to a 75 cm<sup>2</sup> Nunc Easy flask. The cells were subcultured (1:4 – 1:12) every 3-5 days, when they reached near confluence in the 75 cm<sup>2</sup> flasks. The culture medium was discarded and the cells were washed with PBS-B buffer (5 ml). Phosphate buffered saline for biological experiments (PBS-B) was prepared by dissolving 10 PBS tablets in 1 l of Milli-Q water, followed by sterilisation by autoclaving. The cells were dislodged from the flask's bottom by addition of 5 ml of 0.25% trypsin-EDTA solution and incubation for 5 min at 37 °C under a 5 % CO<sub>2</sub> atmosphere (trypsination). After that time the culture medium (5 ml) was added and then removed by centrifugation at 800 rcf for 5 min at 21 °C. The pellet containing the cells was resuspended in the complete cell culture medium (7 ml) and transferred to two 75 cm<sup>2</sup> Nunc Easy flasks (3 ml of cells' solution in each, completed with 9 ml of complete culture medium to a total of 12 ml in each flask) .

Cell count was achieved by trypsination and resuspension of the cells in 3 ml of complete culture medium. The aliquot of cells' solution (20 µl) was pipetted inside the chamber of the Neubauer haemocytometer previously cleaned with 70% ethanol and covered with a coverslip. The gridlines of the haemocytometer were observed under the microscope. The cells in the four corner squares (consisting 16 squares each) were counted with a hand tally counter. The average of the four sets was then multiplied by 10<sup>4</sup> to give the final result in cells per ml (cells/ml).

### **Freezing for long-term storage**

MDA-MB-231 cells were trypsinised and resuspended in a 10.5 ml of freezing medium (9:1 complete culture medium and DMSO of molecular biology grade). The cell suspension was aliquoted in 1.8 ml Nunc cryo tubes (1 ml per tube). The cryo tubes were placed in a cryogenic freezing container previously filled with isopropanol and stored at - 80 °C overnight. The following day, the cryo tubes were removed from the cryogenic container and stored in a sample box in liquid nitrogen.

### ***In vitro* chemosensitivity studies**

Stock solutions of bis(pyridyl)allenes **97a-b** and allene-derived complexes (20 mM) in DMSO (molecular biology grade) were prepared and further diluted with complete culture medium to obtain a range of desired concentrations. MDA-MB-231 cells were washed with PBS-B, trypsinated and counted. The cell suspension of concentration of 2 x 10<sup>4</sup> cell/ml was prepared and used to seed a number of 96-well round bottom plates. Black bottom plates were used for CellTiter-Blue® assay and transparent plates were used for the MTT assay. Each well was filled with 100 µl of cell suspension (2000 cells/well). The plates were incubated for 24 h at 37 °C at 5% CO<sub>2</sub>. After that time, 100 µl of solution of the drug in complete culture medium was

added to each experimental well giving a total of 200  $\mu\text{l}$  per well. Control wells were treated with DMSO solution alone. Additionally, controls not containing cells were added (DMSO solution in complete culture medium, 200  $\mu\text{l}$ ). Drug solutions were added so that the final DMSO concentration did not exceed 0.5% (v/v). The plates were incubated for 24 h at 37  $^{\circ}\text{C}$  at 5%  $\text{CO}_2$ .

### CellTiter-Blue® (CTB) assay

After the incubation with the corresponding compound, 20  $\mu\text{l}$  of CTB reagent was added to each well and the plate was shaken for 10 s. The plate was returned to the incubator (37  $^{\circ}\text{C}$ , 5%  $\text{CO}_2$ ) for 4 h. Fluorescence emission was the measured (excitation – 561 nm, emission – 594 nm). Background fluorescence was corrected by subtracting the average value of fluorescence emission of cell-free wells (media controls).

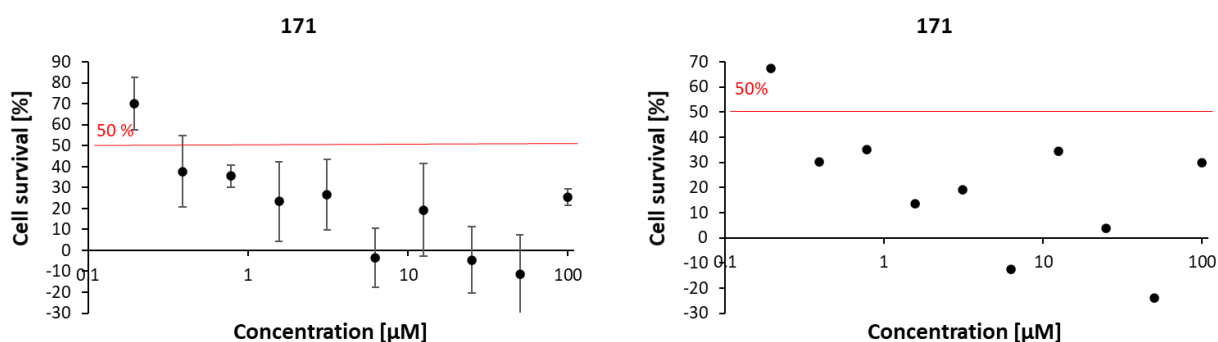
### MTT assay

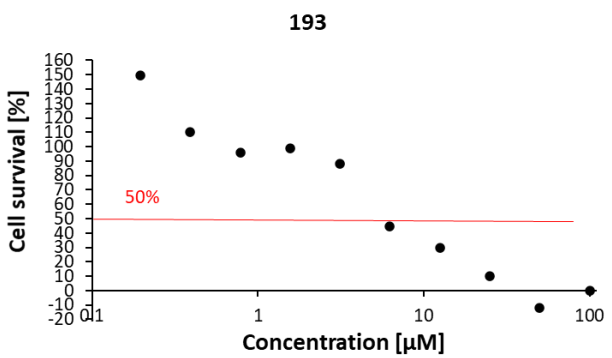
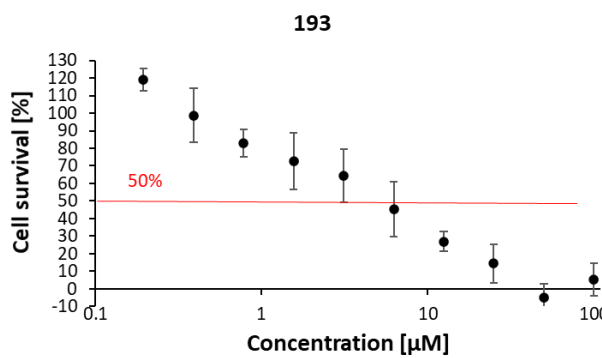
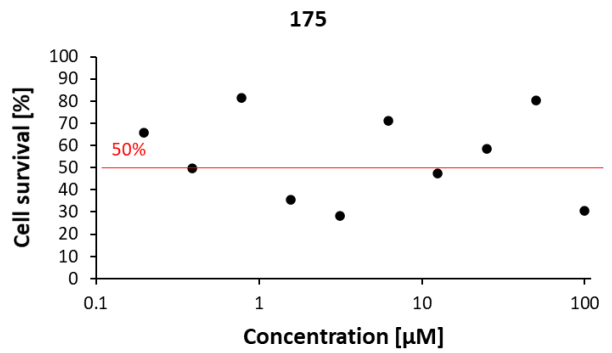
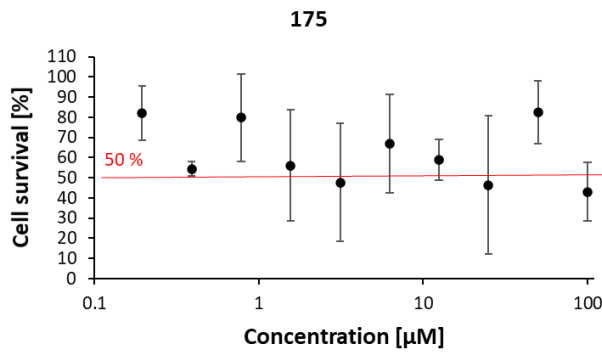
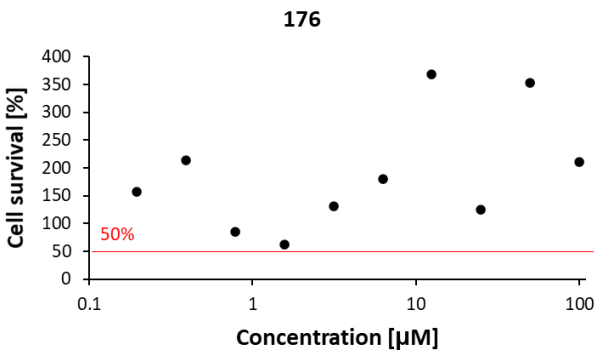
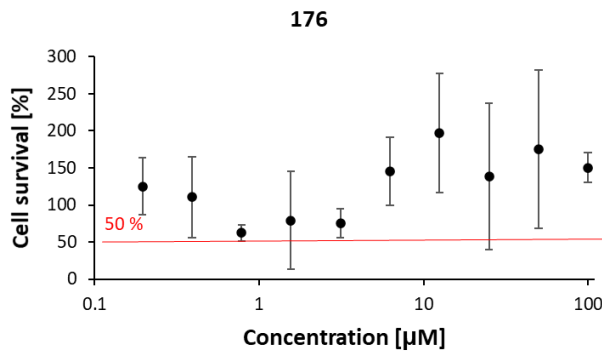
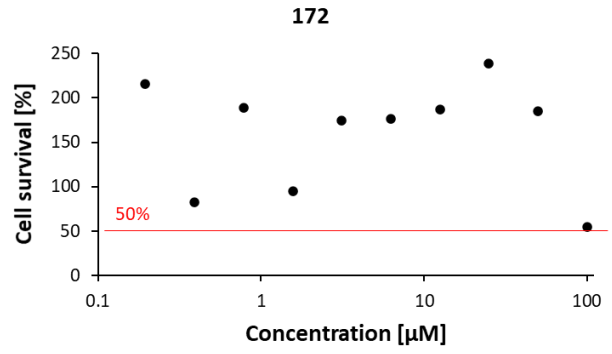
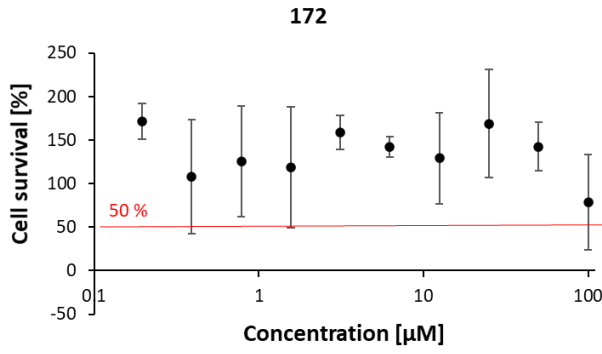
After the incubation with the corresponding compound, 20  $\mu\text{l}$  of a yellow MTT reagent (5mg/ml in PBS-B buffer) was added to each well. The plate was returned to the incubator (37  $^{\circ}\text{C}$ , 5%  $\text{CO}_2$ ) for 3.5 h. The solution was then removed from each well with a pipette. 150  $\mu\text{l}$  of DMSO (molecular biology grade) was added to each well and the plate was shaken resulting in colourless to bright pink solutions. The absorbance intensity was measured at 560 nm. Background absorbance was corrected by subtracting the average value of absorbance intensity of cell-free wells (media controls).

Cell survival was calculated as a percentage of non-treated cells. The half maximal inhibitory concentration ( $\text{IC}_{50}$ ) values were determined from the plots of % cell survival vs concentration. For results presented in the Figure 78 to Figure 81 statistical significance between means was determined using a two-tailed Student's t-test. P values < 0.05 were considered significant, data points with P values > 0.05 are marked with red asterisk.

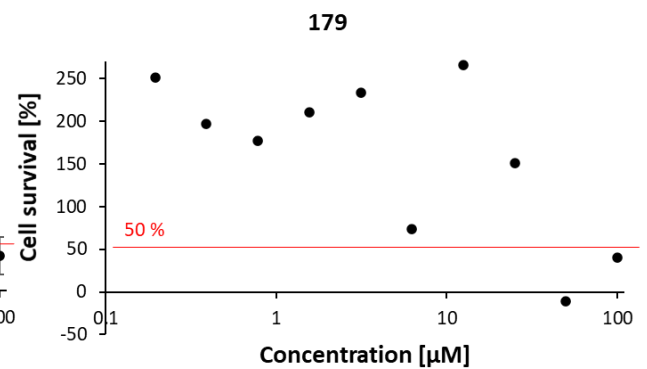
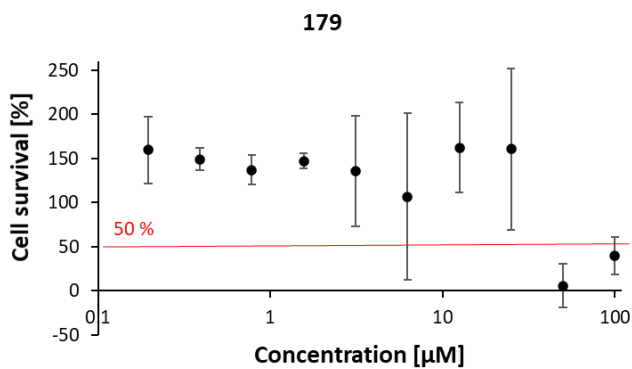
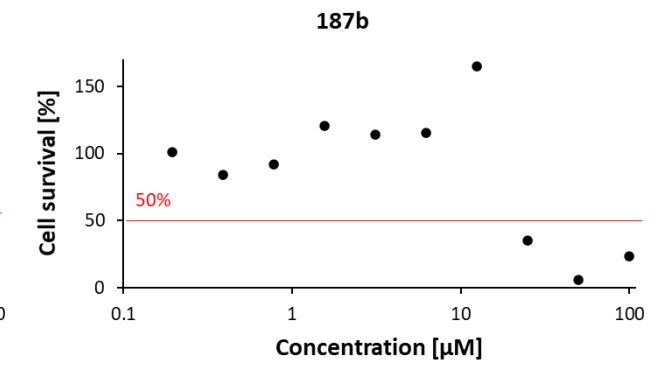
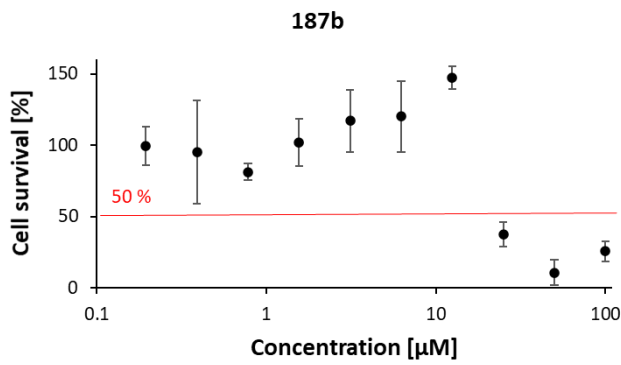
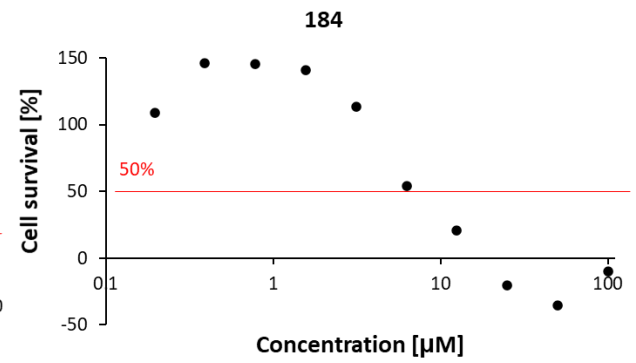
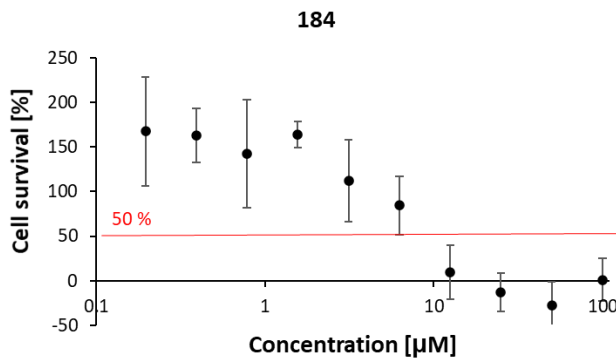
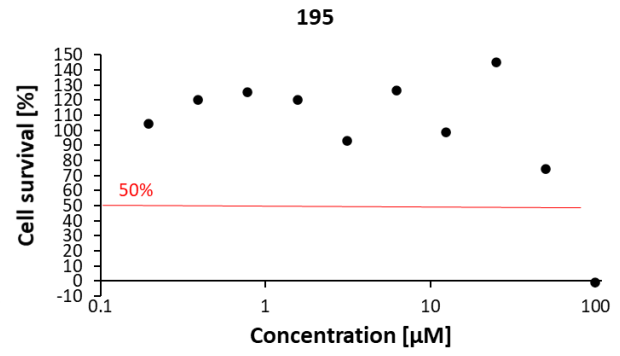
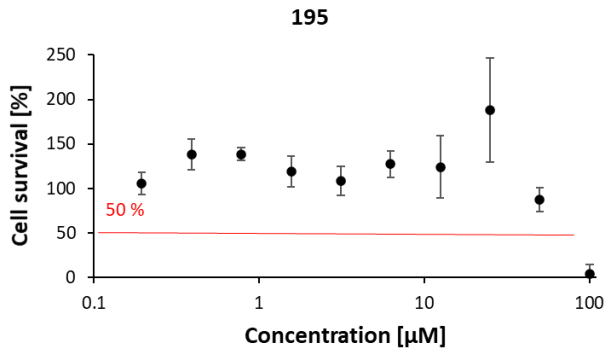
#### a) CellTiter-Blue® (CTB) assay – full library (Figure 75)

The experiment was carried out in technical triplicate.









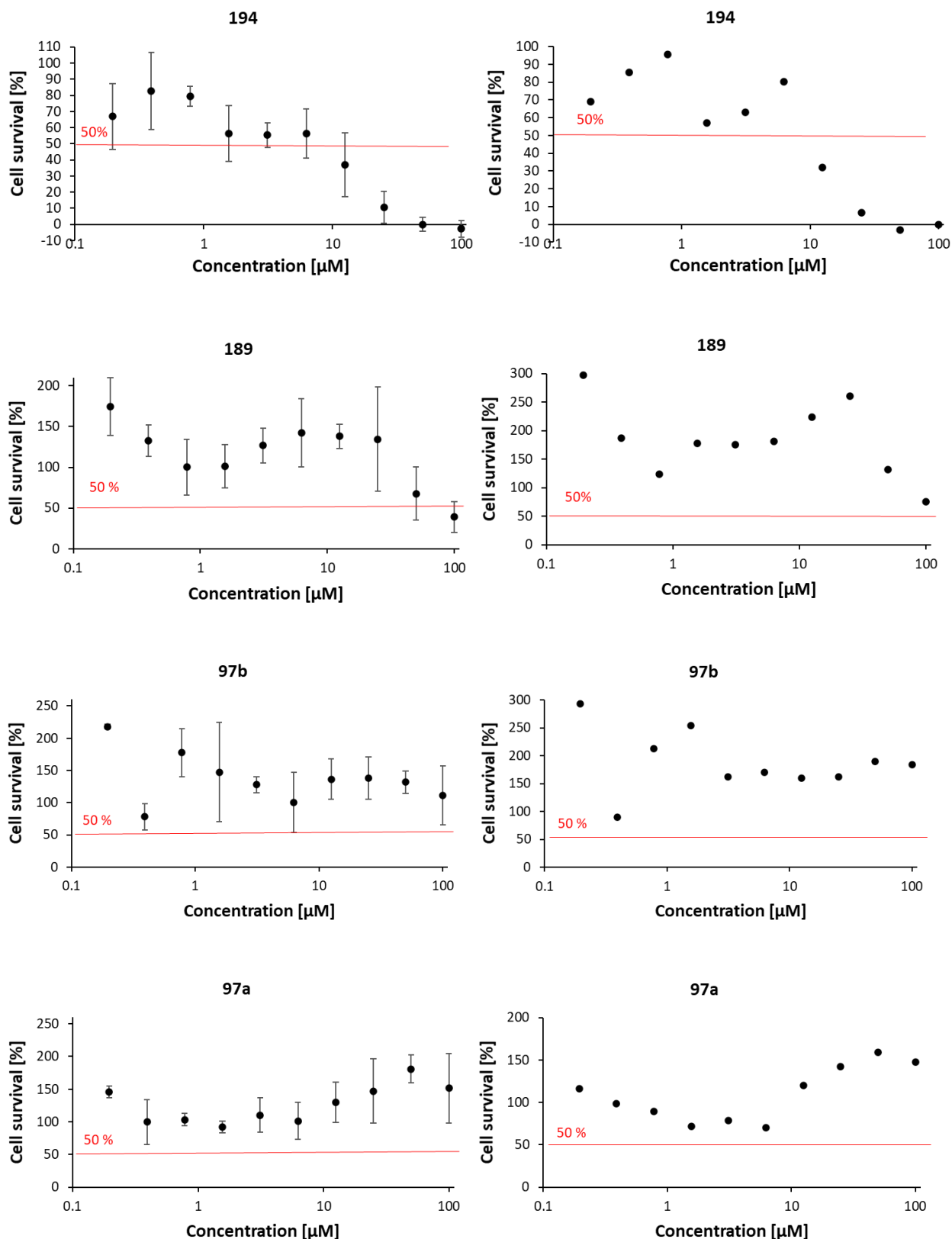


**Figure 75** CTB assay results for the entire library of allene-derived metal complexes and bis(pyridyl)allene ligands in the 0.19 – 100  $\mu\text{M}$  range (left column: data from the technical triplicate repeats, right column: data from the duplicate technical repeats).

b) CellTiter-Blue® (CTB) assay – selected complexes (**193**, **194**, **184**, **171**, Figure 76)

The experiment was carried out in technical triplicate and experimental duplicate.

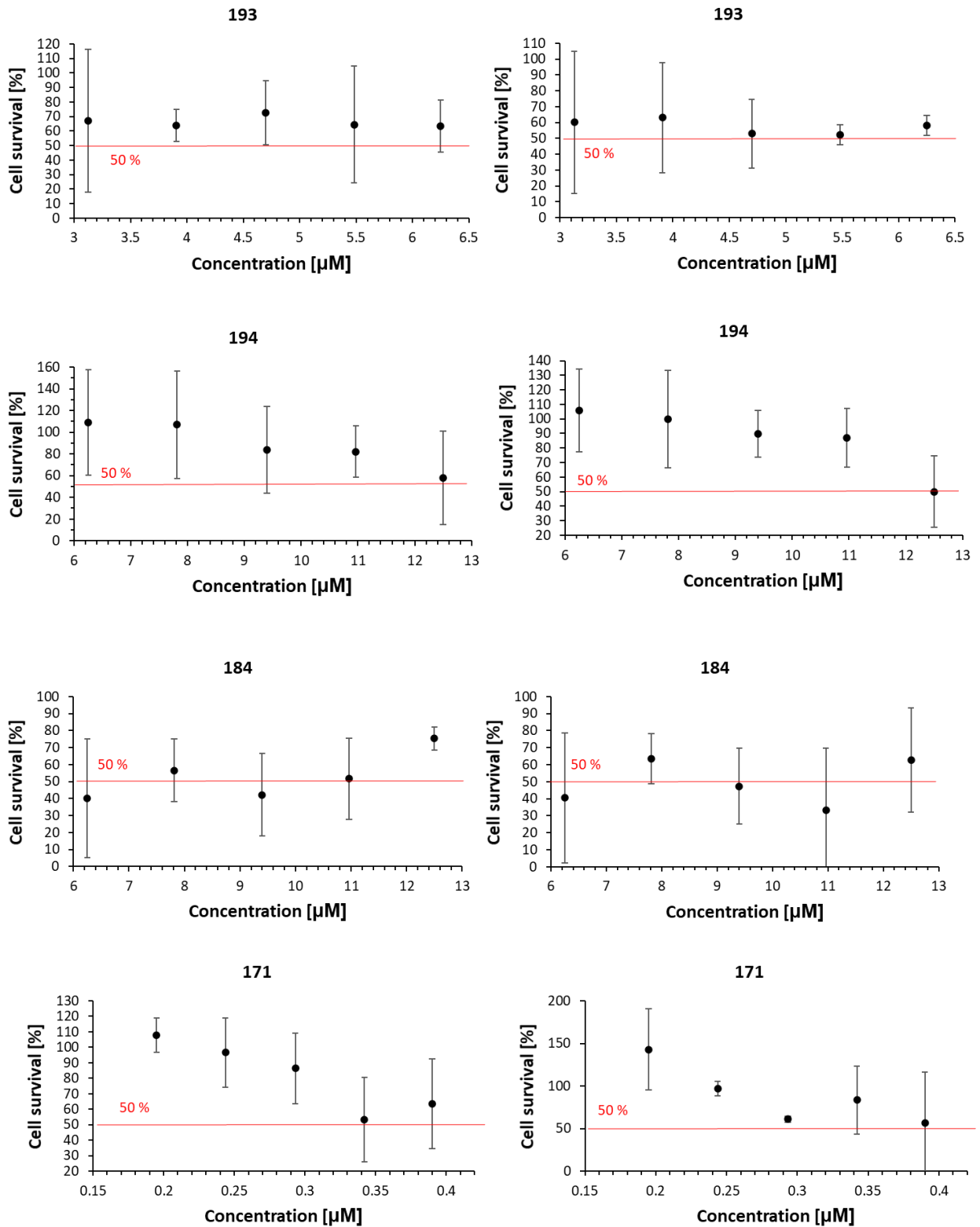


**Figure 76** CTB assay results for complexes **193**, **194**, **184** and **171** at narrowed concentration range (left column: first experimental repeat, right column: second experimental repeat).

c) MTT assay - selected complexes at 0.19 – 100  $\mu\text{M}$  range (**193**, **194**, **184**, **171**, Figure 77)

The experiment was carried out in technical triplicate.

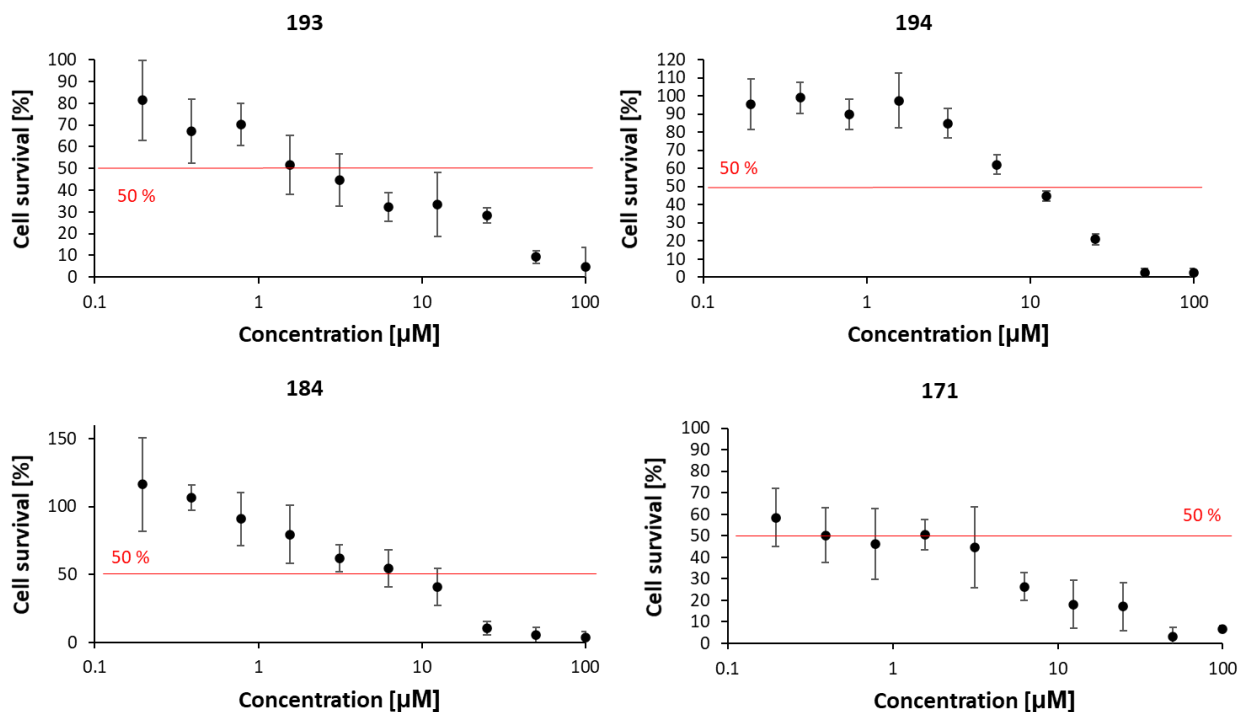


**Figure 77** MTT assay results for complexes **193**, **194**, **184** and **171** at 0.19 – 100  $\mu\text{M}$  concentration range.

d) MTT assay - selected complexes at narrowed concentration range (**194**, **193**, **184**, **171** Figure 78 to Figure 81)

The experiment was carried out in technical and experimental triplicate.

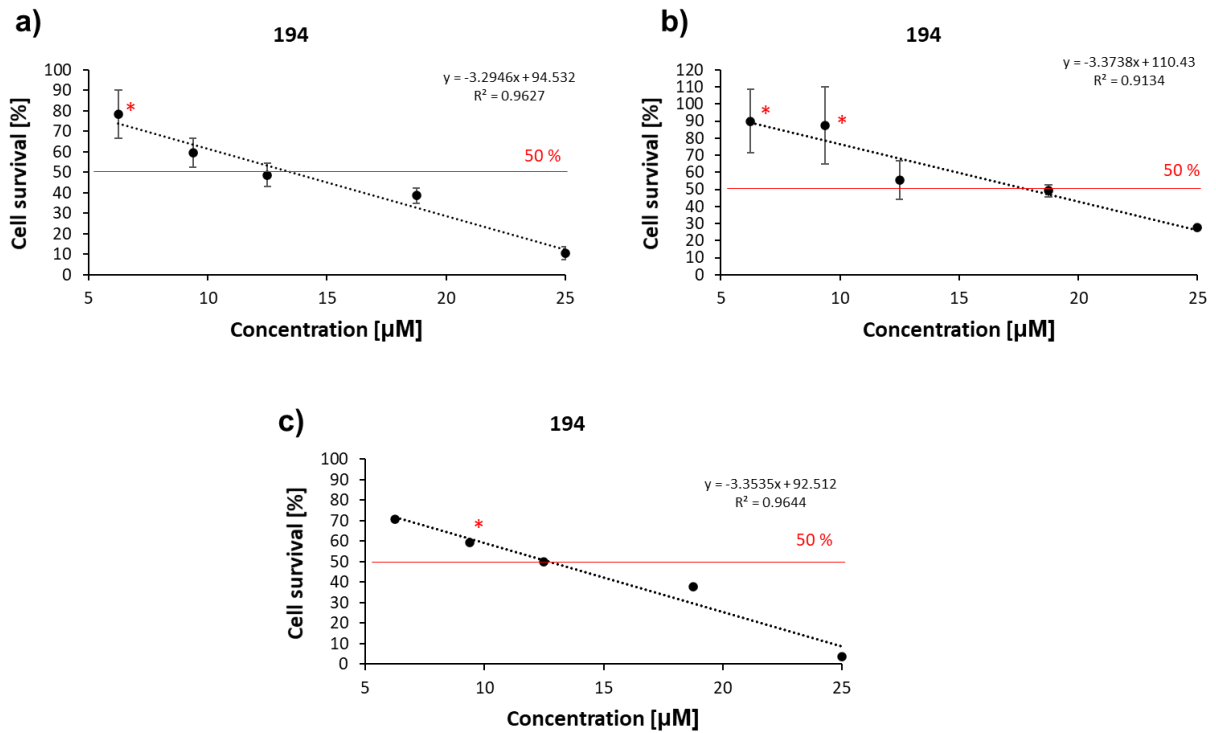


**Figure 78** MTT assay results for complexes **194** at narrowed concentration range: a) first experimental repeat; b) second experimental repeat; c) third experimental repeat (from technical duplicate).

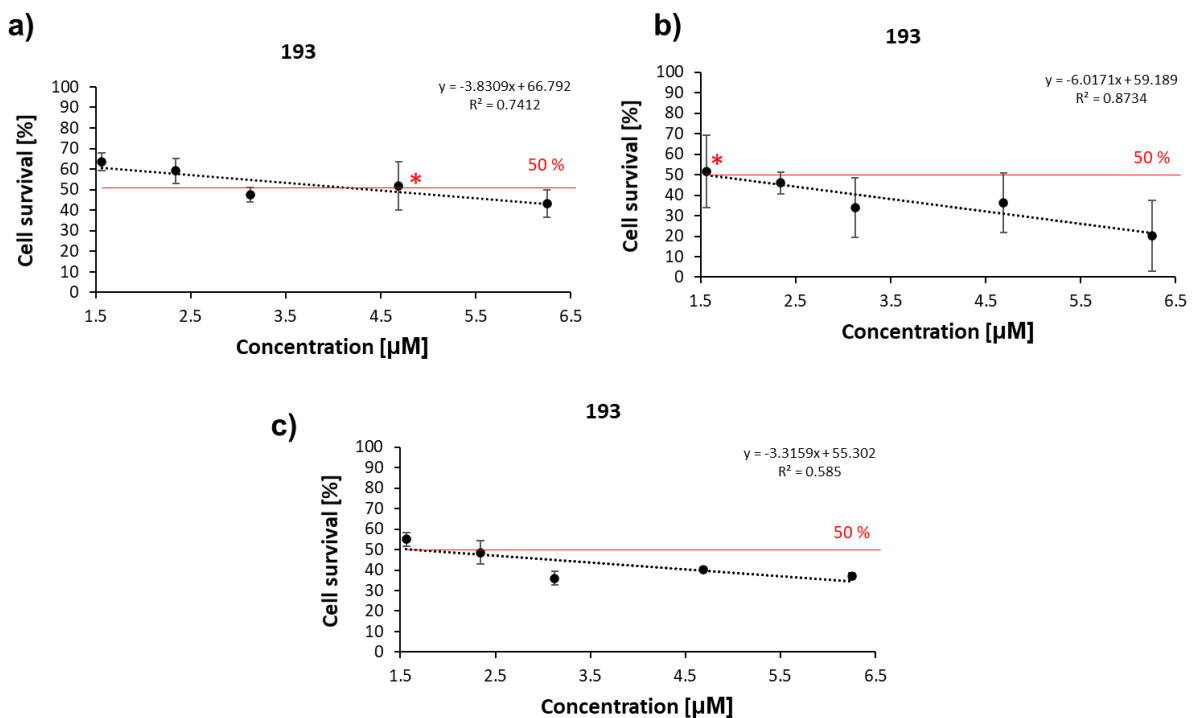


**Figure 79** MTT assay results for complexes **193** at narrowed concentration range: a) first experimental repeat; b) second experimental repeat; c) third experimental repeat (some data points from technical duplicate).

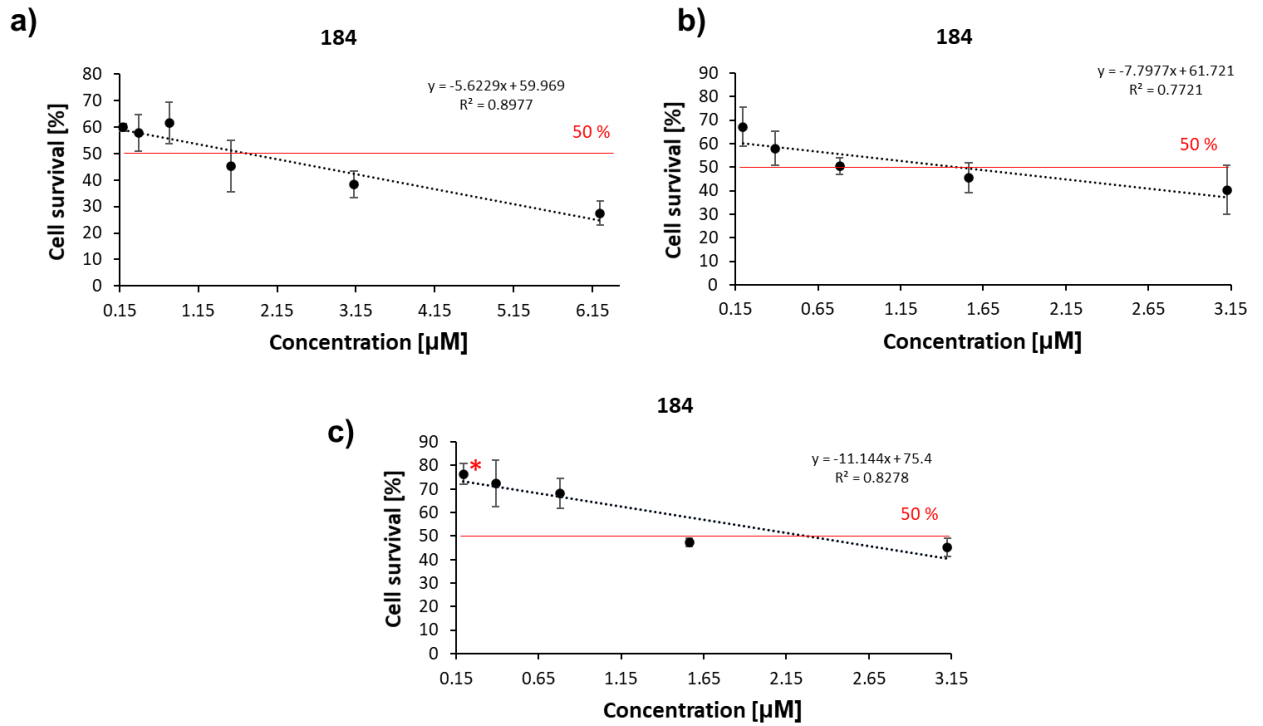


**Figure 80** MTT assay results for complexes **184** at narrowed concentration range: a) first experimental repeat; b) second experimental repeat; c) third experimental repeat.

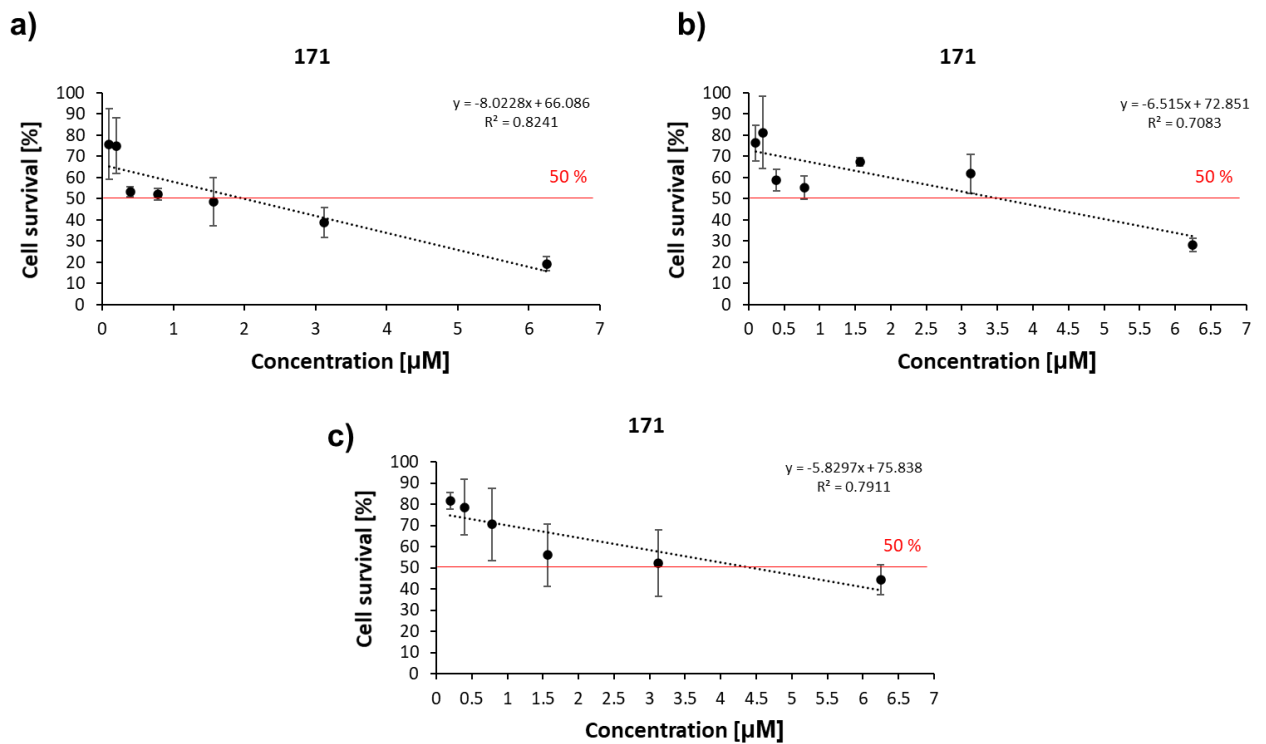


**Figure 81** MTT assay results for complexes **171** at narrowed concentration range: a) first experimental repeat; b) second experimental repeat; c) third experimental repeat.

## Chapter VI - DNA studies

All experimental data presented in this section was provided by Waller's group (while still in the School of Pharmacy at UEA, currently at UCL).

### General Experimental

Custom oligonucleotides (Table 23) were purchased from Eurogentec and were HPLC purified. Solid DNA samples were initially dissolved to give ~100  $\mu\text{M}$  for labelled and 1 mM for unlabelled oligonucleotides stock solutions in ultrapure water (18.2  $\text{M}\Omega\cdot\text{cm}$ ); further dilutions were carried out in the respective sodium cacodylate buffer. The oligonucleotides were dual-labelled for FRET: the donor fluorophore 6 carboxyfluorescein (FAM) was attached at the 5' end and the acceptor fluorophore 6 carboxytetramethylrhodamine (TAMRA) to the 3' end. Samples were prepared to give 400 nM oligonucleotide in 10 mM sodium cacodylate buffer at the respective transitional pH for each sequence. Samples were thermally annealed by placing in a heat block at 95°C for 5 minutes and then allowed to cool slowly to room temperature overnight.

### FRET-melting experiments

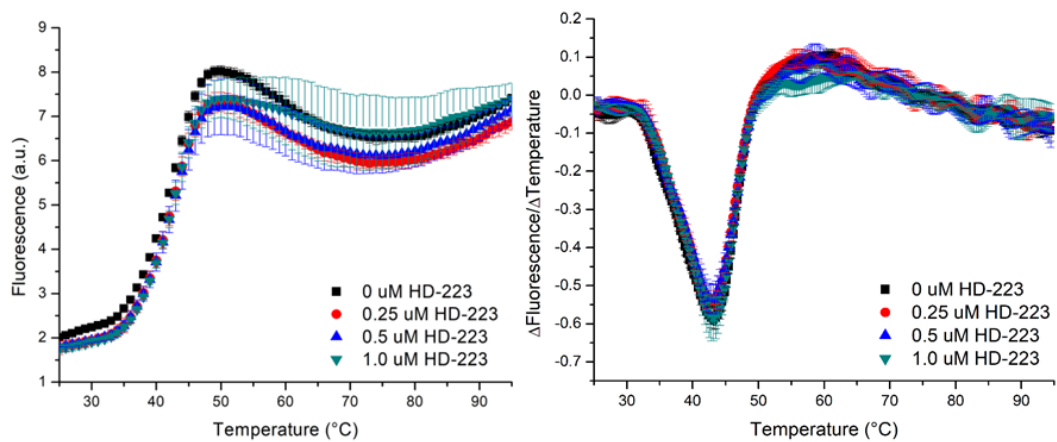
**Table 23** Oligonucleotide sequences used for FRET melting experiments. The double stranded (DS) sequence consists of two complementary 10 base sequences linked by an 18 unit hexaethylene glycol (HEG) polymer.

Name	Sequence modification-5' → 3'-modification
hTeloC	FAM-TAACCCCTAACCCCTAACCCCTAACCC-TAMRA
DAP	FAM-CCCCCGCCCCCGCCCCCGCCCCCGCCCC-TAMRA
hif-1- $\alpha$	FAM-CGCGCTCCCGCCCCCTCTCCCCTCCCGCGC-TAMRA
DS	FAM-TATAGCTATA-HEG(18)-TATAGCTATA-TAMRA
hTeloG	FAM-GGGTTAGGGTTAGGGTTAGGG-TAMRA

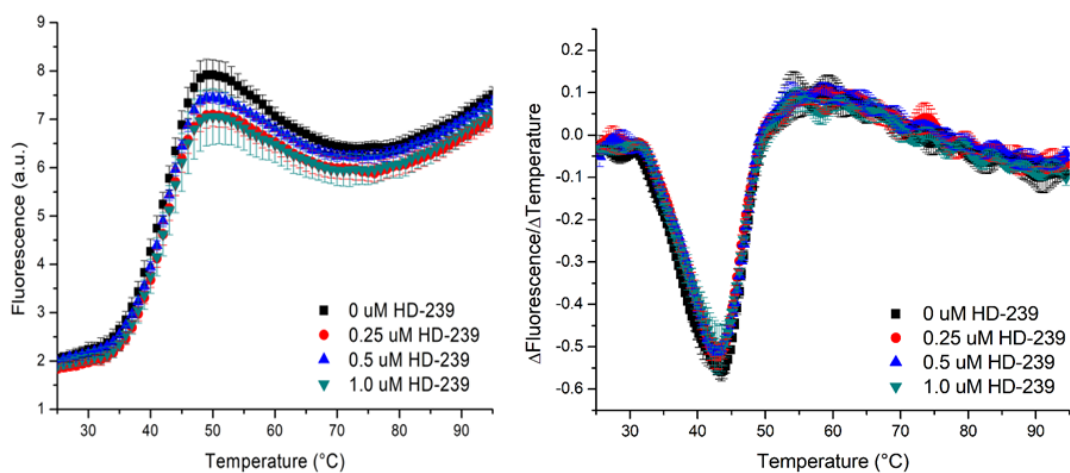
Strip-tubes (QIAGEN) were prepared by aliquoting 10  $\mu\text{L}$  of the annealed DNA followed by addition of 10  $\mu\text{L}$  of solutions of the complexes in buffer at different concentrations (pH values given). This gave a final volume of 20  $\mu\text{L}$  with 200 nM DNA and up to 5 equivalents (1  $\mu\text{M}$ ) of complex across the samples. Control samples for each run were prepared with the same quantity of DMSO with the DNA in buffer. Fluorescence melting curves were acquired in a QIAGEN Rotor Gene Q series PCR machine. Samples were held at 25°C for 5 minutes then ramped to 95 °C in increments of 1 °C, holding the temperature at each step for 1 minute. Measurements were made with excitation at 483 nm and detection at 533 nm. Experiments were performed in triplicate with final analysis of the data carried out using QIAGEN Rotor Gene Q series software and Origin or Excel.  $T_m$  values were determined using the first derivative of the melting curves.

a) carbene-type complexes (Figure 82 to Figure 86)

a) Complex **184** (HD-223)

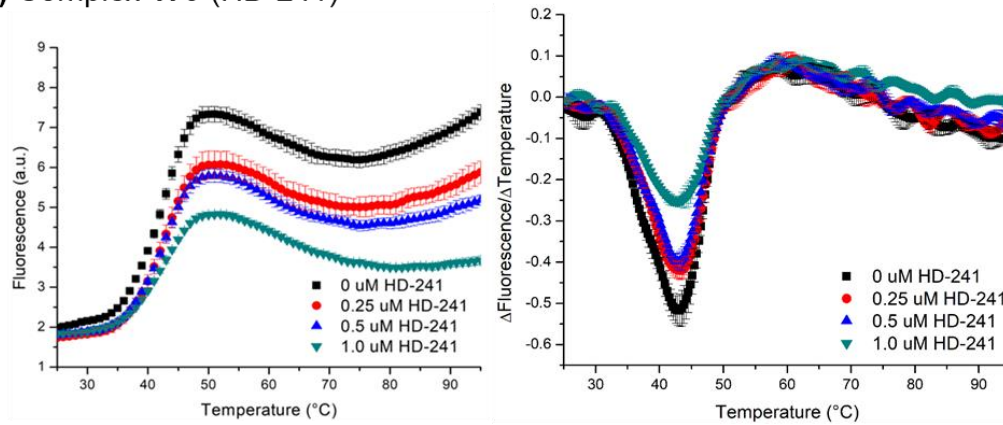


b) Complex **187** (as a mixture of **187a**:**187b**, HD-239)

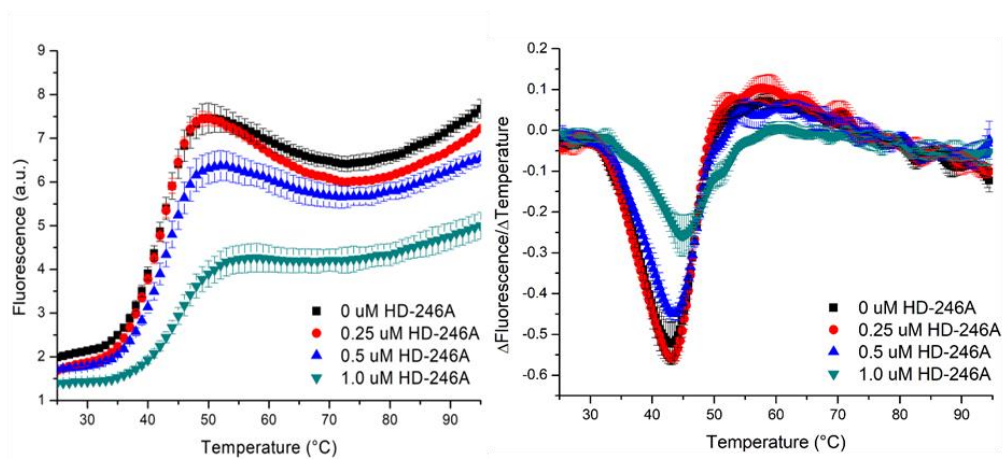




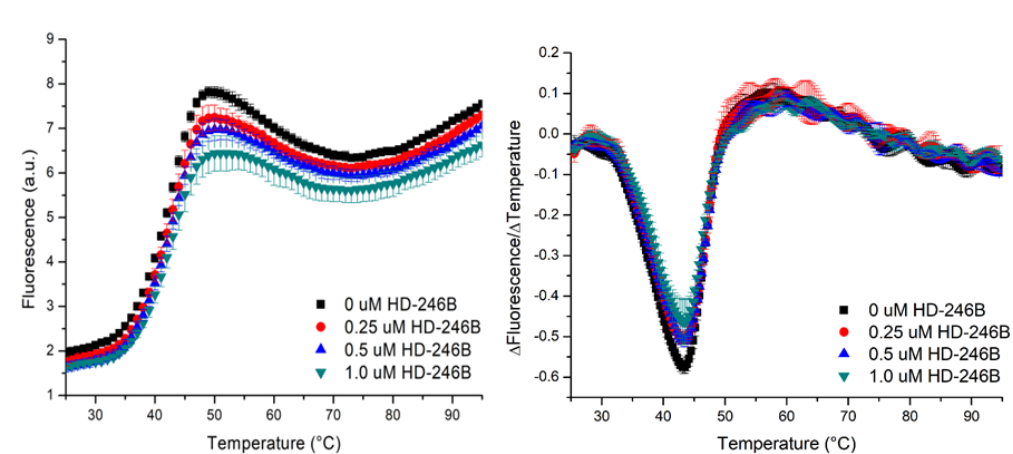
## c) Complex 179 (HD-241)



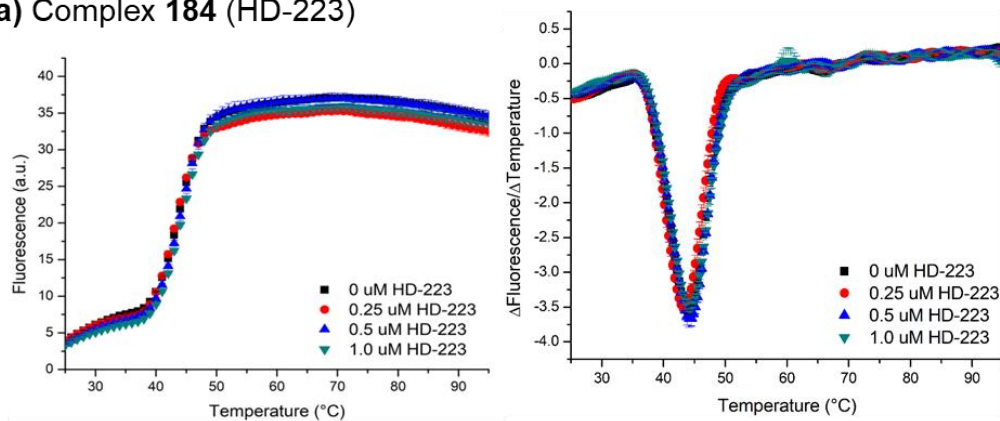
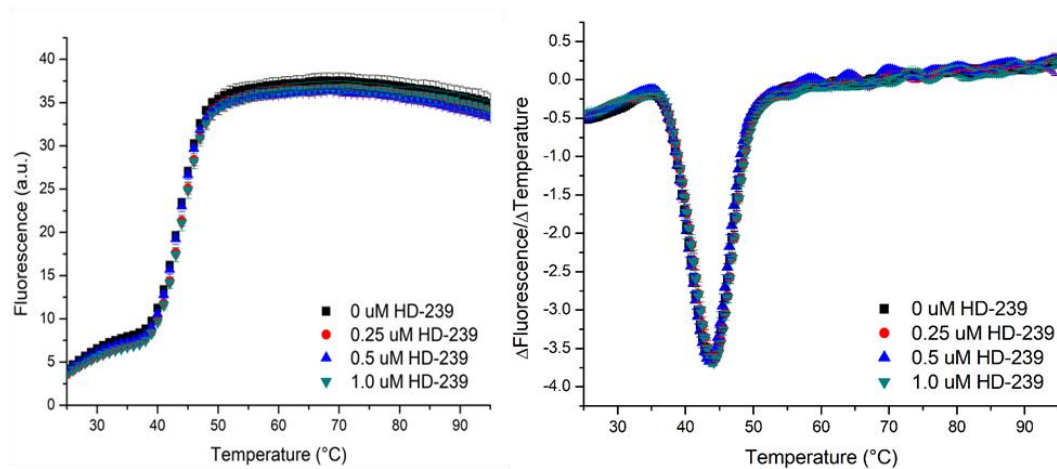
## d) Complex 194 (HD-246A)



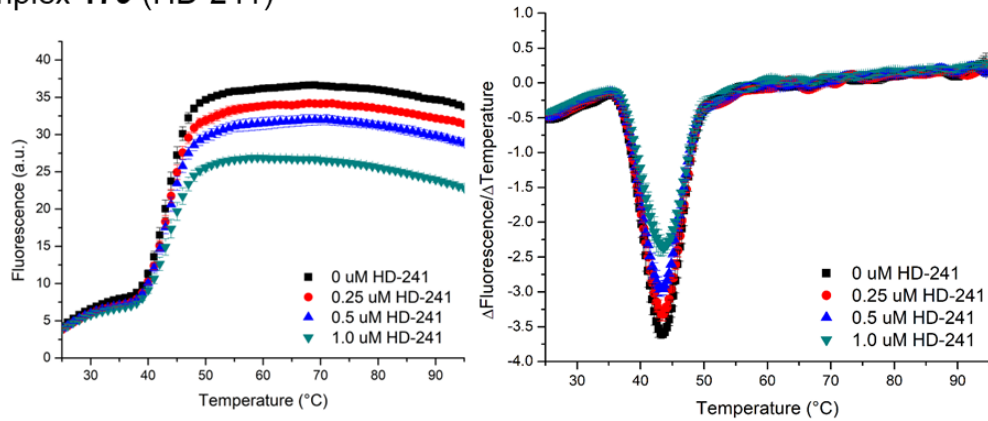
## e) Complex 189 (as a mixture of 189a:189b, HD-264B)



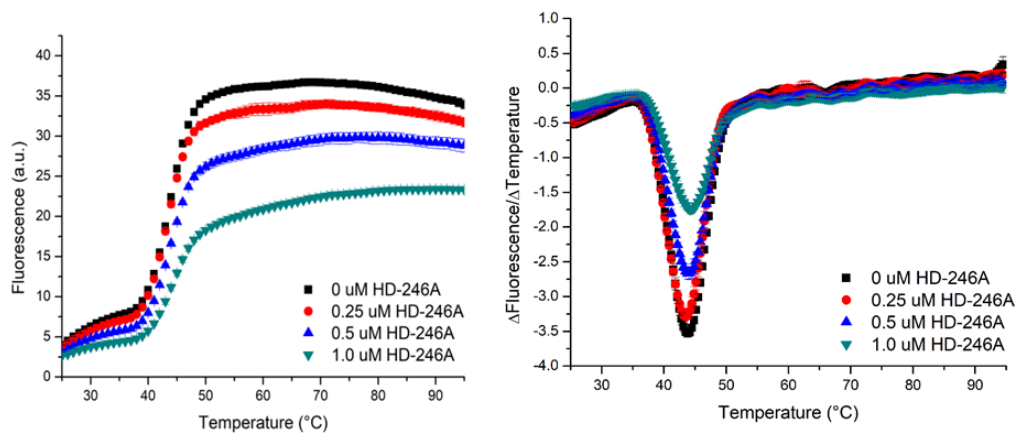
**Figure 82** FRET-melting experiments using 0.2  $\mu\text{M}$  hTeloC in 10 mM sodium cacodylate pH 6.0 with different compounds as indicated in the key and sub-captions (a to e). Melting curves (left), first derivatives (right).

**a) Complex 184 (HD-223)****b) Complex 187 (as a mixture of 187a:187b, HD-239)**

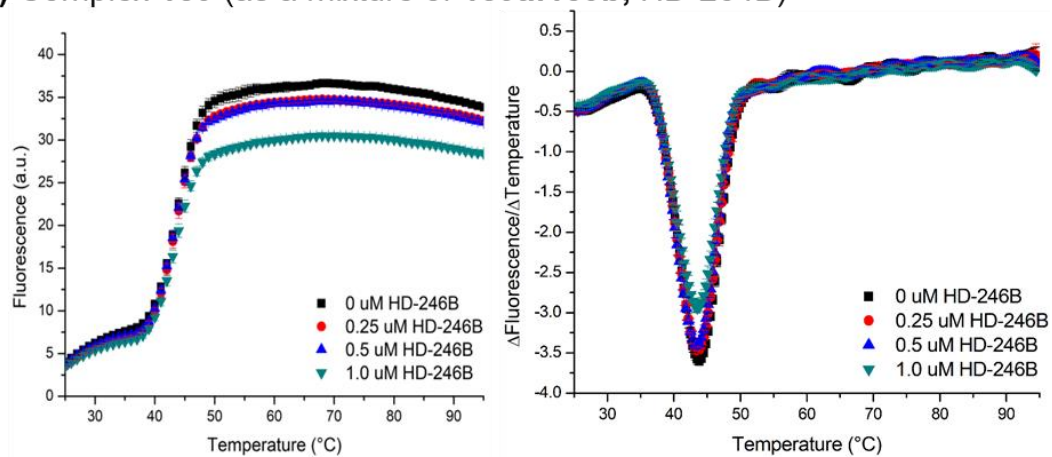
## c) Complex 179 (HD-241)



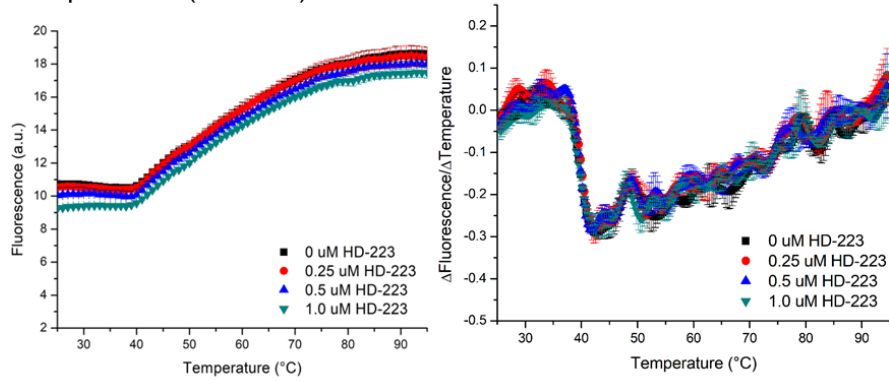
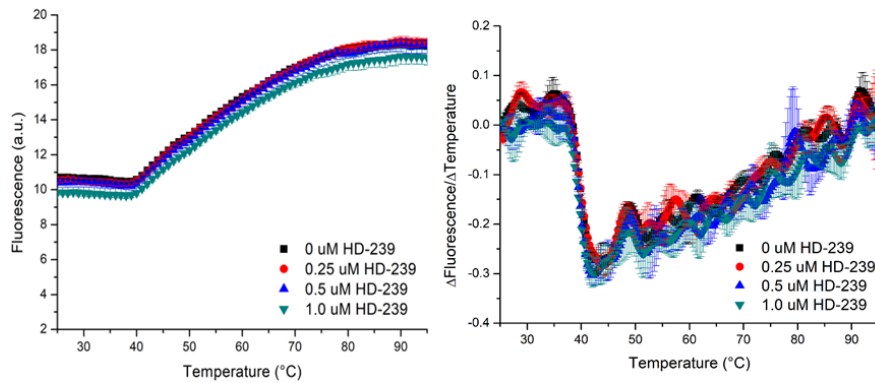
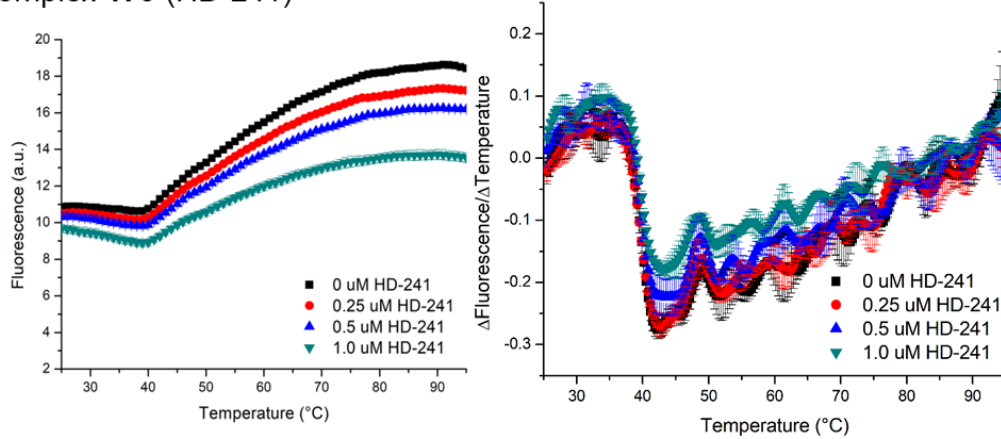
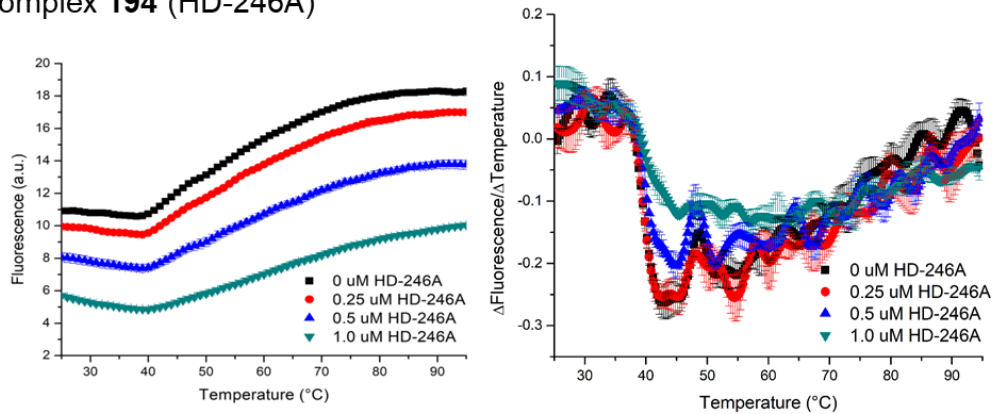
## d) Complex 194 (HD-246A)

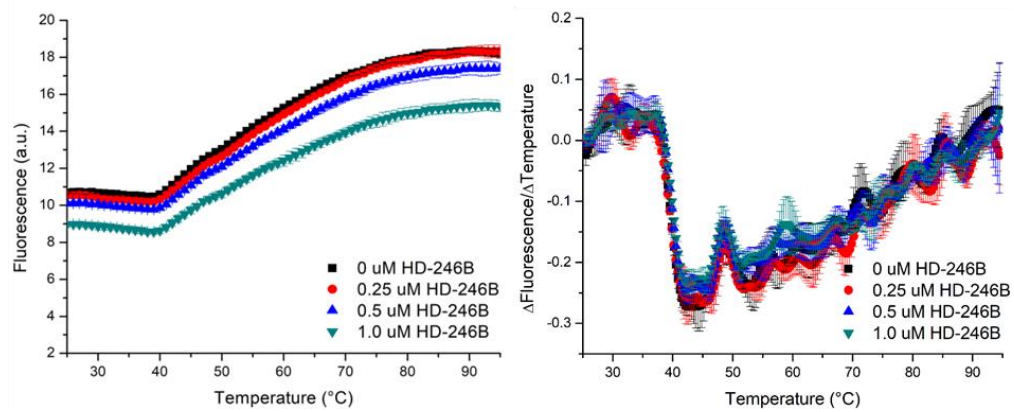


## e) Complex 189 (as a mixture of 189a:189b, HD-264B)

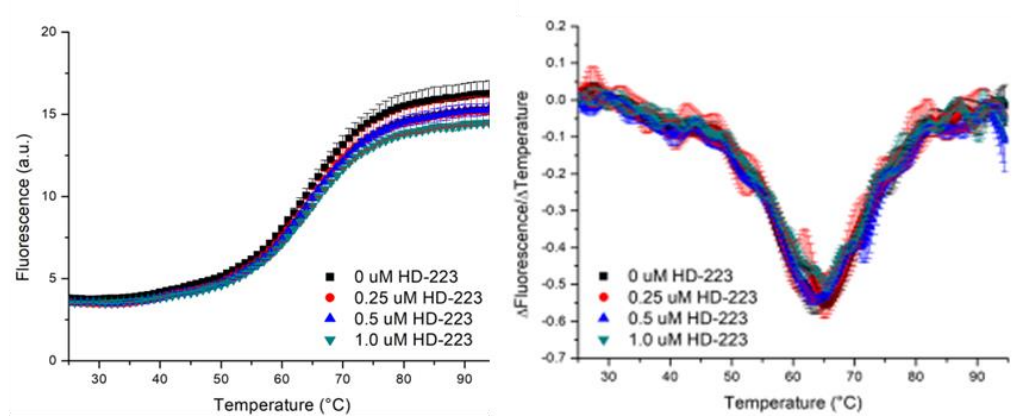
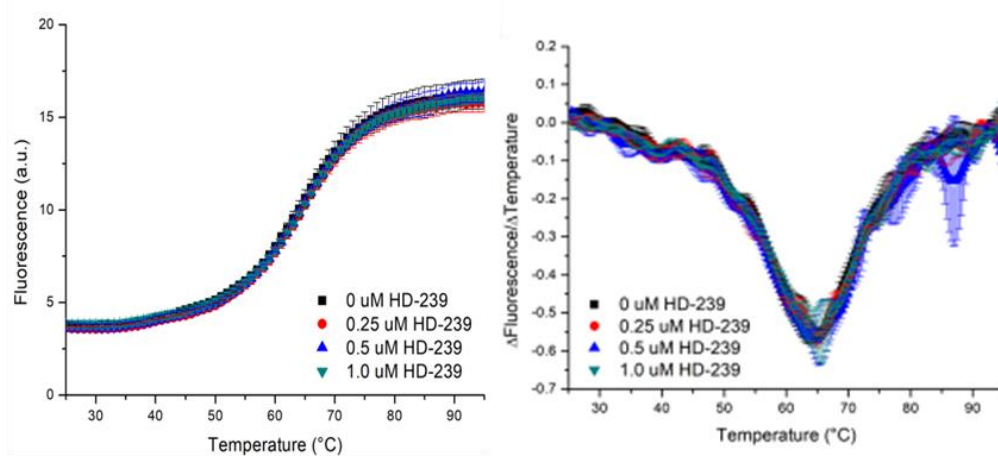


**Figure 83** FRET-melting experiments using 0.2  $\mu\text{M}$  DAP in 10 mM sodium cacodylate pH 7.0 with different compounds as indicated in the key and sub-captions (a to e). Melting curves (left), first derivatives (right).

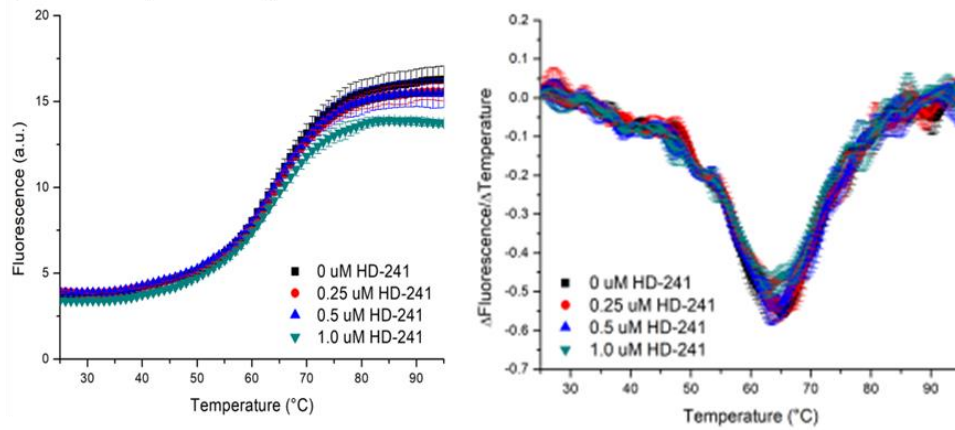
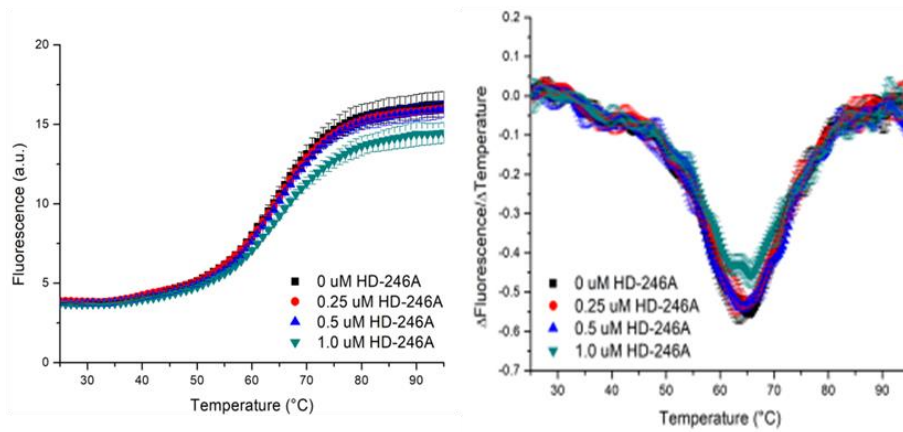
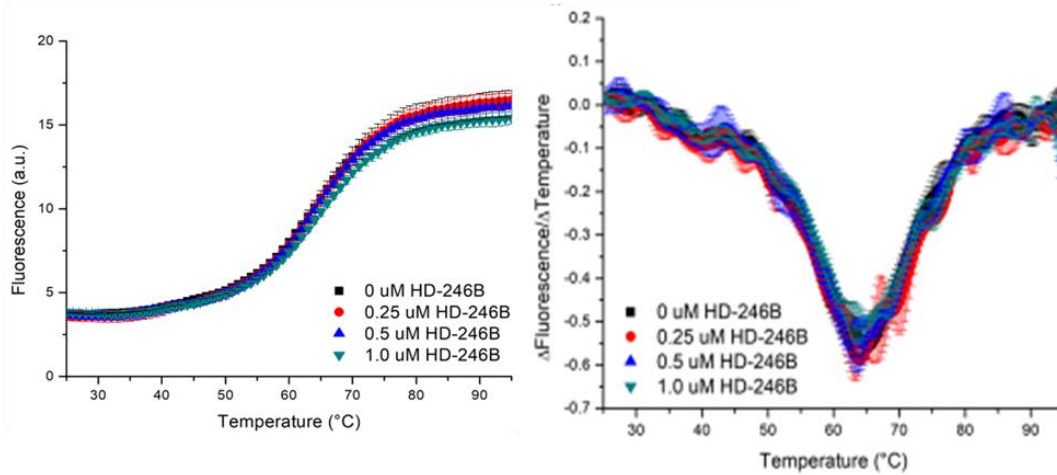
**a) Complex 184 (HD-223)****b) Complex 187 (as a mixture of 187a:187b, HD-239)****c) Complex 179 (HD-241)****d) Complex 194 (HD-246A)**

**e) Complex 189 (as a mixture of 189a:189b, HD-264B)**

**Figure 84** FRET-melting experiments using 0.2  $\mu\text{M}$  hif-1- $\alpha$  in 10 mM sodium cacodylate pH 7.2 with different compounds as indicated in the key and sub-captions (a to e). Melting curves (left), first derivatives (right).

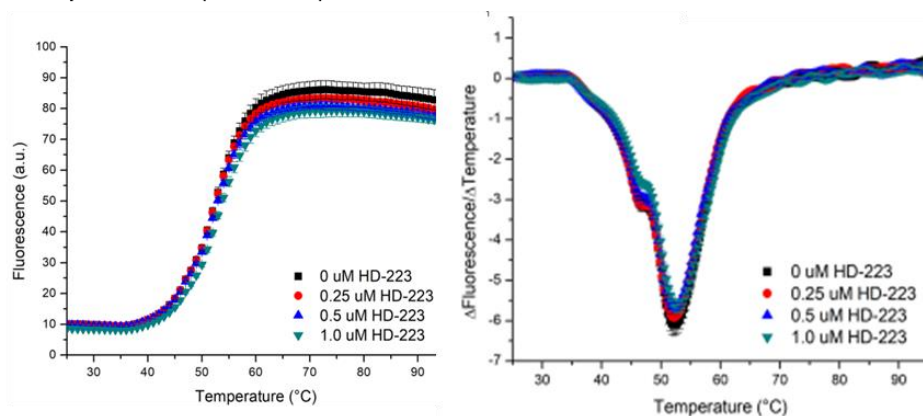
**a) Complex 184 (HD-223)****b) Complex 187 (as a mixture of 187a:187b, HD-239)**



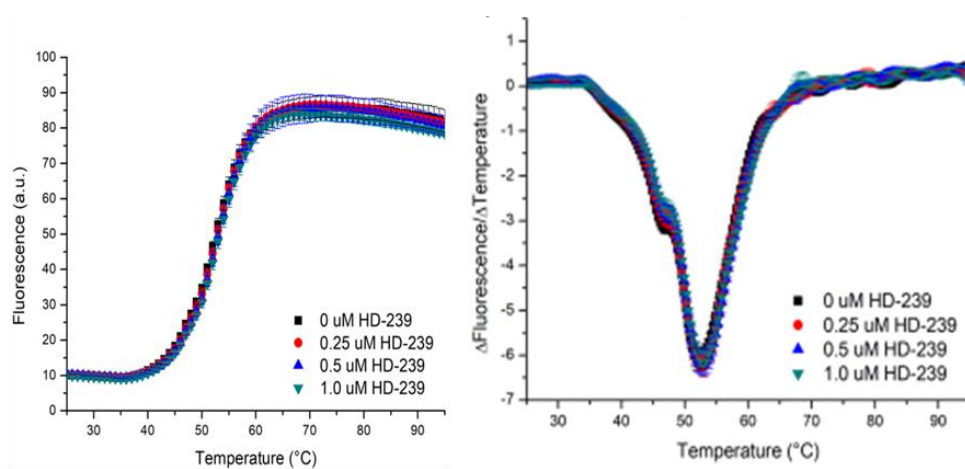
c) Complex **179** (HD-241)d) Complex **194** (HD-246A)e) Complex **189** (as a mixture of **189a**:**189b**, HD-246B)

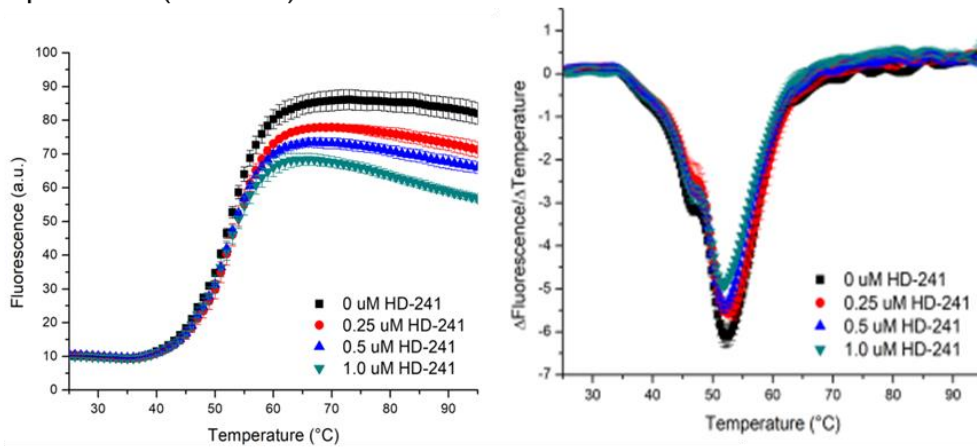
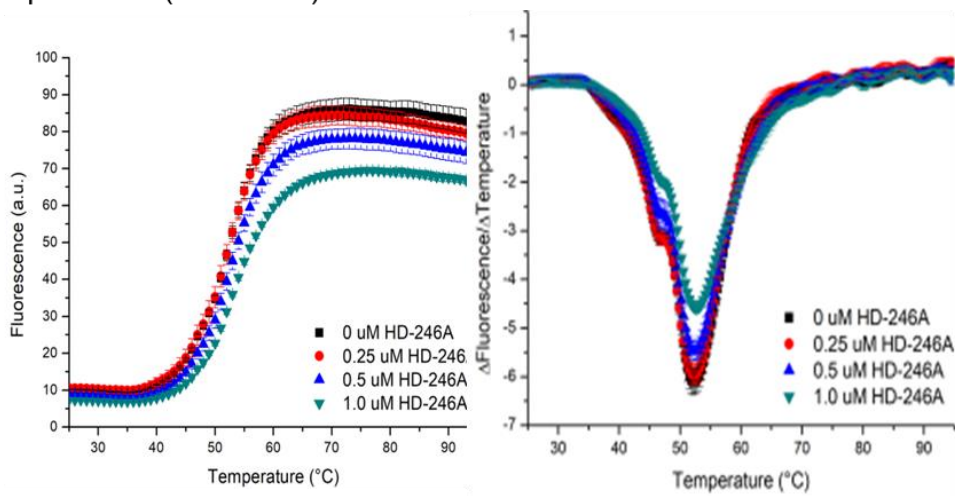
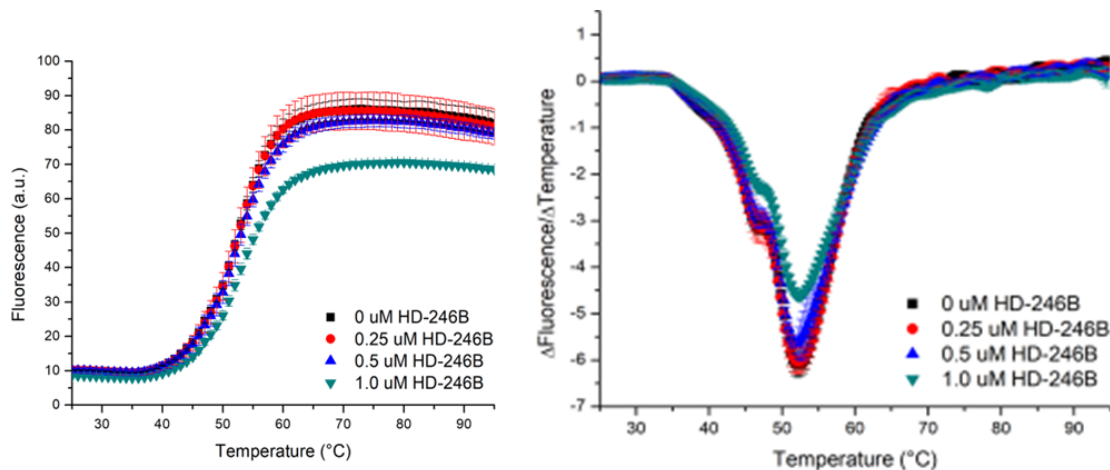
**Figure 85** FRET-melting experiments using 0.2  $\mu$ M hTeloG in 10 mM sodium cacodylate pH 7.0 with different compounds as indicated in the key. Melting curves (left), first derivatives (right).

## a) Complex 184 (HD-223)



## b) Complex 187 (as a mixture of 187a:187b, HD-239)



c) Complex **179** (HD-241)d) Complex **194** (HD-246A)e) Complex **189** (as a mixture of **189a**:**189b**, HD-246B)

**Figure 86** FRET-melting experiments using 0.2  $\mu$ M DS in 10 mM sodium cacodylate pH 7.0 with different compounds as indicated in the key and sub-captions (a to e). Melting curves (left), first derivatives (right).



b) Allene ligands **97a-b** and allene-containing complexes (Figure 87 to Figure 90)

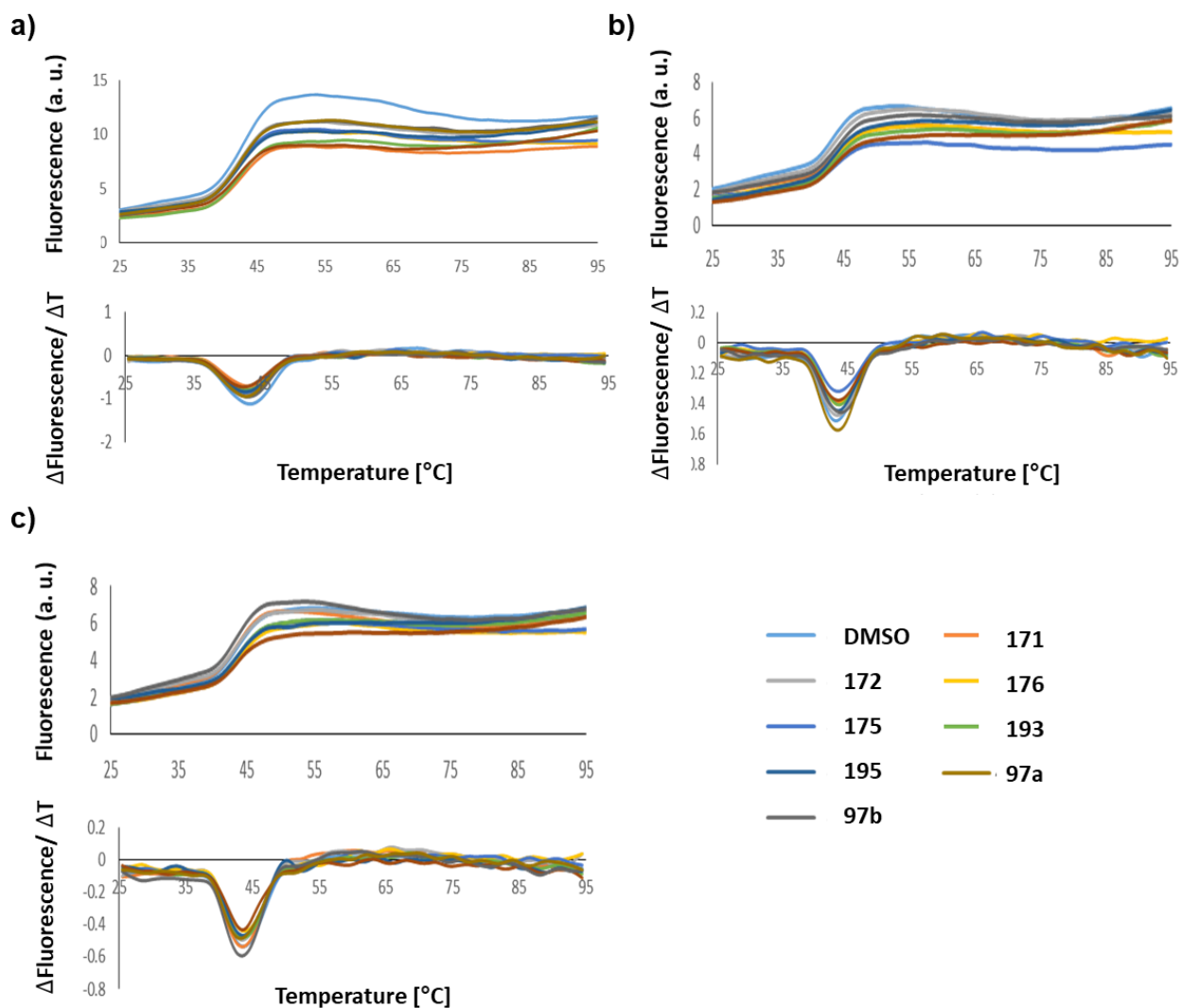


**Figure 87** FRET-melting experiments using 0.2  $\mu\text{M}$  hTeloC in 10 mM sodium cacodylate, 100 mM KCl, pH 5.5 with compounds at 1.0  $\mu\text{M}$ : a) run 1; b) run 2; c) run 3. Top graphs are melting curves, bottom are first derivatives.

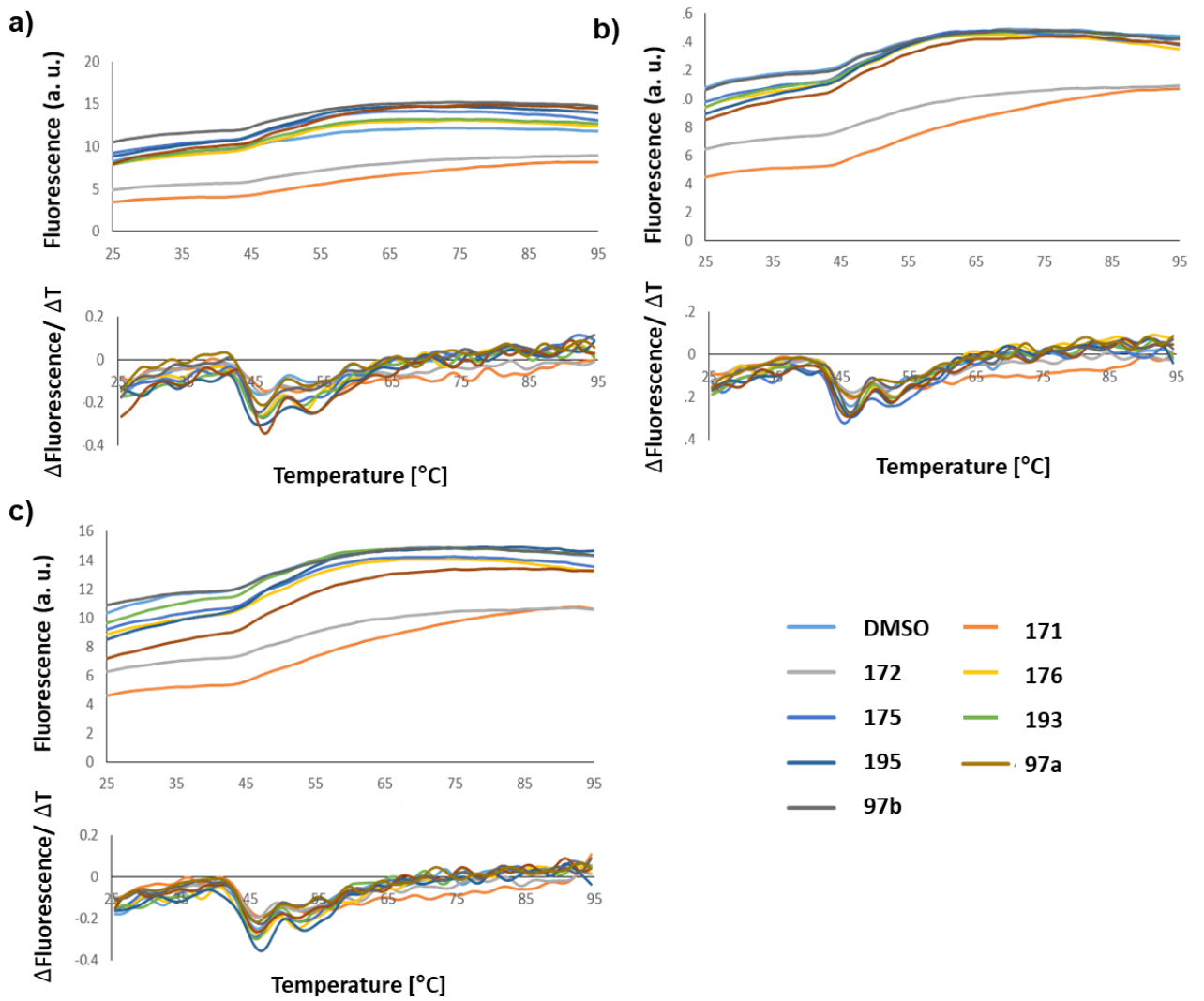


**Figure 88** FRET-melting experiments using 0.2  $\mu\text{M}$  hif-1- $\alpha$  in 10 mM sodium cacodylate, 100 mM KCl, pH 6.8 with compounds at 1.0  $\mu\text{M}$ : a) run 1; b) run 2; c) run 3. Top graphs are melting curves, bottom are first derivatives.

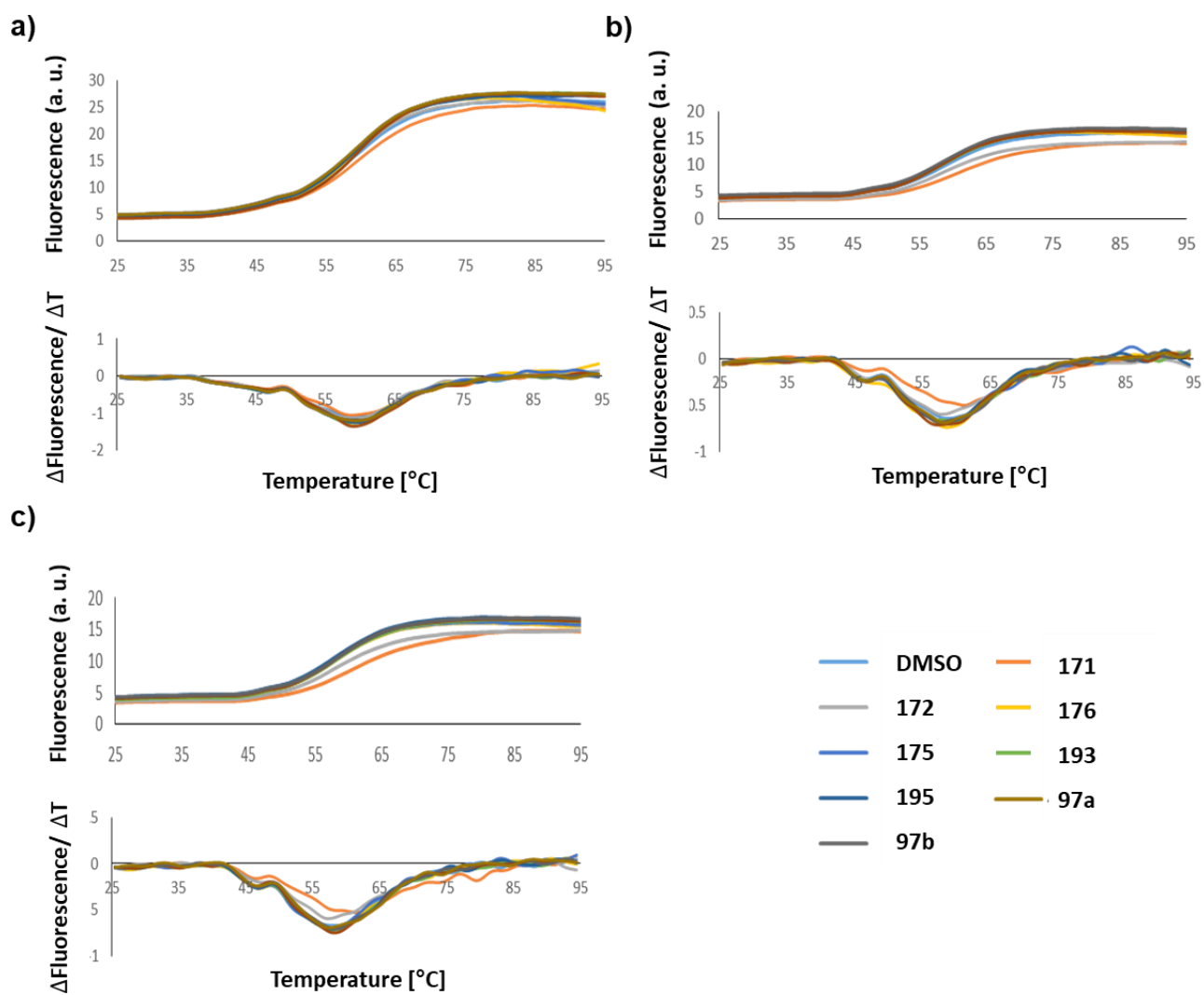


**Figure 89** FRET-melting experiments using 0.2 hTeloG in 10 mM sodium cacodylate, 100 mM KCl, pH 7.0 with compounds at 1.0  $\mu\text{M}$ : a) run 1; b) run 2; c) run 3. Top graphs are melting curves, bottom are first derivatives.

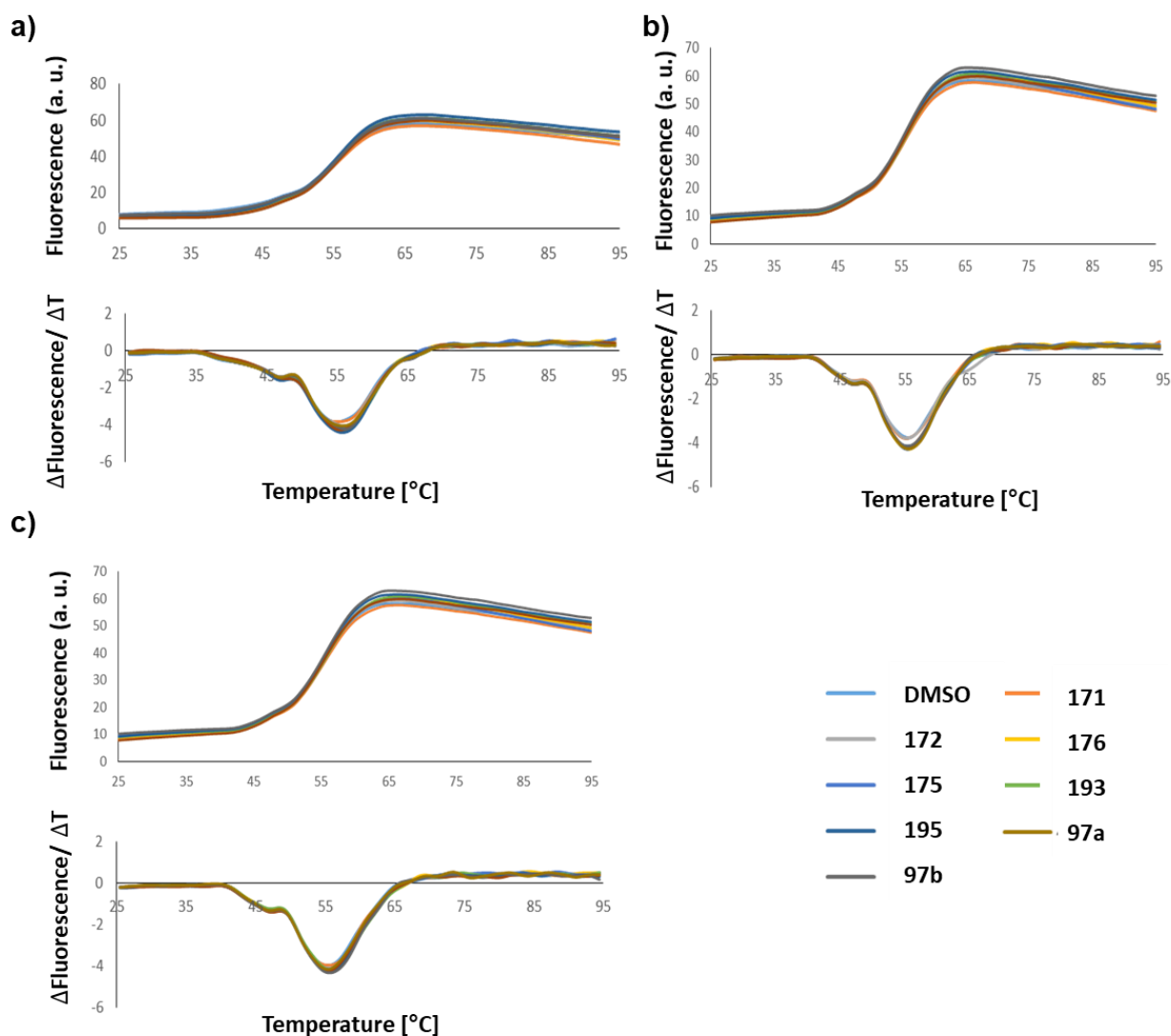


**Figure 90** FRET-melting experiments using 0.2 DS in 10 mM sodium cacodylate, 100 mM KCl, pH 7.0 with compounds at 1.0  $\mu\text{M}$ : a) run 1; b) run 2; c) run 3. Top graphs are melting curves, bottom are first derivatives.

### FID assay

FID experiments were performed on a BMG CLARIOstar plate reader using Corning 96-Well Solid Black Flat Bottom plates. A 10 mM stock solution of TO was prepared in DMSO and diluted to 2  $\mu\text{M}$  in the appropriate buffer. 90  $\mu\text{L}$  of the 2  $\mu\text{M}$  TO solution were added to each well and the fluorescence emission at 450 nm was measured with excitation at 430 nm; this was normalised to 0% representing background fluorescence. 1  $\mu\text{L}$  of 90  $\mu\text{M}$  DNA was then added, shaken using 114 double orbital shaking at 700 rpm in the plate reader for 15 s, and allowed to equilibrate for 15 minutes. After equilibration, fluorescence emission was measured once again and normalised to 100% representing maximum fluorescence enhancement from the TO probe binding the DNA secondary structure. 0.9  $\mu\text{L}$  aliquots of ligand were titrated into each well (in triplicate) and measured as before. Fluorescence measurements after ligand

addition were normalised between the 0 and 100% levels determined per the respective well. Percentage TO displacement was calculated as the difference between the normalised 100% fluorescence level and the normalised fluorescence measured after each ligand addition

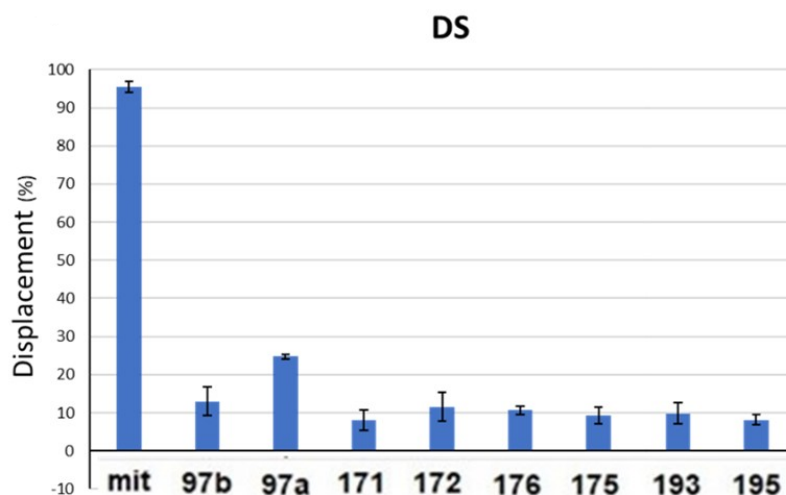


**Figure 91** FID assay for allene ligands **97a-b** and allene-containing complexes at 2.5  $\mu\text{M}$  in 10 mM sodium cacodylate, 100 mM KCl, 0.5  $\mu\text{M}$  DS, pH 7.0.

### CD-melting experiments

Circular dichroism was performed using a Jasco J-810 spectropolarimeter using a 1 mm path length quartz cuvette. Scans were performed with a scanning speed of 200 nm/min, response time of 1 s, 0.5 nm pitch and 2 nm bandwidth. The spectra are an accumulation of either 3 or 4 scans and are zero corrected at the longest wavelength of the measurement. Melting experiments were performed using the same measurement parameters while heating the sample at a rate of 1  $^{\circ}\text{C}/\text{min}$  within the desired temperature range and measuring at 5  $^{\circ}\text{C}$  intervals. The temperature at which 50% of the thermal denaturation had taken place ( $T_m$ ) was calculated using Excel to plot normalised ellipticity at 288 nm against temperature. These data were fitted with sigmoidal curves and the equations of the curves solved for  $y = 0.5$  to give the  $T_m$  values.

a) DMSO

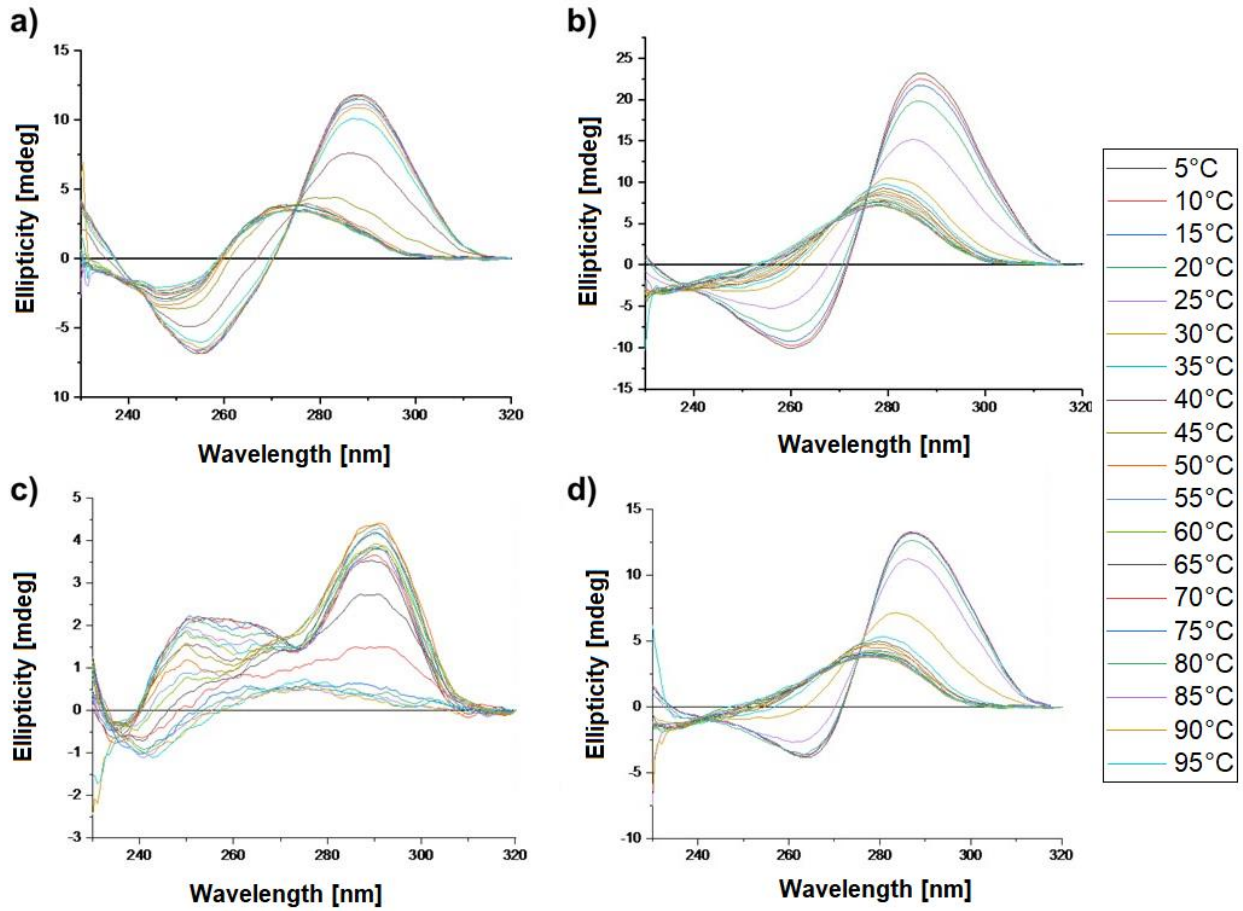


**Figure 92** CD-melting spectra of DMSO in 10 mM sodium cacodylate with 10  $\mu\text{M}$  of DNA: a) hTeloC, 100 mM KCl, pH 5.5; b) hif-1- $\alpha$ , 10 mM KCl, pH 6.8; c) hTeloG, 100 mM KCl, pH 7.0; d) DAP, 100 mM KCl, pH 6.8.

b) Complex **171** (Figure 93 to Figure 96)

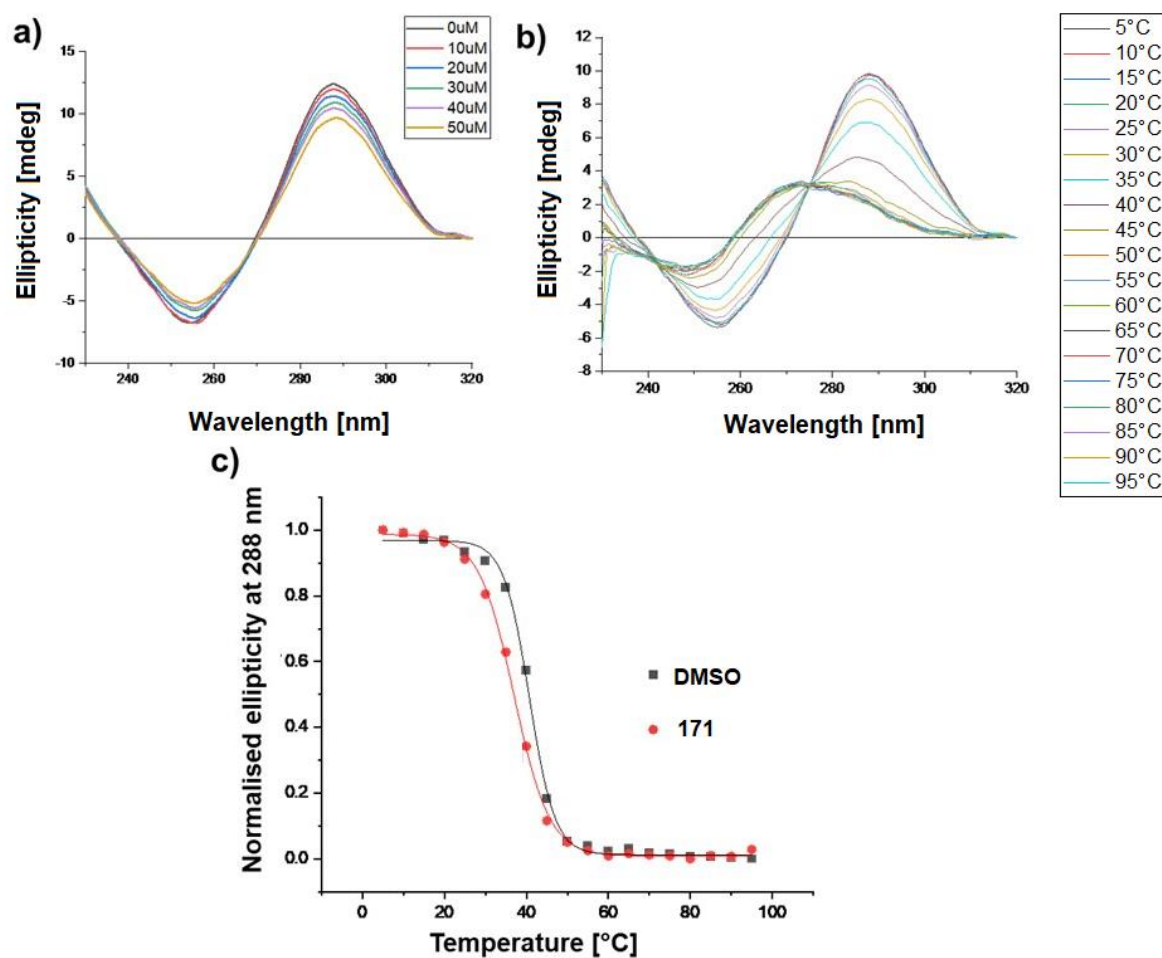


**Figure 93** CD spectra of **171** with 10  $\mu\text{M}$  hTeloC in 10 mM sodium cacodylate, 100 mM KCl, pH 5.5:

a) titration; b) CD-melt with 50  $\mu\text{M}$  of **171**; c) normalised ellipticity.

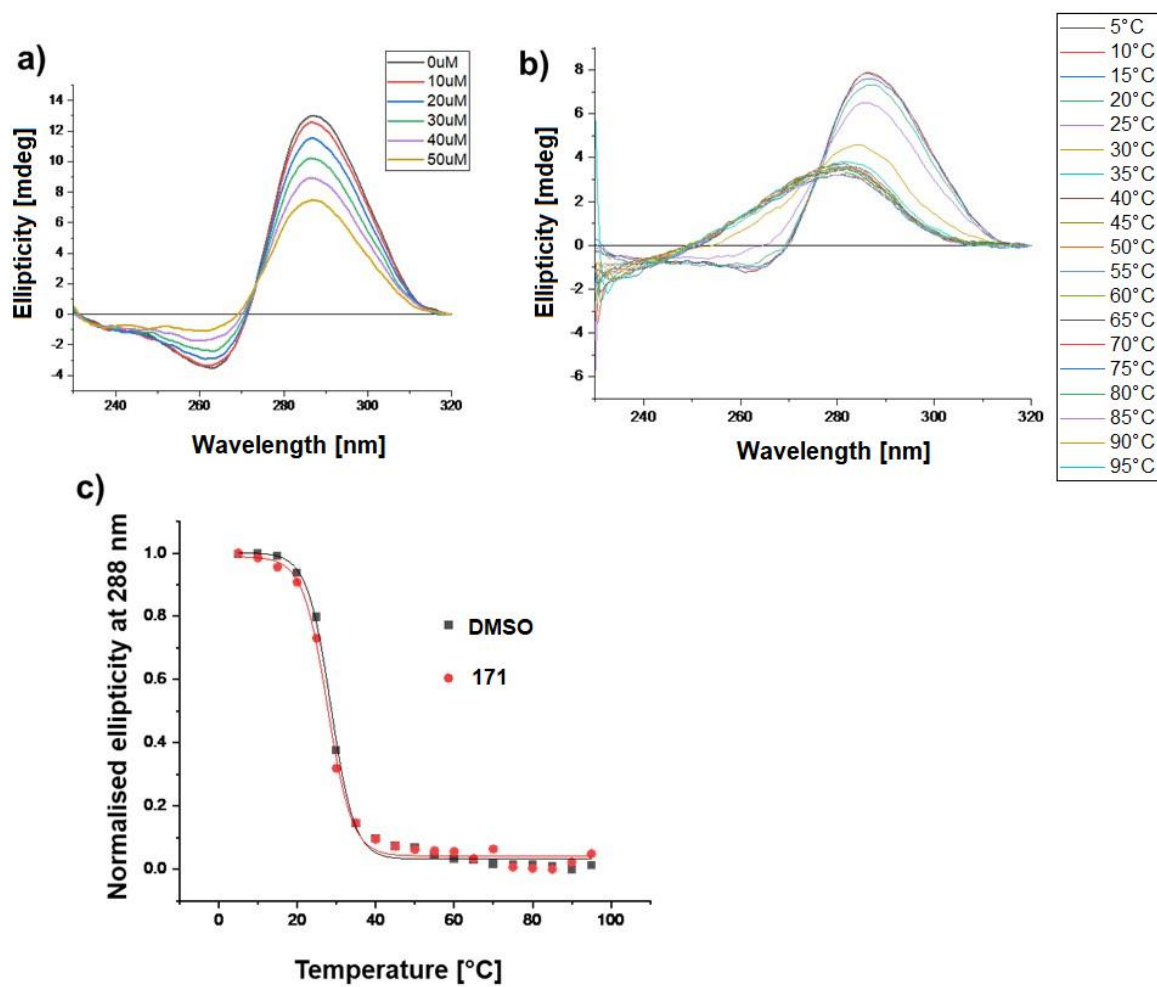


**Figure 94** CD spectra of **171** with 10  $\mu$ M DAP in 10 mM sodium cacodylate, 100 mM KCl, pH 6.8: a) titration; b) CD-melt with 50  $\mu$ M of **171**; c) normalised ellipticity.



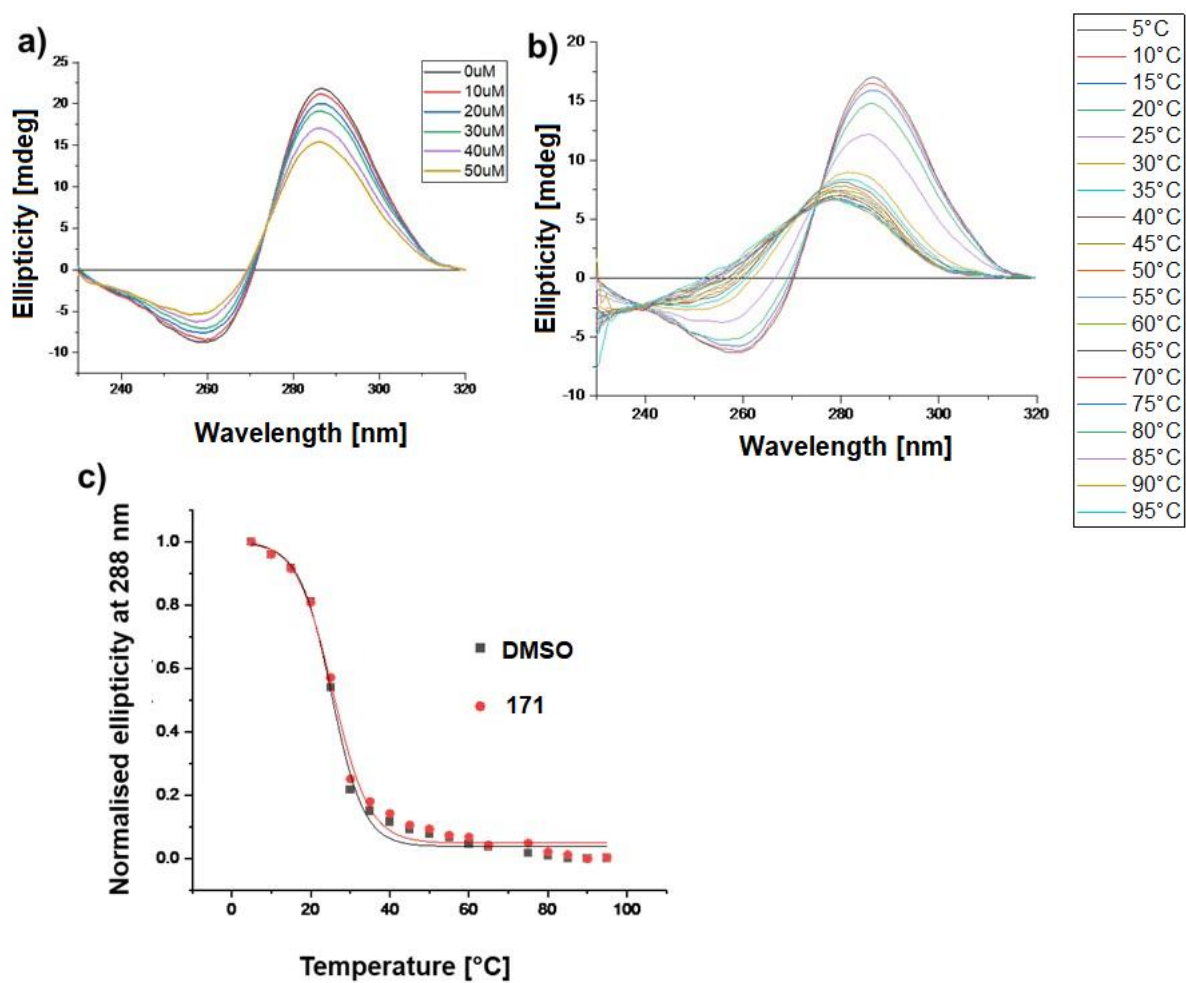


**Figure 95** CD spectra of **171** with 10  $\mu\text{M}$  hif-1- $\alpha$  in 10 mM sodium cacodylate, 100 mM KCl, pH 6.8: a) titration; b) CD-melt with 50  $\mu\text{M}$  of **171**; c) normalised ellipticity.

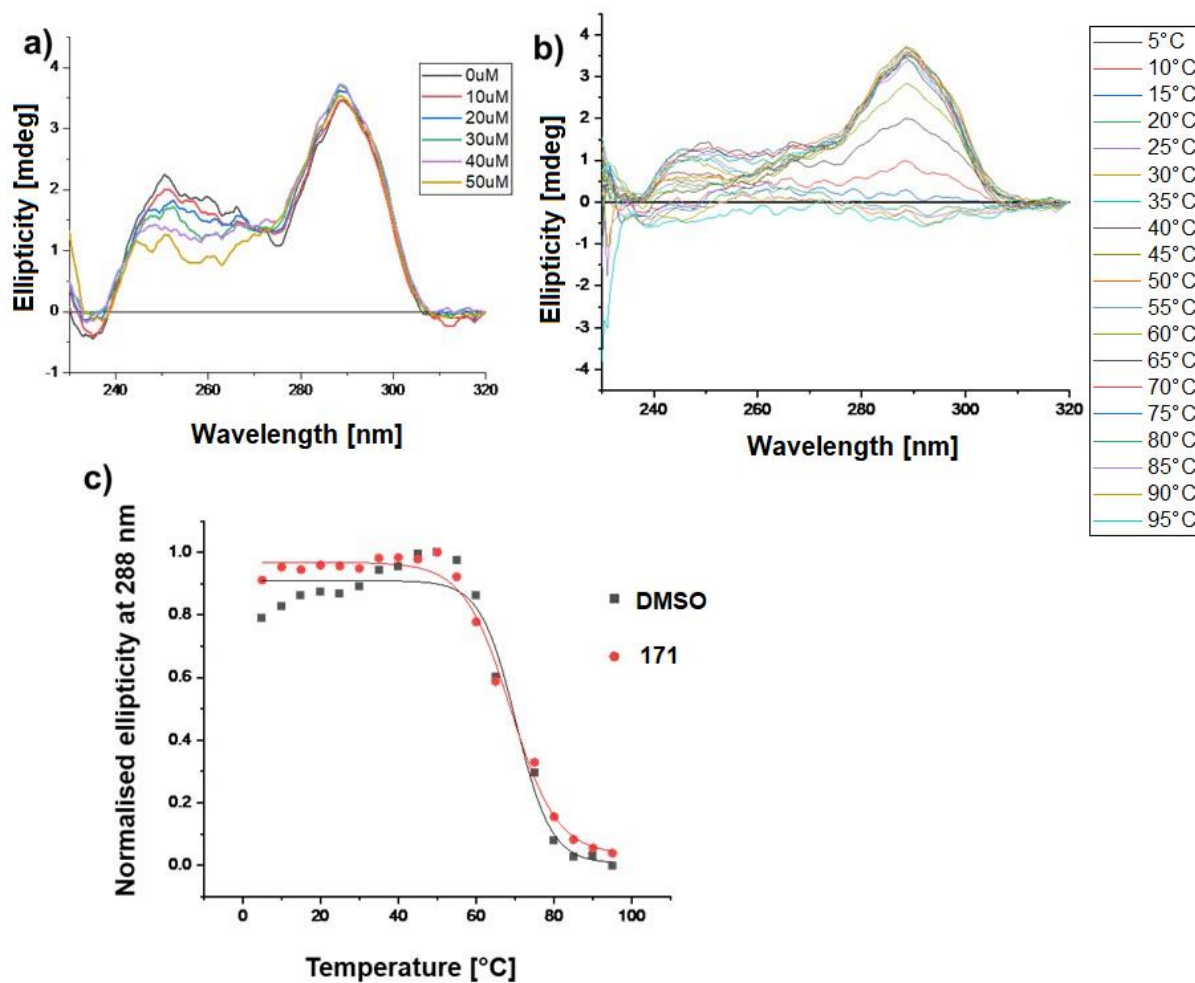


**Figure 96** CD spectra of **171** with 10  $\mu\text{M}$  hTeloG in 10 mM sodium cacodylate, 100 mM KCl, pH 7.0: a) titration; b) CD-melt with 50  $\mu\text{M}$  of **171**; c) normalised ellipticity.

c) Complex **172** (Figure 97 to Figure 100)

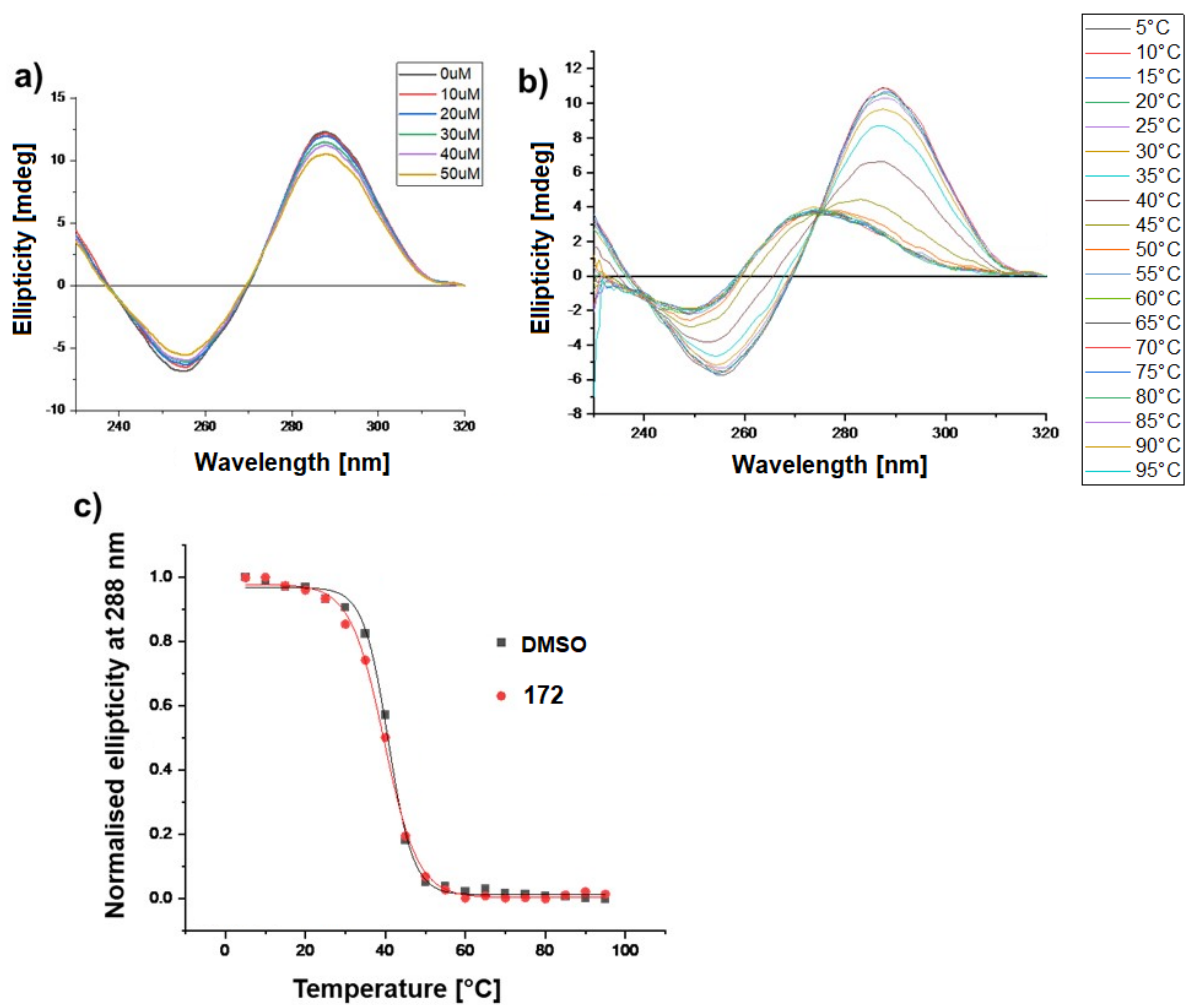


**Figure 97** CD spectra of **172** with 10  $\mu\text{M}$  hTeloC in 10 mM sodium cacodylate, 100 mM KCl, pH 5.5: a) titration; b) CD-melt with 50  $\mu\text{M}$  of **172**; c) normalised ellipticity.

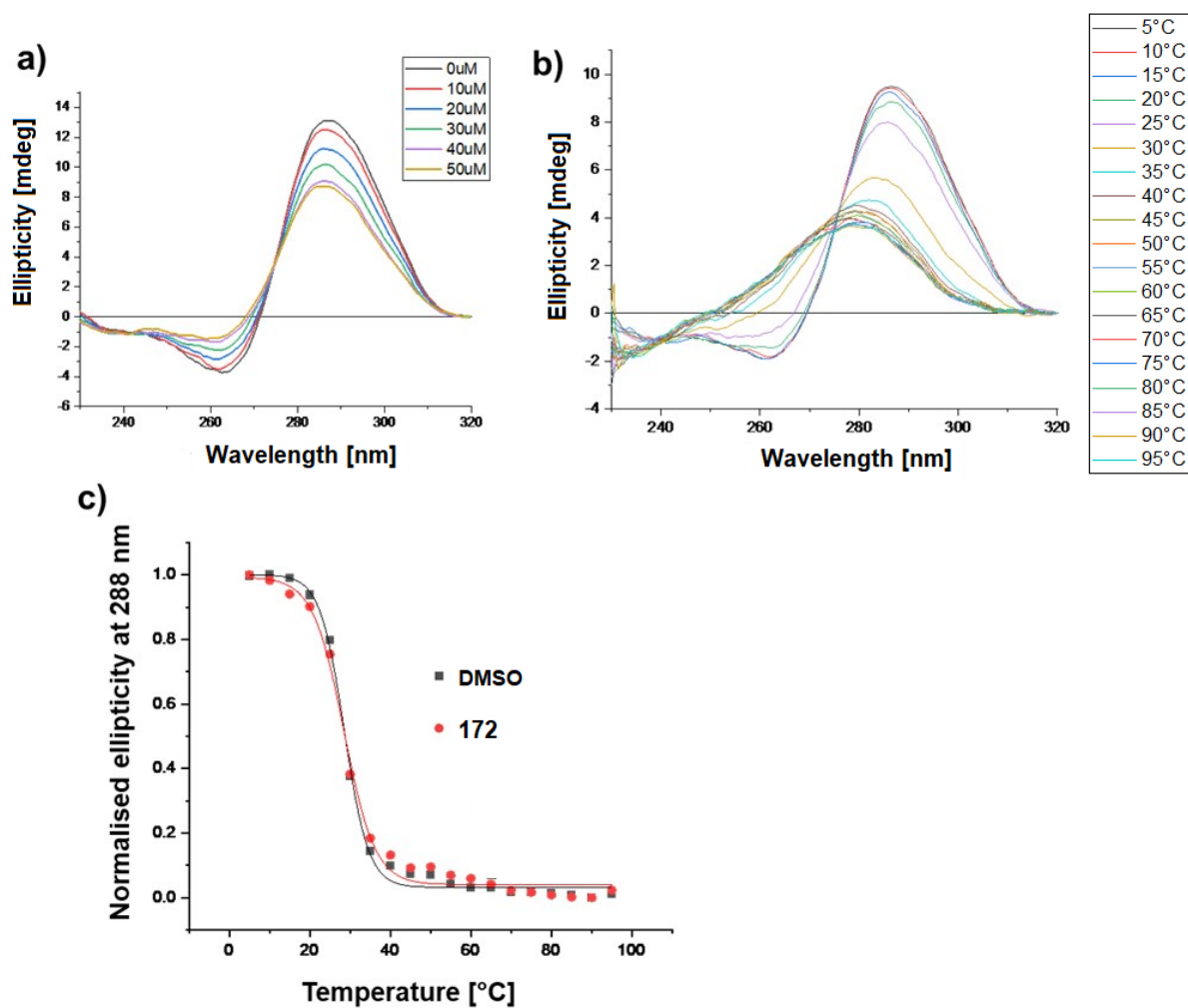
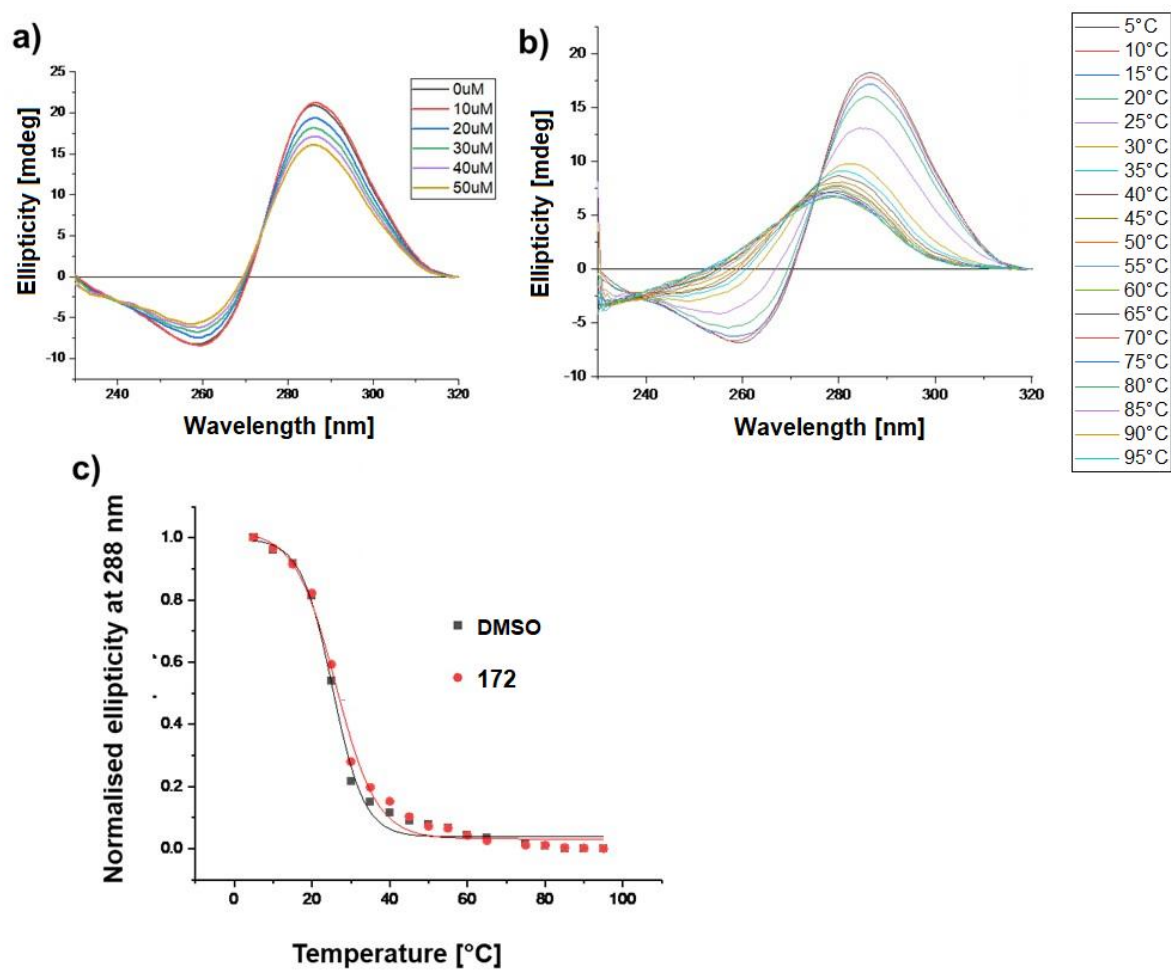
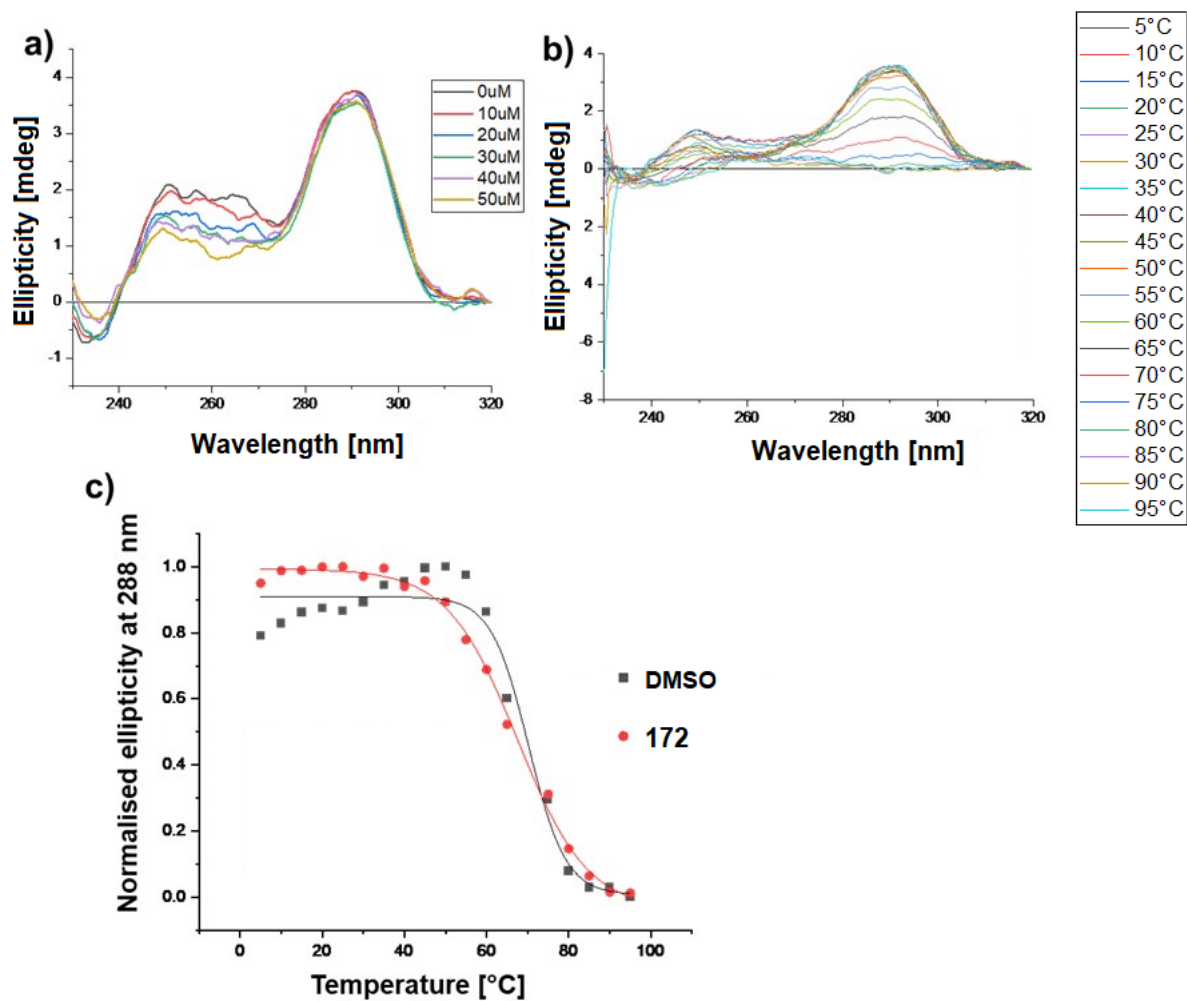


Figure 98 CD spectra of **172** with 10  $\mu$ M DAP in 10 mM sodium cacodylate, 100 mM KCl, pH 6.8: a) titration; b) CD-melt with 50  $\mu$ M of **172**; c) normalised ellipticity.



**Figure 99** CD spectra of **172** with 10 μM hif-1-α in 10 mM sodium cacodylate, 100 mM KCl, pH 6.8: a) titration; b) CD-melt with 50 μM of **172**; c) normalised ellipticity.



**Figure 100** CD spectra of **172** with 10  $\mu\text{M}$  hTeloG in 10 mM sodium cacodylate, 100 mM KCl, pH 7.0: a) titration; b) CD-melt with 50  $\mu\text{M}$  of **172**; c) normalised ellipticity.

## Appendix A - Structures of new complexes

## Appendix B - NMR Spectra

## Appendix C - X-ray data

## Appendix D - Procedures from CO-ADD

## XI. References

- [1] J. A. Januszewski, R. R. Tykwinski, *Chem. Soc. Rev.* **2014**, *43*, 3184–3203.
- [2] J. A. Januszewski, D. Wendinger, C. D. Methfessel, F. Hampel, R. R. Tykwinski, *Angew. Chem. Int. Ed.* **2013**, *52*, 1817–1821.
- [3] J. H. Van't Hoff, *Bazendijk Rotterdam* **1875**.
- [4] B. S. Burton, H. von Pechmann, *Berichte Dtsch. Chem. Ges.* **1887**, *20*, 145–149.
- [5] E. R. H. Jones, G. H. Mansfield, M. C. Whiting, *J. Chem. Soc.* **1954**, 3208–3212.
- [6] E. A. Johnson, K. L. Burdon, *J. Bacteriol.* **1947**, *54*, 281–282.
- [7] W. D. Celmer, I. A. Solomons, *J. Am. Chem. Soc.* **1952**, *74*, 1870–1871.
- [8] A. Hoffmann-Röder, N. Krause, *Angew. Chem. Int. Ed.* **2004**, *43*, 1196–1216.
- [9] M. Bouis, *Ann. Chim.* **1928**, *10*, 402.
- [10] P. Maitland, W. H. Mills, *Nature* **1935**, 994.
- [11] D. R. Taylor, *Chem. Rev.* **1967**, *67*, 317–359.
- [12] S. Patai, *Ketenes, Allenes and Related Compounds*, John Wiley & Sons Ltd., Hoboken; New Jersey, **1980**, 45-98.
- [13] H. F. Schuster, G. M. Coppola, *Allenenes in Organic Synthesis*, Wiley-Interscience, New York, **1984**.
- [14] C. H. Hendon, D. Tiana, A. T. Murray, D. R. Carbery, A. Walsh, *Chem. Sci.* **2013**, *4*, 4278–4284.
- [15] E. Soriano, I. Fernández, *Chem. Soc. Rev.* **2014**, *43*, 3041–3105.
- [16] E. Weber, E. Seichter, B. Hess, G. Will, H. -J. Dasting, *J. Phys. Org. Chem.* **1995**, *8*, 94–96.
- [17] J. D. Price, R. P. Johnson, *Tetrahedron Lett.* **1986**, *27*, 4679–4682.
- [18] M. A. Hofmann, U. Bergsträßer, G. J. Reiß, L. Nyulászi, M. Regitz, *Angew. Chem. Int. Ed.* **2000**, *39*, 1261–1263.
- [19] T. Shimizu, F. Hojo, W. Ando, *J. Am. Chem. Soc.* **1993**, *115*, 3111–3115.
- [20] C. A. Dyker, V. Lavallo, B. Donnadiou, G. Bertrand, *Angew. Chem. Int. Ed.* **2008**, *47*, 3206–3209.
- [21] M. M. Hänninen, A. Peuronen, H. M. Tuononen, *Chem. Eur. J.* **2009**, *15*, 7287–7291.
- [22] V. Lavallo, C. A. Dyker, B. Donnadiou, G. Bertrand, *Angew. Chem. Int. Ed.* **2009**, *48*, 1540–1542.
- [23] L. Radom, W. A. Lathan, W. J. Hehre, J. A. Pople, *J. Am. Chem. Soc.* **1971**, *93*, 5339–5342.
- [24] S. Ma, *Chem. Rev.* **2005**, *105*, 2829–2872.
- [25] M. P. Muñoz, *Chem. Soc. Rev.* **2014**, *43*, 3164–3183.
- [26] R. Zimmer, H.-U. Reissig, *Chem. Soc. Rev.* **2014**, *43*, 2888–2903.
- [27] J. Le Bras, J. Muzart, *Chem. Soc. Rev.* **2014**, *43*, 3003–3040.
- [28] W.-D. Chu, Y. Zhang, J. Wang, *Catal. Sci. Technol.* **2017**, *7*, 4570–4579.
- [29] S. Yu, S. Ma, *Angew. Chem. Int. Ed.* **2012**, *51*, 3074–3112.
- [30] J. M. Alonso, M. T. Quirós, M. P. Muñoz, *Org. Chem. Front.* **2016**, *3*, 1186–1204.
- [31] M. Alcarazo, C. W. Lehmann, A. Anoop, W. Thiel, A. Fürstner, *Nat. Chem.* **2009**, *1*, 295–301.
- [32] P. Rivera-Fuentes, F. Diederich, *Angew. Chem. Int. Ed.* **2012**, *51*, 2818–2828.
- [33] M. O. Bagby, C. R. Smith, I. A. Wolff, *J. Org. Chem.* **1965**, *30*, 4227–4229.
- [34] J. Meinwald, K. Erickson, M. Hartshorn, Y. C. Meinwald, T. Eisner, *Tetrahedron Lett.* **1968**, 2959–2962.

- [35] R. Kinnel, A. J. Duggan, T. Eisner, J. Meinwald, I. Miura, *Tetrahedron Lett.* **1977**, *18*, 3913–3916.
- [36] F. Bohlmann, H. Bornowski, C. Arndt, *Chem. Ber.* **1965**, *98*, 2236–2242.
- [37] M. Ito, Y. Yamano, S. Sumiya, A. Wada, *Pure Appl. Chem.* **1994**, *66*, 939–946.
- [38] M. T. Crimmins, E. A. Tabet, *J. Am. Chem. Soc.* **2000**, *122*, 5473–5476.
- [39] M. T. Crimmins, K. A. Emmitte, *J. Am. Chem. Soc.* **2001**, *123*, 1533–1534.
- [40] J. R. Williams, J. C. Boehm, *Steroids* **1995**, *60*, 699–708.
- [41] A. L. Castelhana, D. H. Pliura, G. J. Taylor, K. C. Hsieh, A. Krantz, *J. Am. Chem. Soc.* **1984**, *106*, 2734–2735.
- [42] S. Phadtare, D. Kessel, T. H. Corbett, H. E. Renis, B. E. Court, J. Zemlicka, *J. Med. Chem.* **1991**, *34*, 421–429.
- [43] P. W. Collins, S. W. Djuric, *Chem. Rev.* **1993**, *93*, 1533–1564.
- [44] N. Omura, H. Kashiwagi, T. Aoki, K. Omura, Y. Fukuchi, *J. Gastroenterol.* **1997**, *32*, 740–746.
- [45] C. Walsh, *Tetrahedron* **1982**, *38*, 871–909.
- [46] H. L. Carrell, J. P. Glusker, D. F. Covey, F. H. Batzold, C. H. Robinson, *J. Am. Chem. Soc.* **1978**, *100*, 4282–4289.
- [47] B. L. Shaw, A. J. Stringer, *Inorg. Chim. Acta* **1973**, *7*, 1–10.
- [48] F. L. Bowden, R. Giles, *Coord. Chem. Rev.* **1976**, *20*, 81–106.
- [49] M. J. S. Dewar, *Bull. Soc. Chim. Fr.* **1951**, *18*, 71–79.
- [50] J. Chatt, L. A. Duncanson, *J. Chem. Soc.* **1953**, 2939–2947.
- [51] A. Fürstner, P. W. Davies, *Angew. Chem. Int. Ed.* **2007**, *46*, 3410–3449.
- [52] M. S. Nechaev, V. M. Rayon, G. Frenking, *J. Phys. Chem. A* **2004**, *108*, 3134–3142.
- [53] T. Cañeque, F. M. Truscott, R. Rodriguez, G. Maestri, M. Malacria, *Chem Soc Rev* **2014**, *43*, 2916–2926.
- [54] V. Gandon, G. Lemièrre, A. Hours, L. Fensterbank, M. Malacria, *Angew. Chem. Int. Ed.* **2008**, *47*, 7534–7538.
- [55] R.-X. Zhu, D.-J. Zhang, J.-X. Guo, J.-L. Mu, C.-G. Duan, C.-B. Liu, *J. Phys. Chem. A* **2010**, *114*, 4689–4696.
- [56] R. J. Harris, K. Nakafuku, R. A. Widenhoefer, *Chem. Eur. J.* **2014**, *20*, 12245–12254.
- [57] H. Li, R. J. Harris, K. Nakafuku, R. A. Widenhoefer, *Organometallics* **2016**, *35*, 2242–2248.
- [58] R. Ben-Shoshan, R. Pettit, *J. Am. Chem. Soc.* **1967**, *89*, 2231–2232.
- [59] B. Foxman, D. Marten, A. Rosan, S. Raghu, M. Rosenblum, *J. Am. Chem. Soc.* **1977**, *99*, 2160–2165.
- [60] T. J. Brown, A. Sugie, M. G. Dickens, R. A. Widenhoefer, *Organometallics* **2010**, *29*, 4207–4209.
- [61] M. T. Quirós, J. Angulo, M. P. Muñoz, *Chem. Commun.* **2015**, *51*, 10222–10225.
- [62] M. T. Quirós, M. P. Muñoz, J. Christensen, S. J. Coles, *Organometallics* **2017**, *36*, 318–330.
- [63] K. Okamoto, Y. Kai, N. Yasuoka, N. Kasai, *J. Organomet. Chem.* **1974**, *65*, 427–441.
- [64] A. L. Colebatch, I. A. Cade, A. F. Hill, M. M. Bhadbhade, *Organometallics* **2013**, *32*, 4766–4774.
- [65] T. G. Hewitt, J. J. De Boer, *J. Chem. Soc. Inorg. Phys. Theor.* **1971**, 817–822.
- [66] O. Kaufhold, F. E. Hahn, *Angew. Chem. Int. Ed.* **2008**, *47*, 4057–4061.
- [67] M. Alcarazo, *Dalton Trans.* **2011**, *40*, 1839–1845.
- [68] C. Esterhuysen, G. Frenking, *Chem. Eur. J.* **2011**, *17*, 9944–9956.



- [69] A. Fürstner, M. Alcarazo, R. Goddard, C. W. Lehmann, *Angew. Chem. Int. Ed.* **2008**, *47*, 3210–3214.
- [70] A. Wojcicki, *Inorg. Chem. Commun.* **2002**, *5*, 82–97.
- [71] N. Krause, A. S. K. Hashmi, *Modern Allene Chemistry*, WILEY-VCH Verlag GmbH & Co. KGaA, Weinheim, **2004**.
- [72] S. Doherty, J.F. Corrigan, A.J. Carty, E. Sappa, *Adv. Organomet. Chem.* **1995**, *37*, 39–125.
- [73] J. M. A. Wouters, R. A. Klein, C. J. Elsevier, L. Haming, C. H. Stam, *Organometallics* **1994**, *13*, 4586–4593.
- [74] M. A. Esteruelas, A. V. Gómez, A. M. López, J. Modrego, E. Oñate, *Organometallics* **1998**, *17*, 5434–5436.
- [75] M. I. Bruce, *Chem. Rev.* **1998**, *98*, 2797–2858.
- [76] S. Rigaut, D. Touchard, P. H. Dixneuf, *Coord. Chem. Rev.* **2004**, *248*, 1585–1601.
- [77] N. Kim, R. A. Widenhoefer, *Angew. Chem. Int. Ed.* **2018**, *57*, 4722–4726.
- [78] E. Wuttke, B. Nägele, B. Weibert, F. Kessler, *Organometallics* **2011**, *30*, 6270–6282.
- [79] K. M. Brummond, J. E. DeForrest, *Synthesis* **2007**, 795–818.
- [80] X. Huang, S. Ma, *Acc. Chem. Res.* **2019**, 1301–1312.
- [81] S. Yu, S. Ma, *Chem. Commun.* **2011**, *47*, 5384–5418.
- [82] E. A. Deutsch, B. B. Snider, *Tetrahedron Lett.* **1983**, *24*, 3701–3704.
- [83] J. A. Marshall, J. Liao, *J. Org. Chem.* **1998**, *63*, 5962–5970.
- [84] H. Hauptmann, *Tetrahedron Lett.* **1974**, 3593–3596.
- [85] J. -P. Dulcere, J. Crandall, R. Faure, M. Santelli, V. Agati, M. N. Mihoubi, *J. Org. Chem.* **1993**, *58*, 5702–5708.
- [86] A. R. Katritzky, S. Zhang, A. H. M. Hussein, Y. Fang, P. J. Steel, *J. Org. Chem.* **2001**, *66*, 5606–5612.
- [87] G. Saucy, R. Marbet, *Helv. Chim. Acta* **1967**, *50*, 1158–1167.
- [88] C. Agami, F. Couty, G. Evano, *Eur. J. Org. Chem.* **2002**, 29–38.
- [89] V. Vaithyanathan, K. Selvakumar, P. Shanmugam, *Synlett* **2009**, 1591–1596.
- [90] A. L. Castelhana, A. J. Krantz, *J. Am. Chem. Soc.* **1984**, *106*, 1877–1879.
- [91] L. F. V. Pinto, P. M. C. Glo'ria, M. J. S. Gomes, H. S. Rzepa, S. Prabhakar, A. M. Lobo, *Tetrahedron Lett.* **2009**, *50*, 3446–3449.
- [92] B. D. Sherry, F. D. Toste, *J. Am. Chem. Soc.* **2004**, *126*, 15978–15979.
- [93] K. Tanaka, E. Okazaki, Y. Shibata, *J. Am. Chem. Soc.* **2009**, *131*, 10822–10823.
- [94] C. Mukai, M. Ohta, H. Yamashita, S. Kitagaki, *J. Org. Chem.* **2004**, *69*, 6867–6873.
- [95] V. C. Christov, J. G. Ivanova, *Synth. Commun.* **2006**, *36*, 2231–2244.
- [96] N. N. B. Kumar, M. Chakravarty, N. S. Kumar, K. V. Sajna, K. C. K. Swamy, *J. Chem. Sci.* **2009**, *121*, 23–36.
- [97] M. Harmata, C. Huang, *Adv. Synth. Catal.* **2008**, *350*, 972–974.
- [98] M. Lahrech, S. Hacini, J. -L. Parrain, M. Santelli, *Tetrahedron Lett.* **1997**, *38*, 3395–3398.
- [99] M. S. Baird, A. V. Nizovtsev, I. G. Bolesov, *Tetrahedron* **2002**, *58*, 1581–1593.
- [100] T. Satoh, Y. Gouda, *Tetrahedron Lett.* **2006**, *47*, 2835–2838.
- [101] K. M. Brummond, D. Chen, *Org. Lett.* **2005**, *7*, 3473–3475.
- [102] J. Yamazaki, T. Watanabe, K. Tanaka, *Tetrahedron: Asymmetry* **2001**, *12*, 669–675.
- [103] P. Crabbe, D. Andre, H. Fillion, *Tetrahedron Lett* **1979**, *20*, 893–896.
- [104] S. Searles, Y. Li, B. Nassim, M. R. Lopes, P. T. Tran, P. Crabbe, *J. Chem. Soc., Perkin Trans. 1* **1984**, 747–751.

- [105] X. Tang, X. Huang, T. Cao, Y. Han,, X. Jiang, W. Lin, Y. Tang, J. Zhang, Q. Yu, C. Fu, S. Ma, *Org. Chem. Front.* **2015**, *2*, 688–691.
- [106] J. Kuang, X. Tang, S. Ma, *Org. Chem. Front.* **2015**, *2*, 470–475.
- [107] M. Ogasawara, H. Ikeda, T. Hayashi, *Angew. Chem. Int. Ed.* **2000**, *39*, 1042–1044.
- [108] M. Ogasawara, H. Ikeda, T. Nagano, T. Hayashi, *Org. Lett.* **2001**, *3*, 2615–2617.
- [109] Y. Watanabe, T. Yamazaki, *Synlett* **2009**, 3352–3354.
- [110] D. R. Fandrick, J. T. Reeves, Z. Tan, H. Lee, J. J. Song,, N. K. Yee, C. H. Senanayake, *Org. Lett.* **2009**, *11*, 5458–5461.
- [111] P. C. Ravikumar, L. Yao, F. F. Fleming, *J. Org. Chem.* **2009**, *74*, 7294–7299.
- [112] A. Claesson, A. Quader, C. Sahlberg, *Tetrahedron Lett.* **1983**, *24*, 1297–1300.
- [113] T. Nishiyama, T. Esumi, Y. Iwabuchi, H. Irie, S. Hatakeyama, *Tetrahedron Lett.* **1998**, *39*, 43–46.
- [114] M. Ogasawara, K. Ueyama, T. Nagano, Y. Mizuhata, T. Hayashi, *Org. Lett.* **2003**, *5*, 217–219.
- [115] M. Ogasawara, H. Murakami, T. Furukawa, T. Takahashi,, N. Shibata, *Chem. Commun.* **2009**, 7366–7368.
- [116] P. Rona, P. Crabbe, *J. Am. Chem. Soc.* **1969**, *91*, 3289–3292.
- [117] S. Ma, E.-i. Negishi, *J. Am. Chem. Soc.* **1995**, *117*, 6345–6357.
- [118] D. Llerena, O. Buisine, C. Aubert, M. Malacria, *Tetrahedron* **1998**, *54*, 9373–9392.
- [119] M. Mae, J. A. Hong, B. Xu,, G. B. Hammond, *Org. Lett.* **2006**, *8*, 479–482.
- [120] N. Krause, A. S. K. Hashmi, *Modern Allene Chemistry*, WILEY-VCH Verlag GmbH & Co. KGaA, Weinheim, **2004**, 54.
- [121] J. D. Buynak, D. Khasnis, B. Bachmann, K. Wu, G. Lamb, *J. Am. Chem. Soc.* **1994**, *116*, 10955–10965.
- [122] S. Thorand, F. Vögtle, N. Krause, *Angew. Chem. Int. Ed.* **1999**, *38*, 3721–3723.
- [123] A. Fürstner, M. Mendez, *Angew. Chem. Int. Ed.* **2003**, *42*, 5355–5357.
- [124] H. Ito, Y. Sasaki, M. Sawamura, *J. Am. Chem. Soc.* **2008**, *130*, 15774–15775.
- [125] J. Li, C. Zhou, C. Fu, S. Ma, *Tetrahedron* **2009**, *65*, 3695–3703.
- [126] D. J. Pasto, G. F. Hennion, R. H. Shults, A. Waterhouse, *J. Org. Chem.* **1976**, *41*, 3496–3496.
- [127] A. Jansen, N. Krause, *Synthesis* **2002**, 1987–2002.
- [128] S. Kobayashi, K. Nishio, *J. Am. Chem. Soc.* **1995**, *117*, 6392–6893.
- [129] I. Matsuda, K.-i. Komori, K. Itoh, *J. Am. Chem. Soc.* **2002**, *124*, 9072–9073.
- [130] D. Girard, S. Broussous,, O. Provot, J.-D. Brion, M. Alami, *Tetrahedron Lett.* **2007**, *48*, 6022–6026.
- [131] M. Yoshida, T. Okada and, K. Shishido, *Tetrahedron* **2007**, *63*, 6996–7002.
- [132] Z. Zhang, S. Mo, G. Zhang, X. Shao, Q. Li, Y. Zhong, *Synlett* **2017**, *28*, 611–614.
- [133] H. Jiang, X. Liu, L. Zhou, *Chem. Eur. J.* **2008**, *14*, 11305–11309.
- [134] D. R. Williams, A. A. Shah, *Chem. Commun.* **2010**, *46*, 4297–4299.
- [135] R. L. Snowden, S. Linder, *Helv. Chim. Acta* **2005**, *88*, 3055–3068.
- [136] N. Furuichi, H. Hara, T. Osaki, M. Nakano, H. Mori, S. Katsumura, *J. Org. Chem.* **2004**, *69*, 7949–7959.
- [137] N. Krause, A. Hoffmann-Röder, J. Canisius, *Synthesis* **2002**, 1759–1774.
- [138] G. Handke, N. Krause, *Tetrahedron Lett.* **1993**, *34*, 6037–6040.
- [139] U. Koop, G. Handke, N. Krause, *Liebigs Ann. Chem.* **1996**, 1487–1499.
- [140] J. W. Han, N. Tokunaga, T. Hayashi, *J. Am. Chem. Soc.* **2001**, *123*, 12915–12916.
- [141] C. Moberg, *Org. Lett.* **2008**, *10*, 2505–2508.
- [142] A. Tillack, D. Michalik, C. Koy, M. Michalik, *Tetrahedron Lett.* **1999**, *40*, 6567–6568.

- [143] Y. Maruyama, K. Yamamura, I. Nakayama, K. Yoshiuchi, F. Ozawa, *J. Am. Chem. Soc.* **1998**, *120*, 1421–1429.
- [144] W. Zhang, H. Xu, H. Xu, W. Tang, *J. Am. Chem. Soc.* **2009**, *131*, 3832–3833.
- [145] R. J. Armstrong, *Curr. Org. Chem.* **2019**, *23*, 3027–3039.
- [146] T. Satoh, N. Hanaki, Y. Kuramochi, Y. Inoue, K. Hosoya, K. Sakai, *Tetrahedron* **2002**, *58*, 2533–2549.
- [147] M. Yokota, K. Fuchibe, M. Ueda, Y. Mayumi, J. Ichikawa, *Org. Lett.* **2009**, *11*, 3994–3997.
- [148] T. Yamazaki, T. Yamamoto, R. Ichihara, *J. Org. Chem.* **2006**, *71*, 6251–6253.
- [149] S. Löhr, J. Averbek, M. Schürmann, N. Krause, *Eur. J. Inorg. Chem.* **2008**, *2008*, 552–556.
- [150] X. Pu, X. Qi, J. M. Ready, *J. Am. Chem. Soc.* **2009**, *131*, 10364–10365.
- [151] F. Cai, X. Pu, X. Qi, V. Lynch, A. Radha, J. M. Ready, *J. Am. Chem. Soc.* **2011**, *133*, 18066–18069.
- [152] M. I. Antczak, F. Cai, J. M. Ready, *Org. Lett.* **2011**, *13*, 184–187.
- [153] F. Cai, N. D. Thangada, E. Pan, J. M. Ready, *Organometallics* **2013**, *32*, 5619–5622.
- [154] A. Vanitcha, G. Gontard, N. Vanthuynne, E. Derat, V. Mouriès-Mansuy, L. Fensterbank, *Adv. Synth. Catal.* **2015**, *357*, 2213–2218.
- [155] E. V. Banide, J. P. Grealis, H. Müller-Bunz, Y. Ortin, M. Casey, C. Mendicute-Fierro, M. Cristina Lagunas, M. J. McGlinchey, *J. Organomet. Chem.* **2008**, *693*, 1759–1770.
- [156] S. Milosevic, E. V. Banide, H. Müller-Bunz, D. G. Gilheany, M. J. McGlinchey, *Organometallics* **2011**, *30*, 3804–3817.
- [157] A. Vanitcha, C. Damelin-court, G. Gontard, N. Vanthuynne, V. Mouriès-Mansuy, L. Fensterbank, *Chem. Commun.* **2016**, *52*, 6785–6788.
- [158] H. Schmidbaur, C. M. Frazão, G. Reber, G. Müller, *Chem. Ber.* **1989**, *122*, 259–263.
- [159] S. E. Denmark, Y. Fan, *Tetrahedron: Asymmetry* **2006**, *17*, 687–707.
- [160] S. Ushijima, S. Dohi, K. Moriyama, H. Togo, *Tetrahedron* **2012**, *68*, 1436–1442.
- [161] D. B. Dess, J. C. Martin, *J. Am. Chem. Soc.* **1991**, *113*, 7277–7287.
- [162] T. Hirayama, S. Ueda, T. Okada, N. Tsurue, K. Okuda, H. Nagasawa, *Chem. Eur. J.* **2014**, *20*, 4156–4162.
- [163] M. Murai, S. Kitabata, K. Okamoto, K. Ohe, *Chem. Commun.* **2012**, *48*, 7622–7624.
- [164] X. Zhang, S. Sarkar, R. C. Larock, *J. Org. Chem.* **2006**, *71*, 236–243.
- [165] Van Overmeire, S. A. Boldin, K. Venkataraman, R. Zisling, S. De Jonghe, S. Van Calenbergh, D. De Keukeleire, A. H. Futerman, P. Herdewijn, *J. Med. Chem.* **2000**, *43*, 4189–4199.
- [166] M. Shimizu, M. Higashi, Y. Takeda, G. Jiang, M. Murai, T. Hiyama, *Synlett* **2007**, *7*, 1163–1165.
- [167] J. Xiao, H. Luo, S. Huang, H. Qian, S. Ma, *Chem. Commun.* **2018**, *54*, 10451–10454.
- [168] H. Kurata, M. Monden, T. Kawase, M. Oda, *Tetrahedron Lett.* **1998**, *39*, 7135–7138.
- [169] S. Kobayashi, Y. Mori, Y. Yamashita, *Comprehensive Coordination Chemistry II*, Elsevier Pergamon, Oxford; San Diego, **2004**, 405–415.
- [170] D. A. Engel, G. B. Dudley, *Org. Biomol. Chem.* **2009**, *7*, 4149–4158.
- [171] V. Cadierno, J. Francos, J. Gimeno, *Tetrahedron Lett.* **2009**, *50*, 4773–4776.
- [172] M. Egi, Y. Yamaguchi, N. Fujiwara, S. Akai, *Org. Lett.* **2008**, *10*, 1867–1870.
- [173] K. A. Nolin, R. W. Ahn, Y. Kobayashi, J. J. Kennedy-Smith, F. D. Toste, *Chem. Eur. J.* **2010**, *16*, 9555–9562.
- [174] D. A. Engel, G. B. Dudley, *Org. Lett.* **2006**, *8*, 4027–4029.

- [175] S. Aiken, B. Armitage, C. D. Gabbutt, B. M. Heron, *Tetrahedron Lett.* **2015**, *56*, 4840–4842.
- [176] N. Cabrera-Lobera, N. Velasco, R. Sanz, M. A. Fernández-Rodríguez, *Tetrahedron* **2019**, *75*, 4071–4080.
- [177] A. R. Ubbelohde, J. A. Burgess, *J. Chem. Soc. (B)* **1970**, 1106–1113.
- [178] P. Maitland, W. H. Mills, *J. Chem. Soc. Resumed* **1936**, 987–998.
- [179] H. Mayr, B. Kempf, A. R. Ofial, *Acc. Chem. Res.* **2003**, *36*, 66–77.
- [180] F. Brotzel, B. Kempf, T. Singer, H. Zipse, H. Mayr, *Chem. Eur. J.* **2007**, *13*, 336–345.
- [181] C. Bazzicalupi, A. Bencini, A. Bianchi, A. Danesi, E. Faggi, C. Giorgi, S. Santarelli, B. Valtancoli, *Coord. Chem. Rev.* **2008**, *252*, 1052–1068.
- [182] F. Fache, E. Schulz, M. L. Tommasino, M. Lemaire, *Chem. Rev.* **2000**, *100*, 2159–2232.
- [183] C. Bazzicalupi, A. Bencini, A. Bianchi, C. Giorgi, B. Valtancoli, *Coord. Chem. Rev.* **1999**, *184*, 243–270.
- [184] A. Togni, L. M. Venanzi, *Angew. Chem. Int. Ed. Engl.* **1994**, *33*, 497–526.
- [185] S. Gladioli, E. Alberico, *Chem Soc Rev* **2006**, *35*, 226–236.
- [186] I. Ott, *Coord. Chem. Rev.* **2009**, *253*, 1670–1681.
- [187] K. M. Deo, D. L. Ang, B. McGhie, A. Rajamanickam, A. Dhiman, A. Khoury, J. Holland, A. Bjelosevic, B. Pages, C. Gordon, J. R. Aldrich-Wright, *Coord. Chem. Rev.* **2018**, *375*, 148–163.
- [188] R. K. Dieter, N. Chen, H. Yu, L. E. Nice, V. K. Gore, *J. Org. Chem.* **2005**, *70*, 2109–2119.
- [189] H. Ohno, A. Toda, N. Fujii, Y. Takemoto, T. Tanaka, T. Ibuka, *Tetrahedron* **2000**, *56*, 2811–2820.
- [190] Y. Ittah, Y. Sasson, I. Shahak, S. Tsaroom, J. Blum, *J. Org. Chem.* **1978**, *43*, 4271–4273.
- [191] L. Pauli, R. Tannert, R. Scheil, A. Pfaltz, *Chem. Eur. J.* **2015**, *21*, 1482–1487.
- [192] D. J. Gallagher, S. Wu, N. A. Nikolic, P. Beak, *J. Org. Chem.* **1995**, *60*, 8148–8154.
- [193] N. Liu, Y. Zhi, J. Yao, J. Xing, T. Lu, X. Dou, *Adv. Synth. Catal.* **2018**, *360*, 642–646.
- [194] D. Qian, L. Wu, Z. Lin, J. Sun, *Nat. Commun.* **2017**, *8*, 1–9.
- [195] P. Zhang, Q. Huang, Y. Cheng, R. Li, P. Li, W. Li, *Org. Lett.* **2019**, *21*, 503–507.
- [196] I. Scheipers, C. Mück-Lichtenfeld, A. Studer, *Angew. Chem. Int. Ed.* **2019**, *58*, 6545–6548.
- [197] Q. Liu, X. Tang, Y. Cai, S. Ma, *Org. Lett.* **2017**, *19*, 5174–5177.
- [198] D. Chernyak, S. B. Gadamsetty, V. Gevorgyan, *Org. Lett.* **2008**, *10*, 2307–2310.
- [199] C.-F. Xu, M. Xu, L.-Q. Yang, C.-Y. Li, *J. Org. Chem.* **2012**, *77*, 3010–3016.
- [200] T. Schwier, A. W. Sromek, D. M. L. Yap, D. Chernyak, V. Gevorgyan, *J. Am. Chem. Soc.* **2007**, *129*, 9868–9878.
- [201] L.-P. Liu, B. Xu, M. S. Mashuta, G. B. Hammond, *J. Am. Chem. Soc.* **2008**, *130*, 17642–17643.
- [202] G. Seidel, A. Fürstner, *Angew. Chem. Int. Ed.* **2014**, *53*, 4807–4811.
- [203] R. J. Harris, R. A. Widenhofer, *Angew. Chem. Int. Ed.* **2014**, *53*, 9369–9371.
- [204] S. Sentets, R. Serres, Y. Ortin, N. Lugan, G. Lavigne, *Organometallics* **2008**, *27*, 2078–2091.
- [205] N. C. Vieira, J. A. Pienkos, C. D. McMillen, A. R. Myers, A. P. Clay, P. S. Wagenknecht, *Dalton Trans.* **2017**, *46*, 15195–15199.
- [206] L. D. Jaques, S. L. McDarmont, M. M. Smart, C. D. McMillen, S. E. Neglia, J. P. Lee, J. A. Pienkos, *Inorg. Chem. Commun.* **2020**, *112*, 107722–107727.
- [207] T. Kawano, T. Shinomaru, I. Ueda, *Org. Lett.* **2002**, *4*, 2545–2547.

- [208] R. D. Shannon, *Acta Cryst.* **1976**, A32, 751–767.
- [209] R. Kuroda, S. Neidle, I. M. Ismail, P. J. Sadler, *Inorg. Chem.* **1983**, 22, 3620–3624.
- [210] M. D. Hall, T. W. Hambley, *Coord. Chem. Rev.* **2002**, 232, 49–67.
- [211] Y. Shi, S.-A. Liu, D. J. Kerwood, J. Goodisman, J. C. Dabrowiak, *J. Inorg. Biochem.* **2012**, 107, 6–14.
- [212] D. Höfer, H. P. Varbanov, M. Hejl, M. A. Jakupec, A. Roller, M. Galanski, B. K. Keppler, *J. Inorg. Biochem.* **2017**, 174, 119–129.
- [213] M. Albrecht, *Chem. Rev.* **2010**, 110, 576–623.
- [214] G. Minghetti, S. Stoccoro, M. A. Cinellu, B. Soro, A. Zucca, *Organometallics* **2003**, 22, 4770–4777.
- [215] G. Minghetti, A. Doppiu, A. Zucca, S. Stoccoro, M. A. Cinellu, M. Manassero, M. Sansoni, *Chem. Heterocycl. Compd.* **1999**, 35, 992–1000.
- [216] S.-X. Guo, D. N. Mason, S. A. Turland, E. T. Lawrenz, L. C. Kelly, G. D. Fallon, B. M. Gatehouse, A. M. Bond, G. B. Deacon, A. R. Battle, T. W. Hambley, S. Rainone, L. K. Webster, C. Cullinane, *J. Inorg. Biochem.* **2012**, 115, 226–239.
- [217] M. C. McCormick, K. Keijzer, A. Polavarapu, F. A. Schultz, M.-H. Baik, *J. Am. Chem. Soc.* **2014**, 136, 8992–9000.
- [218] L.T. Ellis, H.M. Er, T.W. Hambley, *Aust. J. Chem.* **1995**, 48, 793–806.
- [219] A.R. Khokhar, Y. Deng, Y. Kido, A.H. Siddik, *J. Inorg. Biochem.* **1993**, 50, 79–87.
- [220] T.W. Hambley, A.R. Battle, G.B. Deacon, E.T. Lawrenz, G.D. Fallon, B.M. Gatehouse, L.K. Webster, S. Rainone, *J. Inorg. Biochem.* **1999**, 77, 3–12.
- [221] S. Choi, C. Filotto, M. Bisanzo, S. Delaney, D. Lagasee, J. L. Whitworth, A. Jusko, C. Li, N. A. Wood, J. Willingham, A. Schwenker, K. Spaulding, *Inorg. Chem.* **1998**, 37, 2500–2504.
- [222] Y. Kido, A.R. Khokhar, A.H. Siddik, *Biochem. Pharmacol* **1994**, 47, 1635–1642.
- [223] J.J.Z. Zhang, E. Wexselblatt, T.W. Hambley, D. Gibson, *Chem. Commun.* **2012**, 48, 847–849.
- [224] M. Fañanás-Mastral, F. Aznar, *Organometallics* **2009**, 28, 666–668.
- [225] G. Seidel, B. Gabor, R. Goddard, B. Heggen, W. Thiel, A. Fürstner, *Angew. Chem. Int. Ed.* **2014**, 53, 879–882.
- [226] G. Kleinhans, M. M. Hansmann, G. Guisado-Barrios, D. C. Liles, G. Bertrand, D. I. Bezuidenhout, *J. Am. Chem. Soc.* **2016**, 138, 15873–15876.
- [227] J. Chu, D. Munz, R. Jazzar, M. Melaimi, G. Bertrand, *J. Am. Chem. Soc.* **2016**, 138, 7884–7887.
- [228] D. Schneider, O. Schuster, H. Schmidbaur, *Dalton Trans.* **2005**, 1940–1947.
- [229] T. Martinez, I. Alahyen, G. Lemièrre, V. Mouriès-Mansuy, L. Fensterbank, *Org. Process Res. Dev.* **2020**, 24, 817–821.
- [230] M. Melaimi, R. Jazzar, M. Soleilhavoup, G. Bertrand, *Angew. Chem. Int. Ed.* **2017**, 56, 10046–10068.
- [231] H. G. Raubenheimer, S. Cronje, *Chem. Soc. Rev.* **2008**, 37, 1998–2011.
- [232] J. Cure, R. Poteau, I. C. Gerber, H. Gornitzka, C. Hemmert, *Organometallics* **2012**, 31, 619–626.
- [233] B. Bertrand, L. Stefan, M. Pirrotta, D. Monchaud, E. Bodio, P. Richard, P. Le Gendre, E. Warmerdam, M. H. de Jager, G. M. M. Groothuis, M. Picquet, A. Casini, *Inorg. Chem.* **2014**, 53, 2296–2303.
- [234] S. M. Meier-Menches, B. Aikman, D. Döllerer, W. T. Klooster, S. J. Coles, N. Santi, L. Luk, A. Casini, R. Bonsignore, *J. Inorg. Biochem.* **2020**, 202, 110844–110856.
- [235] C. Praveen, *Coord. Chem. Rev.* **2019**, 392, 1–34.

- [236] T. J. Brown, A. Sugie, M. G. D. Leed, R. A. Widenhoefer, *Chem. - Eur. J.* **2012**, *18*, 6959–6971.
- [237] Compound **97e** was prepared by Tino Freestone.
- [238] J. Yang, Y. Zhu, A. K.-W. Tse, X. Zhou, Y. Chen, Y. C. Tse, K. M.-C. Wong, C.-Y. Ho, *Chem. Commun.* **2019**, *55*, 4471–4474.
- [239] V. Sivchik, R. K. Sarker, Z.-Y. Liu, K.-Y. Chung, E. V. Grachova, A. J. Karttunen, P.-T. Chou, I. O. Koshevoy, *Chem. Eur. J.* **2018**, *24*, 11475–11484.
- [240] J. A. Akana, K. X. Bhattacharyya, P. Müller, J. P. Sadighi, *J. Am. Chem. Soc.* **2007**, *129*, 7736–7737.
- [241] A. S. K. Hashmi, A. M. Schuster, F. Rominger, *Angew. Chem. Int. Ed.* **2009**, *48*, 8247–8249.
- [242] Y. Zhu, B. Yu, *Angew. Chem. Int. Ed.* **2011**, *50*, 8329–8332.
- [243] A. G. Nair, R. T. McBurney, M. R. D. Gatus, S. C. Binding, B. A. Messerle, *Inorg. Chem.* **2017**, *56*, 12067–12075.
- [244] M. Pažický, A. Loos, M. J. Ferreira, D. Serra, N. Vinokurov, F. Rominger, C. Jäkel, A. S. K. Hashmi, M. Limbach, *Organometallics* **2010**, *29*, 4448–4458.
- [245] G. Minghetti, F. Bonati, G. Banditelli, *Inorg. Chem.* **1976**, *15*, 1718–1720.
- [246] R. Kumar, J.-P. Krieger, E. Gómez-Bengoia, T. Fox, A. Linden, C. Nevado, *Angew. Chem. Int. Ed.* **2017**, *56*, 12862–12865.
- [247] J. A. González, F. Verdugo, J. L. Mascareñas, F. López, C. Nevado, *Angew. Chem. Int. Ed.* **2020**, *59*, 20049–20054.
- [248] H.-F. Duan, J.-H. Xie, X.-C. Qiao, L.-X. Wang, Q.-L. Zhou, *Angew. Chem. Int. Ed.* **2008**, *47*, 4351–4353.
- [249] C. Nieto-Oberhuber, M. P. Muñoz, E. Buñuel, C. Nevado, D. J. Cárdenas, A. M. Echavarren, *Angew. Chem. Int. Ed.* **2004**, *43*, 2402–2406.
- [250] S. P. Nolan, *Acc. Chem. Res.* **2011**, *44*, 91–100.
- [251] A. Correa, S. P. Nolan, L. Cavallo, *Computational Mechanisms of Au and Pt Catalyzed Reactions; Topics in Current Chemistry*, Springer, Berlin; Heidelberg, **2011**.
- [252] E. Peris, *Chem. Rev.* **2018**, *118*, 9988–10031.
- [253] Á. Vivancos, C. Segarra, M. Albrecht, *Chem. Rev.* **2018**, *118*, 9493–9586.
- [254] M. Soleilhavoup, G. Bertrand, *Acc. Chem. Res.* **2015**, *48*, 256–266.
- [255] J. Tsuji, H. Takahashi, M. Morikawa, *Tetrahedron Lett.* **1965**, *6*, 4387–4388.
- [256] B. M. Trost, T. J. Fullerton, *J. Am. Chem. Soc.* **1973**, 292–294.
- [257] M. E. Krafft, Z. Fu, M. J. Procter, A. M. Wilson, A. Dasse, C. Hirose, *Pure Appl. Chem.* **1998**, *1970*, 1083–1090.
- [258] R. Prétôt, A. Pfaltz, *Angew. Chem. Int. Ed.* **1998**, *37*, 323–325.
- [259] S. Noreen, A. F. Zahoor, S. Ahmad, I. Shahzadi, A. Irfan, S. Faiz, *Curr. Org. Chem.* **2019**, *23*, 1168–1213.
- [260] L. Milhau, P. J. Guiry, *Transition Metal Catalyzed Enantioselective Allylic Substitution in Organic Synthesis*, Springer, Berlin; Heidelberg, **2011**, 95–153.
- [261] G. Chelucci, A. Saba, G. Sanna, F. Soccolini, *Tetrahedron Asymmetry* **2000**, *11*, 3427–3438.
- [262] T. Mizoroki, K. Mori, A. Ozaki, *Bull. Chem. Soc. Jpn.* **1971**, 581–581.
- [263] R. F. Heck, J. P. Nolley, *J. Org. Chem.* **1972**, *37*, 2320–2322.
- [264] C. C. C. Johansson Seechurn, M. O. Kitching, T. J. Colacot, V. Snieckus, *Angew. Chem. Int. Ed.* **2012**, *51*, 5062–5085.
- [265] A. B. Dounay, L. E. Overman, *Chem. Rev.* **2003**, *103*, 2945–2964.
- [266] C. Torborg, M. Beller, *Adv. Synth. Catal.* **2009**, *351*, 3027–3043.

- [267] J. Magano, J. R. Dunetz, *Chem. Rev.* **2011**, *111*, 2177–2250.
- [268] Y. Sato, M. Sodeoka, M. Shibasaki, *J. Org. Chem.* **1989**, *54*, 4738–4739.
- [269] N. E. Carpenter, D. J. Kucera, L. E. Overman, *J. Org. Chem.* **1989**, *54*, 5846–5848.
- [270] M. Shibasaki, E. M. Vogl, T. Ohshima, *Adv. Synth. Catal.* **2004**, *346*, 1533–1552.
- [271] S. Y. Cho, M. Shibasaki, *Tetrahedron Lett.* **1998**, *39*, 1773–1776.
- [272] A. Ortiz, P. Gómez-Sal, J. C. Flores, E. de Jesús, *Organometallics* **2018**, *37*, 3598–3610.
- [273] P. Elumalai, R. Ujjval, M. Nethaji, N. Thirupathi, *Polyhedron* **2018**, *151*, 313–322.
- [274] A. M. Echavarren, C. Nevado, *Chem. Soc. Rev.* **2004**, *33*, 431–436.
- [275] E. Jiménez-Núñez, A. M. Echavarren, *Chem. Rev.* **2008**, *108*, 3326–3350.
- [276] L. Fensterbank, M. Malacria, *Acc. Chem. Res.* **2014**, *47*, 953–965.
- [277] M. T. Quirós, M. P. Muñoz, *Au-Catalyzed Synthesis and Functionalization of Heterocycles*, Springer, Cham, **2016**, 117–174.
- [278] M. E. Krafft, A. M. Wilson, O. A. Dasse, L. V. R. Bonaga, Y. Y. Cheung, Z. Fu, B. Shao, I. L. Scott, *Tetrahedron Lett.* **1998**, *39*, 5911–5914.
- [279] M. Takachi, Y. Kita, M. Tobisu, Y. Fukumoto, N. Chatani, *Angew. Chem.* **2010**, *122*, 8899–8902.
- [280] B. M. Trost, Y. Li, *J. Am. Chem. Soc.* **1996**, *118*, 6625–6633.
- [281] M. Mori, Y. Kozawa, M. Nishida, M. Kanamaru, K. Onozuka, M. Takimoto, *Org. Lett.* **2000**, *2*, 3245–3247.
- [282] C. Nieto-Oberhuber, M. P. Muñoz, S. López, E. Jiménez-Núñez, C. Nevado, E. Herrero-Gómez, M. Raducan, A. M. Echavarren, *Chem. Eur. J.* **2006**, *12*, 1677–1693.
- [283] L. Charruault, V. Michelet, R. Taras, S. Gladiali, J.-P. Genêt, *Chem. Commun.* **2004**, 850–851.
- [284] J.-C. Galland, S. Dias, M. Savignac, J.-P. Genêt, *Tetrahedron* **2001**, *57*, 5137–5148.
- [285] M. P. Muñoz, J. Adrio, J. C. Carretero, A. M. Echavarren, *Organometallics* **2005**, *24*, 1293–1300.
- [286] S. T. Diver, A. J. Giessert, *Chem. Rev.* **2004**, *104*, 1317–1382.
- [287] T. Kitamura, Y. Sato, M. Mori, *Adv. Synth. Catal.* **2002**, *344*, 678–693.
- [288] M. T. Reetz, *Angew. Chem. Int. Ed. Engl.* **1972**, *11*, 130–131.
- [289] N. Cabello, E. Jiménez-Núñez, E. Buñuel, D. J. Cárdenas, A. M. Echavarren, *Eur. J. Org. Chem.* **2007**, *2007*, 4217–4223.
- [290] J. Blum, H. Beer-Kraft, Y. Badrieh, *J. Org. Chem.* **1995**, *60*, 5567–5569.
- [291] A. Fürstner, F. Stelzer, H. Szillat, *J. Am. Chem. Soc.* **2001**, *123*, 11863–11869.
- [292] C. Nevado, C. Ferrer, A. M. Echavarren, *Org. Lett.* **2004**, *6*, 3191–3194.
- [293] S. Díez-González, N. Marion, S. P. Nolan, *Chem. Rev.* **2009**, *109*, 3612–3676.
- [294] M. Michalak, W. Kośnik, *Catalysts* **2019**, *9*, 890–930.
- [295] M. C. Kimber, *Org. Lett.* **2010**, *12*, 1128–1131.
- [296] A. B. Pritzius, B. Breit, *Angew. Chem.* **2015**, *127*, 3164–3168.
- [297] J. M. Alonso, M. P. Muñoz, *Org. Lett.* **2019**, *21*, 7639–7644.
- [298] M. P. Muñoz, M. C. de la Torre, M. A. Sierra, *Adv. Synth. Catal.* **2010**, *352*, 2189–2194.
- [299] M. P. Muñoz, M. C. de la Torre, M. A. Sierra, *Chem. Eur. J.* **2012**, *18*, 4499–4504.
- [300] L. Cooper, J. M. Alonso, L. Eagling, H. Newson, S. Herath, C. Thomson, A. Lister, C. Howsham, B. Cox, M. P. Muñoz, *Chem. Eur. J.* **2018**, *24*, 6105–6114.
- [301] M. T. Quirós, E. Gómez-Bengoa, M. P. Muñoz, *Pure Appl. Chem.* **2020**, *92*, 167–177.
- [302] Menggenbateer, M. Narsireddy, G. Ferrara, N. Nishina, T. Jin, Y. Yamamoto, *Tetrahedron Lett.* **2010**, *51*, 4627–4629.
- [303] W. Yang, A. S. K. Hashmi, *Chem. Soc. Rev.* **2014**, *43*, 2941–2955.

- [304] N. Krause, C. Winter, *Chem. Rev.* **2011**, *111*, 1994–2009.
- [305] Z. Zhang, S. Du Lee, A. S. Fisher, R. A. Widenhoefer, *Tetrahedron* **2009**, *65*, 1794–1798.
- [306] R. E. Kinder, Z. Zhang, R. A. Widenhoefer, *Org. Lett.* **2008**, *10*, 3157–3159.
- [307] Z. Zhang, R. A. Widenhoefer, *Org. Lett.* **2008**, *10*, 2079–2081.
- [308] C. F. Shaw, *Chem. Rev.* **1999**, *99*, 2589–2600.
- [309] T. Lazarević, A. Rilak, Ž. D. Bugarčić, *Eur. J. Med. Chem.* **2017**, *142*, 8–31.
- [310] Z. Guo, P. J. Sadler, *Adv. Inorg. Chem.* **2000**, *49*, 183–306.
- [311] T. W. Hambley, *Dalton Trans.* **2007**, 4929–4937.
- [312] C. G. Hartinger, N. Metzler-Nolte, P. J. Dyson, *Organometallics* **2012**, *31*, 5677–5685.
- [313] J. C. Dabrowiak, *Metals in Medicine*, John Wiley & Sons, Inc., Hoboken, New Jersey, **2017**.
- [314] A. Sigel, H. Sigel, E. Freisinger, R. K. O. Sigel, *Metallo-Drugs: Development and Action of Anticancer Agents*, Walter De Gruyter GmbH, Berlin; Boston, **2018**.
- [315] C. N. Morrison, K. E. Prosser, R. W. Stokes, A. Cordes, N. Metzler-Nolte, S. M. Cohen, *Chem. Sci.* **2020**, *11*, 1216–1225.
- [316] A. Frei, J. Zuegg, A. G. Elliott, M. Baker, S. Braese, C. Brown, F. Chen, C. G. Dowson, G. Dujardin, N. Jung, A. P. King, A. M. Mansour, M. Massi, J. Moat, H. A. Mohamed, A. K. Renfrew, P. J. Rutledge, P. J. Sadler, M. H. Todd, C. E. Willans, J. J. Wilson, M. A. Cooper, M. A. T. Blaskovich, *Chem. Sci.* **2020**, *11*, 2627–2639.
- [317] P. J. Sadler, Z. Guo, *Pure Appl. Chem.* **1998**, *70*, 863–871.
- [318] R. M. Lord, P. C. McGowan, *Chem. Lett.* **2019**, *48*, 916–924.
- [319] G. Gasser, I. Ott, N. Metzler-Nolte, *J. Med. Chem.* **2011**, *54*, 3–25.
- [320] S. A. Patil, S. A. Patil, R. Patil, R. S. Keri, S. Budagumpi, G. R. Balakrishna, M. Tacke, *Future Med. Chem.* **2015**, *7*, 1305–1333.
- [321] C. Saturnino, I. Barone, D. Iacopetta, A. Mariconda, M. S. Sinicropi, C. Rosano, A. Campana, S. Catalano, P. Longo, S. Andò, *Future Med. Chem.* **2016**, *8*, 2213–2229.
- [322] T. Gianferrara, I. Bratsos, E. Alessio, *Dalton Trans.* **2009**, 7588–7598.
- [323] E. Boros, A. B. Packard, *Chem. Rev.* **2019**, *119*, 870–901.
- [324] S. Monro, K. L. Colón, H. Yin, J. Roque, P. Konda, S. Gujar, R. P. Thummel, L. Lilge, C. G. Cameron, S. A. McFarland, *Chem. Rev.* **2019**, *119*, 797–828.
- [325] Z. Yu, J. A. Cowan, *Chem. Eur. J.* **2017**, *23*, 14113–14127.
- [326] E. Meggers, *Chem. Commun.* **2009**, 1001–1010.
- [327] S. P. Fricker, *Metallomics* **2010**, *2*, 366–377.
- [328] D. P. Riley, R. H. Weiss, *J. Am. Chem. Soc.* **1994**, *116*, 387–388.
- [329] J. Maksimoska, L. Feng, K. Harms, C. Yi, J. Kissil, R. Marmorstein, E. Meggers, *J. Am. Chem. Soc.* **2008**, *130*, 15764–15765.
- [330] B. W. Harper, A. M. Krause-Heuer, M. P. Grant, M. Manohar, K. B. Garbutcheon-Singh, J. R. Aldrich-Wright, *Chem. Eur. J.* **2010**, *16*, 7064–7077.
- [331] B. Rosenberg, *Platinum Met. Rev.* **1971**, *15*, 42–51.
- [332] D. Wang, S. J. Lippard, *Nat. Rev. Drug Discov.* **2005**, *4*, 307–320.
- [333] M. Zaki, F. Arjmand, S. Tabassum, *Inorganica Chim. Acta* **2016**, *444*, 1–22.
- [334] P. J. Bednarski, F. S. Mackay, P. J. Sadler, *Anti-Cancer Agents Med. Chem.* **2007**, *75*–93.
- [335] S. Dhar, W. L. Daniel, D. A. Giljohann, C. A. Mirkin, S. J. Lippard, *J. Am. Chem. Soc.* **2009**, *131*, 14652–14653.
- [336] R. Koch, *Dtsch. Med. Wochenschr.* **1890**, *16*, 756.
- [337] J. Forestier, *J. Lab. Clin. Med.* **1935**, *20*, 827–840.



- [338] H. E. Abdou, A. A. Mohamed, J. P. Fackler, A. Burini, R. Galassi, J. M. López-de-Luzuriaga, M. E. Olmos, *Coord. Chem. Rev.* **2009**, *253*, 1661–1669.
- [339] S. P. Fricker, *PATAI'S Chemistry of Functional. Groups*, John Wiley & Sons, Ltd, Chichester, **2009**.
- [340] B. Bertrand, M. R. M. Williams, M. Bochmann, *Chem. Eur. J.* **2018**, *24*, 11840–11851.
- [341] P. Patanjali, R. Kumar, Sourabh, A. Kumar, P. Chaudhary, R. Singh, *Main Group Chem.* **2018**, *17*, 35–52.
- [342] A. Casini, M. C. Diawara, R. Scopelliti, S. M. Zakeeruddin, M. Grätzel, P. J. Dyson, *Dalton Trans.* **2010**, *39*, 2239–2245.
- [343] C.-M. Che, R. W.-Y. Sun, W.-Y. Yu, C.-B. Ko, N. Zhu, H. Sun, *Chem. Commun.* **2003**, 1718–1719.
- [344] J. J. Yan, A. L.-F. Chow, C.-H. Leung, R. W.-Y. Sun, D.-L. Ma, C.-M. Che, *Chem. Commun.* **2010**, *46*, 3893–3895.
- [345] J. H. Leibfarth, R. H. Persellin, *Agents Actions* **1981**, *11*, 458–472.
- [346] M. Navarro, H. Pérez, R. A. Sánchez-Delgado, *J. Med. Chem.* **1997**, *40*, 1937–1939.
- [347] D. L. Shapiro, J. R. Masci, *J. Rheumatol.* **1996**, *23*, 1818–1820.
- [348] T. Okada, B. K. Patterson, S. -Q. Ye, M. E. Gurney, *Virology* **1993**, *192*, 631–642.
- [349] F. Lovering, J. Bikker, C. Humblet, *J. Med. Chem.* **2009**, *52*, 6752–6756.
- [350] R. Twigg, *Nature* **1945**, *155*, 401–402.
- [351] J. L. Sebaugh, *Pharm. Stat.* **2011**, *10*, 128–134.
- [352] I. A. Cree, *Cancer Cell Culture*, Humana Press, Totowa, New Jersey, **2011**.
- [353] R. Czarnomysy, A. Surazyński, B. Popławska, E. Rysiak, N. Pawłowska, A. Czajkowska, K. Bielawski, A. Bielawska, *Mol. Cell. Biochem.* **2017**, *427*, 13–22.
- [354] E. Wong, C. M. Giandomenico, *Chem. Rev.* **1999**, *99*, 2451–2466.
- [355] J. Kasparkova, V. Marini, V. Bursova, V. Brabec, *Biophys. J.* **2008**, *95*, 4361–4371.
- [356] Y. Najajreh, J. M. Perez, C. Navarro-Ranninger, D. Gibson, *J. Med. Chem.* **2002**, *45*, 5189–5195.
- [357] A. R. Kapdi, I. J. S. Fairlamb, *Chem. Soc. Rev.* **2014**, *43*, 4751–4777.
- [358] S. M. Cohen, S. J. Lippard, *Prog. Nucleic Acid Res. Mol. Biol.* **2001**, 93–130.
- [359] C. K. Mirabelli, C.-M. Sung, J. P. Zimmerman, D. T. Hill, S. Mong, S. T. Crooke, *Biochem. Pharmacol.* **1986**, *35*, 1427–1433.
- [360] C. P. Saris, Pj. M. van de Vaart, R. C. Rietbroek, Fa. Bloramaert, *Carcinogenesis* **1996**, *17*, 2763–2769.
- [361] L. Messori, P. Orioli, C. Tempi, G. Marcon, *Biochem. Biophys. Res. Commun.* **2001**, *281*, 352–360.
- [362] S. G. Chaney, S. L. Campbell, B. Temple, E. Bassett, Y. Wu, M. Faldu, *J. Inorg. Biochem.* **2004**, *98*, 1551–1559.
- [363] D. Rhodes, H. J. Lipps, *Nucleic Acids Res.* **2015**, *43*, 8627–8637.
- [364] H. Abou Assi, M. Garavís, C. González, M. J. Damha, *Nucleic Acids Res.* **2018**, *46*, 8038–8056.
- [365] E. P. Wright, J. L. Huppert, Z. A. E. Waller, *Nucleic Acids Res.* **2017**, *45*, 2951–2959.
- [366] A. T. Phan, *Nucleic Acids Res.* **2002**, *30*, 4618–4625.
- [367] W. Lu, Y. Zhang, D. Liu, Z. Songyang, M. Wan, *Exp. Cell Res.* **2013**, *319*, 133–141.
- [368] J. W. Shay, S. Bacchetti, *Eur. J. Cancer* **1997**, *33*, 787–791.
- [369] A. I. H. Murchie, R. M. Clegg, E. von Krtzing, D. R. Duckett, S. Diekmann, D. M. J. Lilley, *Nature* **1989**, *341*, 763–766.
- [370] J.-L. Mergny, *Biochemistry* **1999**, *38*, 1573–1581.
- [371] B. R. Vummidi, J. Alzeer, N. W. Luedtke, *ChemBioChem* **2013**, *14*, 540–558.

- [372] Q. Sheng, J. C. Neaverson, T. Mahmoud, C. E. M. Stevenson, S. E. Matthews, Z. A. E. Waller, *Org. Biomol. Chem.* **2017**, *15*, 5669–5673.
- [373] M. Vorlíčková, I. Kejnovská, K. Bednářová, D. Renčiuk, J. Kypr, *Chirality* **2012**, *24*, 691–698.
- [374] J. Ye, S. Ma, *Org. Chem. Front.* **2014**, *1*, 1210–1224.
- [375] M. Ogasawara, *Tetrahedron Asymmetry* **2009**, *20*, 259–271.
- [376] B. C. N. M. Jones, J. V. Silverton, C. Simons, S. Megati, H. Nishimura, Y. Maeda, H. Mitsuya, J. Zemlicka, *J. Med. Chem.* **1995**, *38*, 1397–1405.
- [377] J. D. Carballeira, P. Krumlinde, M. Bocola, A. Vogel, M. T. Reetz, J.-E. Bäckvall, *Chem. Commun.* **2007**, 1913–1915.
- [378] P. G. Cozzi, S. Alesi, *Chem. Commun.* **2004**, 2448–2449.
- [379] M. Turlington, Y. Yue, X.-Q. Yu, L. Pu, *J. Org. Chem.* **2010**, *75*, 6941–6952.
- [380] X. Lu, G. Xie, T. Li, X. Qu, J. Mao, *Synth. Commun.* **2012**, *42*, 775–783.
- [381] W.-C. Huang, W. Liu, X.-D. Wu, J. Ying, L. Pu, *J. Org. Chem.* **2015**, *80*, 11480–11484.
- [382] D. K. Friel, M. L. Snapper, A. H. Hoveyda, *J. Am. Chem. Soc.* **2008**, *130*, 9942–9951.
- [383] Y. Kita, Y. Takebe, K. Murata, T. Naka, S. Akai, *J. Org. Chem.* **2000**, *65*, 83–88.
- [384] R. Kourist, P. Domínguez de María, U. T. Bornscheuer, *ChemBioChem* **2008**, *9*, 491–498.
- [385] I. Brackenridge, R. McCague, S. M. Roberts, N. J. Turner, *J. Chem. Soc. Perkin 1* **1993**, 1093–1094.
- [386] T. J. Wenzel, *Differentiation of Enantiomers II; Topics in Current Chemistry*, Springer, Cham, **2013**.
- [387] B. Milde, M. Pawliczek, P. G. Jones, D. B. Werz, *Org. Lett.* **2017**, *19*, 1914–1917.
- [388] T. S. Reddy, D. K. Reddy, M. Narasimhulu, D. Ramesh, Y. Venkateswarlu, *Helv. Chim. Acta* **2010**, *93*, 2158–2163.
- [389] D. J. Cassar, G. Ilyashenko, M. Ismail, J. Woods, D. L. Hughes, C. J. Richards, *Chem. Eur. J.* **2013**, *19*, 17951–17962.
- [390] *CrysAlisPro*, Rigaku Oxford Diffraction Ltd., Abingdon, UK, **2017**.
- [391] G. M. Sheldrick, *Acta Cryst.* **2015**, *A71*, 3–8.
- [392] G. M. Sheldrick, *Acta Cryst.* **2015**, *C71*, 3–8.
- [393] *Programs CrysAlisPro*, Rigaku Oxford Diffraction Ltd., Abingdon, UK, **2018**.
- [394] S. E. King, N. J. Ashcroft, *International Tables for Crystallography*, Kluwer Academic Publishers, Dordrecht, **1992**, 193, 219, 500.
- [395] T. M. Keck, M.-F. Zou, P. Zhang, R. P. Rutledge, A. H. Newman, *ACS Med. Chem. Lett.* **2012**, *3*, 544–549.
- [396] L. S. Kallander, Q. Lu, W. Chen, T. Tomaszek, G. Yang, D. Tew, T. D. Meek, G. A. Hofmann, C. K. Schulz-Pritchard, W. W. Smith, C. A. Janson, M. D. Ryan, G.-F. Zhang, K. O. Johanson, R. B. Kirkpatrick, T. F. Ho, P. W. Fisher, M. R. Mattern, R. K. Johnson, M. J. Hansbury, J. D. Winkler, K. W. Ward, D. F. Veber, S. K. Thompson, *J. Med. Chem.* **2005**, *48*, 5644–5647.
- [397] S. Ushijima, S. Dohi, K. Moriyama, H. Togo, *Tetrahedron* **2012**, *68*, 1436–1442.
- [398] T. Hirayama, S. Ueda, T. Okada, N. Tsurue, K. Okuda, H. Nagasawa, *Chem. Eur. J.* **2014**, *20*, 4156–4162.
- [399] A. Nagaki, S. Yamada, M. Doi, Y. Tomida, N. Takabayashi, J. Yoshida, *Green Chem.* **2011**, *13*, 1110–1113.
- [400] J. Mazuela, O. Pàmies, M. Diéguez, *Chem. Eur. J.* **2013**, *19*, 2416–2432.
- [401] G. C. Nandi, B. M. Rathman, K. K. Laali, *Tetrahedron Lett.* **2013**, *54*, 6258–6263.
- [402] I. Pérez, J. P. Sestelo, L. A. Sarandeses, *J. Am. Chem. Soc.* **2001**, *123*, 4155–4160.

- [403] I. Van Overmeire, S. A. Boldin, K. Venkataraman, R. Zisling, S. De Jonghe, S. Van Calenbergh, D. De Keukeleire, A. H. Futerman, P. Herdewijn, *J. Med. Chem.* **2000**, *43*, 4189–4199.
- [404] E. Paegle, S. Belyakov, M. Petrova, E. Liepinsh, P. Arsenyan, *Eur. J. Org. Chem.* **2015**, *2015*, 4389–4399.
- [405] A. F. Asachenko, V. N. Valaeva, V. A. Kudakina, D. V. Uborsky, V. V. Izmer, D. S. Kononovich, A. Z. Voskoboynikov, *Russ. Chem. Bull., Int. Ed.* **2016**, *65*, 456–463.
- [406] C. A. McAdam, M. G. McLaughlin, A. J. S. Johnston, J. Chen, M. W. Walter, M. J. Cook, *Org. Biomol. Chem.* **2013**, *11*, 4488–4502.
- [407] W. Zhao, E. M. Carreira, *Chem. Eur. J.* **2007**, *13*, 2671–2685.
- [408] A. Andicsová-Eckstein, D. Végh, A. Krutošíková, Z. Tokárová, *Arkivoc* **2018**, 124–139.
- [409] R. Moriarty, O. Prakash, M. P. Duncan, *J. Chem. Soc. Perkin Trans. 1* **1987**, 559–561.
- [410] S. Wei, H. Du, *J. Am. Chem. Soc.* **2014**, *136*, 12261–12264.
- [411] H. -Y. Wang, K. Huang, M. De Jesús, S. Espinosa, L. E. Piñero-Santiago, C. L. Barnes, M. Ortiz-Marciales, *Tetrahedron: Asymmetry* **2016**, *27*, 91–100.
- [412] X. Sun, X. Li, S. Song, Y. Zhu, Y.-F. Liang, N. Jiao, *J. Am. Chem. Soc.* **2015**, *137*, 6059–6066.
- [413] R. Munirathinam, D. Joe, J. Huskens, W. Verboom, *J. Flow. Chem.* **2012**, *2*, 129–134.
- [414] H. Shao, Q. Zhu, M. Goodman, *J. Org. Chem.* **1995**, *60*, 790–791.
- [415] Y. V. Shubina, D. A. Tikhomirov, A. V. Eremeev, *Chem. Heterocycl. Compd.* **1982**, *18*, 494–498.
- [416] R. R. Milburn, V. Snieckus, *Angew. Chem.* **2004**, *116*, 910–912.
- [417] K. Zhang, L. Chang, Q. An, X. Wang, Z. Zuo, *J. Am. Chem. Soc.* **2019**, *141*, 10556–10564.
- [418] D. Coucouvanis, *Inorganic Syntheses* 33, John Wiley & Sons, Inc., New York, **2002**, 189–196.
- [419] A. Gaballa, C. Wagner, H. Schmidt, D. Steinborn, *Z. Für Anorg. Allg. Chem.* **2003**, 629, 703–710.
- [420] G.-W. Lin, Y.-C. Lin, S.-C. Lin, Y.-S. Wen, L.-K. Liu, *J. Chin. Chem. Soc.* **2013**, *60*, 281–287.
- [421] M. Sinisi, V. Gandin, T. Saltarella, F. P. Intini, C. Pacifico, C. Marzano, G. Natile, *J. Biol. Inorg. Chem.* **2014**, *19*, 1081–1097.
- [422] J. K. Jawad, H. Adams, M. J. Morris, *Inorganica Chim. Acta* **2010**, *363*, 685–690.
- [423] Z. Chen, Y.-X. Zhang, Y.-H. Wang, L.-L. Zhu, H. Liu, X.-X. Li, L. Guo, *Org. Lett.* **2010**, *12*, 3468–3471.
- [424] W. Zhang, T. Shimanuki, T. Kida, Y. Nakatsuji, I. Ikeda, *J. Org. Chem.* **1999**, *64*, 6247–6251.
- [425] J. Pytkowicz, S. Roland, P. Mangeney, G. Meyer, A. Jutand, *J. Organomet. Chem.* **2003**, *678*, 166–179.
- [426] S. C. Söderman, A. L. Schwan, *J. Org. Chem.* **2012**, *77*, 10978–10984.
- [427] B. M. Trost, R. Braslau, *Tetrahedron Lett.* **1988**, *29*, 1231–1234.
- [428] M. P. Muñoz, M. Méndez, C. Nevado, D. J. Cárdenas, A. M. Echavarren, *Synthesis* **2003**, 2898–2902.
- [429] T. Kataoka, H. Yoshimatsu, Y. Noda, T. Sato, H. Shimazu, M. Hori, *J. Chem. Soc. Perkin Trans. 1* **1993**, *19*, 121–129.
- [430] D. Xing, D. Yang, *Org. Lett.* **2010**, *12*, 1068–1071.
- [431] F. Inagaki, S. Hira, C. Mukai, *Synlett.* **2017**, *28*, 2143–2146.
- [432] B. M. Trost, F. D. Toste, *J. Am. Chem. Soc.* **2002**, *124*, 5025–5036.

- [433] T. R. Hoye, J. A. Suriano, *Organometallics* **1992**, *11*, 2044–2050.
- [434] A. M. Castaño, M. Ruano, A. M. Echavarren, *Tetrahedron Lett.* **1996**, *37*, 6591–6594.
- [435] H.-Y. Lee, H. Y. Kim, H. Tae, B. G. Kim, J. Lee, *Org. Lett.* **2003**, *5*, 3439–3442.
- [436] P. Cao, B. Wang, X. Zhang, *J. Am. Chem. Soc.* **2000**, *122*, 6490–6491.
- [437] M. Méndez, M. P. Muñoz, A. M. Echavarren, *J. Am. Chem. Soc.* **2000**, *122*, 11549–11550.
- [438] F. Schröder, C. Tugny, E. Salanouve, H. Clavier, L. Giordano, D. Moraleda, Y. Gimbert, V. Mouriès-Mansuy, J.-P. Goddard, L. Fensterbank, *Organometallics* **2014**, *33*, 4051–4056.
- [439] C. L. Joe, K. L. Tan, *J. Org. Chem.* **2011**, *76*, 7590–7596.
- [440] A. V. Iosub, *Org. Lett.* **2019**, 7804–7808.
- [441] Y. Quevedo-Acosta, I. D. Jurberg, D. Gamba-Sa, *Org. Lett.* **2020**, *22*, 239–243.